NBSIR 83-2742 (R)

Photonuclear Data - Abstract Sheets 1955 - 1982 Volume I (Hydrogen - Helium)

U.S. DEPARTMENT OF COMMERCE
National Bureau of Standards
National Measurement Laboratory
Center for Radiation Research
Washington, DC 20234

April 1983

DEPARTMENT OF COMMERCE
NAL BUREAU OF STANDARDS

NBSIR 83-2742

PHOTONUCLEAR DATA - ABSTRACT SHEETS 1955 - 1982 VOLUME I (HYDROGEN - HELIUM)

E. G. Fuller, Henry Gerstenberg

U.S. DEPARTMENT OF COMMERCE
National Bureau of Standards
National Measurement Laboratory
Center for Radiation Research
Washington, DC 20234

April 1983

U.S. DEPARTMENT OF COMMERCE, Malcolm Baldrige, *Secretary*
NATIONAL BUREAU OF STANDARDS, Ernest Ambler, *Director*

FOREWORD

This series of reports is the culmination of an effort initiated over 15 years ago to compile and evaluate photonuclear reaction data. Over the years, the NBS Photonuclear Data Center has been almost the sole source of this type of information and as such is recognized for its contribution to nuclear science throughout the world. Its Photonuclear Data Index publications are widely used and acknowledged in the community as an entry point for important information about the field. Consequently, the issuance of these data sheets in tabulated and graphic form, annotated by the authors, will serve to place the overall field in perspective and render in concise form those data which are of value to present and future efforts on nuclear electromagnetic interactions. The Office of Standard Reference Data is pleased to have contributed to the fruition of this effort as represented by the Photonuclear Data Sheets.

D. R. Lide, Jr.

D. R. Lide, Jr., Director
Office of Standard Reference Data

TABLE OF CONTENTS

Photonuclear Data-Abstract Sheets
1955 - 1982

These abstract sheets cover most classes of experimental photonuclear data leading to information of the electromagnetic matrix element between the ground and excited states of a given nucleus. This fifteen volume work contains nearly 7200 abstract sheets and covers 89 chemical elements from hydrogen through americium. It represents a twenty-seven year history of the study of electromagnetic interactions. The sheets are ordered by target element, target isotope, and by an assigned bibliographic reference code. Information is given on the type of measurement, excitation energies studied, source type and energies, detector type, and angular ranges covered in the measurement. For a given reference, the relevant figures and tables are mounted on a separate sheet for each nuclide studied.

I. Introduction

As used in connection with this collection of data-abstract sheets, the term photonuclear data is taken to mean any data leading to information on the electromagnetic matrix element between the ground state and excited states of a given nuclide. The most common types of reactions included in this compilation are: (e,e'), (γ,γ), (γ,γ'), (γ,n), (γ,p), etc. as well as ground-state particle capture reactions, e.g. (α,γ_0). Two reactions which fit the matrix element criterion are not included in the compilation because of their rather special nature. These are heavy particle Coulomb excitation and the thermal neutron capture reaction (n,γ_0). While the energy region of particular interest extends from 0 to 150 MeV, papers are indexed which report measurements in the region from 150 MeV to 4 Gev. Most of the experiments listed are concerned with the excitation energy range from 8 to 30 MeV, the region of the photonuclear giant resonance.

The first set of photonuclear data-abstract sheets was compiled by G. L. Shaw and E. C. Gregg. Copies were distributed to the participants in the conference on photonuclear reactions held at the Case Institute of Technology, Cleveland, Ohio on May 2nd and 3rd, 1955. This compilation consisted of 71 sheets covering 68 elements between hydrogen and uranium. Only three elements, magnesium, copper and bromine, required two sheets to record the data available at the time. The entries made on these sheets were almost equally divided between neutron separation energy and cross section or yield data.

In 1959 Evans Hayward and E. G. Fuller agreed to provide a review article on photonuclear reactions for volume II of the series Nuclear Reactions that was being edited by P. M. Endt and P. B. Smith for the North Holland Publishing Company. In preparing to write this article they updated the Shaw and Gregg file. It soon became obvious that this file of data-abstract sheets was a valuable adjunct to the research programs being carried out in the Betatron Section at the National Bureau

of Standards. The file was maintained informally until January 1963 when a project to compile photonuclear data was established. Later that year, with the establishment of the National Standard Reference Data System under E. L. Brady and M. B. Wallenstein, the Photonuclear Data Center was created. It was one of the first in the System.

After the creation of the Photonuclear Data Project in 1963, it was decided to formalize the data-abstract file, to carry out a systematic literature search to ensure that it covered all experimental papers published after the cut-off date for the Shaw and Gregg compilation, i.e., January 1, 1955, and to maintain it "current" with the published literature for the field. A data-abstract form was devised to systemize the creation of this file. The format adapted was essentially an extension of that which had been used in the Shaw and Gregg compilation. The main modification was to establish a protocol in which, rather than using a single sheet to record all the information about an element, a sheet was made for each nuclide covered in a specific paper. The reference to the paper was given at the top and acknowledged the source of the published data. Photocopies of the pertinent figures and tables from each article were mounted on each sheet. A few of the data-abstract sheets in this collection are in this original format. Most of the sheets, however, are in the format that was developed about a year later when it was decided that a photonuclear data index would be published by the Photonuclear Data Center. In order to facilitate the punching of the 80 column computer cards that would be used to generate this index, the present data-abstract sheet was designed. On the revised form the information for the data-index entry is given in punch-card format at the top of each data-abstract sheet. As with the original format, the complete reference was left at the top. The relevant figures and tables associated with each nuclide are mounted on the bottom of each sheet.

During the close to twenty-year history of the Photonuclear Data Center, its file of data-abstract sheets has proven to be a valuable resource not only for the photonuclear research programs within the Bureau of Standards, but also for visitors from other laboratories and various basic and applied research groups both within as well as outside the United States. With the decision to cease operation of the Center in late 1981, it was decided to reproduce this file of nearly 7200 sheets and make it available free of charge, to the educational and research institutions as well as specialists concerned with the interaction of electromagnetic radiation with nuclei. This volume is the first of 15 that will cover the complete file.

II. Organization of the Photonuclear Data-Abstract File

The hierarchical grouping of the photonuclear data-abstract sheets within the file is by: 1. Target Element, 2. Target Isotope, and 3. by the Bibliographic Reference Code assigned to the paper from which the data on the sheet were abstracted. In this file, colored pages are used to mark the beginning and end of the sheets for each chemical element. A brief historical sketch of the element is given on the divider sheet marking the start of each section; the information for this sketch was derived from the following references: Chapters in the Chemistry of Less Familiar Elements, B. S. Hopkins, Stipes Publishing Co. (1939); Discovery of the Elements, Mary Elvira Weeks, Journal of Chemical Education (1956); Encyclopaedia Britannica, William Benton Publisher, (1966); Encyclopedia of the Chemical Elements, ed. by Clifford A. Hanpel, Reinhold Book Corporation (1968). In those cases where the sheets for a given element make up a major part of a volume, colored pages are also used to delineate sections pertaining to the individual isotopes of the element. Each of the sections of the file, as delineated by two colored divider sheets, represents a 27 year history of the study of electromagnetic interactions in either a specific nuclide or a specific element.

The data-abstract sheets are filed under the element and/or isotope in which the ground-state electromagnetic transition takes place. For example, the abstract sheet for a total neutron yield measurement for a naturally occurring copper sample would appear in the elemental section of the copper file. On the other hand a measurement of the ^{62}Cu 9.73 minute positron activity produced in the same sample by photons with energies below the three-neutron separation energy for ^{65}Cu (28.68 MeV) would be filed with the sheets for ^{63}Cu. Similarly a measurement of the ground-state neutron capture cross section in ^{12}C would be filed uner ^{13}C while the corresponding ground-state alpha-particle capture cross section would be filed under ^{16}O.

At the end of this volume there is a master list of the abbreviations that have been used in the index section of the abstract sheets. The listings are those used in the final published index, Photonuclear Data Index, 1973-1981, NBSIR 82-2543, issued in August 1982 by the U. S. Department of Commerce, National Bureau of Standards, Washington, DC 20234. In some cases two notations are entered for the same quantity. The second entry is the abbreviation that was used in one or more of the earlier published editions of the index.

III. Acknowledgments

Many individuals made significant contributions to the photonuclear data project over the twenty year period it existed. Julia Holland was of invaluable help in setting up the punch-card files used to drive the typewriter that produced the camera-ready copy for the first Photonuclear Data Index (National Bureau of Standards Miscellaneous Publication 277, April 1, 1966). For over thirteen years Theresa Collins Dunn was the mainstay of the project. While ensuring that all entries were made in an uniform and consistent format, she was responsible for maintaining and updating the Center's data-abstract, data-index and bibliographic files. The careful digitizing work of Debra Ann Free during the early 1970's did much to enhance the usefulness of the Center's digital data library. In 1978 Cheryl Campbell willingly stepped in to take on the tedious and exacting work associated with the publication of Photonuclear Data Index, 1973-1977 (NBS Special Publication 380, August 1978). Finally, this set of photonuclear data-abstract sheets would not exist if it were not for the invaluable contributions of Ann Rothgeb who edited and recompiled the master file of data-abstract sheets to produce the camera-ready copy from which the set was produced.

The final acknwledgment is to the physicists at the National Bureau of Standards who for varying time periods over the last 20 years participated in the photonuclear data project. They searched the physics literature to locate and index the pertinent articles and also determined the information that was to appear on each of the data-abstract sheets resulting from an article. In chronological order of their association with the data project these physicist were: J. H. Hubbell, N. V. Baggett, J. S. O'Connell, J. D. Murphy, H. Vander Molen (Nuclear Information Research Associate at NBS, 1972-75) and R. D. Starr.

HYDROGEN
Z=1

Hydrogen is the Greek word for "maker of water." It appears that Theophrastus Paracelsus (Theophrastus Bombastus von Hohenheim) (c. 1490-1541) was familiar with hydrogen since he found that an inflammable gas was evolved when a metal was dissolved in an acid. Paracelsus, born in Switzerland, was a physician and alchemist who established the role of chemistry in medicine. The epithet, Paracelsus, was probably his own invention and was meant to denote his superiority to the great Latin medical writer, Celsus, who lived in the first century A. D.

H
A=1

H
A=1

REF.

C. L. Oxley and V. L. Telegdi
Phys. Rev. 100, 435 (1955)

ELEM. SYM.	A	Z
H	1	1

METHOD

REF. NO.	
55 Ox 1	JOC

REACTION	RESULT	EXCITATION ENERGY	SOURCE		DETECTOR		ANGLE
			TYPE	RANGE	TYPE	RANGE	
G,G	ABX	20 - 98	C	98	TEL-D	20 - 98	DST

Mean energy 64 MeV

Constant efficiency points 40-89 MeV

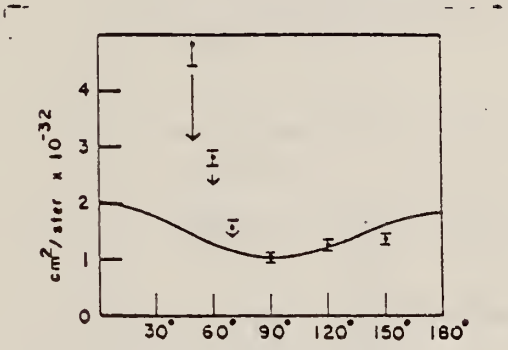

FIG. 1. Experimental points and theoretical curve of differential cross sections.

Ref. C.L. Oxley
Phys. Rev. 110, 733 (1958)

Elem. Sym.	A	Z
H	1	1

Method: counter telescope

Ref. No.: 58 Ox 1 | F/H

Reaction	E or ΔE	E_0	Γ	$\int \sigma dE$	Jπ	Notes
$H^1(\gamma,\gamma)$	87					70-150°. Angular distribution at E_γ = 60±55/2

TABLE III. Values of A, B, and β from the relation $(A+B\sin^2\vartheta^*)\times(1+2\beta\cos\vartheta^*)$ representing the cross section. The isotropic part, the $\sin^2\vartheta^*$ part, and the total cross sections are given in the last three columns.

k_0 Mev	2β	A μb/sterad	B μb/sterad	$4\pi A$ μb	$8\pi B/3$ μb	σ_{total} μb
65	0.25	5.0	5.7	62	47	109
80	0.35	4.5	3.9	56	32	88
105	0.38	3.9	2.2	49	18	67
140	0.40	3.4	1.3	43	11	54
114	0.40	5.3	0.9	67	7	74
149	0.44	3.5	1.2	44	10	54
194	0.22	4.2	2.9	53	24	77
248	0.10	4.2	0.9	53	11	64
220	0.22	4.5	1.3	57	11	68

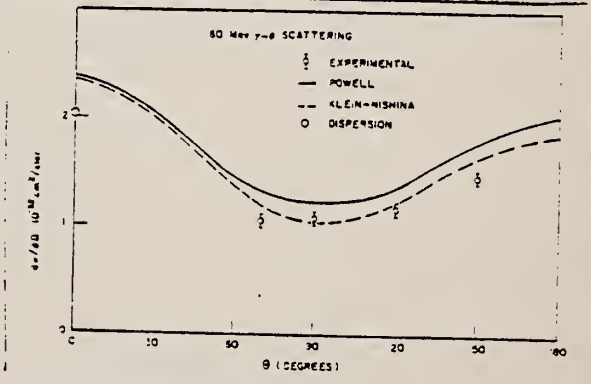

FIG. 6. Experimental and theoretical differential cross sections.

Ref. V.I. Gol'danskii, O.A. Karpukhin, A.V. Kutsenko, V.V. Pavlovskaya
Zhur. Eksp. i Teoret. Fiz. 38, 1695 (1960);
Soviet Phys. JETP 11, 1223 (1960)

Elem. Sym.	A	Z
H	1	1

Method

Ref. No.	
60 Go 1	JHH

Reaction	E or ΔE	E_0	Γ	$\int \sigma dE$	Jπ	Notes
$H^1(\gamma,\gamma)$	40-70 E_B = 75					Cross-section measurements at θ_γ = 45°, 75°, 90°, 120°, 135° and 150°. Magnetic polarizability determined to be much less than electric polarizability. From 90° setting determine proton electric polarizability α_E = $(11\pm4)\ 10^{-43}$ cm^3. From π production, $\alpha_E + \alpha_M$ = 11×10^{-43} cm^3, where $\alpha_E = (9\pm2)\ 10^{-43}$ cm^3 $\alpha_M = (2\pm2)\ 10^{-43}$ cm^3.

Angle ϑ, deg.	$10^{44}\frac{d\sigma}{d\Omega}(\vartheta)$, cm²/sr (without correction)	Correction for absorption of primary and registered γ quanta, Δσ/σ, %	Correction (for extraneous processes (in units of 10^{-44} cm²/sr)) Rutherford scattering of electrons with subsequent radiation	Pair production at large angles with subsequent radiation	Emission of bremsstrahlung radiation at large angles	Total Correction	$10^{44}\frac{d\sigma}{d\Omega}(\vartheta)$, cm²/sr (final values)
45	4.66±0.28	−8.5	−127	−14.1	−5.4	−146	3.40±0.28
75	1.21±0.08	−3.5	−10.7	−1.4	−0.47	−12.6	1.12±0.08
90	1.14±0.05	−3.5	−6.7	−0.7	−0.3	−7.7	1.10±0.05
120	1.30±0.08	−4.5	−1.4	−0.18	−0.06	−1.6	1.34±0.08
135	1.48±0.08	−8.5	−0.89	−0.09	−0.04	−1.0	1.56±0.08
150	1.32±0.07	−8.5	−0.36	−0.04	−0.01	−0.4	1.93±0.07

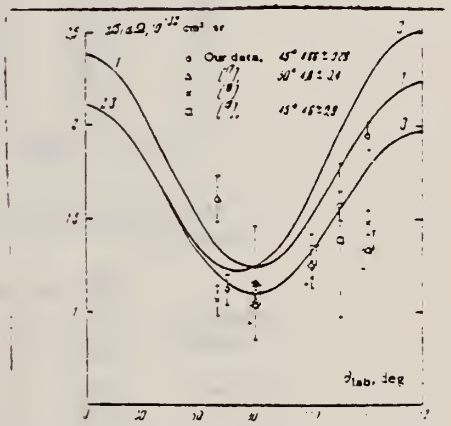

FIG. 5. Experimental data on γp scattering with ~60-Mev γ quanta. Curves – calculated: 1 – for $A_E = A_M = 0$; 2 – for $A_E = 0$, $A_M = 16$; 3 – for $A_E = 16$ and $A_M = 0$. The γp scattering cross sections compatible with the value $A_E + A_M = 16$ ($A_E, A_M > 0$) lies between curves 2 and 3 (ϑ – angle in the laboratory system).

Ref. J.M. Wyckoff, H.W. Koch
Phys. Rev. 117, 1261 (1960)

Elem. Sym.	A	Z
H	1	1

Method: 180 MeV Synchrotron; total absorption; NaI

Ref. No.: 60 Wy 1 JHH

Reaction	E or ΔE	E_o	Γ	$\int \sigma dE$	Jπ	Notes
H (σ_t)	Bremss. 35-90					Difference between graphite and cyclohexane (C_6H_{12}) attenuators. ERRATUM: In Table IV, conversion factor R [= $(cm^2/g)/(barns/atoms)$] should be changed from 0.5997 to 0.5977.

TABLE II. Experimental attenuation coefficients in cm^2/g.

Energy, Mev	Carbon	Aluminum	Water	Hydrogen
13.3	0.01795	0.02213	0.02026	0.02521
17.5	0.01648	0.02219	0.01883	0.02239
21.5	0.01626	0.02268	0.01846	0.02018
25.9	0.01566	0.02193	0.01766	0.01822
30.3	0.01507	0.02208	0.01721	0.01702
34.3	0.01482	0.02231	0.01701	0.01622
38.3	0.01465	0.02259	0.01693	0.01546
42.3	0.01453	0.02279	0.01684	0.01472
46.3	0.01446	0.02300	0.01677	0.01409
50.3	0.01440	0.02322	0.01675	0.01375
54.3	0.01440	0.02351	0.01676	0.01347
58.3	0.01440	0.02367	0.01681	0.01310
62.3	0.01442	0.02392	0.01685	0.01293
66.2	0.01442	0.02409	0.01685	0.01258
70.2	0.01442	0.02429	0.01687	0.01233
74.2	0.01445	0.02454	0.01696	0.01203
78.2	0.01445	0.02472	0.01699	0.01155
82.2	0.01447	0.02500	0.01711	0.01116

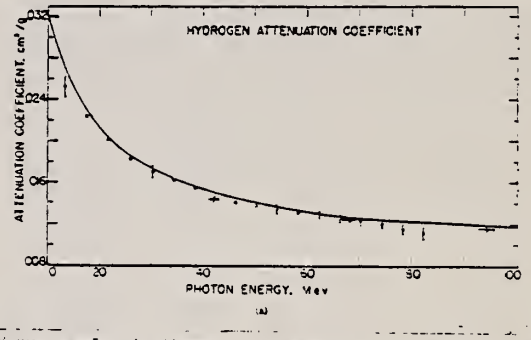

FIG. 7. Detailed plot of attenuation coefficients for (a) hydrogen, (b) carbon, (c) water, and (d) aluminum showing the predicted curves electronic (see text) and the experimental curves. The maximum error is indicated on (a) while only the statistical accuracy is indicated on (b), (c), and (d). The results of the Circular 583 carbon calculation are shown. The carbon curve has been plotted for a pair correction factor of 1.008 and 1.030 in addition to the value 1.0125 used for the water and aluminum curves. The synthesis of a nuclear cross section is shown for carbon, water, and aluminum as well as the experimental nuclear cross section. The latter was obtained by subtracting the predicted curve for the electronic processes only from the experimental points. Experimental points of Lawson at 19 Mev and Morfatt *et al.*[4] at 34, 68, and 82 Mev are shown by triangles as are some of the lower energy results tabulated in reference 1.

TABLE III. Sources of error and estimates of uncertainties.

Material	Energy range Mev	Statistics %	Response function, % Density %	Energy uncertainty	Correction factor	Total %
Hydrogen	13–30	2.4	1.4	0.9	1.6	3.3
	30–80	2.4	1.4	1.6	0.3	3.2
Carbon	13–25	0.8	0.2	0.0	0.7	1.1
	25–30	0.8	0.2	0.4	0.4	1.0
	30–80	0.8	0.2	0.3	0.2	0.9
Water	13–25	0.9	0.1	0.0	0.6	1.1
	25–30	0.9	0.1	0.3	0.3	1.0
	30–80	0.9	0.1	0.3	0.2	1.0
Aluminum	13–25	0.9	0.1	0.0	0.4	1.0
	25–30	0.9	0.1	0.1	0.3	1.0
	30–80	0.9	0.1	0.5	0.3	1.1

[1] G. White Grodstein, *X-Ray Attenuation Coefficients from 10 kev to 100 Mev*, National Bureau of Standards Circular No. 583 (U. S. Government Printing Office, Washington, D. C., 1957). An earlier unpublished NBS report, 1952, also by G. White Grodstein has been duplicated in the following articles: (a) C. M. Davisson and R. D. Evans, Revs. Modern Phys. 24, 102 (1952); (b) R. H. Morgan, *Handbook of Radiology* (The Year-Book Publishers, Inc., Chicago, 1955), pp. 99–117; (c) K. Siegbahn, *Beta- and Gamma-Ray Spectroscopy* (Interscience Publishers, Inc., New York, 1955), pp. 857–874. The basic difference between the two Grodstein reports is in the triplet cross sections used. The 1952 report used the Borsellino cross sections, while NBS Circular 583 used the Votruba results. To illustrate the differences, the present experiment at 60 Mev yields a carbon attenuation coefficient of 0.01441 ±1% cm^2/g to be compared with 0.0142 cm^2/g in the 1952 NBS report and 0.0138 cm^2/g in NBS Circular 583.

REF.

P. S. Baranov, L. I. Slovokhotov, G. A. Sokol, and L. N. Shtarkov
J. Exptl. Theoret. Phys. (USSR) 41, 1713 (1961)
Soviet Phys. JETP 14, 1219 (1962)

ELEM. SYM.	A	Z
H	1	1

METHOD

REF. NO.	
61 Ba 3	EGF

REACTION	RESULT	EXCITATION ENERGY	SOURCE		DETECTOR		ANGLE
			TYPE	RANGE	TYPE	RANGE	
G,G	ABX	247	C	260	TEL-D		DST

Energy of recoil p gave photon energy E = 247±10 MeV.

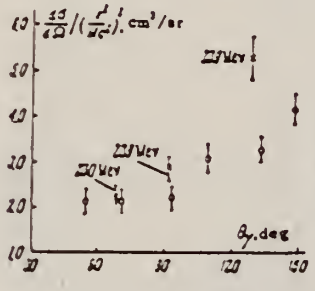

FIG. 4. Angular distribution (c.m.) of γ rays scattered elastically on hydrogen, converted to 247 Mev (lab. system). o – present work; x – from [4].

Ref. R.F. Stiening, R. Loh, M. Deutsch
Phys. Rev. Letters 10, 536 (1963)

Elem. Sym.	A	Z
H	1	1

Method: Synchrotron; 4 spark chambers

Ref. No.: 63 St 1 | JHH

Reaction	E or ΔE	E_0	Γ	$\int \sigma dE$	Jπ	Notes
$H^1(\gamma,\gamma)$	Bremss. 900					Results are for energy range 500-850 MeV.

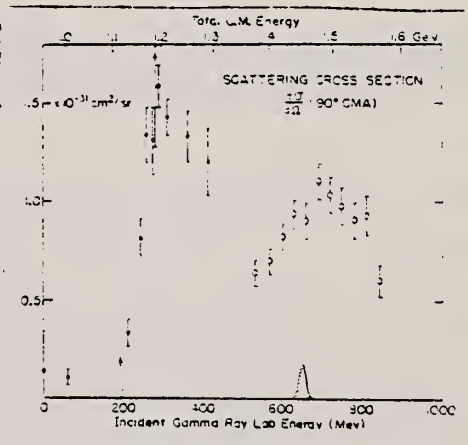

FIG. 1. Differential cross section at 90° for elastic gamma-ray scattering. Open circles show results of this paper. The shaded area indicates the approximate energy resolution.

REF. A. Ito, R. Loe, E. C. Loh, A. Ramanauskas, D. Ritchie, W. Schmidt
Phys. Rev. Letters 24, 687 (1970)

ELEM. SYM.	A	Z
H	1	1

METHOD

REF. NO. 70 It 1 hmg

REACTION	RESULT	EXCITATION ENERGY	SOURCE		DETECTOR		ANGLE
			TYPE	RANGE	TYPE	RANGE	
G,PI+	RLX	600-999	C	600-999	SPK-I		4PI
		(600-1700)		(600-1700)			

Detected pions. R = $\gamma(d,2N)/\gamma(P,N)$ 999=1700 MEV

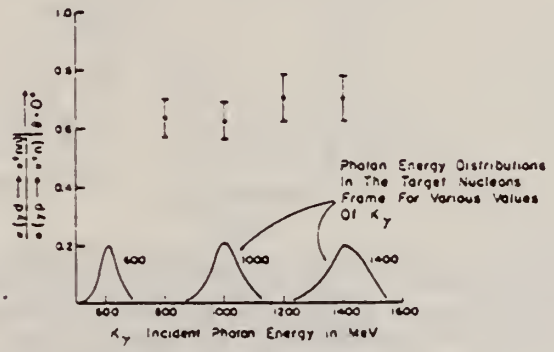

FIG. 4. Ratio $(\gamma + d \rightarrow \pi^+ nn)/(\gamma + p \rightarrow \pi^+ n)$ as a function of incident photon energy.

REF.

V.M. Kuznetsov, O.I. Stukov, E.V. Repenko, V.D. Epaneshnikov, V.N. Zabaev, and A.P. Potylitsyn
Yad. Fiz. 13, 1052 (1971)
Sov. J. Nucl. Phys. 13, 603 (1971)

ELEM. SYM.	A	Z
H	1	1

METHOD

REF. NO.	
71 Ku 4	hmg

REACTION	RESULT	EXCITATION ENERGY	SOURCE		DETECTOR		ANGLE
			TYPE	RANGE	TYPE	RANGE	
$G,PI+	NOX	210-270	D	210-270	TEL-D		DST

N,PI+ COIN. POL. G

We present a procedure and results of the measurements of the asymmetry of the photoproduction of π^+ mesons on a linearly polarized beam of photons for the angles 51, 82, 106, 116, 133, and 134° at photon energies in the region 210–270 MeV.

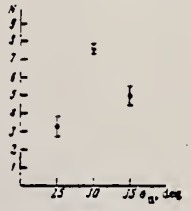

FIG. 2

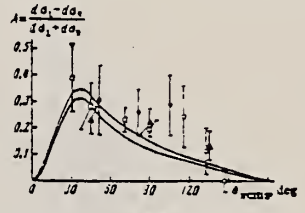

FIG. 3

FIG. 2. Dependence of the counting rate of the π^+n coincidences on the angle of installation of the neutron detector for $\theta_\pi = 90°$ in the l.s. and $E_\gamma = 230$ MeV. The maximum at the point $\theta_\pi = 30°$ corresponds to the kinematics of the reaction $\gamma + p \to \pi^+ + n$.

FIG. 3. Dependence of the asymmetry on the angle of the emission of the π^+ meson in the reaction $\gamma + p \to \pi^+ + n$ at $E_\gamma = 230$ MeV. Points: □–Frascati data [6], Δ–Stanford [11], ●, ○–our data. Curves–theoretical calculation [1].

Table II

E_γ, MeV	θ_π (cms), deg	P	A	$\frac{\nu^H_\perp - \nu^H_\parallel}{\nu^H_\perp + \nu^H_\parallel}$
230±5	51±3.5	0.331±0.046	0.706±0.133	0.103±0.0125
230±5	82±3.5	0.331±0.046	0.254±0.085	0.0875±0.0130
230±5	106±3.5	0.331±0.046	0.287±0.114	0.0930±0.0354
230±10	116±3.5	0.331±0.046	0.240±0.120	0.0795±0.0362
230±10	133±3.5	0.331±0.046	0.110±0.068	0.0364±0.0257
230±10	146±3.5	0.331±0.046	0.010±0.040	0.0033±0.0132

Table I

E_γ, MeV	θ_π (cms), deg	P	A	$\frac{\nu^H_\perp - \nu^H_\parallel}{\nu^H_\perp + \nu^H_\parallel}$
277±13	106±6	0.120	0.14±0.16	0.0168±0.0191
216±9	106±6	0.132	0.17±0.19	0.0224±0.0248
253±9	106±6	0.137	0.30±0.16	0.0411±0.0215
237±10	133±6	0.130	0.16±0.13	0.0208±0.0164
250±7	134±6	0.136	0.19±0.17	0.0258±0.0219

REF. S. Arai, S. Fukui, N. Horikawa, R. Kajikawa, T. Kasuga, H. Kobayakawa, A. Masaike, T. Matsuda, T. Nakanishi, T. Ohshima, M. Saito, S. Sugimoto, T. Yamaki, K. Amako, K. Yoshida
Nucl. Phys. B48, 397 (1972)

ELEM. SYM.	A	Z
H	1	1

METHOD

REF. NO. 72 Ar 9 egf

REACTION	RESULT	EXCITATION ENERGY	SOURCE TYPE	SOURCE RANGE	DETECTOR TYPE	DETECTOR RANGE	ANGLE
$G,PI+	ABX	300-900	C	300-900	MAG-D		90

POLARIZED TARGET

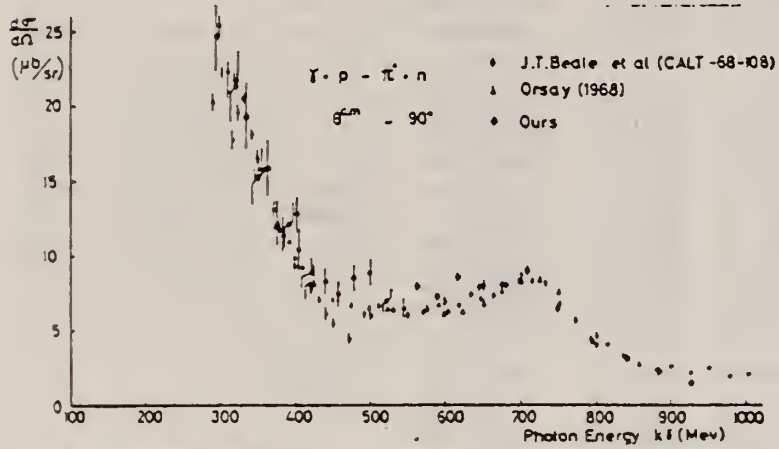

Fig. 8. Differential cross section of $\gamma p \rightarrow \pi^0 n$ at 90° c.m. obtained from the subtraction (CH_2 – C) are shown with other data measured by the hydrogen target.

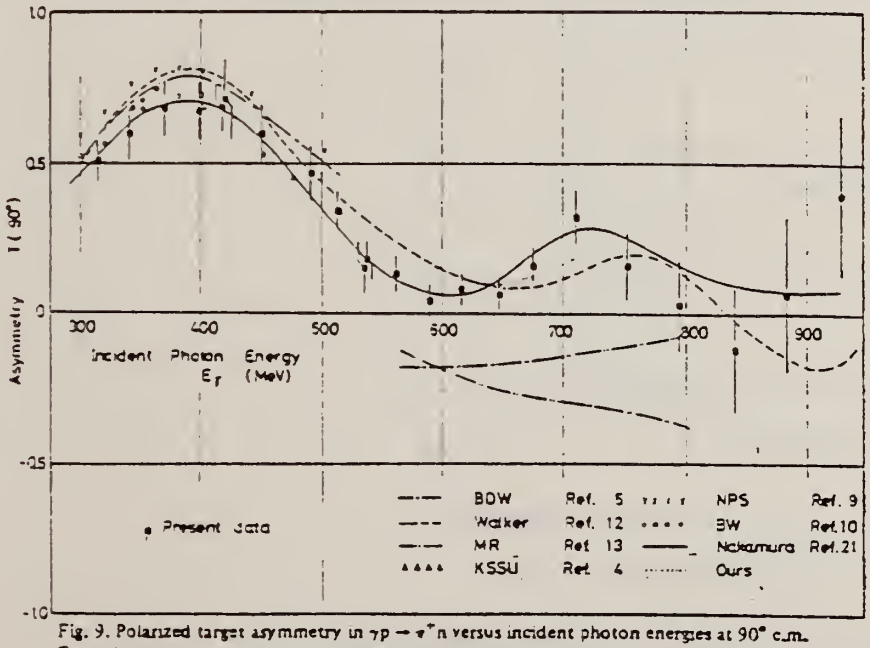

Fig. 9. Polarized target asymmetry in $\gamma p \rightarrow \pi^0 n$ versus incident photon energies at 90° c.m. Errors indicated are statistical only. The results from various analyses are also shown for comparison.

(continued)

Table 3

Results of asymmetries in $\gamma p \to \pi^+ n$ at 90° c.m. The errors shown in the asymmetry column are statistical only. The errors arising from the unknown asymmetries in double pion production processes are quoted in the note column; blank spaces indicate no contribution from the processes. The errors indicated in the incident photon energy and the angle are FWHM of the spectrometer acceptances.

Maximum energy of bremsstrahlung E_{max} (MeV)	Incident photon energy E_γ (MeV)	π^+ c.m. angle θ (deg.)	Asymmetry $T(\theta)$	Note
475	314 ± 16	91.4 ± 2.2	0.510 ± 0.071	
	340 ± 16	89.9 ± 2.5	0.598 ± 0.085	
	369 ± 17	88.6 ± 2.6	0.685 ± 0.094	
	398 ± 18	87.5 ± 2.9	0.678 ± 0.096	
	419 ± 13	86.9 ± 3.1	0.713 ± 0.137	
575	417 ± 22	89.7 ± 3.2	0.690 ± 0.085	
	449 ± 23	87.0 ± 3.3	0.603 ± 0.098	
	490 ± 24	86.7 ± 3.3	0.470 ± 0.089	
	534 ± 25	86.8 ± 3.4	0.156 ± 0.088	
750	513 ± 13	86.6 ± 3.4	0.346 ± 0.066	± 0.066
	537 ± 14	86.5 ± 3.4	0.181 ± 0.065	± 0.029
	561 ± 14	86.6 ± 3.4	0.136 ± 0.062	
	589 ± 15	86.6 ± 3.5	0.043 ± 0.060	
	616 ± 16	86.7 ± 3.5	0.083 ± 0.054	
	646 ± 16	87.1 ± 3.6	0.068 ± 0.053	
	675 ± 16	87.3 ± 3.6	0.171 ± 0.053	
1000	710 ± 23	87.6 ± 3.7	0.322 ± 0.092	± 0.026
	752 ± 24	88.0 ± 3.7	0.161 ± 0.115	± 0.012
	794 ± 25	88.4 ± 3.8	0.029 ± 0.150	~0
	840 ± 26	89.0 ± 3.8	−0.119 ± 0.207	
	883 ± 26	89.3 ± 3.9	0.064 ± 0.258	
	929 ± 27	89.8 ± 3.9	0.395 ± 0.267	

REF.

C. Bacci, R. Baldini-Celio, B. Esposito, C. Mencuccini, A. Reale, G. Sciacca, M. Spinetti and A. Zallo
Lettere al Nuovo Cimento 4, 5 (1972)

ELEM. SYM.	A	Z
H	1	1

METHOD

REF. NO.	
72 Ba 5	egf

REACTION	RESULT	EXCITATION ENERGY	SOURCE		DETECTOR		ANGLE
			TYPE	RANGE	TYPE	RANGE	
G,PIO	RLX	400-800	C	999	TEL-D		DST

999 = 1.1 GEV

TABLE I.

$\theta_\pi^* = 60°$		$\theta_\pi^* = 90°$		$\theta_\pi^* = 135°$	
E'_γ	r	E'_γ	r	E'_γ	r
505	0.78 ± 0.07	430	0.82 ± 0.03	471	0.93 ± 0.06
539	0.84 ± 0.07	476	0.84 ± 0.03	520	0.87 ± 0.07
606	0.85 ± 0.05	508	0.77 ± 0.03	556	0.81 ± 0.06
658	0.79 ± 0.05	547	0.85 ± 0.03	596	0.82 ± 0.07
701	0.83 ± 0.05	591	0.84 ± 0.04	644	0.77 ± 0.08
733	0.98 ± 0.06	623	0.77 ± 0.04	683	0.90 ± 0.08
773	1.08 ± 0.11	667	0.91 ± 0.05	736	0.81 ± 0.09
		710	0.86 ± 0.05		
		738	0.90 ± 0.07		

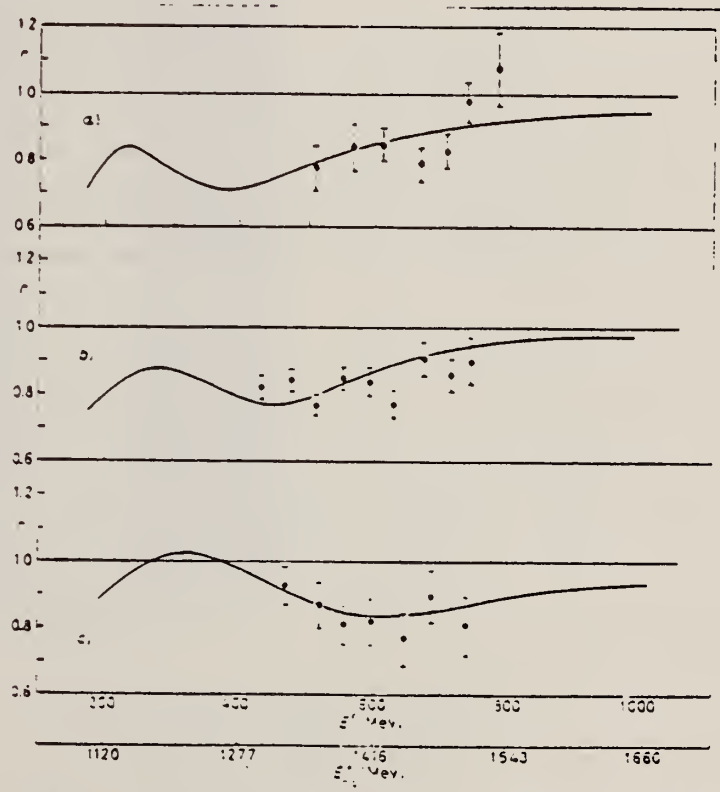

Fig. 1. – Ratio $r = (d\sigma/d\Omega^*(\gamma D \to \pi^+ p(n_s))/(d\sigma/d\Omega^*)\gamma p \to \pi^+ n)$ at different π^+ c.m. angles vs. $E'^*_{\pi_p}$, the total c.m. energy of the $\pi^+ p$ final-state system and also vs. E'_γ, the incident-photon energy which gives on free proton a total c.m. energy $E'^*_{\pi_p}$. a) $\theta_\pi^* = 60°$, b) $\theta_\pi^* = 90°$, c) $\theta_\pi^* = 135°$.

REF.

Yu. I. Titov and E.V. Stepula
Yad. Fiz. 15, 649 (1972)
Sov. J. Nucl. Phys. 15, 361 (1972)

EL EM. SYM.	A	Z
H	1	1

METHOD

REF. NO.	
72 Ti 4	hmg

REACTION	RESULT	EXCITATION ENERGY	SOURCE		DETECTOR		ANGLE
			TYPE	RANGE	TYPE	RANGE	
E,E/	SPC	0-530	D	999	MAG-D		DST

999=1.18 GEV

θ	Li^6 nucleus			Protons, $d\sigma/d\Omega$, cm^2/sr	
	β	$(d\sigma/d\Omega)_{dec.}$, cm^2/sr	$(d\sigma/d\Omega)_{qu.}$, cm^2/sr	Present work	Theory [13]
16°50′	0.65±0.05	(6.45±0.71)·10^{-30}	(1.20±0.08)·10^{-29}	(1.04±0.12)·10^{-29}	0.99·10^{-29}
20°50′	0.66±0.06	(3.01±0.30)·10^{-30}	(4.09±0.30)·10^{-30}	(0.48±0.05)·10^{-29}	0.50·10^{-29}
24°40′	0.70±0.03	(1.39±0.15)·10^{-30}	(1.75±0.16)·10^{-30}	(0.29±0.03)·10^{-29}	0.28·10^{-29}
32°	0.72±0.05	(4.72±0.40)·10^{-31}	(4.65±0.45)·10^{-31}	(0.78±0.10)·10^{-31}	1.02·10^{-31}
40°	0.76±0.05	(1.71±0.15)·10^{-31}	(1.39±0.15)·10^{-31}	—	3.98·10^{-32}
47°	0.81±0.06	(8.61±0.80)·10^{-32}	(6.07±0.61)·10^{-32}	—	1.93·10^{-32}
55°	0.82±0.06	(3.80±0.30)·10^{-32}	(2.52±0.50)·10^{-32}	—	9.31·10^{-33}

Note. The initial electron energy is 1180 MeV.

REF.

R. W. Zdarko and E. B. Dally
Il Nuovo Cimento 10A, 10 (1972)

ELEM. SYM.	A	Z
H	1	1

METHOD

REF. NO.	
72 Zd 1	hmg

REACTION	RESULT	EXCITATION ENERGY	SOURCE		DETECTOR		ANGLE
			TYPE	RANGE	TYPE	RANGE	
$ G,PI +	NOX	150-909	C	390-909	MAG-D		135
$ G,PI0	NOX	150-918	C	426-918	MAG-D		DST

POLARIZED PHOTONS

TABLE I. – *Asymmetry values measured in this experiment.*

$\gamma+p\to n+\pi^-$, $\theta_{c.m.}=135°$	
E_γ	A
390	0.348 ± 0.042
408	0.247 ± 0.044
460	0.321 ± 0.043
485	0.312 ± 0.047
793	0.160 ± 0.076
842	-0.341 ± 0.123
849	-0.171 ± 0.097
909	-0.302 ± 0.156

$\gamma+p\to p+\pi^0$, $\theta_{c.m.}=60°$	
E_γ	A
628	0.417 ± 0.128
653	0.251 ± 0.132
673	0.373 ± 0.126
720	0.493 ± 0.069
731	0.570 ± 0.069
775	0.667 ± 0.075
847	0.361 ± 0.092
886	0.646 ± 0.126
913	0.573 ± 0.130

$\gamma+p\to p+\pi^0$, $\theta_{c.m.}=90°$	
E_γ	A
426	0.517 ± 0.021
440	0.504 ± 0.024
452	0.487 ± 0.026
521	0.565 ± 0.063
541	0.607 ± 0.074
556	0.622 ± 0.089
594	0.528 ± 0.080
617	0.694 ± 0.098
636	0.834 ± 0.114
667	0.629 ± 0.069
694	0.707 ± 0.077
715	0.864 ± 0.084
729	0.622 ± 0.041
729 (*)	0.657 ± 0.083
760	0.682 ± 0.044
760 (*)	0.600 ± 0.077
783	0.750 ± 0.050
783 (*)	0.632 ± 0.085
816	0.664 ± 0.057
851	0.668 ± 0.077
878	0.730 ± 0.099

(*) = coincidence data.

(continued)

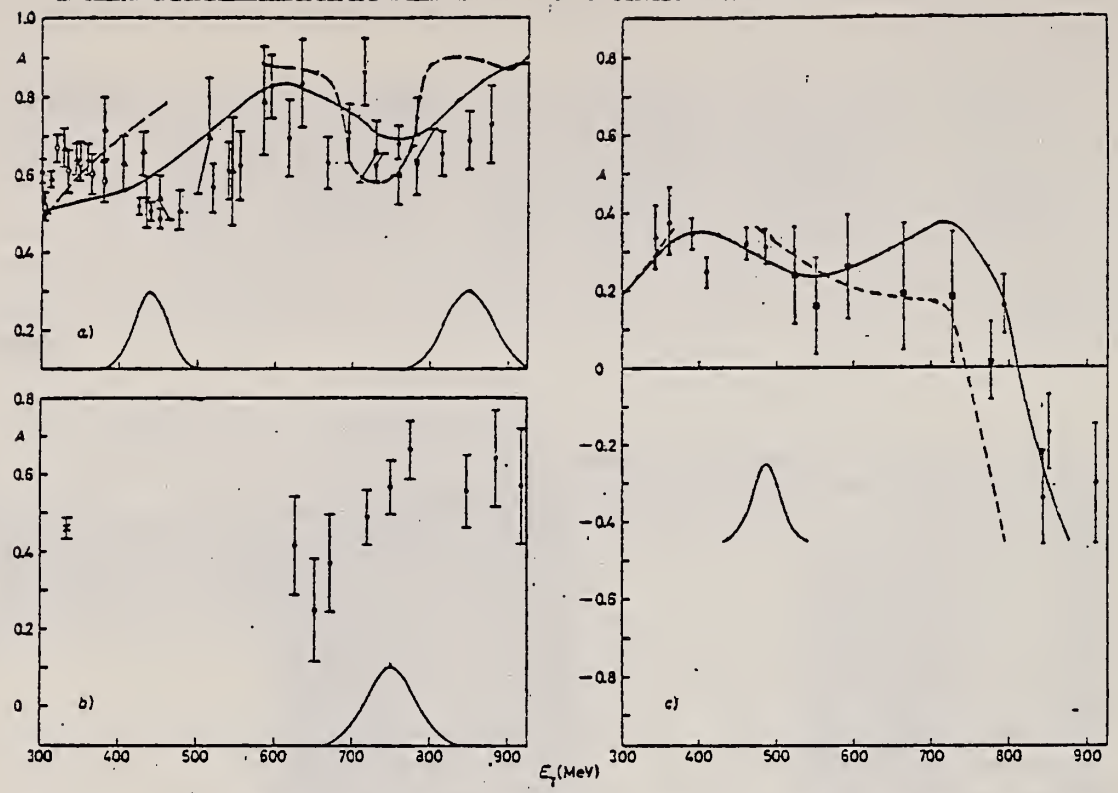

Fig. 3. – Asymmetry values $A = (\sigma_\perp - \sigma_\parallel)/(\sigma_\perp + \sigma_\parallel)$ from this experiment plotted with other data and compared to the theoretical curves of WALKER and SCHMIDT: *a*) π^0 at $\theta_{c.m.} = 90°$, $\gamma + p \to p + \pi^0$; • this experiment, ▪ this experiment with π^0 coincidence, ▲ BOLOGNA *et al.*, × DRICKEY *et al.*, – – – SCHMIDT *et al.*, —— WALKER, ◇ BARBIELLINI *et al.* *b*) π^0 at $\theta_{c.m.} = 60°$, $\gamma + p \to p + \pi^0$; • this experiment, × DRICKEY *et al.* *c*) π^+ at $\theta_{c.m.} = 135°$, $\gamma + p \to n + \pi^+$; • this experiment, ▪ LIU *et al.*, ▲ SMITH *et al.*, – – – SCHMIDT *et al.*, —— WALKER.

REF. Yu. M. Aleksandrov, V.B. Ganenko, V.F. Grushin, I.I. Miroshnichenko, V.M. Sanin, P.V. Sorokin
Yad. Fiz. 20, 915 (1974)
Sov. J. Nucl. Phys. 20, 487 (1975)

ELEM. SYM.	A	Z
H	1	1

METHOD

REF. NO. 74 Al 13 . hmg

REACTION	RESULT	EXCITATION ENERGY	SOURCE		DETECTOR		ANGLE
			TYPE	RANGE	TYPE	RANGE	
G,PI+	RLX	200-400	C	600	MAG-D		DST

The measured values of the ratio of the $\gamma d \to n n \pi^+$ and $\gamma p \to n \pi^+$ differential cross sections are presented in the photon energy region 200–400 MeV for pion emission angles 25°–140°. The average statistical accuracy of the results is ±2.5%; the systematic error is ~ ±3%. The results disagree with theoretical calculations based on the model of Chew and Lewis.

D(G,PI+)/P(G,PI+)

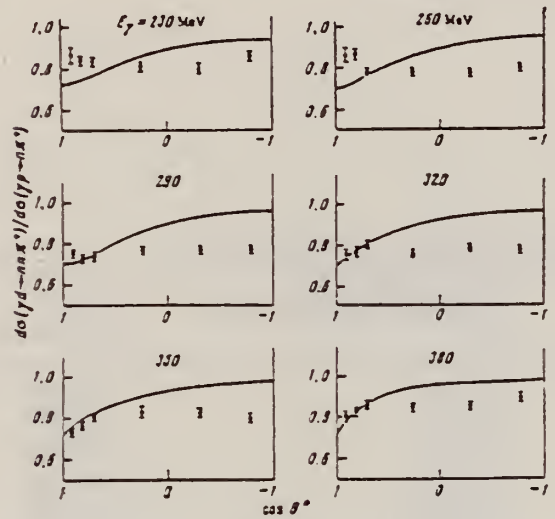

FIG. 2. Experimental results in the form of angular distributions. The solid curves represent calculations based on the theory of Chew and Lewis. [11]

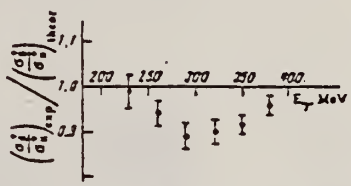

FIG. 3. Ratios of the experimental total photoproduction cross sections from deuterium and hydrogen compared with the theory in [11]. The experimental values were obtained by averaging the data represented in Fig. 2 on the angular distributions of the $\gamma p \to n \pi^+$ process.

$d\sigma(\gamma d \to n n \pi^+)/d\sigma(\gamma p \to n \pi^+)$ for different angles and energies

θ*, deg	E_γ, MeV			
	200	230	260	290
25		0.560±0.025	0.580±0.030	0.735±0.025
33		0.525±0.020	0.670±0.025	0.730±0.020
45		0.570±0.020	0.760±0.020	0.740±0.020
75	0.550±0.025	0.810±0.020	0.785±0.015	0.765±0.020
107		0.900±0.025	0.760±0.015	0.770±0.020
140	0.535±0.025	0.860±0.020	0.905±0.020	0.770±0.020

Continued

θ*, deg	E_γ, MeV			
	320	350	380	400
25	0.735±0.020	0.735±0.020	0.810±0.020	
33	0.770±0.020	0.765±0.015	0.850±0.020	
45	0.805±0.020	0.810±0.020	0.865±0.020	
75	0.760±0.020	0.835±0.020	0.900±0.020	
107	0.790±0.020	0.850±0.020	0.860±0.020	
140	0.780±0.020	0.800±0.020	0.900±0.020	0.905±0.025

[11] G.F. Chew and H.W. Lewis, Phys. Rev. 84, 779 (1951).

REF. P. Baranov, G. Buinov, V. Godin, V. Kuznetzova, V. Petrunkin, L. Tatarinskaya, V. Shirthenko, L. Shtartkov, V. Yurtchenko, and Yu. Yanulis
Phys. Letters 52B, 122 (1974)

ELEM. SYM.	A	Z
H	1	1

METHOD

REF. NO.	
74Ba 9	egf

REACTION	RESULT	EXCITATION ENERGY	SOURCE		DETECTOR		ANGLE
			TYPE	RANGE	TYPE	RANGE	
G,G	ABX	70-110	C	UKN	UKN-D		DST

Monitor cross section $e\gamma \rightarrow e'\gamma'$

The γp-elastic scattering cross section has been measured in the photon energy range 70–110 MeV. As a monitor process the electron Compton-scattering was simultaneously measured. The values of the electric ($\bar{\alpha}$) and magnetic ($\bar{\beta}$) polarizabilities of the proton were obtained from the experimental data: $\bar{\alpha} = (10.7 \pm 1.1) \times 10^{-43}$ cm^3; $\bar{\beta} = (-0.7 \pm 1.6) \times 10^{-43}$ cm^3.

Table 2.
The experimental results on the photon elastic scattering on protons

The different gamma-ray counter sets	ϑ lab. syst. (degree)	ω (MeV)	The ratio of the principal to the monitor process cross sections $\times 10^{-7}$	$(d\sigma/d\Omega)$ 10^{-32} cm^2/st.
I	90	85.4	1.52 ± 0.05	1.09 ± 0.04
II	90	80.9	1.60 ± 0.09	1.15 ± 0.06
I	150	86.3	1.92 ± 0.14	1.37 ± 0.10
II	150	81.9	2.02 ± 0.17	1.44 ± 0.12
I	90	109.9	1.44 ± 0.07	1.03 ± 0.06
I	150	111.1	2.02 ± 0.06	1.44 ± 0.06
II	150	106.7	2.22 ± 0.09	1.60 ± 0.08

REF.	ELEM. SYM.	A	Z
P.S. Baranov, G.M. Buinov, V.G. Godin, V.A. Kuznetsova, V.A. Petrun'kin, L.S. Tatarinskaya, V.S. Shirchenko, L.N. Shtarkov, V.V. Yurchenko, and Yu.P. Yanulis ZhETF Pis. Red 19, 777 (1974); JETP Lett. 19, 398 (1974)	H	1	1

METHOD	REF. NO.
	74 Ba 11 hmg

REACTION	RESULT	EXCITATION ENERGY	SOURCE		DETECTOR		ANGLE
			TYPE	RANGE	TYPE	RANGE	
G,G	ABX	85-107	C	127,148	TEL-D		DST

We measured the differential cross section for elastic scattering of photons by protons at angles 90° and 150° in the energy interval from 70 to 110 MeV. The experimental data were used to determine the coefficients of the electric and magnetic polarizabilities of the proton, $\alpha=(10.7\pm1.1)\times10^{-43}$ cm^3 and $\beta=(-0.7\pm1.6)\times10^{-43}$ cm^3, respectively.

Experimental results for elastic scattering of photons by protons, absolutized against a monitor process.

Variant of assembly of telescope	θ, Lab system, deg.	ω, MeV	Ratio of cross sections of the main and of the monitor process	$\frac{d\sigma}{d\Omega}\,10^{32}$ cm^2/sr
I	90	85.4*	$(1.52\pm0.03)\cdot10^{-7}$	1.09 ± 0.04
II	90	80.9	$(1.60\pm0.09)\cdot10^{-7}$	1.15 ± 0.06
I	150	88.3	$(1.92\pm0.14)\cdot10^{-7}$	1.37 ± 0.20
II	150	81.9	$(2.02\pm0.17)\cdot10^{-7}$	1.44 ± 0.12
I	90	109.9	$(1.44\pm0.07)\cdot10^{-7}$	1.03 ± 0.06
I	150	111.1	$(2.02\pm0.06)\cdot10^{-7}$	1.44 ± 0.06
II	150	106.7	$(2.22\pm0.09)\cdot10^{-7}$	1.60 ± 0.08

REF.

R.W. Clifft, E. Gabathuler, L.S. Littenberg, R. Marshall, S.E. Rock, J.C. Thompson, D.L. Ward, and G.R. Brookes
Phys. Rev. Letters 33, 1500 (1974)

ELEM. SYM.	A	Z
H	1	1

METHOD

REF. NO.: 74 C1 10 hmg

REACTION	RESULT	EXCITATION ENERGY	SOURCE TYPE	SOURCE RANGE	DETECTOR TYPE	DETECTOR RANGE	ANGLE
G,PI0	ABX	150-450	C	250-450	Tel-D		DST
G,PI+	ABX	150-450	C	250-450	Tof-D		DST

TAGGED PHOTONS

Differential cross sections for the reactions $\gamma p \to \pi^0 p, \pi^+ n$ and $\gamma n \to \pi^- p, \pi^0 n$ were measured in a single experiment using tagged photons in the energy region 240–450 MeV incident on $^1H_2$ and $^2H_2$ targets. Results of the ratios $\pi^0 n/\pi^0 p$ and $\pi^- p/\pi^+ n$ are presented. The ratio of isotensor to isovector amplitude is found to be 0.00 ± 0.02.

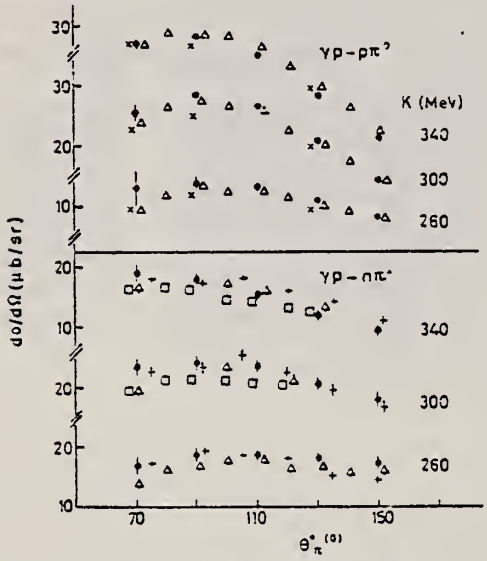

FIG. 3. $d\sigma(\gamma p \to \pi^0 p)/d\Omega$ and $d\sigma(\gamma p \to \pi^+ n)/d\Omega$ from a hydrogen target. Other data are shown for comparison (Ref. 5). The incident photon energy is K (MeV). Circles, present experiment; crosses, T. Fujii *et al.*; triangles, G. Fischer *et al.*; squares, C. Betourne *et al.*; exes, R. Morand *et al.*

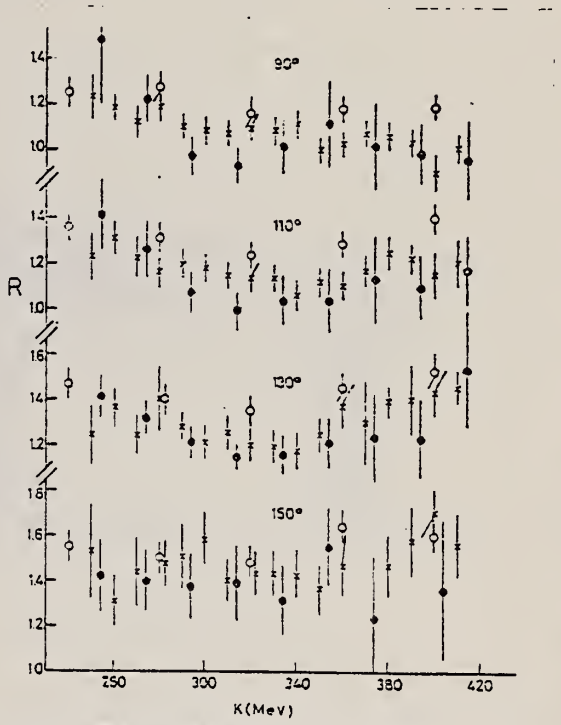

FIG. 4. The ratio $R = [d\sigma(\gamma n \to \pi^- p)/d\Omega][d\sigma(\gamma p \to \pi^+ n)/d\Omega]^{-1}$ from a deuterium target at center-of-mass pion angles of 90°, 110°, 130°, and 150° versus equivalent laboratory photon energy. Filled circles, present data; exes, T. Fujii *et al.*; open circles, G. von Holtey *et al.*

(continued)

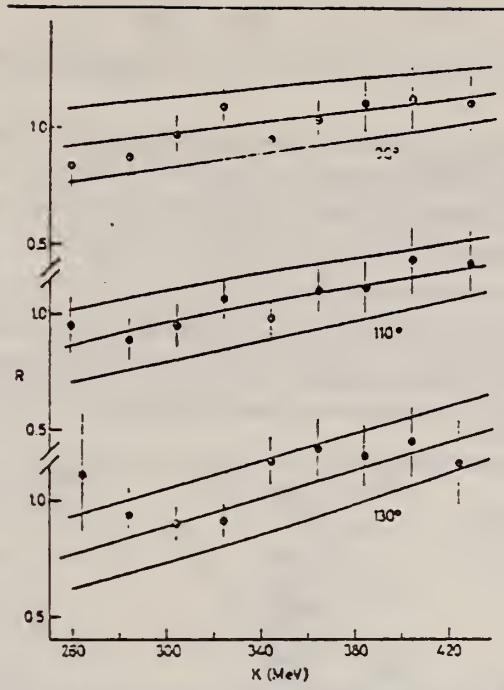

FIG. 5. The ratio $R=[d\sigma(\gamma\pi\to\pi^0 n)/d\Omega][d\sigma(\gamma p\to\pi^0 p)/d\Omega]^{-1}$ from a deuterium target at center-of-mass pion angles of 90°, 110°, and 130° versus equivalent laboratory photon energy. The lines are predictions in which t, the ratio of isotensor to isovector amplitude, is assumed equal to 0 and ±0.05.

REF. J. Deutsch, D. Favart, R. Prieels, B. Van Ostaeyen, G. Audit, N. de Botton, J.L. Faure, Cl. Schuhl, G. Tamas, and C. Tzara
Phys. Rev. Lett. 33, 316 (1974)

ELEM. SYM.	A	Z
H	1	1

METHOD

REF. NO.	
74 De 3	hmg

REACTION	RESULT	EXCITATION ENERGY	SOURCE		DETECTOR		ANGLE
			TYPE	RANGE	TYPE	RANGE	
G,PI+	ABX	145-155	C	145-154	ACT-I		4PI

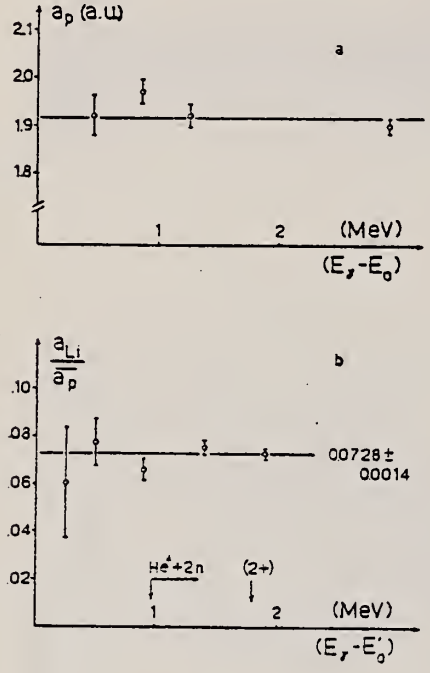

FIG. 1. (a) Coefficient a_p of the photoproduction on proton as a function of the lab photon energy above threshold. The line indicates the best-fit value $\bar{a}_p$. (b) Coefficient a_{Li} of the photoproduction on ^{6}Li normalized to the average a_p as a function of the lab photon energy above threshold. The position of the continuum and the 2^+ level in ^{5}He are also shown.

TABLE I. Photoproduction yield as a function of the energy of the electron beam.

Target	Electron-beam energy (MeV)	Photoproduction yield (arbitrary units)
^{6}Li	145.68	1.38 ± 0.52
	145.93	8.4 ± 1.1
	146.33	26.0 ± 1.6
	146.83	76.3 ± 2.5
	147.33	140.1 ± 3.3
CH_2	151.90	215.6 ± 4.8
	152.30	681.4 ± 9.2
	152.70	1335 ± 17
	154.35	6175 ± 49

9 J.H. Koch and T.W. Donnelly, Nucl. Phys. B64, 478 (1973).

10 M.I. Adamovitch et al., Yad. Fiz. 9, 848 (1969); Sov.J.Nucl.Phys. 9, 496 (1969).

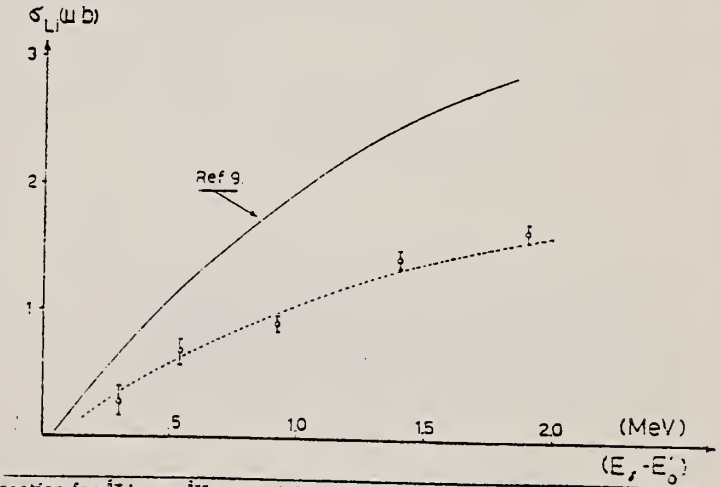

FIG. 2. Total photoproduction cross section for $^6Li+\gamma \rightarrow {}^5He_{g.s.}+\pi^+$ found in this experiment compared to the theoretical prediction, Ref. 9. The errors include the inaccuracy of σ_p, Ref. 10. The dashed curve is our best fit: it is 0.54 times the value from Ref. 9.

REF. A.I. Derebchinskii, S.G. Tonapetyan, O.G. Konovalov, V.P. Nazyrov, and A.E. Tenishev
Zh. Eksp. Teor. Fiz. 66, 68-73 (1974)
Sov. Phys. JETP, 39, 30 (1974)

ELEM. SYM.	A	Z
H	1	1

METHOD

REF. NO. 74 De 13 hmg

REACTION	RESULT	EXCITATION ENERGY	SOURCE TYPE	SOURCE RANGE	DETECTOR TYPE	DETECTOR RANGE	ANGLE
$ G,PIO	ABX	980-999	C	999	SPK-D		UKN

Measurements of proton polarization from the reaction $\gamma+p \rightarrow \pi^0+p$ are reported in the photon-energy range 980–1225 MeV at a center-of-mass angle 90°. A peak is observed in the energy dependence of the polarization with a maximum at $E_\gamma \sim 1090$ MeV. A comparison is given of the polarization values obtained with those calculated by Walker. A disagreement is observed between the experimental and theoretical polarization values.

POL P, 999=1.225 GEV

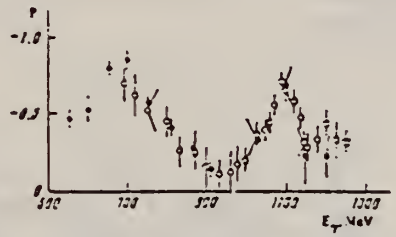

FIG. 2. Experimental energy dependence of polarization of protons from reaction (1) at 90° c.m.s. in the photon-energy interval 550–1250 MeV: hollow circles) results of the present work and ref. 8; solid circles) ref. 1; hollow squares) ref. 5; solid squares) ref. 6.

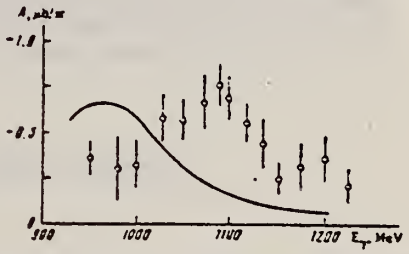

FIG. 3. Energy dependence of the polarization cross section (2). The curve was calculated with use of the amplitudes for photoproduction (1) from ref. 13.

TABLE 1.

$P \pm \Delta P$	E_γ MeV 950	1090	1225
Present work [*]	−0.175±0.115 −0.11±0.13	−0.195±0.065 −0.18±0.13	−0.362±0.084 −0.36±0.13

TABLE 2.

E_γ, MeV	$\pm \Delta E_\gamma$, MeV	$\theta_{c.m.}$, deg	Number of events	$P \pm \Delta P$	$A \pm \Delta A$, μb/sr
950	12	90.9	466	−0.175±0.115	−0.302±0.181
1090	13	90.7	971	−0.195±0.065	−0.313±0.128
1028	13	90.5	1111	−0.362±0.064	−0.570±0.128
1050	14	90.3	1263	−0.302±0.059	−0.581±0.118
1057	14	90.3	1103	−0.442±0.063	−0.404±0.131
1073	15	90.1	1264	−0.547±0.062	−0.630±0.148
1090	15	90.0	1242	−0.701±0.061	−0.747±0.125
1110	15	89.9	1437	−0.636±0.057	−0.678±0.117
1113	16	89.7	996	−0.573±0.070	−0.541±0.111
1135	16	89.6	823	−0.363±0.075	−0.427±0.135
1152	17	89.5	760	−0.280±0.077	−0.244±0.089
1173	18	89.3	502	−0.321±0.085	−0.206±0.127
1194	19	89.1	525	−0.170±0.090	−0.350±0.170
1225	20	88.8	349	−0.375±0.120	−0.195±0.180

TABLE 3.

E, MeV	A, μb/sr	B, μb/sr	C, μb/sr	D, μb/sr
950	−0.267±0.101	−0.751±0.441	0.203±0.406	5.20±2.68
1090	−0.591±0.104	−0.787±0.720	0.353±0.749	6.33±4.23
1150	−0.335±0.139	−1.818±0.762	2.96±0.00	3.27±3.21

[1] D.E. Lundquist et al., Phys. Rev. 168, 1527 (1968).

[5] M.N. Prentice et al., Preprint DNPL/P103, Daresbury, 1971.

[6] P. Blum et al., Proc. XV Intern. Conf. on High Energy Physics) Vol. 1, Kiev, 1970, p. 343.

[8] N.V. Goncharov et al., Zh.Eksp. Teor. Fiz. 64, 67 (1973); Sov. Phys. JETP 37 (1973).

[13] R.L. Walker, Phys. Rev. 182, 1729 (1969).

REF.	V.B. Ganenko, V.G. Gorbenko, Yu.V. Zhebrovskii, L.Ya Kolesnikov, I.I. Miroshnichenko, A.L. Rubashkin, V.M. Sanin, P.V. Sorokin, and S.V. Shalatskii Yad. Fiz. 20, 356 (1974); Sov. J. Nucl. Phys. 20, 189 (1974)	ELEM. SYM.	A	Z
		H	1	1

METHOD	REF. NO.	
	74 Ga 9	hmg

REACTION	RESULT	EXCITATION ENERGY	SOURCE		DETECTOR		ANGLE
			TYPE	RANGE	TYPE	RANGE	
$ G,PIO	NOX	400-650	C	999	UKN-D		DST

999= 1.4 GEV,POL G

Measurements are presented of the asymmetry of the differential cross sections for the reaction $\gamma p \to p\pi^0$ with polarized γ rays. The angular distributions of the asymmetry have been measured in the interval of pion-emission angle 60°–135° in the c.m.s. in the range of primary-photon energies 400–650 MeV. The measurements were made by means of linearly polarized photons obtained from coherent bremsstrahlung of high-energy electrons in a diamond single crystal. The experimental results are compared with theoretical analyses.

$$\sum \equiv \frac{\sigma_\parallel - \sigma_\perp}{\sigma_\perp + \sigma_\parallel} = \frac{1}{P}\,\frac{R-1}{R+1}.$$

E_γ	$\theta^*_{\pi^0}$, deg	R	P, %	Σ	E_γ	$\theta^*_{\pi^0}$, deg	R	P, %	Σ
400	60	1.692	47.7	0.539±0.034		105	1.338	22.7	0.534±0.047
	75	1.605	43.0	0.540±0.032		120	1.228	18.7	0.543±0.035
	90	1.470	39.0	0.485±0.024		135	1.196	15.0	0.503±0.043
	105	1.529	35.9	0.533±0.033					
	120	1.439	28.5	0.622±0.035	550	60	1.234	23.0	0.455±0.061
	135	1.339	27.2	0.533±0.030		75	1.284	22.3	0.561±0.047
						90	1.271	20.9	0.571±0.037
450	60	1.531	39.9	0.525±0.034		105	1.254	19.3	0.584±0.042
	75	1.556	39.0	0.538±0.043		120	1.208	15.0	0.625±0.035
	90	1.550	36.1	0.597±0.027		135	1.146	11.6	0.586±0.056
	105	1.427	31.8	0.553±0.028					
	120	1.357	24.9	0.608±0.024	650	50	1.156	12.5	0.379±0.058
	135	1.292	19.4	0.657±0.032		60	1.183	12.7	0.677±0.091
						75	1.247	15.1	0.723±0.055
500	60	1.273	25.0	0.462±0.044		90	1.222	14.7	0.636±0.035
	75	1.490	27.3	0.721±0.041		105	1.207	13.1	0.716±0.052
	90	1.387	22.8	0.711±0.039		120	1.176	11.0	0.735±0.053
						135	1.085	10.5	0.536±0.044

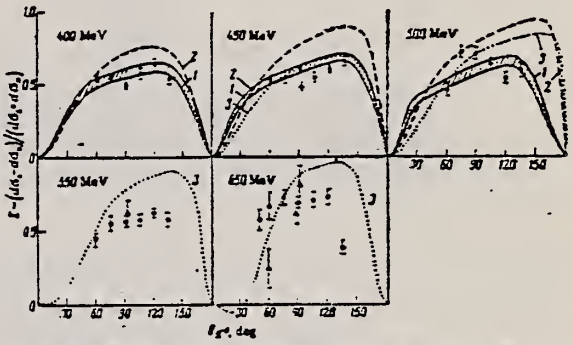

Angular distribution of the asymmetry of the reaction $\gamma p \to p\pi^0$. The theoretical curves have been taken from the following multipole analyses: 1–from ref. 9, 2–from ref. 10, 3–from ref. 1. Points: ●–our data, ▲–data of ref. 3.

[3] R. W. Zdarko and E. B. Dally, Nuovo Cimento 10A, 10 (1972).
[9] F. A. Berends, A. Donnachie, et al., Nucl. Phys. B4, 1, 54, 103 (1968).
[10] D. Schwela, Preprint, Bonn. Univ., P1-2-86, December, 1970.

H. Genzel

REF. Z. Phys. 268, 37 (1974)

EL EM. SYM.	A	Z
H	1	1

METHOD

REF. NO. 74 Ge 2 egf

REACTION	RESULT	EXCITATION ENERGY	SOURCE		DETECTOR		ANGLE
			TYPE	RANGE	TYPE	RANGE	
G,PIO	ABX	400-500	C	500	TEL-D		DST

Table 2. Parametrization of the diff. cross sections by a polynomial in $\cos\theta$ with the fit coefficients A, B and C, the integrated cross section σ_{tot} and the χ^2, n

K MeV	A	B	C	σ_{tot}	χ^2, n
	μb, ster			μb	
440.0 ± 5.0	10.29 ± 0.29	1.97 ± 0.17	−6.35 ± 0.41	94.7 ± 4.0	1.2
450.0 ± 5.0	9.09 ± 0.35	1.71 ± 0.19	−7.15 ± 0.49	84.5 ± 4.9	1.5
460.0 ± 5.0	8.54 ± 0.29	1.61 ± 0.17	−6.67 ± 0.41	79.6 ± 4.0	1.4
470.0 ± 5.0	7.93 ± 0.24	1.57 ± 0.12	−6.20 ± 0.32	73.7 ± 3.3	0.79
480.0 ± 5.0	6.70 ± 0.24	1.37 ± 0.11	−4.94 ± 0.32	63.7 ± 3.4	0.91
490.0 ± 5.0	5.96 ± 0.27	1.32 ± 0.14	−4.24 ± 0.36	57.3 ± 3.8	1.4

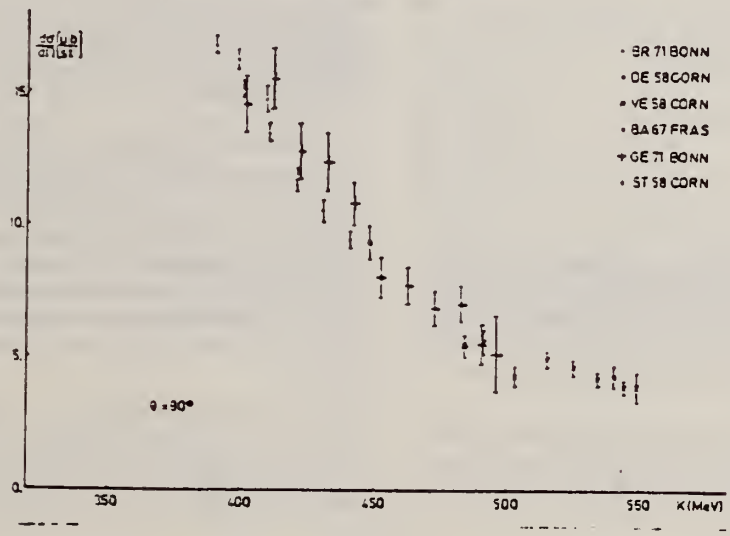

Fig. 2. Excitation curve of π^0-photoproduction at 90°. The data of this experiment are labeled with GE 71 BONN

REF.

V.G. Gobenko, A.I. Derebchinskii, Yu.V. Zhebrovskii,
L.Ya. Kolesnikov, O.G. Konovalov, A.L. Rubashkin, A.E. Tenishev
ZhETF Pis. Red. 19, 659 (1974)
JETP Lett. 19, 340 (1974)

EL EM. SYM.	A	Z
H	1	1

METHOD

REF. NO. 74 Go 3 hmg

REACTION	RESULT	EXCITATION ENERGY	SOURCE		DETECTOR		ANGLE
			TYPE	RANGE	TYPE	RANGE	
$ G,PIO	NOX	150-495	C	600,999	MAG-D		UKN

POL PROTONS PHOTONS

In the case when the photon-polarization vector is directed perpendicular (parallel) to the reaction plane, it becomes possible to measure three experimentally observable quantities[1]:

$$\Sigma = \frac{\mathrm{Re}H_2^{(-)}}{A^{(+)}}\ ; \tag{1}$$

$$P_y^{(\perp,\parallel)} = \frac{\mathrm{Im}H_1^{(+)} \pm \mathrm{Im}H_3^{(-)}}{A^{(+)} \pm \mathrm{Re}H_2^{(-)}} = \frac{P_y^0 \pm T_y}{1 \pm \Sigma}\ ; \tag{2}$$

(the plus and minus signs pertain respectively to perpendicular ($\perp$) and parallel ($\parallel$) polarization-vector directions).

If the angle between the photon polarization vector and the plane of the reaction is 45°, then we can obtain three components of the spatial polarization vector of the nucleon

$$P_x = \frac{\mathrm{Im}H_3^{(-)}}{A^{(+)}}\ ; \tag{3}$$

$$P_y^0 = \frac{\mathrm{Im}H_1^{(+)}}{A^{(+)}}\ ; \tag{4}$$

$$P_z = \frac{\mathrm{Im}H_2^{(-)}}{A^{(+)}}\ , \tag{5}$$

where $H_i^{(\pm)}$ and $A^{(+)}$ are corresponding bilinear combinations of the helicity amplitudes,[1] P_y^0 is the polarization of the nucleon on an unpolarized photon beam, Σ and T_y are the asymmetries of the cross sections on the linearly-polarized photon beam and the polarized nucleon target, respectively.

Thus, measurements with linearly-polarized photons yield information on five bilinear combinations of the photoproduction amplitudes (out of the 10 needed for the complete experiment).

We present here, for the first time, experimental results of the measurement of the polarization of protons from the reaction $\gamma + p \to \pi^0 + p$ on linearly polarized 495-MeV photons with the polarization vector directed perpendicular and parallel to the plane of the reaction. The measurements were made at a pion c.m.s. emission angle $\vartheta_\pi = 105°$.

The experiment was performed with a beam of linearly-polarized photons obtained by coherent bremsstrahlung of electrons from the linear accelerator of our institute in single-crystal diamond.[2] The maximum energy of the photon spectrum was 1380 MeV. The energy resolution in the experiment was $\Delta E_\gamma = \pm 20$ MeV. The experiment was performed with two magnetic spectrometers,[3] in the focus of which the liquid-hydrogen target was located.

The polarization of the protons and the asymmetry Σ were measured with the aid of a telescope of spark chambers[4] mounted at the exit from one of the magnetic spectrometers. The presence of the second spectrometer made is possible to monitor during the course of the experiment the stability of the polarization of the photon beam and of the measured asymmetry, by observing the yield of the photoprotons from the reaction $\gamma + p \to \pi^0 + p$.[5]

In the experiments we performed three independent measurements of the proton polarization: 1) photon polarization vector directed perpendicular to the reaction plane, 2) polarization parallel to this plane, 3) coherent effect, and consequently no photon polarization. The third measurement is essential to take into account the contribution to the proton polarization from the background due to the incoherent bremsstrahlung and to the proton yield from the two-pion photo-production process.

$C_\perp$	$C^\parallel$	C^0	$P_{y(\mathrm{eff})}$	$P^0_{y(\mathrm{meas})}$	Σ	P_y^+	P_y^a	P_y^0	T_y
0.493	0.218	0.666	0.791	−0.257	0.574	−0.43	0.20	−0.32	−0.45
±0.014	±0.011	±0.055	±0.012	±0.031	±0.037	±0.29	±0.52	±0.27	±0.37

340 (continued)

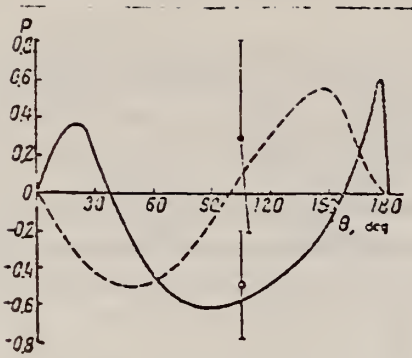

FIG. 1. Dashed lines—results of Walker's analysis,[7] ○—P_y, ●—P_y.

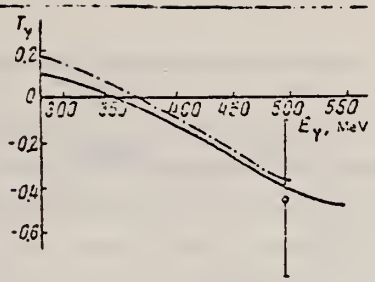

FIG. 2. Solid curve—results of Walker's analysis,[7] dash-dot line—results of Schwela's analysis.[8]

This measurement procedure has made it possible to separate the yields of the protons connected directly with coherent part of the photon spectrum. This yields the effective photon polarization $P_{\gamma(\mathrm{eff})}$ and the value of the proton polarization $P_{\mathrm{coll}}^{\perp(\parallel)}$ pertaining to the coherent spectrum, as well as the asymmetry parameter Σ.

The values of the proton polarization $P_y^{\perp(\parallel)}$ for photons polarized perpendicular (parallel) to the plane of the reaction are obtained from the experimentally measured values $P_{\mathrm{coll}}^{\perp(\parallel)}$, $P_{\gamma(\mathrm{eff})}$, and Σ with the aid of the following relations:

$$P_{\mathrm{coll}}^{\perp} = \frac{(1+\Sigma)(1+P_{\gamma(\mathrm{eff})})P_y^{\perp} + (1-\Sigma)(1-P_{\gamma(\mathrm{eff})})P_y^{0}}{(1+\Sigma)(1+P_{\gamma(\mathrm{eff})}) + (1-\Sigma)(1-P_{\gamma(\mathrm{eff})})};$$
$$P_{\mathrm{coll}}^{\parallel} = \frac{(1+\Sigma)(1-P_{\gamma(\mathrm{eff})})P_y^{\parallel} + (1-\Sigma)(1+P_{\gamma(\mathrm{eff})})P_y^{0}}{(1+\Sigma)(1-P_{\gamma(\mathrm{eff})}) + (1-\Sigma)(1+P_{\gamma(\mathrm{eff})})}. \quad (6)$$

From the values of $P_y^{\perp(\parallel)}$ and Eq. (3) we can obtain P_y^0 and T_y.

To verify the experimental procedure, we carried out a control measurement of the polarization of the protons in the reaction $\gamma + p \to \pi^0 + p$ on unpolarized photons under the same kinematic conditions, with a bremsstrahlung spectrum with $E_\gamma^{\max} = 600$ MeV. The obtained polarization $P_{y(\mathrm{coll})}^{0} = -0.267 \pm 0.031$ is in good agreement with the value obtained with the aid of Eq. (2) and the previously measured data.[6]

$C^{\perp}$, $C^{\parallel}$, and C^0 are the relative yields of the protons for the corresponding directions of the photon polarization vector (the superscript 0 denotes the absence of the coherent effect). The errors given are statistical.

The results of the present paper are listed in the table. The relatively large errors in the measurements of $P_y^{\perp}$ and $P_y^{\parallel}$ are due to the small statistics and to the appreciable contribution of the incoherent background. At a small background, which is possible if thinner diamond crystals are used, these errors can be greatly decreased at the same statistics (1200 events of scattering by the polarization analyzer). Reasonable agreement is observed between the experimentally measured quantity, $P_{y(\mathrm{coll})}^{0}$, and the value P_y^0 obtained from relation (2).

The results are shown in Figs. 1 and 2, where they are compared with the results of multipole analyses.[7,8]

The results are preliminary. Experiments are now under way aimed at obtaining information in a wide range of angles and energies, with much higher accuracy.

In conclusion, the authors thank I.I. Miroshnichenko, V.I. Nikiforov, and P.V. Sorokin for valuable advice during the discussion of the results, and P.I. Glushakov, A.A. Zybalov, and V.N. Shusinets for help with the experiments.

[1]V.I. Nikiforov, Complete kinematic description of the γN → πN reaction, Preprint KhFTI 72-41, Khar'kov, 1972.
[2]V.G. Gorbenko, Yu. V. Khebrovskiĭ, L. Ya. Kolesnikov, *et al.*, Yad. Fiz. 11, 1044 (1970) [Sov. J. Nuc. Phys. 11, 580 (1970)].
[3]N.G. Afanas'ev, V.A. Gol'dshteĭn, and S.V. Dementiĭ, Prib. Tekh. Éksp. No. 3, 30 (1968).
[4]V.I. Derebchinskiĭ, S.G. Tonapetyan, O.G. Kirovalov, *et al.*, *ibid.* No. 6, 36 (1970).
[5]V.D. Ganenko, V.G. Gorbenko, Yu. V. Zhebrovskiĭ, *et al.*, ZhETF Pis. Red. 16, 439 (1972) [JETP Lett. 16, 305 (1972)].
[6]H. Wenzel and W. Pfeil, Photoproduction Data Below 1.5 GeV, Bonn Univ. PIEI-168, February 1972.
[7]R.L. Walker, Phys. Rev. 182, 1729 (1970).
[8]D. Schwela, Preprint, Bonn Univ. PI12-36, 1970.

REF.

E. Hilger, H.-J. Roegler, L.M. Simons, and M. Tonutti
Z. Physik 268, 19 (1974)

ELEM. SYM.	A	Z
H	1	1

METHOD

REF. NO. 74 Hi 5 egf

REACTION	RESULT	EXCITATION ENERGY	SOURCE		DETECTOR		ANGLE
			TYPE	RANGE	TYPE	RANGE	
G,PIO	ABX	340-420	C	412,447	CKV-D		DST

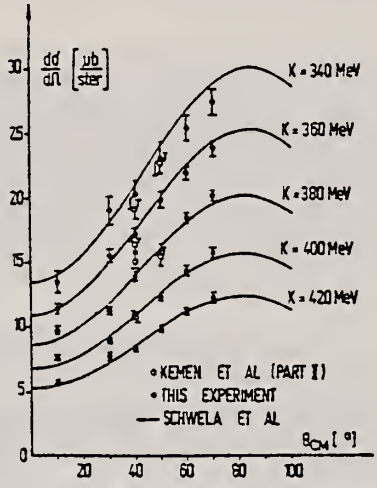

Fig. 5. Angular distributions of π^0-photoproduction showing the data of this experiment together with results of the experiment described in Part II

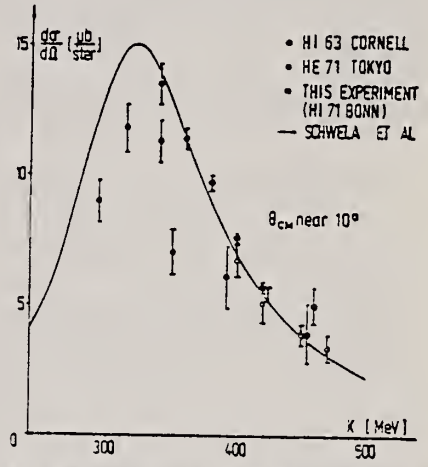

Fig. 6. π^0-photoproduction cross sections near $\theta^*_{CM} = 10°$ showing our date together with those from Refs. 10 and 11. The curve is a theoretical result from Ref. 9

[9] Schwela, D., Weizel, R.: Z. Physik 221, 71 (1969).

[10] Highland, V.L., DeWire, J.: Phys. Rev. 132, 1293 (1963).

[11] Hemmi, Y., Inagaki, T., Inagaki, Y., Maki, A., Miyake, K., Nakamura, T., Tamura, N., Tsukamoto, J., Yamashita, N. Itoh, H., Kobayashi S., Yasumi, S., Yoshida, H.: Phys. Lett. 43B, 79 (1973).

K. Jaeckel, H. Kaiser, H. Kemen, R. Wedemeyer, and H.J. Weyer

REF. Z. Phys. 268, 27 (1974)

ELEM. SYM.	A	Z
H	1	1

METHOD

REF. NO. 74 Ja 3 egf

REACTION	RESULT	EXCITATION ENERGY	SOURCE		DETECTOR		ANGLE
			TYPE	RANGE	TYPE	RANGE	
G,PIO	ABX	240-380	C	455	TEL-D		DST

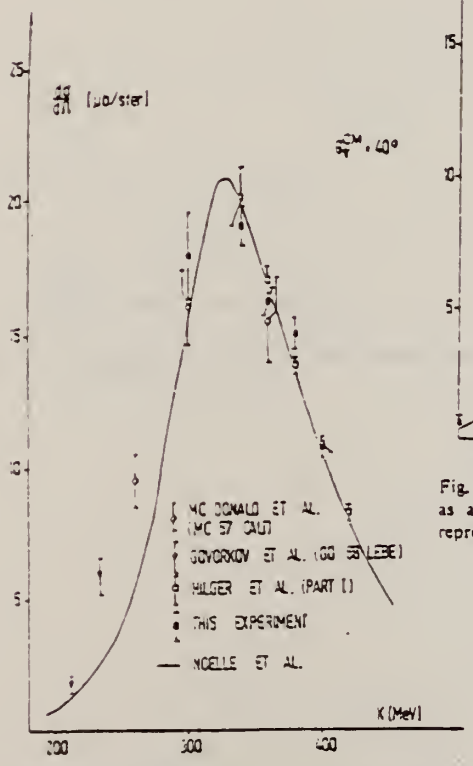

Fig. 9. Measured differential cross sections at $\theta_\gamma^{cm} = 40°$ as a function of the photon energy. The solid line represents a theoretical analysis

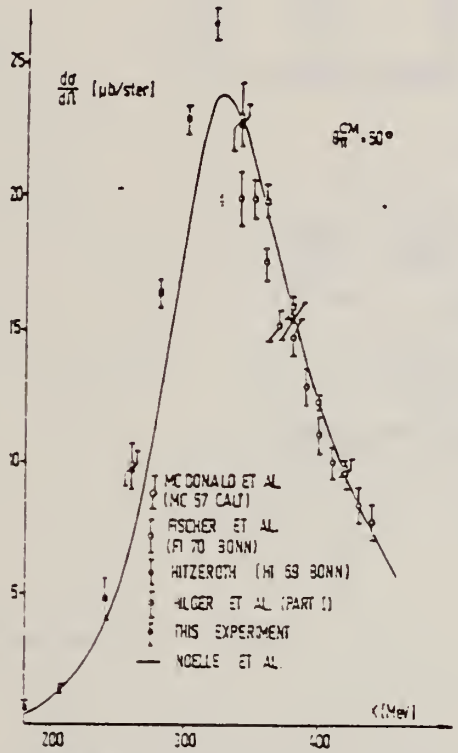

Fig. 10. Measured differential cross sections at $\theta_\gamma^{cm} = 50°$ as a function of the photon energy. The solid line represents a theoretical analysis

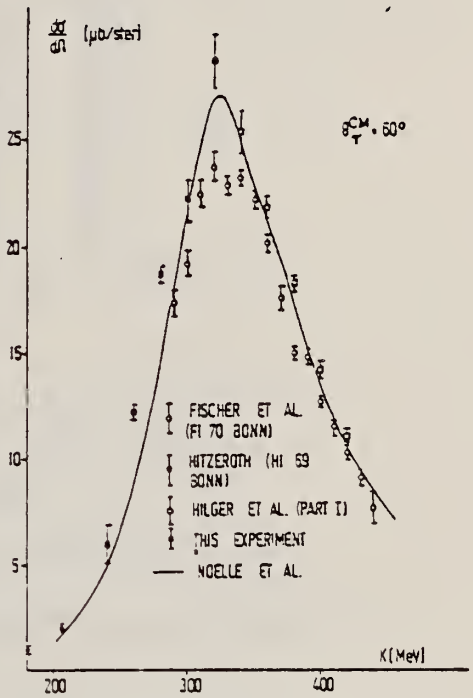

Fig. 11. Measured differential cross sections at $\theta_\gamma^{cm} = 60°$ as a function of the photon energy. The solid line represents a theoretical analysis

(continued)

Table 3. The differential cross sections for $\gamma + p \to p + \pi^0$ and their absolute statistical and systematical errors

θ_π^{cm}	k MeV	$d\sigma/d\Omega_{cm}$ μb/ster	$\Delta\sigma$ statist.	$\Delta\sigma$ system.
40°	300	18.0	±1.6	±1.2
	340	19.1	±0.7	±1.1
	360	16.3	±0.5	±1.0
	380	15.1	±0.6	±0.8
	400	10.8	±0.4	±1.2
50°	240	4.8	±0.8	±0.4
	260	9.7	±0.7	±0.7
	280	16.4	±0.5	±1.3
	300	22.9	±0.5	±1.2
	320	26.5	±0.6	±1.7
	340	22.7	±0.8	±1.3
	380	15.4	±0.7	±0.9
60°	240	5.9	±0.8	±0.5
	260	12.2	±0.4	±0.6
	280	18.7	±0.4	±1.0
	300	22.2	±1.0	±1.2
	320	23.7	±1.2	±1.8
70°	260	13.1	±1.2	±0.7

REF. N.G. Afanas'ev, A.S. Esaulov, A.M. Pilipenko, Yu. I. Titov
Pis'ma Zh. Eksp. Teor. Fiz. 22, 400 (1975)
JETP Lett. 22, 189 (1975)

EL EM. SYM.	A	Z
H	1	1

METHOD

REF. NO. 75 Af 11 hmg

REACTION	RESULT	EXCITATION ENERGY	SOURCE		DETECTOR		ANGLE
			TYPE	RANGE	TYPE	RANGE	
E,E/	ABX	155-225	D	526-913	MAG-D		DST

We report the results of inelastic scattering of electrons by protons at the threshold at $k^2 = 5F^{-2}$. We determine the quantities $|E_{0+}|$ and $|S_{0+}|$ from which we obtain the values of the axial-vector form factor of the nucleon and the form factor of the pion.

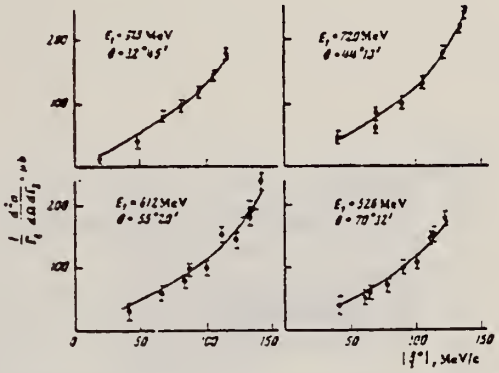

FIG. 1. Pion electroproduction cross section vs. the pion 3-momentum in the c.m.s. Curves—results of best fit.

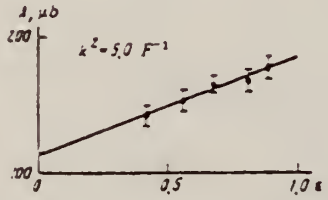

FIG. 2. Plot of $A = |E_{0+}|^2 + \epsilon k^2 |S_{0+}|^2$ against the virtual-photon polarization operator.

REF.		ELEM. SYM.	A	Z
	P. S. Baranov, G. M. Buinov, V. G. Godin, V. A. Kuznetsova, V. A. Petrun'kin, L. S. Tatarinskaya, V. S. Shirchenko, L. N. Shtarkov, V. V. Yurchenko, Yu. P. Yanulis Yad. Fiz. 21, 689 (1975); Sov. J. Nucl. Phys. 21, 355 (1975)	H	1	1
METHOD		REF. NO.		
		75 Ba 2		hmg

REACTION	RESULT	EXCITATION ENERGY	SOURCE		DETECTOR		ANGLE
			TYPE	RANGE	TYPE	RANGE	
G,G	ABX	70-110	C	127,148	TEL-D		DST

The differential cross section for the elastic scattering of photons by protons is measured in the 70–110-MeV energy range at 90° and 150° laboratory angles. Yield data of the $\gamma+e\rightarrow\gamma'+e'$ monitor process, obtained by means of the same experimental apparatus, are used in determining the absolute values of the cross section for the $\gamma+p\rightarrow\gamma'+p'$ reaction. Approximating the experimental values of the photon-proton elastic scattering cross section by a phenomenological expression at low energies, we obtain the electric and magnetic polarizabilities of the proton: $\bar{\alpha}_p^{exp}=(10.7\pm1.1)\times10^{-43}$ cm³ and $\bar{\beta}_p^{exp}=(-0.7\pm1.6)\times10^{-43}$ cm³.

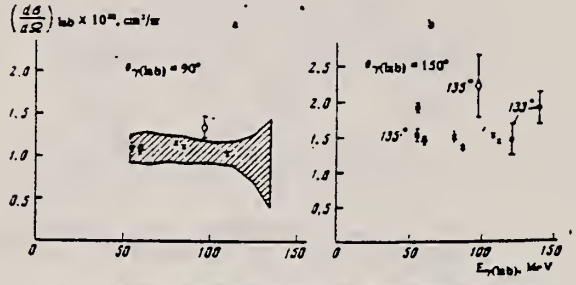

FIG. 2. Energy dependence of the cross section for lab angles 90° (a) and 150° (b). Points: ●–[18], ●–[27], ○–[28], ○–[30], X–present work; shaded region–results in [29].

TABLE II. Experimental results for elastic scattering of photons by protons, absolutized in accordance with the monitor process.

γ-telescope variants	θ_{lab}, deg	ω, MeV	Cross section ratio of the main and monitor processes ($\times10^{-1}$)	$\left(\frac{d\sigma}{d\Omega}\right)_{\theta}$, in units of 10^{-33} cm²/sr
A1234	90	85.4	1.52±0.05	1.09±0.04
A1234A+	90	80.9	1.80±0.09	1.15±0.06
A1234	150	86.3	1.92±0.14	1.37±0.10
A1234A+	150	81.9	2.02±0.17	1.44±0.12
A1234	90	109.9	1.44±0.07	1.03±0.06
A1234	150	111.1	2.02±0.06	1.44±0.06
A1234A+	150	106.7	2.22±0.09	1.60±0.08

[18] V.I. Gol'danskii et al., Zh. Eksp. Teor. Fiz. 38, 1695 (1960); Sov. Phys. JETP 11, 1223 (1960).

[27] C. Oxley, Phys. Rev. 110, 733 (1958).

[28] B.B. Govorkov et al. Dokl.Akad.Nauk SSSR 111, 988 (1956); Sov. Phys. Dokl. 1, 735 (1957).

[29] L.G. Hyman et al., Phys. Rev. Lett. 3, 93 (1959).

[30] G. Bernardini et al, Nuovo Cimento 18, 1203 (1960).

REF.

P. Dougan, T. Kivikas, K. Lugner, V. Ramsay, W. Stiefler
Z. Physik A274, 73 (1975)

ELEM. SYM.	A	Z
H	1	1

METHOD

REF. NO.: 75 Do 1 egf

REACTION	RESULT	EXCITATION ENERGY	SOURCE		DETECTOR		ANGLE
			TYPE	RANGE	TYPE	RANGE	
G,PI0	ABX	360-938	C	999	TEL-D		DST

Table of cross section values in paper.

999=1.2 GEV

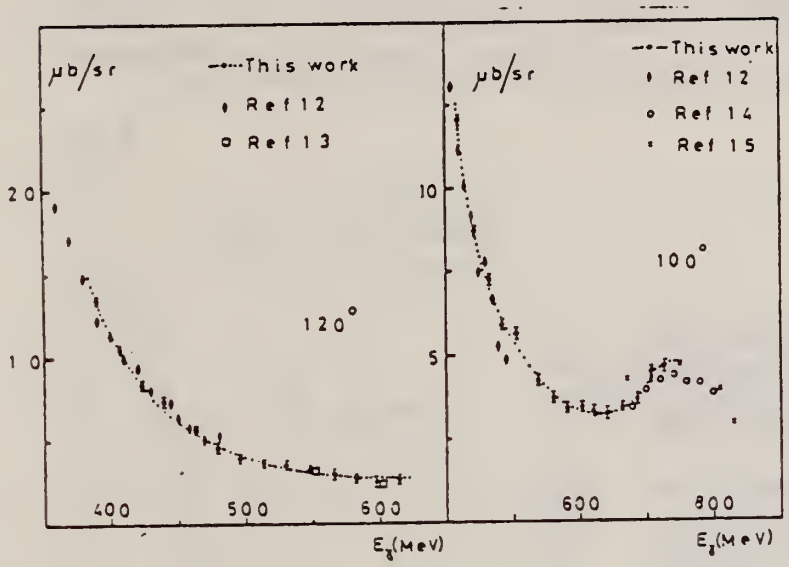

Fig. 5. The cross-sections for π^0-production off protons att 120° and 100° pion c.m. angle obtained in the measurements described here are compared with other recent data. For clarity, only the statistical errors in the present measurements are shown. The total errors in the other data are in the range 6–10%.

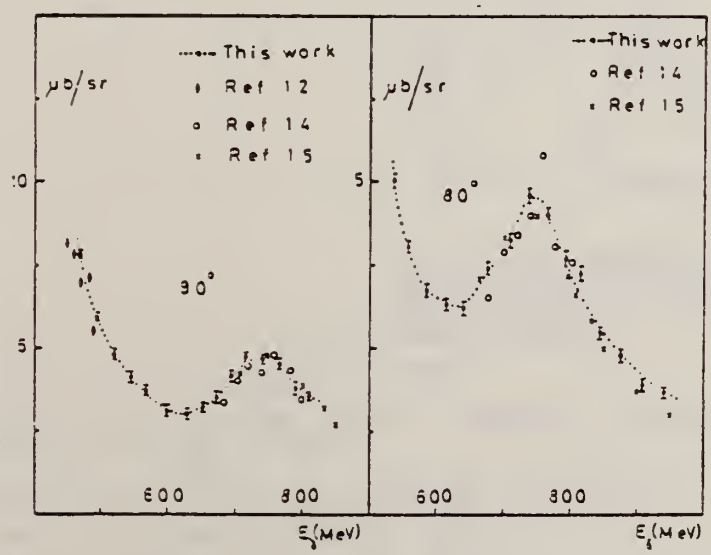

Fig. 6. The cross-sections for π^0-production off protons at pion c.m. angles of 90° and 80° obtained in the measurements described here are compared with other recent data. For clarity, only the statistical errors in the present measurements are shown. The total errors in the other data are in the range 6–10%.

(continued)

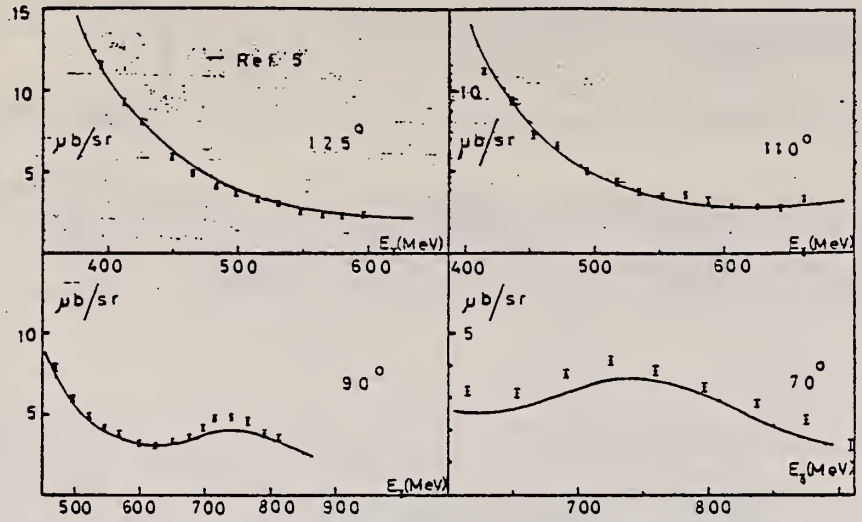

Fig. 7. The cross-section for π^0-production off protons at pion c.m. angles of 125°, 110°, 90° and 70° obtained in the present measurements are compared with predictions based on the MOR phase-shift analysis [5]. The agreement is seen to be best at larger pion c.m. angles

5. Moorhouse, R.G., Oberlack, H., Rosenfeld, A.H.: Lawrence Berkeley Laboratory Preprint. LBL 2410 (1973)
12. Genzel, H., Hilger, E., Knop, G., Keman, H., Wedemeyer, R.: Z. Physik 268, 43 (1974)
13. Feller, P., Herr, H., Hilger, E., Kadansky, V., Menze, D., Miczaika, Th., Opara, U., Schwille, W.J.: Phys. Letters 49 B, 197 (1974)
14. de Staebler, H., Erickson, E.F., Hearn, A.C., Shaerf, C.: Phys. Rev. 140 B. 336 (1965)
15. Barton, J.S., Booth, P.S.L., Carroll, L.J., Holt, J.R., Jackson, J.N., Moscati, G., Wormald, J.R.: Daresbury Internal Report DL/P 208 (1974)

REF.	L.O. Abramyan, R.O. Avakyan, N.Z. Akopov, A.O. Agan'yants, G.A. Vartapetyan, P.I. Galumyan, A.N. Lebedev, E.G. Muradyan, S.E. Piliposyan, A.M. Sirunyan, and A.G. Khudaveryan JETP Lett. 23, 375 (1976) Pis'ma Zh. Eksp. Teor. Fiz. 23, 415 (1976)	ELEM. SYM.	A	Z
		H	1	1
METHOD		REF. NO.		
		76 Ab 7		hmg

REACTION	RESULT	EXCITATION ENERGY	SOURCE		DETECTOR		ANGLE
			TYPE	RANGE	TYPE	RANGE	
$ G,PIO	ABX	900-999	D	900-999	MAG-D		DST

We measured the asymmetry of the cross section of the photoproduction of π^0 mesons from hydrogen at 110° in the c.m.s. at linearly polarized photon energies 0.9–1.65 GeV. The results are compared with the existing model predictions in the resonance region.

999=1.65 GeV,-POL G

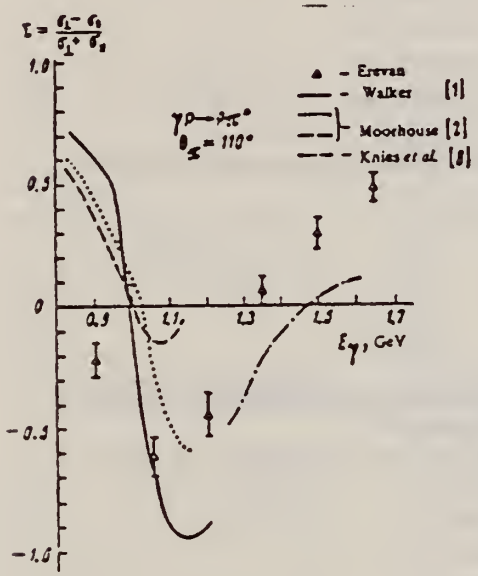

FIG. 2. Energy dependence of the asymmetry of the cross section of the reaction $\gamma P \to P\pi^0$ at $\theta_{\pi^0} = 110°$ in the c. m. s.

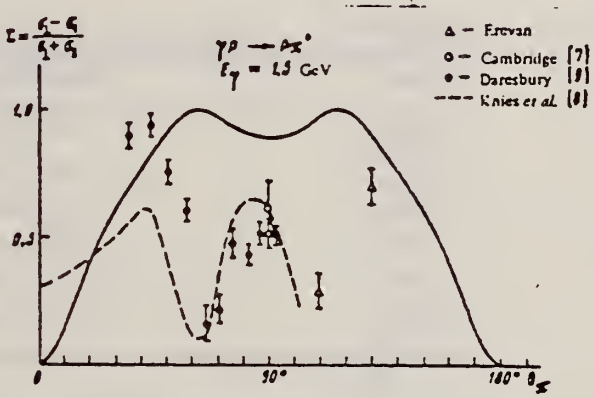

FIG. 3. Angular dependence of the asymmetry of the cross section of the reaction $\gamma P \to P\pi^0$ for $E_\gamma = 1.5$ GeV. The solid curve corresponds to the prediction of the asymmetry Σ in the case of the $F_{37}(1950)$ resonance for pure M_{2+} magnetic excitation.

[1] R.L. Walker, Phys. Rev. 182, 1729 (1969)

[2] R.G. Moorhouse, H. Oberlack, and A.H. Rosenfeld, Preprint LBL-1950, 1973; Phys. Lett. 43B, 44 (1973)

[7] J. Alspector et al., Phys. Rev. Lett. 28, 1403 (1972)

[8] G. Knies et al., Preprint LBL-2673, 1974,

[9] Annual Report, Daresbury, 1974, and Rapporteur's Talk of J.G. Rutherglen to XVII Intern. Conf. on High Energy Physics, London, 1974.

(continued)

The obtained cross section asymmetries

$$\Sigma = \frac{\sigma_\perp - \sigma_\parallel}{\sigma_\perp + \sigma_\parallel} = \frac{1}{P_\gamma} \frac{C_\perp - C_\parallel}{C_\perp + C_\parallel}$$

are listed in Table I. $C_\perp$ and $C_\parallel$ are the numbers of coincidences in the case of photons polarized perpendicular and parallel to the meson production plane, respectively. The errors in the asymmetry include the statistical error in the determination of $C_\perp$ and $C_\parallel$, as well as the error (~10%) in the effective photon polarization (P_γ).

TABLE I.

E_γ, GeV	Σ		
	$\theta_\pi^{cms} = 90°$	$\theta_\pi^{cms} = 110°$	$\theta_\pi^{cms} = 130°$
0.90	...	-0.22 ± 0.07	...
1.05	...	-0.616 ± 0.082	...
1.20	...	-0.44 ± 0.085	...
1.35	...	0.056 ± 0.056	...
1.50	0.52 ± 0.05	0.295 ± 0.063	0.71 ± 0.07
1.65	...	0.48 ± 0.06	...

TABLE II.

E_γ, GeV	$(d\sigma/d\Omega)$ ms (μb/sr)
0.90	1.86 ± 0.074
1.05	1.34 ± 0.054
1.20	0.5 ± 0.024
1.35	0.55 ± 0.022
1.50	0.61 ± 0.02
1.65	0.37 ± 0.015

REF.

P. Blüm, R. Brockmann, and W. Mohr
Z. Physik A278, 275 (1976)

ELEM. SYM.	A	Z
H	1	1

METHOD

REF. NO. 76 B1 9 egf

REACTION	RESULT	EXCITATION ENERGY	SOURCE		DETECTOR		ANGLE
			TYPE	RANGE	TYPE	RANGE	
$ G,PIO	NOX	700-999	C	2*	SPK-D		DST
				(2.5GeV)			

999= 1.2 GEV,*GEV,$P

The polarization of the recoil proton from the reaction $\gamma p \to \pi^0 p$ has been measured for photon energies between 900–1,350 MeV and pion c.m. angles between 70° and 150°. There are significant deviations from recent analysis.

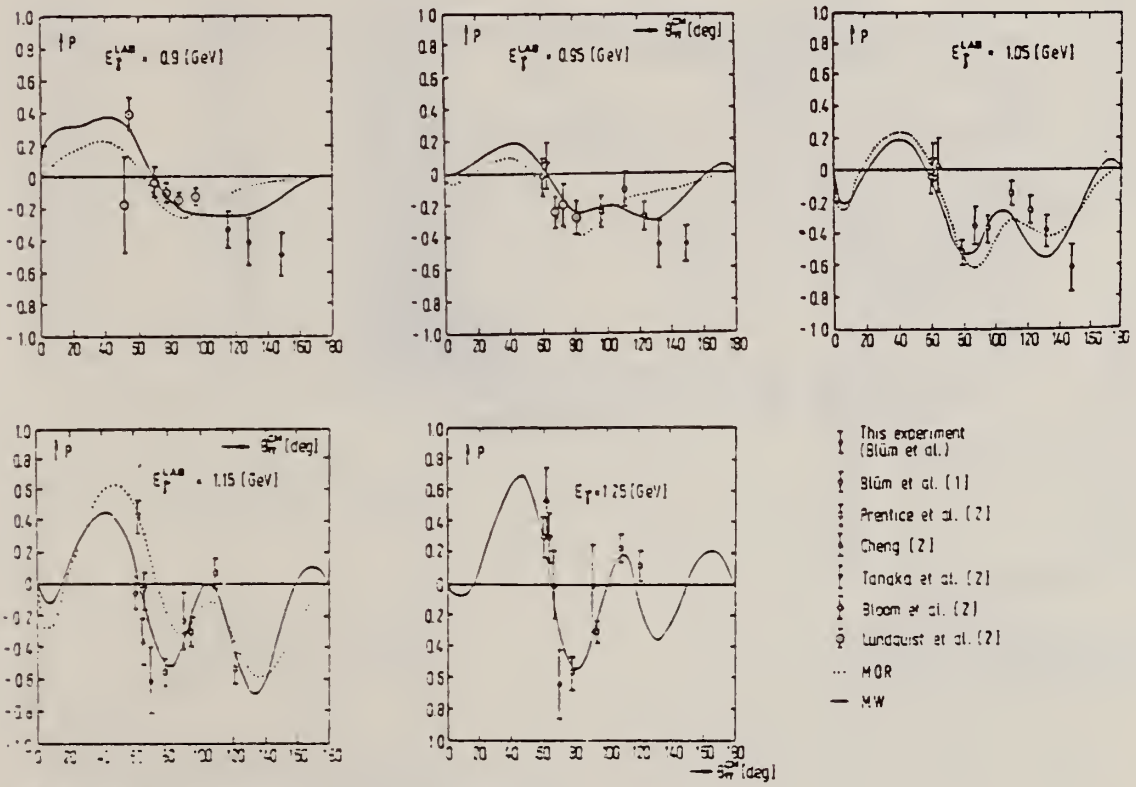

Fig. 4. Angular distributions of recoil proton polarization from $\gamma p \to \pi^0 p$

(continued)

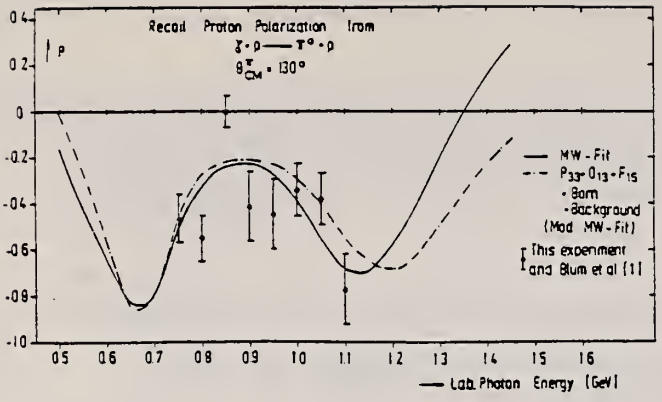

Fig. 6. Energy dependence of recoil proton polarization from $\gamma p \to \pi^0 p$ at $\theta_\pi^{cm} = 130°$. Comparison with a simplified Metcalf-Walker fit

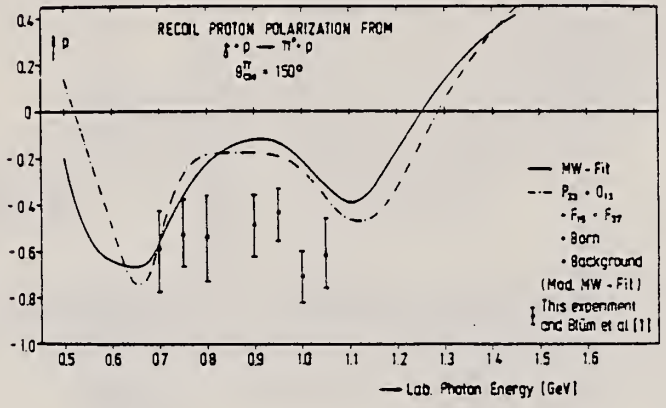

Fig. 7. Like Figure 6, but at $\theta_\pi^{cm} = 150°$

REF. P. Blüm, P. Brinckmann, R. Brockmann, P. Lütter, W. Mohr, and R. Sauerwein
Z. Physik A277, 311 (1976)

ELEM. SYM.	A	Z
H	1	1

METHOD

REF. NO. 76 B1 14 egf

REACTION	RESULT	EXCITATION ENERGY	SOURCE		DETECTOR		ANGLE
			TYPE	RANGE	TYPE	RANGE	
$ G,PIO	NOX	600 - 999	C	2*	MAG-D		DST
				(2.5GeV)			

The polarization of the recoil proton from the reaction $\gamma p \to \pi^0 p$ has been measured for photon energies between 600 and 1,200 MeV and pion c.m. angles between 90° and 150°.

999=1.2GEV,*GEV,$P

Table I

Primary photon energy GeV	c.m. angle	Polarization $P \pm \Delta P$
0.70 ± 0.05	148.5°	−0.595 ± 0.17
0.75 ± 0.05	129.5°	−0.46 ± 0.1
0.75 ± 0.05	150.0°	−0.531 ± 0.16
0.80 ± 0.05	129.5°	−0.55 ± 0.1
0.80 ± 0.05	150.0°	−0.538 ± 0.19
0.85 ± 0.05	115.0°	−0.332 ± 0.09
0.85 ± 0.05	128.8°	0.0 ± 0.07
0.90 ± 0.05	115.0°	−0.335 ± 0.11
0.90 ± 0.05	128.8°	−0.410 ± 0.115
1.05 ± 0.05	87.2°	−0.353 ± 0.11
1.10 ± 0.05	87.2°	−0.668 ± 0.14
1.15 ± 0.05	89.5°	−0.233 ± 0.18
1.20 ± 0.07	89.5°	−0.220 ± 0.144
1.25 ± 0.06	90.0°	−0.030 ± 0.28
0.65 ± 0.05	90.7°	−0.835 ± 0.3 (Hydrogen analyzer)
0.65 ± 0.03	90.0°	−0.650 ± 0.07 (Carbon analyzer)

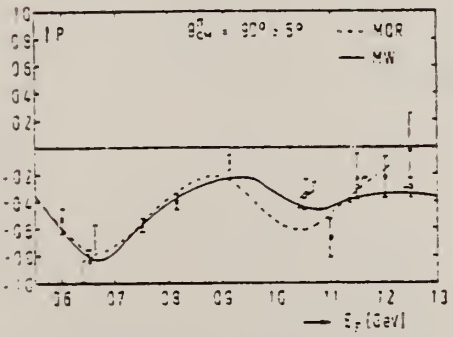

Fig. 8. Energy dependence of the recoil proton polarization from the reaction $\gamma p \to \pi^0 p$. $\theta^*_{CM} = 90° \pm 5°$. ✕ Lundquist et al., ◇ Prentice et al., ● This experiment, Blüm et al., ○ Bloom et al. —— MOR, — — MW

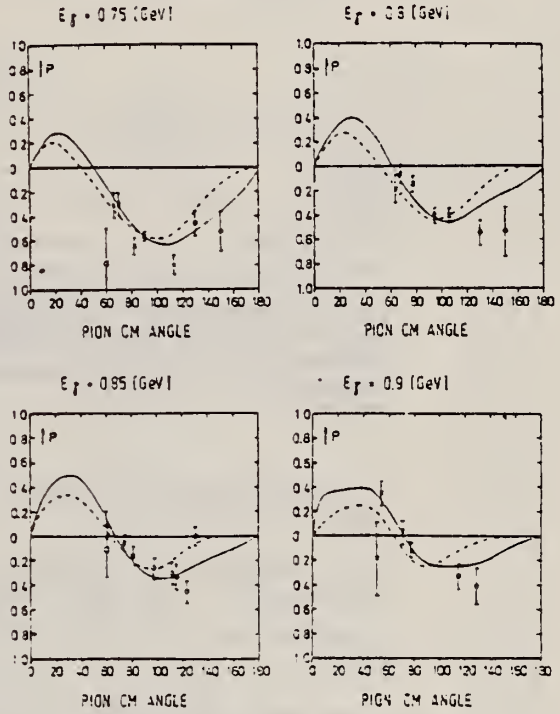

Fig. 9. Angular distributions of the recoil proton polarization from the reaction $\gamma p \to \pi^0 p$. ● This experiment, Blüm et al., ✕ Lundquist et al., ◇ Prentice et al., ○ Bloom et al. ----- MOR, —— MW

REF. A. I. Derebchinskii, A. A. Zybalov, O. G. Konovalov, V. R. Nazyrov, A. E. Tenishev, and S. G. Tonapetyan
Sov. Phys.-JETP 43, 218 (1976)
Zh. Eksp. Teor. Fiz. 70, 423 (1976)

ELEM. SYM.	A	Z
H	1	1

METHOD

REF. NO. 76 De 7 hmg

REACTION	RESULT	EXCITATION ENERGY	SOURCE		DETECTOR		ANGLE
			TYPE	RANGE	TYPE	RANGE	
$ G,PIO	NOX	150-640	C	540-640	MAG-D	-	DST

Measurements are reported of the polarization of protons from the $\gamma + p \rightarrow \pi^0 + p$ reaction at photon energies of 540, 560, 585, 610, and 640 MeV at pion angle of emission of 90° in the center of mass system. The angular dependence of the proton polarization has been investigated for this reaction at a photon energy 600 MeV. The data obtained are compared with the results of the phenomenological analysis reported by Metcalf and Walker (Preprint CALT-68-425, 1974).

$ RECOIL P

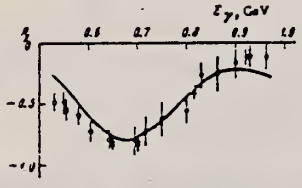

FIG. 1. Energy dependence of the polarization of protons from the $\gamma + p \rightarrow \pi^0 + p$ reaction at $\theta_\pi = 90°$ c.m.s.: —present results and our previously published results[2]; ×—results of Lundquist *et al.*[7]; solid curve—results of the Metcalf-Walker analysis.[2]

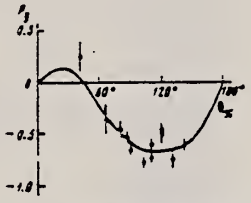

FIG. 2. Angular dependence of polarization at photon energy of 600 MeV: ○—present results; ●—results from the compilation of Genzel and Pfeil[12]; solid curve—results of Metcalf and Walker.[2]

2 W.J. Metcalf and R.L. Walker, Preprint, CALT-68-425, 1974

7 D.E. Lundquist, R.L. Anderson, I.V. Allaby, and D.M. Ritson, Phys. Rev. 168, 1527 (1968)

12 H. Genzel and W. Pfeil, Preprint, Bonn Univ. P1, 81-168 1972.

$E_\gamma \pm \Delta E_\gamma$, MeV:	536±10	560±11	585±12	610±13	640±28
$P \pm \Delta P$:	−0.48±0.09	−0.54±0.10	−0.59±0.09	−0.72±0.08	−0.74±0.07

θ_π (c.m.s.):	90°	110°	120°	142.5°
$P \pm \Delta P$:	−0.660±0.060	−0.603±0.056	−0.445±0.056	−0.393±0.059

θ_π (c.m.s.):	90°	110°	120°	142.5°
$P_1 \pm \Delta P_1$:	−0.590±0.090	−0.528±0.085	−0.424±0.097	−0.624±0.078
$P_2 \pm \Delta P_2$	−0.720±0.081	−0.664±0.084	−0.499±0.095	−0.523±0.092

REF. P. Dougan, V. Ramsay and W. Stiefler
Z. Physik A276, 155 (1976)

ELEM. SYM.	A	Z
H	1	1

REF. NO. 76 Do 6

Comment: Detailed cross section tables given. See samples on back of sheet. egf

REACTION	RESULT	EXCITATION ENERGY	SOURCE TYPE	SOURCE RANGE	DETECTOR TYPE	DETECTOR RANGE	ANGLE
G,PIO	ABX	238 - 922	C	245-922	TEL-D		DST

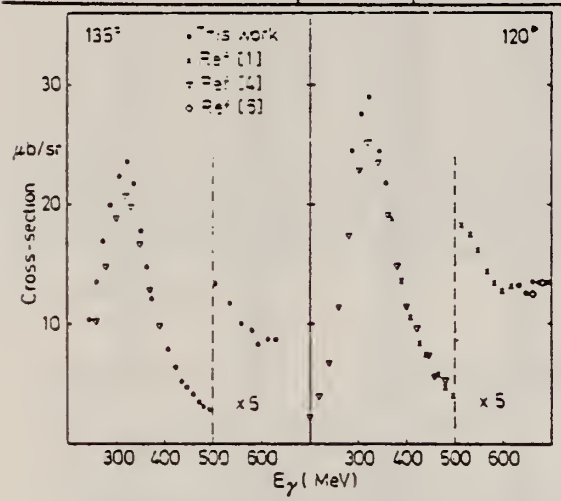

Fig. 2. The cross-sections for π^0-production from hydrogen at pion c.m. angles of 135° and 120° as found in the present experiment and in [1] are compared with selected other data from similar measurements. The statistical errors are not shown explicitly, being for all measurements usually only slightly larger than the dimensions of the symbols used. Note the change of scale to the right of the dotted line in both cases. The scale-factor is as shown in the figure

1. Dougan, P., Kivikas, T., Lugner, K., Ramsay, V., Stiefler, W.: Z. Physik 274, 73 (1975)
4. Genzel, H., Hilger, E., Knop, G., Kemen, H., Wedemeyer, R.: Z. Physik 268, 43 (1974)
6. DeStaebler Jr., H., Ericksen, E.F., Hearn, A.C., Schaerf, C.: Phys. Rev. 140 B, 336 (1965)

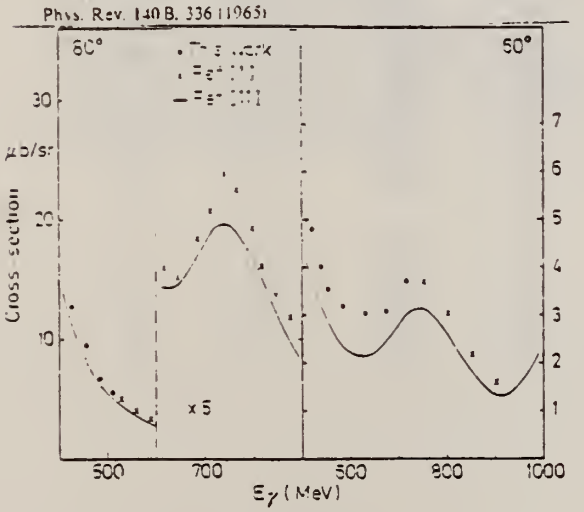

Fig. 3. As Fig. 2, but pion c.m. angles of 60° and 30°. Note the different scales in the two halves of the drawing

1. Dougan, P., Kivikas, T., Lugner, K., Ramsay, V., Stiefler, W.: Z. Physik 274, 73 (1975)
11. Moorhouse, R.G., Oberlack, H., Rosenfeld, A.H.: Lawrence Berkeley Laboratory Report LBL 2410, (1973)

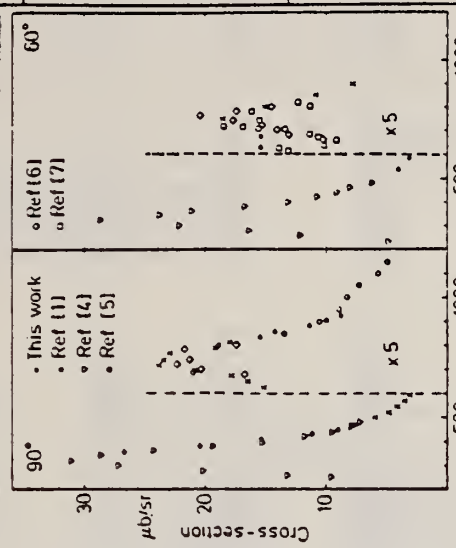

Fig. 3 As Fig. 2, but pion c.m. angles of 90° and 60°

1. Dougan, P., Kivikas, T., Lugner, K., Ramsay, V., Stiefler, W.: Z. Physik 274, 73 (1975)
4. Genzel, H., Hilger, E., Knop, G., Kemen, H., Wedemeyer, R.: Z. Physik 268, 43 (1974)
5. Barton, J.S., Booth, P.S.L., Carroll, L.J., Holt, J.R., Jackson, J.N., Moscati, G., Wormald, J.R.: Daresbury Internal Report DL/P 208, (1974)
6. DeStaebler Jr., H., Ericksen, E.F., Hearn, A.C., Schaerf, C.: Phys. Rev. 140 B, 336 (1965)
7. Bellettini, G., Bemporad, C., Biggs, P.J., Braccini, P.L., Del Prete, T., Foà, L.: Nuovo Cimento 44, 239 (1966)

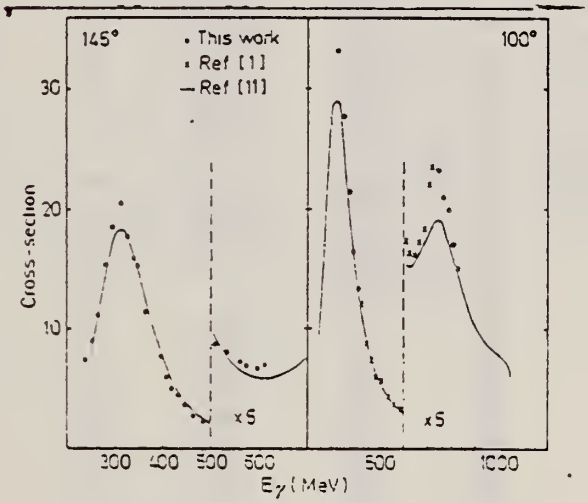

Fig. 4. The cross-sections for π^0-production from hydrogen at pion c.m. angles of 145° and 100° from this work and [1] are compared with results calculated from the phase-shift parameters given by Moorhouse *et al.* [11]. The statistical errors in the experimental points are not shown explicitly, being typically only slightly larger than the dimensions of the symbols. Note the change of scale to the right of the dotted line. The scale-factor is as given in the figure

1. Dougan, P., Kivikas, T., Lugner, K., Ramsay, V., Stiefler, W.: Z. Physik 274, 73 (1975)
11. Moorhouse, R.G., Oberlack, H., Rosenfeld, A.H.: Lawrence Berkeley Laboratory Report LBL 2410, (1973)

Abstract. The results of a comprehensive series of measurements of the cross-sections for the photo-production of π^0-mesons from hydrogen at pion c.m. angles from 47 to 145 degrees are presented. The minimum and maximum photon energies have been 238 and 922 MeV respectively.

(continued)

Table 1. The cross-sections for π^0-production from hydrogen as measured in the present experiment. The values quoted include the contribution from the proton Compton effect

C.M. angle (deg)	Photon energy (MeV)	Cross-section (μb/sr)	Stat. error (%)
45°			
47.2	725.6	2.96	3.5
47.2	794.9	3.04	4.1
47.1	867.6	2.79	4.7
50°			
50.2	668.1	2.45	4.8
50.3	729.3	2.87	4.1
50.2	793.2	2.75	4.6
50.0	854.6	2.12	8.9
60°			
59.4	485.5	6.76	2.2
59.8	521.0	4.82	3.1
59.8	541.4	4.01	2.9
60.1	553.6	3.56	5.2
60.0	587.8	3.18	3.5
60.1	633.4	3.03	4.1
60.1	675.6	3.08	4.9
60.0	716.7	3.72	6.4
70°			
69.5	455.1	8.71	1.7
69.9	490.3	6.43	1.7
70.1	526.0	4.82	2.3
70.2	559.6	3.79	3.0
70.2	590.9	3.35	4.3
75°			
74.5	423.1	12.42	2.9
74.9	454.9	9.29	2.5
75.2	487.0	6.29	3.4
75.4	517.1	5.60	3.6
74.8	529.7	4.87	2.3
75.4	545.1	4.55	4.4
74.8	557.3	4.01	3.9
74.8	583.2	3.46	4.5
74.8	608.3	3.53	5.1
75.7	636.6	3.09	5.1
80°			
79.3	397.2	17.27	0.9
79.8	426.4	12.70	1.3
80.1	455.8	9.49	2.2
80.3	483.2	6.79	2.9
80.4	508.7	5.54	5.1
90°			
89.0	356.3	26.64	0.9
89.6	381.5	20.50	1.0
90.0	406.8	15.42	1.5
90.2	430.2	11.25	2.0
90.4	452.0	9.03	3.0
90.2	334.7	3.13	4.2
90.0	856.5	2.84	4.5
90.0	880.5	2.27	6.7
90.0	903.0	1.98	5.4
89.8	922.0	1.75	8.3
100°			
98.4	297.7	32.63	1.5
99.2	316.0	33.70	1.6
98.9	325.7	33.25	0.9
99.8	332.4	31.69	1.8
99.5	348.1	27.77	1.0
100.3	351.8	27.61	2.4
100.0	370.5	21.41	1.4
100.7	373.5	20.98	3.1
100.3	391.2	16.41	2.2
100.5	410.3	13.42	2.6
100.2	746.7	4.64	2.6
100.1	764.8	4.38	2.8
100.0	786.4	3.99	3.5
99.9	803.7	3.41	4.8
99.8	819.8	3.07	4.0
105°			
103.5	314.3	32.22	1.2
104.1	335.7	29.34	1.2
104.6	357.0	23.90	1.5
104.9	376.8	19.07	2.9
104.5	383.3	18.32	2.0
105.1	395.0	16.84	3.3
104.7	401.0	14.48	2.4
104.8	417.4	11.94	2.9
104.9	433.2	10.09	3.3
105.0	450.8	8.58	3.2
110°			
109.1	302.6	30.69	1.1
109.7	322.9	30.31	1.1
110.2	343.2	27.71	1.5
110.5	361.9	21.25	1.9
110.7	379.2	17.16	3.2
110.2	679.6	3.33	3.8
110.0	697.3	1.67	3.7
110.1	714.7	2.04	4.4
110.1	731.2	2.26	3.0
109.9	745.4	1.60	4.3
120°			
118.6	261.9	16.98	2.8
119.3	277.5	21.35	2.7
118.8	285.5	24.46	1.3
119.9	291.4	25.70	1.9
119.8	305.7	27.74	0.9
120.2	324.1	28.89	1.3
120.2	340.5	24.51	1.4
120.4	356.4	21.81	1.9
120.1	631.6	2.64	4.0
120.0	646.5	2.51	4.0
120.0	660.3	2.71	4.3
120.2	675.9	2.68	3.5
120.1	689.6	2.68	3.6
125°			
123.7	278.5	20.68	1.7
124.4	296.8	24.71	1.5
124.8	315.0	25.47	1.6
125.1	331.7	24.39	1.7
125.2	347.1	22.13	1.5
125.2	611.6	2.26	4.0

REF. V.B. Ganenko, V.G. Gorbenko, L.M. Derkach, Yu.V. Zhebrovskii, L.Ya. Kolesnikov, I.I. Miroshnichenko, V.I. Nikiforov, A.L. Rubashkin, V.M. Sanin, P.V. Sorokin, S.V. Shalatskii
Sov. J. Nucl. Phys. 23, 162 (1976)
Yad. Fiz. 23, 310 (1976)

ELEM. SYM.	A	Z
H	1	1

METHOD

REF. NO.	
76 Ga 6	egf

REACTION	RESULT	EXCITATION ENERGY	SOURCE		DETECTOR		ANGLE
			TYPE	RANGE	TYPE	RANGE	
$ G,PIØ	RLX	250-650	C	1*2	TEL-D		DST

1.15*1.4 GEV, COH-BRMS

Experimental results on the asymmetry of the differential cross sections for the $\gamma p \rightarrow p\pi^0$ reaction with polarized photons in the photon energy range 250–650 MeV (lab system) and the pion escape angle range 60–135° (c.m. system) are presented and are compared with dispersion-theory predictions and with the results of a phenomenological multipole analysis. The asymmetry angular distributions indicate that the S-plus P-wave approximation is valid for the $\gamma p \rightarrow p\pi^0$ reaction at photon energies up to 650 MeV.

PACS numbers: 13.60.Kd

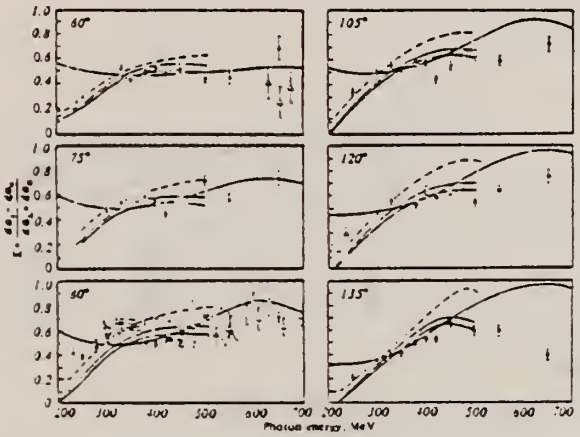

FIG. 9. Excitation functions for the asymmetry at several pion–escape angles (c. m. system). The points represent experimental results: the black circles are from the present work, the open circles and squares from[4], and the triangles from[3]. The dashed curves are from[19], the full curves from from[20], and the hatched bands from[18].

TABLE 1.

E_γ, MeV	$\theta^*_{\pi^0}$, deg	Σ	$\Delta\Sigma$	E_γ, MeV	$\theta^*_{\pi^0}$, deg	Σ	$\Delta\Sigma$	E_γ, MeV	$\theta^*_{\pi^0}$, deg	Σ	$\Delta\Sigma$
250	90	0.387	0.018	350	60	0.506	0.020	500	60	0.482	0.044
	105	0.350	0.016		75	0.589	0.027		75	0.721	0.041
	135	0.210	0.017		90	0.506	0.025		90	0.711	0.039
300	75	0.475	0.015		105	0.380	0.030		105	0.634	0.047
	90	0.541	0.018		120	0.528	0.026		120	0.543	0.035
	105	0.553	0.016		135	0.513	0.024		135	0.395	0.043
	120	0.452	0.014	400	60	0.539	0.034	550	60	0.455	0.061
	135	0.357	0.015		75	0.540	0.032		75	0.561	0.047
330	60	0.522	0.024		90	0.488	0.024		90	0.571	0.037
	75	0.541	0.025		105	0.583	0.033		105	0.584	0.042
	90	0.652	0.027		120	0.632	0.035		120	0.628	0.035
	105	0.560	0.026		135	0.533	0.030		135	0.586	0.056
	120	0.556	0.024	420	60	0.487	0.024	650	50	0.579	0.068
	135	0.391	0.020		75	0.455	0.023		60	0.677	0.091
					90	0.518	0.025		75	0.728	0.055
350	60	0.434	0.031		105	0.444	0.026		80	0.696	0.035
	75	0.555	0.025		120	0.584	0.030		105	0.716	0.052
	90	0.611	0.021		135	0.529	0.026		120	0.735	0.053
	105	0.543	0.022						135	0.388	0.044
	120	0.516	0.024	450	60	0.526	0.034				
	135	0.412	0.030		75	0.558	0.043				
					90	0.597	0.027				
					105	0.553	0.028				
					120	0.608	0.024				
					135	0.657	0.032				

REF. Yu. A. Aleksandrov, V.A. Kozlov, V.N. Maikov, and V.V. Pavlovskaya
Sov. J. Nucl. Phys. 25, 43 (1977)
Yad. Fiz. 25, 80-84 (Jan. 1977)

ELEM. SYM.	A	Z
H	1	1

METHOD

REF. NO. 77 AT 5 hmg

REACTION	RESULT	EXCITATION ENERGY	SOURCE		DETECTOR		ANGLE
			TYPE	RANGE	TYPE	RANGE	
G,PI0	ABX	320	C	350	CKV-D		DST

Differential cross sections for neutral-pion photoproduction from hydrogen are obtained at 320 MeV and pion c.m.s. angles 10, 30, 60, 90, and 120 degrees.

PACS numbers: 13.60.Kd, 14.40.Dt

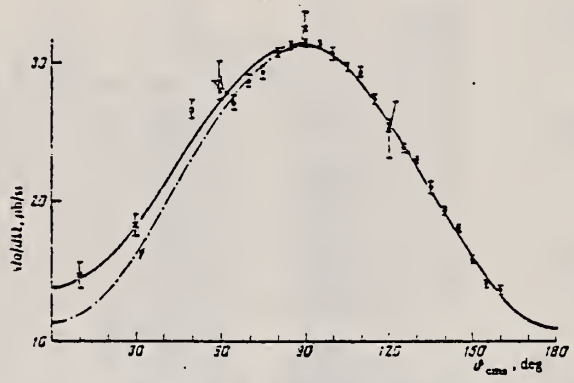

FIG. 1. Differential cross sections for π^0 photoproduction from hydrogen at mean energy 320 MeV. Experimental points: ●—,[1] ○—,[2] x—our data. Curves: dash-dot—approximation of data in Ref. 1, solid—approximation of our results together with the combined results given in Ref. 2.

TABLE II.

$\bar{\vartheta}$, deg	$d\sigma/d\Omega$, μb/sr	Statistical error, μb/sr	Total error, μb/sr
	$\bar{E}=320\pm17$ MeV		
10	14.46	±0.97	±1.32
30	18.3	±0.92	±1.39
60	27.08	±0.85	±1.97
90	22.47	±1.29	±2.53
120	25.0	±1.97	±2.54

REF. I. Arai, H. Fujii, S. Homma, Y. Hoshi, H. Ikeda, T. Ishii, A. Itano, K. Maruyama, E. Ohshima, H. Okuno, A. Sasaki and N. Yamashita
J. Phys. Soc. Japan 43, 363 (1977)

ELEM. SYM.	A	Z
H	1	1

METHOD

REF. NO. 77 Ar 7 egf

REACTION	RESULT	EXCITATION ENERGY	SOURCE		DETECTOR		ANGLE
			TYPE	RANGE	TYPE	RANGE	
G,PI0	ABX	500-930	D	500-930	MAG-D		DST
G,PI+	ABX	500-930	D	500-930	MAG-D		DST

Differential cross sections of the reactions, $\gamma+p\rightarrow p+\pi^0$, and $\gamma+p\rightarrow n+\pi^+$, are measured at about 85° and 65°, respectively, in the incident energy range from 500 MeV to 930 MeV. A tagged photon is used as an incident photon beam. Overall features are consistent with the theoretical analyses by Moorhouse Oberlack and Rosenfeld, and by Metcalf and Walker.

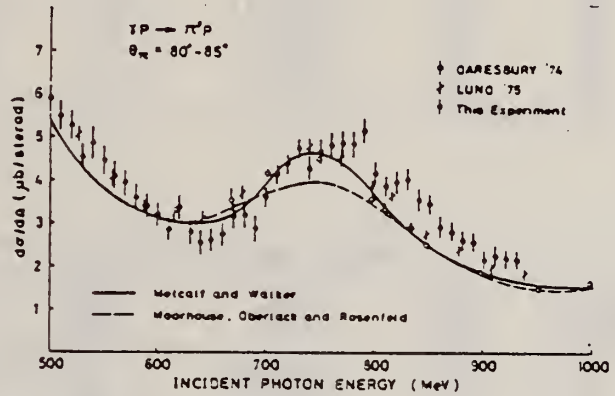

Fig. 4. The differential cross sections in the reaction $\gamma+p\rightarrow p+\pi^0$ at $\theta^*_\pi=80°\sim85°$. The indicated errors are only due to statistical ones.

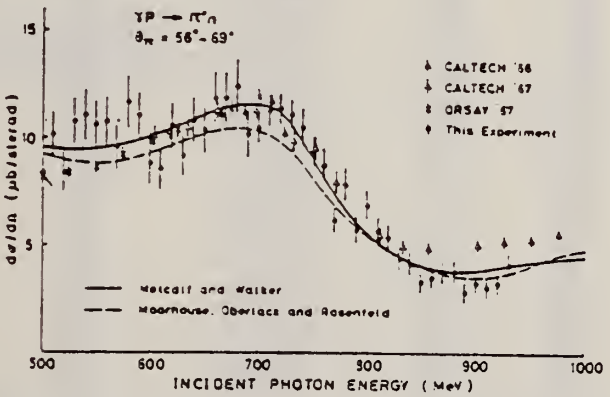

Fig. 5. The differential cross sections in the reaction $\gamma+p\rightarrow n+\pi^+$ at $\theta^*_\pi=56°\sim69°$. The indicated errors are only due to statistical ones.

(continued)

Table I. Cross sections for the reaction $\gamma p \rightarrow p^{\circ}\pi$.

Photon energy (MeV)	CM angle (degree)	Cross section (μb/sr)	Photon energy (MeV)	CM angle (degree)	Cross section (μb/sr)
500	85.6	5.90±0.32	720	83.3	4.41±0.21
510	85.6	5.48±0.34	730	83.1	4.75±0.21
520	85.5	5.26±0.33	740	83.0	4.28±0.28
530	85.5	4.52±0.31	750	82.9	4.66±0.27
540	85.4	4.86±0.37	760	82.7	4.82±0.28
550	85.4	4.42±0.33	770	82.6	4.86±0.26
560	85.3	4.11±0.32	780	82.4	4.83±0.28
570	85.3	3.94±0.30	790	82.3	5.14±0.27
580	85.2	3.59±0.30	800	82.1	4.19±0.25
590	85.1	3.39±0.28	810	81.9	3.88±0.24
600	85.0	3.20±0.27	820	81.8	3.95±0.25
610	84.8	2.85±0.26	830	81.7	4.05±0.25
620	84.7	3.37±0.28	840	81.6	3.56±0.24
630	84.6	2.77±0.26	850	81.4	3.45±0.23
640	84.5	2.53±0.26	860	81.3	2.93±0.22
650	84.4	2.61±0.26	870	81.2	2.83±0.22
660	84.2	2.74±0.27	880	81.1	2.63±0.21
670	84.0	3.16±0.29	890	80.9	2.62±0.21
680	83.9	3.17±0.31	900	80.8	2.19±0.20
690	83.7	2.86±0.29	910	80.7	2.28±0.20
700	83.6	3.63±0.17	920	80.6	2.18±0.20
710	83.4	4.15±0.20	930	80.4	2.17±0.18

Table II. Cross sections for the reaction $\gamma p \rightarrow n\pi^{+}$.

Photon energy (MeV)	CM angle (degree)	Cross section (μb/sr)	Photon energy (MeV)	CM angle (degree)	Cross section (μb/sr)
500	56.6	8.41±0.84	720	63.6	11.36±0.68
510	57.0	10.19±1.02	730	63.8	11.16±0.66
520	57.4	8.41±0.93	740	64.1	10.51±0.88
530	57.7	10.79±1.07	750	64.4	9.35±0.78
540	58.1	11.08±1.20	760	64.7	8.74±0.75
550	58.4	10.62±1.10	770	64.9	6.22±0.60
560	58.8	10.77±1.13	780	65.2	7.86±0.74
570	59.1	9.58±0.99	790	65.5	5.75±0.59
580	59.5	11.70±1.19	800	65.8	6.90±0.67
590	59.8	11.07±1.08	810	66.0	5.72±0.60
600	60.1	8.85±0.99	820	66.3	5.41±0.57
610	60.4	8.57±0.97	830	66.5	4.30±0.52
620	60.7	10.61±1.04	840	66.8	4.16±0.51
630	61.0	9.20±0.94	850	67.0	3.31±0.45
640	61.3	10.86±1.07	860	67.2	3.52±0.48
650	61.6	10.39±1.03	870	67.5	3.77±0.50
660	61.9	11.86±1.17	880	67.7	3.85±0.51
670	62.2	11.90±1.16	890	67.9	2.84±0.42
680	62.5	12.42±1.23	900	68.2	3.31±0.48
690	62.7	10.21±1.11	910	68.4	3.09±0.46
700	63.0	10.50±0.61	920	68.7	3.24±0.47
710	63.3	11.33±0.67	930	68.9	4.13±0.51

REF.	ELEM. SYM.	A	Z
E.C. Booth, B. Chasan, A.M. Bernstein, P. Bosted, J.H. Koch Phys. Lett. 66B, 236 (1977)	H	1	1

METHOD	REF. NO.	
	77 Bo 1	egf

REACTION	RESULT	EXCITATION ENERGY	SOURCE		DETECTOR		ANGLE
			TYPE	RANGE	TYPE	RANGE	
G,PI+	ABY	149-158	C	148-158	ACT-I		4PI

We have measured the excitation function from threshold to 9 MeV above threshold for the reaction $\gamma + d \rightarrow \pi^+ + n + n$ by counting positrons after the bremsstrahlung beam burst. The extracted cross section is compared with a calculation using the impulse approximation, and good agreement is found near threshold.

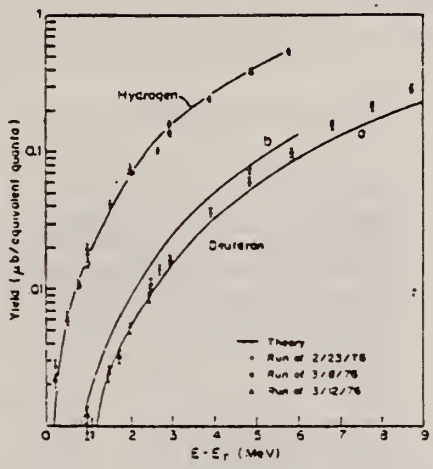

Fig. 1. Yield curves for the reactions $\gamma(p,n)\pi^+$ and $\gamma(d,nn)\pi^+$. The hydrogen data is scaled to fit the yield obtained from $\sigma_2 = a_0 q/k$ shown as a solid line, and deuterium is normalized to hydrogen. Curves a and b are calculated from theoretical cross sections shown in fig. 2.

REF.

P. Dougan, V. Ramsay and W. Stiefler
Z. Physik A280, 341 (1977)

ELEM. SYM.	A	Z
H	1	1

METHOD

REF. NO.	
77 Do 5	egf

REACTION	RESULT	EXCITATION ENERGY	SOURCE		DETECTOR		ANGLE
			TYPE	RANGE	TYPE	RANGE	
G,PIO	ABX	262 - 238	C	375-475	TEL-D		DST

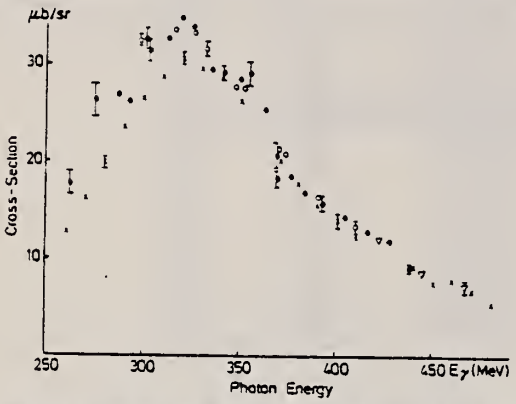

Fig. 1. The cross-sections for π^0-production off protons at 100° c.m. as measured at Lund and Bonn. The Bonn data are fits to the results of several experiments using different techniques. The Lund data have been obtained over a four-year period with major alterations to the experimental set-up. • This work (1975), ○ Lund (1974–1975) [10], ▽ Lund (1972–1973) [9], × Bonn [11]

Table 1. The cross-sections for π^0-production off protons at 100° c.m. found in the present measurements. The groups correspond to the different telescope configurations employed. Within each group, the effective photon energy-resolutions (FWHM) are given to a good approximation by the differences between consecutive values. Systematic errors amount to about 5%

C.M. angle (degrees)	E_γ (MeV)	Cross-section (μb/sr)	Stat. Error (%)	End-point Energy (MeV)
96.7	262.6	17.80	7.6	
97.7	275.4	26.30	6.2	
98.5	286.9	26.93	6.3	
99.3	301.7	32.65	4.5	
100.0	319.2	34.89	4.8	375
100.5	335.2	29.45	5.8	
100.9	350.0	28.60	6.4	
101.2	363.0	25.58	7.6	
98.4	292.3	26.21	3.3	
98.9	302.8	31.48	3.1	
99.3	312.6	33.70	3.3	
99.8	325.5	33.91	2.5	375 and
100.2	341.0	29.25	3.0	
100.6	355.5	29.07	4.2	400
100.8	369.2	20.75	5.6	
99.6	369.4	18.34	4.8	
99.7	376.6	18.55	5.1	
99.8	383.6	16.99	5.4	
100.0	393.2	15.84	4.1	475
100.1	405.2	14.37	4.5	
100.2	416.6	12.93	4.8	
100.3	427.7	11.94	5.3	
100.3	438.3	9.11	6.6	

REF. V.G. Gorbenko, A.I. Derebchinskii, Yu.A. Zhebrovskii, A.A. Zybalov, L.Ya. Kolesnikov, O.G. Konovalov, A.L. Rubashkin, P.V. Sorokin, & A.E. Tenishev
Yad. Fiz. 26, 320 (August 1977)
Sov. J. Nucl. Phys. 26, 167 (August 1977)

ELEM. SYM.	A	Z
H	1	1

METHOD

REF. NO. 77 Go 3

hmg 11/17/80

REACTION	RESULT	EXCITATION ENERGY	SOURCE		DETECTOR		ANGLE
			TYPE	RANGE	TYPE	RANGE	
$ G,PIO	NOX	500	D	500	MSP-D	---	DST

We measured the polarization of the recoil proton in the reaction $\gamma p \to p\pi^0$ with a beam of linearly polarized photons obtained with the aid of coherent bremsstrahlung from a diamond crystal in the Khar'kov linear electron accelerator. The experimental values of the cross-section asymmetry ϵ, of the asymmetry T, on a polarized target, and the recoil-proton polarization components P_y and $P_{x'}$ are obtained at a photon energy 500 MeV and at c.m.s. pion-emission angles 105, 120, and 140° and are compared with the predictions of various multipole analyses.

POL Photons, Protons

TABLE I. Experimental results with photons that are linearly polarized at angles 0 and 90° (Σ, $P_y^{\perp}$, $P_y^{\parallel}$, $P_{y'}$, T_y) and 45 and 135° ($P_{x'}$, $P_{z'}$) to the plane of the reaction $\gamma p \to p\pi^0$ at E_γ = 500 MeV.

Observed quantity	Pion angle in the c.m.s.		
	105°	120°	140°
Σ	0.666±0.062	–	0.513±0.147
$P_y^{\perp}$	−0.451±0.170	–	−0.237±0.152
$P_y^{\parallel}$	0.428±0.378	–	0.189±0.282
T_y	−0.451±0.156	–	−0.215±0.138
$P_{x'}$	−0.28±0.12	−0.53±0.25	−0.05±0.11
$P_{z'}$	−0.42±0.19	−0.31±0.16	0.194±0.202

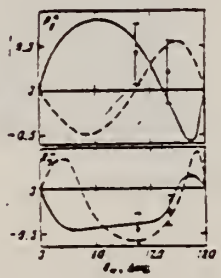

FIG. 3. Angular dependence of the proton polarization $P_y^{\perp(\parallel)}$ at E_γ = 500 MeV for photons that are linearly polarized perpendicular (parallel) to the reaction plane. Solid curves—results of Schwela's analysis,[13] dashed—results of Walker's analysis.[12]

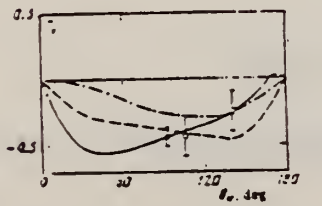

FIG. 4. Angular dependence of the asymmetry T_y of the cross sections on the polarized target at E_γ = 500 MeV. Solid curve—results of Schwela's analysis,[13] dash-dot line—result of Moorhouse's analysis.[21] •—experimental values of T_y obtained in Ref. 3, o—present results.

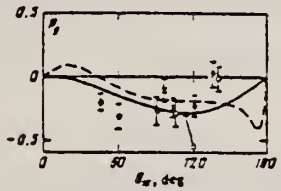

FIG. 5. Angular dependence of the proton polarization P_y with polarized photons at E_γ = 500 MeV. Solid curve—results of Schwela's analysis,[13] dashed—results of Walker's analysis,[12] •—results of Ref. 18, x—results of Ref. 23, o—results of present paper.

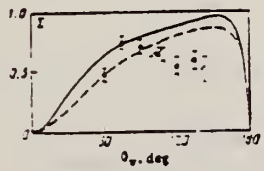

FIG. 6. Angular distribution of the asymmetry Σ with linearly polarized photons at E_γ = 500 MeV. Solid curve—results of Schwela's analysis,[13] dashed—results of Walker's analysis,[12] •—results of Ref. 22, o—results of present work.

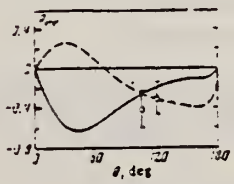

FIG. 7. Angular dependence of the recoil-proton polarization component $P_{y'}$ in the plane of the reaction $\gamma p \to p\pi^0$ at E_γ = 500 MeV. Solid curve—results of Schwela's analysis,[13] dashed—results of Walker's analysis,[12] o—results of present work.

REF. Yu.A. Aleksandrov, V.A. Kozlov and V.V. Pavlovskaya
Yad. Fiz. 28, 670 (1978)
Sov. J. Nucl. Phys. 28, 344 (1978)

EL EM. SYM.	A	Z
H	1	1

METHOD

REF. NO.	
78 A1 12	hg

REACTION	RESULT	EXCITATION ENERGY	SOURCE		DETECTOR		ANGLE
			TYPE	RANGE	TYPE	RANGE	
G,PIØ	ABX	290-360	C	350-563	CKV-D		DST

Analyzed angular distribution in terms of

$$\frac{d\sigma}{d\Omega} = A(E)+B(E)\cos\theta+C(E)\cos^2\theta)+D(E)\cos^3\theta$$

Differential cross sections have been measured for photoproduction of π^0 mesons in hydrogen in the primary-photon energy interval 290–360 MeV at pion emission angles 10,30,50,70, and 90° in the c.m.s. The angular distributions have been analyzed by means of second and third degree polynomials in cos θ.

TABLE I.

E_γ, MeV	$\theta_{cm\pi^0}$, deg				
	10	30	50	70	90
290	11.73±0.60±0.58	13.33±0.47±0.68	15.28±0.61±0.72	21.19±0.81±0.96	25.82±1.05±1.33
300	12.15±0.54±0.53	16.15±0.51±0.72	19.31±0.69±0.87	23.12±0.82±1.12	29.36±1.0±1.35
310	14.22±0.55±0.69	16.92±0.47±0.71	20.22±0.6)±0.86	28.82±0.88±1.24	28.73±1.0±1.31
340	13.72±0.78±0.63	15.11±0.58±0.63	20.07±0.73±0.93	28.05±1.06±1.26	29.49±1.03±1.44
350	10.29±0.51±0.49	14.04±0.51±0.59	19.55±0.67±0.87	24.93±0.85±1.08	26.34±0.81±1.24
360	9.28±0.39±0.41	11.98±0.35±0.52	18.08±0.58±0.79	23.38±0.76±1.03	25.72±0.76±1.23

TABLE II.

Coefficient	E_γ, MeV						
	290	300	310	320	340	350	360
A	23.6±0.78	27.12±0.79	29.08±0.68	31.07±0.69	28.86±0.69	26.54±0.8	25.23±0.09
B	−0.66±0.17	0.48±0.16	0.56±0.16	1.43±0.21	1.42±0.15	0.89±0.16	1.39±0.19
C	−13.69±0.24	−15.89±0.23	−17.74±0.22	−18.68±0.31	−18.8±0.23	−18.02±0.23	−16.23±0.17
χ^2	3.78	1.75	1.95	2.47	1.28	0.97	2.57

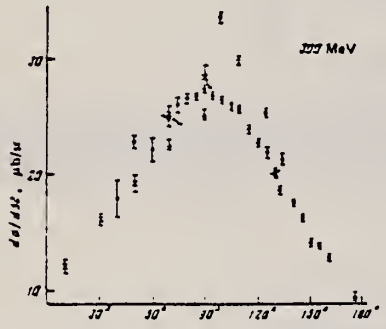

FIG. 1. Differential cross sections for photoproduction of π^0 mesons in hydrogen for an average energy 300 MeV. Points: ×—our measurements, •—Ref. 10, ⌒—Ref. 1, Δ—Ref. 11.

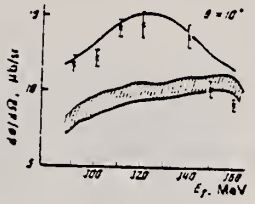

FIG. 2. Energy dependence of differential cross sections near $\theta = 10°$ in the c.m.s.: ×—our measurements, solid line—calculation of Ref. 3, cross-hatched region—calculation of Ref. 4.

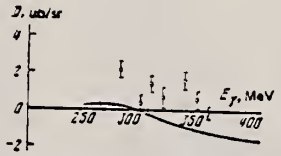

FIG. 3. Energy dependence of the coefficient D. ○—our results, solid line—calculation of Ref. 3.

REF. P. Argan, G. Audit, A. Bloch, P. Bosted, N. de Botton, J.L. Faure, C. Schuhl, G. Tamas, C. Tzara, E. Vincent, J. Deutsch, D. Favart, R. Prieels, and B. Van Oystaeyen
Phys. Rev. Lett. 41, 629 (1978)

ELEM. SYM.	A	Z
H	1	1

METHOD

REF. NO. 78 Ar 2 rs

REACTION	RESULT	EXCITATION ENERGY	SOURCE		DETECTOR		ANGLE
			TYPE	RANGE	TYPE	RANGE	
G,PO	ABY	146-151	C	151	TEL-D		DST

π^0 photoproduction on deuterium has been measured in the region of 1 to 7 MeV above threshold, relative to the same reaction on hydrogen. The comparison of our results with available theoretical predictions shows the necessity to go beyond the impulse approximation.

TABLE I. Experimental yield $A(E_\gamma) = \int_{E_0}^{E_\gamma} \int_\Omega \bar{B}(E, E_\gamma) \epsilon(E, \Omega) (d\sigma/d\Omega) d\Omega\, dE$ in microbarns, normalized to one target nucleus and one equivalent quantum, for different values of the bremsstrahlung endpoint energy E_γ above threshold E_0.

Hydrogen		Deuterium	
$E_\gamma - E_0$ (MeV)	$10^6 A_H$	$E_\gamma - E_0$ (MeV)	$10^6 A_D$
1.04	0.16 ± 0.06	0.88	0.40 ± 0.07
2.04	0.61 ± 0.11	1.88	1.16 ± 0.11
3.04	0.92 ± 0.13	2.38	2.64 ± 0.26
4.04	1.94 ± 0.27	4.88	6.66 ± 0.37
6.04	4.29 ± 0.36	5.88	10.62 ± 0.55
		7.38	16.43 ± 1.50

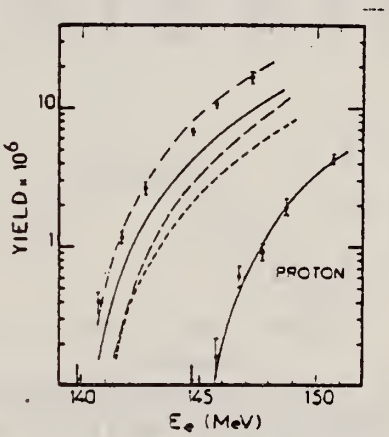

FIG. 2. The measured photoproduction yields as a function of the bremsstrahlung endpoint energy E_γ compared to theoretical estimates for deuterium without rescattering (long dashes, Ref. 6, and short dashes, Ref. 5) and including rescattering (dash-dotted line, Ref. 6, and solid line, Ref. 5). These two theoretical estimates use the same proton cross section; the corresponding yield has been adjusted to the hydrogen data. Arrows indicate the threshold energies. The yields are given in microbarns per equivalent quantum.

[5] P. Bosted and J.M. Laget, Nucl. Phys. A296, 413 (1978).

[6] J.H. Koch and R.M. Woloshyn, Phys. Rev. C 16, 1968 (1977).

REF. A.I. Derebchinskii, A.A. Zybalov, O.G. Konovalov, V.R. Nazyrov, A.E. Tenishev, & S.G. Tonapetyan
Yad. Fiz. 28, 265 (July 1978)
Sov. J. Nucl. Phys. 28, 132 (July 1978)

ELEM. SYM.	A	Z
H	1	1

METHOD

REF. NO. 78 De 9

hmg 11/18/80

REACTION	RESULT	EXCITATION ENERGY	SOURCE		DETECTOR		ANGLE
			TYPE	RANGE	TYPE	RANGE	
$ G,PIØ	NOX	480-800	C	UKN	MAG-D	---	99

Polarized protons

TABLE I.

E_γ^{eff}, MeV	θ_π (in c.m.s.), deg	P	$\pm\Delta P$	E_γ^{eff}, MeV	θ_π (in c.m.s.), deg	P	$\pm\Delta P$
480	99.0	−0.158	0.107	660	99.7	−0.778	0.095
500	99.0	−0.201	0.094	680	99.8	−0.797	0.093
520	99.1	−0.318	0.090	700	99.9	−0.722	0.090
540	99.1	−0.386	0.094	720	100.1	−0.724	0.068
560	99.2	−0.384	0.102	740	100.2	−0.721	0.080
580	99.3	−0.431	0.095	760	100.4	−0.541	0.071
600	99.3	−0.597	0.093	780	100.5	−0.504	0.074
620	99.4	−0.657	0.095	800	100.7	−0.438	0.103
640	99.5	−0.742	0.094				

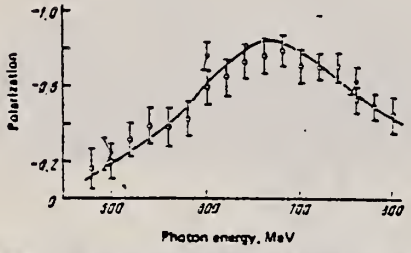

FIG. 1. Energy dependence of proton polarization in the reaction $\gamma p \to \pi^0 p$ at an angle $\theta_\pi = 100°$ c.m.s. The curve is the result of Ref. 1; the points ● are from Ref. 5, and ○ from the present work.

REF. P.I. Vatset, A.I. Derebchinskii, A.A. Zybalov, O.G. Konovalov, V.R. Nazyrov, A.É. Tenishev, and S.G. Tonapetyan
Sov. J. Nucl. Phys. 27, 323 (1978)
Yad. Fiz. 27, 605 (1978)

ELEM. SYM.	A	Z
H	1	1

METHOD

REF. NO.	
78 Va 5	hg

REACTION	RESULT	EXCITATION ENERGY	SOURCE		DETECTOR		ANGLE
			TYPE	RANGE	TYPE	RANGE	
$ G,P1O	NOX	THR-800	C	800	MAG-D		UKN

POL. PROTONS

---SEE REVERSE SIDE---

(continued)

Polarization of protons in interaction of photons with energy up to 800 MeV with deuterium nuclei

P. I. Vatset, A. I. Derebchinskiĭ, A. A. Zybalov, O. G. Konovalov, V. R. Nazyrov, A. É. Tenishev, and S. G. Tonapetyan

Khar'kov Physico-technical Institute, Ukrainian Academy of Sciences
(Submitted 27 May 1977)
Yad. Fiz. 27, 605–606 (March 1978)

The polarization of photoprotons from deuterium has been studied. The data obtained are used to extract information on the polarization of protons in the reaction $\gamma n \to \pi^- p$.

PACS numbers: 13.60.Kd, 25.10.+s

In this article we described an experiment on measurement of the polarization of protons in reactions of photons with energy up to 800 MeV with deuterium nuclei. The purpose of the work was to obtain information on the polarization of protons in the reaction $\gamma n \to \pi^- p$ by a difference method.

The experiment was carried out in the photon beam of the 2-GeV electron linear accelerator by means of a telescope of spark chambers[1] located at the exit of the magnet spectrometer. Protons with momentum 612 ± 24 MeV/c were detected by means of this apparatus. The proton polarization was measured on the basis of the asymmetry in their scattering in the graphite electrodes of the spark chamber.[2]

Three independent measurements were made, in which the relative yields of the protons and their polarization were investigated:

1) measurement in hydrogen at a maximum photon energy 800 MeV;

2) measurement in deuterium under the same conditions;

3) measurement in deuterium at a maximum photon energy 600 MeV.

The kinematic conditions of the first two measurements correspond to an effective photon energy 650 ± 40 MeV for the channels of production of single pions from free nucleions at 90° in the c.m.s.

In the third measurement these channels are kinematically forbidden, and therefore the polarization of the protons measured in this case is determined mainly by the two-particle and three-particle photodisintegration of deuterium (PD).

The polarization obtained in measurement 2) is determined by the contribution of the reactions $\gamma p \to \pi^0 p$, $\gamma n \to \pi^- p$, and PD.

Thus, knowing the relative contributions of these processes, we can obtain a value of the proton polarization in the reaction $\gamma n \to \pi^- p$ from the experimental polarization values:

$$P_1 = (C_2 P_2 - C_{p0} P_{p0} + C_{PD} P_{PD}) / C_{\pi^-}, \qquad (1)$$

where P_1 is the proton polarization measured in experiment 2); P_{p0} and C_{p0} are the polarization and relative yield of protons obtained in experiment 1); P_{PD} and C_{PD} are these same quantities obtained in experiment 3); P_{π^-} and C_{π^-} are the polarization and yield of protons associated with the reaction $\gamma n \to \pi^- p$; $C_2 = C_{\pi^-} + C_{\pi^0} + C_{PD}$ is the yield of protons measured in experiment 2).

TABLE I

C_{π^0}	C_{PD}	C_{π^-}	P_{π^0}	P_{PD}	P_{π^-}
4.7	8.3	8.1	−0.72±0.07	0.22±0.11	−0.49±0.24

The relative yield C_{π^-} is determined from the experimentally measured yield C_{π^0} and the ratio of the cross sections of the reactions $\gamma p \to \pi^0$ and $\gamma n \to \pi^- p$.

In the table we have given the results of the present experiment. The value of P_{π^0} was obtained from Eq. (1). The value of P_1 obtained in the present work is -0.24 ± 0.08. The errors are statistical.

The proton polarization value in the reaction $\gamma n \to \pi^- p$ is in reasonable agreement with the polarization values obtained in experiments in deuterium[3] and carbon[4] with $\pi^- p$ coincidences in this energy region.

The studies carried out have shown an appreciable contribution to the polarization from processes associated with photodisintegration of deuterium. The existence of polarization in the PD process can be explained by the fact that this process is due to a significant degree to creation of a pion from one of the nucleons with subsequent absorption of the produced meson by another nucleon.[5]

The error in determination of the polarization P_{π^-} depends strongly on the contribution of background processes ($\gamma p \to \pi^+ n$ and PD), and therefore even a substantial improvement in the accuracy of the quantities measured in the experiment cannot adequately reduce the error in calculation of P_{π^-}. This method of measurement of polarization permits a qualitative picture to be obtained of the angular and energy dependences and in some cases may be effective in those regions where information on proton polarization in the $\gamma n \to \pi^- p$ reaction cannot be obtained by the coincidence method with its higher accuracy.

[1] S. G. Tonapetyan, O. G. Konovalov *et al.*, Prib. Tekh. Éksp., No. 5, 58 (1970) [Instrum. Exper. Tech.].
[2] S. G. Tonapetyan, O. G. Konovalov, *et al.*, Prib. Tekh. Éksp., No. 2, 61 (1970) [Instrum. Exper. Tech.].
[3] M. Beneventano, S. d'Angelo, *et al.*, XVth Intern. Conf. on High Energy Physics, Kiev, 1, 242, 1970.
[4] V. N. Stibunov, Issledovanie fotoobrazovaniya na yadrakh pionov s vyletom nuklonov, Avtoreferat kandidatskoĭ dissertatsii (Study of Photoreproduction of pions from nuclei with emission of nucleons, author's abstract of candidate's dissertation), Tomsk, 1974.
[5] R. R. Wilson, Phys. Rev. 104, 218 (1956).

Translated by Clark S. Robinson

REF. A.A. Zybalov, A.I. Derebchinskii, O.G. Konovalov, A.S. Bratashevskii, V.R. Nazyrov, A.E. Tenishev, & S.G. Tonapetyan
Yad. Fiz. 28, 105 (1978)
Sov. J. Nucl. Phys. 28, 52 (1978)

ELEM. SYM.	A	Z
H	1	1

METHOD

REF. NO.	
78 Zy 5	hg

REACTION	RESULT	EXCITATION ENERGY	SOURCE		DETECTOR		ANGLE
			TYPE	RANGE	TYPE	RANGE	
$G,PIØ	NOX	650,700	C	UKN	MAG-D		DST

The polarizations of protons from the $\gamma p \rightarrow \pi^0 p$ reaction are measured for photon energies of 650 and 700 MeV and c.m. pion emission angles from 80 to 140°. The results are compared with the predictions of various theoretical analyses.

POL PROTON RECOIL

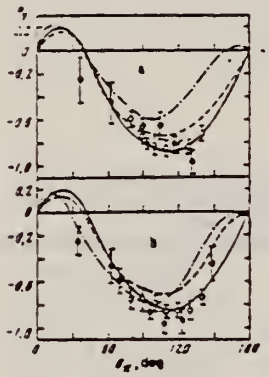

FIG. 1. Angular dependences of polarization at $E_\gamma = 650$ MeV (a) and $E_\gamma = 700$ MeV (b). The curves show the results of the analyses of Ref. 1 (full), Ref. 2 (dash-dot), and Ref. 3 (dashed). The experimental points are from Ref. 6 (●), Ref. 7 ( ), Ref. 9 (⊗), and the present work (○).

TABLE I. Angular dependence of proton polarization for $E_\gamma = 650$ and 700 MeV.

$E_\gamma = 650$ MeV			$E_\gamma = 700$ MeV		
θ_{π}, deg	P_y	$\pm\Delta E_\gamma$, MeV	θ_{π}, deg	P_y	$\pm\Delta E_\gamma$, MeV
78.8	−0.589±0.068	18	80.0	−0.782±0.089	20
90.0	−0.748±0.064	18	90.3	−0.763±0.095	19
100.4	−0.820±0.068	17	100.0	−0.786±0.072	18
110.0	−0.853±0.079	17	110.4	−0.864±0.059	18
119.4	−0.827±0.058	16	119.7	−0.858±0.065	17
129.7	−0.840±0.064	15	130.0	−0.851±0.081	16
140.0	−0.718±0.072	14	140.0	−0.737±0.071	15

Note: the indicated errors are statistical.

REF. P. Argan, G. Audit, A. Bloch, N. de Botton, J.L. Faure, C. Schuhl, G. Tamas, C. Tzara, E. Vincent, J. Deutsch, D. Favart, R. Prieels, B. Van Oystaeyen
Phys. Rev. C20, 242 (1979)

ELEM. SYM.	A	Z
H	1	1

METHOD

REF. NO. 79 Ar 1 hg

REACTION	RESULT	EXCITATION ENERGY	SOURCE		DETECTOR		ANGLE
			TYPE	RANGE	TYPE	RANGE	
G,PI+	ABX	150-156	C	152-156	ACT-I		90

The positive-pion photoproduction yield on ^{3}He was measured near threshold. The transition matrix element of this process is extracted with a $\pm 1.5\%$ accuracy. We discuss the relation of our result, firstly, with magnetic electron scattering on ^{3}He and ^{3}H, secondly, with the properties of pionic ^{3}He atom.

[NUCLEAR REACTION ^{3}He(γ, π^+)^{3}H, measured σ, E = 1–5 MeV.]

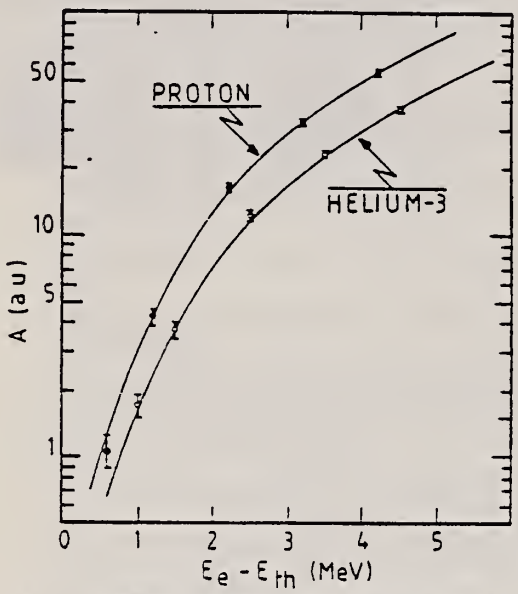

FIG. 1. Measured π^+ photoproduction yields per nucleus as a function of the excess energy above threshold in the laboratory system for hydrogen and ^{3}He. Solid lines are the calculated yields giving the best fit to the experimental data.

TABLE I. Photoproduction yield per nucleus for the hydrogen and ^{3}He targets at different values of the nominal bremsstrahlung end point energy E_e.

E_e (MeV)	$A(p)$ (a.u.)	E_e (MeV)	$A(^3\mathrm{He})$ (a.u.)
152.5	1.05 ± 0.19	145	1.73 ± 0.20
153	4.24 ± 0.39	145.5	3.74 ± 0.29
154	16.4 ± 0.79	146.5	12.3 ± 0.58
155	32.0 ± 1.1	147.5	23.3 ± 0.70
156	54.3 ± 1.4	148.5	37.0 ± 0.93

REF. E.C. Booth, B. Chasan, J. Comuzzi, P. Bosted
Phys. Rev. C20, 1217 (1979)

ELEM. SYM.	A	Z
H	1	1

METHOD

REF. NO.	
79 Bo 1	hg

REACTION	RESULT	EXCITATION ENERGY	SOURCE		DETECTOR		ANGLE
			TYPE	RANGE	TYPE	RANGE	
G,PI+	RLY	151-174	C	151-174	ACT-I		90

The bremsstrahlung yield of the $^2H(\gamma,\pi^-)2p$ reaction is measured from threshold to 25 MeV above threshold. The extracted total cross section relative to the $p(\gamma,\pi^+)n$ cross section is 3–10% greater than the theoretical prediction.

[NUCLEAR REACTIONS $^2H(\gamma,\pi^-)2p$, bremsstrahlung end point energies to 174 MeV, measured π^- yield, deduced $\sigma(E)$.]

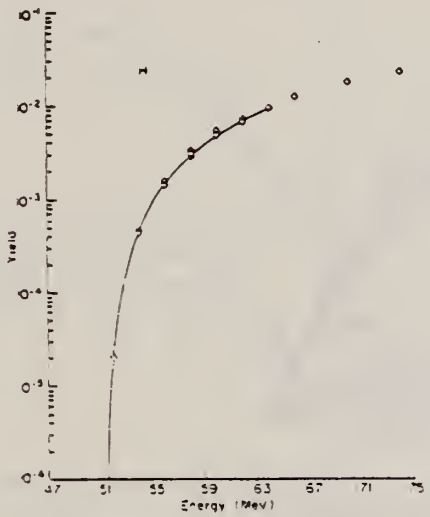

FIG. 1. Yield for the $p(\gamma,\pi^+)n$ reaction vs $E_\gamma - E_{\gamma_0}$ the energy above threshold. The solid line is the calculated yield using the theoretical bremsstrahlung spectrum folded with $\sigma_p = q/k\ 201(1-0.0063\omega)$ as described in the text.

REF. V.A. Get'man, V.G. Gorbenko, V.F. Grushin, A.Ya. Derkach, Yu.V. Zhebrovskii, I.M. Karnaukhov, L.Ya. Kolesnikov, V.S. Kuz'menko, A.A. Lukhanin, Yu.N. Ranyuk, A.L. Rubashkin, V.M. Sanin, P.V. Sorokin, E.A. Sporov, Yu.N. Telegin
JETP Lett. 29, 468 (1979)

ELEM. SYM.	A	Z
H	1	1

METHOD

REF. NO.	
79 Ge 4	hg

REACTION	RESULT	EXCITATION ENERGY	SOURCE		DETECTOR		ANGLE
			TYPE	RANGE	TYPE	RANGE	
$ G,PI+	NOX	150-340	D	340	MAG-D		DST

POL. P,UP/DOWN ASYM

We present the first results of measurement of the asymmetry of the cross section of the reaction $\gamma p \rightarrow n\pi^+$ using a polarized proton target in the region of the first pion-nucleon resonance. The measurements were carried out at a photon energy of 340 MeV for 7 values of the angle of escape of the π^+ meson (30–150°). The obtained results can be used in phenomenological analyses of the processes of single photoproduction of pions by nucleons.

PACS numbers: 13.60.Kd

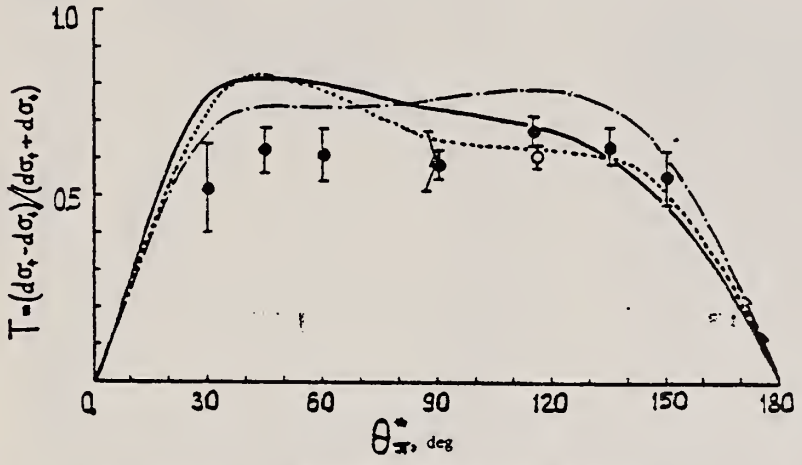

FIG. 1. Angular dependence of the T asymmetry of the cross section of the reaction $\gamma p \rightarrow n\pi^+$ for $E_\gamma = 340$ MeV: ●, results of our work; △ and ○, data of the Japanese group.[1,2] The curves give the predictions of the phenomenological analyses (—, Ref. 10. –, Ref. 11; ..., Ref. 12).

TABLE I.

$\theta^*_{\pi^+}$, deg	30	45	60	90	115	135	150
T	0.520	0.623	0.612	0.588	0.680	0.645	0.554
ΔT	0.117	0.065	0.074	0.033	0.042	0.051	0.070

REF. V.A. Get'man, V.G. Gorbenko, V.F. Grushin, A.Ya. Derkach, Yu.V. Zhebrovskii, I.M. Karnaukhov, L.Ya. Kolesnikov, A.A. Lukhanin, A.L. Rubashkin, V.M. Sanin, P.V. Sorokin, E.A. Sporov, Yu.N. Telegin
JETP Lett. 30, 82 (1979)
Pis'ma Zh. Eksp. Teor. Fiz. 30, 90 (1979)

EL.EM. SYM.	A	Z
H	1	1

METHOD

REF. NO.	
79 Ge 7	hg

REACTION	RESULT	EXCITATION ENERGY	SOURCE		DETECTOR		ANGLE
			TYPE	RANGE	TYPE	RANGE	
$ G,PI+	NOX	340	C.	*1	MAG-D		DST
				(1.25)			

Linearly polarized photon beam was obtained from the 1250 MeV electrons on a diamond monocrystal.

*E IN GEV, $ POL G,P

A two-fold polarization experiment of the "beam-target" type is carried out for the first time for the reaction $\gamma p \to n\pi^+$ for $E_\gamma = 340$ MeV, and the three polarization parameters, Σ, T, and P are determined simultaneously.

PACS numbers: d13.60.Kd

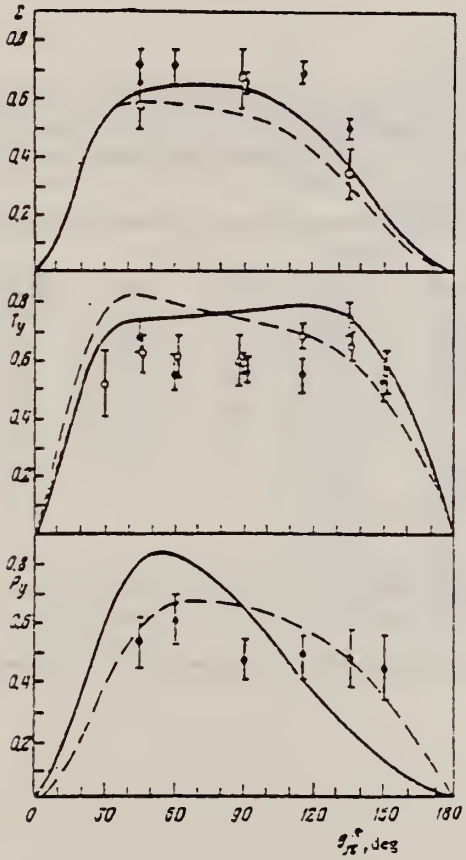

FIG. 1. Polarization data for the $\gamma p \to n\pi^+$ reaction at $E_\gamma = 340$ MeV: filled circles, our work; open circles, Ref. 6; squares, Ref. 7, and triangles, Ref. 8. Dashed curves are for theoretical predictions,[4] solid curves are predictions of the energy-independent analysis.[5]

Σ is cross section assymetry for linearly polarized photons, T is the assymetry for polarized protons, and P is the recoil nucleon polarization

REF. P. Argan, G. Audit, A. Bloch, N. de Botton, J.L. Faure, C. Schuhl, G. Tamas, C. Tzara, E. Vincent, J. Deutsch, D. Favart, R. Prieels, B. Van Oystaeyen
Phys. Rev. C21, 1416 (1980).

ELEM. SYM.	A	Z
H	1	1

METHOD

REF. NO. 80 Ar 2 hg

REACTION	RESULT	EXCITATION ENERGY	SOURCE		DETECTOR		ANGLE
			TYPE	RANGE	TYPE	RANGE	
G,PIØ	ABY	145-153	C	146-153	CKV-D		0

Relative measurements of π^0 photoproduction yields have been performed on hydrogen, deuterium, ^{3}He, and ^{4}He, in the region of 1 to 10 MeV above threshold. A simplified distorted-wave impulse approximation model of the four reactions is described; it leads to an overall understanding of the results. Large rescattering effects are brought to evidence in deuterium and ^{3}He, making the extraction of precise values for the dipole photoproduction amplitudes E_{0+} on nucleons strongly dependent on the theoretical description of the processes.

THRESHOLD MEASUREMENT

Final data in 81Ar2.

[NUCLEAR REACTIONS (γ,π^0), ^{1}H, ^{2}H, ^{3}He, and ^{4}He targets; measured reaction yields, E_{γ^0} = 1–10 MeV.]

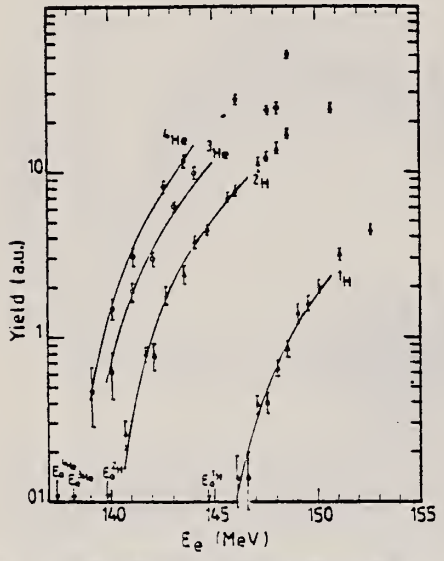

FIG. 5. The measured π^0 photoproduction yields as a function of the end-point bremsstrahlung energy E_e. The curves are the theoretical yields computed with DWIA cross sections, and adjusted to the data up to 6 MeV above threshold as explained in the text.

TABLE III. Experimental yields $Y_A(E_e) = C\int_{E_0}^{E_e}\int_{\Omega_M} B(E,E_e)\epsilon_A(E,\Omega)(d\sigma_A/d\Omega)d\Omega\,dE$ in microbarns, normalized to one target nucleus and one equivalent quantum, for different values of the bremsstrahlung end-point energy E_e above threshold E_0. *Note:* The measurements with empty targets gave $Y_{empty} = 0.00 \pm 0.02$. The average yields measured below threshold amounted to $Y_H = 0.02 \pm 0.02$, $Y_D = 0.07 \pm 0.04$, $Y_{^3He} = 0.01 \pm 0.12$, and $Y_{^4He} = 0.01 \pm 0.15$. All have been taken into account in the table.

Hydrogen		Deuterium		^{3}He		^{4}He	
$E_e - E_0$ (MeV)	$10^6 Y_H$	$E_e - E_0$ (MeV)	$10^6 Y_D$	$E_e - E_0$ (MeV)	$10^6 Y_{^3He}$	$E_e - E_0$ (MeV)	$10^6 Y_{^4He}$
1.41	0.14 ± 0.05	0.88	0.26 ± 0.05	1.87	0.61 ± 0.19	1.72	0.47 ± 0.19
1.91	0.14 ± 0.06	1.88	0.79 ± 0.08	2.87	1.88 ± 0.24	2.72	1.48 ± 0.22
2.41	0.39 ± 0.05	2.26	0.77 ± 0.14	3.87	2.94 ± 0.28	3.72	3.02 ± 0.39
2.91	0.40 ± 0.06	2.88	1.79 ± 0.21	4.87	6.08 ± 0.47	5.22	8.12 ± 0.63
3.41	0.65 ± 0.07	3.76	2.38 ± 0.29	5.87	9.86 ± 0.53	6.22	11.52 ± 0.89
3.91	0.85 ± 0.10	4.26	3.75 ± 0.32	9.37	23.7 ± 1.2	8.72	27.3 ± 1.7
4.41	1.39 ± 0.17	4.88	4.47 ± 0.31	9.87	24.4 ± 1.3	11.22	51.1 ± 3.2
4.91	1.60 ± 0.15	5.88	7.07 ± 0.47				
5.41	2.00 ± 0.16	6.26	7.75 ± 0.55				
6.41	3.15 ± 0.25	7.38	11.13 ± 1.12				
7.91	4.40 ± 0.28	7.76	12.40 ± 0.72				
		8.26	13.9 ± 1.1				
		8.76	16.9 ± 1.1				
		10.38	24.3 ± 1.1				

REF. A.S. Bratashevskij, V.G. Gorbenko, A.I. Derebchinskij, A.Ya. Derkach, Yu.V. Zhebrovskij, A.A. Zybalov, I.M. Karnaukhov, L.Ya. Kolesnikov, O.G. Konovalov, A.A. Likhanin, A.S. Omelaenko, A.L. Rubashkin, P.V. Sorokin, E.A. Sporov, A.E. Tenishev, S.G. Tonapetyan
Nucl. Phys. B166, 525 (1980)

ELEM. SYM.	A	Z
H	1	1

METHOD

REF. NO.: 80 Br 9 egf

REACTION	RESULT	EXCITATION ENERGY	SOURCE		DETECTOR		ANGLE
			TYPE	RANGE	TYPE	RANGE	
$ G,PIØ	NOX	500-800	D	UKN	TEL-D		DST

Measurements of secondary-proton polarization from the reaction $\gamma p \to \pi^0 p$ have been performed in the photon energy range 500–800 MeV at c.m. pion emission angles 100°, 120°, 140°. The experiment was carried out using an optical spark chamber telescope at the output of the magnetic spectrometer. The obtained experimental data are included in a Walker-type analysis in order to verify the parameters of the resonances $P_{11}(1470)$, $D_{13}(1570)$ and $S_{11}(1535)$. Proton polarization in the reaction $\gamma p \to \pi^0 p$ was measured for a photon energy of 450 MeV at a c.m. pion emission angle of 105° using photons linearly polarized at 45° to the reaction plane. A liquid hydrogen target in the field of a superconducting magnet was used for the separation of the P_1- and P_2- components of the secondary-proton polarization vector.

Data are obtained for three components (P_x, P_y, P_z) of the proton polarization. The obtained results are compared with predictions of different multipole analyses of photoproduction.

POL G, POL RECOIL P

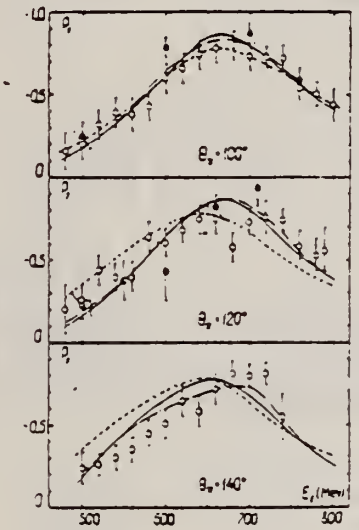

Fig. 2. Energy dependences of the proton polarization from the reaction $\gamma p \to \pi^0 p$ ●, ◒, ○: the data taken from ref. [15]; ○: our present results. The solid curve shows the results of the MW-analysis [2]; the dashed curve, the results of the work [4]; the dash-dotted curve represents fit 1.

REF. T. Ishii, K. Egawa, S. Kato, T. Miyachi, K. Sugano, K. Toshioka, K. Ukai, M. Chiba, K. Joh, T. Shinohara, Y. Yoribayashi, Y. Wada
Nucl. Phys. B165, 189 (1980)

ELEM. SYM.	A	Z
H	1	1

METHOD

REF. NO. 80 Is 7 egf

REACTION	RESULT	EXCITATION ENERGY	SOURCE TYPE	SOURCE RANGE	DETECTOR TYPE	DETECTOR RANGE	ANGLE
G,G	ABX	375-999	C	1*	TEL-D		DST

Differential cross sections of proton Compton scattering have been measured in the energy range between 375 MeV and 1150 MeV in steps of 25 MeV at c.m. angles of 130°, 100° and 70°. The recoil proton was detected with a magnetic spectrometer. In coincidence with the proton, the scattered photon was detected with a lead-glass Čerenkov counter of the total absorption type.

Theoretical calculations based on an isobar model with two components, that is, the resonance plus the background, were practiced. The photon couplings of the second resonance region were determined from the proton Compton data for the first time. The results were that the helicity $\frac{1}{2}$ photon couplings of $P_{11}(1470)$ and $S_{11}(1535)$, and the helicity $\frac{3}{2}$ photon coupling of $D_{13}(1520)$ were consistent with those determined from the single-pion photoproduction data; however, the helicity $\frac{1}{2}$ photon coupling of $D_{13}(1520)$ required a somewhat larger value than that from the single-pion photoproduction data.

999=1.15GEV,1*=1.3GEV

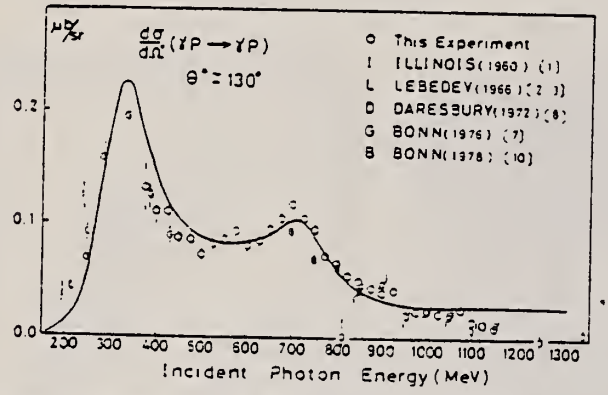

Fig. 3a. Results of the differential cross sections at $\theta^* = 130°$. The solid line represents our analysis.

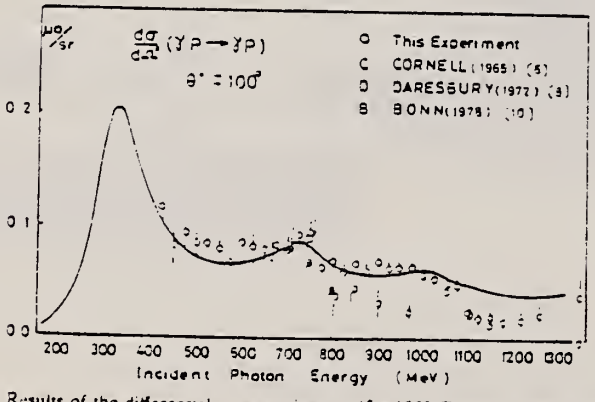

Fig. 3b. Results of the differential cross sections at $\theta^* = 100°$. The solid line represents our analysis.

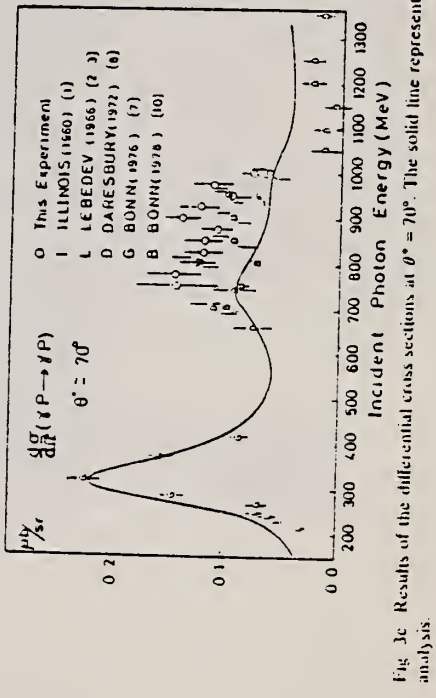

Fig. 3c. Results of the differential cross sections at $\theta^* = 70°$. The solid line represents our analysis.

REF. S. Kato, T. Miyachi, K. Sugano, K. Toshioka, K. Ukai, M. Chiba, K. Egawa, T. Ishii, Y. Yoribayashi, K. Joh, T. Shinohara, Y. Wada Nucl. Phys. B168, 1 (1980)

EL EM. SYM.	A	Z
H	1	1

METHOD

REF. NO.	
80 Ka 4	egf

REACTION	RESULT	EXCITATION ENERGY	SOURCE		DETECTOR		ANGLE
			TYPE	RANGE	TYPE	RANGE	
$ G,PIØ	NOX	400-999	C	600-999	TEL-D		DST

The recoil proton polarization of the reaction $\gamma p \rightarrow \pi^0 p$ was measured at a c.m. angle of 100° for incident photon energies between 451 and 1106 MeV, and at an angle of 130° for energies from 400 to 1142 MeV. One photon, decayed from a π^0 meson, and a recoil proton were detected in coincidence. Two kinds of polarization analyzer were employed. In the range of proton kinetic energy less than 420 MeV and higher than 346 MeV, carbon plates and liquid hydrogen were used for determining the polarization, respectively. The data given by the two polarimeter systems are in good agreement. Results are compared with recent phenomenological analyses. From the comparison between the present data and the polarized target data, the invariant amplitude A_3 can be estimated to be small.

999=1142 MEV, $RCL P

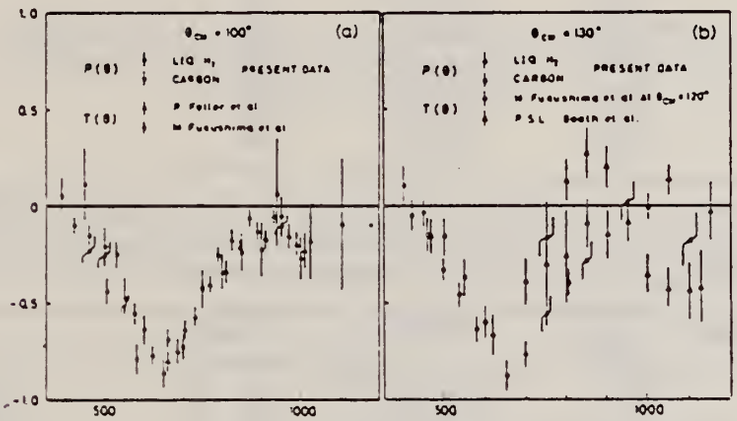

Fig. 10. Comparison of the recoil polarization $P(\theta)$ with the target asymmetry $T(\theta)$ for the process of $\gamma p \rightarrow \pi^0 p$ at a c.m. angle of (a) 100° and (b) 130°.

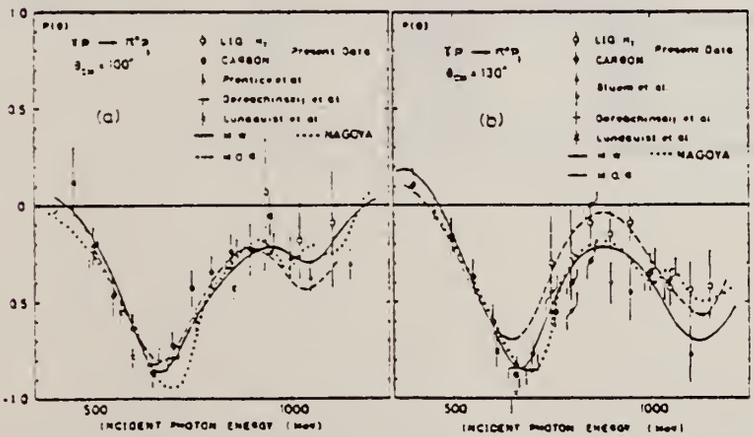

Fig. 11. Results of the polarization as a function of the incident photon energies at a c.m. angle of (a) 100° and (b) 130°. The results of the analyses given by MW, MOR and NAGOYA are also shown for a comparison.

(continued)

TABLE 1a
Results for the carbon polarimeter

Energy bin (MeV)	Average photon energy (MeV)	Average c.m. angle (degrees)	Polarization	Number of events
450 ± 25	451	105 ± 3	+0.12 ± 0.19	1027
500 ± 25	500	104 ± 5	−0.21 ± 0.10	1775
550 ± 25	549	103 ± 5	−0.47 ± 0.11	838
600 ± 25	600	103 ± 5	−0.64 ± 0.08	1181
650 ± 25	650	102 ± 4	−0.86 ± 0.08	739
700 ± 25	699	103 ± 5	−0.73 ± 0.07	972
750 ± 25	750	102 ± 3	−0.43 ± 0.10	544
800 ± 25	799	102 ± 5	−0.34 ± 0.09	554
850 ± 25	849	102 ± 3	−0.24 ± 0.10	522
900 ± 25	898	101 ± 3	−0.22 ± 0.14	254
950 ± 25	950	103 ± 3	−0.05 ± 0.11	477
1000 ± 25	999	100 ± 4	−0.27 ± 0.11	372
400 ± 25	400	133 ± 4	+0.11 ± 0.10	2284
450 ± 25	449	131 ± 6	−0.04 ± 0.07	2430
500 ± 25	497	129 ± 5	−0.16 ± 0.10	697
550 ± 25	550	132 ± 4	−0.37 ± 0.10	675
600 ± 25	599	130 ± 5	−0.61 ± 0.09	550
650 ± 25	654	133 ± 4	−0.88 ± 0.08	558
700 ± 25	700	129 ± 5	−0.77 ± 0.07	1134
750 ± 25	758	132 ± 3	−0.56 ± 0.09	807
800 ± 25	803	130 ± 5	−0.40 ± 0.07	931
850 ± 25	850	131 ± 4	−0.28 ± 0.10	593

TABLE 1b
Results for the hydrogen polarimeter

Energy bin (MeV)	Average photon energy (MeV)	Average c.m. angle (degrees)	Polarization	Number of events
925 ± 50	940	106 ± 2	+0.07 ± 0.28	108
1025 ± 50	1023	103 ± 2	−0.18 ± 0.20	176
1125 ± 50	1106	101 ± 2	−0.09 ± 0.34	59
750 ± 25	751	134 ± 2	−0.30 ± 0.32	92
800 ± 25	800	132 ± 2	−0.26 ± 0.24	138
850 ± 25	849	131 ± 3	−0.09 ± 0.13	419
900 ± 25	900	130 ± 2	−0.15 ± 0.13	338
950 ± 25	950	130 ± 4	−0.09 ± 0.10	578
1000 ± 25	1001	132 ± 3	−0.35 ± 0.10	492
1050 ± 25	1048	131 ± 3	−0.43 ± 0.10	418
1100 ± 25	1099	131 ± 2	−0.44 ± 0.15	185
1150 ± 25	1142	130 ± 2	−0.42 ± 0.19	104

REF. P. Stoler, E.J. Winhold, F. O'Brien, P.F. Yergin, D. Rowley, K. Min, J. LeRose, A.M. Bernstein, K.I. Blomqvist, G. Franklin, N. Paras, M. Pauli
Phys. Rev. C22, 911 (1980)

ELEM. SYM.	A	Z
H	1	1

METHOD

REF. NO. 80 St 3 hg

REACTION	RESULT	EXCITATION ENERGY	SOURCE		DETECTOR		ANGLE
			TYPE	RANGE	TYPE	RANGE	
E,PI+	RLY	175-199	C	230	MAG-D		90
G,PI+	RLY	175-199	C	230	MAG-D		90

TEST VIRTUAL PHOTONS

The virtual photon spectrum shape and intensity within several MeV of the kinematic limit was measured for ^{9}Be$(e,\pi^+)^9$Li.e' and ^{16}O$(e,\pi^+)^{16}$N.e'($T_\pi = 28$ MeV, $\theta_\pi = 90°$). The intensity over this interval is 1.25 ± 0.10 times plane-wave virtual photon theory predictions; the shape agrees with theory within errors. Measurements on the proton 30 to 55 MeV below the end point agree with the intensity predictions of virtual photon theory within the errors ($\pm 8\%$).

[NUCLEAR REACTIONS ^{16}O(e,π^+), $E = 180.4$ MeV; ^{9}Be(e,π^+), $E = 184.8$ MeV; measured $\sigma(E_\pi, 90°_{lab})$ relative to (γ,π^+), near $E_\pi = 28$ MeV. ^{1}H(e,π^+), $E = 230$ MeV; measured $\sigma(E_\pi, 90°_{lab})$ relative to (γ,π^+), near $E_\pi = 18$, 30 MeV. Compared to PWBA virtual photon theory.]

TABLE I. Results for R/V, the real-to-virtual ratio as defined in the text. The quantity E_0 is the incident electron total energy, T_π the pion kinetic energy, k the virtual photon energy, and ΔT_π the averaging interval over pion energy in the experiment (corresponding to the range of k). Note that k is close to the end point for ^{16}O and ^{9}Be but 30 to 55 MeV below for ^{1}H.

	^{16}O(e,π^+)	^{9}Be(e,π^+)	^{1}H(e,π^+)	
E_0(MeV)	180.4	184.8	230	230
T_π(MeV)	28	28	18	30
k(MeV)	176.8–179.9	182.2–184.3	174.7–181.7	188.3–199.4
ΔT_π(MeV)	3.0	2.0	4.9	7.5
$(R/V)_{expt}$	78 ± 9	72 ± 8	71 ± 6	80 ± 6
$(R/V)_{theor}$	91	96	70	77
$(R/V)_{theor}/(R/V)_{expt}$	1.17 ± 0.14	1.33 ± 0.15	0.99 ± 0.08	0.96 ± 0.08

REF. M. Yoshioka, A. Noda, M. Daigo, Y. Hemmi, R. Kikuchi, M. Minowa, K. Miyake, T. Nakamura, M. Ono, Y. Suzuki, S. Kato, K. Ukai, K. Toshioka, K. Sugano, T. Shimomura, T. Shinohara, M. Chiba, Y. Hoshi
Nucl. Phys. B168, 222 (1980)

ELEM. SYM.	A	Z
H	1	1

METHOD

REF. NO.	
80 Yo 3	egf

REACTION	RESULT	EXCITATION ENERGY	SOURCE		DETECTOR		ANGLE
			TYPE	RANGE	TYPE	RANGE	
G,PIØ	ABX	390-975	C	550-999	TEL-D		DST

The differential cross sections of the reaction $\gamma p \rightarrow \pi^0 p$ have been measured at photon energies between 390 MeV and 975 MeV with an energy step of 20 or 25 MeV. The angular region covers 11 angles between 15° and 130° in the c.m.s. A combination of a magnetic spectrometer and photon detector was used for the measurement in the angular region from 50° to 130°. At forward angles of 15°, 35° and 50°, π^0 mesons were detected using a π^0 detector consisting of a pair of photon detectors. The data obtained with two different detection systems overlap at the angle of 50° and coincide with each other within the experimental error. The results are compared with those of phenomenological partial-wave analyses.

999=1.GEV

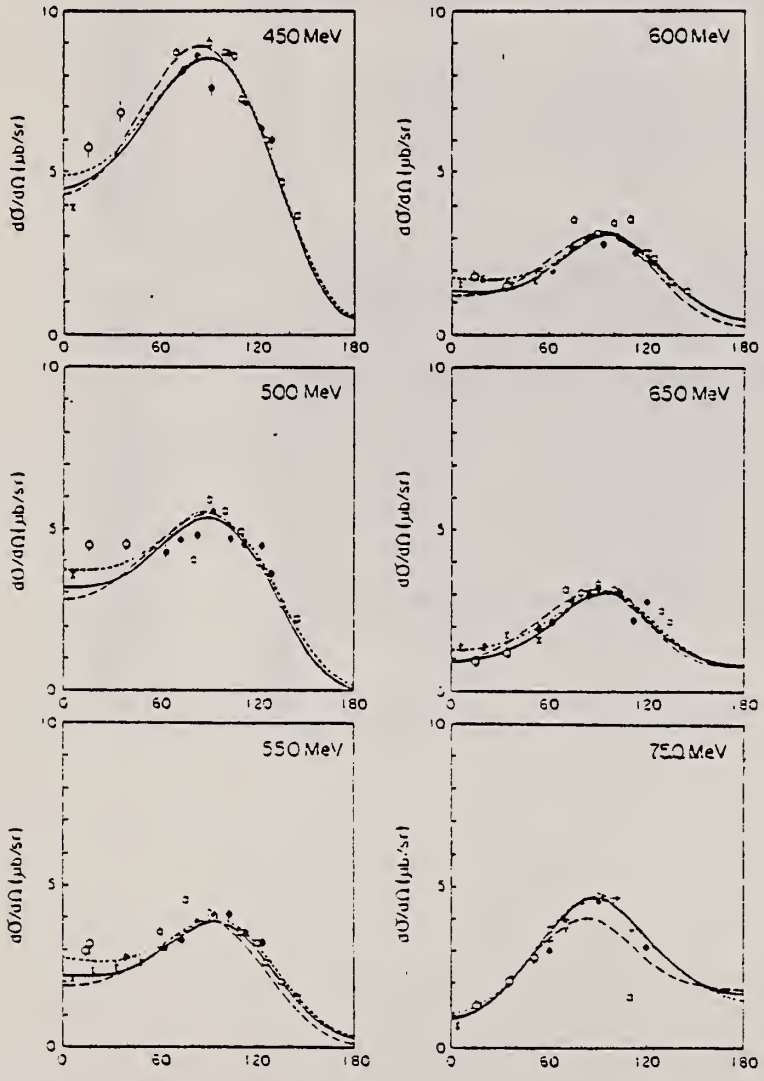

Fig. 6. The angular distribution of the differential cross section at the photon energies of 450, 500, 550, 600, 650 and 750 MeV. Reference sources are the same as in fig. 5.

(continued)

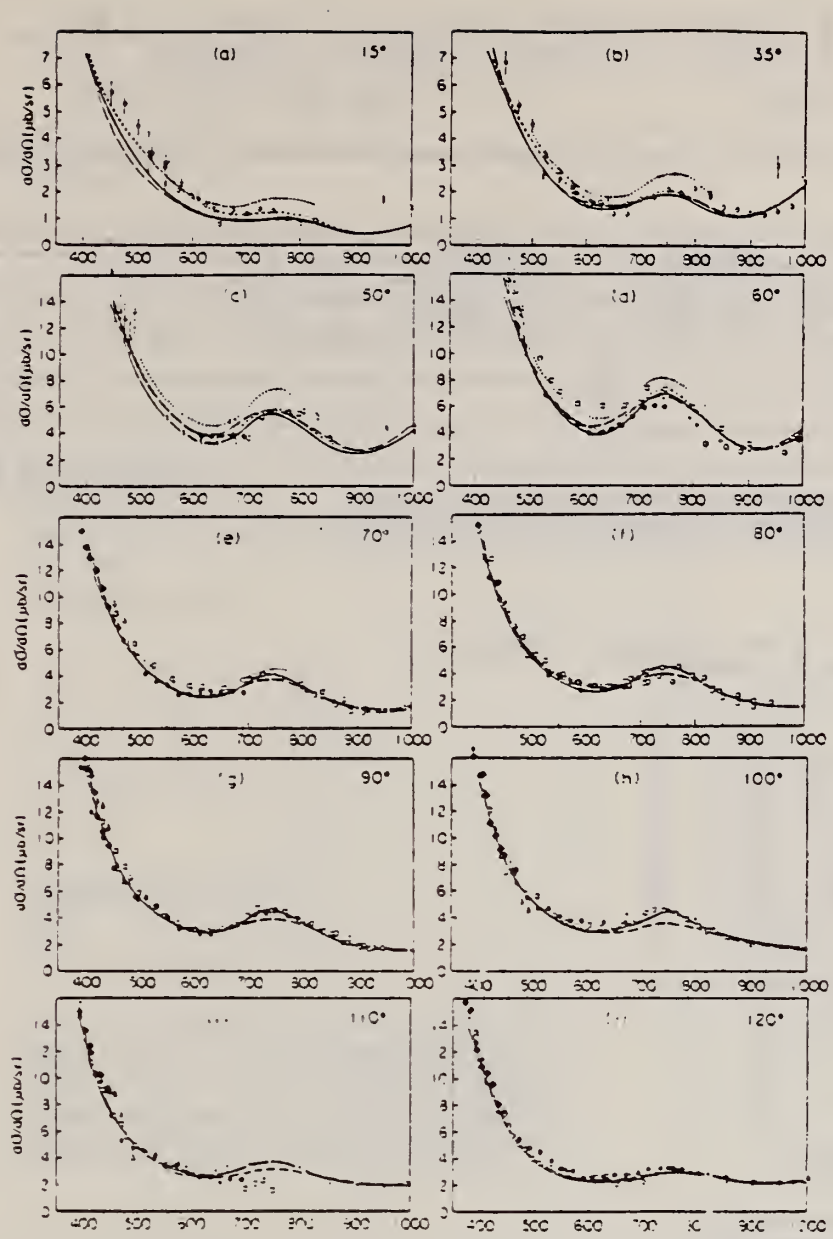

Fig. 5. The energy dependences of the differential cross sections at eleven angles between 15° and 130° in the c.m.s. Reference sources for curves are: full curve, Metcalf-Walker [2]; long dashed curve, Moorhouse et al. [5]; dotted curve, Noelle [9]; short dashed curve, present analysis. Reference sources for the cross sections are: ×, ref. [23]; △, ref. [19]; □, ref. [11]; ⇔, ref. [20]; −, ref. [22]; ○, ref. [21]; ◇, ref. [10]; ⇒, ref. [17]; ◆, ref. [18]; ■, present results obtained by the π^+ detection method; ●, present results obtained by the p–γ coincidence method.

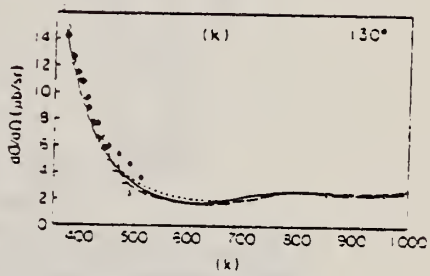

Fig. 5 (continued).

REF. P. Argan, G. Audit, A. Bloch, N. de Botton, J.L. Faure, C. Schuhl, G. Tamas, C. Tzara, E. Vincent, J. Deutsch, D. Favart, R. Prieels, B. Van Oystaeyen
Phys. Rev. C24, 300 (1981)

ELEM. SYM.	A	Z
H	1	1

METHOD

REF. NO. 81 Ar 2 egf

REACTION	RESULT	EXCITATION ENERGY	SOURCE		DETECTOR		ANGLE
			TYPE	RANGE	TYPE	RANGE	
G,PIØ	ABY	146-153	C	146-153	CKV-D		Ø

REANALYSIS OF 80AR2

Our recently published π^0 photoproduction data at threshold have been reanalyzed with the use of a more refined detection efficiency calculation. The high energy points appear to be consistent with the threshold measurements; the effective threshold amplitudes remain unchanged, and are now supported by the complete set of experimental data.

[NUCLEAR REACTIONS (γ,π^0), ^{1}H, ^{2}H, ^{3}He, and ^{4}He targets; measured reaction yields, E_{π^0}=1–10 MeV.]

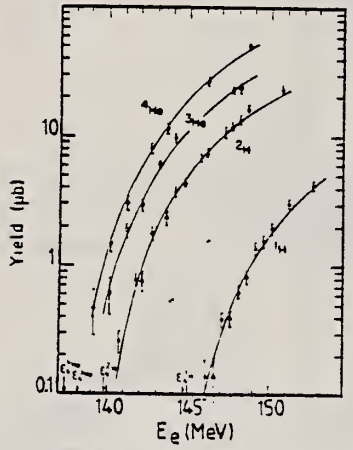

FIG. 2. The measured π^0 photoproduction yields in microbarns, normalized to one target nucleus and one equivalent quantum, as functions of the Bremsstrahlung end-point energy E_e. The curves are the theoretical yields computed with DWIA cross sections, and adjusted to the complete set of data as explained in the text.

REF. A.S. Bratashevskiĭ, A.A. Zybalov, A.I. Derebchinskiĭ, O.G. Konovalov, P.V. Sorokin, A.E. Tenishev
Sov. J. Nucl. Phys. 33, 538 (1981)
Yad. Fiz. 33, 1020 (1981)

EL EM. SYM.	A	Z
H	1	1

METHOD

REF. NO.	
81 Br 3	egf

REACTION	RESULT	EXCITATION ENERGY	SOURCE		DETECTOR		ANGLE
			TYPE	RANGE	TYPE	RANGE	
$ G,PIØ	NOX	800-999	C	2*	SPK-D		60

999,2*=1.3,2 GEV $RCL

The proton polarization has been measured in the reaction $\gamma + p \rightarrow p + \pi^0$ for the angle $\theta_\pi^* = 60°$ over the photon energy range 800–1300 MeV. The experimental results are compared with theoretical analyses for this energy range.

PACS numbers: 13.60.Kd

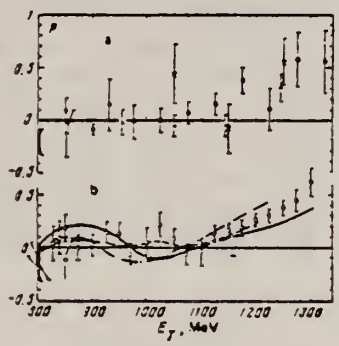

FIG. 1. Energy dependence of the proton polarization in the reaction $\gamma + p \rightarrow p + \pi^0$ for the pion-emission angle $\theta_\pi^* = 60°$. a—Results of earlier work. ●) Data from Ref. 1; +) Ref. 3; ⊖) Ref. 4; ⊖) Ref. 5; ×) Ref. 6. b—Results of the present experiments (open circles) and some results of some analyses. Solid curve) Results of the analysis of Ref. 8; dashed curve) results of Ref. 9; dot-dashed curve) results of Ref. 10.

TABLE I.

$E_{\gamma eff}$, MeV	θ_π^*, deg	P	$\pm\Delta P$	$E_{\gamma eff}$, MeV	θ_π^*, deg	P	$\pm\Delta P$
800	58.3	−0.119	0.152	1125	60.3	−0.066	0.098
825	58.5	0.039	0.156		61.8	0.131	0.071
850	58.6	0.183	0.125	1150	60.5	0.086	0.114
875	58.8	−0.007	0.125		61.4	0.157	0.004
900	58.9	0.025	0.118				
925	59.0	0.143	0.1	1175	60.6	0.14	0.1
950	59.2	0.137	0.106		61.2	0.175	0.073
975	59.3	−0.061	0.1	1200	60.8	0.317	0.125
1000	59.5	0.043	0.097		61.0	0.264	0.039
1025	59.7	0.233	0.097				
1050	59.8	0.078	0.106	1225	60.9	0.305	0.063
1075	60.0	−0.060	0.099	1250	60.7	0.374	0.071
1100	60.1	−0.192	0.098	1275	60.5	0.441	0.068
	61.8	−0.04	0.129	1300	60.3	0.612	0.125

Note: $\Delta E = \pm 12.5$ MeV.

REF.

A.S. Bratashevskiĭ, A.A. Zybalov, A.I. Derebchinskiĭ, O.G. Konovalov, P.V. Sorokin, A.E. Tenishev
Sov. J. Nucl. Phys. 33, 538 (1981)
Yad. Fiz. 33, 1020 (1981)

ELEM. SYM.	A	Z
H	1	1

METHOD

REF. NO.: 81 Br 8 hg

REACTION	RESULT	EXCITATION ENERGY	SOURCE		DETECTOR		ANGLE
			TYPE	RANGE	TYPE	RANGE	
$ G,PIØ	NOX	150-999	C	800-999	MAG-D		60

999=1.3 GEV POL P OUT

The proton polarization has been measured in the reaction $\gamma + p \rightarrow p + \pi^0$ for the angle $\theta^*_\pi = 60°$ over the photon energy range 800–1300 MeV. The experimental results are compared with theoretical analyses for this energy range.

PACS numbers: 13.60.Kd

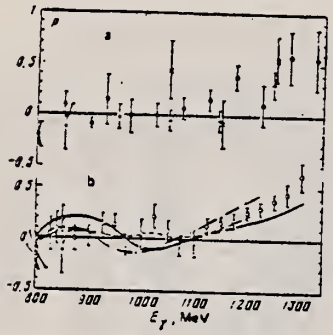

FIG. 1. Energy dependence of the proton polarization in the reaction $\gamma + p \rightarrow p + \pi^0$ for the pion-emission angle $\theta^*_\pi = 60°$. a—Results of earlier work. ●) Data from Ref. 1; +) Ref. 3; ⊖) Ref. 4; ⊖) Ref. 5; ×) Ref. 6. b—Results of the present experiments (open circles) and some results of some analyses. Solid curve) Results of the analysis of Ref. 8; dashed curve) results of Ref. 9; dot-dashed curve) results of Ref. 10.

TABLE I.

E_{γ}, MeV	θ^*_π, deg	P	±ΔP	E_{γ}, MeV	θ^*_π, deg	P	±ΔP
800	58.3	−0.119	0.182	1125	60.3	−0.068	0.076
825	58.5	0.039	0.156		61.8	0.131	0.071
850	58.8	0.183	0.120	1150	60.5	0.086	0.114
875	58.8	−0.007	0.125		61.4	0.157	0.064
900	58.9	0.025	0.118				
925	59.0	0.143	0.1	1175	60.6	0.14	0.1
950	59.2	0.137	0.106		61.2	0.173	0.075
975	59.3	−0.061	0.1	1200	60.8	0.317	0.125
1000	59.5	0.045	0.097		61.0	0.264	0.059
1025	59.7	0.225	0.097				
1050	59.8	0.078	0.106	1225	60.9	0.305	0.053
1075	60.0	−0.060	0.099	1250	60.7	0.374	0.071
1100	60.1	−0.192	0.098	1275	60.5	0.441	0.084
	61.8	−0.04	0.129	1300	60.3	0.612	0.125

Note: $\Delta E = \pm 12.5$ MeV.

REF. Y. Wada, S. Kato, T. Miyachi, K. Sugano, K. Toshioka, K. Ukai, T. Ishii, K. Egawa, M. Chiba, K. Joh, T. Shinohara, Y. Yoribayashi
Il Nuovo Cimento 63A, 57 (1981)

ELEM. SYM.	A	Z
H	1	1

METHOD

REF. NO. 81 Wa 4 hg

REACTION	RESULT	EXCITATION ENERGY	SOURCE		DETECTOR		ANGLE
			TYPE	RANGE	TYPE	RANGE	
$ G,G	NOX	400-999	C	400-999	MAG-D		DST

$H $P, P-G COIN

Summary. — The recoil proton polarization of proton Compton scattering ($\gamma p \to \gamma p$) was measured in the photon energy range from 500 MeV to 1000 MeV at $\theta^* = 100°$ and from 400 MeV to 800 MeV at $\theta^* = 130°$. A recoil proton and a scattered photon were detected in coincidence with a magnetic spectrometer and a photon detector. The recoil proton polarization was measured with a carbon polarimeter. The results are compared with a phenomenological analysis based on an isobar model and a dynamical analysis based on the dispersion relation.

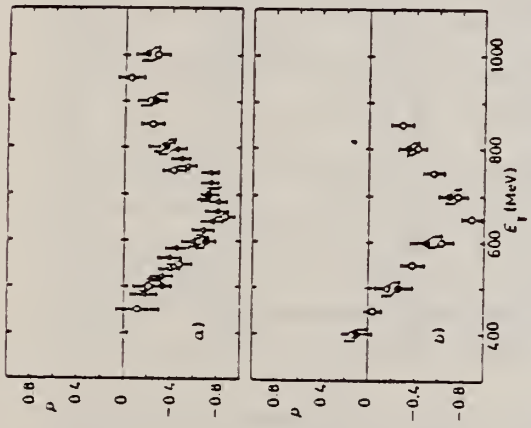

Fig. 4. – Results of the recoil proton polarization of the $\gamma + p \to \pi^0 + p$ reactions. Present data agree well with other recent experiment (12,13). *a)* $P(\gamma p \to \gamma p)$, $\theta^* = 100°$; *b)* $P(\gamma p \to \gamma p)$, $\theta^* = 130°$; • present results, ○ KATO *et al.* (12), ▲ DERBENEVSKIJ *et al.* (13).

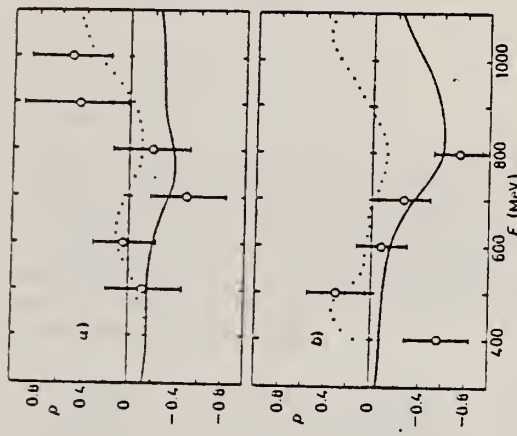

Fig. 5. – Results of the recoil proton polarization of proton Compton scattering. The solid line and the dotted line are the phenomenological analysis (14) and the dynamical analysis (11), respectively. *a)* $P(\gamma p \to \gamma p)$, $\theta^* = 100°$; *b)* $P(\gamma p \to \gamma p)$, $\theta = 130°$.

(12) S. KATO, T. MIYACHI, K. SUGANO, K. TOSHIOKA, K. UKAI, M. CHIBA, K. EGAWA, T. ISHII, T. YORIBAYASHI, K. JOH, T. SHINOHARA and Y. WADA: *Nucl. Phys. B*, 168, 1 (1980). 80 Ka 4

(13) A. S. BRATASHEVSKIJ, A. I. DERBENEVSKIJ, A. A. ZYBALOV, O. B. KONOVALOV, A. S. OMELAENKO, A. E. TENISHEV and S. G. TOSAFETYAN: contributed paper to *Lepton Photon Symposium at Fermilab* (1979).

(continued)

TABLE II. – *Polarization of proton Compton scattering a) at* $\theta^* = 100°$ *and b)* $\theta^* = 130°$.

E_γ (MeV)	Average of E_γ (MeV)	Average of θ^* (degrees)	p_c
a) $\theta^* = 100°$			
500 ± 50	501.9	104 ± 3	-0.108 ± 0.335
600	596.4	103 ± 3	$+0.042 \pm 0.270$
700	702.5	102 ± 3	-0.495 ± 0.327
800	796.6	102 ± 4	-0.185 ± 0.331
900	876.3	100 ± 3	$+0.425 \pm 0.324$
1000	977.2	100 ± 3	$+0.514 \pm 0.344$
b) $\theta^* = 130°$			
400	406.0	134 ± 3	-0.548 ± 0.286
500	504.4	132 ± 4	$+0.295 \pm 0.245$
600	593.3	131 ± 4	-0.074 ± 0.218
700	693.6	131 ± 4	-0.287 ± 0.227
800	788.8	131 ± 3	-0.727 ± 0.219

REF. A.A. Belyaev, V.A. Get'man, V.G. Gorbenko, V.A. Gushchin, A.Ya. Derkach, Yu.V. Zhebrovskii, I.M. Karnaukhov, L.Ya. Kolesnikov, A.A. Lukhanin, A.L. Rubashkin, P.V. Sorokin, E.A. Sporov, Yu.N. Telegin
Yad. Fiz. 35, 693 (1982)
Sov. J. Nucl. Phys. 35, 401 (1982)

ELEM. SYM.	A	Z
H	1	1

METHOD

REF. NO. 82 Be 4 egf

REACTION	RESULT	EXCITATION ENERGY	SOURCE TYPE	SOURCE RANGE	DETECTOR TYPE	DETECTOR RANGE	ANGLE
$ G,PIØ	NOX	300-420	D	300-420			DST

tabular Data given

$ G+TARGET, COH BREMS

We report an experimental study of the Σ, T, and P parameters of the cross section for the reaction $\gamma p \to p\pi^0$ for photon energies 300, 320, 350, 380, 400, 420 MeV in the range of pion emission angles 60–135° c.m.s. The technique of a double polarization experiment with use of linearly polarized photons and a polarized proton target is described. The experimental results are compared with the predictions of theoretical analyses.

PACS numbers: 13.60.Le

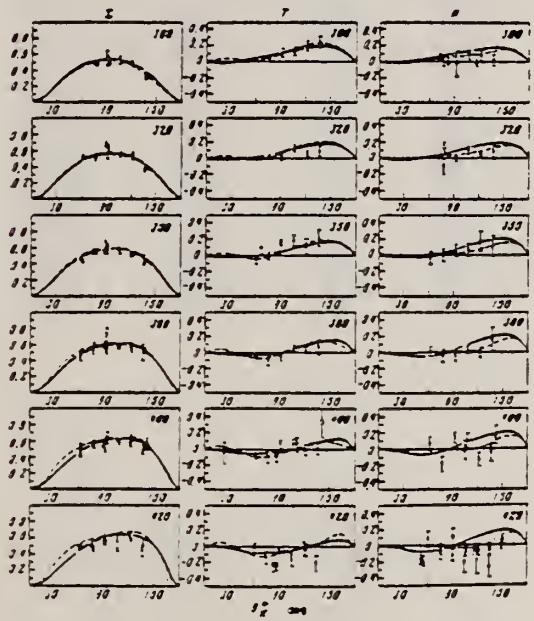

FIG. 1. Angular distributions of the Σ, T, and P parameters for the reaction $\gamma p \to p\pi^0$. Experimental results: •— present work, ○— Ref. 1, ■— Ref. 15, □— Ref. 16, ▽— Ref. 17, ▼— Ref. 2, △— Ref. 18, ▲— Ref. 3, ◇— Ref. 23; the remaining data were taken from the compilations of Refs. 19 and 20, where they are designated as follows: ♦— MI 73 BONN, ▽— TR 72 BONN, ◇— B2 69 BONN, ●— AN 71 KHAR. The theoretical curves are as follows: solid curves from Ref. 21, dashed curves from Ref. 22.

In this case measurements of the total yields of protons from the polarized proton target for the different combinations of directions of the polarization vectors of the target (↑—up and ↓—down with respect to the normal to the reaction plane) and the photons (⊥—perpendicular and ∥—parallel to the reaction plane: $\phi = 90°$ and 0°, respectively) give four quantities:

$$\begin{aligned} C_{\perp}^{\uparrow} &= C_0^{\perp}(1+\Sigma_{\perp}\bar{\rho}_{\perp}) + C_0^{\parallel}(1+\Sigma\rho_{\perp}+T\rho_y+P\rho_{\perp}\rho_y), \\ C_{\perp}^{\downarrow} &= C_0^{\perp}(1-\Sigma_{\perp}\bar{\rho}_{\perp}) + C_0^{\parallel}(1-\Sigma\rho_{\perp}-T\rho_y-P\rho_{\perp}\rho_y), \\ C_{\parallel}^{\uparrow} &= C_0^{\perp}(1-\Sigma_{\perp}\bar{\rho}_{\perp}) + C_0^{\parallel}(1-\Sigma\rho_{\perp}+T\rho_y-P\rho_{\perp}\rho_y), \\ C_{\parallel}^{\downarrow} &= C_0^{\perp}(1-\Sigma_{\perp}\bar{\rho}_{\perp}) - C_0^{\parallel}(1-\Sigma\rho_{\perp}-T\rho_y+P\rho_{\perp}\rho_y), \end{aligned} \tag{2}$$

where $C_0^{\perp}$ and $C_0^{\parallel}$ are respectively the yield from the target nuclei and from polarized free protons, averaged over the photon and proton spin directions, $\Sigma_{\perp}$ is the asymmetry of the cross sections for photoproduction of pions in the target nuclei for polarized photons, and $\bar{\rho}_{\perp}$ is the value of photon polarization averaged over the photon spectrum with inclusion of the Fermi motion of the nucleons.

As is easy to show from Eqs. (2)–(5), the Σ, T, and P parameters are obtained from the experimental yield values by means of the following expressions:

$$\begin{aligned} \Sigma &= \frac{1}{k_{\perp}\bar{\rho}_{\perp}} \frac{C_{\perp}^{\parallel} - C_{\parallel}^{\parallel}}{C_{\perp}^{\parallel} - C_{\parallel}^{\parallel} - 2C^{\parallel}}, \\ T &= \frac{1}{p_y} \frac{C_{\perp}^{\uparrow} + C_{\parallel}^{\uparrow} - C_{\perp}^{\downarrow} - C_{\parallel}^{\downarrow}}{2\eta(C_{\perp}^{\parallel} + C_{\parallel}^{\parallel})}, \\ P &= \frac{1}{p_{\perp}k_{\perp}\bar{\rho}_{\perp}} \frac{C_{\perp}^{\uparrow} - C_{\parallel}^{\uparrow} - C_{\perp}^{\downarrow} + C_{\parallel}^{\downarrow}}{2\eta(C_{\perp}^{\parallel} + C_{\parallel}^{\parallel} - 2C^{\parallel})}. \end{aligned} \tag{6}$$

REF. A.A. Belyaev, V.A. Get'man, V.G. Gorbenko, V.A. Gushchin, A.Ya. Derkach, Yu.V. Zhebrovskii, A.A. Zayats, I.M. Karnaukhov, L.Ya. Kolesnikov, A.A. Lukhanin, A.L. Rubashkin, M.V. Sobol', P.V. Sorokin, E.A. Sporov, Yu.N. Telegin
Yad. Fiz. 35, 373 (1982)
Sov. J. Nucl. Phys. 35, 213 (1982)

ELEM. SYM.	A	Z
H	1	1

METHOD

REF. NO. 82 Be 6 egf

REACTION	RESULT	EXCITATION ENERGY	SOURCE		DETECTOR		ANGLE
			TYPE	RANGE	TYPE	RANGE	
$ G,PI-	NOX	660	C	750	TEL-D		DST

We have measured for the first time the asymmetry of the cross section for the reaction $\gamma p \to \Delta^{++}\pi^-$ on polarized protons. The measurements were made at $E_\gamma = 660$ MeV in the range of pion emission angles 45–120° c.m.s. The experimental data obtained are compared with the theoretical predictions.

$ PROTON, POL ASYM

PACS numbers: 13.60.Le, 13.60.Rj

The following quantities were directly measured in the experiment: C' and C'—the yields of pions from the polarized target with the direction of proton polarization along (↑) and opposite to (↓) the normal to the reaction plane ($n = [k \times q]$, where k and q are the momenta of the photon and π^- meson, respectively), C_2—the yield of pions from a liquid-hydrogen target, and C_1—the background yield for the empty appendix.

The desired T-asymmetry was determined as follows:

$$T = \frac{1}{P_t} \frac{C' - C'}{2\eta(C_2 - C_1)},$$

TABLE I.

θ_{π^-}, deg	T	ΔT	θ_{π^-}, deg	T	ΔT
45	0.23	0.20	90	0.28	0.55
60	−0.25	0.25	120	−0.06	0.13

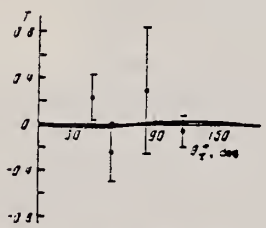

FIG. 1. Angular distribution of the T-asymmetry at photon energy 660 MeV. The points are the experimental data of the present work, and the curve is a calculation according to the model of Ref. 4.

REF. A.S. Bratashevskii, A.I. Derebchinskii, A.A. Zybalov, S.P. Karasev, O.G. Konovalov, P.V. Sorokin, A.E. Tenishev
Yad. Fiz. 35, 56 (1982)
Sov. J. Nucl. Phys. 35, 33 (1982)

EL EM. SYM.	A	Z
H	1	1

METHOD

REF. NO. 82 Br 8 egf

REACTION	RESULT	EXCITATION ENERGY	SOURCE TYPE	SOURCE RANGE	DETECTOR TYPE	DETECTOR RANGE	ANGLE
$ G,PIØ	NOX	650-999	700-999	C	MAG-D		70

– Measurements of the proton polarization in the reaction $\gamma + p \rightarrow p + \pi^0$ are reported for an angle $\theta_\pi^{c.m.} = 70°$ in the photon energy range 0.65–1.4 GeV. The results of the measurements are compared with the
– phenomenological analysis of Metcalf and Walker.

– PACS numbers: 13.60.Le

999=1.4 GEV, $ PROTON

TABLE I.

E_γ, GeV	$\theta_\pi^{c.m.}$, deg	P	±ΔP
0.650±0.0125	74.5±0.56	−0.278	±0.158
0.675±0.0125	74.3±0.56	−0.341	±0.12
0.700±0.0125	74.2±0.56	−0.446	±0.1
0.725±0.0125	74.1±0.56	−0.3	±0.1
0.750±0.0125	73.9±0.56	−0.254	±0.12
0.775±0.0125	73.8±0.56	−0.17	±0.13
0.800±0.0125	73.7±0.56	+0.103	±0.114
0.825±0.0125	73.6±0.56	+0.157	±0.121
0.850±0.0125	73.45±0.56	+0.216	±0.054
0.875±0.0125	73.15±0.56	−0.061	±0.098
0.900±0.0125	72.9±0.56	−0.17	±0.104
0.925±0.0125	72.7±0.56	−0.087	±0.085
0.950±0.0125	72.55±0.56	−0.1	±0.094
0.975±0.0125	72.4±0.56	−0.22	±0.091
1.000±0.0125	72.2±0.56	−0.232	±0.09
1.025±0.0125	72.0±0.56	−0.277	±0.09
1.050±0.0125	71.8±0.56	+0.172	±0.081
1.075±0.0125	71.6±0.56	−0.27	±0.072
1.100±0.0125	71.4±0.56	−0.3	±0.067
1.125±0.0125	71.2±0.56	−0.244	±0.065
1.150±0.0125	71.0±0.56	−0.5	±0.062
1.175±0.0125	70.9±0.56	−0.42	±0.108
1.200±0.0125	70.8±0.56	−0.14	±0.09
1.240±0.0155	70.5±0.56	−0.04	±0.08
1.275±0.02	70.0±0.56	+0.001	±0.13
1.315±0.02	69.9±0.56	−0.03	±0.1
1.355±0.02	69.6±0.56	−0.14	±0.13

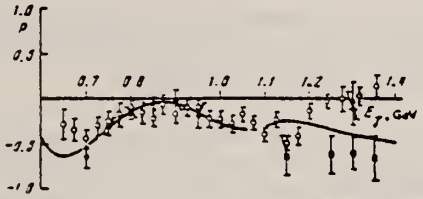

FIG. 1. Proton polarization in the reaction $\gamma + p \rightarrow p + \pi^0$ as a function of the γ-ray energy for an angle $\theta_\pi^{c.m.} = 70°$. The points are as follows: •—our data,[4] ▪—Ref. 5, +—Ref. 6, ▲—Ref. 7, ○—data of the present work. The curve is the result of the Metcalf-Walker analysis.[8]

[5]P. Blum, R. Brokmann, and W. Mohr, Preprint Bonn-He-76-2, 1976.
[6]P. J. Bussey, C. Raine, J. G. Rutherglen, *et al.*, Nucl. Phys. B154, 492 (1979).
[7]N. Tanaka, M. M. Castro, *et al.*, Phys. Rev. D8, 1 (1973).

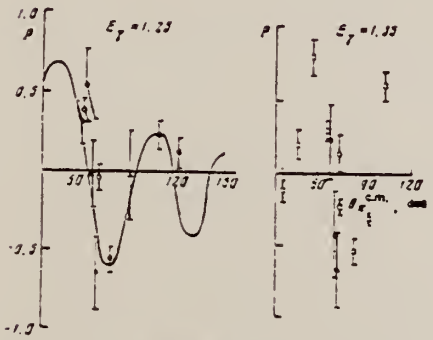

FIG. 2. Angular dependence of proton polarization in the reaction $\gamma + p \rightarrow p + \pi^0$ for photon energies 1.25 and 1.35 GeV. The points are as follows: •—data of Ref. 9, ▪—Ref. 10, ▲—Ref. 5, ○—Ref. 11, ◐—data of the present work. The curve is the result of the Metcalf-Walker analysis.[12]

[9]E. D. Bloom, C. A. Heusch, *et al.*, Thesis, Caltech, 1967.
[10]M. N. Prentice, R. Raitoo, *et al.*, Nucl. Phys. B41, 353 (1972).
[11]P. J. Bussey, J. G. Rutherglen, *et al.*, Contribution to Stanford Conf., 1975.

REF. R.M. Sealock, H.S. Caplan, B.W. Zulkoskey, A. Szyjewicz, E.L. Tomusiak
Can. J. Phys. 60, 1257 (1982)

ELEM. SYM.	A	Z
H	1	1

METHOD

REF. NO. 82 Se 1 egf

REACTION	RESULT	EXCITATION ENERGY	SOURCE		DETECTOR		ANGLE
			TYPE	RANGE	TYPE	RANGE	
E,PI+	ABX	7*12	D	200	TEL-D		DST

*PION ENERGY

Differential cross sections were measured for the electro-pion production from H and ^{3}He at an incident energy of 200 MeV and pion energies from 7.3 to 12.1 MeV. Pion-angular distributions are presented and compared with theory. For hydrogen there is good agreement. A simple three-channel calculation performed for the pion production from ^{3}He was found to overestimate the cross section at forward pion angles.

On a mesuré les sections efficaces différentielles d'électroproduction de pions à partir de H et ^{3}He, pour une énergie incidente de 200 MeV et des énergies des pions allant de 7.3 à 12.1 MeV. Les distributions angulaires des pions sont présentées et comparées avec la théorie. Dans le cas de l'hydrogène, l'accord est bon. Un calcul simple, à trois voies, a été effectué pour la production de pions à partir de ^{3}He, et l'on a trouvé qu'il surestime la section efficace pour la production de pions dirigés vers l'avant.

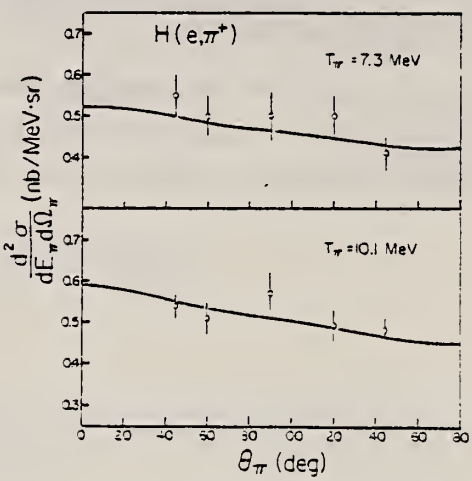

FIG. 1. Pion-angular distributions (in the lab frame) for the reaction H(e,π⁺)e' at 200 MeV incident energy: our measurements and predictions (solid line).

TABLE 1. ^{1}H(e,π⁺) $d^2\sigma/dE_\pi d\Omega_\pi$ nb/(MeV sr) for T_e = 200 MeV

E_π/θ_π	45°	60°	90°	120°	145°
7.3	0.55±0.05	0.50±0.05	0.50±0.06	0.50±0.05	0.41±0.04
10.1	0.54±0.03	0.51±0.04	0.57±0.05	0.48±0.04	0.48±0.03
12.1	—	—	—	—	0.41±0.03

H
A=2

H
A=2

H
A=2

Ref. Lew Allen, Jr.
Phys. Rev. 98, 705 (1955)

Elem. Sym.	A	Z
H	2	1

Method Plates; Betatron

Ref. No. 55 Al 1 F/H

Reaction	E or ΔE	E_o	Γ	$\int \sigma dE$	Jπ	Notes
$H^2(\gamma,p)$	20-65	95				$f(\theta) = (\alpha + \sin^2\theta)(1 + 2\beta \cos\theta)$

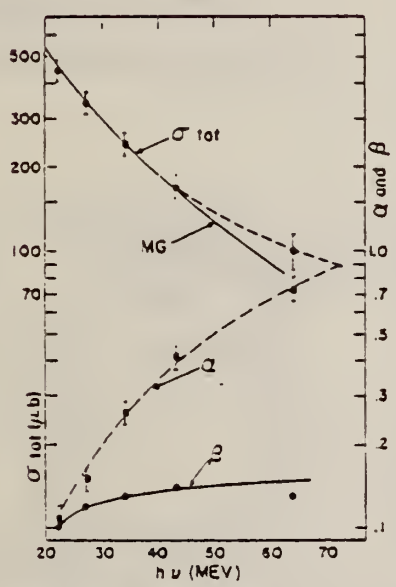

FIG. 4. Total cross section (c.m.) *versus* photon energy (c.m.). Each point represents about 1000 proton tracks. Errors are statistical plus the probable error arising from the integration of the observed angular distribution. The solid curve is that calculated by Marshall and Guth for central forces. The experimentally determined values of the angular distribution parameters are also plotted *versus* photon energy. No error in β is shown since it is not determined independently of α; however, for the plotted value of α and σ_{tot}, β is determined to within about 10 percent.

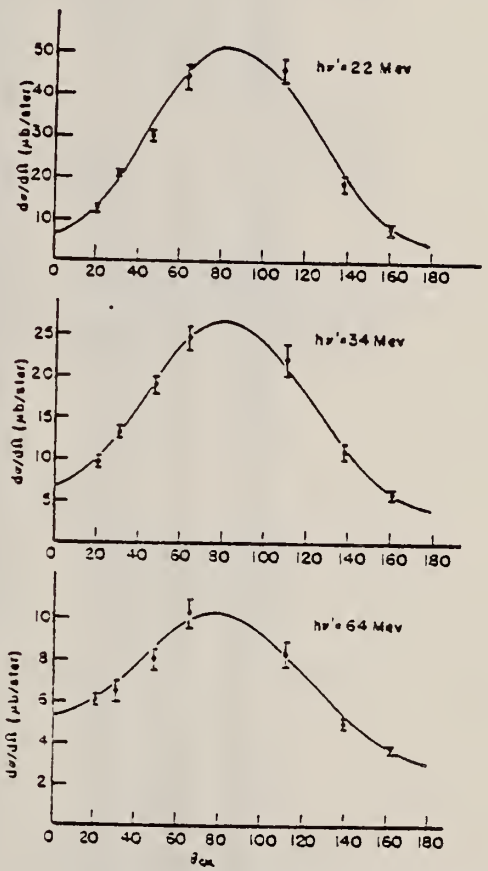

FIG. 3. Sample plots of differential cross sections (c.m.) *versus* ϑ (c.m.) for a constant mean photon energy. The points are the experimental points as shown in Fig. 2, except that when interpolation was necessary the dotted curve of Fig. 2 was used as a guide. Errors displayed are statistical only. The solid curve is of the form of $f(\vartheta) = (\alpha + \sin^2\vartheta)(1 + 2\beta \cos\vartheta)$ and has been fitted to the observed points.

REF.

D. R. Dixon, K. C. Bandtel
Phys. Rev. 104, 1730 (1956)

ELEM. SYM.	A	Z
H	2	1

METHOD

Synchrotron; ion chamber monitor

REF. NO. 56 Di 1 NVB

REACTION	RESULT	EXCITATION ENERGY	SOURCE		DETECTOR		ANGLE
			TYPE	RANGE	TYPE	RANGE	
G,P	ABX	136-293	C	342	TEL-D	40-230	DST

TABLE I. Differential cross sections for photodisintegration of deuterons at various energies and angles (θ=lab angle; θ'=c.m. angle).

θ (deg)	(E_γ) (Mev)	θ' (deg)	Photons in ΔE_γ per unit beam	$d\sigma/d\Omega$ (μb)	$d\sigma/d\Omega'$ (μb)
36	150	42.8	0.503×10⁸	12.7±0.9	9.6±0.7
	165	43.2	0.490	8.8±0.9	6.6±0.7
	182	43.5	0.482	8.5±1.1	6.3±0.8
	200	43.9	0.471	6.9±1.0	5.1±0.8
	220	44.4	0.462	9.9±1.0	7.1±0.7
	242	44.8	0.454	8.6±0.9	6.1±0.6
	266	45.3	0.443	10.6±1.0	7.4±0.7
	293	45.7	0.417	8.5±0.9	5.9±0.6
49 (Run II)	136	57.3	0.518×10⁸	9.7±1.2	7.8±0.9
	150	57.7	0.503	10.1±1.4	8.1±1.1
	165	58.2	0.490	8.4±1.1	6.7±0.9
	182	58.6	0.482	7.9±1.2	6.2±0.9
	200	59.1	0.471	6.6±1.2	5.2±0.9
	220	59.7	0.462	8.3±1.0	6.4±0.8
	242	60.2	0.454	8.7±1.0	6.7±0.8
	266	60.8	0.443	8.0±1.2	6.1±0.9
	293	61.4	0.417	7.5±1.2	5.8±0.9
49 (Run I)	136	57.3	2.41×10⁸	10.0±1.0	8.1±0.8
	150	57.7	2.34	7.3±1.0	5.8±0.8
	165	58.2	2.28	8.0±0.9	6.4±0.7
	182	58.6	2.24	8.9±0.9	7.0±0.7
	200	59.1	2.19	6.5±0.8	5.1±0.6
	220	59.7	2.15	7.8±0.9	6.1±0.7
	242	60.2	2.11	8.1±0.8	6.3±0.6
	266	60.8	2.06	8.9±0.9	6.8±0.7
	293	61.4	1.94	9.2±0.9	7.0±0.7
75	136	85.7	2.41×10⁸	6.7±0.7	6.4±0.7
	150	86.2	2.34	8.0±0.7	7.7±0.6
	165	86.8	2.28	7.2±0.7	6.9±0.7
	182	87.3	2.24	6.2±0.7	6.0±0.7
	200	87.9	2.19	6.8±0.7	6.5±0.6
	220	88.6	2.15	6.2±0.7	6.1±0.7
	242	89.2	2.11	6.9±0.7	6.7±0.7
	266	89.9	2.06	7.5±0.7	7.3±0.7
	293	90.6	1.94	6.2±0.7	6.0±0.6
106	136	116.5	2.41×10⁸	4.2±0.6	4.9±0.7
	150	117.0	2.34	3.7±0.5	4.4±0.6
	165	117.5	2.28	3.7±0.5	4.4±0.6
	182	118.1	2.24	3.3±0.5	4.0±0.6
	200	118.7	2.19	4.5±0.5	5.5±0.6
	220	119.3	2.15	4.7±0.5	5.9±0.6
	242	120.0	2.11	3.5±0.6	4.5±0.7
	266	120.7	2.06	4.8±0.5	6.1±0.6
	293	121.3	1.94	4.8±0.5	6.2±0.7
141	165	148.5	2.28×10⁸	1.7±0.4	2.3±0.6
	182	148.8	2.24	1.8±0.5	2.5±0.7
	200	149.2	2.19	1.8±0.4	2.5±0.6
	220	149.6	2.15	2.6±0.5	3.8±0.7
	242	150.0	2.11	2.1±0.5	3.2±0.7
	266	150.4	2.06	3.1±0.5	4.8±0.7
	293	150.8	1.94	1.8±0.5	2.8±0.8

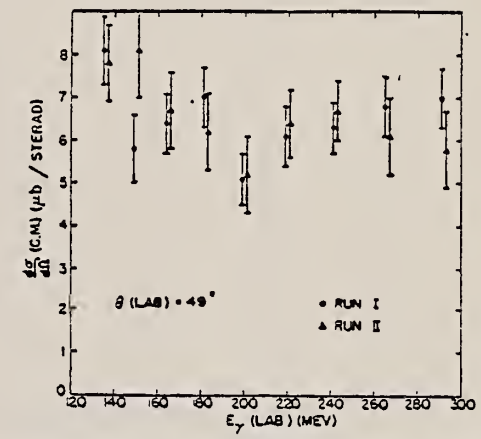

FIG. 6. Differential cross sections *versus* photon energy for θ=49°.

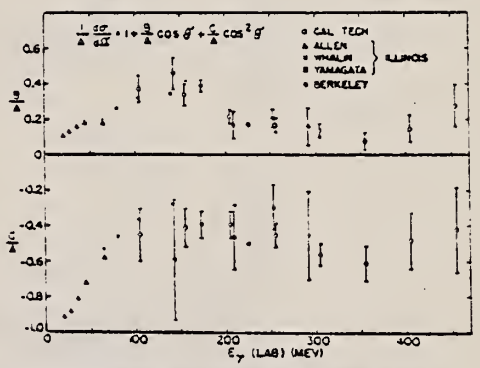

FIG. 7. Angular distributions as functions of energy.

(continued)

REACTION	RESULT	EXCITATION ENERGY	SOURCE TYPE	SOURCE RANGE	DETECTOR TYPE	DETECTOR RANGE	ANGLE

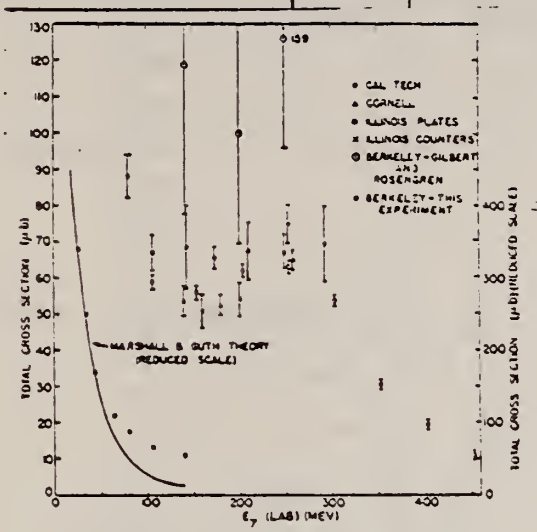

FIG. 8. Total cross sections as functions of energy.

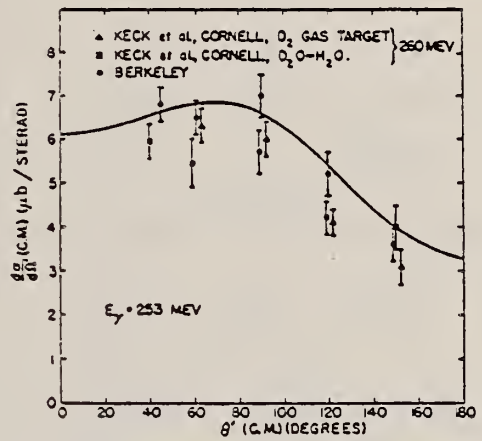

FIG. 9. Angular distribution for $E_\gamma = 173$ Mev.

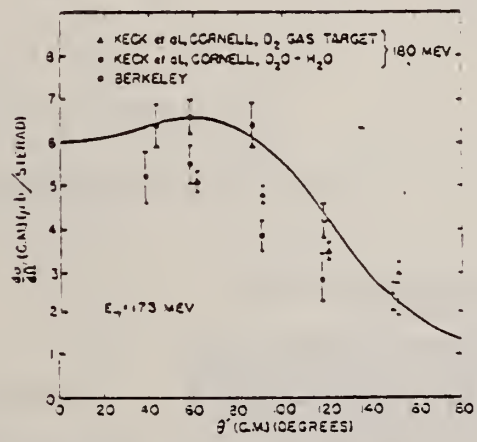

FIG. 10. Angular distribution for $E_\gamma = 253$ Mev.

Ref. J.C. Keck, A.V. Tollestrop
Phys. Rev. 101, 360 (1956)

Elem. Sym.	A	Z
H	2	1

Method: Counter telescope

Ref. No.: 56 Ke 1 F/H

Reaction	E or ΔE	E_o	Γ	$\int \sigma dE$	Jπ	Notes
$H^2(\gamma,p)$	75-450					Measured θ_L: 39° 93° 56° 115° 74° 138°

$$\frac{d\sigma}{dr} = (a + b\cos\theta) + (c\cos^2\theta)$$

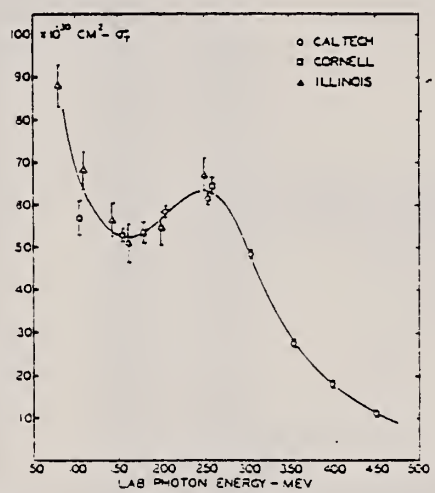

FIG. 10. Total cross sections for photodissociation of the deuteron as a function of laboratory energy. The CalTech and Cornell cross sections were taken from Table II and are subject to a quoted uncertainty of 10% in absolute value. The Illinois data were kindly communicated to the authors by A. O. Hanson. The solid curve is drawn through the experimental points.

[n] L. I. Schiff, Phys. Rev. 78, 733 (1951); J. F. Marshall and E. Guth, Phys. Rev. 78, 738 (1950).

[=] California Institute of Technology experiments on pion production in *H* and *D*.

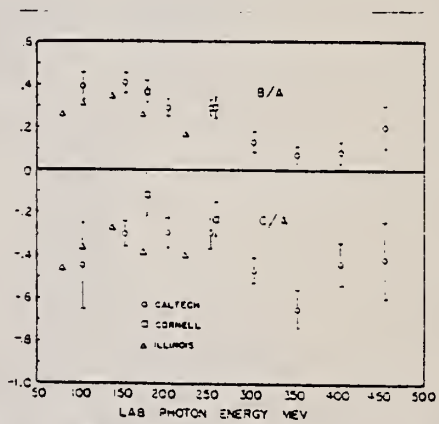

FIG. 11. Coefficients obtained by fitting CalTech, Cornell, and Illinois angular distributions with the empirical expression $(1+(B/A)\cos\theta+(C/A)\cos^2\theta)$. The CalTech and Cornell points are taken from Table II. The Illinois data were kindly communicated to the authors by A. O. Hanson.

FORM NBS-418
(8-1-63)
USCOMM-OC 18556-P63

U.S. DEPARTMENT OF COMMERCE
NATIONAL BUREAU OF STANDARDS

REF.

A.C. Odian, P.C. Stein, A. Wattenberg, B. T. Feld, and R. Weinstein
Phys. Rev. 102, 837 (1956)

ELEM. SYM.	A	Z
H	2	1

METHOD

Synchrotron; plastic scintillator proton telescope, liquid scintillator neutron detector, also integrating neutron detector

REF. NO.	
56 Od 1	NVB

REACTION	RESULT	EXCITATION ENERGY	SOURCE		DETECTOR		ANGLE
			TYPE	RANGE	TYPE	RANGE	
G,NP	RLX	140-260	C	340	TEL-D	70-125	DST

NP COINCIDENCE

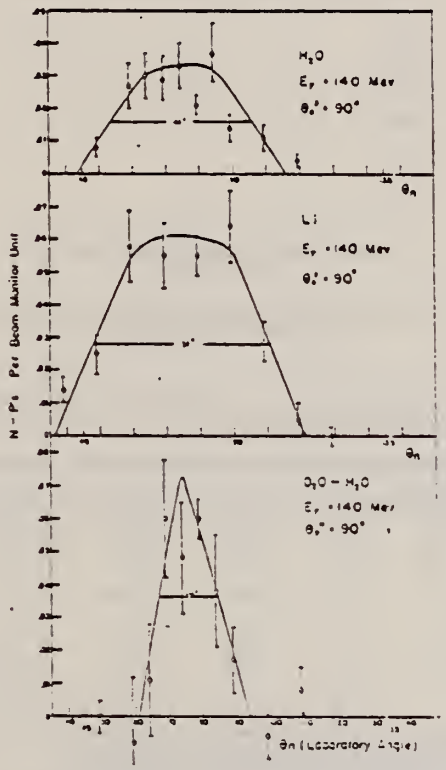

FIG. 2. Variation of neutron-proton coincidences with neutron angle. Gamma-ray energy is 140 Mev.

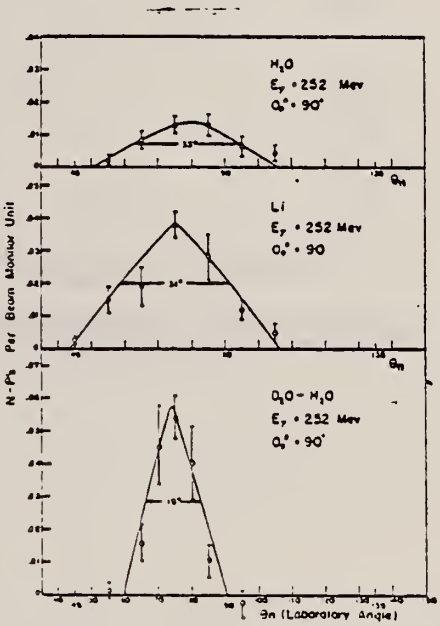

FIG. 3. Variation of neutron-proton coincidences with neutron angle. Gamma-ray energy is 252 Mev.

(continued)

REF.
1. A.C. Odian, P.C. Stein, A. Wattenberg, B.T. Feld, and R. Weinstein
Phys. Rev. 102, 837 (1956)

ELEM. SYM.	A	Z
H	2	1

METHOD

REF. NO. 56 Od 1 NVB

REACTION	RESULT	EXCITATION ENERGY	SOURCE TYPE	SOURCE RANGE	DETECTOR TYPE	DETECTOR RANGE	ANGLE

NP COINCIDENCE

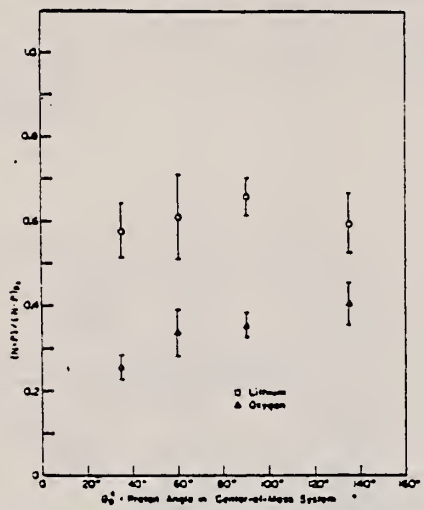

FIG. 6. Angular distribution of photoneutron proton pairs from lithium and oxygen relative to deuterium. $E_\gamma = 260$ Mev.

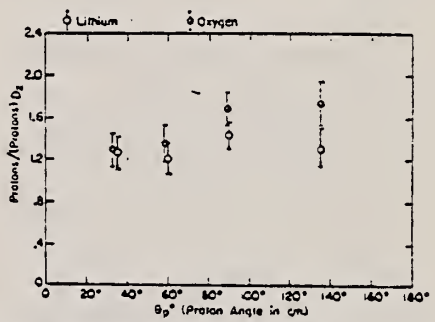

FIG. 7. Proton rates for oxygen and lithium relative to deuterium for various laboratory angles.

TABLE II. Summary of data[a] for lithium and oxygen. $E_\gamma = 260$ Mev; $\theta_P^* = 90°$; $\theta_P = \theta_N = \theta_{lab} = 76°$; $E_P = 129$ Mev; $E_N = 129$ Mev.[b]

Substance	Run[b]	P/M	$(N-P)/M$	$(N-P)/P$
Li	1	5.42	0.244	0.0450
	2	5.42	0.244	0.0450
	3	6.07	0.257	0.0423
	Av	5.64	0.248	0.0441
O_2	1	7.00	0.142	0.0203
	2	7.00	0.142	0.0203
	3	7.55	0.150	0.0198
	Av	7.18	0.145	0.0201

[a] Large counter uo close (10 in.).
[b] Each run corresponds to about 2000 monitor units.

TABLE I. Summary of data[a] for H_2O and D_2O. $E_\gamma = 260$ Mev; $\theta_P^* = 90°$; $\theta_P = \theta_N = \theta_{lab} = 76°$; $E_P = 129$ Mev; $E_N = 129$ Mev.

Run[b]	Prot / M_{H_2O}	Prot / M_{D_2O}	$\Delta P / M$	$N-P / M_{H_2O}$	$N-P / M_{D_2O}$	$\Delta(N-P) / M$	$\Delta(N-P) / P$	$N-P / P_{H_2O}$	$N-P / P_{D_2O}$
1	7.112	7.964	0.852	0.042	0.140	0.098	0.115	0.0060	0.0176
2	7.353	8.521	0.968	0.048	0.143	0.095	0.098	0.0064	0.0168
3	7.021	8.078	1.057	0.049	0.157	0.108	0.102	0.0070	0.0194
4	7.753	8.520	0.767	0.048	0.148	0.100	0.130	0.0061	0.0174
Av	7.360	8.271	0.91	0.047	0.147	0.100	0.110	0.0064	0.0178
Correction of 0.02 H_2O[c]			0.15			0.001			

Corrected av value: Prot/$M_{D_2} = 1.06$ · $N-P/M_{D_2} = 0.101$

[a] Large conuter far away (51 in.).
[b] Each run corresponds to about 2000 monitor units.
[c] The correction of 0.02 H_2O is to correct for the H_2O cell having a thickness that is 0.98 of the thickoess of the D_2O cell.

FORM NBS-418 (REV. 7-14-64) USCOMM-DC 26(

MERCE DARDS

Ref. E.A. Whalin, B.D. Schriever, A.O. Hanson
Phys. Rev. 101, 377 (1956)

Elem. Sym.	A	Z
H	2	1

Method: plates

Ref. No.: 56 Wh 1 | F/H

Reaction	E or ΔE	E_0	Γ	$\int \sigma dE$	Jπ	Notes
$H^2(\gamma,p)$	60-250					In Figure 4: $\frac{d\sigma}{dr} = (a + b \sin^2\theta)(1 + 2\beta \cos\theta)$

TABLE III. Values of A, B, and β from the relation $(A - B\sin^2\theta^*) \times (1 - 2\beta\cos\theta^*)$ representing the cross section. The isotropic part, the $\sin^2\theta^*$ part, and the total cross sections are given in the last three columns.

ϵ_γ Mev	2β	A μb/sterad	B μb/sterad	$4\pi A$ μb	$8\pi B/3$ μb	σ_{total} μb
65	0.25	5.0	5.7	62	47	109
80	0.35	4.5	3.9	56	32	88
105	0.38	3.9	2.2	49	18	67
140	0.40	3.4	1.3	43	11	54
114	0.40	5.3	0.9	67	7	74
149	0.44	3.5	1.2	44	10	54
194	0.22	4.2	2.9	53	24	77
248	0.10	4.2	0.9	53	11	64
220	0.22	4.5	1.3	57	11	68

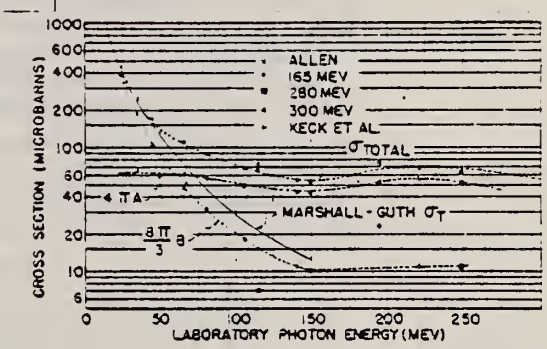

FIG. 4. The total cross section as given by $4\pi A + 8\pi B/3$. The isotropic component $4\pi A$ and the $\sin^2\theta^*$ component $8\pi B/3$ are shown as a function of energy. The solid line is the total cross section as calculated by Marshall and Guth.

REF.

Iu. A. Aleksandrov, N. B. Delone, L. I. Slovokhotov, G. A. Sokol, and L. N. Shtarkov
J. Exptl. Theoret. Phys. (USSR) 33, 614 (1957)
Soviet Phys. JETP 6, 472 (1958)

ELEM. SYM.	A	Z
H	2	1

METHOD

REF. NO.	
57 A1 1	EGF

REACTION	RESULT	EXCITATION ENERGY	SOURCE		DETECTOR		ANGLE
			TYPE	RANGE	TYPE	RANGE	
G,P	ABX	50 - 150	C	170,264	TEL-D	20-75	DST

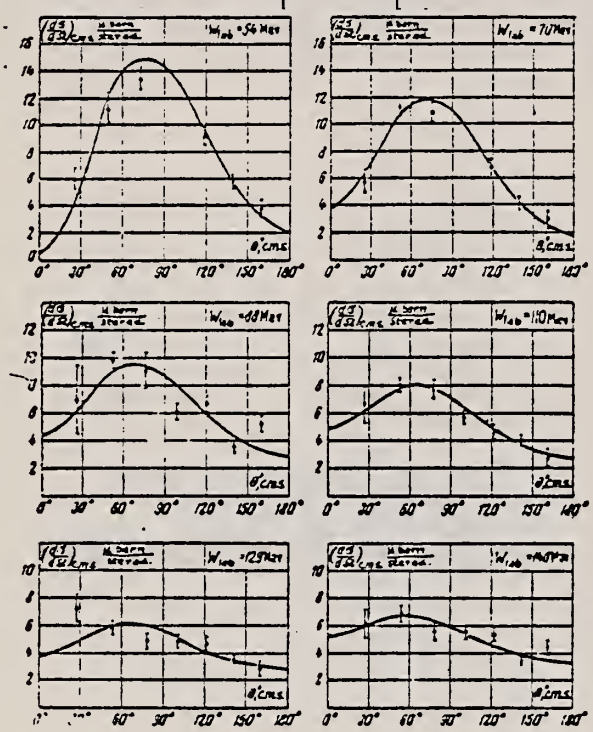

FIG. 1. Differential cross section vs. angle of the emitted proton in the c.m.s. for γ-rays of various energies (W_{lab} = 54, 70, 88, 110, 129 and 148 Mev, respectively). The solid curve corresponds to the approximate form $d\sigma/d\Omega = (d\sigma/d\Omega)_{M.G.} + P + Q\cos\theta$. Energy values have a definition of approximately 7.5 Mev. Errors of the experimental points are standard statistical errors.

TABLE I. Values of the parameters obtained in approximating the angular distributions by $d\sigma/d\Omega = (A + B\sin^2\theta)$ $(1 = 2\beta\cos\theta)$.

W_{lab}, Mev	2β	A, $\frac{\mu barn}{sterad.}$	B, $\frac{\mu barn}{sterad.}$
54	0.30	3.9	8.6
70	0.40	3.4	6.7
88	0.36	4.7	4.1
110	0.40	4.4	2.5
129	0.40	5.0	0.0
148	0.36	5.0	0.7

TABLE II. Values of the parameters, obtained in approximating the angular distributions by $d\sigma/d\Omega = (d\sigma/d\Omega)_{M.G.} + P + Q\cos\theta$. The uncertainty in the parameters correspond to the standard statistical error in the proton yield.

W_{lab}, Mev	P, $\frac{\mu barn}{sterad.}$	$\pm\Delta P$	Q, $\frac{\mu barn}{sterad.}$	$\pm\Delta Q$
54	1.30	0.11	−0.76	0.55
70	2.72	0.28	0.92	0.41
88	3.50	0.37	0.81	0.36
110	3.80	0.28	1.11	0.43
129	3.27	0.29	0.42	0.43
148	4.27	0.32	1.00	0.48

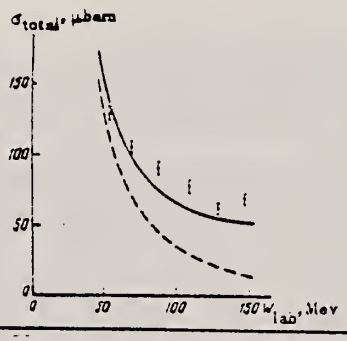

FIG. 2. Total cross section as a function of γ-ray energy W in the l.s. The solid curve is from the calculation of Wilson;[16] the dotted one, from the calculation of Marshall and Guth.[7] The errors in the experimental points are standard statistical ones.

REF.

P. S. Baranov, V. I. Gol'Danskii, and V. S. Roganov
J. Exptl. Theoret. Phys. (USSR) 33, 1123 (1957)
Soviet Phys. JETP 6, 865 (1958)

ELEM. SYM.	A	Z
H	2	1

METHOD

REF. NO.	
57 Ba 1	EGF

REACTION	RESULT	EXCITATION ENERGY	SOURCE		DETECTOR		ANGLE
			TYPE	RANGE	TYPE	RANGE	
G,N	ABY	30 - 260	C	120-260	THR-I	21	DST

$^{12}C(N,2N)^{11}C$ threshold detector.

REL YLDS D TO C

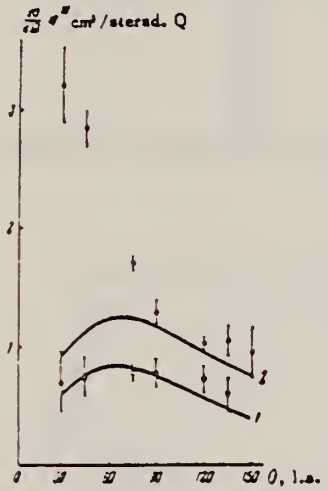

FIG. 3. Angular distributions of photoneutrons of energy > 20 Mev from deuterium; ○ — $E_{\gamma m}$ = 170 Mev, ● — $E_{\gamma m}$ = 255 Mev. The solid curve gives the results of the experiments, Refs. 4 — 10, transposed for neutrons: 1 — for $E_{\gamma m}$ = 170 Mev, 2 — for $E_{\gamma m}$ = 255 Mev.

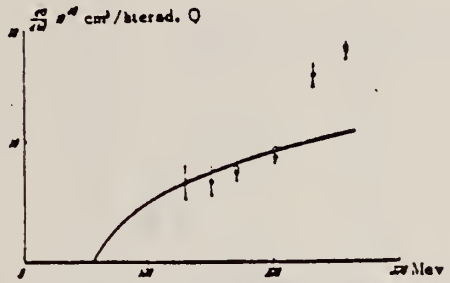

FIG. 2. Yield of fast photo neutrons from deuterium at 75° in the l.s. vs. maximum energy of the photon bremsstrahlung spectrum. The solid curve gives the results of the experiments, Refs. 4 — 10, transposed for neutrons; ● — yield of fast neutrons from deuterium, ○ — yield of fast neutrons from carbon.

TABLE I. Yield of photoneutrons of energy $\gtrsim$ 20 Mev from deuterium and carbon

$E_{\gamma m}$ (Mev)	Yield from deuterium (without meson production) according to Refs. 4-10 10^{-28} cm^2/Q	Total yield from deuterium $\sigma_D \times 10^{28}$ cm^2/Q	Total cross section from carbon $\sigma_C \times 10^{28}$ cm^2/Q	σ_C/σ_D
170	0.82	0.84±0.07	7.2±0.25	8.58±0.66
255	1.27	2.06±0.06	18.9±1.35	9.18±1.44

Ref. P.S. Baranov, V.I. Gol'danskii, V.S. Roganov
Phys. Rev. 109, 1801 (1958)

Elem. Sym.	A	Z
H	2	1

Method: $C^{12}(n,2n)$ scintillator

Ref. No.: 58 Ba 1 — F/H

Reaction	E or ΔE	E_o	Γ	$\int \sigma dE$	Jπ	Notes
$H^2(\gamma,n!)$						In figure 2 and 3, solid curves have been calculated for neutrons using Illinois and Cornell data on $d(\gamma,p)$. In figure 3, the rise in yield at small angles for $(E_\gamma)_{max}$=255 MeV is attributed to neutron production associated with photopion production.

[4] E. Whalin, Phys. Rev. 95, 1362 (1954).
[5] J. C. Keck and R. M. Littauer, Phys. Rev. 93, 527 (1954).
[6] L. Allen and A. Hanson, Phys. Rev. 95, 629 (1954).
[7] L. Allen, Phys. Rev. 98, 705 (1955).
[8] Tollestrup, Keck, and Smythe, Phys. Rev. 96, 550(A) (1954); J. C. Keck and A. V. Tollestrup, Phys. Rev. 101, 360 (1956).
[9] Whalin, Schriever, and Hanson, Phys. Rev. 101, 377 (1956).
[10] Aleksandrov, Delone, Slovokhotov, Sokol, and Shtarkov, J. Exptl. Theoret. Phys. U.S.S.R. (to be published).

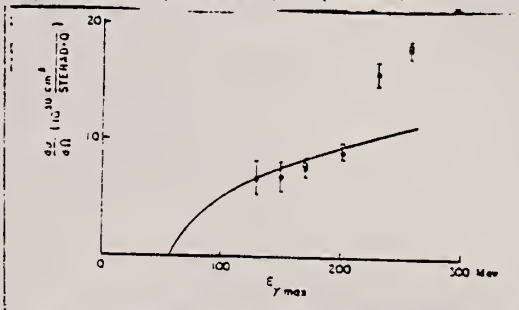

FIG. 2. Dependence of yield of fast photoneutrons emitted from deuterium at 75° in the l.s. on the peak bremsstrahlung energy. Solid curve—results from references 4–10 recalculated for neutrons. ●—fast neutron yield from deuterium; ○—fast neutron yield from carbon. The carbon neutron yields are normalized with respect to total cross section to the deuteron data assuming $\sigma_C = 9\sigma_D$.

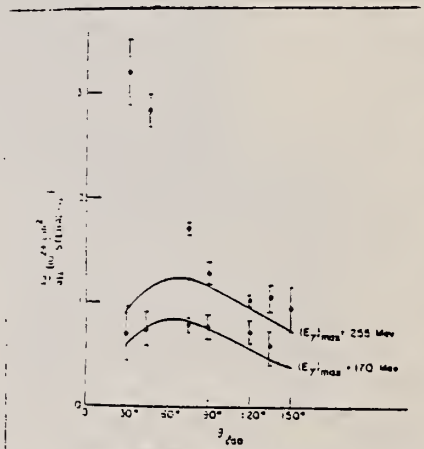

FIG. 3. Angular distributions of >20.6-Mev photoneutrons from deuterium produced by bremsstrahlung of 170- and 255-Mev peak energy. The upper and lower solid curves represent the experimental results obtained in references 4–10 recalculated for neutrons with $E_{\gamma m}$ = 170 Mev and $E_{\gamma m}$ = 255 Mev, respectively.

REF.

C. A. Tatro, T. R. Palfrey, Jr., R. M. Whaley, and R. O. Haxby
Phys. Rev. 112, 932 (1958)

ELEM. SYM.	A	Z
H	2	1

METHOD

Synchrotron; scintillation counter telescope; ion chamber monitor

REF. NO.: 58 Ta 2 NVB

REACTION	RESULT	EXCITATION ENERGY	SOURCE		DETECTOR		ANGLE
			TYPE	RANGE	TYPE	RANGE	
G,P	ABX	146-238	C	146-238	TEL-D	51-166	DST

TABLE II. Results

$\theta_{c.m.}$	Mean photon energy (Mev)	$(d\sigma/d\Omega)_{c.m.}$ (μbarns/sterad)
11°	192	5.84±0.7
	211	6.42±0.6
	227	6.15±0.9
100°	146	5.90±1.0
	172	5.50±0.5
	206	5.92±0.5
176°	190	4.00±0.7
	238	5.42±0.6

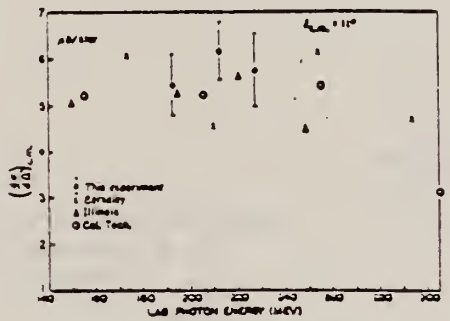

FIG. 3. Comparison of the energy dependence of the Purdue 11° c.m. data with extrapolated values from other laboratories.

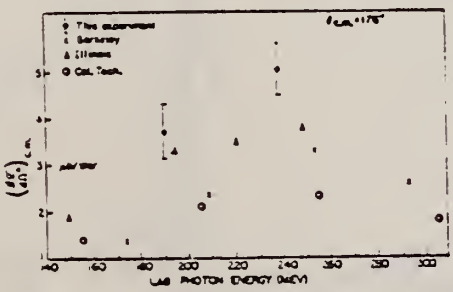

FIG. 4. Comparison of the energy dependence of the Purdue 176° c.m. data with extrapolated values from other laboratories.

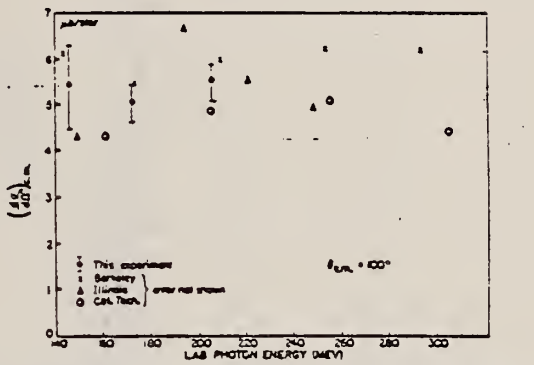

FIG. 5. Comparison of the energy dependence of the Purdue 100° c.m. data with interpolations of data from other laboratories.

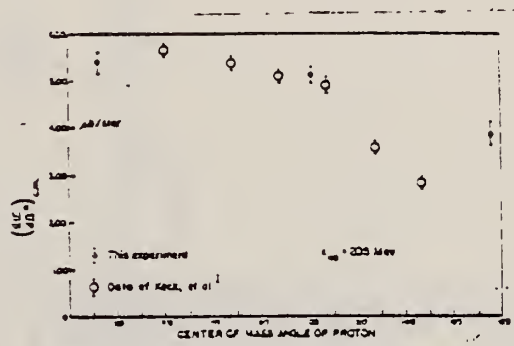

FIG. 6. Comparison of angular distributions for a photon energy of 205 Mev.

Ref. A. Whetstone, J. Halpern
Phys. Rev. 109, 2072 (1958)

Elem. Sym.	A	Z
H	2	1

Method NaI Detector

Ref. No. 58 Wh 1 F/H

Reaction	E or ΔE	E_o	Γ	$\int \sigma dE$	Jπ	Notes
$H^2(\gamma,p)$	9-23					Data fited to an angular distribution: $f(\theta) = (A + B \sin^2\theta)(1 + 2\beta \cos\theta)$ The ratio A/B rises from a value of 0.015±0.041 for 9-12 MeV photon group to one of 0.133±0.020 for the 20-22 MeV group.

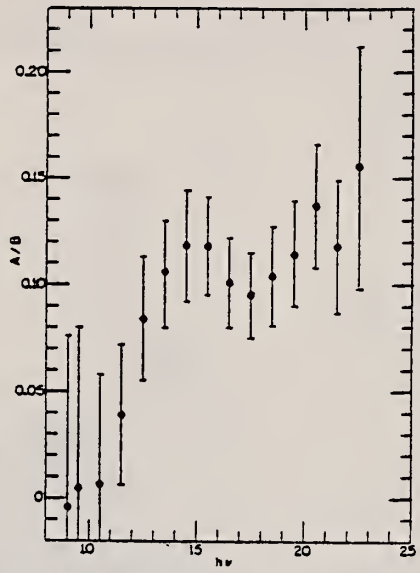

FIG. 7. A/B vs energy. The errors shown are the standard deviation plus systematic errors combined additively.

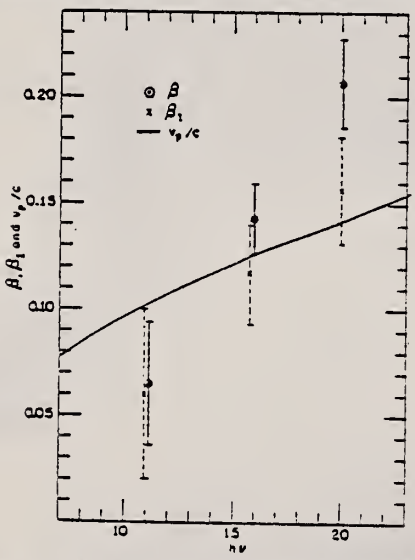

FIG. 9. β and β_1 are determined by fitting the data to Eqs. (1) and (2) after a previous determination of A/B. The errors shown are statistical plus systematic. For comparison the function v_p/c is plotted.

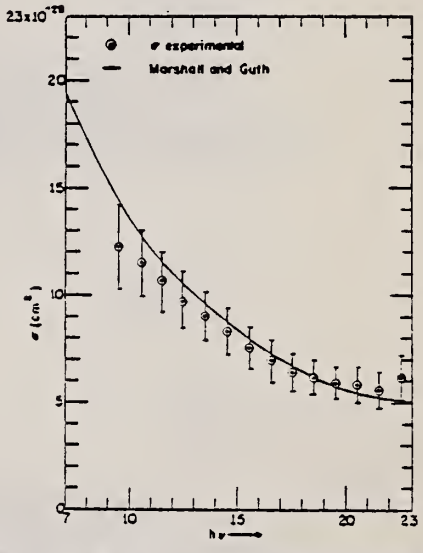

FIG. 10. The solid curve is the Marshall-Guth calculation for 50% exchange. The Schiff bremsstrahlung spectrum is used with the data to obtain the experimental points. The error indicated is largely systematic and is due to the difficulty of ascertaining the number of photons involved.

REF.
J.I. Friedman
Phys. Rev. 116, 1257 (1959)

EL EM. SYM.	A	Z
H	2	1

METHOD
Linac

REF. NO.
59 Fr 1
NVB

REACTION	RESULT	EXCITATION ENERGY	SOURCE		DETECTOR		ANGLE
			TYPE	RANGE	TYPE	RANGE	
E,E/	SPC	0-95	D	175	MAG-D		DST

Q = 206MEV/C

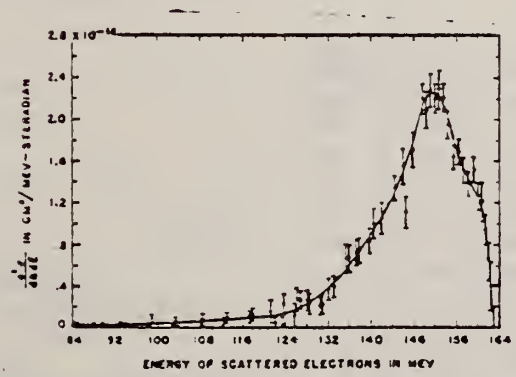

FIG. 3. The inelastic spectrum from electron-deuteron scattering at an incident energy of 175 Mev and a momentum transfer of 206 Mev/c. The data shown here have been corrected for the contributions from the radiative tail of the elastic peak and for the radiative broadening of the inelastic distribution.

TABLE II. Theoretical values of σ_E for various central π-ρ potentials. The experimental value of σ_E is 20.6 Mev with a statistical error of ± 1.1 Mev (one standard deviation) and an additional uncertainty of ± 1.1 Mev.

Potential	Calculated value of σ
Central Wigner	15.7 Mev
Rosenfeld interaction with a Yukawa shape	19.6 Mev
Rosenfeld interaction with a Gaussian shape	19.6 Mev
Central part of the Gartenhaus potential	14.4 Mev

Drell-Schwartz sum rule

Ref. B.T. Feld, B.C. Maglic, J. Parks
Nuovo Cimento 17, Suppl. 2, 241 (1960)

Elem. Sym.	A	Z
H	2	1

Method: Cyclotron; emulsions, polarization measurement

Ref. No.: 60 Fe 2 | JHH

Reaction	E or ΔE	E_o	Γ	$\int \sigma dE$	Jπ	Notes
$H^2(\gamma, p)$	150-300					

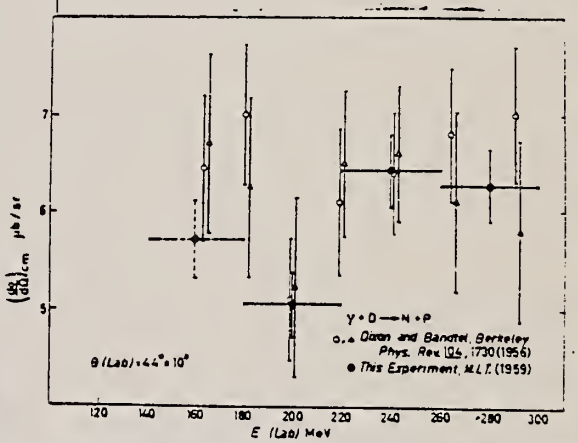

Fig. 6. – Excitation function for the $\gamma + d \to n + p$ reaction.

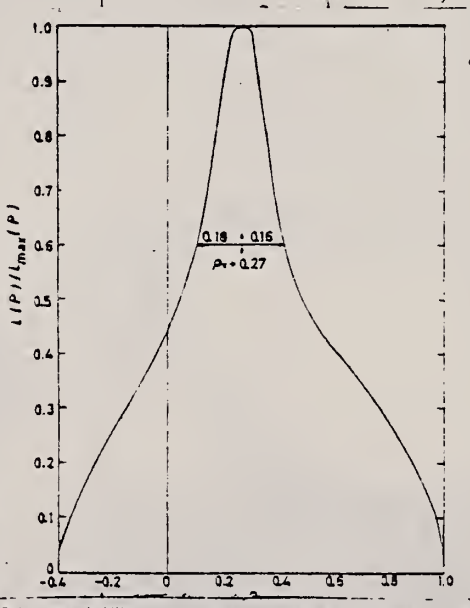

Fig. 7. – Relative probability vs. proton polarization in $\gamma + d \to n + p$, a) with 177 scattering events at an energy > 75 MeV;

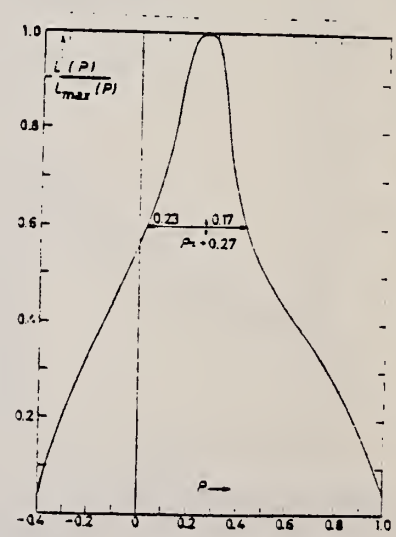

b) with 47 scattering events at an energy > 120 MeV.

Ref. J.A. Galey
Phys. Rev. 117, 763 (1960)

Elem. Sym.	A	Z
H	2	1

Method

100 MeV betatron; counter telescope with plastic scint., NaI as detectors

Ref. No. 60 Ga 1 | JH

Reaction	E or ΔE	E_o	Γ	$\int \sigma dE$	Jπ	Notes
(γ,p)	Bremss.; $E_{\gamma max}$= 93.5±.5MeV					Angular distribution data at 45°, 75°, 90°, 135°, photon energies 50-90 Mev. Smoothed data in Table 2 (center-of-mass coords.); parameters for fitted cubic $\sigma(\theta) = a_o + A_1 \cos\theta_c + a_2\cos^2\theta_c + A_3\cos^3\theta_c$ are in Table 3, with total cross section σ_t in microbarns.

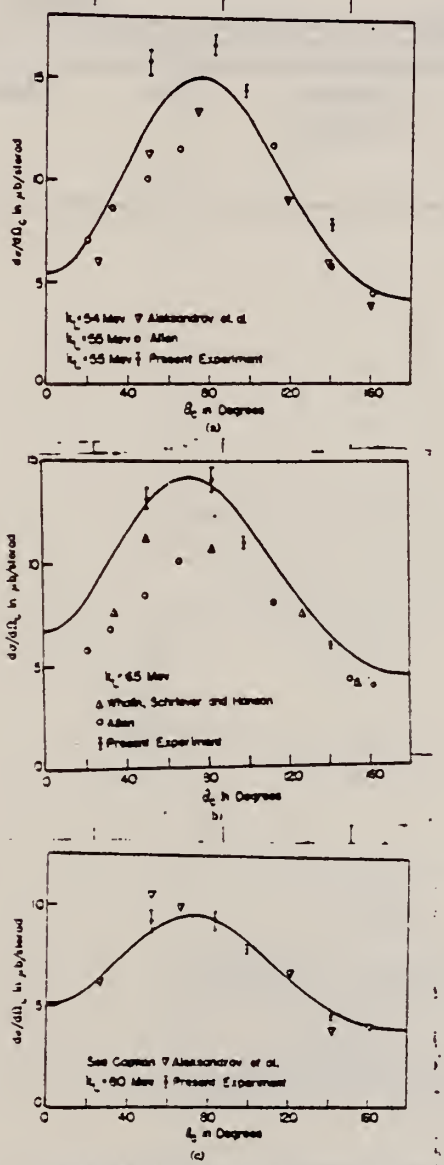

FIG. 6. Angular distribution plots: (a) the 53.7-Mev calculation of de Swart and Marshak; (b) the 64.4-Mev calculation of Zernik, Rustgi, and Breit in their approximation E; (c) the 80.4-Mev calculation of de Swart and Marshak. The values of Aleksandrov et al. are the averages of their 70- and 90-Mev values.

TABLE II. Values of the center-of-mass differential cross section.*

E_γ	θ_c degrees	$d\sigma/d\Omega_c$	θ_c degrees	$d\sigma/d\Omega_c$	θ_c degrees	$d\sigma/d\Omega_c$	θ_c degrees	$d\sigma/d\Omega_c$
50	49.31	17.0 0.6	81.48	19.5 0.6	96.76	16.9 0.25	139.78	8.3 0.5
55	50.03	15.8 0.6	81.31	17.2 0.5	97.08	14.6 0.3	140.00	7.5 0.3
60	50.25	14.4 0.6	82.14	15.6 0.6	97.36	12.35 0.3	140.22	6.5 0.2
65	50.46	13.2 0.6	82.43	13.6 0.6	97.67	11.0 0.3	140.43	5.9 0.2
70	50.65	11.9 0.6	82.71	12.4 0.5	97.96	9.8 0.3	140.61	5.6 0.2
75	50.84	10.45 0.5	82.97	10.7 0.5	98.24	8.9 0.3	140.81	5.15 0.2
80	51.01	9.2 0.5	82.23	9.25 0.5	98.49	7.9 0.2	141.00	4.6 0.2
85	51.18	8.1 0.5	83.48	8.0 0.4	98.74	6.5 0.4	141.17	3.8 0.3
90	51.34	7.1 0.5	83.73	6.3 0.6	98.98	5.7 0.6	141.35	3.2 0.3

* The second entry in alternate columns is the uncertainty associated with the quantity directly above it. These uncertainties do not include the effect of the uncertainty in the calibration of the Kerst-Edwards chamber. E is the laboratory photon energy in Mev. $d\sigma/d\Omega_c$ is given in units of $d\sigma/d\Omega_c$ sterad.

TABLE III. Values of the parameters a_o, A_1, a_2, A_3, and σ_t.*

E_γ	a_o	A_1	a_2	A_3	σ_t
50	18.3 0.3	10.3 2.4	12.0 1.4	11.0 5.1	179 7
55	16.0 0.3	10.2 2.3	9.4 1.3	10.7 4.9	162 7
60	14.1 0.3	12.6 2.2	5.7 1.4	16.0 4.7	140 7
65	12.4 0.35	10.0 2.6	6.6 1.5	11.2 5.5	128 8
70	11.3 0.3	9.9 2.0	6.2 1.4	12.4 4.3	116 7
75	9.95 0.3	6.8 2.0	4.9 1.3	7.3 4.3	104.5 6.5
80	8.72 0.25	5.0 1.7	3.9 1.3	4.6 3.8	93 6
85	7.4 0.3	5.6 2.2	3.3 1.2	5.9 4.6	79 6
90	6.39 0.4	4.1 1.0	2.6 1.7	5.4 6.8	69 9

* The second entry in every section of the table is the uncertainty associated with the next entry. a_o, A_1, a_2, and A_3 are in microbarns per steradian, σ_t is in microbarns. None of the uncertainties quoted here include the effect of the uncertainty in the calibration of the Kerst-Edwards chamber.

FORM NBS-418
(8-1-63)
USCOMM-DC 18556-P63

U.S. DEPARTMENT OF COMMERCE
NATIONAL BUREAU OF STANDARDS

REF.

K. N. Geller, J. Halpern, and E. G. Muirhead
Phys. Rev. 118, 1302-12 (1960)

ELEM. SYM.	A	Z
H	2	1

METHOD

Betatron; neutron threshold; ion chamber

REF. NO. 60 Ge 3 NVB

REACTION	RESULT	EXCITATION ENERGY	SOURCE		DETECTOR		ANGLE
			TYPE	RANGE	TYPE	RANGE	
G,N	NØX	THR	C THR		BF3-I		4 PI

THRESHØLD

TABLE I. Summary and comparison of neutron separation energies inferred from present threshold measurements with values predicted from mass data and reaction energies. All energies are expressed in the center-of-mass system in Mev.

Reaction	No. runs	Present results	Other results	Method	Reference
$D^2(\gamma,n)H^1$	10	2.226±0.001 (calib)	2.226±0.001	LSA	a

[a] J. Mattauch, L. Waldmann, R. Bieri, and F. Everling, *Annual Review of Nuclear Science* (Annual Reviews, Inc., Palo Alto, 1956), Vol. 6, p. 179.

Ref. W. John, F.V. Martin
Phys. Rev. 124, 830 (1961)

Elem. Sym.	A	Z
H	2	1

Method Na^{24} γ source; CD_2 primary target; polarimeter of Mg scatterer, BF_3 counter.

Ref. No. 61 Jo 1 JHH

Reaction	E or ΔE	E_o	Γ	$\int \sigma dE$	Jπ	Notes
(γ,n)	2.75	239.5 - 284.5 kev				Photoneutron polarization, P_1, data in Table I; compared with Kramer calculations in Figure 2.

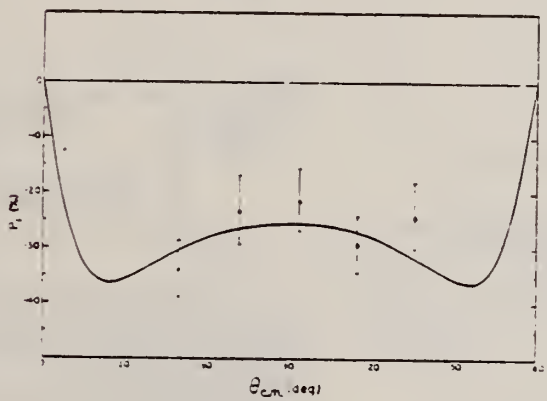

Figure 2: Polarization of the neutrons from the reaction $D(\gamma,n)H$ with E_γ=2.753 MeV. The solid curve is from a theoretical calculation by Kramer (private communication) as explained in the text.

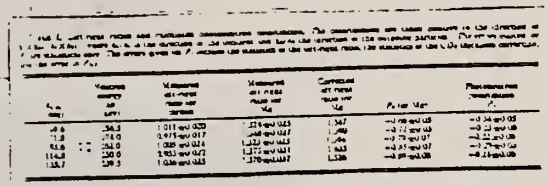

Ref. 14: A.J. Elwyn, R.O. Lane, A.S. Langsdorf, Jr. (Private communication)

Ref. H.W. Kendall, J.I. Friedman, E.F. Erickson, P.A.M. Gram
Phys. Rev. 124, 1596 (1961)

Elem. Sym.	A	Z
H	2	1

Method Linac; magnetic spectrometer

Ref. No. 61 Ke 3 JHH

Reaction	E or ΔE	E_0	Γ	$\int \sigma dE$	Jπ	Notes
$H^2(e,e')$	204-500 E_x = 0-20					

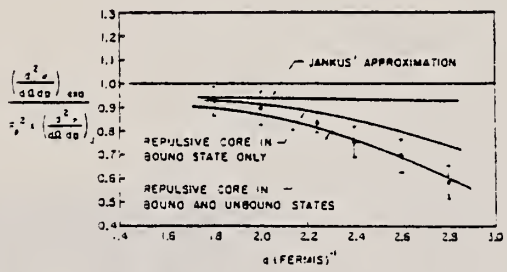

FIG. 10. The points plotted here show the ratio of observed inelastic cross sections at $E_0 = 500$ Mev (see Figs. 1–6) to the predictions of the Jankus theory, modified by the inclusion of the proton form factors and the experimental resolution of the equipment. The ratio is given as a function of q for ϵ approximately 2 Mev. The solid lines show the predictions of the Jankus calculation incorporating repulsive-core wave functions either in just the bound state or in the bound and the ^1S and ^3S unbound states; predictions of the approximate theory [see text following Eq. (12) of reference 6] are also shown. The observed yields have about equal contributions from spin-dip and non-spin-dip processes leading to ^1S and ^3S final n-p states, respectively. Errors are discussed in the text.

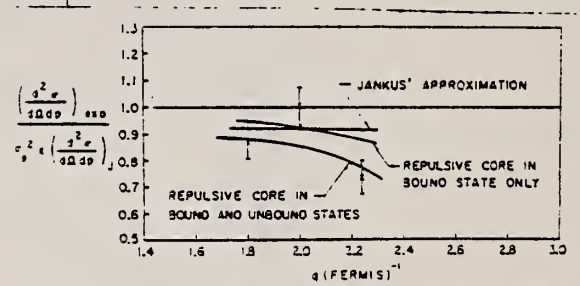

FIG. 11. This figure displays the data for $\theta = 145°$ from Fig. 7 and two other points at $\theta = 145°$: $q = 1.8$ f^{-1} and $q = 2.0$ f^{-1}. The major contributions to the yields at this large angle are from the spin-dip disintegration of the deuteron to the final ^1S n-p state. See the caption for Fig. 10.

FIG. 10. The points plotted here show the ratio of observed inelastic cross sections at $E_0 = 500$ Mev (see Figs. 1–6) to the predictions of the Jankus theory, modified by the inclusion of the proton form factors and the experimental resolution of the equipment. The ratio is given as a function of q for ϵ approximately 2 Mev. The solid lines show the predictions of the Jankus calculation incorporating repulsive-core wave functions either in just the bound state or in the bound and the ^1S and ^3S unbound states; predictions of the approximate theory [see text following Eq. (12) of reference 6] are also shown. The observed yields have about equal contributions from spin-dip and non-spin-dip processes leading to ^1S and ^3S final n-p states, respectively. Errors are discussed in the text.

Ref 6: V.Z. Jankus - Phys. Rev. 102, 1586 (1956).

Ref. H. Myers, R. Gomez, D. Guinier, A.V. Tollestrup
Phys. Rev. 121, 630 (1961)

Elem. Sym.	A	Z
H	2	1

Method CalTech electron synchrotron; liquid deutrium target; counter telescope to measure proton.

Ref. No. 61 My 1 JHH

Reaction	E or ΔE	E_o	Γ	$\int \sigma dE$	Jπ	Notes
(γ,p)	500-900					Excitation measurement at 90° (Figure 6); Angular distributions at E_γ=500 and 700 Mev (Figure 7). Total $\sigma(\gamma,p)$ decreased smoothly from 7μb at 500 MeV to 1μb at 900 MeV (Figure 8).

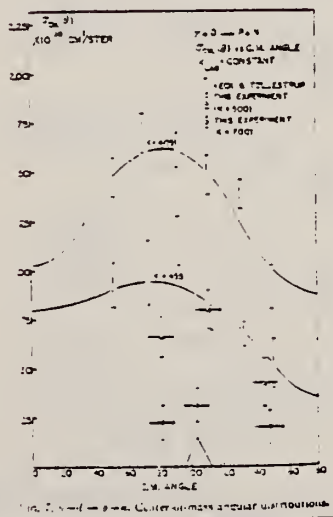

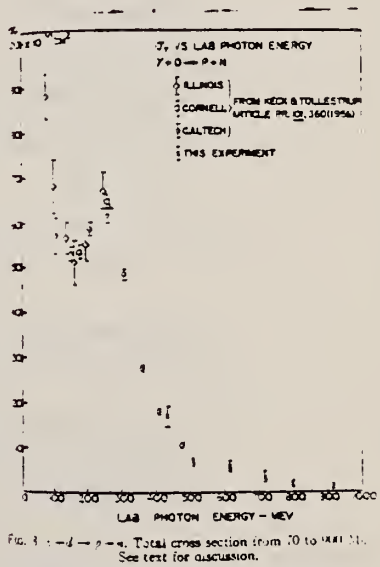

See text for discussion.

FORM NBS-418
(6-1-63)
USCOMM-DC 18856-P63

U.S. DEPARTMENT OF COMMERCE
NATIONAL BUREAU OF STANDARDS

REF.

G. A. Peterson and W. C. Barber
Proc. Ruth. Int. Conf. Manchester 831 (1961)

ELEM. SYM.	A	Z
H	2	1

METHOD

REF. NO. 61 Pe 2 JDM

REACTION	RESULT	EXCITATION ENERGY	SOURCE		DETECTOR		ANGLE
			TYPE	RANGE	TYPE	RANGE	
E,E/	ABX	0-12	D	41	MAG-D		DST

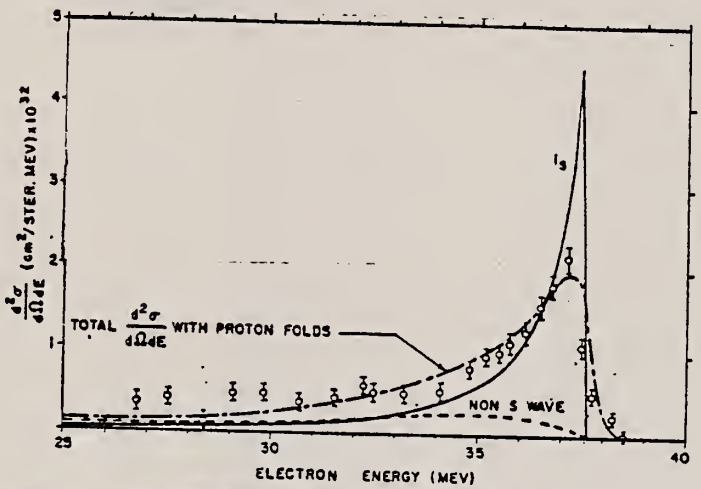

Figure 1. Cross-section for the 180° inelastic scattering of electrons of 41·4 MeV initial energy from the deuteron

Ref. F. Tagliabue, J. Goldemberg
Nuclear Phys. 23, 144 (1961)

Elem. Sym.	A	Z
H	2	1

Method 22 MeV betatron; $Si^{28}(n,p)Al^{28}$ threshold detector.

Ref. No. 61 Ta 1 | JHH

Reaction	E or ΔE	E_o	Γ	$\int \sigma dE$	Jπ	Notes
(γ,n)	Bremss. 22					$E_n > 6$ MeV. $W(\theta_n) = A + B \sin^2\theta$ where B/A = 6.5

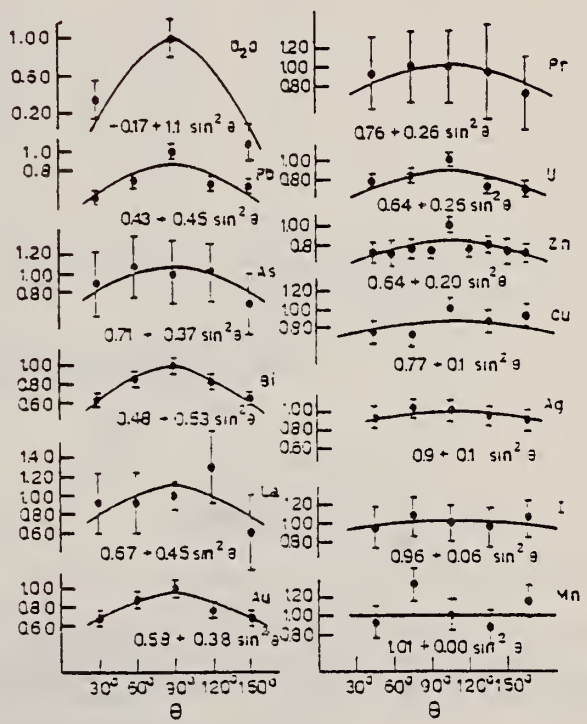

Fig. 4. Angular distributions of fast photoneutrons as observed with the $Si^{28}(n, p)Al^{28}$ detector. Data normalized at 90° in each case.

Ref. G.A. Peterson, W.C. Barber
Phys. Rev. 128, 812 (1962)

Elem. Sym.	A	Z
H	2	1

Method Linac (Stanford Mark II); 3 double coincidence counter telescope; magnet.

Ref. No. 62 Pe 1 BG

Reaction	E or ΔE	E_o	Γ	$\int \sigma dE$	Jπ	Notes
H^2(e,e')	41.5					Deutron magnetic dipole disintegration by 180° electron scattering. In Figure 5, sharp rise at 37 MeV is onset of magnetic dipole disintegration of D; 26 MeV peak due to C excitation (inelastic scattering from 15.1 MeV level).

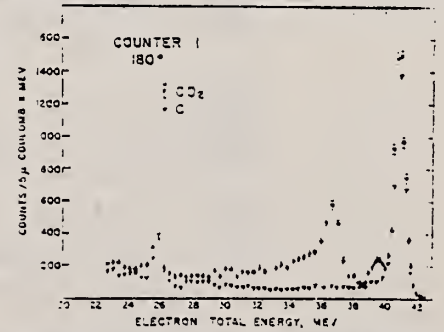

FIG. 5. Energy distribution of electrons, which were initially 41.5 MeV, after scattering through 180° from a CD_2 target.

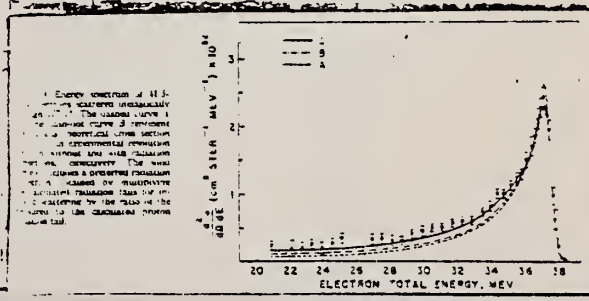

Ref.	Elem. Sym.	A	Z
W.C. Barber, J. Goldemberg, G.A. Peterson, Y. Torizuka Nuclear Phys. 41, 461 (1963); erratum to be published (as of 9/5/63)	H	2	1

Method	Ref. No.	
Linac (Stanford Mark II) - counter telescope	63Bal	BG

Reaction	E or ΔE	E_o	Γ	$\int \sigma dE$	Jπ	Notes
(e,e')	41.5					gas target used. inelastic scattering at 180°.

resonances

*) The results in this column were derived in the "long wave approximation"

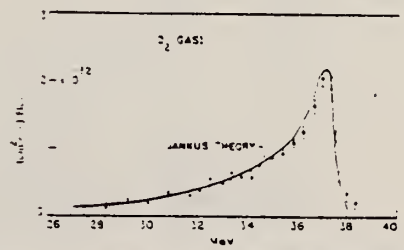

Fig. 3. Spectrum of 41.5 MeV electrons inelastically scattered from deuterium gas at 180°.

It is realized immediately by inspection of the curves that large radiation tails e present. This point is discussed in more detail in sect. 4.

The integrated inelastic scattering cross section $I_n = \int (d\sigma(\theta)\, d\Omega) d\varepsilon$ for each level is defined as the area above a smooth line drawn through the points in the adjacent

Ref. W. Bertozzi, P.T. Demos, S. Kowalski, C.P. Sargent, W. Turchinetz, R. Fullwood, J. Russell
Phys. Rev. Letters 10, 106 (1963)

Elem. Sym.	A	Z
H	2	1

Method: Linac; He-Xe filled gas scintillator counter surrounded by liquid scintillator counters for neutron spectrometer - polarimeter

Ref. No.: 63 Be 7 | JHH

Reaction	E or ΔE	E_o	Γ	$\int \sigma dE$	Jπ	Notes
$H^2(\gamma,n)$	Bremss. 30					CD_2 target

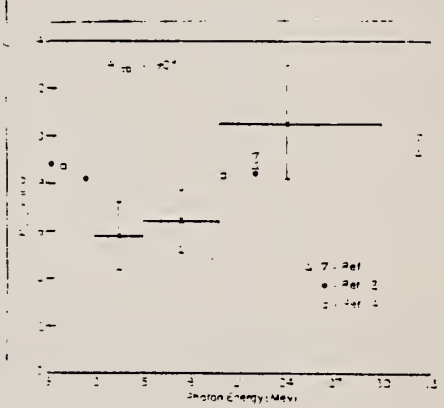

FIG. 1. Percent polarization of photoneutrons from deuterium. ($-P_{nD} \times 100$).

Table I. $P_{He^3 n D} \times 100$ after correcting for contribution from carbon.

E_γ (MeV) \ θ	47°	87°	117°	137°
12–15	+0.53 ± 3.67	+1.21 ± 0.96	−6.21 ± 1.63	−4.06 ± 1.4
15–20	+2.06 ± 1.00	−4.35 ± 1.02	−5.68 ± 1.93	−1.27 ± 1.4
20–30	+5.00 ± 0.89	−5.75 ± 1.45	−5.71 ± 2.73	−4.10 ± 2.1

REF. R. Bosch, J. Lang, R. Muller, W. Wolfli
Helva. Phys. Acta 36, 657 (1963)

EL EM. SYM.	A	Z
H	2	1

METHOD: Radioactive source; neutron angular distribution; scintillator

REF. NO.: 63 Bo 4 nvb

REACTION	RESULT	EXCITATION ENERGY	SOURCE TYPE	SOURCE RANGE	DETECTOR TYPE	DETECTOR RANGE	ANGLE
$ G,N	SPC	3- 9	D	3- 9	SCI-D		DST
		(2.75-9.0)					

N POL

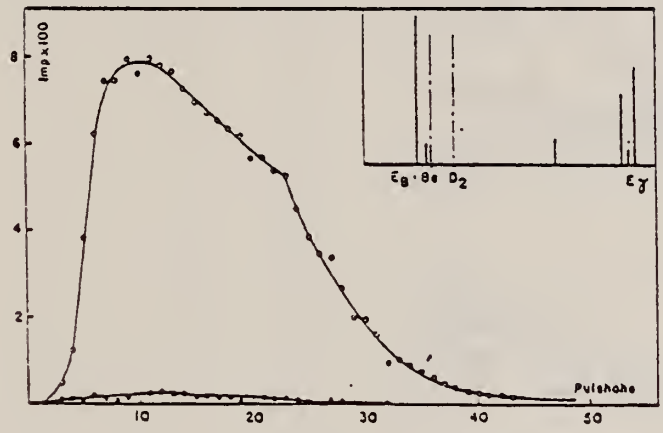

Figur 6

Impulsspektrum der Photoneutronen der Reaktion $H^2(\gamma, n)$, ($E_n = 2{,}2$ MeV) mit zugehörigem Untergrund. Oben rechts: Verwendetes Gammaspektrum der Reaktion $Ti(n, \gamma)$. Energieschwerpunkt der hochenergetischen Liniengruppe: $E_\gamma = 6{,}6$ MeV) und Schwellenenergien E_n der Reaktionen $Be^9(\gamma, n)$ und $H^2(\gamma, n)$.

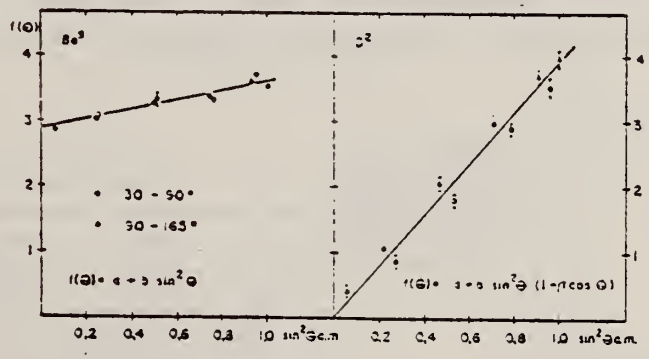

Figur 5

Winkelverteilung der Photoneutronen von Be^9 und H^2 bei einer Gammaenergie von 9,0 MeV.

(continued)

17) A.J. Siegert, Phys. Rev. 52, 787 (1937).
18) Proc. Int. Symposium on Polarization Phenomena of Nucleons, Helv. Phys. Acta. Suppl. VI, 436 (1961).
19) G. Kramer and O. Muller, Z. Phys. 158, 204 (1960).
49) A. Donnachie, Nucl. Phys. 32, 637 (1962).
50) L. Jarczyk, H. Knopfel, J. Lang, R. Muller and W. Wolfli, Nucl. Instr. Meth. 17, 310 (1962).

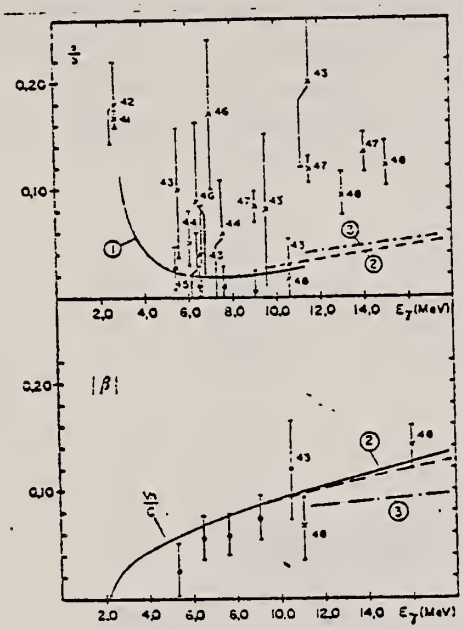

Figur 9

Deuterium: Vergleich der theoretischen Werte für a/b mit den experimentellen Resultaten. ⊙ Theoretischer Verlauf nach KRAMER *et al.*[19]), ○ nach SWART und MARSHAK[6]), ∃ nach DONNACHIE[49]). • : vorliegende Arbeit; ×: übrige bekannten experimentellen Resultate. Die Ziffern an den Fehlerbalken verweisen auf die entsprechenden Literaturangaben.

Unten: Verlauf von $|\beta|$. Zeichenerklärung wie vorhin. Die Kurven ∃ und ∋ entsprechen in den theoretischen Arbeiten $\beta_2/2$.

Tabelle IV

Asymmetrie und Polarisation der Photoneutronen vom H^4

Θc.m.	$E_{n_{lab}}$ (keV)	Asymmetrie A' gemessen	Asymmetrie A korrigiert	P_2 für Mg	Pol. P_1 der Photoneutronen	P_1 nach [4])
44,4°	287,5	1,314 ± 0,050	1,362	−0,658 ± 0,045	−0,33 ± 0,06	−0,34 ± 0,05 *)
93,6°	263,0	1,235 ± 0,035	1,376	−0,794 ± 0,065	−0,20 ± 0,04	−0,22 ± 0,06

*) Dieser Wert wurde unter einem Winkel von Θc.m. = 49,6° gemessen.

Ref. D.E. Frederick
Phys. Rev. 130, 1131 (1963)

Elem. Sym.	A	Z
H	2	1

Method 24 MeV Betatron; emulsions, cloud chamber

Ref. No.	
63 Fr 1	JHH

Reaction	E or ΔE	E_o	Γ	$\int \sigma dE$	$J\pi$	Notes
(γ,n)	11-23					

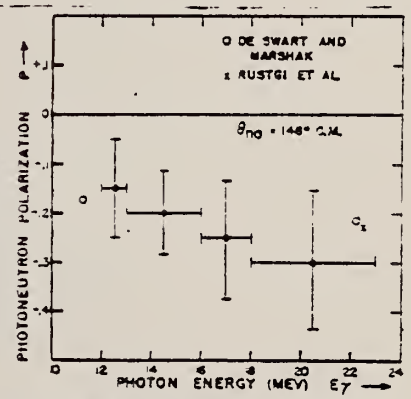

FIG. 7. Photoneutron polarizations measured in this experiment. The theoretical predictions at about 11 and 22 MeV are also shown.

TABLE III. D(γ,n)H polarizations and errors.

Energy (MeV)	Angle (prod)	Polarization	ΔP(D$_x$)	Major contributions to the total error ΔP(P$_{3/2}$−P$_{3/2}$)	ΔP(XCT)	ΔP$_{fit}$	ΔP$_{normalization}$
11.3–11.9	Forward	+0.051±0.091	0.077	0.042	0.009	13%	3%
12.0–12.9		−0.149±0.100	0.068	0.042	0.009	13%	3%
13.0–13.9		−0.198±0.086	0.067	0.042	0.009	13%	3%
14.0–17.9		−0.254±0.120	0.105	0.042	0.009	13%	3%
18.0–22.9		−0.296±0.177	0.122	0.042	0.009	13%	3%
14.0–17.9	Rear	−0.078±0.158	0.125	0.056	0.017	13%	3%
18.0–22.9		+0.038±0.135	0.120	0.056	0.017	13%	3%

Ref. F.J. Loeffler, T.R. Palfrey, Jr., T.O. White Jr.
Phys. Rev. 131, 1844 (1963)

Elem. Sym.	A	Z
H	2	1

Method: 320 MeV synchrotron; carbon plate spark chamber

Ref. No.: 63 Lo 1 | JHH

Reaction	E or ΔE	E_0	Γ	$\int \sigma dE$	Jπ	Notes
$ (γ,p)	294					Protons viewed at $\theta_{lab} = 58^\circ$ from primary γ beam. Polarization of proton determined by observing scattering in carbon.

TABLE I. Polarization of protons from the photodisintegration of deuterons.

$\bar{E}_\gamma$ (lab) (MeV)	$\bar{\theta}_p$ (lab)	$\bar{\theta}_p$ (c.m.)	$P_{\parallel}$	$P_{\perp}$
294	58°	72°	−0.03±0.11	−0.12±0.11

REF.	ELEM. SYM.	A	Z
W. Bertozzi, P. Demos, F. Hanser, S. Kowalski, C. Sargent and W. Turchinetz, R. Fullwood and J. Russell Proc. Paris Conf. 1026 (1964)	H	2	1

METHOD	REF. NO.	
Polarization Data	64 Be 8	JDM

REACTION	RESULT	EXCITATION ENERGY	SOURCE		DETECTOR		ANGLE
			TYPE	RANGE	TYPE	RANGE	
$G,N	NOX	THR-32	C	32	SCI-D		DST

In energy range 6 MeV < E_γ < 22 MeV at 90° results indicate a theoretical overestimate of $|P_n|$ by about .02±.01. For 45°, same tendency shows at $E_\gamma \sim 14$ MeV. In other energy ranges theory and experiment agree within experimental uncertainties, $\Delta P_n \geq \pm .04$.

REF.

F. F. Liu
Phys. Letters 11, 306 (1964)

ELEM. SYM.	A	Z
H	2	1

METHOD
Linac; ion chamber monitor

REF. NO.
64 Li 1 JOC

REACTION	RESULT	EXCITATION ENERGY	SOURCE		DETECTOR		ANGLE
			TYPE	RANGE	TYPE	RANGE	
$ G,P	RLX	80-140	C	400-500	MAG-D		90

POL PHOTONS

Table 1

K (MeV)	A	P	Σ
80	-0.0549 ± 0.0235	0.370	0.1480 ± 0.0635
95	-0.0369 ± 0.0275	0.360	0.1025 ± 0.0764
80	-0.0803 ± 0.0141	0.390	0.2059 ± 0.0362
95	-0.0519 ± 0.0177	0.380	0.1366 ± 0.0466
110	-0.0128 ± 0.0066	0.374	0.0342 ± 0.0176
120	-0.0025 ± 0.0075	0.368	0.0069 ± 0.0204
130	+0.0227 ± 0.0092	0.348	-0.0652 ± 0.0264
140	+0.0127 ± 0.0103	0.338	-0.0376 ± 0.0305

K - photon energy, A - measured asymmetry,
P - polarization of the photon beam,
Σ - asymmetry function.

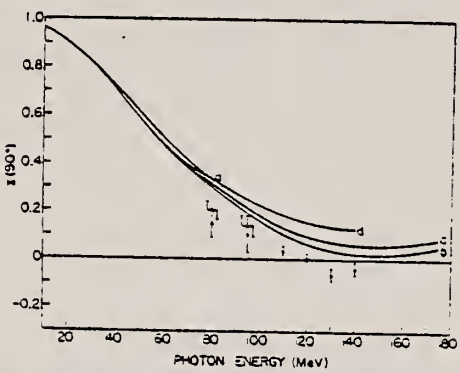

Fig. 1. The result of this experiment is indicated. The theoretical curves are taken from the following works: a - ref. 1, b - ref. 3, d - ref. 4.

REF. M. R. Yearian and E. B. Hughes
Phys. Letters 10, 234 (1964)

ELEM. SYM.	A	Z
H	2	1

METHOD

REF. NO. 64 Ye 2 JOC

REACTION	RESULT	EXCITATION ENERGY	SOURCE		DETECTOR		ANGLE
			TYPE	RANGE	TYPE	RANGE	
E,E/	ABX	0-40	D	150	MAG-D		135

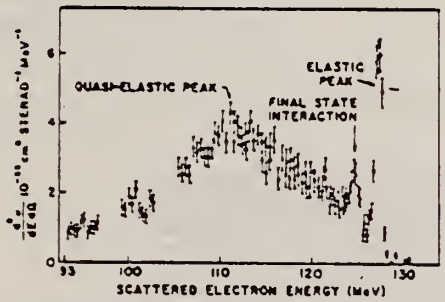

Fig. 1. Energy distribution of electrons scattered elastically and inelastically from the deuteron for an incident energy of 146.9 MeV and a scattering angle of 135°.

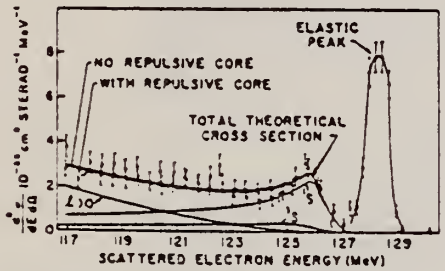

Fig. 2. Variation of the inelastic electron-deuteron cross section of fig. 1 near the disintegration threshold after correction for radiation effects. The experimental points are compared with the predictions of the Jankus theory with and without a repulsive core in the deuteron and final state wave functions.

REF.

P. Bounin and M. Croissiaux
Nuclear Phys. 70, 401 (1965)

ELEM. SYM.	A	Z
H	2	1

METHOD

REF. NO.	
65 Bo 1	EGF

REACTION	RESULT	EXCITATION ENERGY	SOURCE		DETECTOR		ANGLE
			TYPE	RANGE	TYPE	RANGE	
E,E/P	ABX	0-100	D	350	MAG-D	250-350	60,90

Cross section based on elastic scattering by protons.

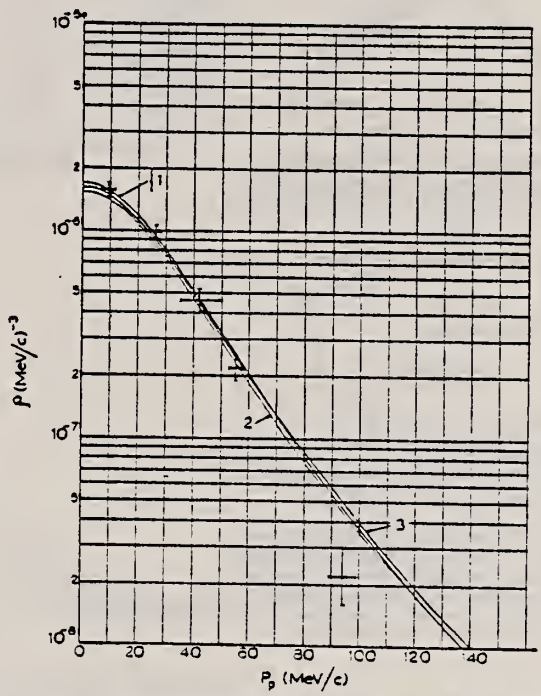

Fig. 7. Regroupement des résultats. Nous reportons sur cette figure les résultats du tableau 2. Nous y avons également reporté une portion de la fig. 8.
1. Breit, Glendenning-Kramer No. 8 2. Hamada 3. Huithén.

REF. Paul Bounin
Ann. Phys. 10, 475 (1965)

ELEM. SYM.	A	Z
H	2	1

METHOD

REF. NO. 65 Bo 3 egf

REACTION	RESULT	EXCITATION ENERGY	SOURCE		DETECTOR		ANGLE
			TYPE	RANGE	TYPE	RANGE	
E,E/P	ABX	50-100	D	235-300	MAG-D	100-300	DST

P IN COINC

$$\rho = \frac{d^3\sigma_{exp}}{\sigma_{ep}(\text{theory}) \times \mu p^2}$$

p = momentum of protons in coincidence

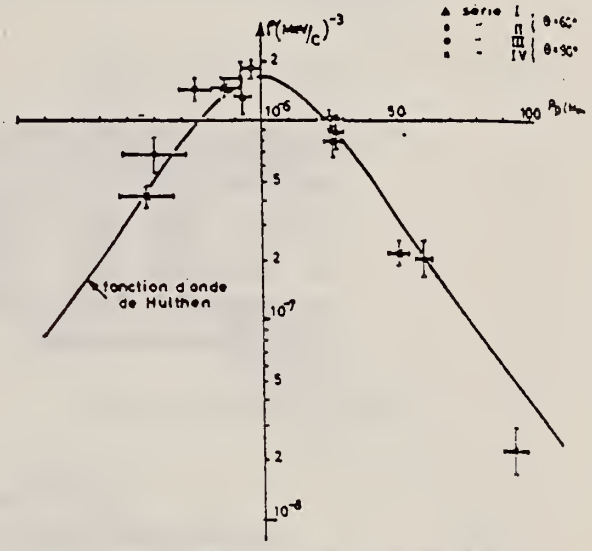

FIG. V-9. — *Résultats de l'expérience des coincidences.*

REF.

R. W. Jewell, W. John, J. E. Sherwood, and D. H. White
Phys. Rev. 139, B71 (1965)

EL EM. SYM.	A	Z
H	2	1

METHOD: Na^{24} source; solenoid to rotate neutron spins 180°, to cancel false asymmetries

REF. NO.: 65 Je 1 NVB

REACTION	RESULT	EXCITATION ENERGY	SOURCE TYPE	SOURCE RANGE	DETECTOR TYPE	DETECTOR RANGE	ANGLE
$G,N	NØX	2-3	D	3	BF3-I		DST
				(2.75)			

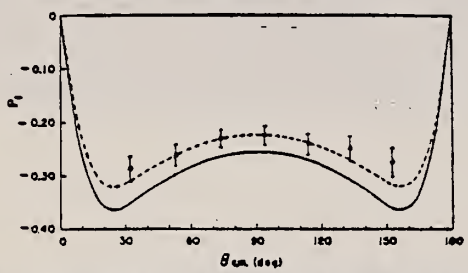

FIG. 7. Polarization of the neutrons from the D(γ,n) reaction with $E_\gamma = 2.754$ MeV. The solid curve is from a theoretical calculation by Kramer. The dashed curve is the theoretical curve multiplied by an arbitrary factor of 0.879 for comparison to the data points.

PØL NEUT, ASYMM.

TABLE II. Errors in the photoneutron polarization P_1. The errors from this experiment include statistics and systematics; the uncertainty in P_2 is from Ref. 20.

$\theta_{c.m.}$ (deg)	Error from this experiment (%)	Uncertainty in P_2 for Mg (%)	Total error in P_1 (%)
31.8	6.1	5.4	8.2
52.7	4.3	7.0	8.2
73.3	3.3	6.8	7.6
93.5	2.4	8.3	8.6
113.3	3.3	7.7	8.4
132.7	3.7	9.4	10.1
151.8	4.4	9.4	10.4

[20] A. J. Elwyn and R. O. Lane, Nucl. Phys. 31, 78 (1962).

TABLE III. Photoneutron polarization and cross sections calculated by Kramer[18] for the D(γ,n) reaction at $E_\gamma = 2.759$ MeV.

Set	r_n, F	γ_0, μb	a, μb	b, μb	a/b	σ_T, μb
1	2.0	−41.2	23.8	136.9	0.174	1446
2	2.4	−40.9	23.0	136.9	0.168	1436
3	2.8	−40.3	22.0	136.9	0.161	1423

[18] G. Kramer (private communication).

TABLE I. Measured left-right ratios ϵ, corrected ratios, and calculated photoneutron polarization. Positive polarization is taken in the direction $\mathbf{k}_\gamma \times \mathbf{k}_n$.

$\theta_{c.m.}$ (deg)	Measured ϵ with statistical error	ϵ corrected for Mg thickness	ϵ corrected for CD_2 thickness	P_2 for Mg	Photoneutron polarization P_1	Final P_1 corrected for geometry with total error
31.8	1.296±0.011	1.332	1.375	−0.605	−0.261	−0.287±0.024
52.7	1.317±0.011	1.359	1.388	−0.661	−0.246	−0.260±0.021
73.3	1.320±0.009	1.365	1.384	−0.730	−0.221	−0.231±0.018
93.5	1.348±0.004	1.395	1.414	−0.795	−0.216	−0.225±0.019
113.3	1.408±0.012	1.454	1.484	−0.842	−0.231	−0.242±0.020
132.7	1.426±0.013	1.469	1.514	−0.865	−0.236	−0.250±0.025
151.8	1.427±0.010	1.463	1.550	−0.865	−0.249	−0.275±0.029

REF.

F. F. Liu
Phys. Rev. 138, B1443 (1965)

ELEM. SYM.	A	Z
H	2	1

METHOD Linac; polarized photons by selecting off-axis bremsstrahlung; ion chamber monitor

REF. NO. 65 Li 1 NVB

REACTION	RESULT	EXCITATION ENERGY	SOURCE		DETECTOR		ANGLE
			TYPE	RANGE	TYPE	RANGE	
$G,P	NØX	75 - 250	C	75 - 250	MAG-D		DST

PØL PHØTØN, ASYMM.

Σ = asymmetry function, defined by:

$$\sigma(\theta) = \sigma_0(\theta)[1 + P\Sigma(\theta) \cos 2\chi]$$

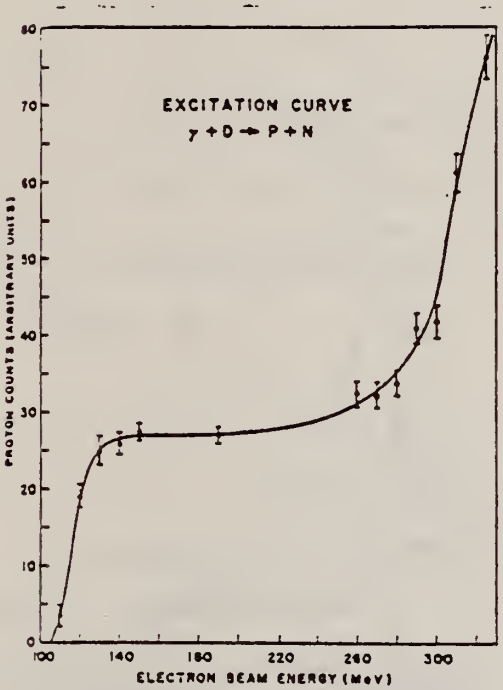

FIG. 5. The excitation function at $K = 115$ MeV, 39.6° proton recoil angle in the laboratory. Single π^0 production is clearly noticeable above 250 MeV.

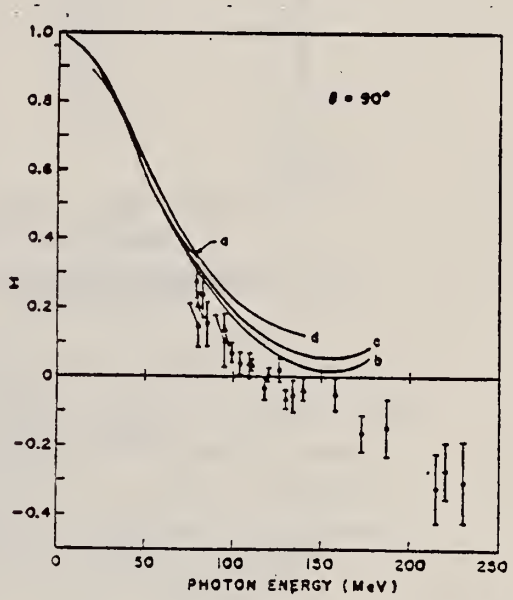

FIG. 6. Σ, the asymmetry function, at 90° in the c.m. system. Curve a is that of Ref. 7, b and c are from Ref. 8, and d is from Ref. 3, approximation *I*.

(continued)

REF.

F. F. Liu
Phys. Rev. 138, B1443-49 (1965)

ELEM. SYM.	A	Z
H	2	1

METHOD

Linac; polarized photons by selecting off-axis bremsstrahlung; ion chamber monitor

REF. NO. 65 Li 1 NVB

REACTION	RESULT	EXCITATION ENERGY	SOURCE		DETECTOR		ANGLE
			TYPE	RANGE	TYPE	RANGE	

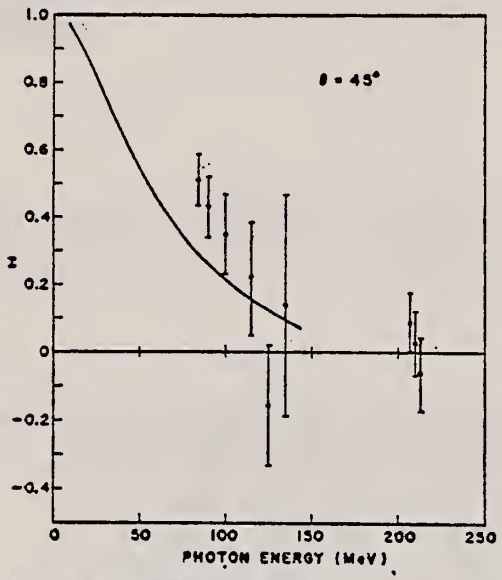

FIG. 7. Σ, the asymmetry function, at 45° in the c.m. system. The fit is that of Partovi.

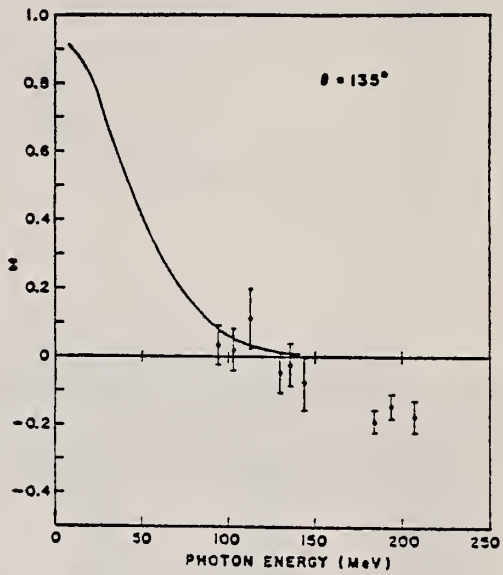

FIG. 8. Σ, the asymmetry function, at 135° in the c.m. system. The fit is that of Partovi.

REF.

J. Goldemberg and C. Schaerf
Phys. Letters 20, 193 (1966)

EL EM. SYM.	A	Z
H	2	1

METHOD

REF. NO.	
66 Go 1	EGF

REACTION	RESULT	EXCITATION ENERGY	SOURCE		DETECTOR		ANGLE
			TYPE	RANGE	TYPE	RANGE	
E,E/	ABX	0 - 6	D	54,70	MAG-D	48 - 70	180

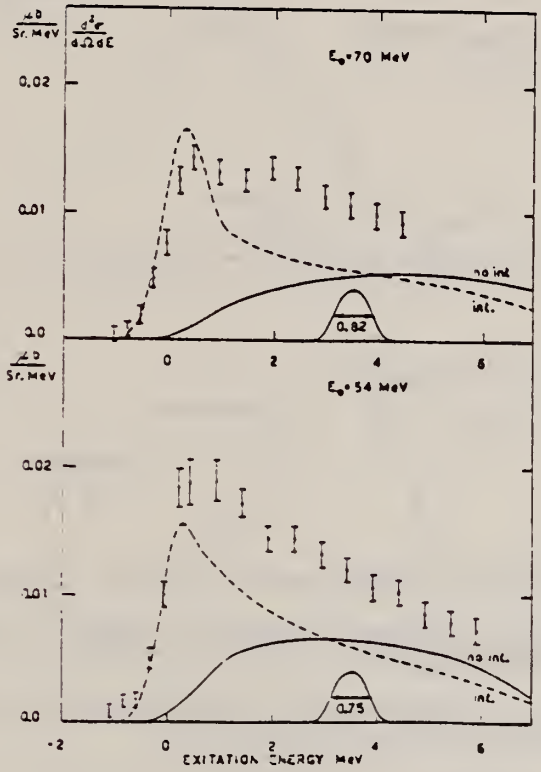

Fig. 1. Energy spectrum of electrons scattered inelastically on deuterium at $\vartheta = 180^0$. The solid lines indicate the theoretical result with no final state interaction. The broken lines indicate the results of the theoretical calculations of Durand when the final state interaction is taken into account. The excitation energy is defined as minus the difference between the energy of the scattered electron and the energy of the scattered electron at the electrodisintegration threshold.

References

1. J. Goldemberg and C. Schaerf, Phys. Rev. Letters 12 (1964) 298.
2. D. Drickey, D. Frerejacque and D. Benaksas, Phys. Rev. Letters 13 (1964) 353.
3. R. J. Adler and S. D. Dreil, Phys. Rev. Letters 13 (1964) 349.
4. G. A. Peterson and W. C. Barber, Phys. Rev. 128 (1962) 812.
5. W. C. Barber, J. Goldemberg, G. A. Peterson and Y. Torizuka, Nuclear Phys. 41 (1963) 1586.
6. V. Z. Jankus, Phys. Rev. 102 (1956) 1586.
7. L. Durand, Phys. Rev. 123 (1961) 1393.

REF.	ELEM. SYM.	A	Z
R.C. Greenwood, and W. W. Black Phys. Letters 21, 702 (1966)	H	2	1

METHOD	REF. NO.	
	66 Gr 1	JDM

REACTION	RESULT	EXCITATION ENERGY	SOURCE		DETECTOR		ANGLE
			TYPE	RANGE	TYPE	RANGE	
N,G	SBC	2	D	1	SCD-D		

BINDING ENERGY

Binding Energy of Deuteron is 2224.61 ± 0.07 keV.

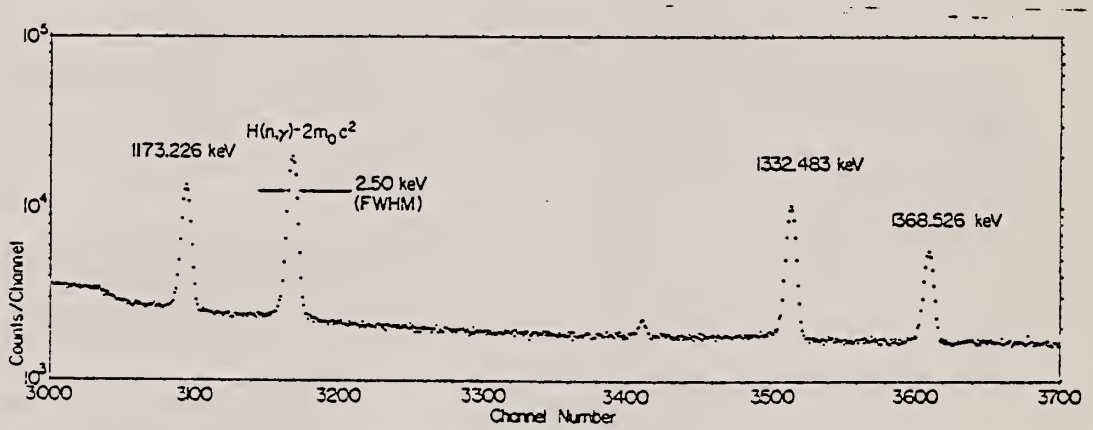

Fig. 1. The neutron capture gamma-ray spectrum of hydrogen measured with a 2.5 cm^2 × 4 mm lithium-drifted germanium detector. Included in the spectrum are ^{60}Co and ^{24}Na calibration lines.

REF.

B. Grossetête, S. Jullian, and P. Lehmann
Phys. Rev. 141, B1435 (1966)

ELEM. SYM.	A	Z
H	2	1

METHOD

REF. NO. 66 Gr 2 JDM

REACTION	RESULT	EXCITATION ENERGY	SOURCE		DETECTOR		ANGLE
			TYPE	RANGE	TYPE	RANGE	
E,E/	ABX	0 - 60	D	219 - 447	MAG-D		DST

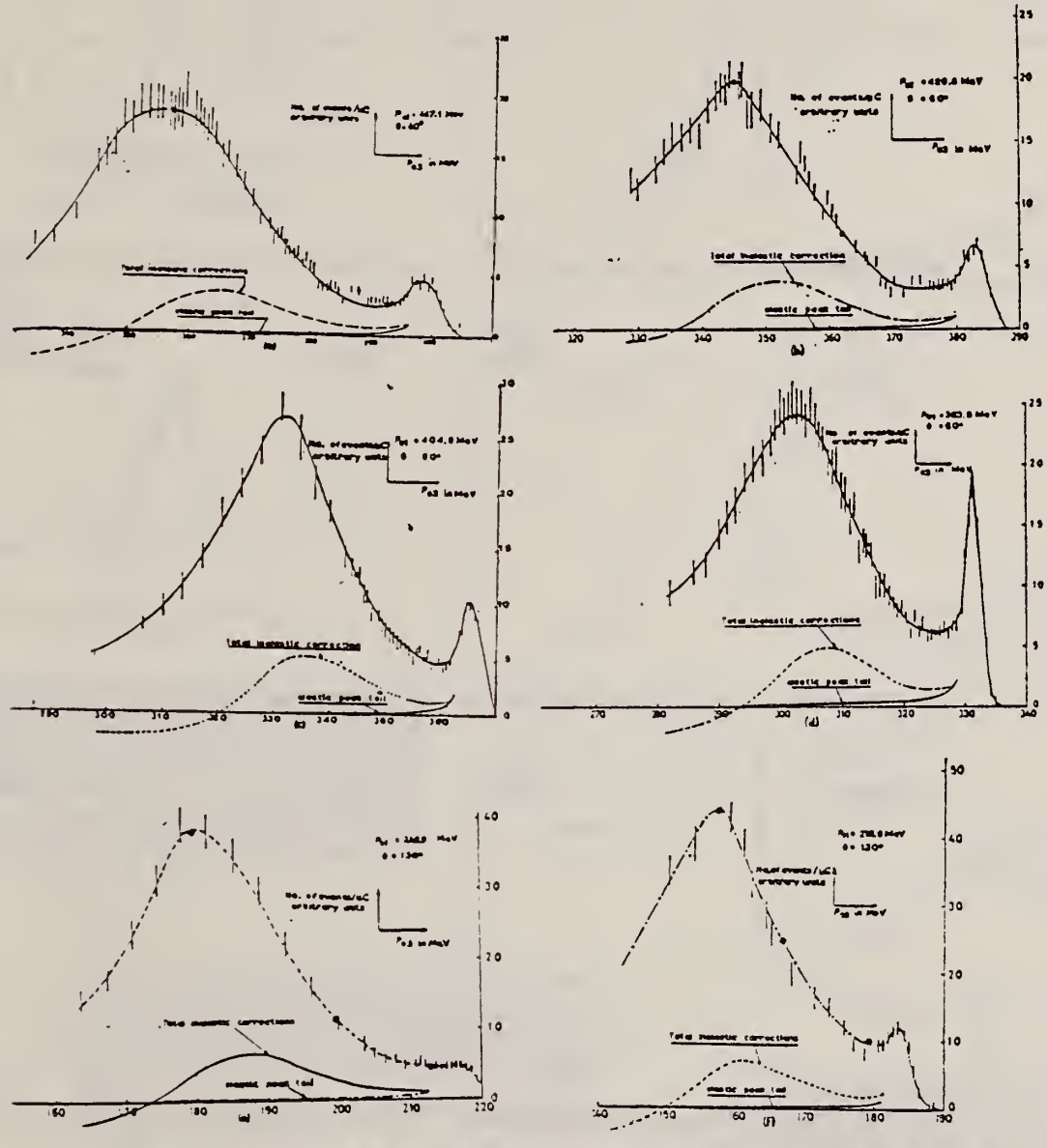

FIG. 3. Deuteron data. The more accurate points are represented by a dot. For the others, statistical errors are indicated. A smooth curve is drawn across all points. Corrections to the cross sections are given by two curves.

Note: See B. Bosco, B. Grossetête and P. Quarati, Phys. Rev. 141, B1441 (1966) for analysis of inelastic spectra.

(continued)

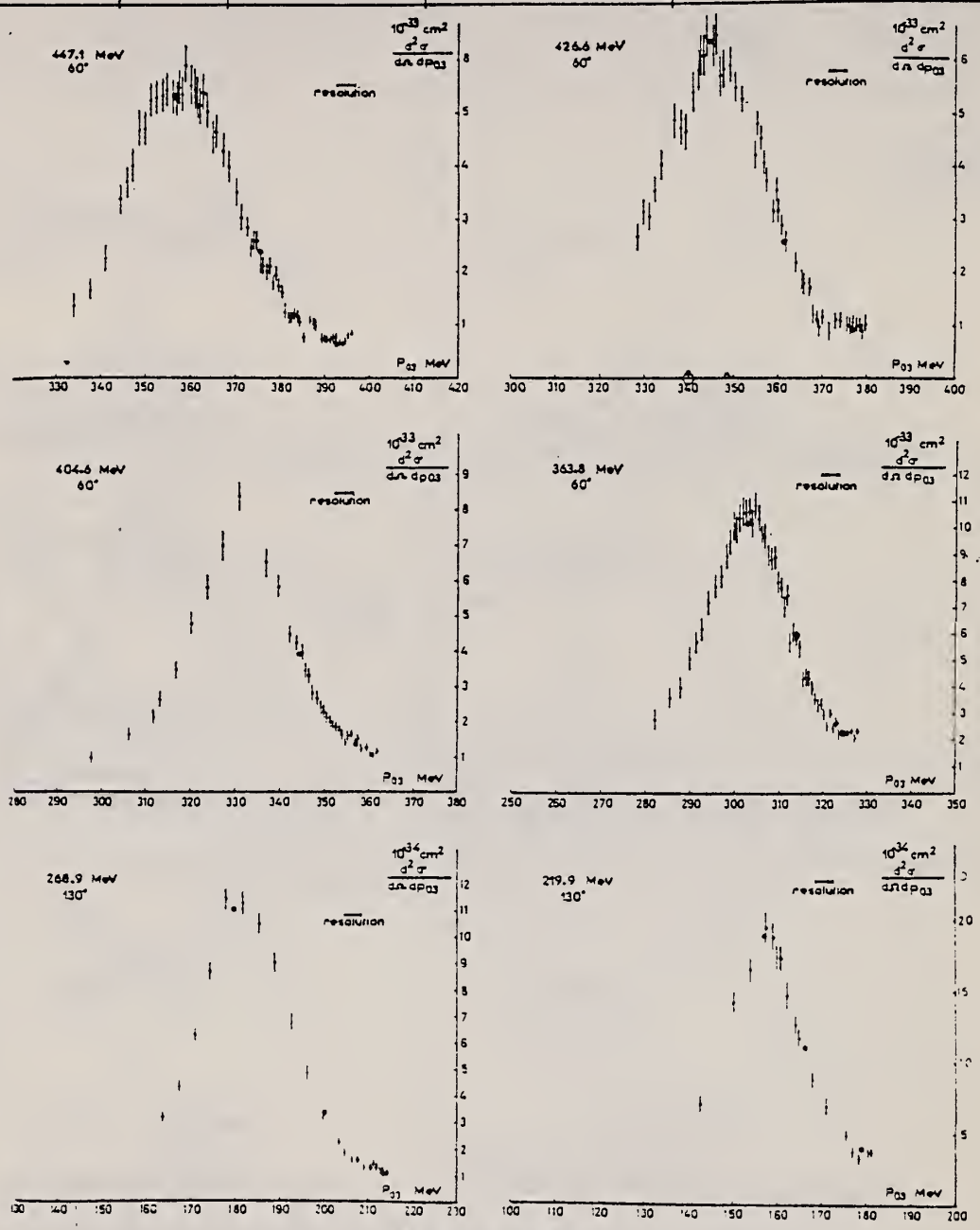

FIG. 4. Corrected spectra.

equations to obtain the right cross sections. The method used permitted us to know, in a satisfactory way, the cross-sections corrected for radiative effects. The bremsstrahlung corrections have been calculated in the same manner. It is well known that the bremsstrahlung formula is very similar to the radiative-emission formula. Thus the bremsstrahlung correction can be calculated as proportional to the radiative correction.

REF.

E.B. Hughes, T.A. Griffy, R. Hofstadter and M.R. Yearian
Phys. Rev. 146, B973 (1966)

ELEM. SYM.	A	Z
H	2	1

METHOD

REF. NO.	
66 Hu 1	JDM

REACTION	RESULT	EXCITATION ENERGY	SOURCE		DETECTOR		ANGLE
			TYPE	RANGE	TYPE	RANGE	
E,E/	FMF	0 - 70		146-475	MAG-D		DST

Range of q^2 is 1.5 - 7.5 F^{-2}.

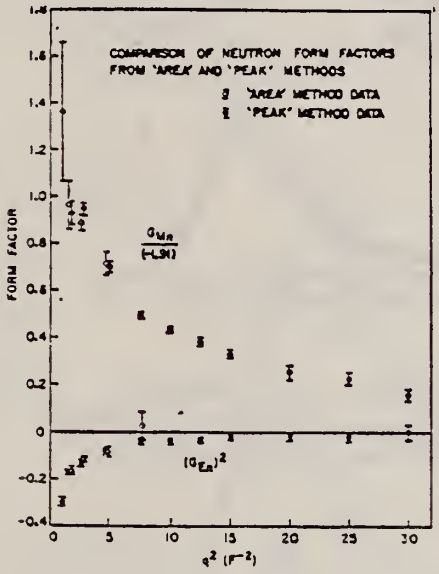

FIG. 6. The square of the neutron's charge form factor $(G_{En})^2$ and magnetic form factor G_{Mn} as a function of q^2 according to the area method. For comparison this figure also shows the neutron form factors found by Hughes *et al.* from the peak method using the simplest form of the Durand theory; namely a pure $^3S_1$ deuteron with no account taken of the final-state interaction. At $q^2 = 7.5$ F^{-2} where the data of the present experiment is restricted to 120° we have shown the value of $(G_{En})^2$ which corresponds to the value of G_{Mn} given by Hughes *et al.* The error bars include the statistical errors and a 4% uncertainty in the absolute electron-proton cross sections.

TABLE II. The neutron form factors $(G_{En})^2$ and G_{Mn} as a function of q^2. The value of G_{Mn} at $q^2 = 7.5$ F^{-2} is taken from Ref. 7. The quantities G_{En} and G_{Mn} are also frequently called $F_{1n}{}^2$ and $\mu_n F_{2n}{}^2$ respectively, where μ_n is the magnetic moment of the neutron. The errors shown include the statistical errors in σ_+/σ_p and a 4% uncertainty in the absolute electron-proton cross sections.

q^2 (F^{-2})	$(G_{En})^2$	$-(G_{Mn}/\mu_n)$
1.5	-0.163 ± 0.021	0.968 ± 0.102
2.5	-0.114 ± 0.010	0.888 ± 0.032
4.6	-0.084 ± 0.019	0.714 ± 0.051
7.5	-0.024 ± 0.057	(0.496 ± 0.013)

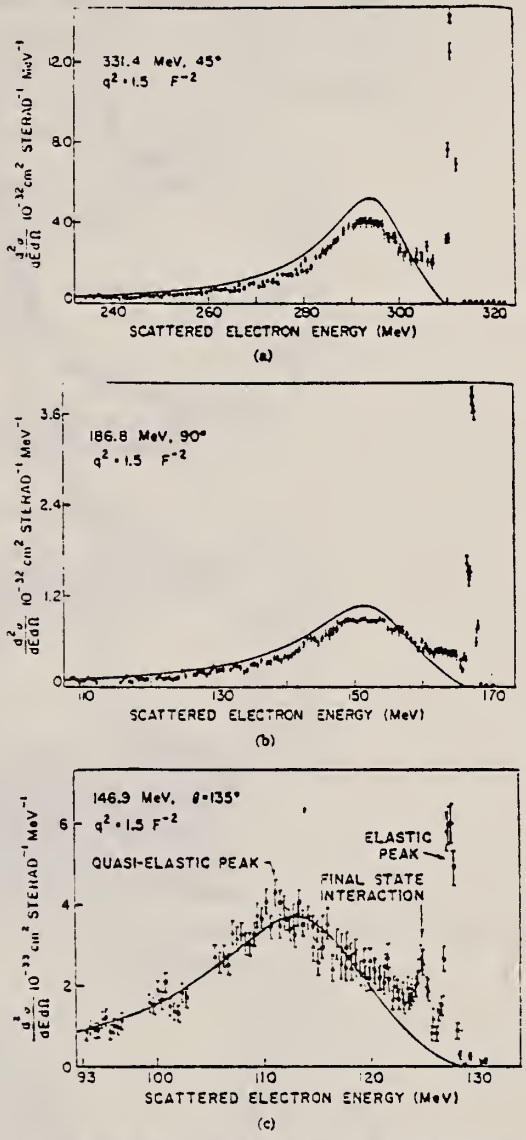

FIG. 1. Examples of the measured momentum distribution of electrons scattered elastically and inelastically from deuterium for scattering angles in the range 45° to 135° and for values of $q^2 = 1.5$ F^{-2}. The full curves represent the expected variation of the inelastic-cross-section calculated according to the formula given by Durand. No corrections are included in the theory for the effects of the *D*-state component of the deuteron wave function, the final-state interaction, or meson-exchange currents. The experimental resolution function and the radiative corrections are folded into the theoretical curves.

(continued)

REACTION	RESULT	EXCITATION ENERGY	SOURCE		DETECTOR		ANGLE
			TYPE	RANGE	TYPE	RANGE	

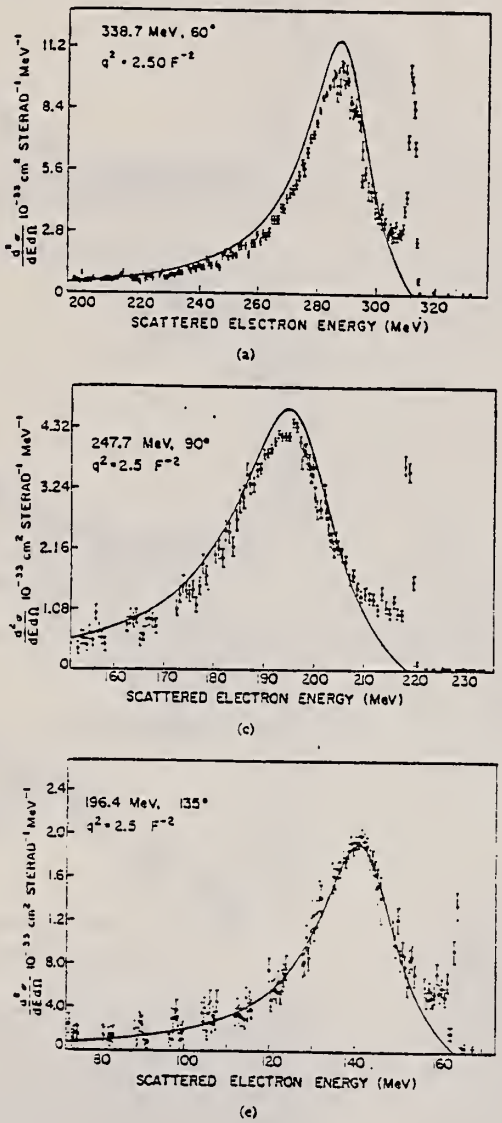

FIG. 2. Examples of the measured momentum distribution of electrons scattered elastically and inelastically from deuterium for scattering angles in the range 45° to 135° and for values of $q^2 = 2.5$ F^{-2}. The full curves represent the expected variation of the inelastic-cross-section calculated according to the formula given by Durand. No corrections are included in the theory for the effects of the *D*-state component of the deuteron wave function, the final-state interaction, or meson-exchange currents. The experimental resolution functions and the radiative corrections are folded into the theoretical curves.

(continued)

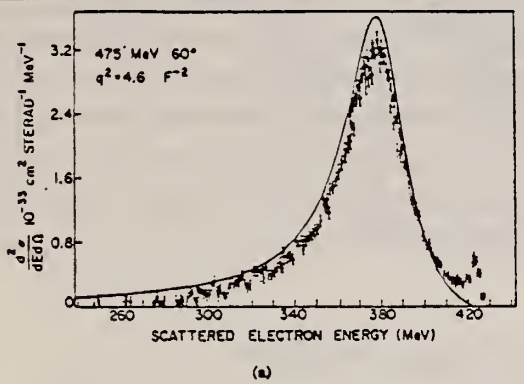

(a)

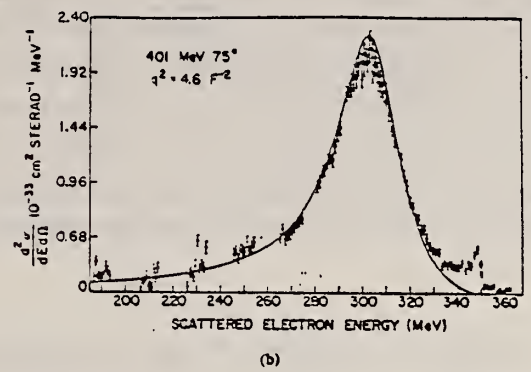

(b)

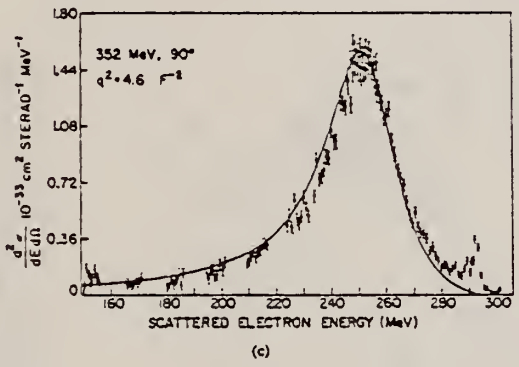

(c)

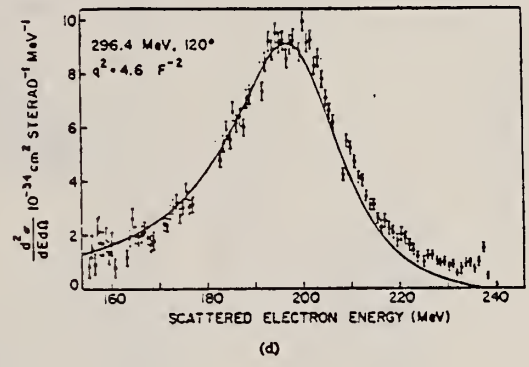

(d)

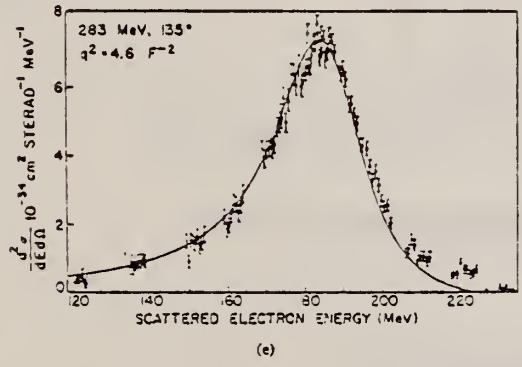

(e)

FIG. 3. Examples of the measured momentum distribution of electrons scattered elastically and inelastically from deuterium for scattering angles in the range 45° to 135° and for values of $q^2 = 4.6$ F^{-2}. The full curves represent the expected variation of the inelastic-cross-section calculated according to the formula given by Durand. No corrections are included in the theory for the effects of the *D*-state component of the deuteron wave function, the final-state interaction, or meson-exchange currents. The experimental resolution function and the radiative corrections are folded into the theoretical curves.

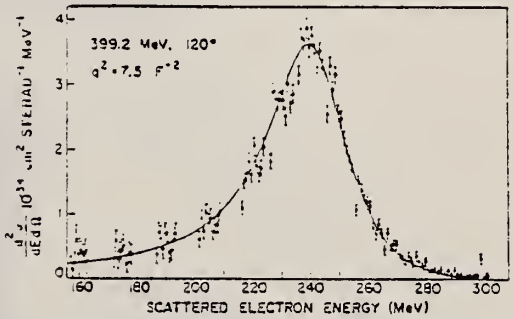

FIG. 4. The measured momentum distribution of electrons scattered elastically and inelastically from deuterium at a scattering angle of 120° and for $q^2 = 7.5$ F^{-2}. The full curve represents the expected variation of the inelastic-cross-section calculated according to the formula given by Durand. No corrections are included in the theory for the effects of the *D*-state component of the deuteron-wave function, the final-state interaction, or meson-exchange currents. The experimental resolution function and the radiative corrections are folded into the theoretical curve.

REF.	ELEM. SYM.	A	Z
G. Barbiellini, C. Bernardini, F. Felicetti, and G. P. Murtas Phys. Rev. 154, 988 (1967)	H	2	1

METHOD	REF. NO.	
Electron synchrotron, polarized γ-ray beam using crystal technique.	67 Ba 1	JDM

REACTION	RESULT	EXCITATION ENERGY	SOURCE		DETECTOR		ANGLE
			TYPE	RANGE	TYPE	RANGE	
$G,N	NOX	200-400	C	1 GEV	TEL-D		90

Measured asymmetry parameter at 90° in the center-of-mass system.

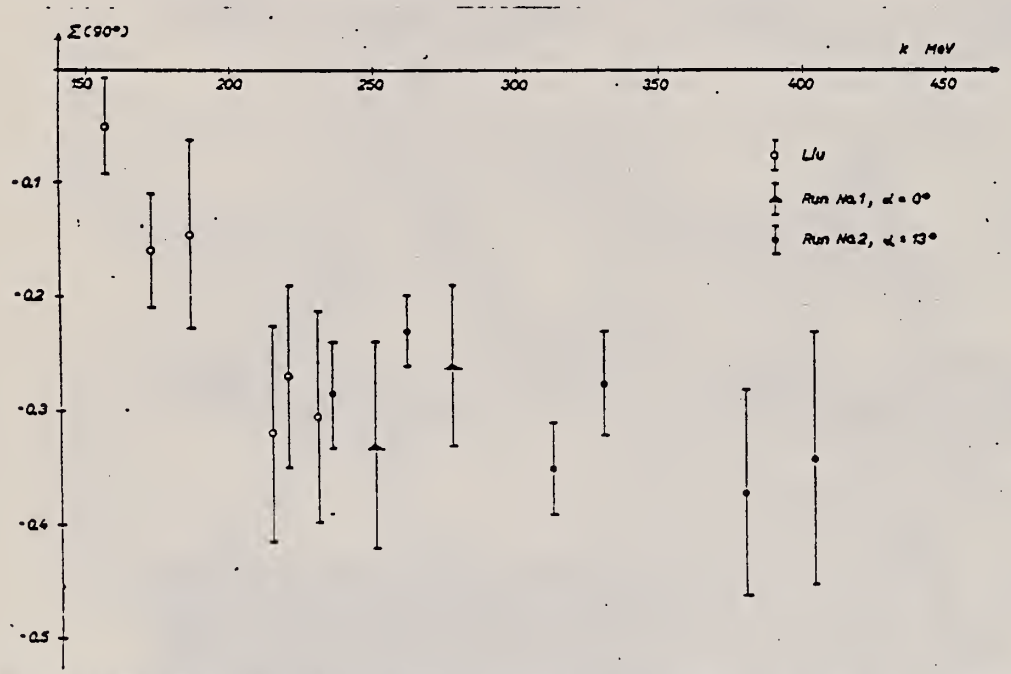

FIG. 7. Experimental results for the asymmetry function Σ at 90° in the c.m. system. Symbols are as follows: hollow circle—Liu (Ref. 7); solid triangle—present experiment, run No. 1; solid circle—present experiment, run No. 2.

TABLE I. Experimental results for the asymmetry function Σ at $\vartheta = 90°$ (c.m. proton angle) for various laboratory photon energies k, with the error for Σ and k. P gives the polarization of the linearly polarized γ rays.

k (MeV)	P	Σ	$\delta\Sigma$	Δk (MeV)
235	0.29	0.276	±0.038	24
253	0.25	0.330	±0.090	19
260	0.37	0.228	±0.028	21
277	0.30	0.260	±0.070	22
310	0.30	0.350	±0.040	11
330	0.34	0.275	±0.045	19
380	0.22	0.370	±0.090	22
404	0.27	0.340	±0.110	24

REF.

R. Kose, W. Paul, K. Stockhorst and K. H. Kissler
Z. Physik 202, 364 (1967)

ELEM. SYM.	A	Z
H	2	1

METHOD

REF. NO.	
67 Ko 3	egf

REACTION	RESULT	EXCITATION ENERGY	SOURCE		DETECTOR		ANGLE
			TYPE	RANGE	TYPE	RANGE	
G,P	ABX	100-420	C	500	TEL-D	50-250	DST

Tabular data given.

N IN COINC

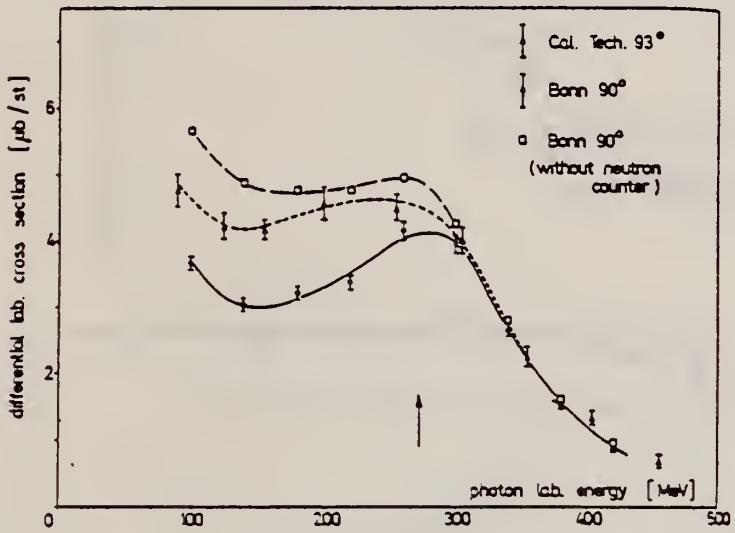

Fig. 13. Excitation curve at proton lab. angle 90°

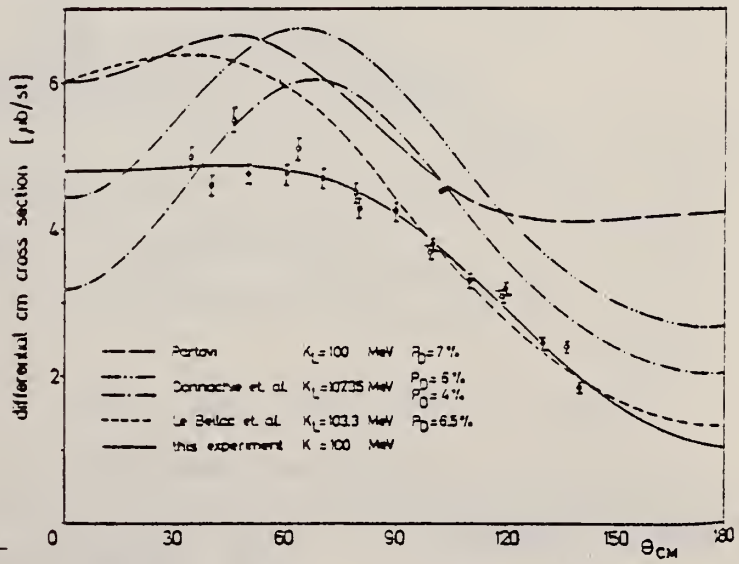

Fig. 14. Angular distribution at photon lab. energy $K_L = 100$ MeV

(continued)

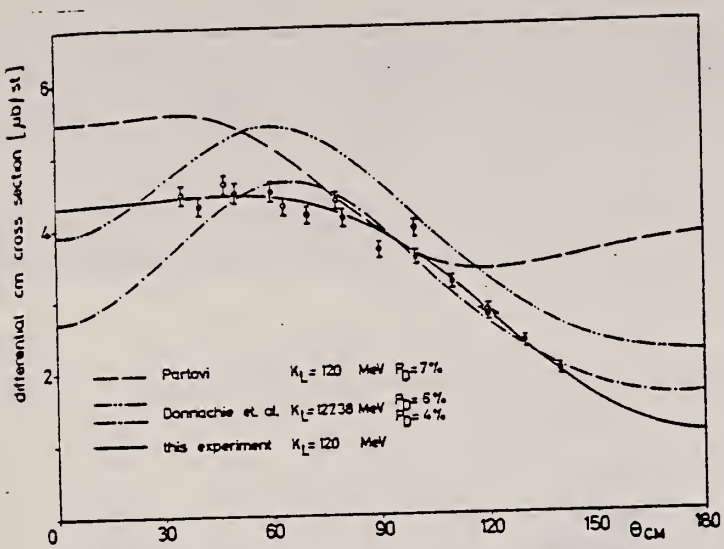

Fig. 15. Angular distribution at photon lab. energy $K_L = 120$ MeV

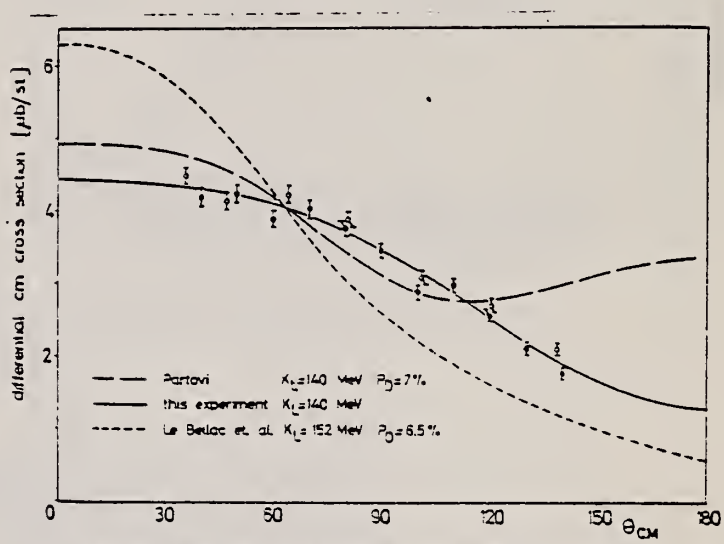

Fig. 16. Angular distribution at photon lab. energy $K_L = 140$ MeV

(continued)

REF. R. Kose, W. Paul, K. Stockhorst and K. H. Kissler
Z. Physik 202, 364 (1967)

EL EM. SYM.	A	Z
H	2	1

METHOD

REF. NO. 67 Ko 3

egf

REACTION	RESULT	EXCITATION ENERGY	SOURCE		DETECTOR		ANGLE
			TYPE	RANGE	TYPE	RANGE	

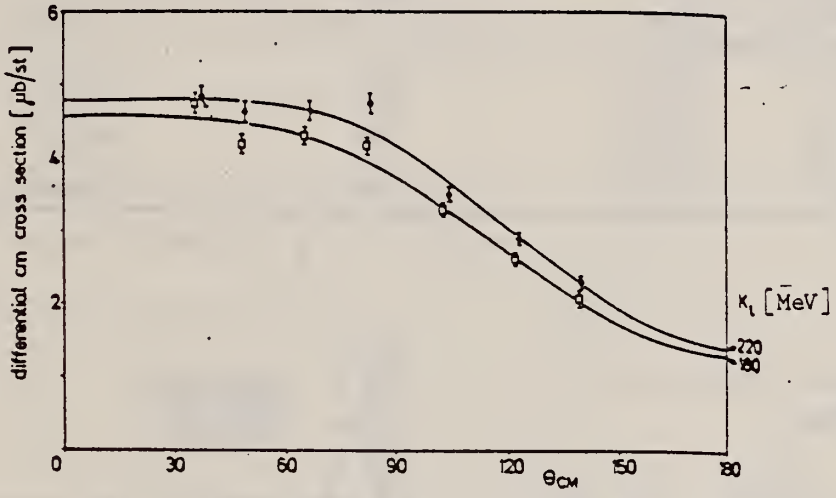

Fig. 17. Angular distributions at photon lab. energies $K_L = 180$, 220 MeV

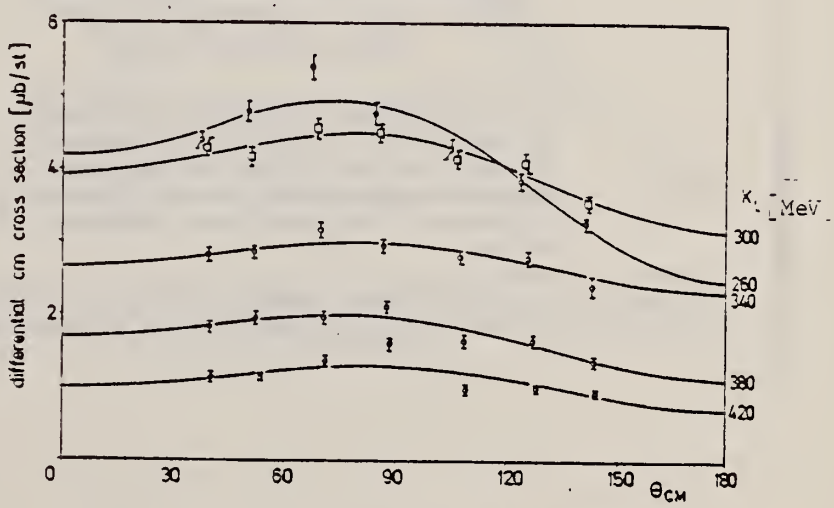

Fig. 18. Angular distributions at photon lab. energies $K_L = 260$, 300, 340, 380, 420 MeV

REF. R. E. Rand, R. F. Frosch, C. E. Littig, and M. R. Yearian
Phys. Rev. Letters 18, 469 (1967)

ELEM. SYM.	A	Z
H	2	1

METHOD: Linac

REF. NO.: 67 Ra 1 JDM

REACTION	RESULT	EXCITATION ENERGY	SOURCE TYPE	SOURCE RANGE	DETECTOR TYPE	DETECTOR RANGE	ANGLE
E,E/	ABX	0-8	D	250-370	MAG-D		180

E_0 (MeV)	q^2 (F^{-2})	σ/σ_J	$d\sigma_J/db$ [10^{-36} cm^2 sr^{-1} (MeV/c)$^{-1}$]	σ_{el} (10^{-36} cm^2/sr)
250	5.07	1.08±0.07	50.4	83±9
275	6.01	1.25±0.08	25.9	56±7
300	7.01	1.20±0.35	13.4	•••
325	8.06	1.38±0.12	6.36	24.5±2.6
350	9.17	1.62±0.18	3.49	13.9±2.4
370	10.09	2.17±0.20	2.01	6.9±1.4

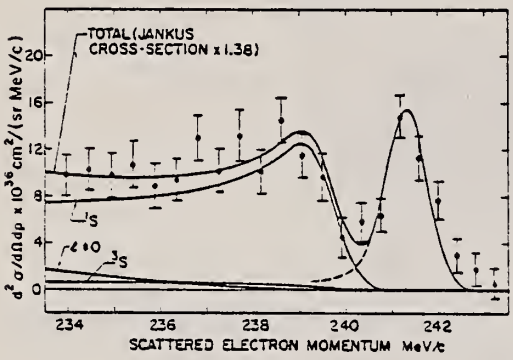

FIG. 1. Differential cross section for 325-MeV electrons scattered at 180° from the deuteron. The modified Jankus (see text) calculations for the separate ^1S, ^3S, and $l > 0$ final states are shown with experimental resolution and radiation effects folded in. These cross sections and the folded elastic peak are normalized to the data.

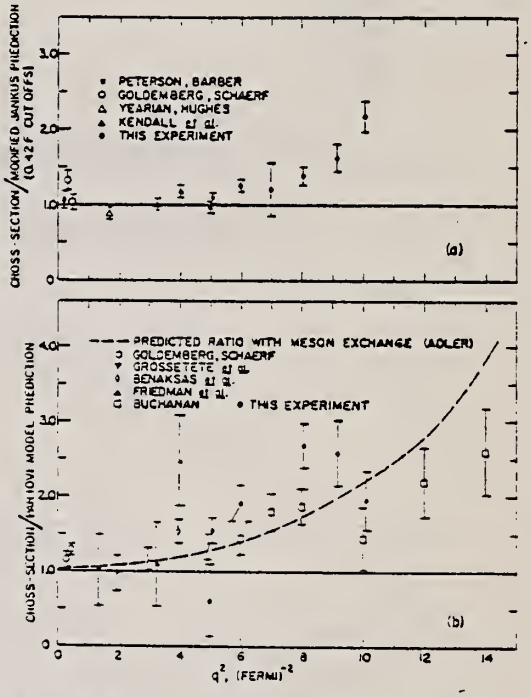

FIG 2. (a) Inelastic (mainly $M1$) e-D experimental cross section normalized to the modified Jankus theory (see text) using 0.42-F hard cores in initial and final states. (b) Magnetic elastic e-D experimental cross sections normalized to the Partovi-model predictions. Also shown is the calculation of Adler and Drell including the $\rho\pi$ exchange current.

REF.

J. Tudoric-Ghemo
Nucl. Phys. A92, 233 (1967)

ELEM. SYM.	A	Z
H	2	1

METHOD

REF. NO.	
67 Tu 1	JDM

REACTION	RESULT	EXCITATION ENERGY	SOURCE		DETECTOR		ANGLE
			TYPE	RANGE	TYPE	RANGE	
N,G	ABX	9	D	14	TEL-D	5-9	0
		(9.4)					

$\sigma_{cap} = 30.6 \pm 1.8$ μb

Deuteron detected in forward direction. Angular distribution of γ-rays determined from energy distribution of deuterons.

$$\frac{d\sigma_{ph}}{d\Omega} = a + (b + d\cos\theta)\sin^2\theta$$

Isotropy Ratio $a/b = 0.08 \pm 0.06$

Asymmetry Parameter $\frac{d}{b} = 0.12 \pm 0.09$

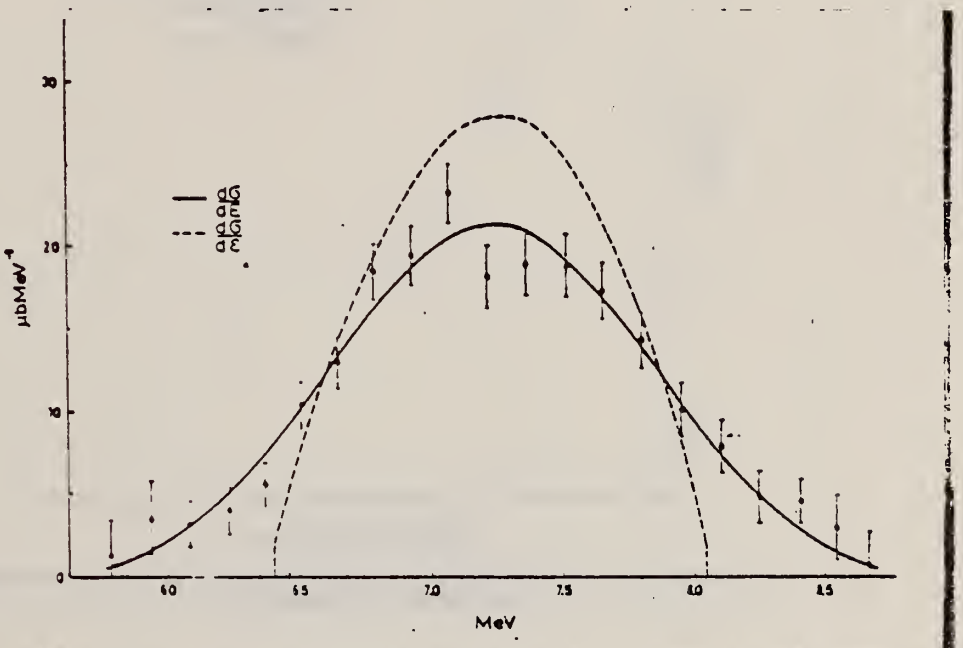

Fig. 4. The measured energy distributions of deuterons from the H(n, d)γ reaction with the results of fitting the theoretical expression to the experimental points. The dashed curve is the theoretical differential cross section. The solid curve represents the theoretical distribution folded with the detector response curve (see the text).

(continued)

REF. J. Tudoric-Ghemo
Nucl. Phys. A92, 233 (1967)

ELEM. SYM.	A	Z
H	2	1

METHOD

REF. NO. 67 Tu 1

JDM

REACTION	RESULT	EXCITATION ENERGY	SOURCE		DETECTOR		ANGLE
			TYPE	RANGE	TYPE	RANGE	

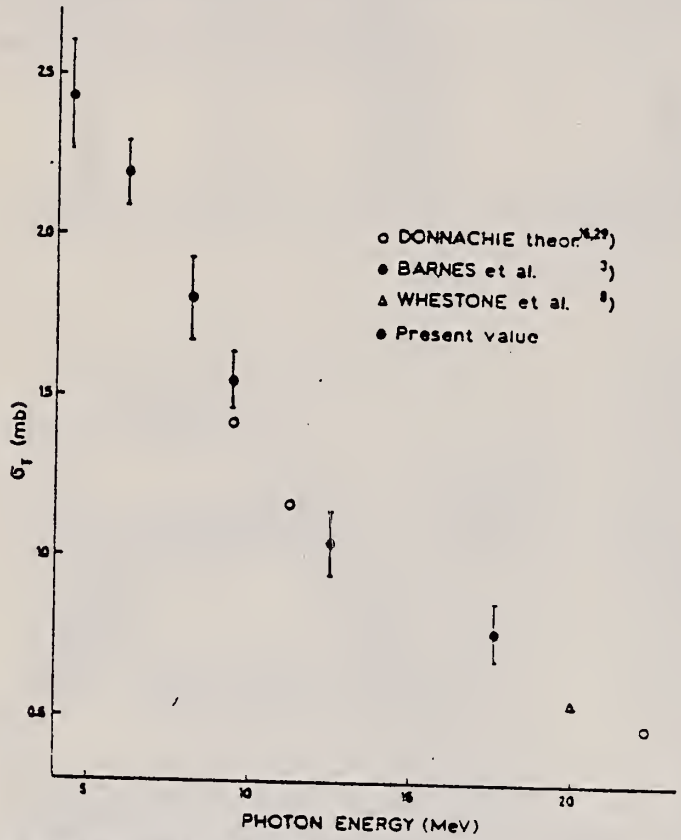

Fig. 5. The theoretical results of Donnachie and the total photodisintegration cross section measurements compared to the present value.

REF. P. M. Tutakin
J. Nucl. Phys. (USSR) 5, 701 (1967)
Sov. J. Nucl. Phys. 5, 497 (1967)

ELEM. SYM.	A	Z
H	2	1

METHOD

REF. NO. 67 Tu 2 HMG

REACTION	RESULT	EXCITATION ENERGY	SOURCE		DETECTOR		ANGLE
			TYPE	RANGE	TYPE	RANGE	
G,P	NOX	9	D	9	EMU		DST
				(8.719)			
				(8.721)			

$$\frac{d\sigma}{d\Omega} = a(1+\beta_1'\cos\theta) + b\sin^2\theta(1+\beta_2'\cos\theta)$$

β_m^0	L_μ	Number of tracks	a/b
15	$L \pm 5$	468	0.088±0.032
15	$L \pm 10$	631	0.099±0.019
30	$L \pm 5$	848	0.096±0.030
30	$L \pm 10$	1189	0.112±0.016

REF. J. Buon, V. Gracco, J. Lefrancois, P. Lehmann, B. Merkel and Ph. Roy
Phys. Letters 26B, 595 (1968)

ELEM. SYM.	A	Z
H	2	1

METHOD

REF. NO. 68 Bu 2 EGF

REACTION	RESULT	EXCITATION ENERGY	SOURCE		DETECTOR		ANGLE
			TYPE	RANGE	TYPE	RANGE	
G,P	ABX	140-400	C	400	MAG-D	50-200	DST

$$\frac{d\sigma}{d\Omega} = a + b\cos\theta + c\cos^2\theta + d\cos^3\theta$$

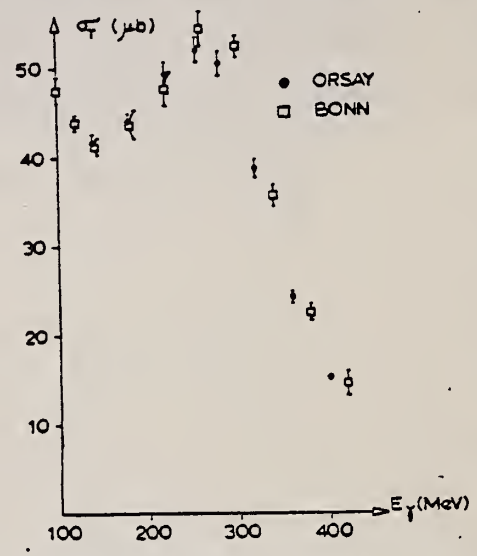

Fig. 3. Total cross section as a function of γ energy. The errors do not include a ± 4% absolute error.

Table 1
Measured center of mass differential cross sections (μb/sr)

E_γ \ θ	30°	55°	70°	90°	110°	130°
100		5.42 ± 0.135				
140	4.00 ± 0.1	4.32 ± 0.11	3.91 ± 0.098	3.48 ± 0.087	2.86 ± 0.071	2.41 ± 0.06
180	4.23 ± 0.105	4.45 ± 0.11	4.17 ± 0.10	3.57 ± 0.089	2.99 ± 0.075	2.53 ± 0.063
220	4.56 ± 0.114	4.85 ± 0.121	4.82 ± 0.12	4.19 ± 0.105	3.54 ± 0.088	2.99 ± 0.075
255	4.64 ± 0.116	5.06 ± 0.128	4.84 ± 0.12	4.49 ± 0.11	3.83 ± 0.096	3.29 ± 0.082
280	4.44 ± 0.11	4.83 ± 0.12	4.75 ± 0.12	4.36 ± 0.11	3.80 ± 0.095	3.24 ± 0.081
320	3.42 ± 0.085	3.62 ± 0.091	3.77 ± 0.094	3.42 ± 0.085	2.86 ± 0.071	2.47 ± 0.061
360	2.04 ± 0.05	2.32 ± 0.058	2.37 ± 0.059	2.15 ± 0.054	1.82 ± 0.045	1.53 ± 0.038
400	1.34 ± 0.033	1.48 ± 0.036	1.45 ± 0.036	1.34 ± 0.033	1.08 ± 0.03	0.94 ± 0.03

Table 2
Results of the fit using formula (1) (μb/sr) and corresponding values for the total cross section (μb)

E_γ	a	b	c	d	σ_T
140	3.78 ± 0.06	1.55 ± 0.19	-0.94 ± 0.14	-0.75 ± 0.35	41.6 ± 1
180	3.98 ± 0.06	1.62 ± 0.2	-0.973 ± 0.15	-0.796 ± 0.36	43.9 ± 0.8
220	4.61 ± 0.07	1.36 ± 0.23	-1.37 ± 0.17	-0.54 ± 0.41	49.3 ± 1.4
255	4.82 ± 0.075	1.07 ± 0.24	-1.38 ± 0.18	-0.32 ± 0.43	51.9 ± 1.4
280	4.70 ± 0.073	0.857 ± 0.24	-1.38 ± 0.18	-0.15 ± 0.42	50.4 ± 1.4
320	3.65 ± 0.056	0.56 ± 0.18	-1.15 ± 0.13	-0.05 ± 0.32	38.6 ± 1.1
360	2.33 ± 0.04	0.33 ± 0.11	-0.86 ± 0.09	-0.035 ± 0.21	23.9 ± 0.7
400	1.44 ± 0.02	0.25 ± 0.07	-0.49 ± 0.05	-0.015 ± 0.13	15.0 ± 0.4

REF. L. Katz, G. Ricco, T. E. Drake and H. S. Caplan
Phys. Letters 28B, 114 (1968)

ELEM. SYM.	A	Z
H	2	1

METHOD

REF. NO. 68 Ka 2 egf

REACTION	RESULT	EXCITATION ENERGY	SOURCE		DETECTOR		ANGLE
			TYPE	RANGE	TYPE	RANGE	
E,E/	ABX	2-4	D	38-90	MAG	30-90	155

q .35 - .84 fm^{-1}

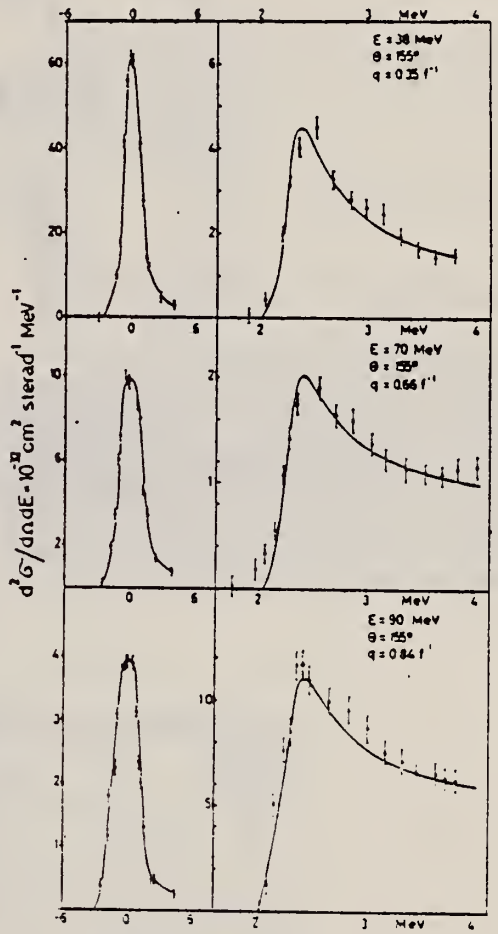

Fig. 1. The elastic peaks and the inelastic cross section obtained at a scattering angle of 155° and incident electron energies of 38, 70 and 90 MeV. The curve through the points in the inelastic region is the theoretical prediction with the experimental resolution taken into account.

REF.

A. M. Smith, S. J. Hall, B. Mann and D. T. Stewart
J. Phys. A. (Proc. Phys. Soc.) 1, 553 (1968)

ELEM. SYM.	A	Z
H	2	1

METHOD

REF. NO.	
68 Sm 1	egf

REACTION	RESULT	EXCITATION ENERGY	SOURCE		DETECTOR		ANGLE
			TYPE	RANGE	TYPE	RANGE	
G,P	ABX	100-320	C	210-330	TEL-D	60-180	DST

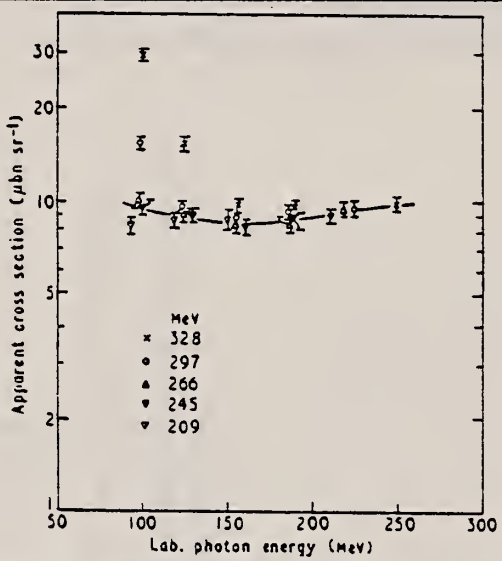

Figure 1. Apparent cross section measured at 40° to the beam for five different bremsstrahlung end-point energies.

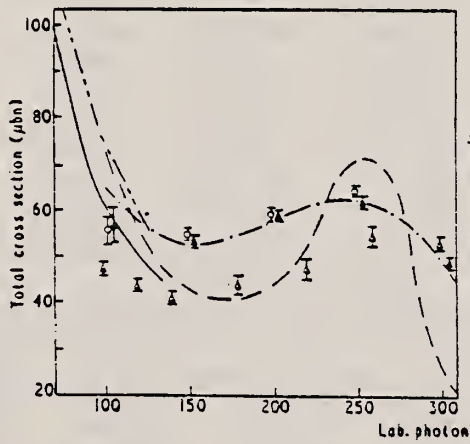

Figure 3. Total cross section. Results: ○ of present experiment; ▲ Keck and Tollestrup 1956; △ Kose *et al.* 1967. Predictions: – – – – Donnachie and O'Donnell 1964; ——— Le Bellac *et al.* 1964; — · — Wilson 1956; — — Pearlstein and Klein 1960.

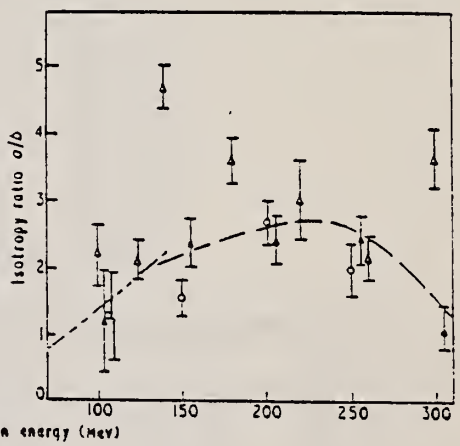

Figure 4. Variation of the isotropy ratio with energy. Results: ○ of present experiments; ▲ Keck and Tollestrup 1956; △ Kose *et al.* 1967. Predictions: – – – – Donnachie and O'Donnell 1964; — — Pearlstein and Klein 1960.

FORM NBS-418
(REV. 7-1-64)
USCOMM-DC 26010-P64

REF. R. L. Anderson, R. Prepost and B. H. Wiik
Phys. Rev. Letters 22, 651 (1969)

EL.EM. SYM.	A	Z
H	2	1

METHOD

REF. NO. 69 An 1 hmg

REACTION	RESULT	EXCITATION ENERGY	SOURCE TYPE	SOURCE RANGE	DETECTOR TYPE	DETECTOR RANGE	ANGLE
G.P	ABX	THR-342	C	222-342	MAG-D		DST

Data taken to test time-reversal invariance in electromagnetic interactions of hadrons.

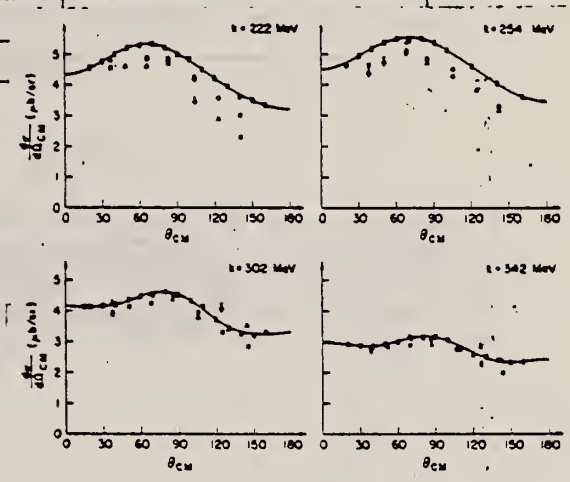

FIG. 2. The c.m. differential cross sections for four photon energies. The solid lines are a least-squares polynomial fit to our data (solid squares) and the four sets of least-squares coefficients are given in Table I. Open triangles, Bonn data at 220, 260, 300, and 340 MeV. Open squares, Orsay data at 220, 255, 302, and 342 MeV. The cross sections at the two last energies were determined by interpolating between the measured values. Typical errors are shown for each energy. The angle plotted is the angle of the recoil proton.

Table I. Coefficients of the polynomial fits.[a]

k MeV	N	a_0 ub/sr.	a_1 ub/sr.	a_2 ub/sr.	a_3 ub/sr.	a_4 ub/sr.	a_5 ub/sr.	σ_T ub	χ^2/Deg. of Freedom
222	3	5.04 ± .02	1.26 ± .05	-1.23 ± .04	-.70 ± .08	--	--	58.2 ± .3	.812
222	4	5.03 ± .02	1.27 ± .05	-1.05 ± .15	-.71 ± .08	-.21 ± .18	--	58.2 ± .8	.810
222	5	5.03 ± .02	1.16 ± .09	-1.09 ± .15	-.19 ± .38	-.17 ± .18	-.50 ± .36	58.2 ± .8	.775
254	3	5.37 ± .02	1.02 ± .05	-1.33 ± .04	-.47 ± .08	--	--	61.9 ± .3	.960
254	4	5.34 ± .02	1.02 ± .05	-1.07 ± .15	-.48 ± .08	-.30 ± .16	--	61.9 ± .8	.725
254	5	5.34 ± .02	.92 ± .10	-1.07 ± .15	-.02 ± .40	-.31 ± .16	-.42 ± .36	61.9 ± .8	.673
302	3	4.39 ± .02	.76 ± .06	-.93 ± .04	-.26 ± .08	--	--	51.3 ± .3	6.35
302	4	4.52 ± .03	.84 ± .06	-2.06 ± .15	-.42 ± .08	1.26 ± .16	--	51.3 ± .8	.988
302	5	4.53 ± .03	.71 ± .10	-2.15 ± .16	+.18 ± .39	1.37 ± .17	-.55 ± .34	51.3 ± .9	.637
342	3	3.04 ± .02	.35 ± .04	-.64 ± .04	-.007 ± .066	--	--	35.6 ± .3	7.15
342	4	3.13 ± .02	.41 ± .04	-1.52 ± .12	-.14 ± .07	1.07 ± .14	--	35.7 ± .7	1.32
342	5	3.13 ± .02	.44 ± .08	-1.53 ± .12	-.31 ± .31	1.08 ± .14	.17 ± .28	35.7 ± .7	1.34

[a] In addition to the quoted errors there is an overall normalization uncertainty of 7%.

REF.

J. P. Didelez, H. Langevin-Joliot, G. Duhamel, L. Marcus and P. Narboni
Nucl. Phys. A139, 69 (1969)

EL.EM. SYM.	A	Z
H	2	1

METHOD

REF. NO.	
69 Di 2	egf

REACTION	RESULT	EXCITATION ENERGY	SOURCE		DETECTOR		ANGLE
			TYPE	RANGE	TYPE	RANGE	
P,G	ABX	77	D	156	MAG-D		DST

QUASI-FREE N

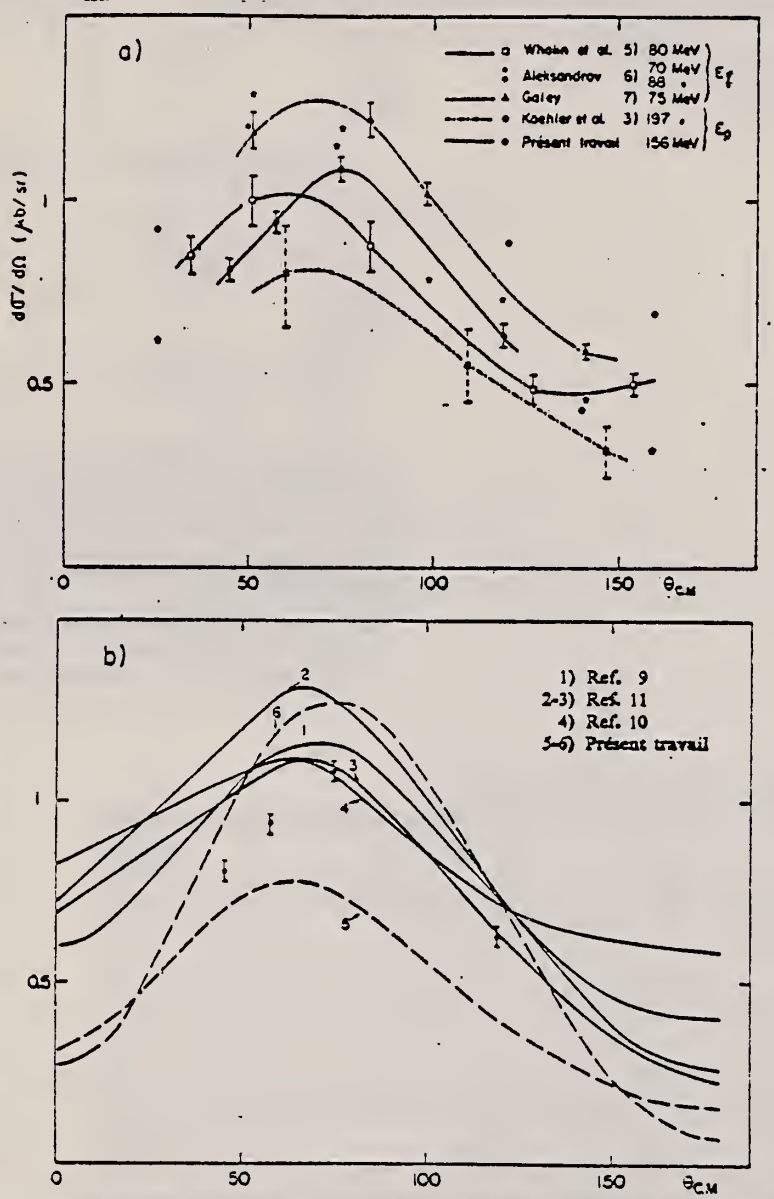

Fig. 4. (a) Distribution angulaire de la capture radiative dans le centre de masse p–n. Les courbes sont un tracé destiné à faciliter la compréhension. (b) Distribution angulaire théorique. 1) Donnachie *et al.* (courbe moyenne sur différentes solutions avec 6 % d'état D), 2) Le Bellac *et al.* (Born-relativiste), 3) Le Bellac *et al.* (Déphasage), 4) Partovi, 5) Born non relativiste 0 % d'état D, 6) Born non relativiste 5 % d'état D.

(continued)

TABLEAU I

Sections efficaces différentielles dans le laboratoire et dans le c.m. de la réaction $D(p,\gamma)P_{pp}$ D à 156 MeV

θ_γ(lab)	$(d\sigma/d\Omega)_{lab}$ (μb)	θ_γ(c.m.)	$(d\sigma/d\Omega)_{c.m.}$ (μb)
35°	1.25±0.04	45.43	0.81±0.02
45°	1.34±0.04	57.61	0.94±0.02
60°	1.35±0.04	74.94	1.08±0.03
105°	0.51±0.05	119.95	0.63±0.03

Abstract: The radiative capture of 156 MeV protons by neutrons has been investigated using liquid deuterium as a "quasi-free" neutron target. The angular and momentum distributions of deuterons measured in coincidence with the emitted γ-ray are in agreement with the distributions calculated in the impulse approximation. Photon differential cross sections are given for four angles and are found to be reduced by a factor 0.85±0.20 from the values inferred from photodisintegration data. Experimental cross sections are compared with theoretical predictions for free capture.

REF.

R. Kose, B. Martin, R. Runkel, H. Wahlen and K. H. Kissler
Z. Physik 220, 305 (1969)

ELEM. SYM.	A	Z
H	2	1

METHOD

REF. NO.	
69 Ko 1	egf

REACTION	RESULT	EXCITATION ENERGY	SOURCE		DETECTOR		ANGLE
			TYPE	RANGE	TYPE	RANGE	
$G,P	NOX	282-405	C	500	TEL-D	280-420	DST
							(60,80)

PROTON POLARIZATION

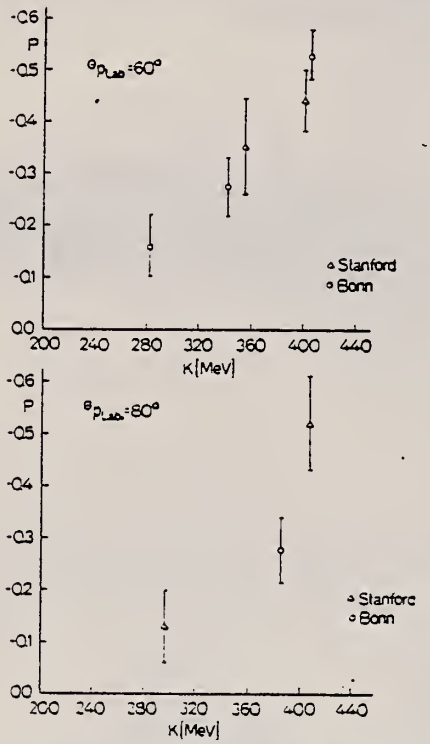

Fig. 7. Polarization of the proton at 60° lab. and 80° lab. as a function of photon energy

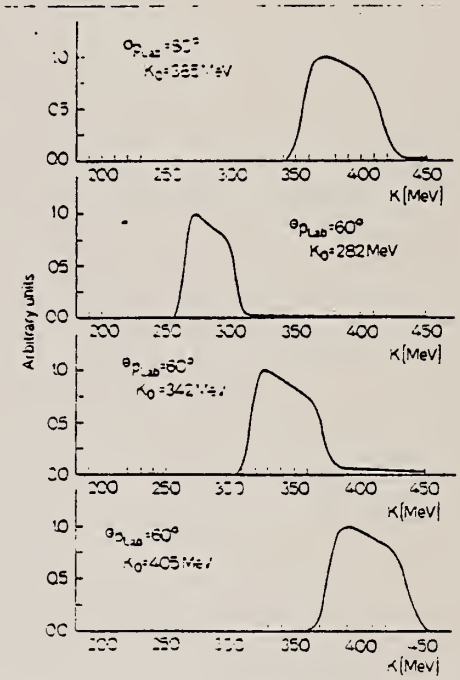

Fig. 2. Photon energy resolution for the different measurements

Table 5

$\theta_{P\,Lab}$	K [MeV]	$\theta_{P_{CM}}$	$\varepsilon \cdot 100$	$\bar{A} \cdot 100$	$P \cdot 100$
60°	282 ± 20	73.9°	− 6.35 ± 2.3	40.8	−15.6 ± 5.6
60°	342 ± 28	75.3°	−15.0 ± 3.0	57.2	−26.2 ± 5.2
60°	405 ± 30	76.7°	−35.4 ± 3.3	69.2	−51.2 ± 4.8
80°	385 ± 30	98.2°	−14.4 ± 3.2	54.2	−26.6 ± 5.9

REF.

D. I. Sober, D. G. Cassel, A. J. Sadoff, K. W. Chen and P. A. Crean
Phys. Rev. Letters 22, 430 (1969)

EL EM. SYM.	A	Z
H	2	1

METHOD

REF. NO.	
69 So 1	hmg

REACTION	RESULT	EXCITATION ENERGY	SOURCE		DETECTOR		ANGLE
			TYPE	RANGE	TYPE	RANGE	
G,N	ABX	230-330	C	350,450	SPK-D		DST

Data taken to test time-reversal invariance in electromagnetic interactions of hadrons.

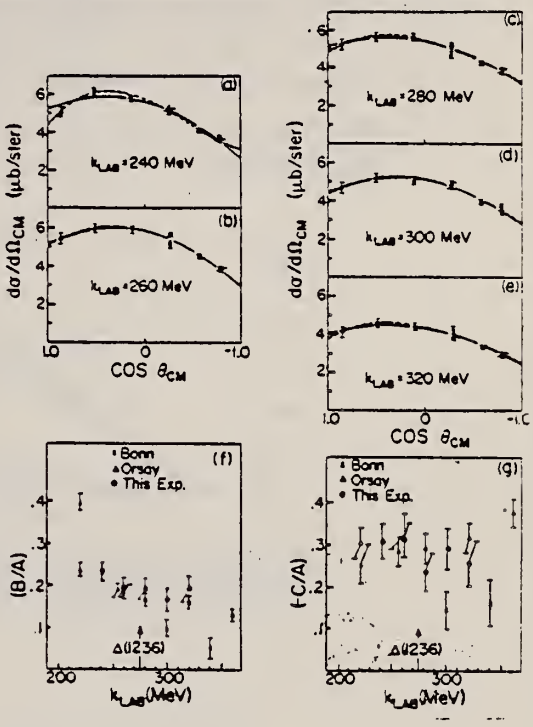

FIG. 2. (a)–(e) $\gamma+d\rightarrow\pi+p$ angular distributions versus $\theta_{c.m.}$ at various incident energies. The circles represent data taken at 350-MeV synchrotron energy, the squares 450-MeV. The solid curve is a fit with the form $d\sigma/d\Omega=A+B\cos\theta_{c.m.}+C\cos\theta_{c.m.}$. The dashed curve is a fit including the term $D\cos^3\theta_{c.m.}$. (f), (g) Normalization-independent ratios B/A and $-C/A$ versus photon energy for least-squares fits with the form $d\theta/d\Omega=A+B\cos\theta_{c.m.}+C\cos^2\theta_{c.m.}$. The Bonn and Orsay points are fits to the data of Refs. 4 and 5, respectively. The errors include the correlations between coefficients.

Table I. Cross sections and angular distribution coefficients for $\gamma+d\rightarrow\pi+p$. The errors listed are statistical only. Additional systematic errors totaled a maximum of 5.4%.

Photon Energy (MeV)	$E^{tot}_{c.m.}$ (MeV)	$\left(\frac{d\sigma}{d\Omega}\right)_{c.m.}$ (μb/ster) Laboratory Angle, θ_L						Coefficients of Least Square Fits[b]				
		23.8°	47.5°	68.2°	90.0°[a]	110.2°	130.0°[a]	A	B	C	B/A	C/A
230 - 250	2102	5.45 ±.30	6.59 ±.22	6.22 ±.20	5.60 ±.20	4.42 ±.12	3.89 ±.09	6.03 ±.10	1.41 ±.14	-1.86 ±.26	.234 ±.023	-.309 ±.039
250 - 270	2120	5.83 ±.31	6.38 ±.24	6.33 ±.21	5.88 ±.12	4.83 ±.13	4.12 ±.09	6.25 ±.11	1.23 ±.15	-1.96 ±.27	.197 ±.023	-.313 ±.039
270 - 290	2137	5.62 ±.31	6.05 ±.26	6.05 ±.22	5.38 ±.13	4.58 ±.13	4.12 ±.10	5.79 ±.12	1.13 ±.15	-1.37 ±.28	.193 ±.026	-.237 ±.044
290 - 310	2155	5.04 ±.31	5.60 ±.25	5.45 ±.22	5.19 ±.13	4.26 ±.14	3.79 ±.10	5.48 ±.12	0.91 ±.15	-1.61 ±.28	.167 ±.027	-.293 ±.046
310 - 330	2172	4.41 ±.30	4.93 ±.26	4.74 ±.22	4.30 ±.13	3.61 ±.13	3.21 ±.10	4.65 ±.12	0.90 ±.15	-1.20 ±.26	.193 ±.031	-.257 ±.052

[a] Combined cross sections measured at 350- and 450-MeV synchrotron energy. Other angles were measured at 350 MeV only.

[b] Assuming $(d\theta/d\Omega)_{c.m.}=A+B\cos\theta_{c.m.}+C\cos^2\theta_{c.m.}$. The errors in B/A and C/A include correlations between coefficients.

REF. D. Harder, R. Mehling, A. C. England
Phys. Lett. 32B, 610 (1970)

ELEM. SYM.	A	Z
H	2	1

METHOD

REF. NO. 70 Ha 2 egf

REACTION	RESULT	EXCITATION ENERGY	SOURCE		DETECTOR		ANGLE
			TYPE	RANGE	TYPE	RANGE	
E,N	ABX	5- 18	D	5- 18	BF3-I		4PI

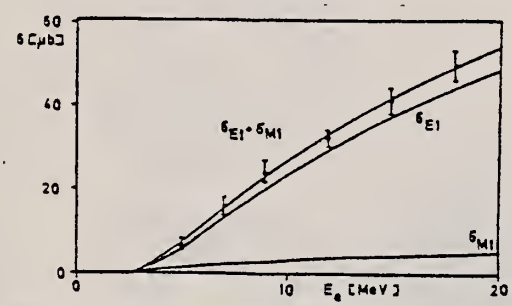

Fig. 3. Cross section of the D(e, e'n)H process. Full curves: theory of Guth and Mullin [4], evaluated for deuterium. Open circles: present experiment.

[4] E. Guth and C. J. Mullin, Phys. Rev. 76, 234 (1949)

REF. A. Ito, R. Loe, E. C. Loh, A. Ramanauskas, D. Ritchie, W. Schmidt
Phys. Rev. Letters 24, 687 (1970)

ELEM. SYM.	A	Z
H	2	1

METHOD

REF. NO. 70 It 1 hmg

REACTION	RESULT	EXCITATION ENERGY	SOURCE		DETECTOR		ANGLE
			TYPE	RANGE	TYPE	RANGE	
G,PI+	RLX	600-999	C	600-999	SPK-I		4PI
		(600-1700)		(600-1700)			
G,PI-	RLX	600-999	C	600-999	SPK-I		4PI
		(600-1700)		(600-1700)			

Detected pions. $R = \gamma(d,2P)/\gamma(d,2N)$ 999=1700 MEV

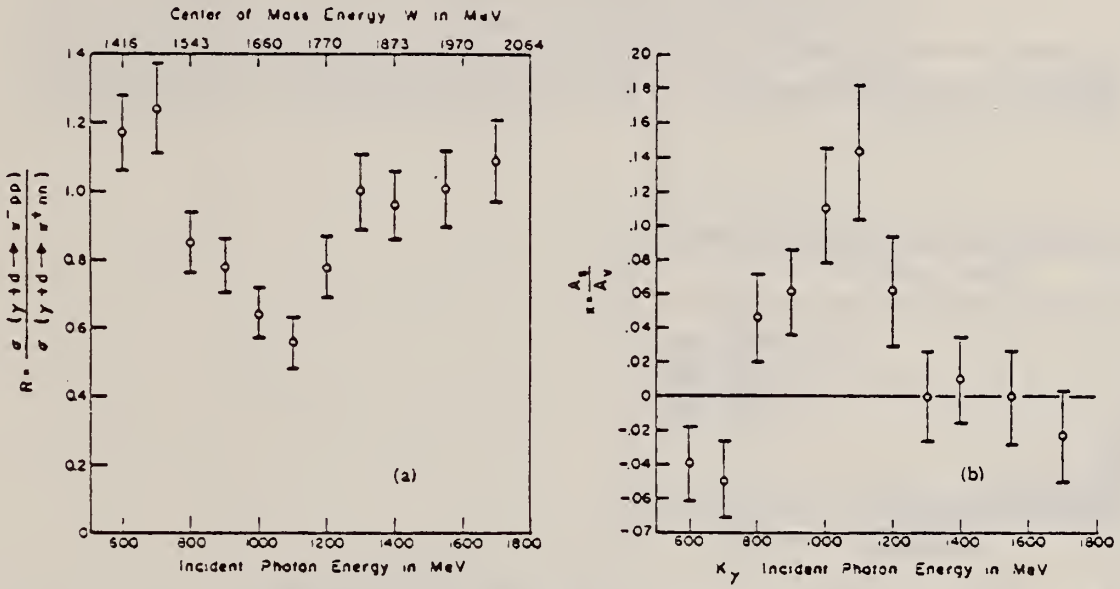

FIG. 2. (a) Ratio $\sigma(\gamma+d\to\pi^-pp)/\sigma(\gamma+d\to\pi^+nn)$ as a function of incident photon energy. (b) Ratio of $\mathrm{Re}A_V$ to $\mathrm{Re}A_S$ as a function of incident photon energy.

Table I. Ratio $R=\sigma(\gamma+d\to\pi^-pp)/\sigma(\gamma+d\to\pi^+nn)$ as a function of incident photon energy together with various corrections.

K_γ (MeV)	π^+ deadtime correction	π^+ beamspot shift correction	π^+ nuclear absorption correction	π^- deadtime correction	π^- beamspot shift correction	π^- nuclear absorption correction	$R=\frac{\sigma(\gamma d\to\pi^-pp)}{\sigma(\gamma d\to\pi^+nn)}_{\vartheta=0^\circ}$	Combined statistical and systematic error(%)
600	1.045	0.981	1.153(±0.016)	1.058	1.019	1.175(±0.019)	1.17±0.11	9.6
700	1.043	0.983	1.154(±0.016)	1.052	1.014	1.175(±0.019)	1.24±0.13	10.4
800	1.039	0.989	1.156(±0.016)	1.047	1.011	1.181(±0.020)	0.85±0.09	10.4
900	1.034	0.992	1.171(±0.018)	1.032	1.009	1.201(±0.022)	0.78±0.08	9.7
1000	1.030	0.993	1.190(±0.020)	1.027	1.007	1.220(±0.023)	0.64±0.07	11.0
1100	1.026	0.995	1.197(±0.022)	1.025	1.006	1.222(±0.023)	0.56±0.07	12.1
1200	1.021	0.995	1.195(±0.022)	1.020	1.005	1.208(±0.022)	0.78±0.09	11.7
1300	1.021	0.996	1.198(±0.022)	1.023	1.004	1.199(±0.022)	1.00±0.11	11.1
1400	1.019	0.997	1.198(±0.022)	1.017	1.003	1.202(±0.022)	0.96±0.10	10.2
1550	1.016	0.998	1.212(±0.023)	1.013	1.002	1.207(±0.022)	1.01±0.11	10.9
1700	1.009	0.998	1.213(±0.023)	1.010	1.002	1.207(±0.022)	1.09±0.12	11.4

REF. J. W. Jury, J. S. Hewitt, and K. G. McNeill
Can. J. Phys. 48, 1635 (1970)

ELEM. SYM.	A	Z
H	2	1

METHOD

REF. NO. 70 Ju 1 egf

REACTION	RESULT	EXCITATION ENERGY	SOURCE		DETECTOR		ANGLE
			TYPE	RANGE	TYPE	RANGE	
G,N	NOX	17-30	C	23-30	TOF-D		DST

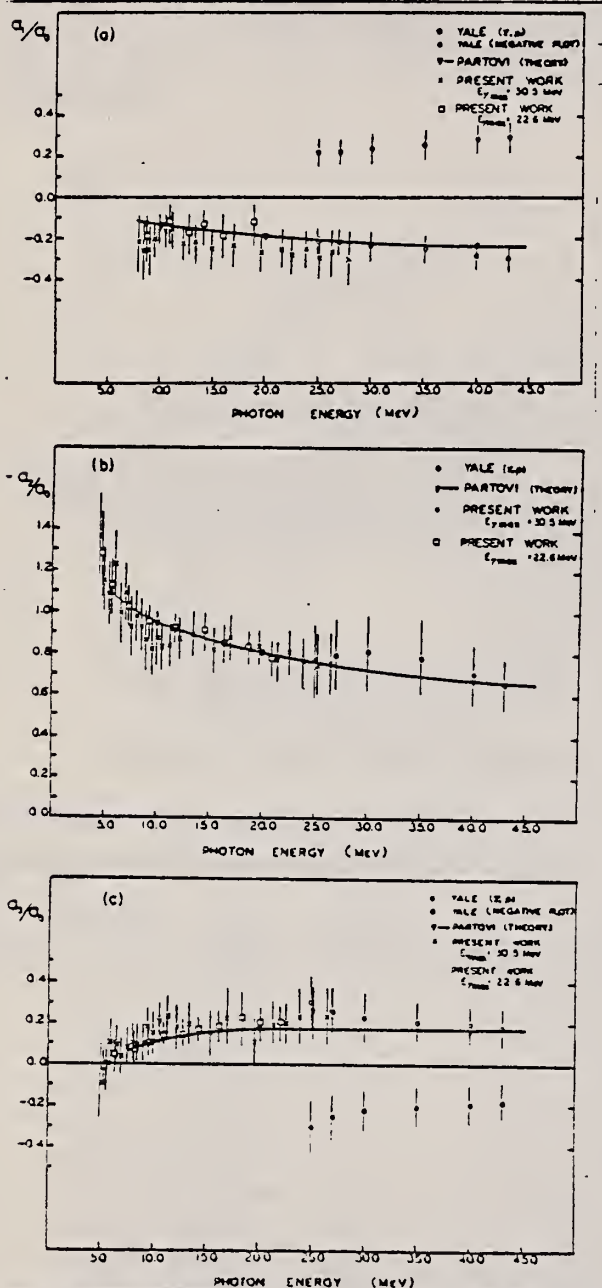

FIG. 2. Photoneutron angular distribution coefficients for the $^2H(\gamma,n)^1H$ reaction. The normalized coefficients a_1/a_0, $-a_2/a_0$, and a_3/a_0 are shown as functions of the incident photon energy in (*a*), (*b*), and (*c*) respectively.

REF. G. Ricco, T. E. Drake, L. Katz, and H. S. Caplan
Phys. Rev. C 1, 391 (1970)

ELEM. SYM.	A	Z
H	2	1

METHOD

REF. NO. 70 Ri 1 hmg

REACTION	RESULT	EXCITATION ENERGY	SOURCE		DETECTOR		ANGLE
			TYPE	RANGE	TYPE	RANGE	
E,E/	ABX	0-4	D	38-90	MAG-D	34-90	DST
							(125,140,
							155)

The electrodisintegration of the deuteron near threshold has been investigated by inelastic electron scattering at momentum transfers $q = 0.35$ F^{-1} and $q = 0.66$ F^{-1} and scattering angles $\theta = 125°$, 140°, and 155°. The longitudinal and transverse matrix elements to the final $^1S_0$ and $^3S_1$ states have been compared with the Jankus-Durand theory using repulsive-core wave functions. The repulsive-core parameter, corresponding to a radius of about 0.2 F, has been adjusted to fit the elastic deuteron form factors up to $q = 6$ F^{-1}. The computed inelastic cross sections give a satisfactory description of the existing data in the whole momentum-transfer range experimentally investigated: (0.35 F$^{-1} \leq q \leq 3$ F^{-1}).

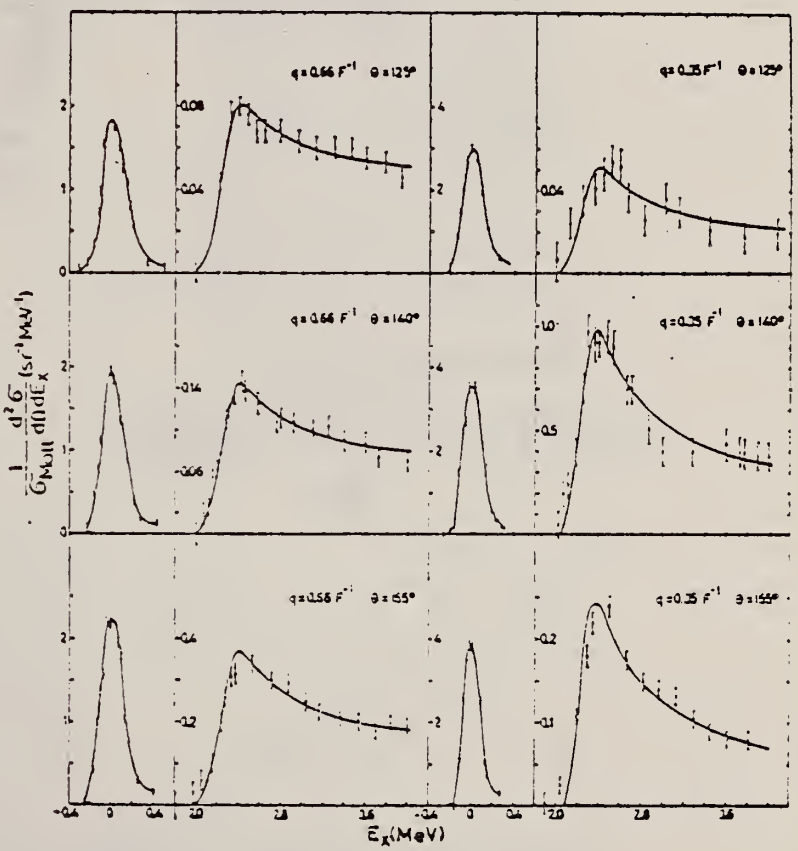

FIG. 2. The elastic peaks and the inelastic differential form factors obtained at $q = 0.34$ F^{-1} and $q = 0.66$ F^{-1} and $\theta = 125°$, 140°, 155°. The curve through the points in the inelastic region is the theoretical prediction with the experimental resolution taken into account.

(continued)

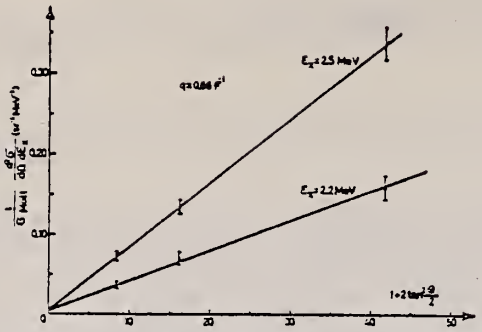

FIG. 3. Angular distribution of the electrons inelastically scattered at $q=0.66$ F^{-1} and excitation energy E_x.

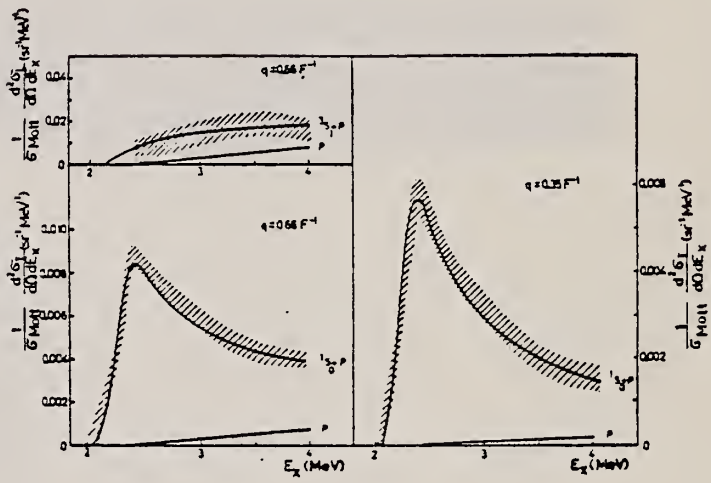

FIG. 4. Longitudinal and transverse differential inelastic form factors at $q=0.35$ F^{-1} and $q=0.66$ F^{-1}. The shaded area represents the uncertainty on the measured form factors, the solid curve is the theoretical prediction.

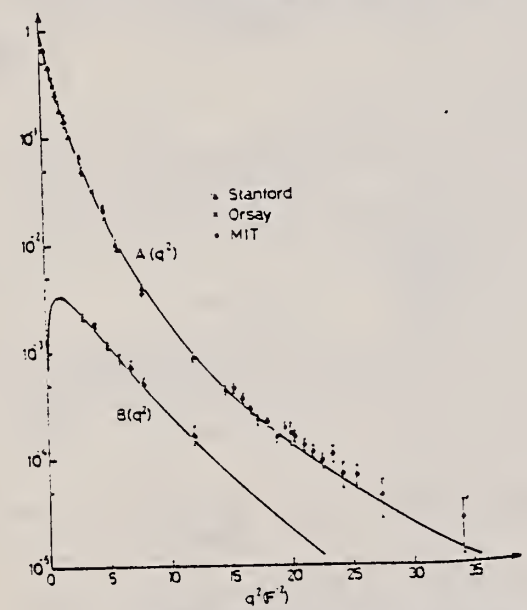

FIG. 5. Longitudinal $A(q^2)$ and transverse $B(q^2)$ elastic deuteron form factors. The curves have been calculated using Hulthén repulsive-core wave functions with the parameters of Table II (P_D=6.0%). Stanford data: Refs. 18–21. Orsay data: Refs. 17 and 22. MIT data: Ref. 23.

REF. P. E. Scheffler and P. L. Walden
Phys. Rev. Letters 24, 952 (1970)

ELEM. SYM.	A	Z
H	2	1

METHOD

REF. NO.	
70 Sc 2	hmg

REACTION	RESULT	EXCITATION ENERGY	SOURCE		DETECTOR		ANGLE
			TYPE	RANGE	TYPE	RANGE	
G,PI-	ABX	600-999	C	600-999	MAG-D		DST
		(600-1250)		(600-1250)			

999=1.2 GEV, PI DET

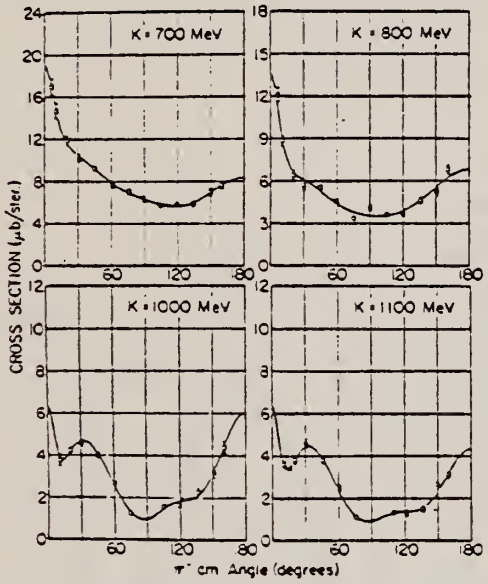

FIG. 1. Angular distributions for π^- photoproduction from deuterium. The solid lines are Moravcsik fits to the data.

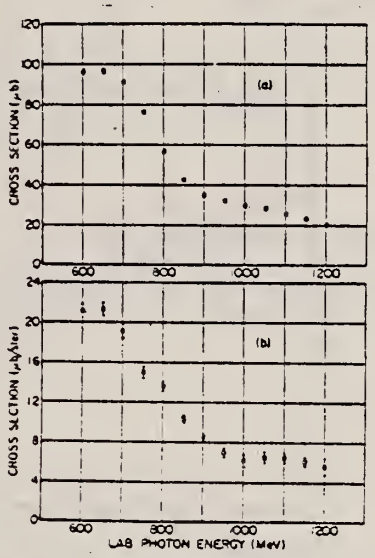

FIG. 2. π^- photoproduction cross sections as a function of energy. (a) Total cross section, (b) $\theta_\pi = 0°$ c.m. cross section.

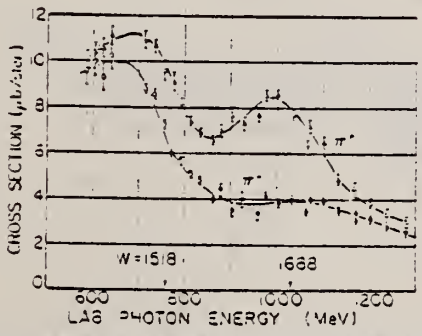

FIG. 3. Energy dependence of the differential cross section at 45° for π^- and π^+ photoproduction from deuterium.

REF. Y. M. Shin, J. A. Rawlins, W. Buss, A. O. Evwaraye
Nucl. Phys. A154, 482 (1970)

ELEM. SYM.	A	Z
H	2	1

METHOD

REF. NO.	
70 Sh 3	egf

REACTION	RESULT	EXCITATION ENERGY	SOURCE		DETECTOR		ANGLE
			TYPE	RANGE	TYPE	RANGE	
G,N	NOX	10-95	C	125	TOF-D	5-45	DST

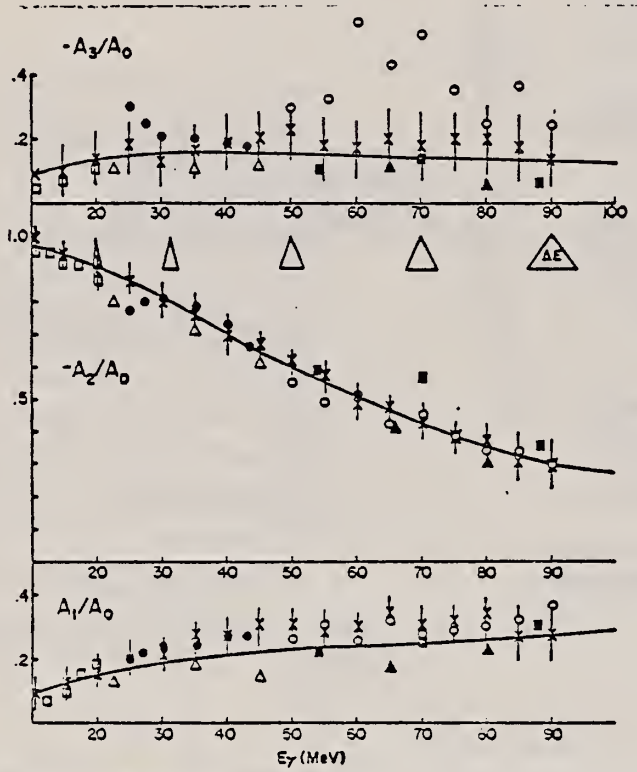

Fig. 5. Coefficients of Legendre polynomials. The solid curve is the prediction of Partovi's calculation in his approximation I. The experimental values are shown as follows: crosses for the present work; solid curves for Weissman and Schultz; solid squares for Alexandrov *et al.*; open circles for Galey; open triangles for Allen, Jr.; solid triangles for Whalin *et al.*; open squares for Whestone and Halpern; cross and circles for our 83 MeV data.

(continued)

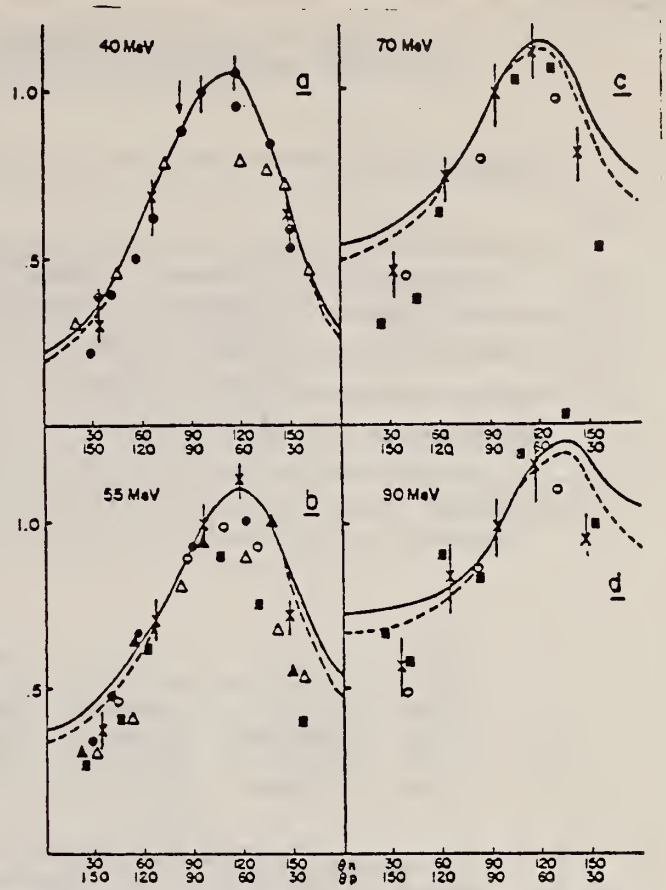

Fig. 8. Comparison of angular distributions at 40, 55, 70 and 90 MeV. Symbols used ar
in fig. 5.

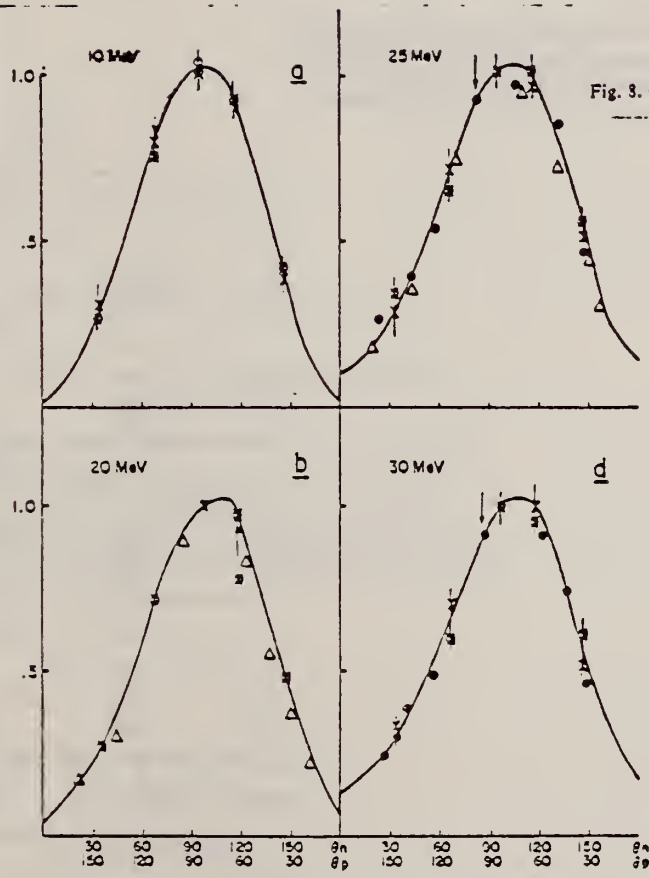

Fig. 7. Comparison of angular distributions at 10, 20, 25 and 30 MeV. Symbols used are the same as in fig. 5. The upward arrow in *b* indicates normalization of 112° point. Downward arrows in the figure indicate the normalization point of the result of the Yale group.

REF. D. F. Bartlett, C. E. Friedberg, P. E. Goldhagen, K. Goulianos
Phys. Rev. Letters 27, 881 (1971)

ELEM. SYM.	A	Z
H	2	1

METHOD

REF. NO. 71 Ba 3 hmg

REACTION	RESULT	EXCITATION ENERGY	SOURCE		DETECTOR		ANGLE
			TYPE	RANGE	TYPE	RANGE	
N,G	DST	239-378	D	475-750	SPK-I		DST

D AND G COINC

Table. Center-of-mass angular distribution is given by $A_0 + A_1 P_1(\cos\theta) + A_2 P_2(\cos\theta)$ where $A_0 = 1$.

T_n (MeV)	A_1	A_2	χ^2/N
475	0.14 ± 0.02	−0.30 ± 0.04	8.2/6
560	0.09 ± 0.02	−0.17 ± 0.03	4.9/6
625	0.15 ± 0.03	−0.22 ± 0.04	3.6/6
750	0.21 ± 0.03	−0.17 ± 0.04	4.5/6

The angular distribution for the reaction $n + p \rightarrow d + \gamma$ has been measured at neutron energies of 475, 560, 625, and 750 MeV. Results based on 31 000 events at nine scattering angles are reported and compared with existing data for the inverse reaction, $\gamma + d \rightarrow n + p$. The angular distributions are found to agree, as predicted by time-reversal invariance.

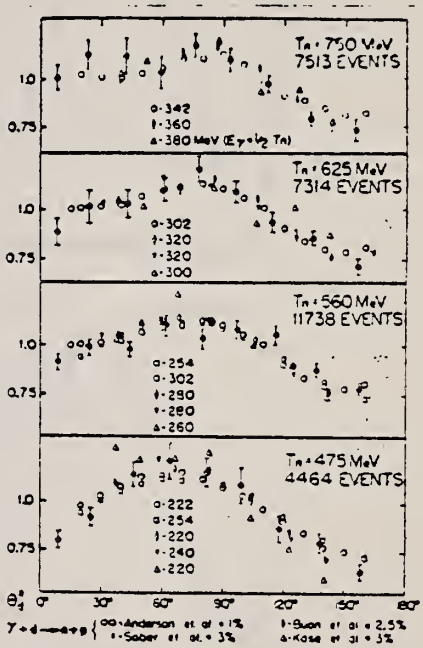

FIG. 3. Angular distributions for $n + p \rightleftharpoons d + \gamma$.

REF. T. Fujii, H. Okuno, S. Orito, H. Sasaki, T. Nozaki, F. Takasaki, K. Takikawa, K. Amako, I. Endo, K. Yoshida, M. Higuchi, M. Sato
Phys. Rev. Letters 26, 1672 (1971)

ELEM. SYM.	A	Z
H	2	1

METHOD

REF. NO.	
71 Fu 3	hmg

REACTION	RESULT	EXCITATION ENERGY	SOURCE		DETECTOR		ANGLE
			TYPE	RANGE	TYPE	RANGE	
G,PI+	ABX	200-999	C	200-999	MAG-D		180
G,PI-	ABX	200-999	C	200-999	MAG-D		180

999 = 1.2 GEV

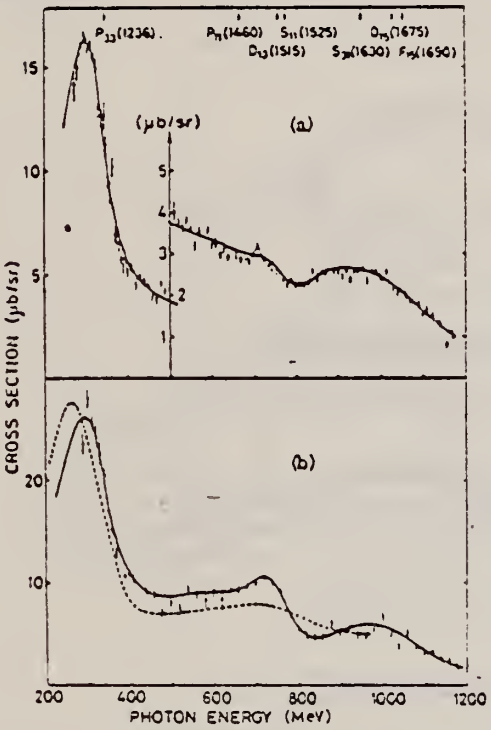

FIG. 1. Differential cross sections at 180° as functions of photon energy (a) for $\gamma + p \rightarrow \pi^0 + n$, and (b) for $\gamma + n \rightarrow \pi^- + p$. The solid curves are the resonance-model fits. The dashed line in (a) is a result of the multichannel analysis for a cusp effect. The dashed line in (b) is calculated with the amplitudes of Walker's analysis.

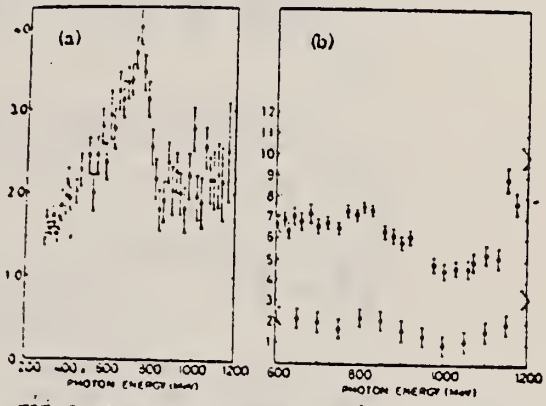

FIG. 2. Energy dependence of the ratios of cross sections. (a) $\sigma_{\gamma p}(180°)/\sigma_{\gamma p}(180°)$; (b) closed circles for $\sigma_{\gamma p}(0°)/\sigma_{\gamma p}(180°)$ and open circles for $\sigma_{\gamma n}(0°)/\sigma_{\gamma n}(180°)$.

REF. B.L. Schrock, R.P. Haddock, J.A. Helland, M.J. Longo, S.S. Wilson, K.K. Young, D. Cheng, V. Perez-Mendez
Phys. Rev. Letters 26, 1659 (1971)

ELEM. SYM.	A	Z
H	2	1

METHOD

REF. NO. 71 Sc 1 hmg

REACTION	RESULT	EXCITATION ENERGY	SOURCE		DETECTOR		ANGLE
			TYPE	RANGE	TYPE	RANGE	
N,G	NOX	300-720	D	300-720	SPK-D	100-500	DST

TIME-REVERSAL TEST

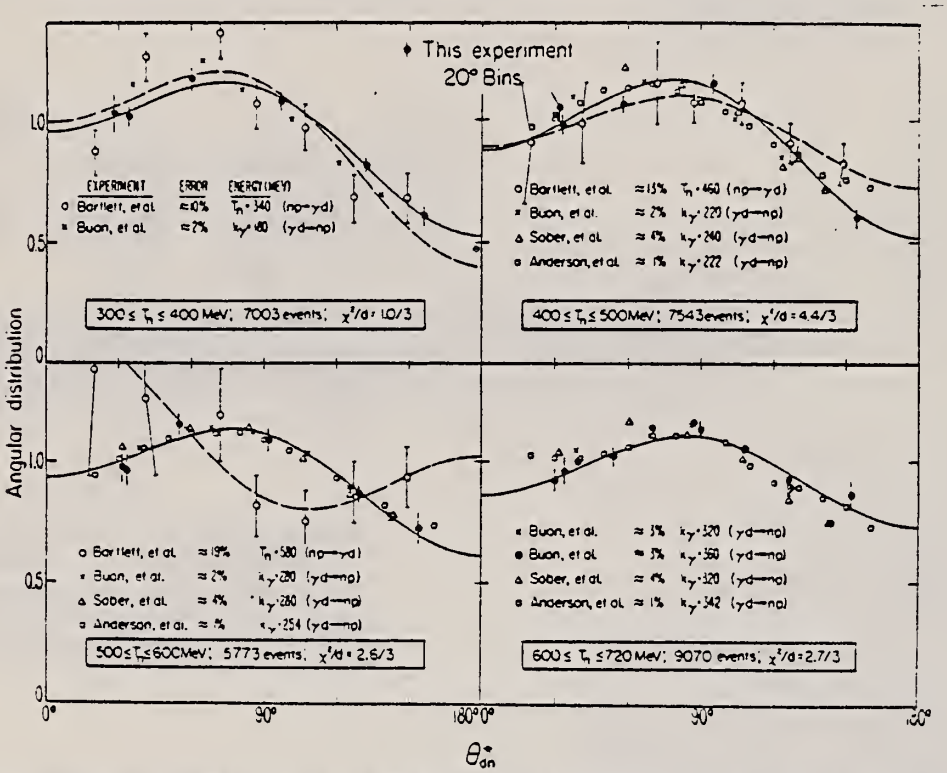

FIG. 2. Angular distributions for $n+p \rightleftharpoons \gamma+d$ as a function of θ_{dn}^*, the c.m. scattering angle of the deuteron relative to the neutron. The solid curve is a second-degree fit in Legendre polynomials to our data for which the χ^2 per degree of freedom is indicated. The dashed curve is a similar fit to the data of Bartlett *et al.*, Ref. 12. For the $\gamma+d \rightarrow n+p$ experiments, see Refs. 4-6.

[4]B. L. Schrock *et al.*, in *High-Energy Physics and Nuclear Structure*, edited by S. Devons (Plenum, New York, 1970), pp. 727-738. This preliminary result based on ≈15% of the data indicated a discrepancy of ≈3σ between $n+p \rightleftharpoons \gamma+d$. Subsequent analysis of the entire data sample allowed a more detailed investigation of systematic errors in the determination of T_n. Removal of these systematic errors in the 15% sample reduced the discrepancy to ≈1σ.

[5]D. I. Sober, D. G. Cassel, A. J. Sadoff, K. W. Chen, and P. A. Crean, Phys. Rev. Lett. 22, 430 (1969).

[6]J. Buon, V. Graceo, J. Lefrancois, P. Lehmann, B. Merkel, and Ph. Roy, Phys. Lett. 26B, 595 (1968).

[12]D. F. Bartlett, C. E. Friedberg, K. Goulianos, I. S. Hammerman, and D. P. Hutchinson, Phys. Rev. Lett. 23, 893 (1969).

(continued)

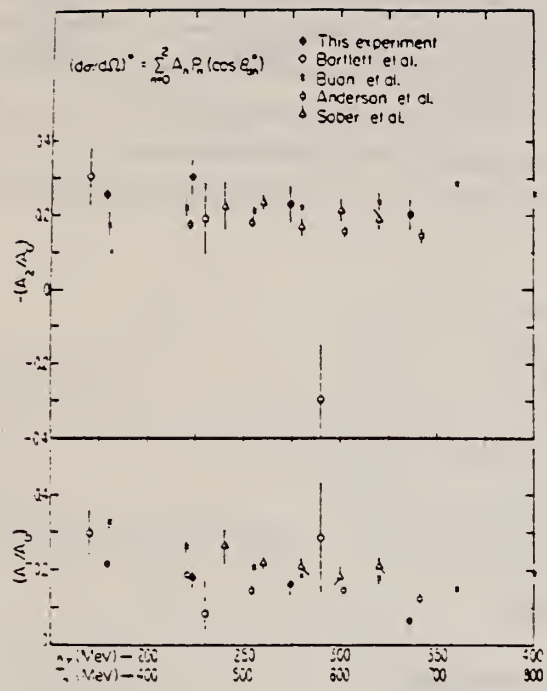

FIG. 3. Normalization-independent ratios, A_1/A_0 and A_2/A_0, resulting from fits of a second-degree Legendre polynomial series to data from recent $\pi^+ p$ $= \gamma - d$ experiments.

REF. K. Tietze, H. Reich and J. O. Trier
Z. Physik 242, 328 (1971)

ELEM. SYM.	A	Z
H	2	1

METHOD

REF. NO. 71 Ti 1 egf

REACTION	RESULT	EXCITATION ENERGY	SOURCE		DETECTOR		ANGLE
			TYPE	RANGE	TYPE	RANGE	
G,P	ABX	20-35	C	60	TEL-D	9-16	90

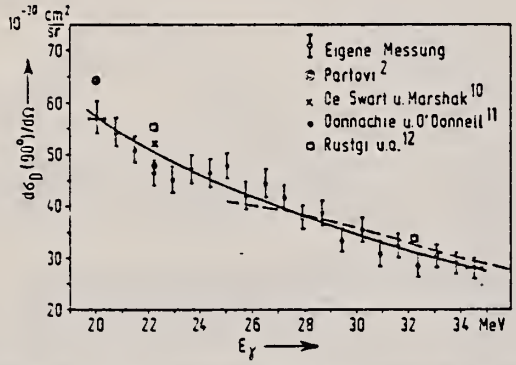

Fig. 1. Differentieller Wirkungsquerschnitt der Photospaltung des Deuterons unter 90° im Laborsystem; E_γ Photonenenergie. Die ausgezogene Linie ist eine Ausgleichskurve durch die eigenen Meßwerte, die gestrichelte eine durch die Meßwerte von Weissman[7]

[7] Weissman, B: Dissertation, Yale University, 1969; New Haven, Connecticut 06520

REF.

B. Weissman and H. L. Schultz
Nucl. Phys. A174, 129 (1971)

ELEM. SYM.	A	Z
H	2	1

METHOD -

REF. NO. 71 We 2

egf

REACTION	RESULT	EXCITATION ENERGY	SOURCE		DETECTOR		ANGLE
			TYPE	RANGE	TYPE	RANGE	
G,P	ABX	25-55	C	60	SCD-D		DST

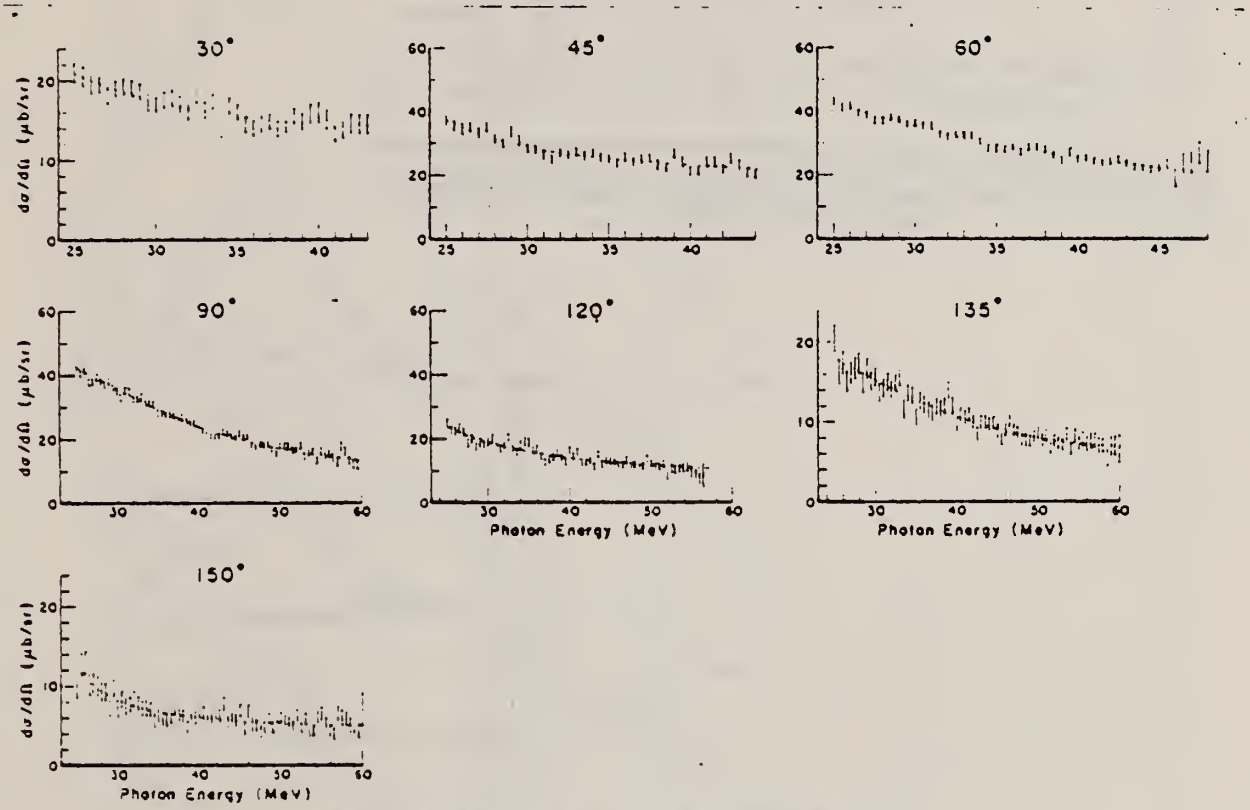

Fig. 3. Differential cross sections (c.m.) versus photon energy (lab).

(continued)

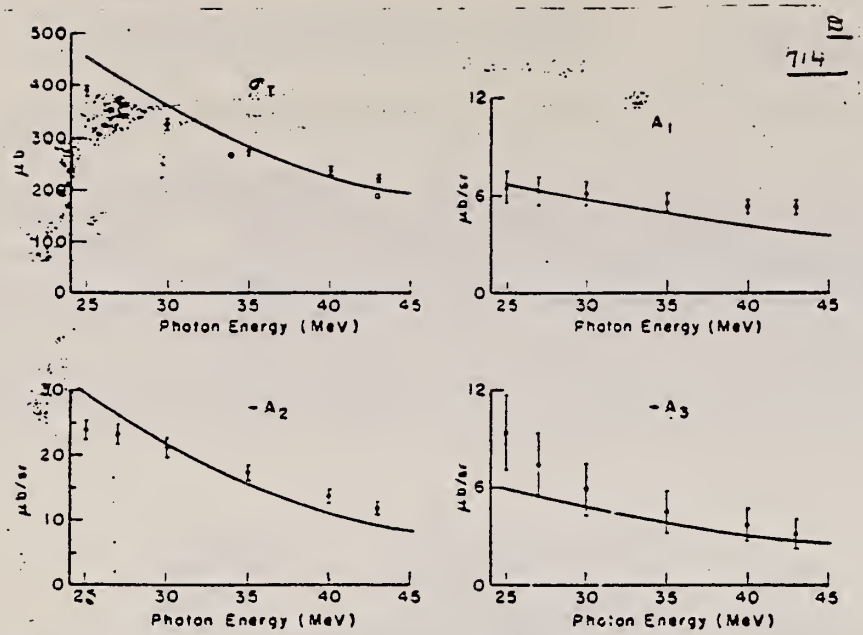

Fig. 5. Total cross section σ_t ($= 4\pi A_0$) and Legendre coefficients A_1, A_2, A_3 as functions of photon energy. Solid circles, present results. Error bars do not reflect a ±3 % uncertainty affecting all cross sections equally. Open circles, σ_t values of Allen (after 9 % increase). Curves, theoretical prediction based on Partovi's calculation.

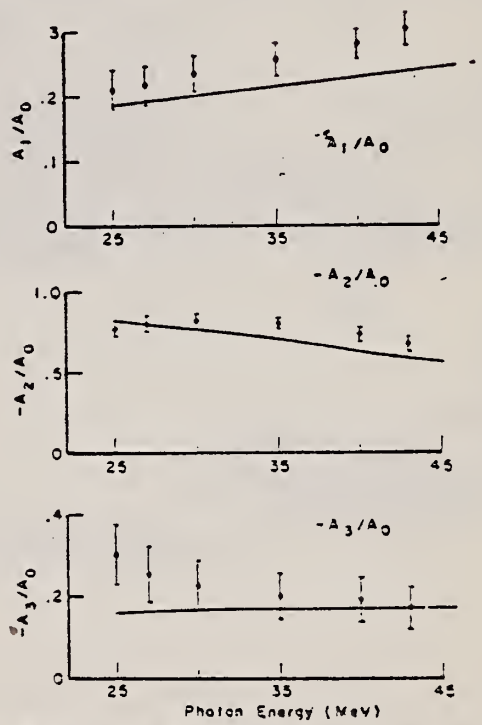

Fig. 6. Legendre coefficients divided by A_0. Solid circles, present results. Curves, theoretical predictions.

(continued)

REF. B. Weissman and H. L. Schultz
Nucl. Phys. A174, 129 (1971)

EL EM. SYM.	A	Z
H	2	1

METHOD

REF. NO. 71 We 2 egf

REACTION	RESULT	EXCITATION ENERGY	SOURCE		DETECTOR		ANGLE
			TYPE	RANGE	TYPE	RANGE	

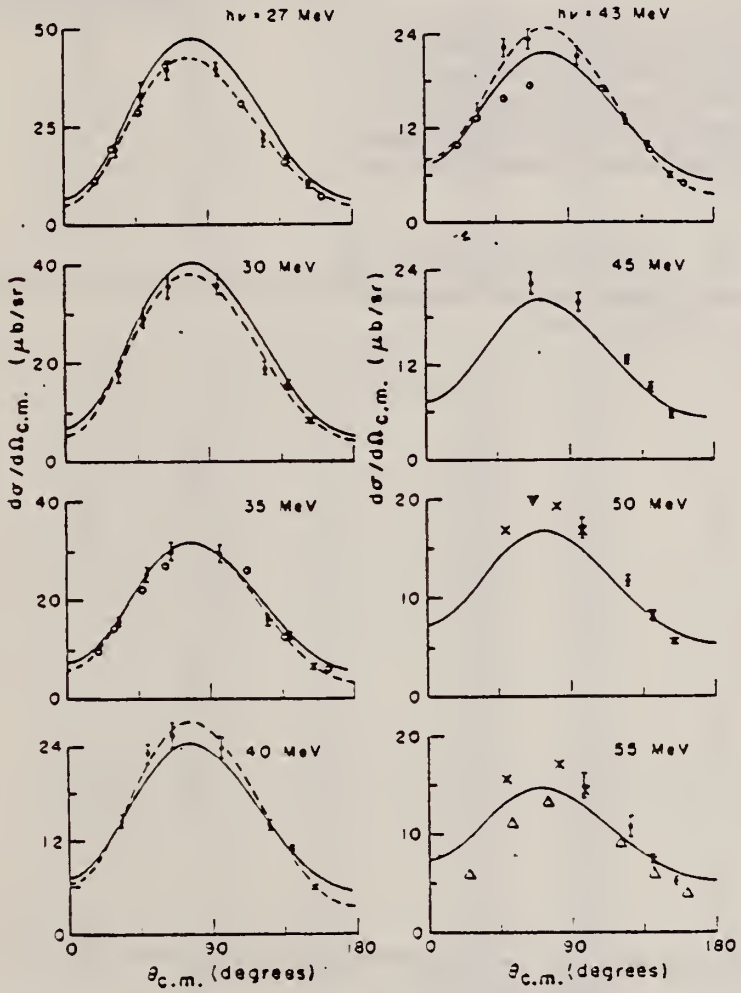

Fig. 4. Angular distributions. Solid circles, present results. Error bars do not include a ±3% uncertainty affecting all points equally. Open circles, results of Allen (after 9% increase). Crosses, results of Galey. Open triangles, results of Aleksandrov *et al.* Solid inverted triangle, cross section obtained by extrapolation of 60° differential cross section versus energy curve in fig. 3. Dotted curves, analytical fits to present results. Solid curves, theoretical predictions from Partovi's calculation (see text).

REF. T.A. Armstrong, W.R. Hogg, G.M. Lewis, A.W. Robertson, G.R. Brookes, A.S. Clough, J.H. Freeland, W. Galbraith, A.F. King, W.R. Rawlinson, N.R.S. Tait, J.C. Thompson, D.W.L. Tolfree
Nucl. Phys. B41, 445 (1972)

EL EM. SYM.	A	Z
H	2	1

METHOD

REF. NO. 72 Ar 14 egf

REACTION	RESULT	EXCITATION ENERGY	SOURCE		DETECTOR		ANGLE
			TYPE	RANGE	TYPE	RANGE	
G,HAD	ABX	265-999	D	265-999	TEL-I		4PI

999=4.215 GEV

Abstract: The total cross section for photoproduction of hadrons on the deuteron, σ_T^d, has been measured for photon energies in the range 0.265–4.215 GeV. From this, using results for the proton total cross section, obtained previously with the same apparatus, the neutron total cross section has been determined in the resonance region. The resonant structure is found to be quite different from that for the proton. Thereafter the neutron cross section falls off steadily with energy, and the values obtained are consistently lower than those for the proton. Forward scattering amplitudes have been evaluated for the deuteron.

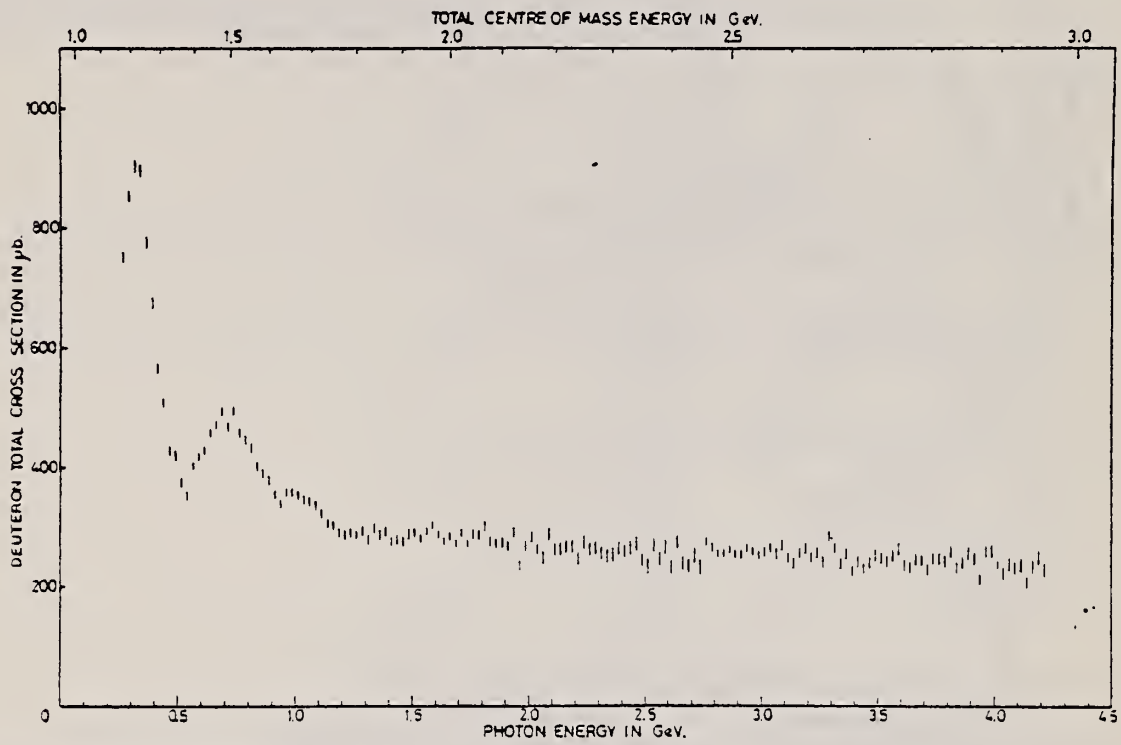

Fig. 4. The total photon-deuteron cross section for hadron production σ_T^d, as a function of γ-ray energy. The numerical values are listed in table 1. (The c.m. energy of a photon interaction with a stationary nucleon is also shown.)

(continued)

Table 1
Total cross section results for deuteron σ_T^d.

ν (GeV)	σ_T^d (μb)	$\Delta\sigma_T^d$ (μb)	ν (GeV)	σ_T^d (μb)	$\Delta\sigma_T^d$ (μb)	ν (GeV)	σ_T^d (μb)	$\Delta\sigma_T^d$ (μb)
0.265	752.4	8.9	1.590	303.8	7.0	2.915	254.4	7.6
0.290	853.7	9.6	1.615	287.6	6.9	2.940	265.9	7.5
0.315	904.2	10.1	1.640	276.3	6.7	2.965	258.9	7.5
0.340	895.7	10.2	1.665	285.1	6.8	2.990	253.2	7.6
0.365	776.0	10.1	1.690	273.1	6.6	3.015	259.4	9.1
0.390	676.2	9.8	1.715	290.7	6.8	3.040	265.6	9.2
0.415	566.8	9.2	1.740	274.0	6.9	3.065	254.7	9.2
0.440	509.0	8.8	1.765	287.8	8.2	3.090	270.3	9.3
0.465	428.8	8.6	1.790	286.8	8.3	3.115	248.9	8.9
0.490	421.9	8.6	1.815	302.2	8.4	3.140	239.3	8.9
0.515	375.7	8.2	1.840	275.5	8.4	3.165	257.2	9.3
0.540	354.5	8.1	1.865	272.0	8.4	3.190	265.2	9.5
0.565	404.1	6.6	1.890	275.1	8.5	3.215	249.5	9.3
0.590	419.4	6.6	1.915	268.7	8.3	3.240	257.2	9.3
0.615	429.4	6.7	1.940	291.4	8.6	3.265	240.5	9.6
0.640	458.1	7.0	1.965	236.2	8.4	3.290	284.1	10.0
0.665	473.3	7.2	1.990	268.7	8.6	3.315	264.8	9.4
0.690	494.7	7.5	2.015	283.6	8.8	3.340	239.7	9.2
0.715	469.6	7.6	2.040	263.7	8.7	3.365	255.7	9.6
0.740	496.0	7.7	2.065	249.4	10.8	3.390	226.6	9.2
0.765	458.4	7.7	2.090	288.5	11.0	3.415	242.7	9.7
0.790	447.0	7.8	2.115	264.0	10.7	3.440	230.5	9.3
0.815	432.4	7.8	2.140	264.0	10.6	3.465	240.8	9.6
0.840	402.2	7.8	2.165	268.8	10.8	3.490	252.9	9.9
0.865	390.7	7.7	2.190	267.7	11.1	3.515	248.7	9.8

Table 1 (Continued)

ν (GeV)	σ_T^d (μb)	$\Delta\sigma_T^d$ (μb)	ν (GeV)	σ_T^d (μb)	$\Delta\sigma_T^d$ (μb)	ν (GeV)	σ_T^d (μb)	$\Delta\sigma_T^d$ (μb)
0.890	378.9	7.5	2.215	246.9	10.9	3.540	242.4	9.6
0.915	355.8	7.6	2.240	275.7	11.6	3.565	252.8	10.0
0.940	340.0	7.5	2.265	263.7	11.2	3.590	263.3	10.5
0.965	359.9	7.6	2.290	265.3	11.8	3.615	235.8	10.1
0.990	358.6	7.7	2.315	256.6	11.5	3.640	231.7	9.6
1.015	354.7	7.9	2.340	251.1	12.0	3.665	245.5	10.1
1.040	346.6	7.9	2.365	254.8	11.6	3.690	244.5	10.2
1.065	342.9	8.0	2.390	264.7	11.5	3.715	228.2	10.1
1.090	336.1	8.1	2.415	260.9	11.6	3.740	246.9	9.9
1.115	323.9	7.9	2.440	266.1	11.8	3.765	247.3	10.5
1.140	306.7	7.7	2.465	272.8	11.8	3.790	242.2	10.1
1.165	302.4	7.9	2.490	244.7	11.3	3.815	258.8	10.5
1.190	291.0	8.0	2.515	234.1	12.3	3.840	231.8	9.8
1.215	287.5	8.2	2.540	269.3	11.7	3.865	240.4	10.4
1.240	291.5	8.0	2.565	247.4	12.2	3.890	257.3	10.6
1.265	286.7	8.1	2.590	267.8	11.7	3.915	246.2	10.1
1.290	294.2	8.3	2.615	233.6	11.6	3.940	213.5	10.1
1.315	279.4	8.2	2.640	274.4	11.7	3.965	259.5	10.7
1.340	299.1	8.6	2.665	239.1	11.9	3.990	260.6	11.0
1.365	287.0	8.4	2.690	235.1	12.2	4.015	234.8	10.5
1.390	293.3	8.8	2.715	252.9	12.1	4.040	222.3	10.2
1.415	275.4	8.4	2.740	232.3	12.9	4.065	238.2	11.0
1.440	279.5	8.4	2.765	276.0	7.7	4.090	232.2	10.9
1.465	275.7	8.7	2.790	266.4	7.5	4.115	237.0	11.2
1.490	289.3	9.0	2.815	255.0	7.1	4.140	207.1	10.6
1.515	291.2	6.7	2.840	256.6	7.5	4.165	233.4	10.9
1.540	280.6	6.6	2.865	263.1	7.2	4.190	249.3	11.7
1.565	293.2	6.6	2.890	255.0	7.3	4.215	228.0	11.4

REF.

C. Bacci, R. Baldini-Celio, B. Esposito, C. Mencuccini, A. Reale, G. Sciacca, M. Spinetti and A. Zallo
Lettere al Nuovo Cimento 4, 5 (1972)

ELEM. SYM.	A	Z
H	2	1

METHOD

REF. NO. 72 Ba 5 egf

REACTION	RESULT	EXCITATION ENERGY	SOURCE TYPE	SOURCE RANGE	DETECTOR TYPE	DETECTOR RANGE	ANGLE
G,PIO	RLX	400-800	C	999	TEL-D		DST

999 = 1.1 GEV

TABLE I.

$\theta_\pi^* = 60°$		$\theta_\pi^* = 90°$		$\theta_\pi^* = 135°$	
E_γ	r	E'_γ	r	E'_γ	r
505	0.78 ± 0.07	430	0.82 ± 0.03	471	0.93 ± 0.06
559	0.84 ± 0.07	476	0.84 ± 0.03	520	0.87 ± 0.07
606	0.85 ± 0.05	508	0.77 ± 0.03	556	0.81 ± 0.06
653	0.79 ± 0.05	547	0.85 ± 0.03	596	0.82 ± 0.07
701	0.83 ± 0.05	591	0.84 ± 0.04	644	0.77 ± 0.08
733	0.98 ± 0.06	623	0.77 ± 0.04	683	0.90 ± 0.08
773	1.08 ± 0.11	667	0.91 ± 0.05	736	0.81 ± 0.09
		710	0.86 ± 0.05		
		738	0.90 ± 0.07		

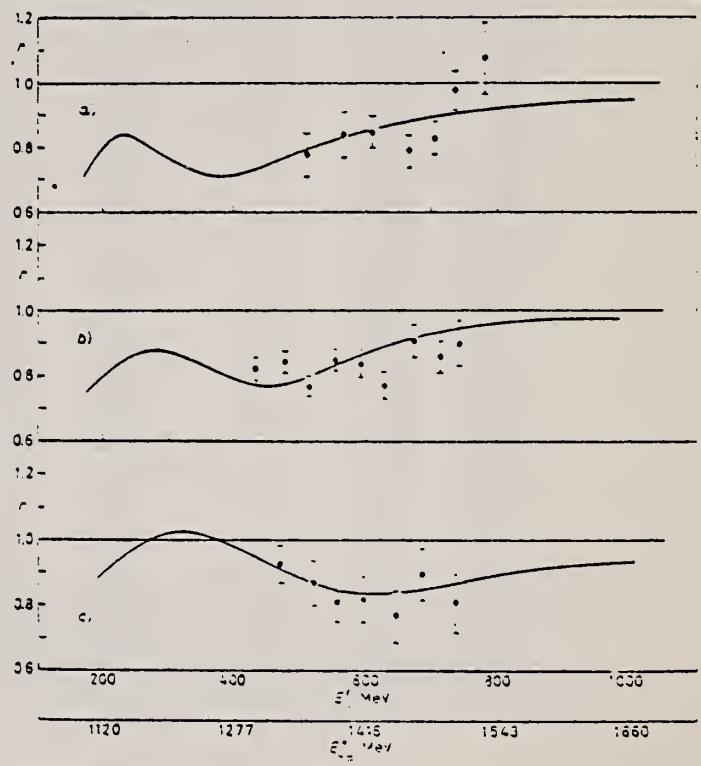

Fig. 2. – Ratio $r = (d\sigma/d\Omega^*)(\gamma D \to \pi^+ p(n_s))/(d\sigma/d\Omega^*)(\gamma p \to \pi^+ p)$ at different π^+ c.m. angles vs. $E^*_{\pi^+}$, the total c.m. energy of the $\pi^+ p$ final-state system and also vs. E'_γ, the incident-photon energy which gives on free proton a total c.m. energy $E^*_{\pi^+}$. a) $\theta^*_\pi = 60°$. b) $\theta^*_\pi = 90°$. c) $\theta^*_\pi = 135°$.

REF.

T. Fujii, S. Homma, K. Huke, S. Kato, H. Okuno, F. Takasaki, T. Kondo, S. Yamada, I. Endo and H. Fujii
Phys. Rev. Letters 28, 1672 (1972)

EL EM. SYM.	A	Z
H	2	1

METHOD

REF. NO.	
72 Fu 2	hmg

REACTION	RESULT	EXCITATION ENERGY	SOURCE		DETECTOR		ANGLE
			TYPE	RANGE	TYPE	RANGE	
G,PI-	NOX	260-800	C	999	MAG-D		DST

REL PI+, 999=1.3 GEV

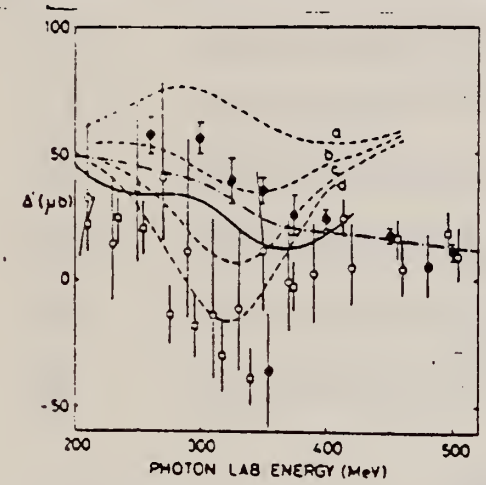

FIG. 2. Energy dependence of $\Delta^*(k)$. Closed circles, obtained from our π^-/π^+ ratio data (see text); open circles, from Ref. 18; squares, from Ref. 19; and double circles, from the data of inverse reaction (Ref. 20). Dashed lines show predictions by Sanda and Shaw (Ref. 4), where a, b, c, and d correspond $x = 0.0$, -0.1, -0.2, and -0.3, respectively. The solid line is a prediction by Noelle and Pfeil (Ref. 8), dot-dashed line is by Walker (Ref. 14).

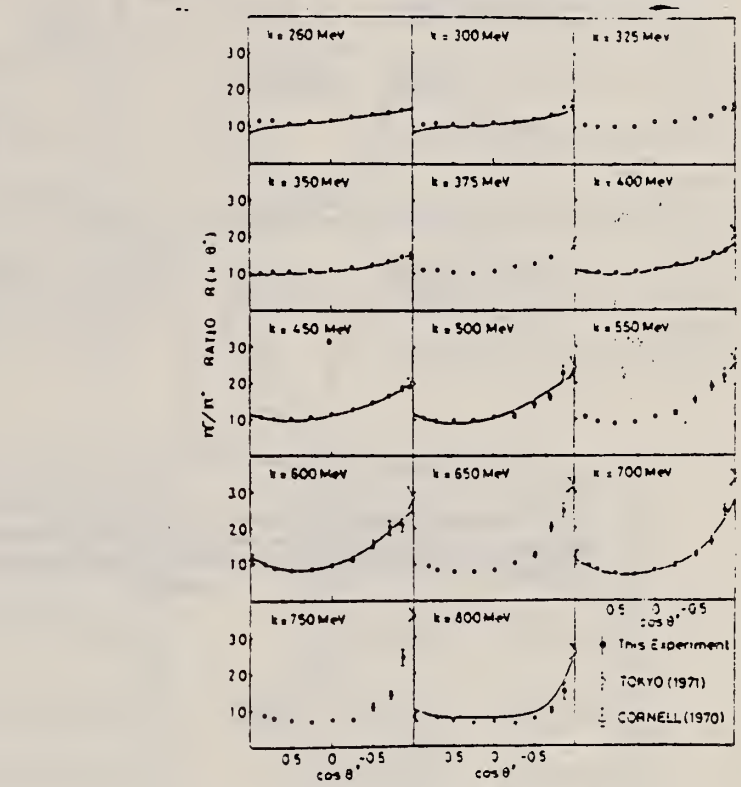

FIG. 1. π^-/π^+ ratio from deuterium as a function of $\cos\theta^*$ at fourteen photon energies from 260 to 800 MeV. Solid curves, calculated with the amplitudes of Walker's analysis (Ref. 14).

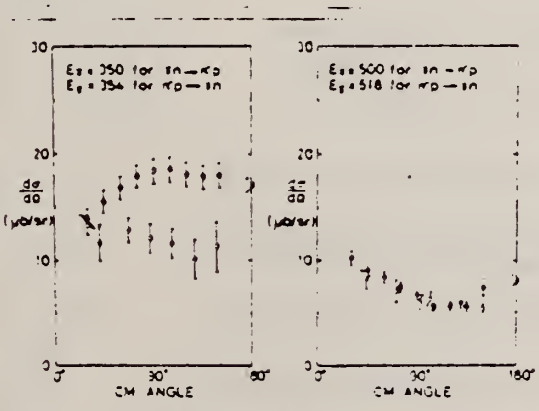

FIG. 3. Differential cross section for $\gamma n \to \pi^- p$ at k = 350 and 500 MeV. Closed circles, results calculated using our π^-/π^+ ratios; closed square, a result of direct measurement at 180° (Ref. 10); open circles and a diamond, results obtained from the inverse reactions by Berardo *et al.* (Ref. 20) and Favier *et al.* (Ref. 21), respectively.

[8] P. Noell et al., Nucl. Phys. B31, 1 (1971).

[10] T. Fujii et al., Phys. Rev. Lett. 26, 1672 (1971), & 27, 223 (1971).

[14] R. L. Walker, Phys. Rev. 182, 1729 (1969).

[18] Aachen-Berlin-Bonn-Hamburg-Heidelberg-Munich (ABBHHM) Collaboration, Nucl. Phys. B8, 535 (1968); H. Butenschon, DESY Rept No. DESY R1-70/1, 1970 (to be published).

[19] Pavia-Frascati-Roma-Napoli (PFRN) Collaboration, Lett. Nuovo Cimento 3, 697 (1970).

[20] P.A. Berardo et al., Phys. Rev. Lett. 26, 201, 205'71.

[21] J. Favier et al., Phys. Lett. 31B, 609 (1970).

REF.

D. Ganichot, B. Grossetete, and D.B. Isabelle
Nucl. Phys. A178, 545 (1972)

EL EM. SYM.	A	Z
H	2	1

METHOD

REF. NO.	
72 Ga 2	egf

REACTION	RESULT	EXCITATION ENERGY	SOURCE		DETECTOR		ANGLE
			TYPE	RANGE	TYPE	RANGE	
E,E/	ABX	0-80	D	70-280	MAG-D		180

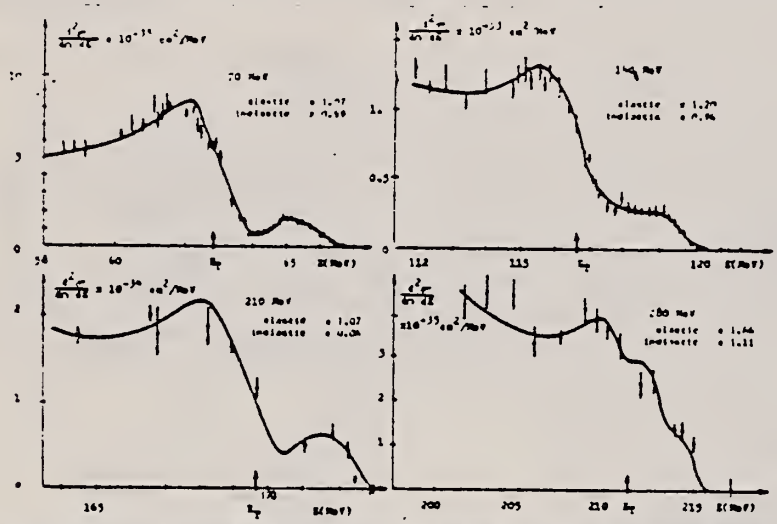

Fig. 7. Comparison between the measured and "predicted" spectra for the electron scattering on deuterium at 180°. The normalization factor corresponding to each spectrum as obtained by a χ^2 fit is indicated in brackets. The point labelled E_T on the energy axis is the electro-disintegration threshold.

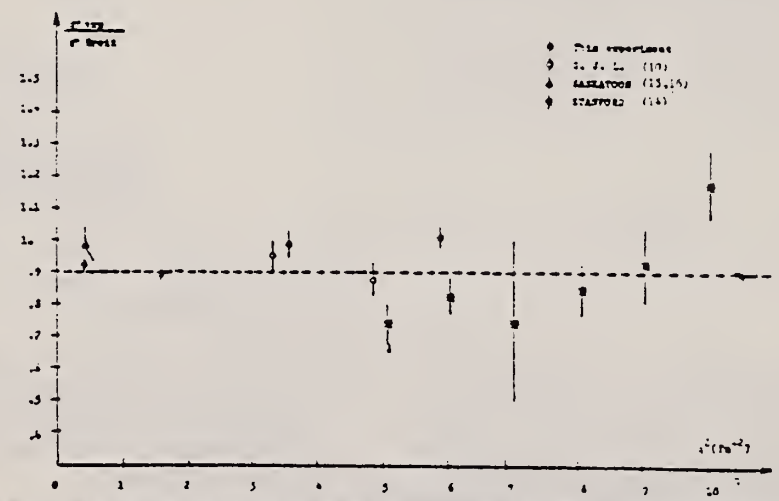

Fig. 8. Ratio of the experimental cross section for inelastic e-d scattering to the theoretical cross section obtained using the Breit wave function.

(continued)

TABLE 5a

Data pertaining to our measurements of the inelastic e-d scattering

E_3-E_T (MeV)	$\frac{d^3\sigma}{d\Omega dE_3}$ exp.	Statistical error (±)	Elastic tail	$\frac{d^3\sigma}{d\Omega dE_3}$ measured	Statistical error (±)	$\frac{d^3\sigma}{d\Omega dE_3}$ expected	$\frac{d^3\sigma}{d\Omega dE_3}$ theoretical Durand/Breit	Contributions to theoretical: without final-state interaction	S-wave final-state interaction	P-wave final-state interaction	D-wave final-state interaction
−1.1	0.69	0.13	0.47	0.22	0.16	0.13					
−1.0	0.68	0.14	0.34	0.34	0.14	0.43					
−0.8	1.29	0.20	0.25	1.04	0.20	0.86					
−0.7	1.67	0.23	0.20	1.47	0.23	1.44					
−0.5	2.49	0.27	0.16	2.33	0.27	2.42					
−0.2	5.18	0.40	0.12	5.06	0.40	4.24					
−0.1	5.81	0.40	0.11	5.70	0.40	5.17					
0.1	5.69	0.32	0.10	5.59	0.32	6.04	20.22	0.86	19.36	0.0	0.0
0.2	5.81	0.42	0.10	5.71	0.42	6.56	17.66	1.18	16.48	0.0	0.0
0.4	6.52	0.43	0.09	6.43	0.43	7.46	14.99	1.58	13.41	0.0	0.0
0.5	6.90	0.45	0.08	6.82	0.45	7.90	13.74	1.83	11.91	0.0	0.0
0.6	7.88	0.46	0.07	7.81	0.46	8.18	12.76	2.06	10.70	0.0	0.0
0.8	7.58	0.43	0.07	7.51	0.43	8.29	10.81	1.99	8.82	0.0	0.0
1.2	7.80	0.21	0.05	7.75	0.21	7.84	9.52	3.31	6.21	0.0	0.0
1.3	8.20	0.55	0.04	8.16	0.55	7.63	9.21	3.49	5.72	0.0	0.0
1.5	7.57	0.53	0.03	7.54	0.53	7.40	8.85	3.92	4.92	0.01	0.0
1.6	7.19	0.53	0.03	7.16	0.53	7.19	8.48	4.00	4.47	0.01	0.0
1.7	8.04	0.55	0.03	8.01	0.55	6.99	8.29	4.15	4.13	0.01	0.0
1.9	6.83	0.51	0.02	6.81	0.51	6.74	7.95	4.44	3.49	0.01	0.01
2.3	6.87	0.56	0.02	6.85	0.56	6.39	7.39	4.93	2.44	0.01	0.01
2.6	6.33	0.31	0.01	6.32	0.31	6.20	7.07	5.26	1.79	0.01	0.01
3.6	5.48	0.46	0.00	5.48	0.46	5.61	6.23	5.87	0.33	0.02	0.01
4.0	5.63	0.45	0.00	5.63	0.45	5.43	5.93	5.97	−0.07	0.02	0.01
4.3	5.50	0.41	0.00	5.50	0.41	5.28	5.71	5.99	−0.31	0.02	0.01

Incident energy = 70.2 MeV, threshold energy = 63.3 MeV. Resolution of the incident beam 0.3 %, and that of the detector = 1.6 %.

TABLE 5c

E_3-E_T (MeV)	$\frac{d^3\sigma}{d\Omega dE_3}$ exp.	Statistical error (±)	Elastic tail	$\frac{d^3\sigma}{d\Omega dE_3}$ measured	Statistical error (±)	$\frac{d^3\sigma}{d\Omega dE_3}$ expected	$\frac{d^3\sigma}{d\Omega dE_3}$ theoretical Durand/Breit	Contributions to theoretical: without final-state interaction	S-wave final-state interaction	P-wave final-state interaction	D-wave final-state interaction
0.0	1.16	0.14	0.12	1.04	0.14	0.81					
0.8	1.66	0.09	0.03	1.63	0.09	1.64	3.12	0.15	2.97	0.0	0.0
1.4	1.87	0.23	0.01	1.86	0.23	2.03	2.53	0.22	2.30	0.1	0.0
2.8	1.78	0.31	0.00	1.78	0.31	1.77	2.12	0.40	1.67	0.04	0.01
3.0	2.02	0.10	0.00	2.02	0.10	1.74	2.10	0.43	1.61	0.05	0.01
5.1	1.76	0.11	0.00	1.76	0.11	1.68	2.14	0.79	1.25	0.08	0.02

Incident energy = 210.2 MeV, threshold energy = 169.9 MeV. Resolution of the incident beam = 0.2 %, and that of the detector = 1.2 %.

TABLE 5b

E_3-E_T (MeV)	$\frac{d^3\sigma}{d\Omega dE_3}$ exp.	Statistical error (±)	Elastic tail	$\frac{d^3\sigma}{d\Omega dE_3}$ measured	Statistical error (±)	$\frac{d^3\sigma}{d\Omega dE_3}$ expected	$\frac{d^3\sigma}{d\Omega dE_3}$ theoretical Durand/Breit	Contributions to theoretical: without final-state interaction	S-wave final-state interaction	P-wave final-state interaction	D-wave final-state interaction
−1.1	0.28	0.04	0.15	0.13	0.01	0.15					
−0.9	0.31	0.03	0.09	0.22	0.03	0.26					
−0.7	0.40	0.04	0.06	0.34	0.04	0.39					
−0.6	0.44	0.03	0.05	0.39	0.01	0.49					
−0.5	0.49	0.06	0.04	0.45	0.06	0.54					
−0.4	0.67	0.05	0.04	0.63	0.05	0.61					
−0.3	0.63	0.08	0.03	0.62	0.08	0.71					
−0.1	0.89	0.09	0.02	0.87	0.09	0.87					
0.2	1.02	0.09	0.02	1.00	0.09	1.02	3.04	0.08	2.96	0.0	0.0
0.4	1.16	0.10	0.02	1.14	0.10	1.15	2.50	0.11	2.39	0.0	0.0
0.6	1.12	0.07	0.01	1.11	0.07	1.26	2.18	0.14	2.04	0.0	0.0
0.8	1.29	0.07	0.01	1.28	0.07	1.29	1.98	0.17	1.81	0.0	0.0
0.9	1.20	0.08	0.01	1.19	0.08	1.31	1.89	0.19	1.70	0.0	0.0
1.0	1.27	0.11	0.01	1.26	0.11	1.32	1.80	0.20	1.60	0.0	0.0
1.2	1.21	0.10	0.01	1.20	0.10	1.32	1.69	0.23	1.46	0.0	0.0
1.4	1.29	0.11	0.00	1.29	0.11	1.29	1.59	0.26	1.33	0.0	0.0
1.6	1.26	0.11	0.00	1.26	0.11	1.25	1.53	0.29	1.24	0.0	0.0
1.8	1.16	0.07	0.00	1.16	0.07	1.22	1.48	0.31	1.17	0.0	0.0
2.4	1.20	0.10	0.00	1.20	0.10	1.15	1.38	0.41	0.96	0.01	0.0
3.0	1.06	0.07	0.00	1.06	0.07	1.13	1.34	0.53	0.80	0.01	0.0
3.8	1.25	0.11	0.00	1.25	0.11	1.14	1.36	0.67	0.67	0.02	0.0
4.1	1.16	0.05	0.00	1.16	0.05	1.16	1.39	0.74	0.62	0.02	0.01
4.5	1.30	0.10	0.00	1.30	0.10	1.18	1.42	0.83	0.56	0.02	0.01
5.1	1.20	0.07	0.00	1.20	0.07	1.23	1.49	0.98	0.48	0.02	0.01

Incident energy = 136.3 MeV, threshold energy = 117.0 MeV. Resolution of the incident beam = 0.2 %, and that of the detector = 1.6 %.

TABLE 5d

E_3-E_T (MeV)	$\frac{d^3\sigma}{d\Omega dE_3}$ exp.	Statistical error (±)	Elastic tail	$\frac{d^3\sigma}{d\Omega dE_3}$ measured	Statistical error (±)	$\frac{d^3\sigma}{d\Omega dE_3}$ expected	$\frac{d^3\sigma}{d\Omega dE_3}$ theoretical Durand/Breit	Contributions to theoretical: without final-state interaction	S-wave final-state interaction	P-wave final-state interaction	D-wave final-state interaction
−2.8	1.41	0.14	1.38	0.03	0.19	0.0					
−2.1	2.06	0.16	1.40	0.66	0.21	0.09					
−1.2	2.52	0.31	1.42	1.10	0.34	1.00					
−0.5	2.43	0.36	0.74	1.69	0.37	1.79					
0.2	3.31	0.33	0.12	3.19	0.33	2.45	8.21	0.07	8.12	0.0	0.02
0.9	3.71	0.24	0.06	3.65	0.24	3.05	4.97	0.17	4.77	0.01	0.02
1.6	3.89	0.28	0.05	3.84	0.28	3.29	4.11	0.29	3.73	0.06	0.03
2.3	4.20	0.31	0.04	4.16	0.31	3.01	3.72	0.40	3.17	0.12	0.03
3.6	3.41	0.16	0.03	3.38	0.16	2.73	3.51	0.62	2.61	0.24	0.04
5.0	3.40	0.36	0.02	3.38	0.36	2.71	3.56	0.89	2.30	0.31	0.06
6.4	4.46	0.40	0.02	4.44	0.40	2.84	3.72	1.23	2.02	0.38	0.09
7.8	4.55	0.40	0.02	4.53	0.40	3.07	4.03	1.63	1.87	0.42	0.11
9.2	4.29	0.40	0.01	4.28	0.40	3.39	4.50	2.13	1.78	0.34	0.13

Incident energy = 275.8 MeV, threshold energy = 211.4 MeV. Resolution of the incident beam = 0.2 %, and that of the detector = 1.6 %.

REF. O.Y. Mafra, S. Kuniyoshi and J. Goldemberg
Nucl. Phys. A186, 110 (1972)

ELEM. SYM.	A	Z
H	2	1

METHOD

REF. NO. 72 Ma 1 egf

REACTION	RESULT	EXCITATION ENERGY	SOURCE		DETECTOR		ANGLE
			TYPE	RANGE	TYPE	RANGE	
G,N	ABX	5-9	D	5-9	BF3-I		4PI

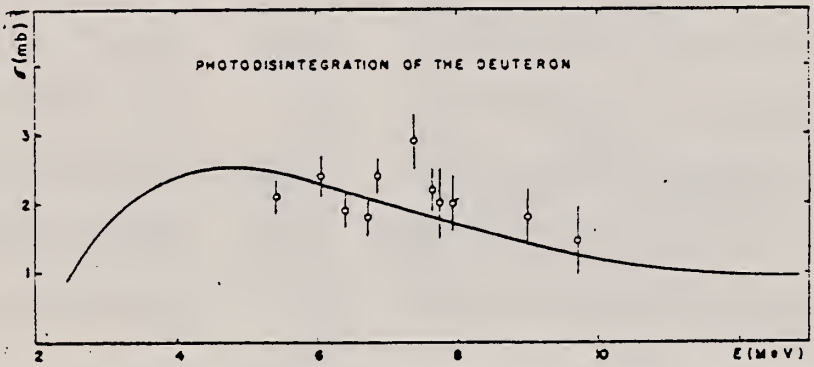

Fig. 4. Deuterium cross sections obtained from neutron capture sources compared with the theoretical values.

REF.

R. Nath, F.W.K. Firk and H.L. Schultz
Nucl. Phys. A194, 49 (1972)

ELEM. SYM.	A	Z
H	2	1

METHOD

REF. NO. 72 Na 2 egf

REACTION	RESULT	EXCITATION ENERGY	SOURCE		DETECTOR		ANGLE
			TYPE	RANGE	TYPE	RANGE	
$ G,N	NOX	7-30	C	65	TOF-D		DST

N POLARIZATION

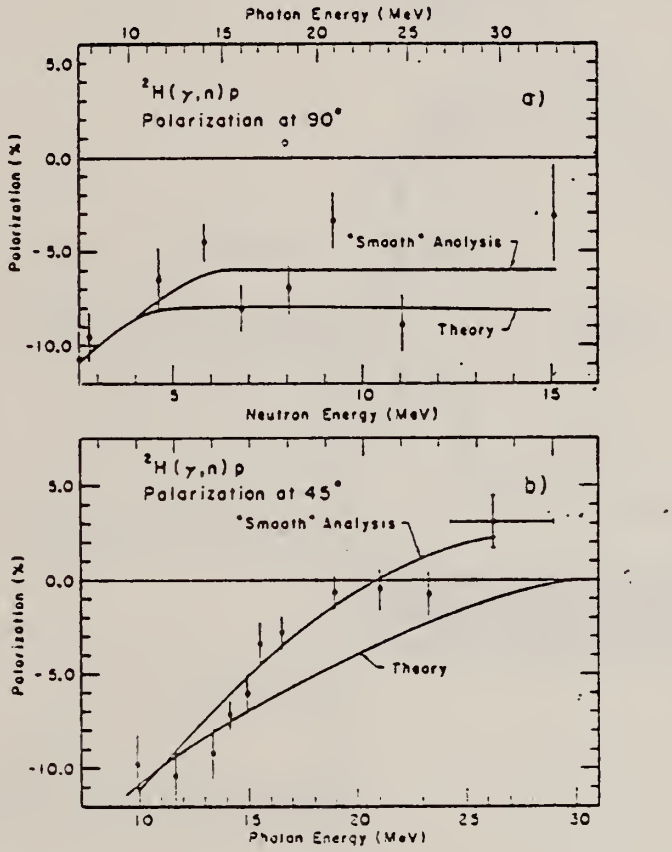

Fig. 5. Polarization of photoneutrons from deuterium at 45° and 90°. Data obtained by using the ^{4}He analyser are shown by solid circles ● and those by using the ^{12}C analyser (subsect. 2.4) by open circles ○.

REF.

R.G. Arnold, B.T. Chertok, I.G. Schroder, and J.L. Alberi
Phys. Rev. C8, 1179 (1973)

ELEM. SYM.	A	Z
H	2	1

METHOD

REF. NO.	
73 Ar 11	hmg

REACTION	RESULT	EXCITATION ENERGY	SOURCE		DETECTOR		ANGLE
			TYPE	RANGE	TYPE	RANGE	
N,2G	ABX	2	D	0 (thermal)	NAI-D		180

Upper limit on $\sigma_{2\gamma} \leq 1.0$ mb placed on doubly radiative np capture cross section.

ANG BTW DET, SIG LIM

REF.

J.R.E. Baglin, R.W. Carr, E.J. Bentz,Jr., C.P. Wu
Nucl. Phys. A201, 593 (1973)

ELEM. SYM.	A	Z
H	2	1

METHOD

REF. NO.	
73 Ba 3	egf

REACTION	RESULT	EXCITATION ENERGY	SOURCE		DETECTOR		ANGLE
			TYPE	RANGE	TYPE	RANGE	
G,P	ABX	17- 25	C	25	SCD-D		DST

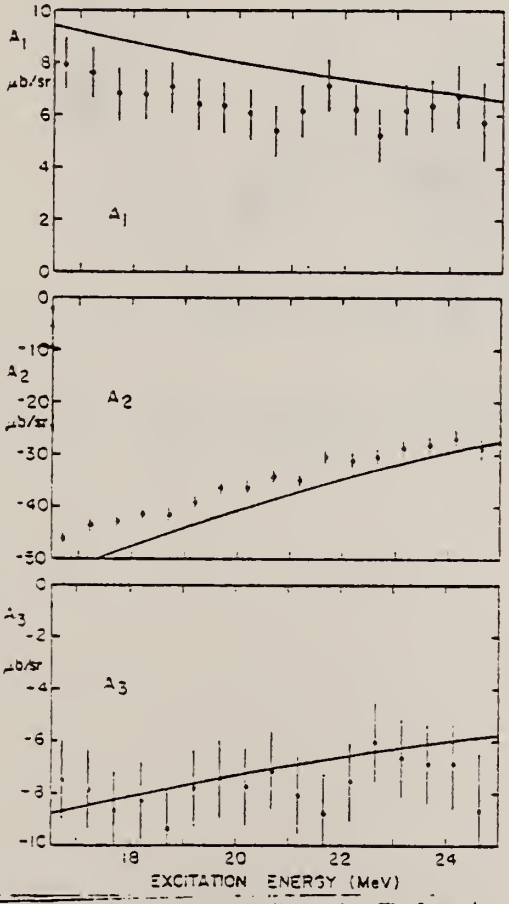

Fig. 4. The $^2H(\gamma, p)n$ angular distribution. The Legendre coefficients A_1, A_2 and A_3 are displayed as functions of energy. Comparison is made with the predictions of Partovi [8]. (Error bars reflect statistical errors and estimated uncertainties in relative $G(\theta)$ among detectors. They do not include a 6% scale uncertainty.)

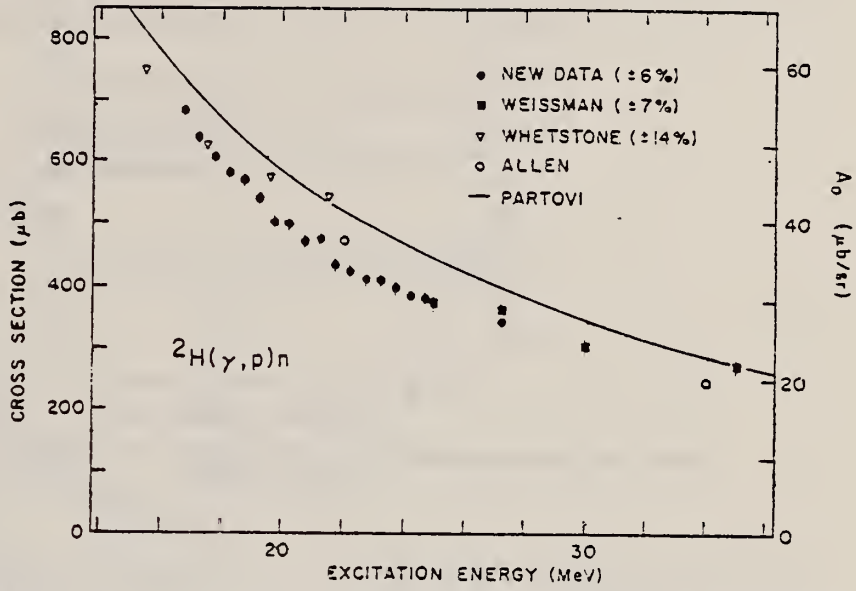

Fig. 3. Total $^2H(\gamma, p)n$ cross section: Results of present experiment and of other experiments in adjoining energy ranges. Systematic departure from the theoretical results of ref. [8]) (solid line) is noted. The ordinate scale at right shows the Legendre coefficient A_0 (= cross section /4π). (Error bars reflect statistical uncertainties only; an additional scale uncertainty of 6% applies to the present data.)

(continued)

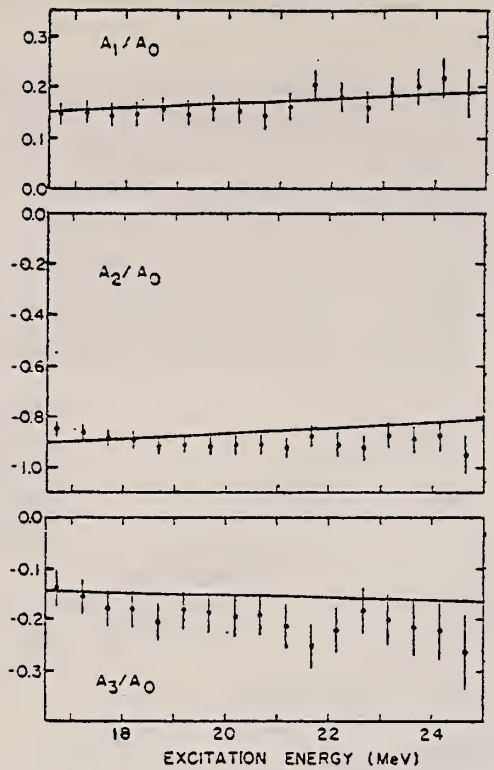

Fig. 5. The $^2H(\gamma, p)n$ angular distribution. The ratio of Legendre coefficients A_N/A_0 is displayed as a function of energy.

REF. K. F. Chong, M. C. Phenneger, Y. M. Shin, D. M. Skopik, and E. L. Tomusiak
PICNS-73, p. 467 (1973) Asilomar

ELEM. SYM.	A	Z
H	2	1

METHOD

REF. NO. 73 Ch 4 hmg

REACTION	RESULT	EXCITATION ENERGY	SOURCE		DETECTOR		ANGLE
			TYPE	RANGE	TYPE	RANGE	
E,P	ABX	5- 24	D	38,107	MAG-D		DST

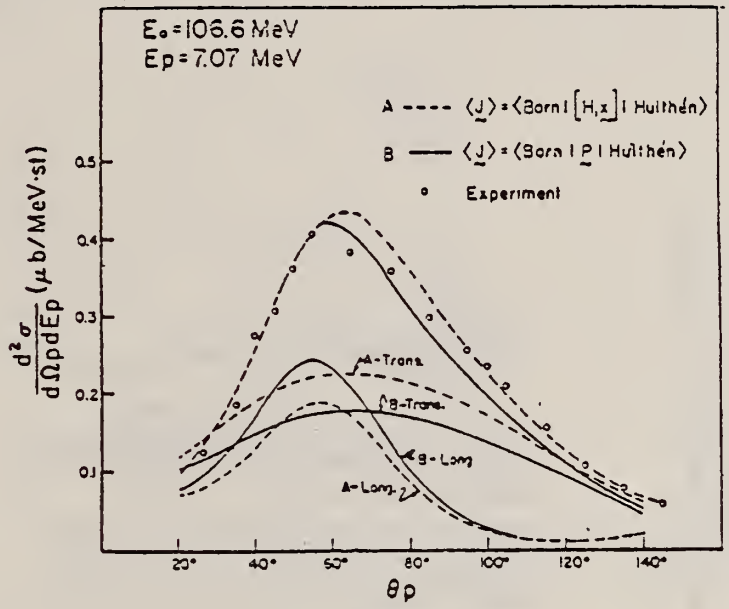

Fig. 1 Angular distribution of protons at an incident electron energy of 106.6 MeV.

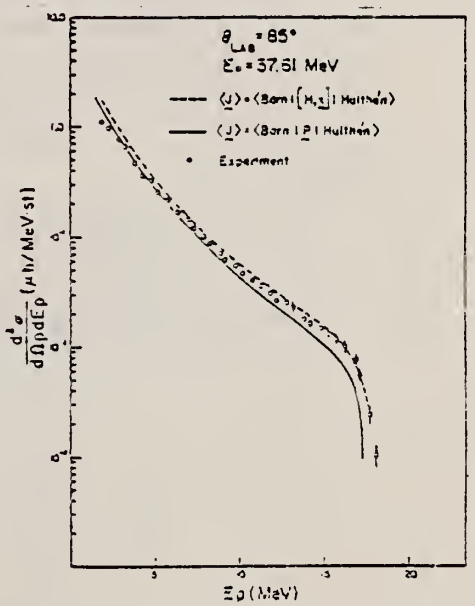

Fig. 2 Energy distribution of protons at an incident electron energy of 37.61 MeV.

REF. Y.M. Shin, D.M. Skopik, and E.L. Tomusyak
Izv. Akad. Nauk SSSR Ser. Fiz. 37, 1863 (1973)
Bull. Acad. Sci. USSR Phys. Ser. 37, 60 (1973)

EL EM. SYM.	A	Z
H	2	1

METHOD

REF. NO.	
73 Sh 18	hmg

REACTION	RESULT	EXCITATION ENERGY	SOURCE		DETECTOR		ANGLE
			TYPE	RANGE	TYPE	RANGE	
E,E/P	ABX	18, 35	D	38,106	MAG-D		DST

E_p = 7.07 MeV (E_x = 18 MeV)

COINC E,P

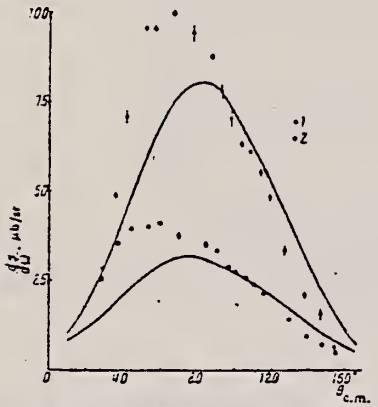

Fig. 5. Differential cross section for the ^{2}H(ep)e'n reaction at E_γ = 18.0 ± 0.5 MeV (1) and 35.0 ± 0.5 MeV (2); the curves were calculated with Partovi's theory.

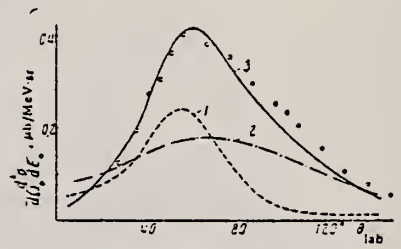

Fig. 6. Experimental differential cross section at E_p = 7.07 MeV (points) and the corresponding cross section as calculated with the simple model including only the longitudinal terms S_L (1), only the transverse terms S_T (2), and all the terms S_L, S_T, and S_I (3).

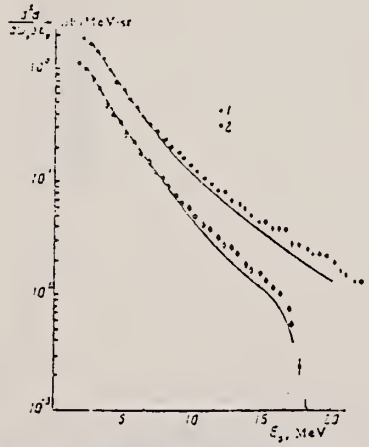

Fig. 7. Experimental proton energy spectrum at θ_p = 35° and E_0 = 106.6 ± 1.0 MeV (1) and 37.6 ± 0.4 MeV (2); the curves were calculated with the simple theory.

REF.

D.M. Skopik, Y.M. Shin, E.L. Tomusiak, M.C. Phenneger, K.F. Chong
Phys. Letters 43B, 481 (1973)

ELEM. SYM.	A	Z
H	2	1

METHOD

REF. NO.	
73 Sk 1	egf

REACTION	RESULT	EXCITATION ENERGY	SOURCE		DETECTOR		ANGLE
			TYPE	RANGE	TYPE	RANGE	
E,P	ABX	4- 46	D	38,107	MAG-D		DST

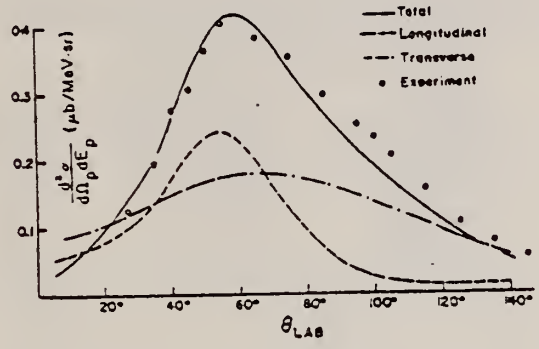

Fig. 1. Angular distribution at a proton energy of $E_p = 7.07 \pm 0.07$ MeV. The solid curve is the prediction of the present model.

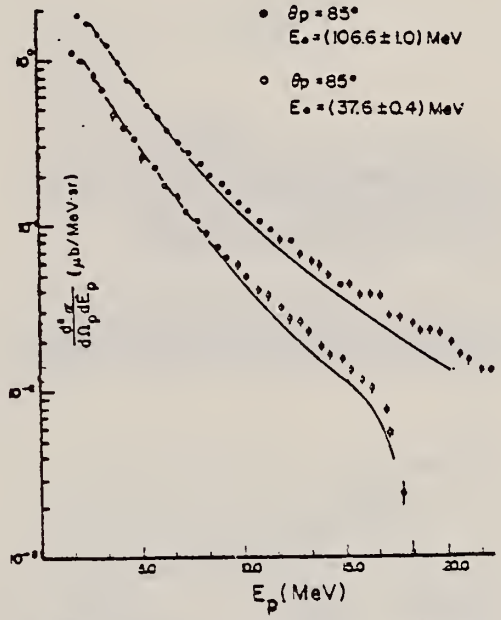

Fig. 2. Energy distribution of protons at two incident electron energies, with the present calculations indicated by the solid lines.

REF. J. Ahrens, H.B. Eppler, H. Gimm, M. Kroning, P. Riehn, H. Waffler, A. Zieger and B. Ziegler
Phys. Lett. 52B, 49 (1974)

ELEM. SYM.	A	Z
H	2	1

METHOD

REF. NO. 74 Ah 9 egf

REACTION	RESULT	EXCITATION ENERGY	SOURCE		DETECTOR		ANGLE
			TYPE	RANGE	TYPE	RANGE	
G,MU-T	ABX	15- 25	C	UKN	MGC-D		4PI

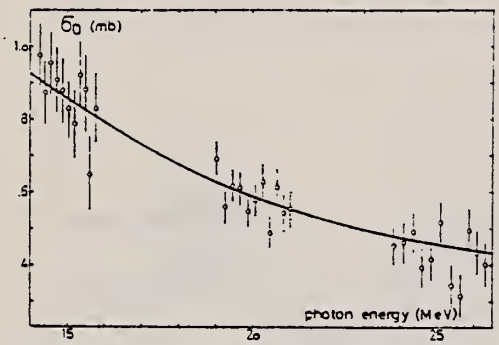

Fig. 1. The measured total cross sections σ_D for the photodisintegration of the deuteron (open circles) compared with the calculation of Partovi [3] (full line). A systematic error of ± 18 μb is to be assigned to the measured values.

Table 1
Absorber characteristics and contributions to the relative systematic error in % (last column) at 20 MeV

Length	109.85 ± 0.01 cm	0.001
Density $\varrho(H_2O)$	(0.99712 ± 10^{-5}) g/cm^3	0.001
$\varrho(D_2O)/\varrho(H_2O)$	1.107360 ± 5 × 10^{-5}	0.003
^{18}O in D_2O	0.399 ± 0.002 %	0.002
D_2 in D_2O	0.99479 ± 0.00054	2.35
Temperature	24.7 ± 0.05 °C	0.2
$\sigma_{tot}(H_2O)$	550 ± 1 mb	0.3

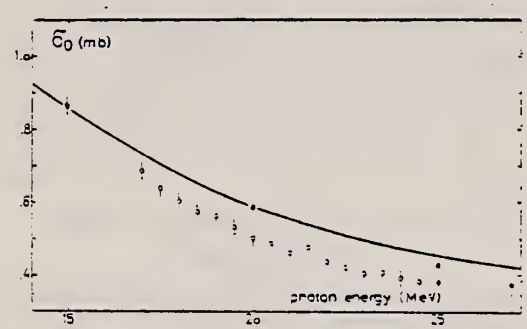

Fig. 2. The statistically weighted average cross sections from table 2 (closed squares) compared with the calculation of Partovi [3] (full line) and the experimental results of Baglin et al. [1] (open circles) and Weissman and Schultz [2] (closed circles).

Table 2
The statistically weighted average total cross sections for the photodisintegration of the deuteron σ_D and their corresponding energies and systematic errors.

Energy (MeV)	cross section (μb)	systematic error (μb)
15.0 ± 0.1	867 ± 27	19
20.0 ± 0.1	535 ± 14	18
25.0 ± 0.1	428 ± 17	16

[1] J.E.E. Baglin et al., Nucl. Phys. A201 (1973) 593.
[2] B. Weissman et al., Nucl. Phys. A174 (1971) 129.
[3] F. Partovi, Ann. Phys. 27 (1964) 79.

REF. Yu. M. Aleksandrov, V.B. Ganenko, V.F. Grushin, I.I. Miroshnichenko, V.M. Sanin, P.V. Sorokin
Yad. Fiz. 20, 915 (1974)
Sov. J. Nucl. Phys. 20, 487 (1975)

ELEM. SYM.	A	Z
H	2	1

METHOD

REF. NO.	
74 A1 13	hmg

REACTION	RESULT	EXCITATION ENERGY	SOURCE		DETECTOR		ANGLE
			TYPE	RANGE	TYPE	RANGE	
G,PI+	RLX	200-400	C	600	MAG-D		DST

D(G,PI+)/P(G,PI+)

The measured values of the ratio of the $\gamma d \to n n \pi^+$ and $\gamma p \to n \pi^+$ differential cross sections are presented in the photon energy region 200–400 MeV for pion emission angles 25°–140°. The average statistical accuracy of the results is ±2.5%; the systematic error is ~±3%. The results disagree with theoretical calculations based on the model of Chew and Lewis.

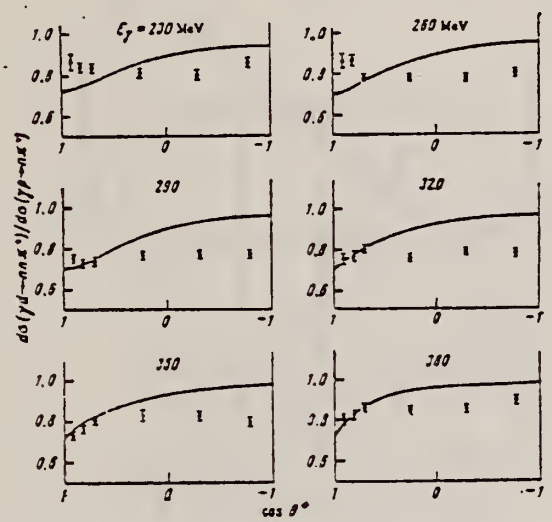

FIG. 2. Experimental results in the form of angular distributions. The solid curves represent calculations based on the theory of Chew and Lewis. [11]

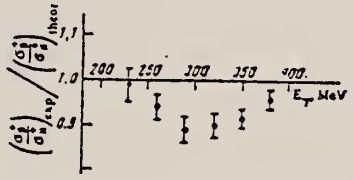

FIG. 3. Ratios of the experimental total photoproduction cross sections from deuterium and hydrogen compared with the theory in [11]. The experimental values were obtained by averaging the data represented in Fig. 2 on the angular distributions of the $\gamma p \to n\pi^+$ process.

$d\sigma(\gamma d \to nn\pi^+)/d\sigma(\gamma p \to n\pi^+)$ for different angles and energies

θ*, deg.	E_γ, MeV			
	220	230	250	290
25		0.560±0.035	0.660±0.030	0.735±0.025
45		0.805±0.020	0.870±0.025	0.790±0.020
75		0.670±0.020	0.780±0.020	0.740±0.020
105	0.630±0.025	0.810±0.020	0.735±0.015	0.765±0.020
135		0.800±0.025	0.750±0.015	0.770±0.020
140	0.535±0.035	0.860±0.020	0.805±0.020	0.775±0.020

Continued

θ*, deg	E_γ, MeV			
	320	350	380	400
25	0.735±0.030	0.705±0.020	1.810±0.030	
45	0.770±0.020	0.755±0.015	0.850±0.020	
75	0.805±0.020	0.810±0.020	0.875±0.020	
105	0.760±0.020	0.835±0.020	0.805±0.020	
135	0.790±0.020	0.830±0.020	0.860±0.020	
140	0.739±0.020	0.800±0.020	0.900±0.020	0.905±0.025

REF.

Yu.P. Antuf'ev, V.L. Agranovich, V.S. Kuz'menko, P.V. Sorokin
ZhETF Pis. Red. 19, 657 (1974)
JETP Lett. 19, 339 (1974)

ELEM. SYM.	A	Z
H	2	1

METHOD

REF. NO. 74 An 5 hmg

REACTION	RESULT	EXCITATION ENERGY	SOURCE		DETECTOR		ANGLE
			TYPE	RANGE	TYPE	RANGE	
E,E/P	ABX	95	C	999	MAG-D		DST

Electron registration angle = 20°. 999 =1.2 GEV

We measured the cross section of the reaction $D(e, e'p)n$ at 1200 MeV as a function of the proton emission angle at a constant proton momentum. Within the framework of the plane-wave impulse approximation, we determined the momentum distribution in the deuterium nucleus, and compared it with the Hulthen distribution.

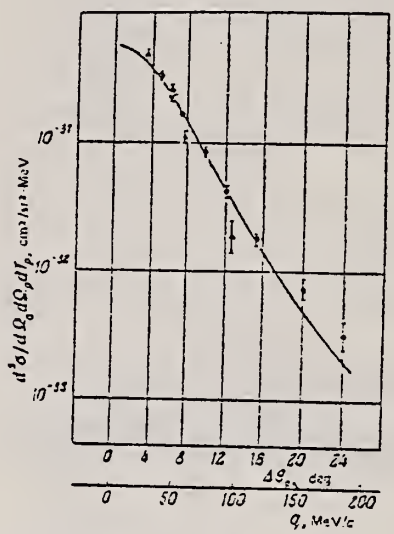

Angular distribution of the protons in the reaction $D(e, e'p)n$; •—our data, ▲—data of Bounin.[5] The angles $\Delta\theta$ are relative to the kinematics of free scattering.

REF.

K.F. Chong, M.C. Phenneger, Y.M. Shin, D.M. Skopik, and E.L. Tomusiak
Nucl. Phys. A218, 43 (1974)

ELEM. SYM.	A	Z
H	2	1

METHOD

REF. NO. 74 Ch 2 egf

REACTION	RESULT	EXCITATION ENERGY	SOURCE		DETECTOR		ANGLE
			TYPE	RANGE	TYPE	RANGE	
E,P	ABX	5- 44	D	30-107	MAG-D		DST

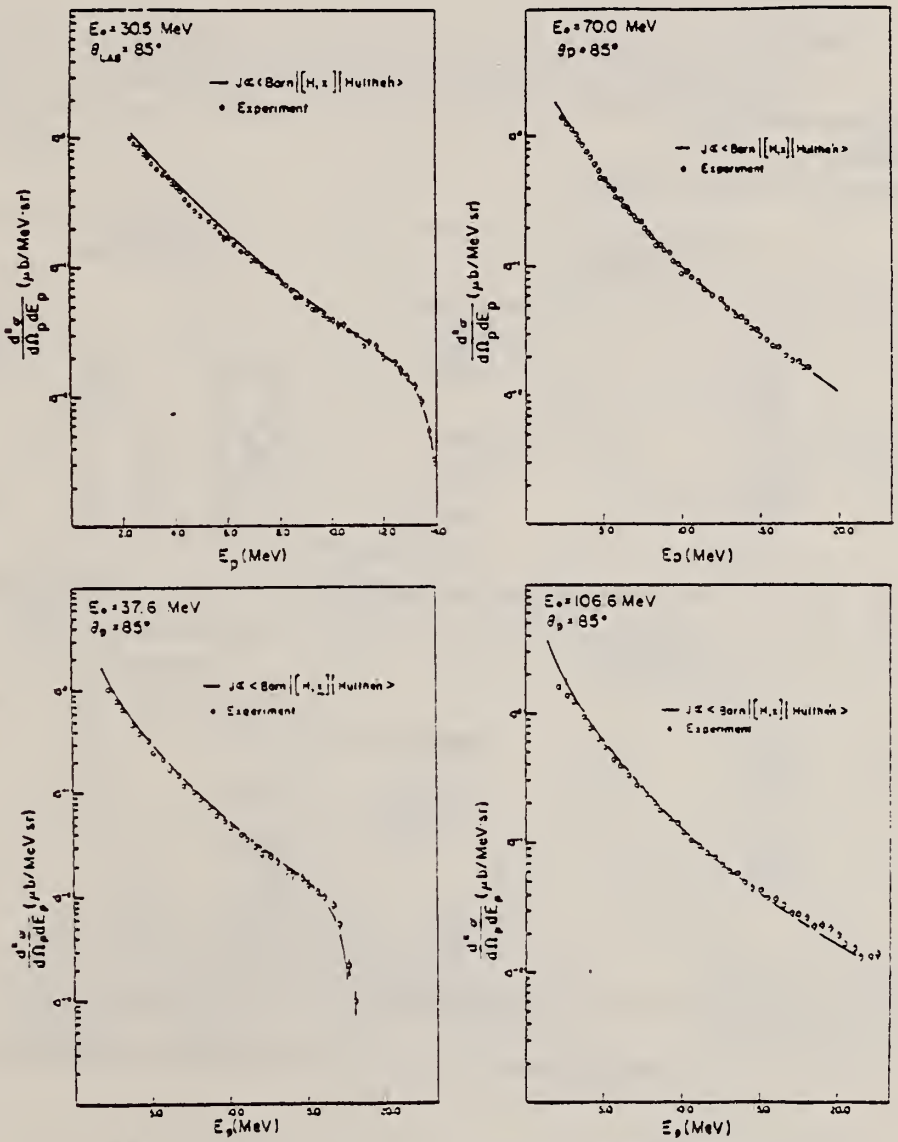

Fig. 5. Proton energy spectra at 35° as a function of the incident electron energy.

(continued)

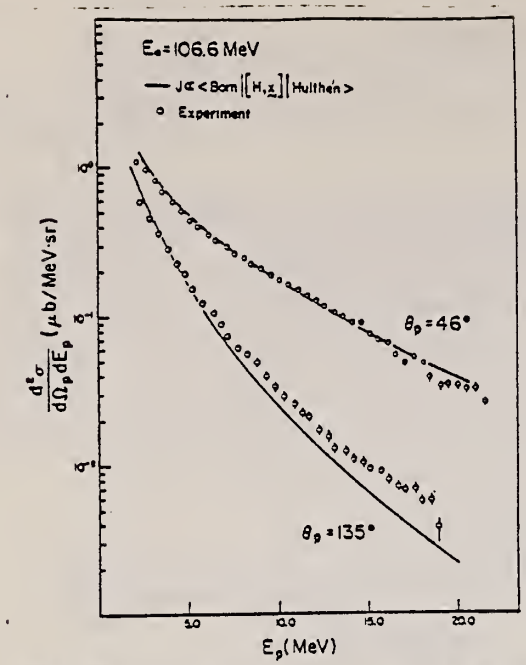

Fig. 6. Proton energy spectra at 46° and 135° for $E_0 = 106.6$ MeV.

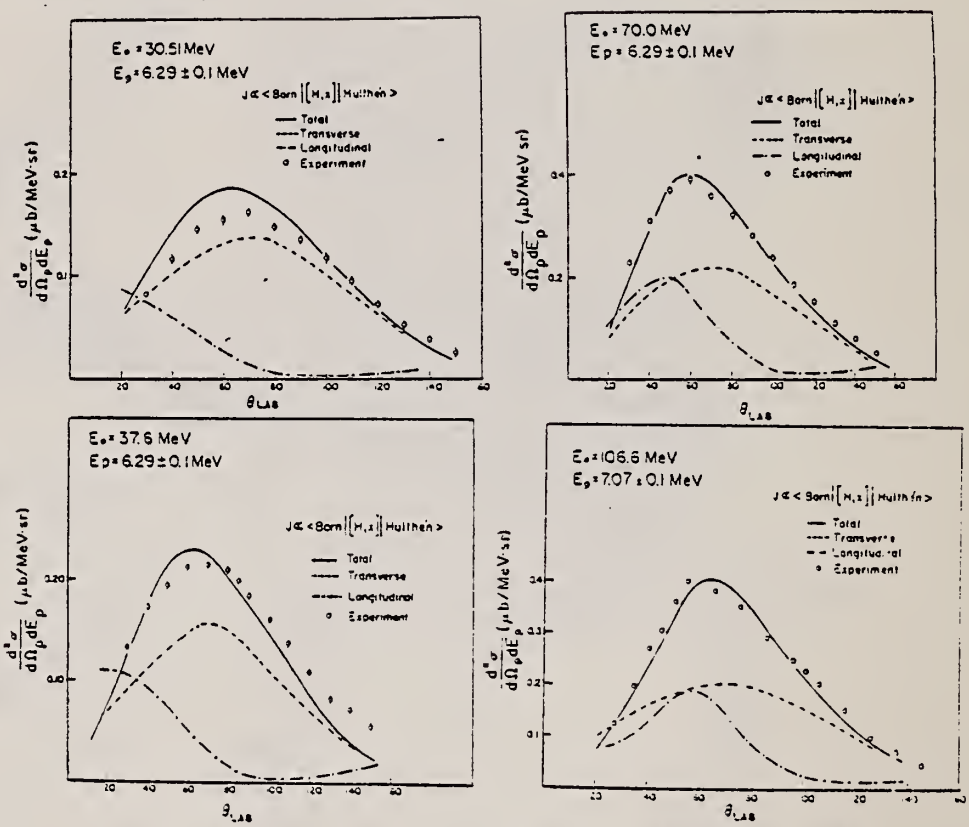

Fig. 4. The angular distribution of protons as a function of the incident electron energy.

REF.

R.W. Clifft, E. Gabathuler, L.S. Littenberg, R. Marshall, S.E. Rock, J.C. Thompson, D.L. Ward, and G.R. Brookes
Phys. Rev. Letters 33, 1500 (1974)

ELEM. SYM.	A	Z
H	2	1

METHOD

REF. NO.: 74 C1 10 hmg

REACTION	RESULT	EXCITATION ENERGY	SOURCE		DETECTOR		ANGLE
			TYPE	RANGE	TYPE	RANGE	
G,PI-	RLX	150-450	C	250-450	Tel-D		DST
G,PI+	RLX	150-450	C	250-450	Tof-D		DST
G,PI0	RLX	150-450	C	250-450	Tel-D		DST

TAGGED PHOTONS

Differential cross sections for the reactions $\gamma p \to \pi^0 p, \pi^+ n$ and $\gamma n \to \pi^- p, \pi^0 n$ were measured in a single experiment using tagged photons in the energy region 240–450 MeV incident on $^1H_2$ and $^2H_2$ targets. Results of the measurements of the ratios $\pi^0 n/\pi^0 p$ and $\pi^- p/\pi^+ n$ are presented. The ratio of isotensor to isovector amplitude is found to be 0.03 ± 0.02.

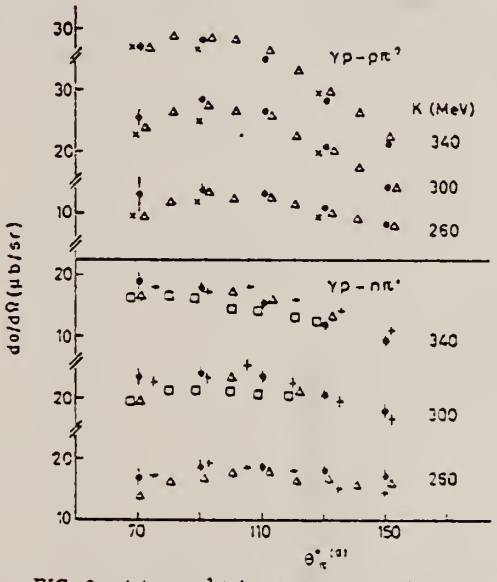

FIG. 3. $d\sigma(\gamma p \to \pi^0 p)/d\Omega$ and $d\sigma(\gamma p \to \pi^+ n)/d\Omega$ from a hydrogen target. Other data are shown for comparison (Ref. 5). The incident photon energy is K (MeV). Circles, present experiment; crosses, T. Fujii *et al.*; triangles, G. Fischer *et al.*; squares, C. Betourne *et al.*; exes, R. Morand *et al.*

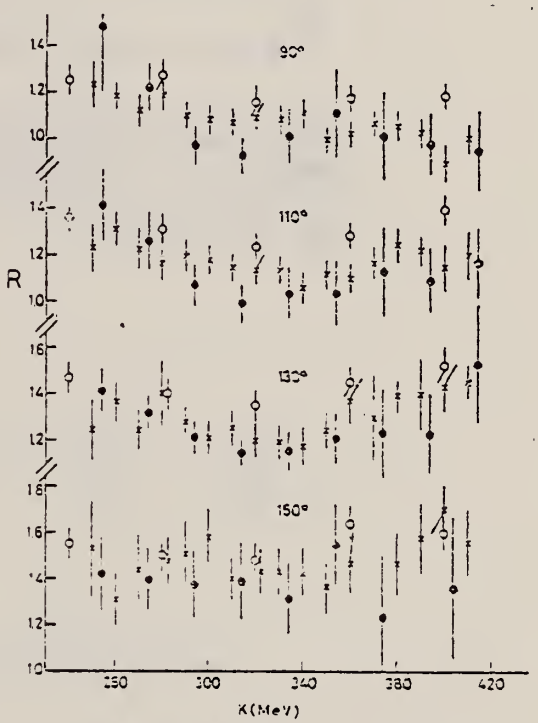

FIG. 4. The ratio $R = [d\sigma(\gamma n \to \pi^- p)/d\Omega][d\sigma(\gamma p \to \pi^+ n)/d\Omega]^{-1}$ from a deuterium target at center-of-mass pion angles of 90°, 110°, 130°, and 150° versus equivalent laboratory photon energy. Filled circles, present data; exes, T. Fujii *et al.*; open circles, G. von Holtey *et al.*

(continued)

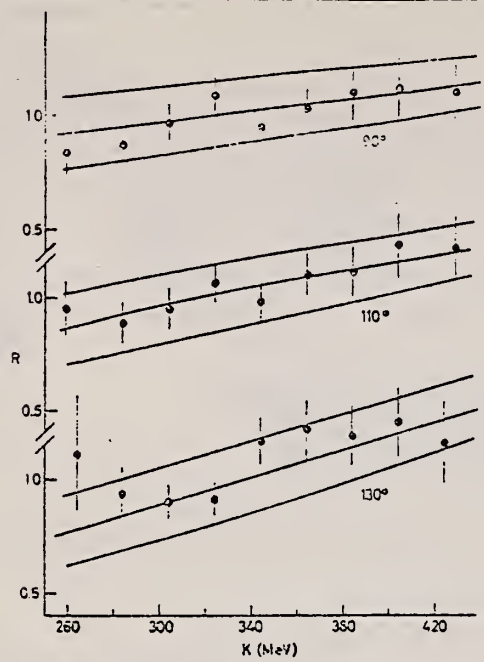

FIG. 5. The ratio $R=[d\sigma(\gamma n\to\pi^0 n)/d\Omega][d\sigma(\gamma p\to\pi^0 p)/d\Omega]^{-1}$ from a deuterium target at center-of-mass pion angles of 90°, 110°, and 130° versus equivalent laboratory photon energy. The lines are predictions in which t, the ratio of isotensor to isovector amplitude, is assumed equal to 0 and ±0.05.

REF. M. C. Phenneger and R. G. Winter
Nucl. Phys. A219, 589 (1974)

ELEM. SYM.	A	Z
H	2	1

METHOD

REF. NO.: 74 Ph 1 egf

REACTION	RESULT	EXCITATION ENERGY	SOURCE		DETECTOR		ANGLE
			TYPE	RANGE	TYPE	RANGE	
E,N	NOX	4- 11	D	4- 11	MOD-I		4PI

RATIO (G,N)/(E,N)

TABLE 1
Ratio R of photodisintegration to electrodisintegration for an 89.5 mg/cm² Cu converter

Incident electron energy E (MeV)	Experimental $R(E)$	Theoretical $R(E)$
4.15	0.569±0.027	0.558
5.20	0.566±0.023	0.561
8.15	0.521±0.010	0.537
10.25	0.537±0.008	0.515

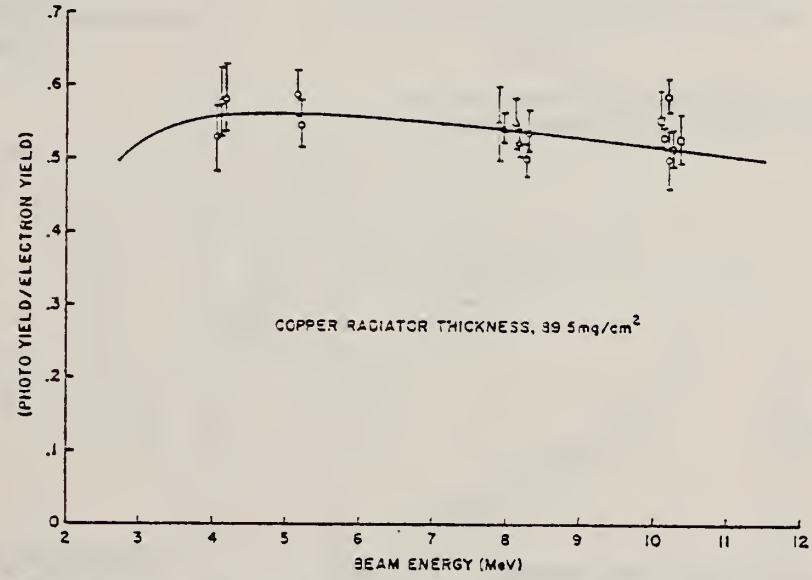

Fig. 2. The ratio R of photodisintegration to electrodisintegration yields as a function of incident electron energy. The curve shows the theoretical result.

REF.

D.M. Skopik, Y.M. Shin, M.C. Phenneger, and J.J. Murphy,II
Phys. Rev. C9, 531 (1974)

ELEM. SYM.	A	Z
H	2	1

METHOD

REF. NO.	
74 Sk 1	hmg

REACTION	RESULT	EXCITATION ENERGY	SOURCE		DETECTOR		ANGLE
			TYPE	RANGE	TYPE	RANGE	
E,P	ABX	17- 28	D	29	MAG-D		DST
				(29.7)			

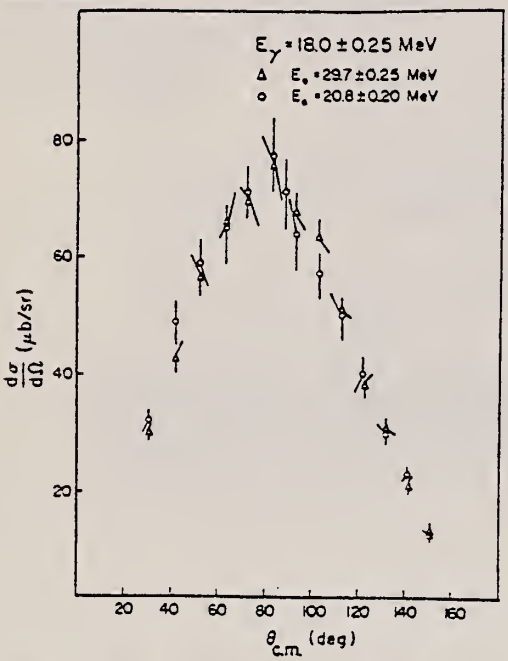

FIG. 4. Angular distribution of protons at E_γ = 18.0 ± 0.25 MeV for two incident electron energies.

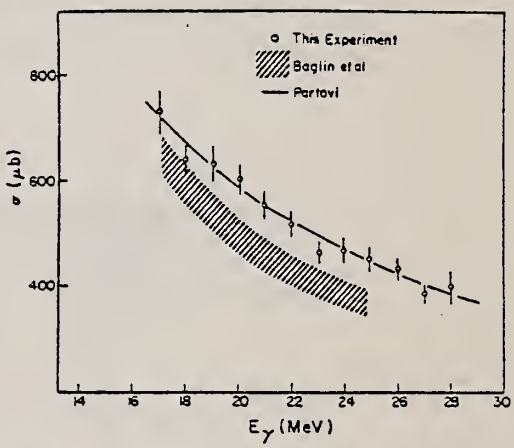

FIG. 6. Total cross section for the $^2H(\gamma,p)n$ reaction showing our results, those of Baglin *et al.* (Ref. 5), and Partovi's calculation. The total error is shown for both experiments.

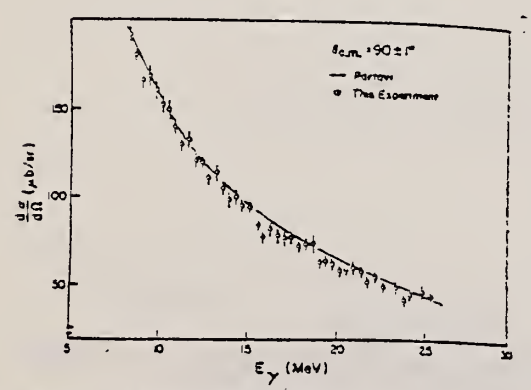

FIG. 7. Differential cross section at a c.m. angle of 90 ± 1°. The errors shown are statistical only.

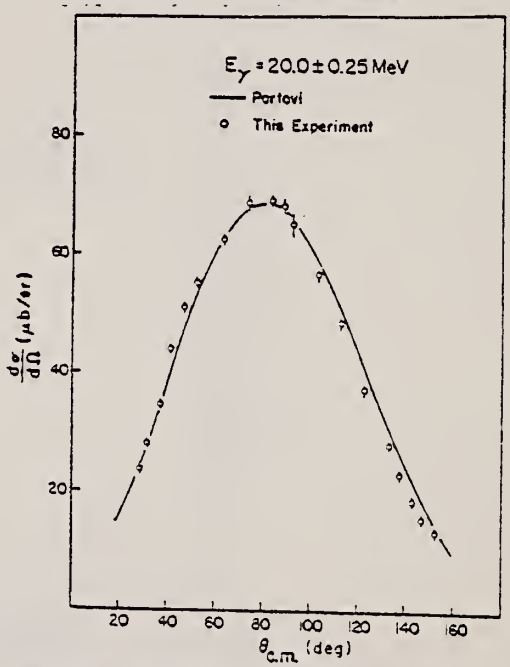

FIG. 5. Angular distribution of protons at E_γ = 20.0 ± 0.25 MeV. The solid line is the prediction of Partovi.

(continued)

TABLE II. Angular-distribution coefficients (μb/sr) of the form $d\sigma/d\Omega = A_\gamma + B_\gamma \sin^2\theta + C_\gamma \sin^2\theta \cos\theta + D_\gamma \sin^2\theta \cos^2\theta$ at $E_\gamma = 20.0 \pm 0.25$ MeV.

	A_γ	B_γ	C_γ	D_γ	σ_{tot} (μb)
Partovi	5.4	61.3	18	4.2	588
Solution of Eqs. (7)	4.8 ± 2.1	63 ± 2	26 ± 1	7.8 ± 1.2	604
Using Eqs. (8) for the virtual photon spectrum	4.0 ± 2.2	64 ± 2	30 ± 1	10 ± 2	605
Baglin *et al.*[a]	2.8 ± 0.9	55 ± 2	20 ± 4	(4.2)[b]	502

[a] Reference 5.
[b] Assumed Partovi's value.

TABLE III. Total-cross-section results determined from the angular-distribution data combined in 1.0-MeV intervals. Error assigned to each point is the total error determined by adding the percentage statistical and systematic errors in quadrature.

E_γ (MeV)	$\sigma \pm \Delta\sigma$ (μb)
17.0	730 ± 42
18.0	640 ± 31
19.0	637 ± 31
20.0	604 ± 29
21.0	534 ± 26
22.0	496 ± 24
23.0	460 ± 23
24.0	465 ± 23
25.0	445 ± 22
26.0	430 ± 21
27.0	377 ± 20
28.0	400 ± 29

[5] J.E. Baglin, R.W. Carr, E.J. Bentz, Jr., and C.P. Wu, Nucl. Phys. A201, 593 (1973).

REF. Yu. P. Antuf'ev, V.L. Agranovich, V.S. Kuz'menko, and P.V. Sorokin
Yad. Fiz. 22, 236 (1975)
Sov. J. Nucl. Phys. 22, 121 (1976)

ELEM. SYM.	A	Z
H	2	1

METHOD

REF. NO. 75 An 9 hmg

REACTION	RESULT	EXCITATION ENERGY	SOURCE TYPE	SOURCE RANGE	DETECTOR TYPE	DETECTOR RANGE	ANGLE
E,E/P	ABX	0*185	D	816,999	MAG-D		DST

999= 1.195 GEV,*MEV/C

Magnetic spectrometers, scintillation counters, and fast electronics including time-to-pulse-height converters have been used to study the reaction $d(e,e'p)n$ with detection of coincidences between the scattered electron and the ejected proton. We have measured the angular distribution of protons for an incident-electron energy of 1195 MeV and have obtained the momentum distribution of nucleons in deuterium in the momentum range from 0 to 185 MeV/c. We have also measured the dependence of the cross section for the $d(e,e'p)n$ reaction on the energy of the ejected proton for electron energies of 816 and 1195 MeV and on the polar angle of neutron emission. The latter experiment permitted a model-independent check of the applicability of the plane-wave impulse approximaion for description of the reaction for recoil-neutron momenta less than 100 MeV/c.

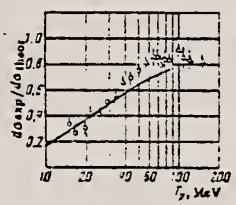

FIG. 3. Ratio of cross sections measured in (p, 2p) experiments [13] (points ○) and in (e, e'p) experiments (points △) to that calculated in the plane-wave impulse approximation, as a function of the energy of the emitted protons. The smooth curve is a calculation from ref. 13.

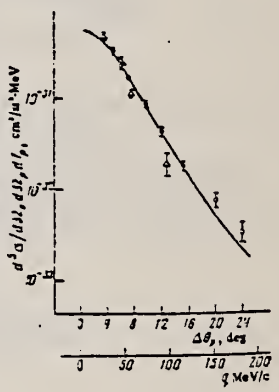

FIG. 1. Cross section for the d(e, e'p)n reaction as a function of the proton-emission angle. The reference angle is from the kinematics of free scattering. The smooth curve is a calculation with the Hulthén wave function; the triangles are the data of ref. 5, normalized to our points (circles). The errors shown are only statistical.

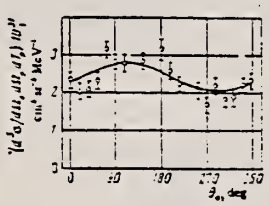

FIG. 5. Cross section for the d(e, e'p)n reaction as a function of neutron-emission angle relative to the primary electron. The positive direction in computation of the angle θ_n is given by the vector $k_1 \times k_0$. The errors are only statistical.

5 P. Bounin, Ann. Phys. (Paris) 10, 400 (1965).
13 R.D. Haracz and T.K. Lim, Phys. Rev. Lett. 31, 1263 (1973).

REF. G. Chiefari, E. Drago, M. Napolitano, C. Sciacca, L. Votano
Nuovo Cimento Lett. 13, 129 (1975)

ELEM. SYM.	A	Z
H	2	1

METHOD

REF. NO. 75 Ch 3 egf

REACTION	RESULT	EXCITATION ENERGY	SOURCE		DETECTOR		ANGLE
			TYPE	RANGE	TYPE	RANGE	
G,PI-	ABX	200-450	C	450	BBL-D		4PI

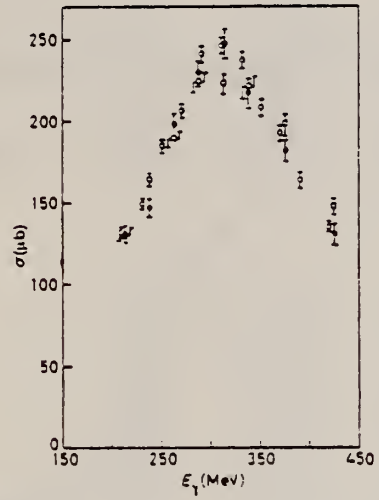

Fig. 1.

Fig. 1. – Total cross-section of the reaction $\gamma+D\to p+p+\pi^-$: • this experiment, ▫ ref. (4), ○ ref. (5).

[1] G. Susinno: Proc. Informal Meeting on Electromagnetic Interactions, Frascati, May 2-3, 1972.

[5] P. Benz et al., Nucl. Phys. 65B, 158 (1973).

TABLE I. – *Total cross-section of the reaction* $\gamma D\to pp\pi^-$.

E_γ (MeV)	σ (μb)
200÷225	131.3 ± 5.2
225÷250	147.1 ± 5.9
250÷275	197.9 ± 7.3
275÷300	229.8 ± 8.3
300÷325	247.8 ± 9.0
325÷350	217.5 ± 8.9
350÷400	181.7 ± 6.4
400÷450	131.0 ± 6.3

REF.

P. Dougan, T. Kivikas, K. Lugner, V. Ramsay and W. Stiefler
Z. Physik A276, 55 (1976)

ELEM. SYM.	A	Z
H	2	1

METHOD

REF. NO.: 76 Do 5 egf

REACTION	RESULT	EXCITATION ENERGY	SOURCE		DETECTOR		ANGLE
			TYPE	RANGE	TYPE	RANGE	
G,P	ABX	139 - 832	C	999	TEL-D		DST

Abstract. The cross-sections for deuteron photo-disintegration have been measured at nine c.m. angles from 37 to 143 degrees. The minimum and maximum photon energies have been 139 and 832 MeV respectively. The results are in agreement with earlier data above 300 MeV, but are significantly larger below 200 MeV, the discrepancies being up to 50% at the lowest energies measured.

999=1.2GEV

Fig. 3. The cross-sections for deuteron photo-disintegration at proton c.m. angles of 53°, 78°, 101° and 127° found in the present measurements are compared with other values reported in the literature. As can be seen, there are large variations in the values from different laboratories below 300 MeV

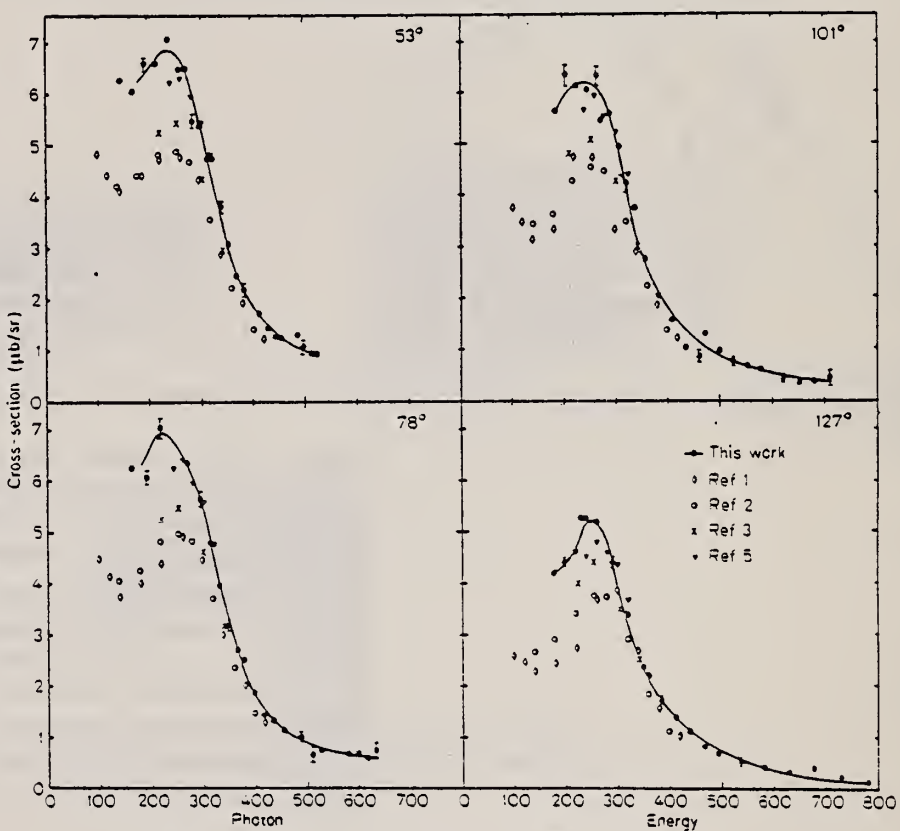

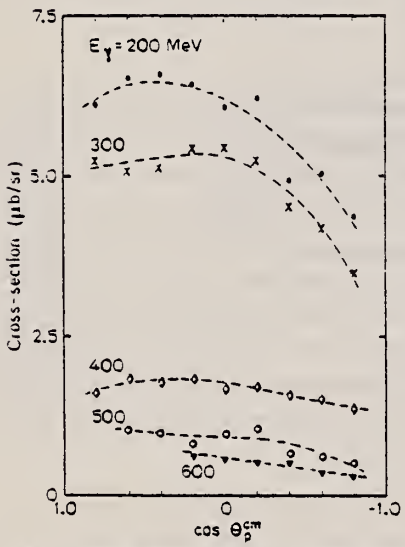

Fig. 2. Angular distributions of the cross-sections for deuteron photo-disintegration obtained by interpolation in the data of Table I in steps of 100 MeV from 200 to 600 MeV. The curves through the points show third-order fits in cos θ_p^{cm} to the data

[1] Kose,R., Paul, W., Stockhorst, K., Kissler, K.H.: Z. Physik 202, 364 (1967)

[2] Buon,J., Gracco, V., Lefrancois, J., Lehmann, P., Merkel, B., Roy, Ph.: Phys. Lett. 26B, 595 (1968)

[3] Anderson, R.L., Prepost, R., Wiik, B.H.: Phys. Rev. Lett. 22, 651 (1969)

(cont.)

[5] Sober, D.I., Cassel, D.G., Sadoff, A.J., Chen, K.W., Crean, P.A.: Phys. Rev. Lett. 22, 430 (1969)

Table 1. The cross-sections for deuteron photo-disintegration obtained in the present measurements

C.M. angle	Photon energy (MeV)	Cross-section (μb/sr)	Stat error (%)	C.M. angle	Photon energy (MeV)	Cross-section (μb/sr)	Stat error (%)
36.9				66.5	305.8	5.318	2.4
36.0	139.1	5.944	2.8	66.9	321.5	4.343	2.8
36.4	160.4	5.299	3.5	67.2	336.7	3.815	3.2
36.7	180.9	5.880	2.5	65.7	349.0	3.541	4.6
37.2	201.2	6.233	3.9	66.1	365.6	2.720	5.6
37.5	219.9	6.113	4.3	66.4	381.8	2.175	6.5
36.5	239.7	6.390	4.3	66.7	397.7	1.766	7.3
36.7	253.4	6.438	3.0	67.0	413.2	1.847	8.8
36.9	266.4	6.280	3.2	66.2	446.5	1.273	8.6
37.1	279.1	6.156	3.3	66.5	463.4	1.127	9.2
37.3	291.3	5.496	3.6	66.8	480.0	0.991	10.3
36.6	303.6	5.253	2.9	67.1	496.4	1.004	11.2
36.7	316.9	4.265	3.4	66.0	526.6	1.101	12.0
36.9	329.9	3.795	3.2	66.2	541.9	0.803	14.4
37.1	342.6	3.265	3.6	66.5	557.0	0.593	17.4
37.3	354.9	3.071	4.7	66.8	572.0	0.650	17.4
36.9	383.8	1.854	9.4				
37.0	397.1	1.808	9.7	*78.5*			
37.2	410.1	1.406	8.5	76.7	164.1	6.250	3.1
37.3	422.9	1.404	8.6	77.6	192.0	6.061	3.8
36.7	450.0	1.172	14.4	78.4	219.3	7.031	3.5
36.8	462.0	0.944	17.1	79.2	246.8	6.291	4.1
37.0	473.7	1.095	15.2	80.0	272.6	6.333	4.3
37.1	485.3	1.121	15.6	77.8	295.3	5.652	2.5
				78.2	314.2	4.787	2.9
53.1				78.7	332.5	3.960	3.2
52.0	146.2	6.261	3.0	79.1	350.4	3.174	3.6
52.6	169.3	6.040	3.5	79.5	367.9	2.700	5.5
53.2	191.6	6.576	3.4	77.8	380.3	2.500	4.1
53.7	213.8	6.597	3.7	78.2	399.4	1.865	5.4
54.2	234.4	7.050	3.8	78.6	418.0	1.412	6.8
52.6	254.8	6.456	3.7	79.0	436.4	1.306	8.4
52.9	269.9	6.477	4.0	79.4	454.4	1.125	9.6
53.2	284.3	5.460	4.6	78.2	489.8	0.986	14.8
53.5	298.3	5.364	4.8	78.5	509.3	0.644	20.3
53.8	311.8	4.707	5.3	78.9	528.6	0.747	19.2
52.7	324.3	4.703	3.3	78.1	580.8	0.677	14.3
52.9	339.1	3.791	3.9	78.4	598.7	0.689	14.6
53.2	353.5	3.056	4.6	78.7	616.5	0.580	16.4
53.5	367.5	2.463	5.5	79.0	634.1	0.711	15.4
53.7	381.3	2.168	6.4				
53.0	412.0	1.717	7.7	*900*			
53.2	426.3	1.408	8.5	87.9	176.0	5.812	3.0
53.5	441.4	1.276	8.8	88.9	207.2	6.114	3.4
53.7	455.8	1.224	8.9	89.9	238.0	6.700	3.3
52.8	484.4	1.288	15.3	90.8	269.5	6.406	3.7
53.0	497.8	1.059	17.9	91.6	299.2	5.588	4.3
53.2	511.0	0.939	15.4	89.0	322.8	4.434	2.9
53.4	524.0	0.907	16.4	89.5	344.7	3.684	3.5
				90.0	365.9	2.544	4.5
56.4				90.5	386.8	2.125	7.2
64.9	154.3	5.925	3.0	91.0	407.2	1.450	9.4
65.7	179.6	6.298	3.3	88.9	419.0	1.769	4.4
66.4	204.1	6.774	3.2	89.4	441.3	1.251	5.7
67.1	228.6	6.992	3.4	89.9	463.2	1.142	8.0
67.7	251.5	6.827	3.8	90.3	484.8	1.031	8.7
65.7	272.9	6.432	1.9	90.8	506.2	0.974	13.0
66.1	289.7	6.048	2.1	89.6	546.0	0.761	10.1

REF. E.D. Earle, A.B. McDonald, and M.A. Lone
Phys. Rev. C14, 1298 (1976)

ELEM. SYM.	A	Z
H	2	1

METHOD

REF. NO. 76 Ea 3 hmg

REACTION	RESULT	EXCITATION ENERGY	SOURCE		DETECTOR		ANGLE
			TYPE	RANGE	TYPE	RANGE	
N,2G	ABX	2	D	0	SCD-D		85
		(2.223)					

ANG BTW DET, SIG LIM

A value of $(-0.8 \pm 2.5) \times 10^{-5}$ has been measured for the ratio of double-photon to single-photon emission following neutron capture in hydrogen for 600 keV $< E_\gamma <$ 1620 keV. The two Ge(Li) detectors used in the experiment subtended an angle of 85° at the H_2O target and were shielded from each other to reduce the background from the cross registration of single γ rays. The upper limit of the measured two-photon cross section ($-3 \pm 8\ \mu$b) is two orders of magnitude larger than the most recent theoretical predictions ($\approx 0.07\ \mu$b) for this energy range.

REF.

R. J. Hughes, A. Zieger, H. Waffler, B. Ziegler
Nucl. Phys. A267, 329 (1976)

ELEM. SYM.	A	Z
H	2	1

METHOD

REF. NO.: 76 Hu 4 | egf

REACTION	RESULT	EXCITATION ENERGY	SOURCE		DETECTOR		ANGLE
			TYPE	RANGE	TYPE	RANGE	
G,P	ABX	20-120	D	20-120	MAG-D		0

Abstract: The absolute differential cross section for the photodisintegration of the deuteron at 0° for the outgoing protons has been measured at lab photon energies of 20, 30, 40, 75, 100 and 120 MeV using a magnetic spectrometer and a bremsstrahlung beam. The absolute cross-section values have an error of ±6 % and were determined with an angular resolution of 1.5°. A serious discrepancy is found to exist between the measured 0° cross sections and those predicted by calculations using the Hamada-Johnston and the boundary condition potential models.

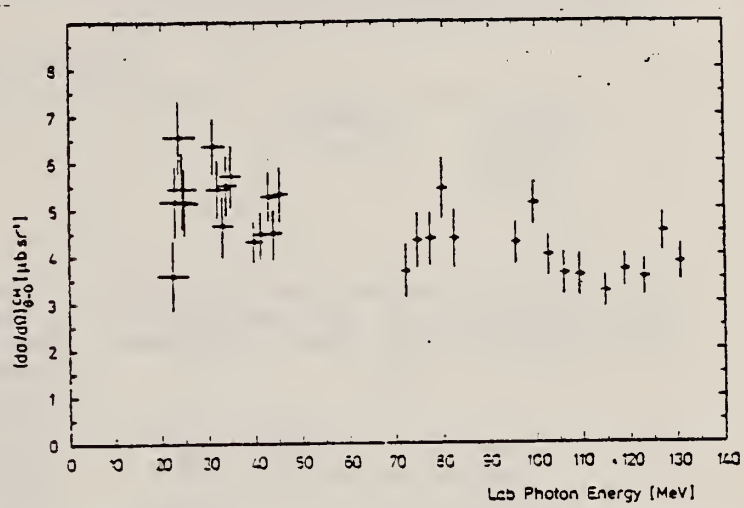

Fig. 9. Measured differential cross-section values $(d\sigma(\theta)\, d\Omega)^{CM}_{\theta=0}$ from the five proton detectors at the six spectrometer energy settings. The errors shown are from counting statistics. A further ±3 % systematic error is to be assigned to each value.

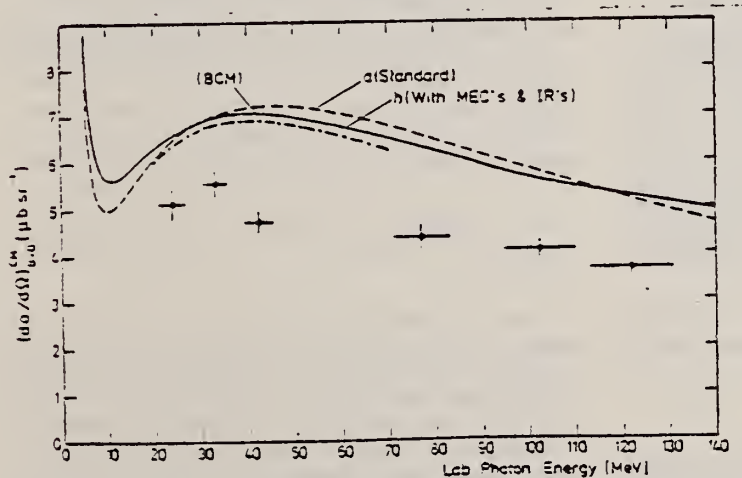

Fig. 10. Statistically weighted average differential cross-section values $(d\sigma(\theta), d\Omega)^{CM}_{\theta=0}$ for the six spectrometer energy settings. The errors shown are from counting statistics. A further ±3 %, systematic error is to be assigned to each value. Curves (a) and (b) are the 0° differential cross sections from the calculation of Arenhövel *et al.* [2]), respectively, without and with the inclusion of the effects due to meson exchange currents and isobar resonance admixtures. The dot-dashed curve [8]) is $(d\sigma(\theta), d\Omega)^{CM}_{\theta=0}$ as calculated by the method of Partovi using the boundary condition model (BCM) potential of Loman and Wilson [9]).

[2] H. Arenhovel et al., Phys. Lett. 52B (1974) 303; W. Fabian, Doctoral thesis (Mainz 1976).
[8] R. Wilson, priv. commun.
[9] E. Loman et al., Phys. Rev. C9 (1974) 1329.

REF.

G.G. Simon, F. Borkowski, Ch. Schmitt, V.H. Walther,
H. Arenhövel, and W. Fabian
Phys. Rev. Lett. 37, 739 (1976)

ELEM SYM.	A	Z
H	2	1

METHOD

REF. NO. 76 SI 11 hmg

REACTION	RESULT	EXCITATION ENERGY	SOURCE		DETECTOR		ANGLE
			TYPE	RANGE	TYPE	RANGE	
E,E/	ABX	2 - 80	D	80-300	MAG-D		DST

Electrodisintegration of the deuteron has been measured for an incident energy of 300 MeV at 30° and 90° scattering angles. The maximum energy transfer was 116 MeV. Very good agreement with theory was achieved when the pionic-exchange currents were included. Near the threshold and for momentum transfer $\vec{q}_{c.m.}^{\,2} = 3.9$ fm^{-2}, the meson-exchange currents contribute about 40% to the total cross section.

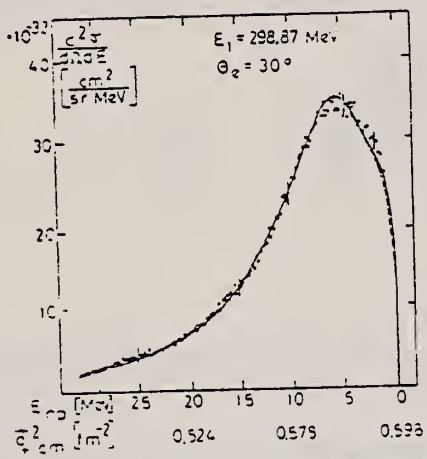

FIG. 2. The double differential cross section at 30° versus the neutron-proton relative energy E_{np}. The corresponding momentum transfer is also indicated. The error bars include both the statistical and systematical errors. The theoretical calculation with (without) the interaction effects is given by the solid (dashed) line.

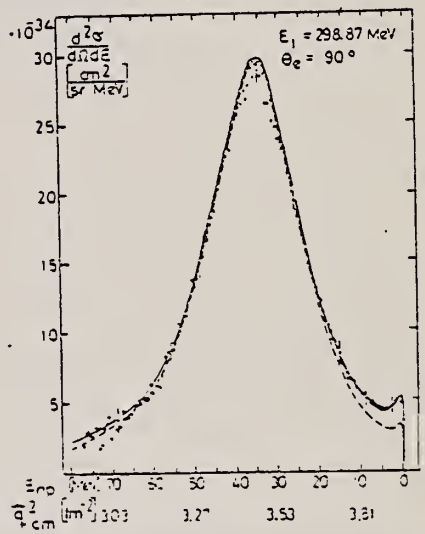

FIG. 3. Same as Fig. 2, but for a scattering angle of 90°.

REF. V.L. Agranovich, V.S. Kuz'menko, P.V. Sorokin
Yad. Fiz. 25, 1123 (1977)
Sov. J. Nucl. Phys. 25, 595 (1977)

ELEM. SYM.	A	Z
H	2	1

METHOD

REF. NO. 77 Ag 8 hg

REACTION	RESULT	EXCITATION ENERGY	SOURCE		DETECTOR		ANGLE
			TYPE	RANGE	TYPE	RANGE	
E,E/P	SPC	160*300	D	999	MAG-D		20

*MEV/C 999=1180 MEV

Momentum distribution of nucleons in deuterium from the $D(e,e'p)n$ reaction

V. L. Agranovich, V. S. Kuz'menko, and P. V. Sorokin

Khar'kov Physicotechnical Institute. Academy of Sciences of the Ukrainian SSR
(Submitted May 10, 1976)
Yad. Fiz. 25, 1123–1124 (May 1977)

PACS numbers: 25.10.+s, 25.30.Cg

Measurements of the quasielastic-scattering cross section of deuterium in the region of large spectator momenta ($p_s > 150$ MeV/c) can provide valuable information on the nuclear wave function, mesonic effects in the nucleon–nucleon interaction, and the reaction mechanism. Up to now, no such data on the $D(e, e'p)n$ reaction have been available. Here we present the results of the first experiment on the $D(e, e'p)n$ reaction in the region of large spectator-neutron momentum (160–300 MeV/c).

We have described the apparatus employed and the experimental technique elsewhere.[1] The kinematic conditions of the measurements (electron scattering angle $\theta_e = 20°$, initial electron energy $k_0 = 1180$ MeV, and ejected proton momentum $p_p = 550$ MeV/c) were so chosen that the energy of the scattered electron would be 70 MeV lower than the energy at the maximum of the quasielastic peak. This made it possible to reduce the accidental-coincidence background several-fold and to make measurements at considerably higher spectator-neutron momenta than we did in our earlier work.[1]

The results of the measurements, together with earlier data obtained by us[1] and by Bounin,[2] are shown in Fig. 1. Radiative corrections amounting to as much as 26% have been made. The cross sections were measured with an accuracy of 20%. The curves show the results of plane-wave impulse-approximation calculations, made using only the Hulthén S-state wave function (full curve) and a wave function containing a 5% D-state admixture (dashed curve). It will be seen that the new measurements agree well with the earlier results[1] in the momentum region around 160 MeV/c. It is also evident that the ratio of the measured cross section to the calculated one increases systematically as p_s rises above 120 MeV/c, the ratio reaching 3 at $p_s = 300$ MeV/c.

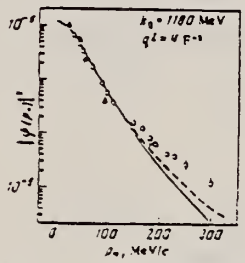

FIG. 1. Momentum distribution of the spectator nucleon in the $D(e, e'p)n$ reaction. The open circles represent our data, and the black triangles, those of Bounin.[2] Only the statistical errors are indicated. The full curve was calculated in the plane-wave impulse approximation with the experimental apparatus bins taken into account; the dashed curve was calculated with allowance for a 5% D-state admixture in the Hulthén wave function.

We wish to express our gratitude to S. V. Dementii for pointing out the usefulness of investigating the $(e, e'p)$ reaction at large p_s under the kinematic conditions described above.

[1]Yu. P. Antuf'ev, V. L. Agranovich, V. S. Kuz'menko, and P. V. Sorokin, Pis'ma Zh. Eksp. Teor. Fiz. 19, 657 (1974) [JETP Lett. 19, 339 (1974)]; Yad. Fiz. 22, 236 (1975) [Sov. J. Nucl. Phys. 22, 121 (1976)].
[2]P. Bounin, Ann. Phys. (Paris) 10, 475 (1965).

Translated by E. Brunner

REF. G. Audit, A. Bloch, N. de Botton, J.L. Faure, C. Schuhl, G. Tamas, C. Tzara, E. Vincent, J. Deutsch, D. Favart R. Prieels, and B. Van Oystaeyen
Phys. Rev. C 16, 1517 (1977)

ELEM. SYM.	A	Z
H	2	1

METHOD

REF. NO. 77 Au 4 hmg

REACTION	RESULT	EXCITATION ENERGY	SOURCE		DETECTOR		ANGLE
			TYPE	RANGE	TYPE	RANGE	
(G,PI+)	RLX	148 - 155	C	150-155	ACT-I		4PI

The π^+ photoproduction on deuterium near threshold was measured and compared to the same process in hydrogen. The cross section for deuterium was extracted with a ± 2.5% accuracy for energies ranging from 1 to 4 MeV above threshold. The comparison of our result with theoretical estimates shows that the process is correctly understood in the frame of the impulse approximation.

D(G,PI+)/P(G,PI+)

TABLE I. Photoproduction yield per nucleus and beam intensity unit, and percentage of background which was subtracted for different values of the nominal bremsstrahlung end point energy for the H_2O and D_2O targets.

E_e (MeV)	$A_p(E_e)$ (a.u.)	Background (%)	E_e (MeV)	$A_d(E_e)$ (a.u.)	Background (%)
152.5	1.05 ± 0.15	6	150.0	0.14 ± 0.03	49
153.0	4.05 ± 0.27	3	150.5	0.42 ± 0.04	7
153.3	3.78 ± 0.42	1	151.0	1.21 ± 0.08	7
154.0	16.09 ± 0.55	0.4	151.5	2.06 ± 0.11	6
155.0	34.27 ± 1.00	0.4	152.0	3.54 ± 0.14	4
			152.5	5.40 ± 0.21	3
			153.0	7.82 ± 0.25	2
			153.5	10.22 ± 0.32	1
			154.0	14.33 ± 0.60	0.6

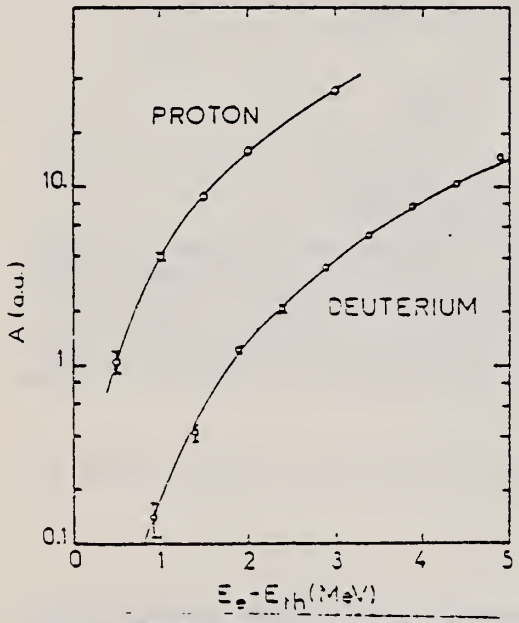

FIG. 1. Measured π^+ photoproduction yields per nucleus as a function of the excess energy above threshold in the laboratory system for deuterium and hydrogen. Solid lines are the calculated yields giving the best fit to the experiment.

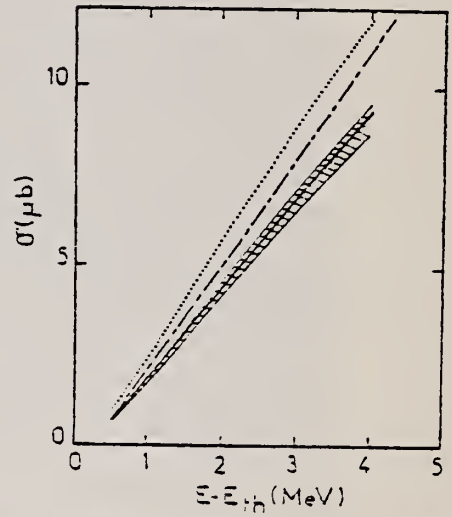

FIG. 2. Cross section of the (γ,π^+) reaction on deuterium deduced from this experiment. $E - E_{th}$ is the excess energy above threshold in the laboratory system. The shaded area corresponds to the experimental determination: the uncertainty on $a_2 = 4\pi E_\gamma^2$ is included in addition to the uncertainty on a_1. Dotted (Ref. 4), dash-dotted (Ref. 7), and solid (Ref. 11) lines are the theoretical predictions.

[4] C. Tzara, Nucl. Phys. A256, 381 (1976)
[7] J.S. O'Connell, Bull. Am. Phys. Soc. 21, 983 (1976); and private communication -
[11] J.V. Noble, Phys. Lett. 67B, 39 (1977)

REF.

E.C. Booth, B. Chasan, A.M. Bernstein, P. Bosted, J.H. Koch
Phys. Lett. 66B, 236 (1977)

ELEM. SYM.	A	Z
H	2	1

METHOD

REF. NO.	
77 Bo 1	egf

REACTION	RESULT	EXCITATION ENERGY	SOURCE		DETECTOR		ANGLE
			TYPE	RANGE	TYPE	RANGE	
G,PI+	ABX	149-158	C	148-158	ACT-I		4PI

We have measured the excitation function from threshold to 9 MeV above threshold for the reaction $\gamma + d \rightarrow \pi^+ + n + n$ by counting positrons after the bremsstrahlung beam burst. The extracted cross section is compared with a calculation using the impulse approximation, and good agreement is found near threshold.

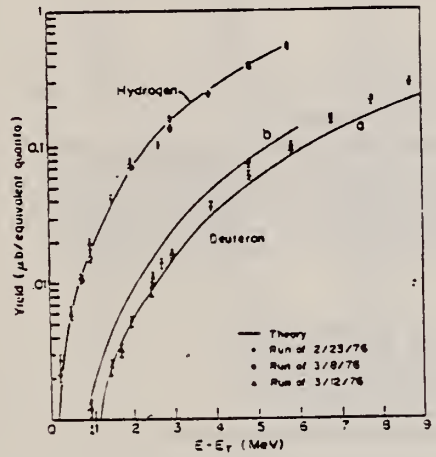

Fig. 1. Yield curves for the reactions $\gamma(p,n)\pi^+$ and $\gamma(d,nn)\pi^+$. The hydrogen data is scaled to fit the yield obtained from $\sigma_p = a_p q/k$ shown as a solid line, and deuterium is normalized to hydrogen. Curves a and b are calculated from theoretical cross sections shown in fig. 2.

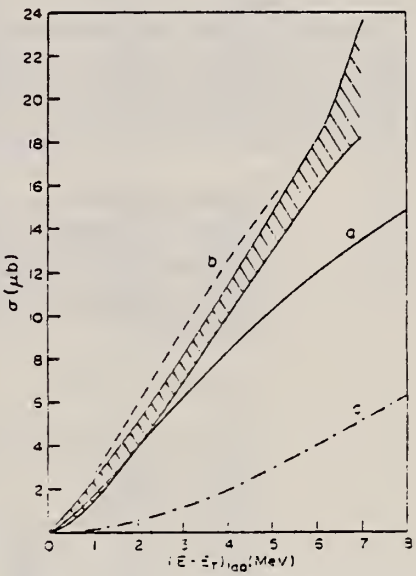

Fig. 2. The $\gamma(d,nn)\pi^+$ cross section deduced from the yield curve in fig. 1. The shaded area shows the limit of the statistical errors, to which a 6% systematic error must be added. Curves a, b, and c are defined in the text.

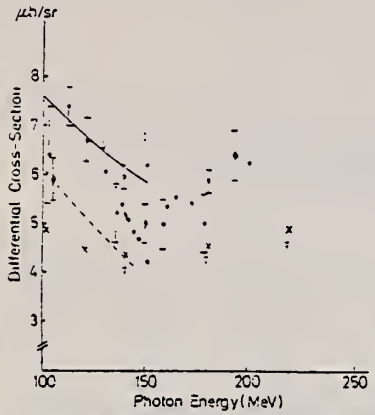

Fig. 2. Cross-sections for deuteron photo-disintegration at 37° c.m. from experiments at Lund and from various sources in the literature. The results of calculations by Fabian and Arenhövel [18] are also shown. The abbreviations are as in the text. • This work, ○ Lund (1973–1974) [2], ◇ Moscow [13], ▽ Orsay [4], × Bonn [3], ♦ Illinois [14], —— RSC + IC + MEC [18], – – – BS [18]

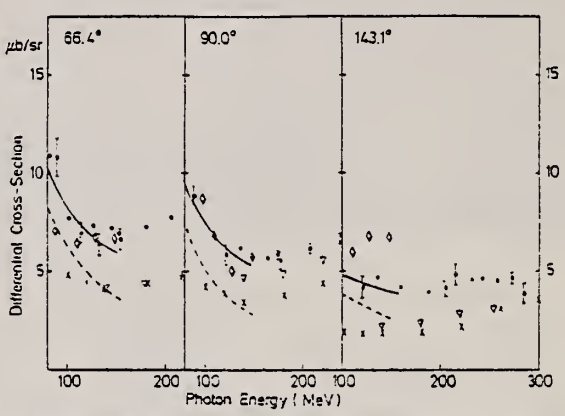

Fig. 3. Cross-sections for deuteron photo-disintegration at nominal proton c.m. angles of 66.4°, 90.0° and 143.1° from experiments at Lund and elsewhere. As in Figure 2, the reproducibility of the earlier Lund data is clearly seen, as is the systematic discrepancy with Bonn-Orsay data. • This work, ○ Lund [1, 2], ◇ Moscow [13], ▽ Orsay [4], × Bonn [3], —— RSC + IC + MEC [18], – – – BS [18]

Table 3. The coefficients of third-order fits in the variable $x = \cos\theta_\gamma^{cm}$ to interpolated fits derived from the complete Lund data-set. The results given by fits of other orders are similar. At energies up to 275 Mev, the data given here replace those in Table 3.2 of [1]. Note that at 100 MeV and above 475 MeV, the angular range covered by the measurements is less than at the other energies, so that the values of total cross-sections can be slightly inaccurate. At the other energies, the total cross-sections should be accurate to better than 10%

$$\frac{d\sigma}{d\Omega} = a + bx + cx^2 + dx^3$$

Photon Energy (MeV)	Angular Range (degrees)	a	b	c	d	σ (μb)
100	37–114	7.63	3.97 ± 0.68	−0.94 ± 1.38	−6.3 ± 2.8	91.9
125	37–143	6.02	2.10 ± 0.45	−0.84 ± 0.34	−1.1 ± 0.8	72.1
150	37–143	5.35	2.78 ± 0.63	−2.01 ± 0.47	−4.3 ± 1.2	65.1
175	37–143	5.95	2.05 ± 0.54	−1.94 ± 0.45	−2.1 ± 1.1	66.6
200	37–143	6.24	1.51 ± 0.41	−1.54 ± 0.34	−0.5 ± 0.8	71.9
225	37–143	6.39	1.96 ± 0.37	−1.40 ± 0.31	−1.6 ± 0.7	74.4
250	37–143	6.60	1.33 ± 0.25	−1.73 ± 0.21	−0.1 ± 0.5	75.6
275	37–143	5.88	0.29 ± 0.80	−1.00 ± 0.67	1.1 ± 1.6	69.7
300	37–143	5.20	0.52 ± 0.32	−1.61 ± 0.27	0.9 ± 0.6	59.8
325	37–143	4.34	0.83 ± 0.29	−1.43 ± 0.25	−0.2 ± 0.6	48.6
350	37–143	3.24	0.75 ± 0.20	−0.94 ± 0.17	−0.2 ± 0.4	36.8
375	37–143	2.40	0.61 ± 0.14	−0.94 ± 0.12	−0.7 ± 0.3	26.2
400	37–143	1.77	0.35 ± 0.12	−0.38 ± 0.12	−0.3 ± 0.2	20.7
425	37–143	1.45	0.36 ± 0.11	−0.38 ± 0.10	−0.2 ± 0.4	16.6
450	37–143	1.16	0.30 ± 0.11	−0.26 ± 0.10	−0.1 ± 0.2	13.5
475	37–143	1.08	0.18 ± 0.18	−0.41 ± 0.15	0.3 ± 0.4	11.9
500	53–143	0.93	0.13 ± 0.27	−0.20 ± 0.34	0.4 ± 0.7	10.9
525	53–143	0.80	0.33 ± 0.26	−0.09 ± 0.33	−0.1 ± 0.7	9.7
550	66–143	0.72	0.14 ± 0.17	0.07 ± 0.49	0.4 ± 0.7	9.3
575	66–143	0.69	0.11 ± 0.13	−0.43 ± 0.39	−0.1 ± 0.6	6.9
600	78–143	0.60	0.34 ± 0.12	0.19 ± 0.62	0.3 ± 0.7	8.3
625	78–143	0.51	0.60 ± 0.15	1.08 ± 0.74	0.9 ± 0.8	10.9

(continued)

Table 2. Cross-sections for deuteron photo-disintegration as measured in this experiment. A certain grouping of data has been made at some values to improve the statistical accuracy. At any one angle, the photon energy-resolutions (FWHM) are given approximately by the differences between successive entries in the table. At some angles, runs have been made at several end-point energies to be certain that protons from direct meson-production processes were not being counted. Systematic errors for any value are about 5%

C.M. angle (degrees)	E_γ (MeV)	Cross-section (μb/sr)	Stat. Error (%)
Nominal angle 36.9°			
36.1	73.8	10.73	12.2
36.4	81.8	9.55	14.7
36.6	91.3	8.37	11.8
36.9	102.9	6.41	17.5
36.9	111.7	7.41	6.0
37.1	121.2	6.66	6.9
37.3	130.1	6.23	7.2
37.2	138.6	5.41	5.9
37.2	147.7	4.52	6.9
37.2	157.9	5.00	9.8
37.3	165.0	5.53	7.8
37.5	171.8	5.41	8.3
37.6	178.3	5.01	11.3
Nominal angle 53.1°			
52.9	102.1	8.48	7.2
53.3	113.6	7.77	8.2
53.6	124.2	7.46	9.6
53.9	134.2	6.50	11.8
54.2	143.5	6.21	13.6
Nominal angle 66.4°			
64.8	80.2	10.91	6.4
65.2	89.0	10.81	6.8
65.6	100.0	7.70	7.3
66.2	113.4	6.91	8.2
66.6	125.3	7.36	8.8
66.8	133.3	6.38	7.6
67.2	144.0	7.13	6.6
67.6	154.2	6.59	7.5
Nominal angle 78.5			
77.1	84.2	9.93	9.6
77.5	93.7	9.19	10.7
78.0	105.7	7.98	9.4
78.6	120.3	6.25	12.3
79.1	133.4	6.05	14.9
79.6	145.6	5.80	13.9
80.0	157.2	6.20	13.7
80.4	168.2	5.29	18.2
Nominal angle 90.0			
88.2	88.6	8.87	5.2
88.6	98.9	7.71	6.5
89.1	108.4	6.73	7.0
89.6	120.7	5.86	6.2
90.2	135.7	6.16	6.7
90.8	149.7	5.77	7.7
91.3	163.0	5.67	8.4
91.7	175.7	5.52	8.9
Nominal value 113.6			
111.5	100.8	6.26	5.7
112.0	113.4	5.57	6.8
112.5	125.2	5.26	7.6
113.1	140.8	5.14	5.7
113.8	160.0	4.61	7.3
114.4	178.2	4.89	6.7
115.0	195.9	5.25	7.7
115.6	212.9	5.76	6.9
Nominal value 143.1			
139.4	120.2	4.19	9.9
139.9	137.0	4.67	9.1
140.5	159.4	4.18	6.2
141.2	187.9	3.99	9.1
141.8	214.9	4.86	8.2
142.4	241.4	4.61	8.1

REF. T. Kamae, I. Arai, T. Fujii, H. Ikeda, N. Kajiura, S. Kawabata, K. Nakamura, K. Ogawa, H. Takeda, Y. Watase
Phys. Rev. Lett. 38, 468 (1977)

ELEM. SYM.	A	Z
H	2	1

METHOD

REF. NO.	
77 Ka 1	hmg

REACTION	RESULT	EXCITATION ENERGY	SOURCE		DETECTOR		ANGLE
			TYPE	RANGE	TYPE	RANGE	
$ G,P	ABX	350-700	C	325-725	MAG-D		90

POLARIZED PROTONS

Proton polarization in $\gamma d \rightarrow pn$ has been measured at c.m. angle around 90° and photon energies from 325 to 725 MeV. The polarization increases sharply with the photon energy, reaching a high maximum of $(-80 \pm 8)\%$ around 500–550 MeV. Such a high polarization with a sharp energy dependence seems to indicate a new effect in the dibaryon system.

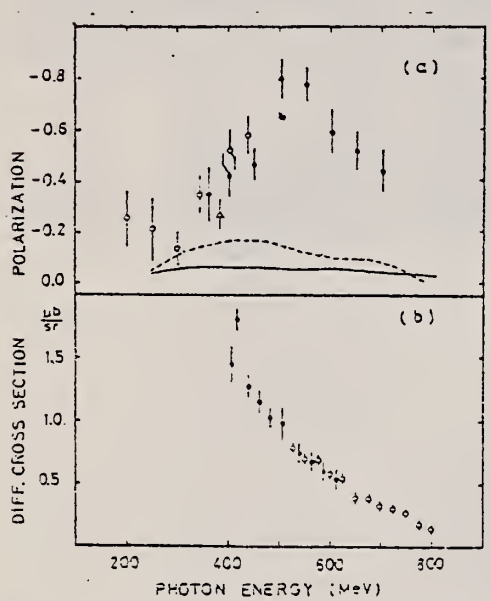

FIG. 3. (a) Proton polarization at 90° c.m. system as a function of the photon energy. The solid and the dashed curves are the results of a relativistic-covariant computation and a phenomenological analysis respectively (see Ref. 10). Data points are from Ref. 5 (open circles), Ref. 6 (triangle), and the present experimental (filled circles). (b) Differential cross section at 90° c.m. system as a function of the photon energy. Data points are taken from Ref. 1 (open circles) and Ref. 2 (closed circles).

TABLE I. Summary of experimental results. The angular acceptance in the center-of-mass system was about ± 1.0°. The errors in polarization refer to the half-width at half-maximum of the likelihood function.

Energy bin, E_γ (MeV)	Average E_γ (MeV)	Average $\theta_{c.m.}$ (deg)	Polarization, P (%)
330 ± 25	352	87.0	−35 ± 12
400 ± 25	398	88.4	−42 ± 9
450 ± 25	448	88.8	−47 ± 7
500 ± 25	496	90.2	−80 ± 8
550 ± 25	548	89.2	−78 ± 7
600 ± 25	597	90.1	−60 ± 10
650 ± 25	652	89.1	−53 ± 9
700 ± 25	697	90.0	−45 ± 9

[1] R. Ching et al., Phys. Rev. 141, 1320 (1965).
[2] P. Dougan et al., Z. Phys. A276, 55 (1976).
[5] F. F. Liu et al., Phys. Rev. 165, 1478 (1968).
[6] R. Kose et al., Z. Phys. 220, 305 (1969).
[10] Ogawa et al., (to be published).

REF. E.A. Kolomenskii, V.B. Kopeliovich, V.M. Lobashev, V.A. Nazarenko, A.I. Okorokov, A.N. Pirozhkov, L.M. Smotritskii, G.I. Kharkevich, and A.F. Shchebetov
Sov. J. Nucl. Phys. 25, 127 (1977)
Yad. Fiz. 25, 233 (1977)

ELEM. SYM.	A	Z
H	2	1

METHOD

REF. NO. 77 Ko 5 hmq

REACTION	RESULT	EXCITATION ENERGY	SOURCE TYPE	SOURCE RANGE	DETECTOR TYPE	DETECTOR RANGE	ANGLE
$ (N,G)	NOX	2	D	1	NAI-D		90
		(2.23)					

POL OF G

A method is proposed for determination of the contribution of the $^3S_1$ state in radiative np capture by measurement of the circular polarization of the γ rays on capture of a polarized neutron by a proton. Experiments carried out with this method are described. It is shown that the circular polarization is $P_\gamma \leq 1.5\%$, which limits the possible contribution of the triplet state to the cross section of the reaction under study to a level of $\sigma_t \leq 2\times10^{-4}\sigma_s$.

REF. P.E. Argan, G. Audit, A. Bloch, J.L. Faure, J.M. Laget, J. Martin, G. Tamas, and E. Vincent
Phys. Rev. Lett. 41, 86 (1978)

ELEM. SYM.	A	Z
H	2	1

METHOD

REF. NO. 78 Ar 1 rs eqf

REACTION	RESULT	EXCITATION ENERGY	SOURCE TYPE	SOURCE RANGE	DETECTOR TYPE	DETECTOR RANGE	ANGLE
G,PI-	ABX	365-460	C	400, 500	MAG-D		DST

By detecting in coincidence the two emitted protons, we have studied the reaction $D(\gamma, pp)\pi^-$ in a kinematical region where the pion-nucleon single-rescattering mechanism is dominant. We have also observed the onset of the photoproduction of two pions on one nucleon followed by the reabsorption of one of them by the other nucleon.

(P,π-,P)COINC

TABLE I. The experimental conditions and the measured yields.

Q MeV	p_2 MeV/c	θ_2 deg	p_1 MeV/c	θ_1 deg	$\Delta N/\Delta\Omega_1\Delta\Omega_2\Delta p_1\Delta p_2$ 10^{-5} μb/(Sr²MeV²) a	b	c
1200	400	30	359	-83	.21	.53	1.23 ± .23
		40	414	-76.5	.25	.45	2.19 ± .19
		50	470	-70	.30	.41	2.51 ± .23
		60	528	-63.9	.34	.40	1.85 ± .15
		70	588	-57.7	.37	.38	1.76 ± .12
		80	651	-51.8	.43	.42	1.56 ± .09
1100	550	37.5	380	-93.5	.078	.313	1.62 ± .38
		42.5	380	-93.5	.085	.301	3.48 ± .54
		47.5	441	-82.3	.093	.248	1.93 ± .21
		52.5	441	-82.3	0.101	.252	2.61 ± .24
		57.5	509	-72	.112	.216	2.36 ± .27
		62.5	509	-72	.125	.221	3.85 ± .32
		67.5	585	-62.5	.136	.195	3.46 ± .33
		72.5	585	-62.5	.159	.204	4.21 ± .42

[a] Spectator-nucleon model without Pauli corrections.
[b] Spectator-nucleon model with Pauli corrections.
[c] Experimental values.

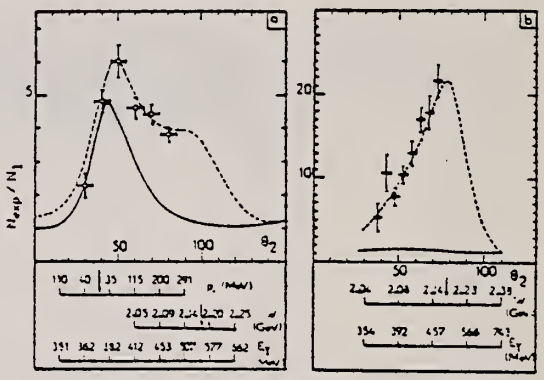

FIG. 2. (a) The ratio of the measured yields to the yield computed when only one-nucleon mechanisms are considered. The solid-line curve includes the pion-nucleon single-rescattering mechanism and the broken-line curve includes also the double-pion-photoproduction mechanism. The experimental conditions are $p_2 = 400$ MeV/c, $Q = 1200$ MeV, and $\omega = 90°$. The arrow on the scale of the lower bound p_- for a physical rescattering shows the origin. The arrow on the scale of the two-nucleon invariant mass shows the value $W = M + m$. The energy E_γ of the incoming photon is also plotted as the abscissa. (b) The same as in (a) but for $p_2 = 550$ MeV/c, $Q = 1100$ MeV, and $\omega = 90°$.

REF. P. Argan, G. Audit, A. Bloch, P. Bosted, N. de Botton, J.L. Faure, C. Schuhl, G. Tamas, C. Tzara, E. Vincent, J. Deutsch, D. Favart, R. Prieels, and B. Oystaeyen
Phys. Rev. Lett. 41, 629 (1978)

ELEM. SYM.	A	Z
H	2	1

METHOD

REF. NO. 78 Ar 2 rs

REACTION	RESULT	EXCITATION ENERGY	SOURCE		DETECTOR		ANGLE
			TYPE	RANGE	TYPE	RANGE	
G,P π^0	ABY	141-147	C	147	TEL-D		DST

π^0 photoproduction on deuterium has been measured in the region of 1 to 7 MeV above threshold, relative to the same reaction on hydrogen. The comparison of our results with available theoretical predictions shows the necessity to go beyond the impulse approximation.

TABLE I. Experimental yield $A(E_e) = \int_{E_0}^{E_e}\int_{\Omega_q} B(E, E_e)\epsilon(E,\Omega)(d\sigma/d\Omega)d\Omega\,dE$ in microbarns, normalized to one target nucleus and one equivalent quantum, for different values of the bremsstrahlung endpoint energy E_e above threshold E_0.

Hydrogen		Deuterium	
$E_e - E_0$ (MeV)	$10^3 A_H$	$E_e - E_0$ (MeV)	$10^3 A_D$
1.04	0.16 ± 0.06	0.88	0.40 ± 0.07
2.04	0.61 ± 0.11	1.88	1.16 ± 0.11
3.04	0.92 ± 0.13	2.88	2.64 ± 0.26
4.04	1.94 ± 0.27	4.88	6.66 ± 0.37
6.04	4.29 ± 0.36	5.88	10.62 ± 0.55
		7.38	16.48 ± 1.50

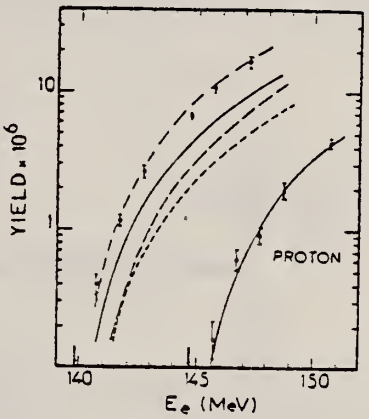

FIG. 2. The measured photoproduction yields as a function of the bremsstrahlung endpoint energy E_e, compared to theoretical estimates for deuterium without rescattering (long dashes, Ref. 6, and short dashes, Ref. 5) and including rescattering (dash-dotted line, Ref. 6, and solid line, Ref. 5). These two theoretical estimates use the same proton cross section; the corresponding yield has been adjusted to the hydrogen data. Arrows indicate the threshold energies. The yields are given in microbarns per equivalent quantum.

[5] P. Bosted and J.M. Laget, Nucl. Phys. A296, 413 (1978)

[6] J.H. Koch and R.M. Woloshyn, Phys. Rev. C 16, 1968 (1977).

REF. P.E. Argan, G. Audit, A.Bloch, J.L. Faure, J.M. Laget, J. Martin, G. Tamas & C.Schuhl
Nucl. Phys. A296, 373 (1978)

ELEM. SYM.	A	Z
H	2	1

METHOD

REF. NO.: 78 Ar 8 hmg

REACTION	RESULT	EXCITATION ENERGY	SOURCE TYPE	SOURCE RANGE	DETECTOR TYPE	DETECTOR RANGE	ANGLE
G,PI-	ABX	150-500	C	250-500	MAG-D	---	DST

PI- in coin. with P

Abstract The $\gamma D \rightarrow pp\pi^-$ reaction cross section, in the $\Delta(1236)$ region, is measured in a counter experiment with high statistical accuracy. Particular emphasis is put on the accurate determination of the complete kinematics. For low values of the undetected nucleon momentum ($p_r \approx 50$ MeV/c), the validity of the spectator nucleon model is experimentally checked and the $\gamma n \rightarrow p\pi^-$ elementary reaction cross section is extracted and compared with other experimental data. When the recoiling nucleon momentum increases ($p_r \approx 150$ MeV/c), significant departures from the spectator nucleon model are found. Presumably they are the signature of final state interaction effects.

E NUCLEAR REACTION D(γ, $p\pi^-$), $250 \leq E \leq 500$ MeV; measured $\sigma(E_p, \theta_p, E_\pi, \theta_\pi)$; deduced $\sigma(\gamma n \rightarrow p\pi^-)$, final state interaction effects.

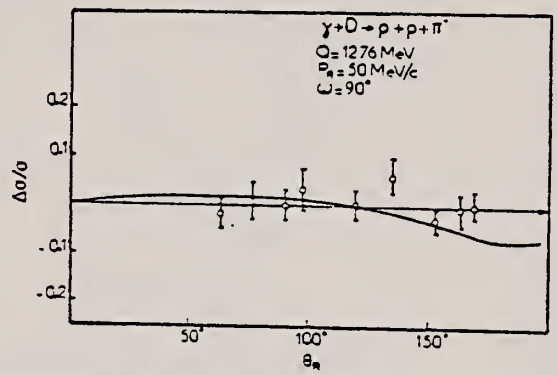

Fig. 7. The measured distribution of the undetected nucleon, when $p_r \approx 50$ MeV/c, $Q = 1276$ MeV and $\omega = 90°$. The relative difference between the measured yield and the prediction of the spectator-nucleon model is plotted. The curve is taken from ref. [12]).

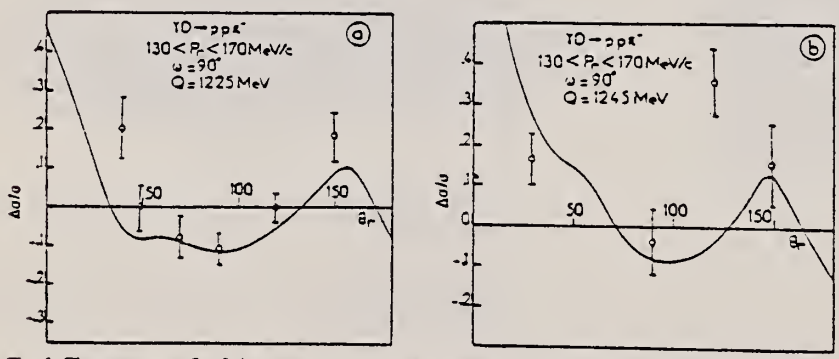

Fig. 8. The same as in fig. 7, but when $p_r \approx 150$ MeV/c and $Q = 1225$ MeV (a) or $Q = 1245$ MeV (b).

(continued)

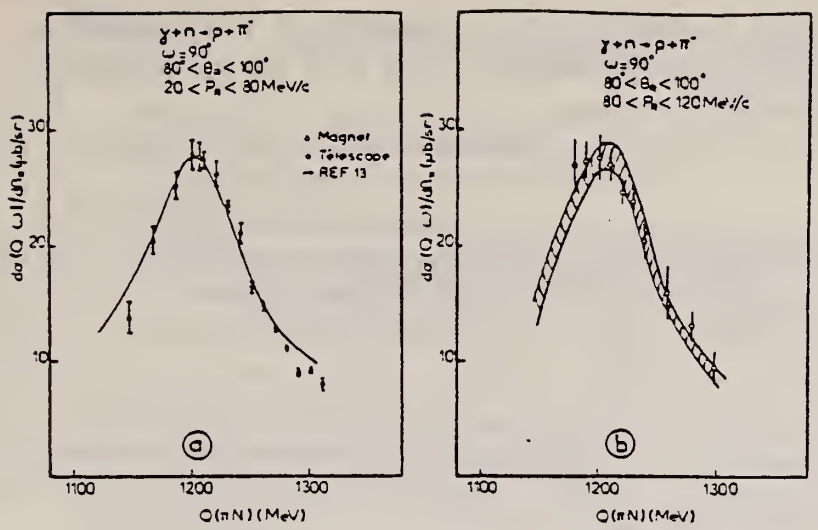

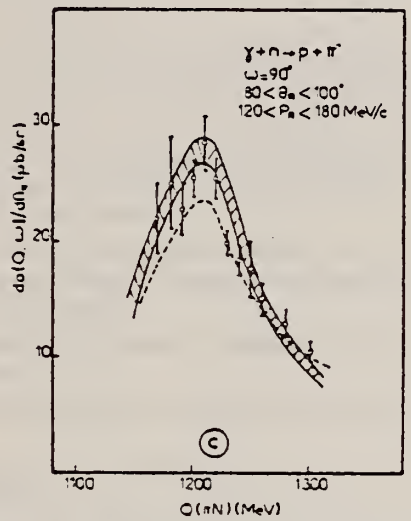

Fig. 9. The mass distribution, at $\omega = 90°$, of the $\gamma n \to p\pi^-$ elementary reaction cross section, as extracted from the $\gamma D \to pp\pi^-$ reaction yield when $p_s \approx 50$ MeV/c (a), $p_s \approx 100$ MeV/c (b) and $p_s \approx 150$ MeV/c (c). In (a) the curve is the prediction (multiplied by 0.95) of ref. [13]). The triangles are obtained when the protons are detected in the magnet, and the circles when they are detected in the range telescope. In (b) and (c) the shaded area corresponds to the experimental points plotted in (a). In (c) the broken line curve is obtained from ref. [13]) when the rescattering effects are taken into account.

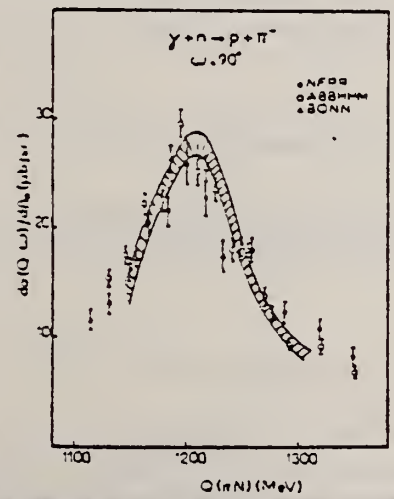

Fig. 10. The comparison between the $\gamma n \to p\pi^-$ reaction cross section (shaded area) extracted from the $\gamma D \to pp\pi^-$ yield when $p_s \approx 50$ MeV/c, and the bubble chamber data [full circles [5a]), open circles [5b])] or as deduced from the π^+/π^- ratio measurements (open triangles [6])).

TABLE 2

The values of the $\gamma n \to p\pi^-$ reaction c.m. cross section at $\omega = 90$

Q (MeV)	$[d\sigma/d\Omega]_{c.m.}$ (μb/sr)	Q (MeV)	$[d\sigma/d\Omega]_{c.m.}$ (μb/sr)
1148	13.7±1.5	1242	21.1±0.9
1168	20.5±1.2	1252	16.4±0.4
1188	25.2±1.2	1262	14.8±0.4
1202	27.9±1.3	1272	12.8±0.4
1208	27.7±1.2	1282	11.1±0.2
1212	27.4±0.8	1292	9.0±0.4
1222	26.2±1.2	1302	9.2±0.4
1232	23.5±0.5	1312	8.0±0.6

REF. P.I. Vatset, A.I. Derebchinskii, A.A. Zybalov, O.G. Konovalov, V.R. Nazyrov, A.E. Tenishev, and S.G. Tonapetyan
Sov. J. Nucl. Phys. 27, 323 (1978)
Yad. Fiz. 27, 605 (1978)

ELEM. SYM.	A	Z
H	2	1

METHOD

REF. NO.	
78 Va 5	hg

REACTION	RESULT	EXCITATION ENERGY	SOURCE		DETECTOR		ANGLE
			TYPE	RANGE	TYPE	RANGE	
$ G,P	NOX	THR-800	C	600, 800	MAG-D		UKN

POL. PROTONS

---SEE REVERSE SIDE---

(continued)

Polarization of protons in interaction of photons with energy up to 800 MeV with deuterium nuclei

P. I. Vatset, A. I. Derebchinskiĭ, A. A. Zybalov, O. G. Konovalov, V. R. Nazyrov, A. É. Tenishev, and S. G. Tonapetyan

Khar'kov Physico-technical Institute, Ukrainian Academy of Sciences
(Submitted 27 May 1977)
Yad. Fiz. 27, 605–606 (March 1978)

The polarization of photoprotons from deuterium has been studied. The data obtained are used to extract information on the polarization of protons in the reaction $\gamma n \to \pi^- p$.

PACS numbers: 13.60.Kd, 25.10.+s

In this article we described an experiment on measurement of the polarization of protons in reactions of photons with energy up to 800 MeV with deuterium nuclei. The purpose of the work was to obtain information on the polarization of protons in the reaction $\gamma n \to \pi^- p$ by a difference method.

The experiment was carried out in the photon beam of the 2-GeV electron linear accelerator by means of a telescope of spark chambers[1] located at the exit of the magnet spectrometer. Protons with momentum 612 ± 24 MeV/c were detected by means of this apparatus. The proton polarization was measured on the basis of the asymmetry in their scattering in the graphite electrodes of the spark chamber.[2]

Three independent measurements were made, in which the relative yields of the protons and their polarization were investigated:

1) measurement in hydrogen at a maximum photon energy 800 MeV;

2) measurement in deuterium under the same conditions;

3) measurement in deuterium at a maximum photon energy 600 MeV.

The kinematic conditions of the first two measurements correspond to an effective photon energy 650 ± 40 MeV for the channels of production of single pions from free nucleions at 90° in the c.m.s.

In the third measurement these channels are kinematically forbidden, and therefore the polarization of the protons measured in this case is determined mainly by the two-particle and three-particle photodisintegration of deuterium (PD).

The polarization obtained in measurement 2) is determined by the contribution of the reactions $\gamma p \to \pi^0 p$, $\gamma n \to \pi^- p$, and PD.

Thus, knowing the relative contributions of these processes, we can obtain a value of the proton polarization in the reaction $\gamma n \to \pi^- p$ from the experimental polarization values:

$$P_1 = (C_2 P_2 - C_{p0} P_{p0} + C_3 P_3)/C_1, \qquad (1)$$

where P_2 is the proton polarization measured in experiment 2); P_{p0} and C_{p0} are the polarization and relative yield of protons obtained in experiment 1); P_{PD} and C_{PD} are these same quantities obtained in experiment 3); P_{π^-} and C_{π^-} are the polarization and yield of protons associated with the reaction $\gamma n \to \pi^- p$; $C_2 = C_{\pi^-} + C_{\pi^0} + C_{PD}$ is the yield of protons measured in experiment 2).

TABLE I

C_{π^0}	C_{PD}	C_{π^-}	P_{π^-}	P_{PD}	P_{π^-}
4.7	8.3	8.5	−0.72±0.07	0.22±0.11	−0.49±0.21

The relative yield C_{π^-} is determined from the experimentally measured yield C_{π^0} and the ratio of the cross sections of the reactions $\gamma p \to \pi^0$ and $\gamma n \to \pi^- p$.

In the table we have given the results of the present experiment. The value of P_{π^0} was obtained from Eq. (1). The value of P_1 obtained in the present work is −0.24 ± 0.08. The errors are statistical.

The proton polarization value in the reaction $\gamma n \to \pi^- p$ is in reasonable agreement with the polarization values obtained in experiments in deuterium[3] and carbon[4] with $\pi^- p$ coincidences in this energy region.

The studies carried out have shown an appreciable contribution to the polarization from processes associated with photodisintegration of deuterium. The existence of polarization in the PD process can be explained by the fact that this process is due to a significant degree to creation of a pion from one of the nucleons with subsequent absorption of the produced meson by another nucleon.[5]

The error in determination of the polarization P_{π^-} depends strongly on the contribution of background processes ($\gamma p \to \pi^0 p$ and PD), and therefore even a substantial improvement in the accuracy of the quantities measured in the experiment cannot adequately reduce the error in calculation of P_{π^-}. This method of measurement of polarization permits a qualitative picture to be obtained of the angular and energy dependences and in some cases may be effective in those regions where information on proton polarization in the $\gamma n \to \pi^- p$ reaction cannot be obtained by the coincidence method with its higher accuracy.

[1] S. G. Tonapetyan, O. G. Konovalov *et al.*, Prib. Tekh. Éksp., No. 5, 58 (1970) [Instrum. Exper. Tech.].
[2] S. G. Tonapetyan, O. G. Konovalov, *et al.*, Prib. Tekh. Éksp., No. 2, 61 (1970) [Instrum. Exper. Tech.].
[3] M. Beneventano, S. d'Angelo, *et al.*, XVth Intern. Conf. on High Energy Physics, Kiev, 1, 242, 1970.
[4] V. N. Stibunov, Issledovanie fotoobrazovaniya na yadrakh pionov s vyletom nuklonov, Avtoreferat kandidatskoĭ dissertatsii (Study of Photoreproduction of pions from nuclei with emission of nucleons, author's abstract of candidate's dissertation), Tomsk, 1974.
[5] R. R. Wilson, Phys. Rev. 104, 218 (1956).

Translated by Clark S. Robinson

REF. E.C. Booth, B. Chasan, J. Comuzzi, P. Bosted
Phys. Rev. C20, 1217 (1979)

ELEM. SYM.	A	Z
H	2	1

METHOD

REF. NO. 79 Bo 1 hg

REACTION	RESULT	EXCITATION ENERGY	SOURCE		DETECTOR		ANGLE
			TYPE	RANGE	TYPE	RANGE	
G,PI+	ABX	149-174	C	149-174	ACT-I		90

The bremsstrahlung yield of the $^2H(\gamma,\pi^+)2n$ reaction is measured from threshold to 25 MeV above threshold. The extracted total cross section relative to the $p(\gamma,\pi^+)n$ cross section is 3–10% greater than the theoretical prediction.

[NUCLEAR REACTIONS $^2H(\gamma,\pi^+)2n$, bremsstrahlung end point energies to 174 MeV, measured π^+ yield, deduced $\sigma(E)$.]

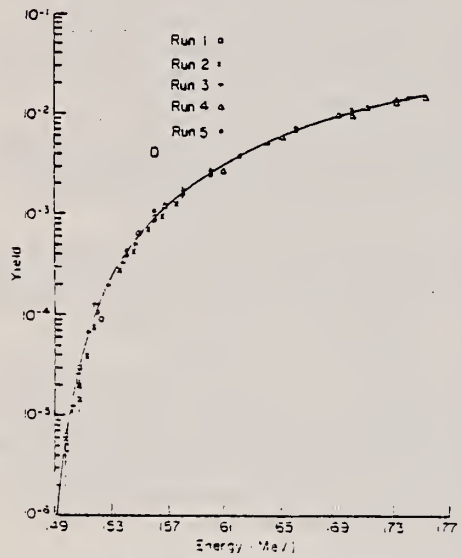

FIG. 2. Yield for the $d(\gamma,\pi^+)2n$ reaction vs E_0-E_T. The solid curve is the theoretical calculation described in the text scaled to the $p(\gamma,\pi^+)n$ yield shown in Fig. 1.

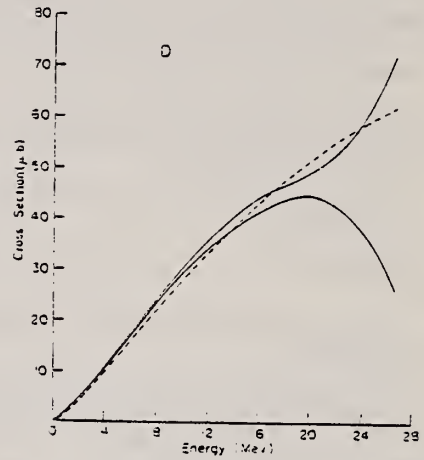

FIG. 3. The $d(\gamma,\pi^+)2n$ cross section. It is the polynomial in powers of E_0-E_T required to give the best fit to the yield shown in Fig. 2.

TABLE I. Theoretical and experimental values of the total cross section σ_t for $^2H(\gamma\pi^+)2n$. The theoretical cross sections are from Dressler (Ref. 3) (interpolated) and Laget (Ref. 4), scaled up by the factor (201/191) to agree with the experimental value for $^2H(\gamma\pi^+)n$ at threshold. σ_t(exp) is the cross section derived using runs 4 and 5 with a 12.3 cm target. σ_t^*(exp) was obtained from runs 1–3 with a 2.54 cm target (Ref. 5) and $\Delta E < 9$ MeV. σ_t^{**}(exp) was obtained using the Saclay data (Ref. 6). The errors shown are only statistical; ±3 % and ±6 % systematic error should be applied to σ_t(exp) and σ_t^*(exp).

ΔE	2.00	3.00	4.00	6.00	8.00	10.00	12.00	14.0	16.0	20.0
σ_t^3	4.21	6.97	9.81	16.0	22.1	28.1	33.3	38.5	43.9	52.0
σ_t^4	4.20	6.90	9.76	15.8	21.6	27.7	33.3	38.6	43.3	51.7
σ_t (exp)	4.31	7.65	10.6	17.1	23.5	29.5	34.7	39.2	42.7	46.7
± error	0.16	0.13	0.13	0.29	0.39	0.47	0.73	1.1	1.4	2.0
σ_t^* (exp)	4.45	7.23	9.53							
± error	0.15	0.28	0.24							
σ_t^{**} (exp)	4.35	7.10	9.05							
± error	0.20	0.24	1.0							

REF. M. Bosman, A. Bol, J.F. Gilot, P. Leleux, P. Lipnik, P. Macq
Phys. Lett. 82B, 212 (1979)

ELEM. SYM.	A	Z
H	2	1

METHOD

REF. NO. 79 Bo 10 egf

REACTION	RESULT	EXCITATION ENERGY	SOURCE		DETECTOR		ANGLE
			TYPE	RANGE	TYPE	RANGE	
N,G	ABX	20-39	D	37-73	TOF-D	37-73	4PI

The total cross section for radiative neutron–proton capture has been measured at 37, 42, 47, 52, 63 and 73 MeV. The inverse process, the photodisintegration of the deuteron, was measured in the same energy range by different authors with contradictory results, some of them in large disagreement with all theoretical predictions of the cross section. The submitted data are in agreement with theory and the results of a recent total absorption experiment.

Table 1
Experimental results for the n–p radiative capture cross section with the c.m. value of the differential elastic cross section at 173° used for normalization. The two last columns translate the present results, by application of detailed balance, into the corresponding photodisintegration energy and cross section.

E_n (MeV)	$\sigma_{capture}$ (μb)	$d\sigma/d\Omega(173°)$ (mb/sr)	E_γ(MeV) corresponding to E_n	$\sigma_{photodisintegration}$ (μb)
37.0 ± 1.4	21.2 ± 1.6	23.2	20.8	582 ± 44
42.2 ± 1.3	20.6 ± 1.4	20.4	23.4	511 ± 35
47.3 ± 1.2	17.0 ± 0.7	18.2	25.9	385 ± 16
52.4 ± 1.1	17.6 ± 0.9	16.7	28.5	367 ± 19
57.4 ± 1.0	15.8 ± 1.1	15.4	31.0	306 ± 21
62.5 ± 1.0	14.6 ± 1.1	14.4	33.5	264 ± 20
72.6 ± 0.9	14.7 ± 1.1	12.8	38.6	234 ± 18

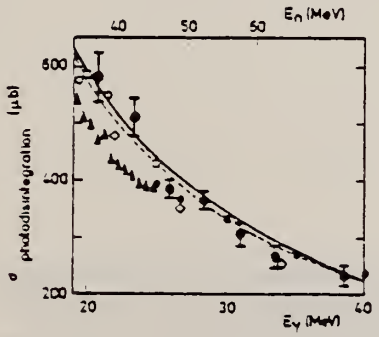

Fig. 3. Experimental cross section measured in the present experiment (•) compared, by means of the detailed-balance theorem, to photodisintegration data of ref. [1] (○), ref. [2] (○), ref. [3] (○), ref. [4] (▲) and ref. [5] (⊂). The error bars do not include systematic errors from the normalization (± 5%). The continuous line represents Partovi's calculation [9], and the dashed one the results from the Low-theorem approach with the triplet effective range value r_{0t} = 1.70 fm. The horizontal scales show either the neutron (E_n) or the corresponding γ-ray (E_γ) energy in the laboratory system.

[1] L. Allen, Phys. Rev. 98 (1955) 705.
[2] A. Whetstone and J. Halpern, Phys. Rev. 109 (1958) 2072.
[3] B. Weissman and H.L. Schultz, Nucl. Phys. A174 (1971) 129.
[4] J.E.E. Baglin, R.W. Carr, E.J. Bentz and C.P. Wu, Nucl. Phys. A201 (1973) 593.
[5] J. Ahrens et al., Phys. Lett. 52B (1974) 49.
[6] M. Bosman et al., Nucl. Instr. Meth. 148 (1978) 363.

REF. V. B. Ganenko, I. I. Miroshnichenko, V. M. Sanin, P. V. Sorokin, S. V. Shalatskii, A. V. Shebeko
Sov. J. Nucl. Phys. 29, 287 (1979)
Yad. Fiz. 29, 565 (1979)

EL EM. SYM.	A	Z
H	2	1

METHOD

REF. NO. 79Ga3 hg

REACTION	RESULT	EXCITATION ENERGY	SOURCE		DETECTOR		ANGLE
			TYPE	RANGE	TYPE	RANGE	
G,PI+	RLY	150-560	C	150-560	TEL-D		DST

D(G,PI+)/H(G,PI+)

An experimental study has been carried out of the energy spectra of π^+ mesons in the reaction $\gamma d \to nn\pi^+$ at pion-emission angles in the range 19–127° lab in the pion-energy interval corresponding to excitation of the Δ_{33} resonance in the πN in the final state. The results of the experiment are compared with calculations in the impulse approximation with inclusion of corrections for the NN and πN interactions of the reaction products in the final state.

PACS numbers: 13.60.Kd

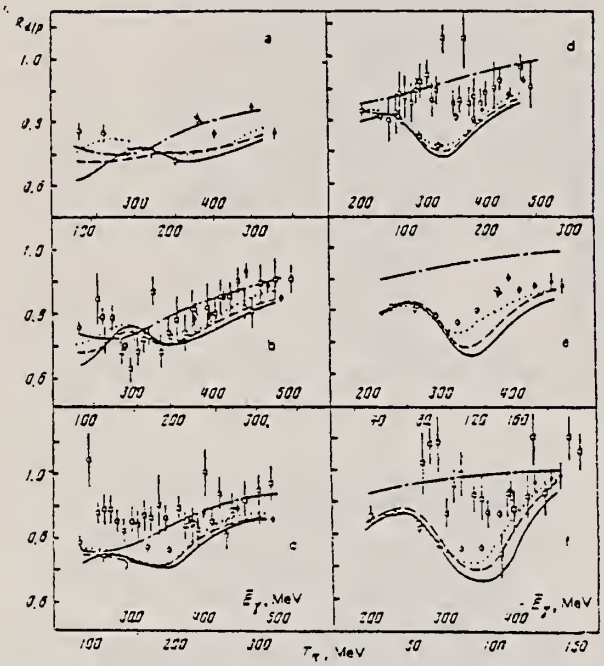

FIG. 1. Ratio of yields of pions in single photoproduction of π^+ mesons in deuterium and hydrogen $R_{d/p}$ in a bremsstrahlung beam as a function of the kinetic energy of the pion (lower scale). On the upper scale we have shown the effective photon energy $\bar{E}_\gamma$. Points: ●—our data, ○—Ref. 2, □—Refs. 9 and 10; (a)—ϑ_π = 19° lab, (b)—ϑ_π = 26.5° lab, data of Refs. 9 and 10 for 30° c.m.s.; (c)—ϑ_π = 33.5° lab, data of Refs. 9 and 10 for 60° c.m.s.; (d)—ϑ_π = 60° lab, data of Refs. 9 and 10 for 90° c.m.s.; (e)—ϑ_π = 90° lab; (f)—ϑ_π = 127° lab, data of Refs. 9 and 10 for 135° c.m.s. Theoretical curves: solid—calculation in the impulse approximation; dashed—calculation in the impulse approximation with inclusion of the $\pi\pi$ correction; dotted—with inclusion of $\pi\pi$ and πN corrections; dot-dash—calculation by the model Chew and Lewis.[15]

(continued)

TABLE I

E_p, MeV	θ_π=19°		θ_π=28.5°		θ_π=33.5°	
	T_π, MeV	$R_{d/p}$	T_π, MeV	$R_{d/p}$	T_π, MeV	$R_{d/p}$
380	230	0.806±0.024	224	0.778±0.023	216	0.843±0.019
400	250	0.759±0.02	243	0.795±0.019	233	0.873±0.023
420			260	0.849±0.024		
450	297	0.845±0.022	288	0.930±0.029	278	0.884±0.023
460	315	0.760±0.024	315	0.831±0.024	302	0.838±0.025
500			332	0.840±0.021	319	0.849±0.018

E_p, MeV	θ_π=40°		θ_π=30°		θ_π=127°	
380	152	0.789±0.015	139	0.844±0.022	104	0.853±0.047
400	192	0.828±0.015	147	0.893±0.020	111	0.928±0.037
420			157	0.857±0.020		
450	225	0.875±0.017	170	0.568±0.028	128	0.948±0.035
480	244	0.920±0.022	183	0.586±0.030	138	0.960±0.050
500			192	0.867±0.030	142	0.970±0.050

REF. V.G. Gorbenko, Yu.V. Zhebrovskii, L.Ya. Kolesnikov, A.L. Rubashkin, P.V. Sorokin
JETP Lett. 30, 118 (1979)
Pis'ma Zh. Eksp. Teor. Fiz. 30, 130 (1979)

ELEM. SYM.	A	Z
H	2	1

METHOD

REF. NO. 79 Go 8 hg

REACTION	RESULT	EXCITATION ENERGY	SOURCE		DETECTOR		ANGLE
			TYPE	RANGE	TYPE	RANGE	
$ G,NP	NOX	400-600	C	1*2	MAG-D		DST
				(1.5*1.6)			

Data given in table and plotted in figure represent the cross section assymetry $\Sigma \equiv \frac{d\sigma_{11} - d\sigma_2}{d\sigma_{11} + d\sigma_2}$, wehre 11 and 1 indicate the polarization of the photon beam with respect to the reaction plane.

*E GEV, POL G, NP COIN

This paper presents the first results of an investigation of the asymmetry of the cross sections of the deuteron photodisintegration reaction, obtained in a beam of linearly polarized photons in the 400–600 MeV energy interval. The measurements were made in conjunction with a search for two-nucleon resonances with masses of 2200–2400 MeV.

PACS numbers: 13.60.Rj, 14.20.Gk

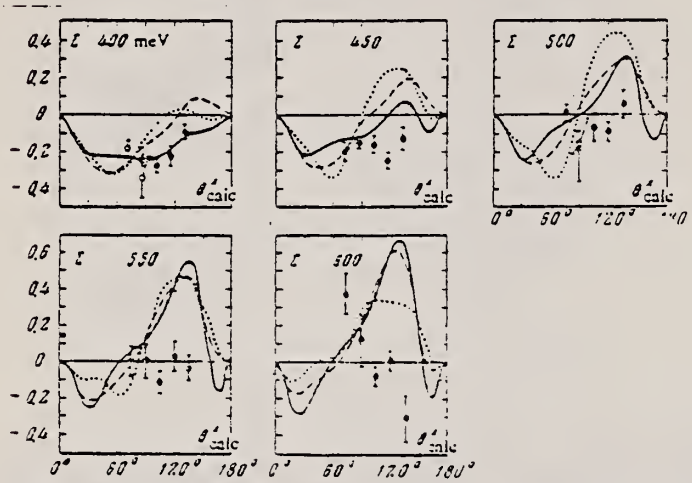

FIG. 1. Angular distributions of the cross section asymmetry of the reaction $\gamma d \to np$: ● ▼ are the results of this work, ○ are the data from Ref. 3.

(continued)

TABLE I.

E_γ, mev	θ^*				
	75°	90°	105°	120°	135°
400	−0,18 ±0,04	−0,25 ±0,03	−0,27 ±0,04	−0,23 ±0,05	−0,09 ±0,04
450	−0,21 ±0,05	−0,16 ±0,03	−0,17 ±0,04	−0,26 ±0,04	−0,15 ±0,06
500	0,02 ±0,04	−0,15 ±0,06	−0,07 ±0,07	−0,09 ±0,05	−0,06 ±0,07
550	0,01 ±0,08	0,00 ±0,09	−0,12 ±0,07	0,03 ±0,08	−0,04 ±0,07
600	0,38 ±0,11	0,13 ±0,14	−0,07 ±0,05	0,02 ±0,05	−0,30 ±0,13

REF. H. Ikeda, I. Arai, H. Fujii, T. Fujii, H. Iwasaki, N. Kajiura, T. Kamae, K. Nakamura, T. Sumiyoshi, H. Takeda, K. Ogawa, and M. Kanazawa
Phys. Rev. Lett. 42, 1321 (1979)

ELEM. SYM.	A	Z
H	2	1

METHOD

REF. NO. 79 Ik 1 hg

REACTION	RESULT	EXCITATION ENERGY	SOURCE TYPE	SOURCE RANGE	DETECTOR TYPE	DETECTOR RANGE	ANGLE
$ G,P	ABX	400-650	C	UKN	MAG-D		DST

POL. PROTONS

The angular dependence of proton polarization in $\gamma d \rightarrow pn$ has been measured at photon energies between 400 and 650 MeV. The polarization and differential-cross-section data are consistently explained by introducing a dibaryon resonance $I(J^P) = 0(3^+)$ or $0(1^+)$ at ≈ 2360 MeV.

TABLE I. Summary of the experimental results. The positive direction of the proton polarization is defined to be parallel to (photon direction) × (proton direction). The errors are given by the quadratic sum of the 1-standard-deviation error in the maximum-likelihood analysis and the error due to the uncertainty in the analyzing power A of the carbon, $P\Delta A/A \approx 0.05P$.

E_γ (MeV) \ $\theta_{c.m.}$	45°	70°	90°	120°	135°
400		−0.44 ± 0.09			
450	−0.24 ± 0.08	−0.54 ± 0.10		−0.35 ± 0.21	
500	−0.24 ± 0.09	−0.61 ± 0.11	−0.77 ± 0.13	−0.46 ± 0.12	−0.35 ± 0.24
550	−0.34 ± 0.10	−0.62 ± 0.11	−0.51 ± 0.09	−0.54 ± 0.10	−0.55 ± 0.20
600	+0.10 ± 0.13	−0.42 ± 0.11	−0.58 ± 0.12	−0.59 ± 0.11	
650				−0.38 ± 0.15	

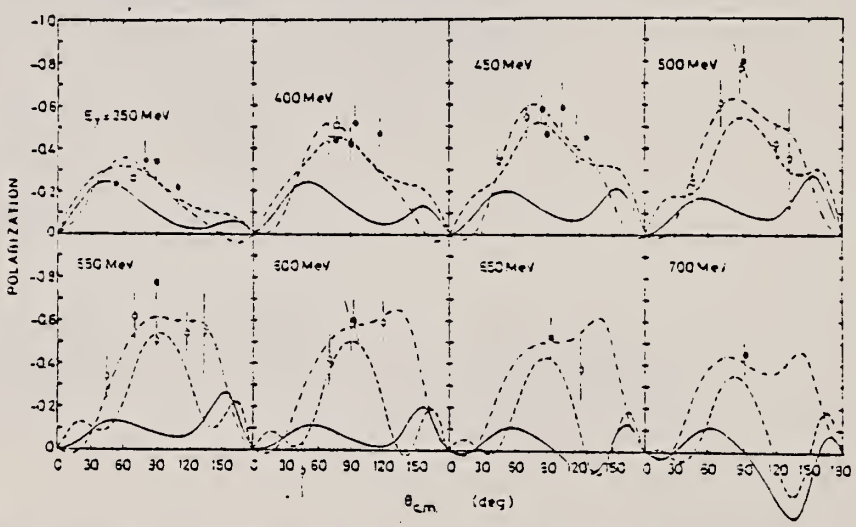

FIG. 1. Angular distributions of the proton polarization. The results of the present experiment (empty circles) are plotted together with the previous data (filled circles, Liu *et al.*, Ref. 12; empty squares, Kose *et al.*, Ref. 12; filled squares, Kamae *et al.*, Ref. 1) used for the χ^2-minimization fits. The dashed curves are the results of the fit including $1(3^-)$ and $0(3^+)$. The dot-dashed curves are the results of the fit including $1(3^-)$ and $0(1^+)$. The solid curves are the calculated results with the nonresonant amplitudes only.

(continued)

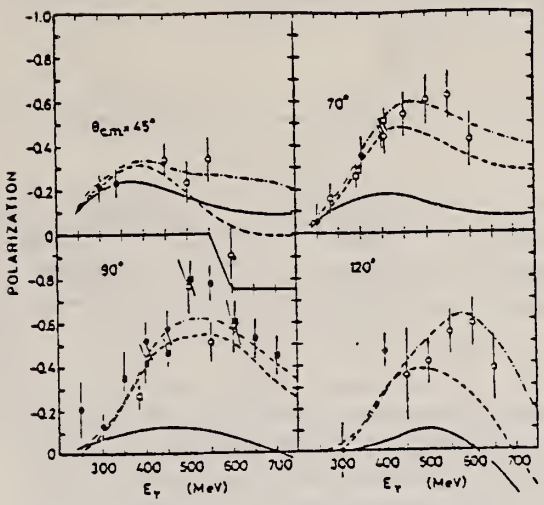

FIG. 2. Proton polarization plotted vs E_γ. The data outside the fitted region are also shown. The curves and symbols are coded as in Fig. 1.

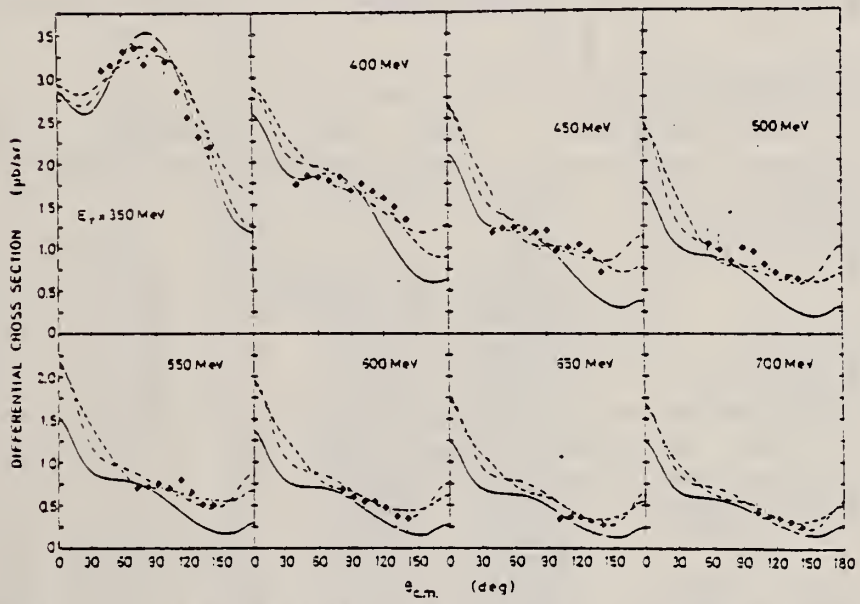

FIG. 3. The differential-cross-section data used for the χ^2-minimization fits and the fitted curves. The curves are coded as in Fig. 1; here the diamonds are data from Dugan *et al.*, Ref. 13.

REF. G. G. Simon, F. Borkowski, Ch. Schmitt, V. H. Walther, H. Arenhövel, W. Fabian
Nucl. Phys. A324, 277 (1979)

ELEM. SYM.	A	Z
H	2	1

METHOD

REF. NO. 79Si5 hg

REACTION	RESULT	EXCITATION ENERGY	SOURCE TYPE	SOURCE RANGE	DETECTOR TYPE	DETECTOR RANGE	ANGLE
E,E/	FMF	2-12	C	80-300	MAG-D		DST

Abstract: Electrodisintegration of the deuteron has been measured for energy transfers from threshold up to 10 MeV at different angles ($30° \leq \theta \leq 160°$) and different incident energies ($80 \leq E_1 \leq 350$ MeV). The longitudinal and transverse form factors have been separated in a momentum region between 0.5 and 4 fm^{-2}. Theoretical calculations including interaction effects give good agreement with the experimental data. The dependence on various nucleon–nucleon potentials was found to be small. The contributions from meson exchange currents and isobar configurations give an enhancement of about 90% of the normal cross section at the highest momentum transfer at backward angles.

Q= .71-2 FM-1

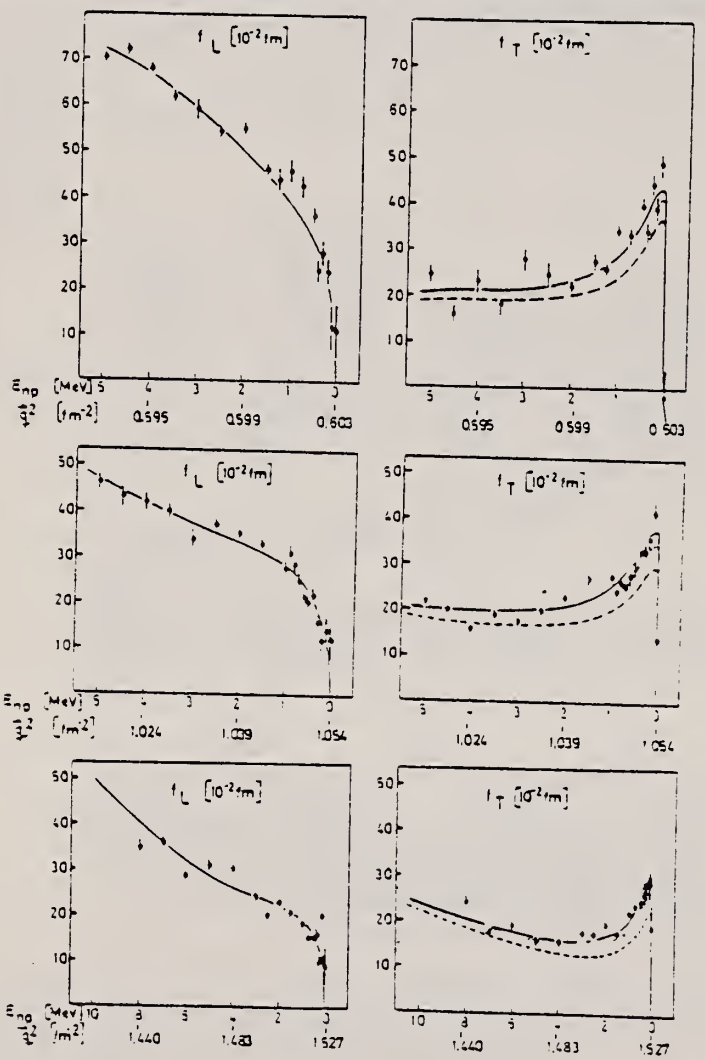

Fig. 4. Inelastic form factors f_L and f_T as a function of E_{no} around $(q^{c.m.})^2 = 0.6$, 1.0 and 1.4 fm^{-2}. The dashed curves are obtained by using the Reid soft-core potential without interaction effects, while the dotted curves include MEC and the full curves both MEC and IC.

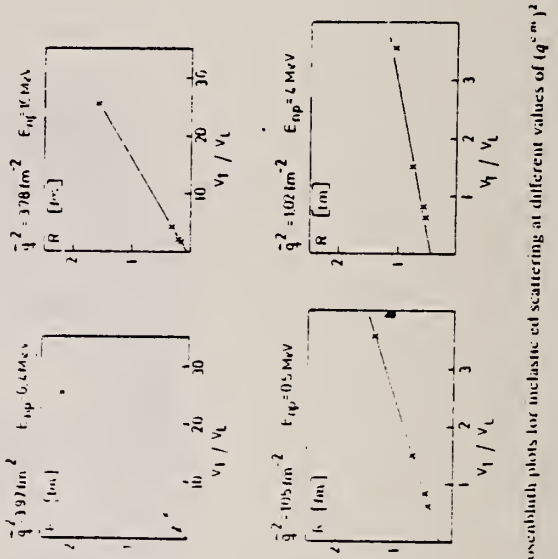

Fig. 2 Rosenbluth plots for inelastic ed scattering at different values of $(q^{c.m.})^2$ and E_{no}.

(continued)

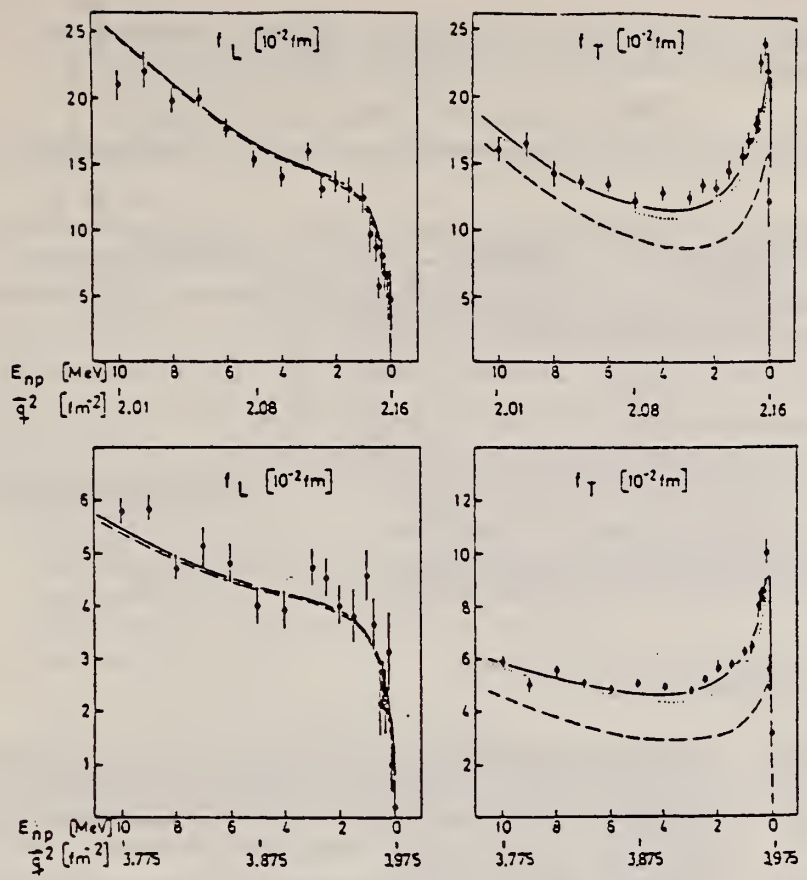

Fig. 5. Same as fig. 4 but around $(q^{c.m.})^2 = 2$ and 4 fm^{-2}.

TABLE 2

Same as table 1 but around $(q^{c.m.})^2 = 2$ and 4 fm^{-2}

E_{np} (MeV)	$q^2_{c.m.}$ (fm^{-2})	f_L (fm)	f_T (fm)	$q^2_{c.m.}$ (fm^{-2})	f_L (fm)	f_T (fm)
0.0	2.156	0.047 ± 0.025	0.122 ± 0.024	3.975	0.002 ± 0.005	0.032 ± 0.005
0.1	2.154	0.050 ± 0.020	0.220 ± 0.014	3.973	0.010 ± 0.006	0.056 ± 0.005
0.2	2.153	0.065 ± 0.019	0.240 ± 0.009	3.971	0.032 ± 0.008	0.101 ± 0.006
0.3	2.151	0.080 ± 0.015	0.226 ± 0.007	3.969	0.022 ± 0.006	0.086 ± 0.006
0.4	2.150	0.057 ± 0.010	0.183 ± 0.010	3.967	0.025 ± 0.005	0.083 ± 0.006
0.5	2.149	0.087 ± 0.014	0.180 ± 0.008	3.965	0.021 ± 0.006	0.080 ± 0.003
0.75	2.145	0.098 ± 0.015	0.168 ± 0.007	3.960	0.037 ± 0.005	0.065 ± 0.002
1.0	2.141	0.124 ± 0.013	0.156 ± 0.011	3.955	0.046 ± 0.006	0.063 ± 0.002
1.5	2.134	0.130 ± 0.010	0.145 ± 0.009	3.949	0.038 ± 0.005	0.058 ± 0.002
2.0	2.127	0.135 ± 0.009	0.132 ± 0.009	3.935	0.040 ± 0.004	0.056 ± 0.003
2.5	2.119	0.131 ± 0.009	0.133 ± 0.006	3.925	0.046 ± 0.004	0.053 ± 0.002
3.0	2.112	0.159 ± 0.007	0.125 ± 0.007	3.915	0.047 ± 0.004	0.049 ± 0.002
4.0	2.098	0.140 ± 0.006	0.128 ± 0.006	3.895	0.039 ± 0.004	0.049 ± 0.002
5.0	2.083	0.154 ± 0.005	0.122 ± 0.008	3.875	0.040 ± 0.004	0.051 ± 0.003
6.0	2.069	0.178 ± 0.006	0.134 ± 0.007	3.855	0.048 ± 0.004	0.049 ± 0.003
7.0	2.054	0.201 ± 0.007	0.136 ± 0.007	3.835	0.052 ± 0.004	0.050 ± 0.003
8.0	2.040	0.198 ± 0.010	0.143 ± 0.008	3.815	0.047 ± 0.003	0.055 ± 0.002
9.0	2.026	0.220 ± 0.014	0.165 ± 0.012	3.796	0.058 ± 0.003	0.050 ± 0.003
10.0	2.011	0.210 ± 0.015	0.160 ± 0.014	3.775	0.058 ± 0.004	0.059 ± 0.002

TABLE 1

Inclusive longitudinal and transverse form factors f_L and f_T around $(q^{c.m.})^2 = 0.6$, 1.0 and 1.4 fm^{-2}

E_{np} (MeV)	$q^2_{c.m.}$ (fm^{-2})	f_L (fm)	f_T (fm)	$q^2_{c.m.}$ (fm^{-2})	f_L (fm)	f_T (fm)	$q^2_{c.m.}$ (fm^{-2})	f_L (fm)	f_T (fm)
0.0	0.603	0.110 ± 0.060	−0.022 ± 0.045	1.054	0.124 ± 0.040	0.144 ± 0.060	1.527	0.089 ± 0.040	0.190 ± 0.050
0.1	0.603	0.120 ± 0.050	0.484 ± 0.025	1.053	0.144 ± 0.030	0.418 ± 0.028	1.526	0.108 ± 0.021	0.288 ± 0.031
0.2	0.602	0.240 ± 0.030	0.394 ± 0.030	1.053	0.120 ± 0.025	0.361 ± 0.024	1.524	0.202 ± 0.018	0.293 ± 0.025
0.3	0.602	0.283 ± 0.028	0.446 ± 0.025	1.052	0.160 ± 0.018	0.339 ± 0.015	1.523	0.101 ± 0.014	0.260 ± 0.022
0.4	0.602	0.242 ± 0.025	0.343 ± 0.020	1.051	0.220 ± 0.025	0.336 ± 0.020	1.522	0.163 ± 0.016	0.287 ± 0.018
0.5	0.601	0.364 ± 0.022	0.400 ± 0.019	1.050	0.203 ± 0.016	0.298 ± 0.018	1.521	0.155 ± 0.020	0.249 ± 0.017
0.75	0.601	0.427 ± 0.024	0.334 ± 0.026	1.049	0.251 ± 0.020	0.259 ± 0.012	1.518	0.155 ± 0.012	0.239 ± 0.015
1.0	0.601	0.460 ± 0.027	0.341 ± 0.020	1.047	0.278 ± 0.018	0.277 ± 0.014	1.516	0.185 ± 0.014	0.224 ± 0.014
1.5	0.600	0.469 ± 0.016	0.279 ± 0.022	1.043	0.332 ± 0.016	0.274 ± 0.016	1.510	0.209 ± 0.012	0.179 ± 0.013
2.0	0.599	0.550 ± 0.017	0.227 ± 0.015	1.039	0.354 ± 0.014	0.231 ± 0.012	1.505	0.235 ± 0.014	0.198 ± 0.014
2.5	0.598	0.545 ± 0.018	0.248 ± 0.032	1.035	0.370 ± 0.015	0.204 ± 0.016	1.500	0.204 ± 0.013	0.175 ± 0.012
3.0	0.597	0.591 ± 0.012	0.288 ± 0.026	1.032	0.339 ± 0.022	0.177 ± 0.012	1.494	0.245 ± 0.014	0.178 ± 0.015
4.0	0.595	0.684 ± 0.013	0.239 ± 0.028	1.024	0.423 ± 0.020	0.159 ± 0.016	1.483	0.301 ± 0.015	0.158 ± 0.010
5.0	0.593	0.703 ± 0.014	0.246 ± 0.020	1.017	0.465 ± 0.022	0.218 ± 0.014	1.472	0.310 ± 0.018	0.161 ± 0.014
6.0	0.591	0.732 ± 0.016	0.164 ± 0.024				1.461	0.289 ± 0.025	0.191 ± 0.016
7.0	0.589	0.697 ± 0.015	0.201 ± 0.034				1.450	0.360 ± 0.020	0.175 ± 0.013
8.0	0.587	0.713 ± 0.018	0.137 ± 0.030				1.440	0.349 ± 0.018	0.244 ± 0.013

REF. P. Argan, G. Audit, A. Bloch, N. de Botton, J.L. Faure, C. Schuhl, G. Tamas, C. Tzara, E. Vincent, J. Deutsch, D. Favart, R. Prieels, B. Van Oystaeyen
Phys. Rev. C21. 1416 (1980)

ELEM. SYM.	A	Z
H	2	1

METHOD

REF. NO.	
80 Ar 2	hg

REACTION	RESULT	EXCITATION ENERGY	SOURCE		DETECTOR		ANGLE
			TYPE	RANGE	TYPE	RANGE	
G,PIØ	ABY	140-151	C	141-151	CKV-D		0

Relative measurements of π^0 photoproduction yields have been performed on hydrogen, deuterium, ^{3}He, and ^{4}He, in the region of 1 to 10 MeV above threshold. A simplified distorted-wave impulse approximation model of the four reactions is described; it leads to an overall understanding of the results. Large rescattering effects are brought to evidence in deuterium and ^{3}He, making the extraction of precise values for the dipole photoproduction amplitudes E_{0+} on nucleons strongly dependent on the theoretical description of the processes.

THRESHOLD MEASUREMENT

Final data in 81Ar2.

[NUCLEAR REACTIONS (γ,π^0), ^{1}H, ^{2}H, ^{3}He, and ^{4}He targets; measured reaction yields, E_{π^0} = 1–10 MeV.]

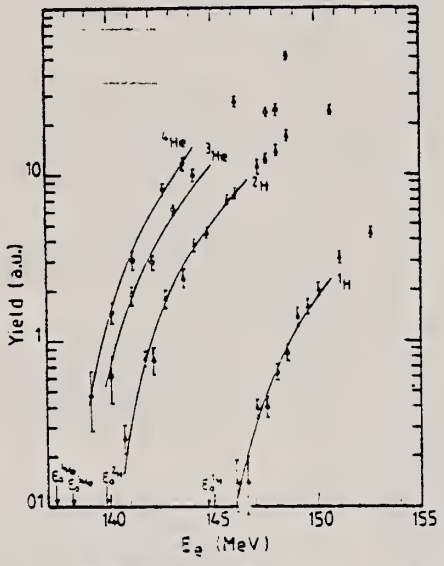

FIG. 5. The measured π^0 photoproduction yields as a function of the end-point bremsstrahlung energy E_e. The curves are the theoretical yields computed with DWIA cross sections, and adjusted to the data up to 6 MeV above threshold as explained in the text.

TABLE III. Experimental yields $Y_A(E_e) = C\int_{E_0}^{E_e}\int_{\Omega_\pi} B(E,E_e)\epsilon_A(E,\Omega)(d\sigma_A/d\Omega)d\Omega\,dE$ in microbarns, normalized to one target nucleus and one equivalent quantum, for different values of the bremsstrahlung end-point energy E_e above threshold E_0. *Note:* The measurements with empty targets gave $Y_{empty} = 0.00 \pm 0.02$. The average yields measured below threshold amounted to $Y_H = 0.02 \pm 0.02$, $Y_D = 0.07 \pm 0.04$, $Y_{^3He} = 0.01 \pm 0.12$, and $Y_{^4He} = 0.01 \pm 0.15$. All have been taken into account in the table.

Hydrogen		Deuterium		^{3}He		^{4}He	
$E_e - E_0$ (MeV)	$10^6 Y_H$	$E_e - E_0$ (MeV)	$10^6 Y_D$	$E_e - E_0$ (MeV)	$10^6 Y_{^3He}$	$E_e - E_0$ (MeV)	$10^6 Y_{^4He}$
1.41	0.14 ± 0.05	0.88	0.26 ± 0.05	1.87	0.61 ± 0.19	1.72	0.47 ± 0.19
1.91	0.14 ± 0.06	1.88	0.79 ± 0.08	2.87	1.38 ± 0.24	2.72	1.48 ± 0.22
2.41	0.39 ± 0.05	2.26	0.77 ± 0.14	3.37	2.94 ± 0.28	3.72	3.02 ± 0.39
2.91	0.40 ± 0.06	2.88	1.79 ± 0.21	4.37	6.08 ± 0.47	5.22	8.12 ± 0.63
3.41	0.63 ± 0.07	3.76	2.38 ± 0.29	5.37	9.86 ± 0.33	6.22	11.52 ± 0.39
3.91	0.85 ± 0.10	4.26	3.75 ± 0.32	9.37	23.7 ± 1.2	8.72	27.3 ± 1.7
4.41	1.39 ± 0.17	4.88	4.47 ± 0.31	9.87	24.4 ± 1.3	11.22	51.1 ± 3.2
4.91	1.60 ± 0.15	5.38	7.07 ± 0.47				
5.41	2.00 ± 0.16	6.26	7.75 ± 0.35				
6.41	3.15 ± 0.25	7.38	11.13 ± 1.12				
7.91	4.40 ± 0.23	7.76	12.40 ± 0.72				
		9.26	13.9 ± 1.1				
		8.76	16.9 ± 1.1				
		10.38	24.3 ± 1.1				

TABLE VII. The deuterium and ^{3}He threshold amplitudes in units of $10^{-3} m_{\pi^+}^{-1}$.

	Experiment	PWIA [a]	Rescattering amplitudes computed in FSA
D	−7.23 ± 0.36	$E_{0+}^{\pi^0 n} - E_{0+}^{\pi^+ n} = -1.5 \pm 0.5$	−6.3
^{3}He	−4.35 ± 0.43	$E_{0+}^{\pi^+ t} = 0.5 \pm 0.5$	−5.4

[a] The E_{0+} values from Sec. V.A.

REF. A.S. Bratashevskii, A.I. Derebchinskii, A.A. Zybalov, O.G. Konovalov, P.V. Sorokin, A.E. Tenishev
JETP Lett. 31, 270 (1980)
Pis'ma Zh. Eksp. Teor. Fiz. 31, 295 (1980)

ELEM. SYM.	A	Z
H	2	1

METHOD

REF. NO. 80 Br 6 hg

REACTION	RESULT	EXCITATION ENERGY	SOURCE		DETECTOR		ANGLE
			TYPE	RANGE	TYPE	RANGE	
$ G,P	NOX	375-700	C	UKN	MAG-D		DST

Proton polarization was determined from the asymmetry of their scattering by carbon nuclei POL PROTONS

The energy dependences of proton polarization at angles of 43, 78 and 120° were investigated in the c.m.s. in the energy range of 400 to 700-MeV photons. The obtained results are compared with the data of other papers.

PACS numbers: 13.60.Rj

TABLE I. Polarization values obtained in our experiment.

E, MeV	43°	78°	120°
375	0.47 ± 0.11	–	–
400	– 0.39 ± 0.07	–	– 0.53 ± 0.13
425	– 0.31 ± 0.08	– 0.40 ± 0.07	–
450	– 0.24 ± 0.08	– 0.45 ± 0.06	– 0.53 ± 0.10
475	– 0.38 ± 0.08	– 0.48 ± 0.06	–
500	– 0.37 ± 0.09	– 0.62 ± 0.07	– 0.50 ± 0.10
525	– 0.27 ± 0.09	– 0.57 ± 0.09	–
550	– 0.20 ± 0.09	– 0.59 ± 0.08	– 0.53 ± 0.10
575	– 0.29 ± 0.10	– 0.55 ± 0.06	–
600	– 0.23 ± 0.14	– 0.62 ± 0.06	– 0.54 ± 0.08
625	–	– 0.68 ± 0.06	–
650	–	– 0.65 ± 0.08	– 0.52 ± 0.08
675	–	– 0.55 ± 0.11	–
700	–	–	– 0.43 ± 0.10

(continued)

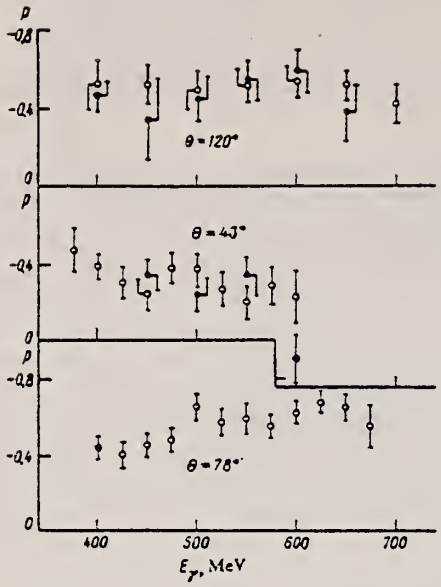

FIG. 1. Energy dependences of the proton polarization in the $\gamma d \rightarrow np$ reaction. ○-Results of Ref. 3; ●-results of Refs. 4 and 5; ▫-our results.

REF. A.S. Bratashevskii, A.I. Derebchinskii, A.A. Zybalov, O.G. Konovalov, P.V. Sorokin, A.E. Tenishev
Sov. J. Nucl. Phys. 31, 444 (1980)
Yad. Fiz. 31, 860 (1980)

ELEM. SYM.	A	Z
H	2	1

METHOD

REF. NO.: 80 Br 7 hg

REACTION	RESULT	EXCITATION ENERGY	SOURCE		DETECTOR		ANGLE
			TYPE	RANGE	TYPE	RANGE	
$ G,P	NOX	375-460	C	UKN	MAG-D		90

POL PROTONS

The energy dependence of the proton polarization in the reaction $\gamma d \rightarrow np$ at 90° c.m.s. has been studied in the photon-energy region 375–650 MeV. The results are compared with calculations based on various models.

PACS numbers: 25.20. + y, 25.10. + s, 13.60. − r

TABLE I

E_γ, MeV	$p \pm \Delta p$ *	E_γ, MeV	$p \pm \Delta p$ *
375	−0.200±0.097	525	−0.549±0.070
400	−0.414±0.080	550	−0.527±0.068
425	−0.491±0.040	575	−0.458±0.074
450	−0.530±0.056	600	−0.406±0.084
475	−0.609±0.077	625	−0.488±0.007
500	−0.692±0.066	650	−0.497±0.119

*The errors are statistical.

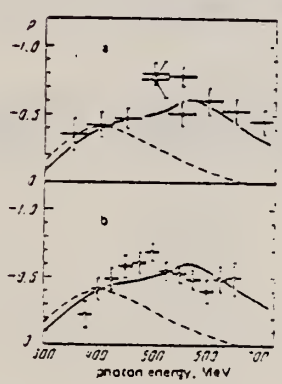

FIG. 1. Energy dependence of proton polarization in the reaction $\gamma d \rightarrow np$ at 90°. Points: •—results of Ref. 3, ○—results of Ref. 4, ▫—results of the present work. The solid curve shows the calculations of Ref. 3; the dashed curve shows the calculations of Ref. 5.

REF.

A.S. Bratashevskiĭ, A.I. Derebchinskiĭ, A.A. Zybalov, O.T. Konovalov, P.V. Sorokin, A.É. Tenishev
Sov. J. Nucl. Phys. 32, 216 (1980)
Yad. Fiz. 32, 418 (1980)

ELEM. SYM.	A	Z
H	2	1

METHOD

REF. NO. 80 Br 8 hg

REACTION	RESULT	EXCITATION ENERGY	SOURCE		DETECTOR		ANGLE
			TYPE	RANGE	TYPE	RANGE	
$ G,P	NOX	375-700	C	UKN	MAG-D		DST

POLARIZED PROTONS

The proton polarization has been studied in the reaction $\gamma d \rightarrow np$ in the photon-energy range 400–700 MeV at proton-emission angles 45, 78, and 120° in the c.m.s. The experimental data obtained are compared with the results of a phenomenological analysis carried out on the basis of various model assumptions.

PACS numbers: 25.20. + y, 25.10. + s

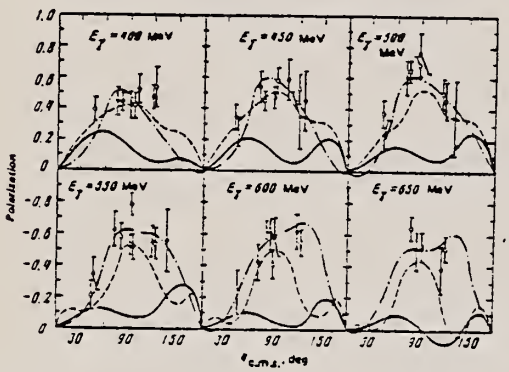

FIG. 1. Angular dependence of proton polarization in the reaction $\gamma d \rightarrow np$. Points: ○—results of Ref. 5, ●—Ref. 6, ◓—Ref. 11, ◑—results of the present work. The solid curves are calculations not taking into account dibaryon resonances, the dashed curves are calculations in which the contribution of 1(3⁻) and 0(3⁺) resonances was taken into account, and the dot-dash curves are calculations in which the contribution of 1(3⁻) and 0(1⁺) resonances was taken into account.

TABLE I.

	$\theta_{c.m.s.}$, deg		
E_γ, MeV	45	78	120
375	−0.472±0.107		
400	−0.393±0.074		−0.523±0.120
425	−0.305±0.083	−0.396±0.071	
450	−0.241±0.091	−0.324±0.064	−0.527±0.096
475	−0.377±0.082	−0.461±0.065	
500	−0.372±0.047	−0.625±0.072	−0.504±0.100
525	−0.273±0.086	−0.572±0.094	
550	−0.204±0.092	−0.566±0.082	−0.529±0.095
575	−0.293±0.097	−0.549±0.064	
600	−0.229±0.140	−0.625±0.058	−0.543±0.081
625		−0.676±0.065	
650		−0.648±0.075	−0.516±0.082
675		−0.532±0.107	
700			−0.431±0.103

Note. The energy resolutions for the angles 45° and 78° were $\Delta E_\gamma = \pm 12.5$ MeV, and for 120° $\Delta E = \pm 25$ MeV. The errors are statistical.

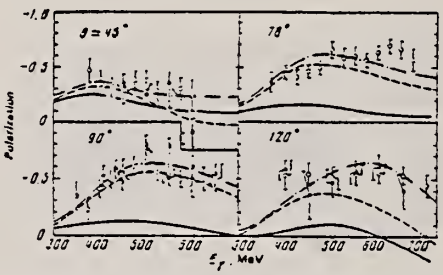

FIG. 2. Energy dependence of proton polarization in the reaction $\gamma d \rightarrow np$. The data at 90° are from Ref. 12. The notation is the same as in Fig. 1.

[12]A. S. Bratashevskiĭ *et al.*, Yad. Fiz. 31, 860 (1980) [Sov. J. Nucl. Phys. 31, 444 (1980)]. 80 Br 7

REF. W. Del Bianco, H. Jeremie, M. Irshad, G. Kajrys
Nucl. Phys. A343, 121 (1980)

ELEM. SYM.	A	Z
H	2	1

METHOD

REF. NO. 80 De 4 hg

REACTION	RESULT	EXCITATION ENERGY	SOURCE		DETECTOR		ANGLE
			TYPE	RANGE	TYPE	RANGE	
$ G,N	RLY	21	D	21	TOF-D		90
		(20.3)		(20.3)			

Re(ϕn) is photoneutron yield at angle ϕn relative to neutron yield at ϕn=0°. ϕn is photoneutron emission angle relative to photon polarization vector.

POLARIZED PHOTONS,

Abstract: Linearly polarized γ-rays from the $^{3}H(p,\gamma)^{4}He$ reaction have been used to measure the relative neutron yield of the $^{2}H(\gamma,n)H$ reaction at $\theta_n = 90°$ and at $\phi_n = 0°$, 45° and 90°. The 20.3 MeV γ-rays were monitored by a 12.7 diameter × 15.2 cm long NaI(Tl) crystal. A 6.3 cm diameter × 6.3 cm long NE230 scintillator was used both as a deuterium target and a proton detector, and a 30.5 cm diameter × 15.2 cm long NE213 scintillator was employed to detect the photoneutrons. The energy of the protons and the time of flight of the neutrons from the $^{2}H(\gamma,n)H$ reaction were measured in coincidence and the events recorded in a bidimensional spectrum. The ratio a/b of the coefficients of the angular distribution of the $^{2}H(\gamma,n)H$ reaction and the quantity $\Sigma(90°)$ were obtained from the ratio of the photoneutron yields at $\phi_n = 90°$ and 0° and found to be $a/b = 0.063–0.076 \pm 0.036$ and $\Sigma = 0.913–0.925 \pm 0.051$.

E NUCLEAR REACTIONS $^{2}H(\gamma,n)$, $E = 20.3$ MeV, measured $\sigma(\theta_n, \phi_n)$. Enriched target.

TABLE 4

Deuteron photodisintegration: ratio $R_E(\phi_n)$ and correction $\Gamma(\phi_n)$

Angle ϕ_n (deg)	$R_E(\phi_n)$ (exp)	P degree of linear polarization	$\Gamma(\phi_n)$	$R_E(\phi_n)$ (calc)
0		$P = 0.978$	17.3	
		$P = 0.989$	17.7	
45	0.470 ± 0.095	$P = 0.978$	10.6	0.54
		$P = 0.989$	10.6	0.54
90	0.106 ± 0.016	$P = 0.978$	6.24	0.114
		$P = 0.989$	6.16	0.109

REF. V.G. Gorbenko, Yu.V. Zhebrovskii, L.Ya. Kolesnikov, A.L. Rubashkin, P.V. Sorokin
JETP Lett. 32, 362 (1980)
Pis'ma Zh. Eksp. Teor. Fiz. 32, 387 (1980).

ELEM. SYM.	A	Z
H	2	1

METHOD

REF. NO.	
80 Go 6	hg

REACTION	RESULT	EXCITATION ENERGY	SOURCE		DETECTOR		ANGLE
			TYPE	RANGE	TYPE	RANGE	
$ G,NP	NOX	80-400	C	600-999	MAG-D		DST

999=1.2 GEV, COH-BRMS

The measurement results of the asymmetry of the cross sections for the $\gamma d \rightarrow np$ reaction with 80 to 600 MeV polarized photons for proton angles of 75°–150° in the c.m.s. are presented. The experimental data are compared with the predictions of theoretical analyses with allowance for dibaryon resonance states.

PACS numbers: 25.20. + y, 24.70. + s, 25.10. + s

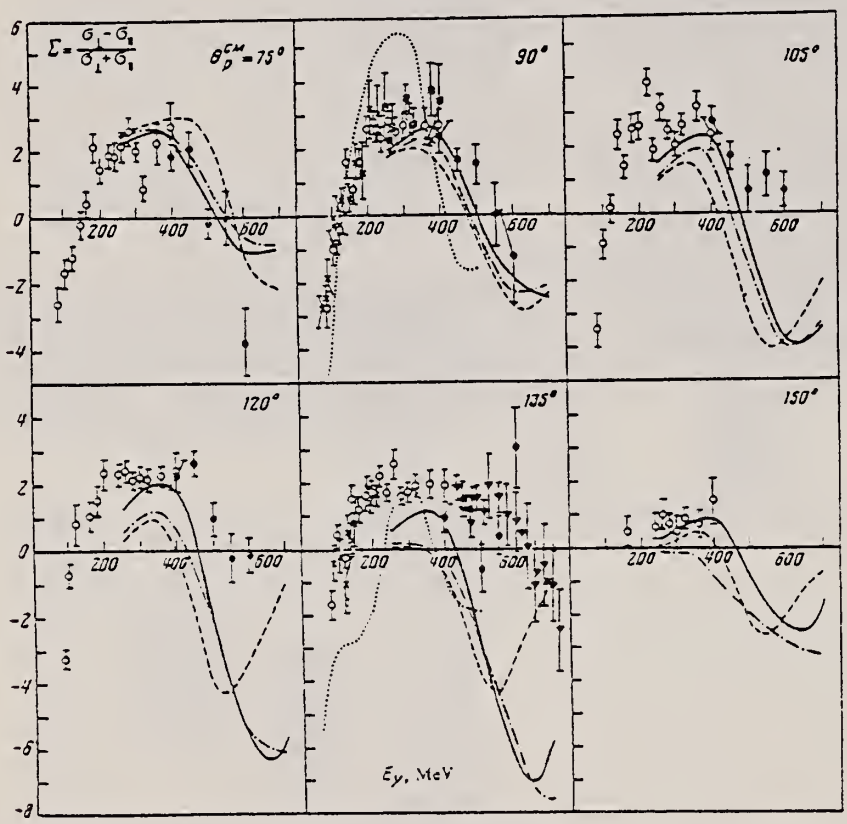

FIG. 1. Photon asymmetry excitation functions of the $\gamma d \rightarrow np$ process for angles of emission of a proton in the c.m.s. θ_p = 75°, 90°, 105°, 120°, 135°, and 150°. ×, Stanford 65 (Ref. 4); □, Frascati 66 (Ref. 5); ▽, Bonn 79 (Ref. 6); ●, Khar'kov 79 (Ref. 7); ○, our work. The dotted curve represents Laget's calculation[1] and the dot-dash curve represent the results of Ref. 3.

REF. H. Ikeda, I. Arai, H. Fujii, T. Fujii, H. Iwasaki, N. Kajiura, T. Kamae, K. Nakamura, T. Sumiyoshi, H. Takeda, K. Ogawa, M. Kanazawa
Nucl. Phys. B172, 509 (1980)

ELEM. SYM.	A	Z
H	2	1

METHOD

REF. NO.: 80 Is 3 | hg

REACTION	RESULT	EXCITATION ENERGY	SOURCE		DETECTOR		ANGLE
			TYPE	RANGE	TYPE	RANGE	
$ G,NP	NOX	400-650	C	UKN	MAG-D		DST

POLARIZED PROTONS

Paper also contains an extensive section on analysis of the data using dibaryon resonances and partial wave analysis.

The proton polarization in deuteron photodisintegration has been measured at photon energies between 400 and 650 MeV and at c.m. angles between 45° and 135°. To explain the polarization and differential cross-section data consistently, we have introduced dibaryon resonances and performed a partial-wave analysis at photon energies between 350 and 700 MeV. It has been shown that the existence of at least two dibaryon resonances is required in this energy range: one at ~2380 MeV with $I(J^P) = 0(3^-)$ or $0(1^-)$, and the other at ~2260 MeV with $I(J^P) = 1(3^-)$ or $1(2^-)$.

TABLE 2

Summary of the experimental results

Spectrometer setting no.	Average E_γ (E_γ) (MeV)	Average $\theta_{c.m.}$ ($\theta_{c.m.}$) (deg)	Polarization $P \pm \Delta P$
1	449.2	44.7 ± 1.9	−0.34 ± 0.08
2	501.7	44.7 ± 1.9	−0.24 ± 0.09
3	551.1	44.6 ± 1.9	−0.34 ± 0.10
4	603.5	44.7 ± 1.9	0.10 ± 0.13
5	403.3	69.6 ± 1.8	−0.44 ± 0.09
5	446.6	71.8 ± 1.6	−0.54 ± 0.10
6	503.3	69.6 ± 1.8	−0.61 ± 0.11
6	547.6	71.6 ± 1.6	−0.62 ± 0.11
7	599.0	69.7 ± 1.7	−0.42 ± 0.11
8	511.4	87.6 ± 1.4	−0.77 ± 0.13
8	549.0	89.7 ± 1.6	−0.51 ± 0.08
8	597.3	91.4 ± 1.5	−0.58 ± 0.12
9	452.3	118.0 ± 1.3	−0.35 ± 0.21
10	503.3	116.7 ± 1.3	−0.46 ± 0.12
10	549.2	118.3 ± 1.3	−0.54 ± 0.10
10	597.9	119.8 ± 1.3	−0.59 ± 0.11
10	646.2	121.0 ± 1.2	−0.38 ± 0.15
11	500.6	132.3 ± 1.1	−0.35 ± 0.24
11	548.6	133.1 ± 1.1	−0.55 ± 0.20

(continued)

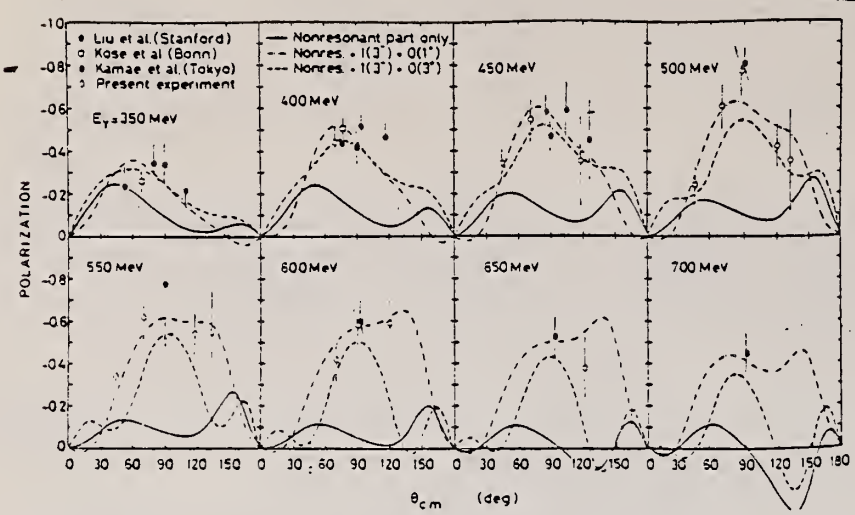

Fig. 4. Angular distribution of the proton polarization. The results of the present experiment (open circles) are plotted together with the previous data (closed circles, Liu et al. [19]; open squares, Kose et al. [20]; closed squares, Kamae et al. [3]) used for the χ^2-minimization fits. The dot-dashed curves show the results of the solution A. The dashed curves show the results of the solution B. The solid curves show the results with the non-resonant amplitudes only.

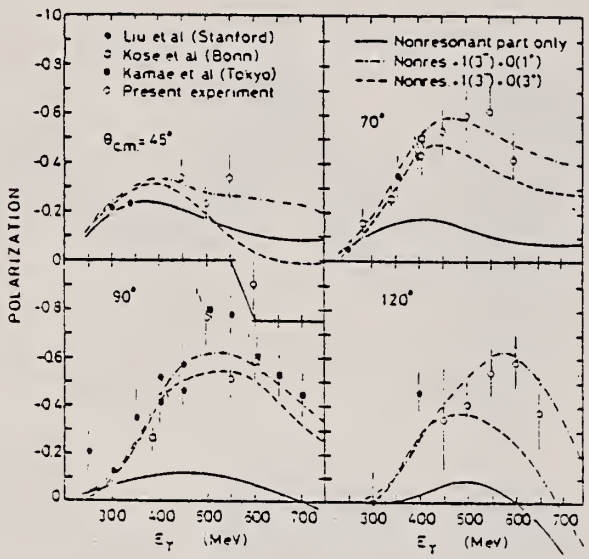

Fig. 5. Proton polarization plotted versus E_γ. The data outside the fitted region are also shown. The curves and symbols are coded as in fig. 4.

REF. E.C. Jones, Jr., W.L. Bendel, L.W. Fagg, R.A. Lindgren
Phys. Rev. C21, 1162 (1980)

ELEM. SYM.	A	Z
H	2	1

METHOD

REF. NO. 80 Jo 2 hg

REACTION	RESULT	EXCITATION ENERGY	SOURCE		DETECTOR		ANGLE
			TYPE	RANGE	TYPE	RANGE	
E,E/	ABX	0-19	C	56	MAG-D		180
				(56.4)			

The elastic and inelastic cross sections of deuterium for 56.4 MeV electrons scattered at 180°, have been measured up to an excitation energy of 19 MeV. The experimental cross sections are compared with those calculated by Miller, by Durand, and by Arenhövel and Fabian, and also with the sum rules of O'Connell. The results indicate that the contribution of meson exchange currents at this low-momentum transfer is significant.

FMF

[NUCLEAR REACTIONS ^{2}H(e,e'); $\theta = 180°$, $E = 56.4$ MeV; measured σ for $E_x = 0$ to 19 MeV. Deduced elastic magnetic form factor.]

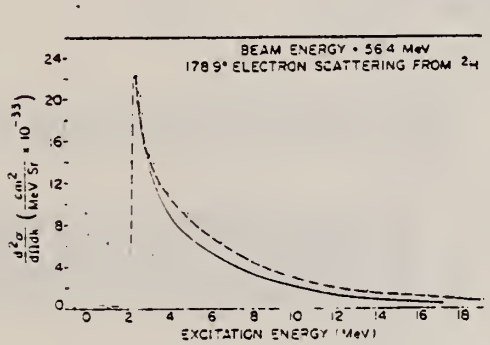

FIG. 1. Cross section values for 56.4-MeV electrons scattered at 180° from ^{2}H. The solid curve is based on the calculation of Miller (Ref. 5) up to 3-MeV excitation and Durand (Ref. 6) above this energy. The dashed curve is the result of a calculation of Arenhövel (Ref. 7) which includes meson-exchange and isobar configuration effects.

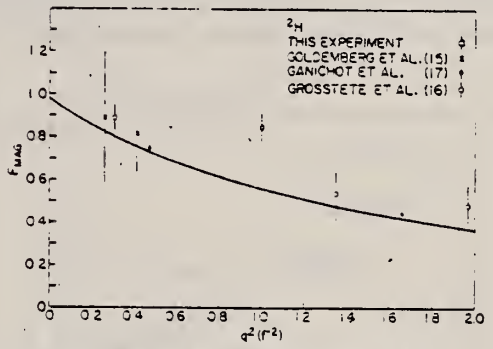

FIG. 2. Magnetic form factors for elastic electron scattering from ^2D from different experiments plotted vs q^2. The solid line is a calculation of F_{MAG} using the Reid soft-core potential with 6.5% D state (Ref. 13).

TABLE I. The factor $J - M$ of the sum rule expression of O'Connell (Ref. 3) is compared with experimental values of the factor corresponding to the elastic, inelastic, and total cross sections. The errors shown on the $J - M$ total are chiefly due to the inelastic part. The experimental sums were taken up to 19-MeV excitation energy.

	Experiment	Theory
	$J - M$	$J - M$
elastic	0.0042	
inelastic	0.0535	
total	0.0577 ± 0.0033	0.078

REF. H. Takeda, I. Arai, T. Fujii, H. Ikeda, H. Iwasaki, N. Kajiura, T. Kamae, S. Kawabata, K. Ogawa, T. Sumiyoshi, H. Fujii, S. Homma, M. Kanazawa, N. Yamashita
Nucl. Phys. B168, 17 (1980)

ELEM. SYM.	A	Z
H	2	1

METHOD

REF. NO.	
80 Ta 5	egf

REACTION	RESULT	EXCITATION ENERGY	SOURCE		DETECTOR		ANGLE
			TYPE	RANGE	TYPE	RANGE	
$ G,PI-P	NOX	700-999	C	999	TEL-D		DST

999=1.2GEV, POL P

The recoil proton polarization for $\gamma n \to \pi^- p$ was measured around the third resonance region. Both momentum vectors of the proton and the pion were determined by the magnetic spectrometers. The proton polarization was measured by means of proton-carbon scattering in the polarization analyzer located behind the proton spectrometer. Below 900 MeV incident photon energy, our data are consistent with the other existing experimental data ($\theta^*_\pi = 90°$) and the predictions of partial-wave analyses. Above 1000 MeV, however, a large discrepancy was observed between our data and the predictions of the partial-wave analyses. This discrepancy stands out as the pion c.m. angle increases. A new partial-wave analysis was made for $\gamma n \to \pi^- p$ including our polarization data, and the accuracy of the experimentally determined electromagnetic coupling constants of the third resonances were greatly improved. In particular, a finite amount of the helicity $\frac{3}{2}$ amplitude for the $\gamma n \to F_{15}(1688)$ resonance was obtained against the predictions of the quark models, by Copley, Karl and Obryk and by Feynman, Kislinger and Ravendal but in agreement with the relativistic quark models of Sugimoto and Toya, and Kubota and Ohta.

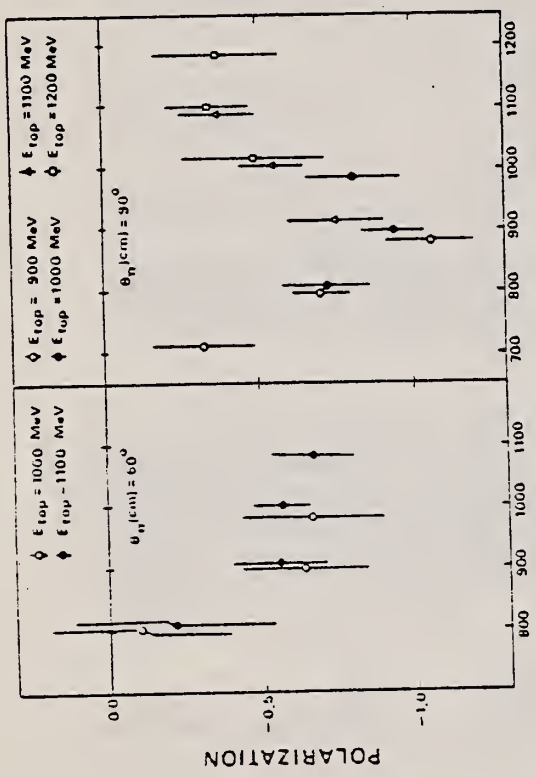

Fig. 4. Consistency of our polarization data in the overlapped region: the energy excitation plots at (a) $\theta_\pi(\mathrm{CM}) = 60°$ and (b) $\theta_\pi(\mathrm{CM}) = 90°$.

TABLE 2
Final results of polarization

Energy bin (MeV)	Average photon energy (MeV)	Pion c.m. angle (degrees)	Polarization	Number of events
750 – 850	807.1	59.6 ± 1.8	−0.15 ± 0.22	283
850 – 950	904.2	60.1 ± 2.0	−0.58 ± 0.13	712
950 – 1050	992.4	60.5 ± 2.0	−0.57 ± 0.09	945
1050 – 1150	1082.0	60.6 ± 1.9	−0.66 ± 0.14	375
850 – 950	909.6	69.8 ± 1.9	−0.45 ± 0.17	242
950 – 1050	1002.9	70.1 ± 1.9	−0.64 ± 0.10	623
1050 – 1150	1083.6	70.5 ± 1.9	−0.34 ± 0.14	327
850 – 950	908.8	79.8 ± 1.9	−0.77 ± 0.21	123
950 – 1050	1001.9	80.2 ± 1.9	−0.55 ± 0.13	306
1050 – 1150	1085.3	80.5 ± 1.8	−0.29 ± 0.18	209
650 – 750	717.9	89.6 ± 1.8	−0.32 ± 0.17	194
750 – 850	803.9	90.0 ± 1.9	−0.71 ± 0.08	817
850 – 950	897.9	90.3 ± 1.8	−0.93 ± 0.08	780
950 – 1050	1008.6	90.3 ± 1.9	−0.54 ± 0.10	515
1050 – 1150	1093.9	90.5 ± 1.9	−0.36 ± 0.10	417
1150 – 1250	1186.0	90.5 ± 1.8	−0.37 ± 0.21	99
850 – 950	912.8	100.0 ± 2.0	−0.83 ± 0.18	117
950 – 1050	1003.0	100.4 ± 1.8	−0.48 ± 0.12	296
1050 – 1150	1086.0	100.6 ± 1.8	−0.34 ± 0.15	184

(continued)

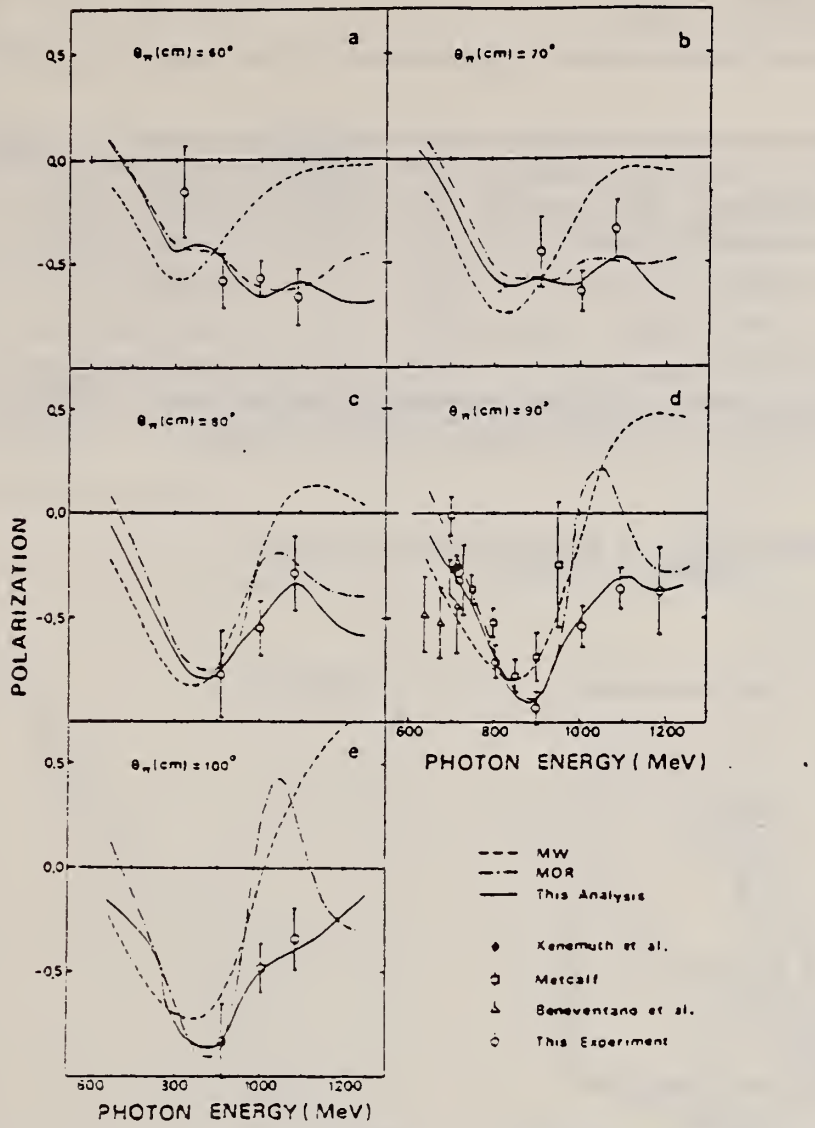

Fig. 5 Photon energy excitation plot of the polarization at θ_π(CM) = 60°(a), 70°(b), 80°(c), 90°(d), 100°(e).

REF. P. Argan, G. Audit, A. Bloch, N. de Botton, J.L. Faure, C. Schuhl, G. Tamas, C. Tzara, E. Vincent, J. Deutsch, D. Favart, R. Prieels, B. Van Oystaeyen
Phys. Rev. C24, 300 (1981)

ELEM. SYM.	A	Z
H	2	1

METHOD

REF. NO. 81 Ar 2 egf

REACTION	RESULT	EXCITATION ENERGY	SOURCE		DETECTOR		ANGLE
			TYPE	RANGE	TYPE	RANGE	
G,PIØ	ABY	141-149	C	141-149	CKV-D		Ø

Our recently published π^0 photoproduction data at threshold have been reanalyzed with the use of a more refined detection efficiency calculation. The high energy points appear to be consistent with the threshold measurements; the effective threshold amplitudes remain unchanged, and are now supported by the complete set of experimental data.

REANALYSIS OF 80AR2

[NUCLEAR REACTIONS (γ,π^0), ^{1}H, ^{2}H, ^{3}He, and ^{4}He targets; measured reaction yields, E_{π^0}=1–10 MeV.]

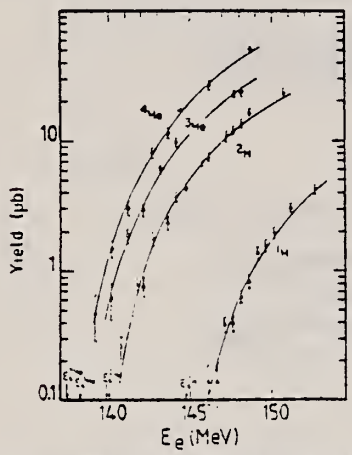

FIG. 2. The measured π^0 photoproduction yields in microbarns, normalized to one target nucleus and one equivalent quantum, as functions of the Bremsstrahlung end-point energy E_e. The curves are the theoretical yields computed with DWIA cross sections, and adjusted to the complete set of data as explained in the text.

REF. M. Bernheim, E. Jans, J. Mougey, D. Royer, D. Tarnowski, S. Turck-Chieze, I. Sick, G.P. Capitani, E. De Canctis, S. Frullani
Phys. Rev. Lett. 46, 402 (1981)

ELEM. SYM.	A	Z
H	2	1

METHOD

REF. NO. 81 Be 1 hg

REACTION	RESULT	EXCITATION ENERGY	SOURCE		DETECTOR		ANGLE
			TYPE	RANGE	TYPE	RANGE	
E,E/	ABX	0-15	D	280-535	MAG-D		155

Electroexcitation of the singlet S state of the deuteron has been measured for the range of momentum transfer $q^2 = 6-19$ fm^{-2}, where meson-exchange current contributions dominate the cross section.

PACS numbers: 25.30.Cg, 21.30.+y, 25.10.+s

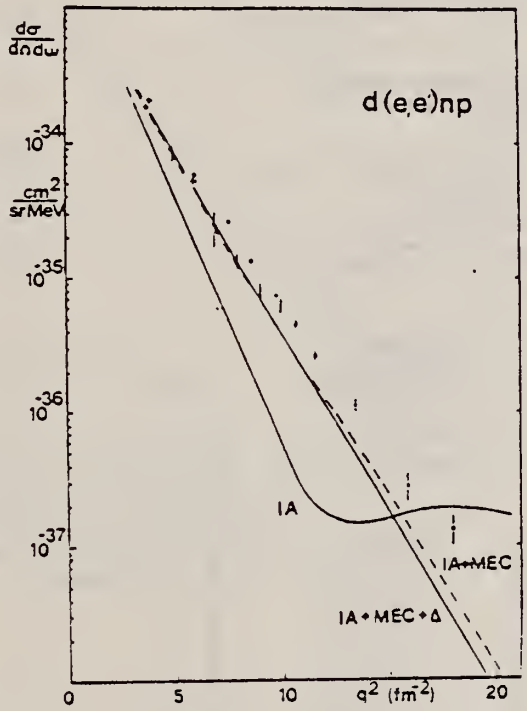

FIG. 2. Cross sections for 0–3 MeV above threshold and $\vartheta = 155°$. Crosses are from Refs. 7 and 8. The comparison with the bars (Ref. 6) is qualitative only (see text). The predicted curves of Fabian and Arenhövel are labeled according to the diagrams included: impulse approximation (IA), pionic current and pair (π), ρ exchange (ρ), total MEC (MEC), and ground-state isobar component (Δ).

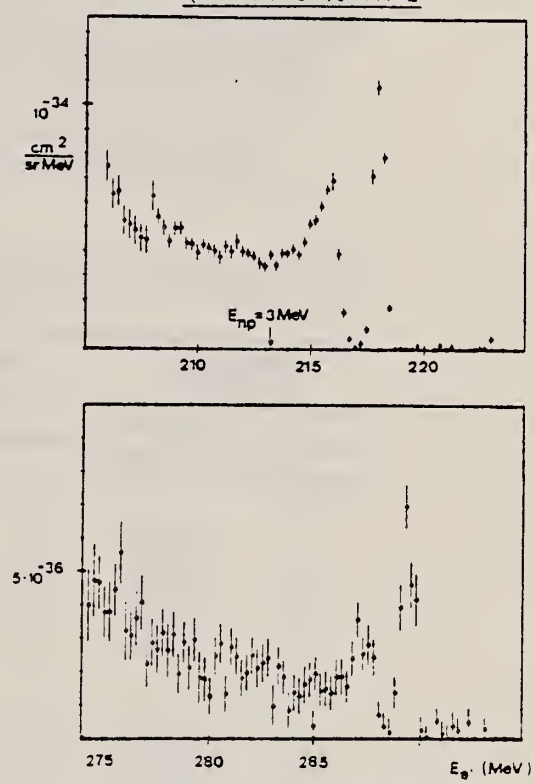

FIG. 1. Cross sections (in cm^2/sr MeV) for e–d scattering at $\vartheta = 155°$ and electron energies of 280 and 410 MeV ($q^2 = 5.9$ and 11.5 fm^{-2}).

TABLE I. Inelastic cross sections for $d(e,e')$ at $\vartheta = 155°$ averaged over threshold region ($E_{np} = 0-3$ MeV) as a function of electron energy E_1.

E_1 (MeV)	q_1^2 (fm^{-2})	$d\sigma/d\Omega_e d\omega_{lab}$ (cm^2/sr MeV)
280	5.89	$(0.602 \pm 0.005) \times 10^{-34}$
320	7.47	$(0.266 \pm 0.007) \times 10^{-34}$
350	8.74	$(0.136 \pm 0.004) \times 10^{-34}$
370	9.63	$(0.751 \pm 0.030) \times 10^{-35}$
390	10.55	$(0.445 \pm 0.030) \times 10^{-35}$
410	11.50	$(0.261 \pm 0.029) \times 10^{-35}$
430	12.47	$(0.113 \pm 0.009) \times 10^{-35}$
495	15.82	$(0.286 \pm 0.072) \times 10^{-36}$
535	18.00	$(0.134 \pm 0.037) \times 10^{-36}$

REF. M. Bernheim, A. Bussière, J. Mougey, D. Royer, D. Tarnowski, S. Turck-Chieze, S. Frullani, G.P. Capitani, E. De Sanctis, E. Jans
Nucl. Phys. A365, 349 (1981)

ELEM. SYM.	A	Z
H	2	1

METHOD

REF. NO. 81 Be 11 hg

REACTION	RESULT	EXCITATION ENERGY	SOURCE		DETECTOR		ANGLE
			TYPE	RANGE	TYPE	RANGE	
E,E/P	ABX	105,147	D	500	MAG-D		DST

Abstract: The nucleon momentum distribution in the deuteron has been determined up to 340 MeV/c by measuring the d(e, e'p)n reaction at an incident electron energy of 500 MeV. The data are well described even above $p = 200$ MeV/c by the most recent deuteron wave functions, in contrast with previous (e, e'p) and (p, 2p) results.

COINCIDENCE

E NUCLEAR REACTION ^{2}H(e, e'p), $E = 500$ MeV; measured σ, missing energy, recoil momentum. ^{2}H deduced effective nucleon momentum distribution. Liquid target.

TABLE 3

Coincidence cross sections $d\sigma/de'd\Omega_e\, d\Omega_p$ for the CD_2 (two sets of measurements) and liquid deuterium targets as a function of the recoil momentum n', and for the $k = 450$ MeV/c and $k = 350$ MeV/c kinematics

Solid CD_2 target $k = 450$ MeV/c		Liquid target (low n') $k = 450$ MeV/c		Liquid target (high n') $k = 350$ MeV/c	
n' (MeV/c)	cross section (nb · sr^{-2} · MeV^{-1})	n' (MeV/c)	cross section (nb · sr^{-2} · MeV^{-1})	n' (MeV/c)	cross section (nb · sr^{-2} · MeV^{-1})
Set I					
5	112.4 ± 8.3	5	80.3 ± 2.1	155	0.883 ± 0.050
15	73.3 ± 3.8	15	76.9 ± 1.2	165	0.612 ± 0.039
25	55.1 ± 2.8	25	60.6 ± 0.8	175	0.452 ± 0.033
35	37.9 ± 2.5	35	42.5 ± 0.8	185	0.389 ± 0.023
45	23.5 ± 2.4	45	26.9 ± 0.8	195	0.320 ± 0.019
55	14.7 ± 2.3	55	13.73 ± 0.44	205	0.260 ± 0.017
Set II					
5	140.3 ± 13.0	65	9.59 ± 0.22	215	0.195 ± 0.014
15	106.5 ± 6.0	75	6.04 ± 0.18	225	0.172 ± 0.011
25	60.8 ± 4.8	85	4.11 ± 0.13	235	0.113 ± 0.007
35	42.0 ± 4.8	95	2.96 ± 0.11	245	0.123 ± 0.010
45	26.4 ± 7.2	105	1.851 ± 0.095	255	0.095 ± 0.007
		115	1.210 ± 0.040	265	0.072 ± 0.005
		125	0.982 ± 0.019	275	0.063 ± 0.005
		135	0.779 ± 0.019	285	0.050 ± 0.006
		145	0.499 ± 0.026	295	0.037 ± 0.003
		155	0.369 ± 0.024	305	0.025 ± 0.003
		165	0.317 ± 0.013	315	0.028 ± 0.003
		175	0.170 ± 0.012	325	0.022 ± 0.003
				335	0.015 ± 0.003

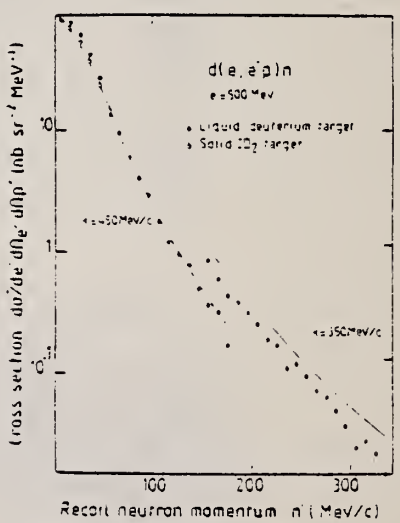

Fig. 9. Coincidence cross section $d\sigma/de'd\Omega_e\, d\Omega_p$ for the d(e, e'p)n reaction, as a function of the recoil momentum n', for the two sets of kinematical conditions given in table 3. Open circles corresoond to measurements on a solid CD_2 target. The solid curve is a PWIA calculation using eq. (1) and a deuteron wave function from the Reid soft core potential, normalized to the low momentum data, as discussed in sect. 5.

REF. W. Del Bianco, L. Federici, G. Giordano, G. Matone, G. Pasquariello, P. Picozza, R. Caloi, L. Casano, M. P. De Pascale, L. Ingrosso, M. Mattioli, E. Poldi, C. Schaerf, P. Pelfer, D. Prosperi, S. Frullani, B. Girolami, H. Jeremie
Phys. Rev. Lett. 47, 1118 (1981)

ELEM. SYM.	A	Z
H	2	1

METHOD

REF. NO. 81 De 1 egf

REACTION	RESULT	EXCITATION ENERGY	SOURCE		DETECTOR		ANGLE
			TYPE	RANGE	TYPE	RANGE	
$ G,N	NOX	10-70	D	10-70	TOF-D		90

The asymmetries $\Sigma(\theta_{c.m.}=\pi/2)$ for the reaction $^2H(\gamma,n)p$ have been measured with use of a monochromatic and linearly polarized γ-ray beam, obtained by backward Compton scattering of laser light against high-energy electrons. Contributions from meson exchange currents must be included in the theoretical calculations to reproduce our data.

$G: CIRCULAR; LINEAR

PACS numbers: 25.20.+g

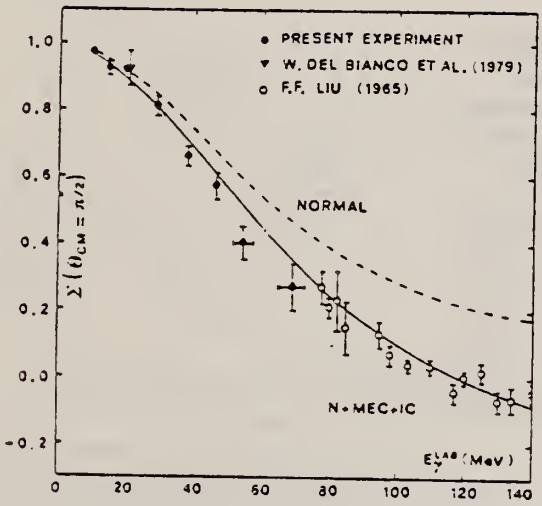

FIG. 2. Plot of the ratio $\Sigma(\theta_{c.m.}=\pi/2)$ vs E_γ for the reaction $^2H(\gamma,n)p$. Dashed and full curves are the Arenhövel calculations in approximations I and II (see text), respectively.

REF. J.F. Gilot, A. Bol, P. Leleux, P. Lipnik, P. Macq
Phys. Rev. Lett. 47, 304 (1981)

ELEM. SYM.	A	Z
H	2	1

METHOD

REF. NO. 81 Gi 4 hg

REACTION	RESULT	EXCITATION ENERGY	SOURCE		DETECTOR		ANGLE
			TYPE	RANGE	TYPE	RANGE	
N,G	ABX	38	D	72	TEL-D		DST
		(38.2)					

SIGMA 0 AND 180 DEG

The neutron-proton capture differential cross section has been measured at extreme forward and backward angles for 72-MeV neutron energy corresponding to a γ-ray energy of 38.2 MeV in the inverse reaction. The results agree well with recent photodisintegration data at forward angles, but only partially with potential model calculations.

PACS numbers: 21.30.+y, 25.10.+s, 13.75.Cs

TABLE I. Results of the present experiment, converted into photodisintegration cross section ($E_\gamma = 38.2 \pm 0.5$ MeV), compared with data of Hughes *et al.* and Weissman and Schultz (WS) at the same energy and with calculations using a Humada-Johnston (HJ) potential, or a Feschbach-Lomon (FL) potential with a 5.2% D-state term ($E_\gamma = 40$ MeV). All numbers are in μb/sr. The quoted experimental errors for the present experimental values are statistical and are obtained from a combination of three independent runs.

	This experiment	Hughes *et al.*[a]	WS[b]	HJ[c]	FL[d]
$d\sigma/d\Omega(0°)$	5.7 ± 0.6	5.2 ± 0.3	6.0 ± 0.8	7.2	6.9
$d\sigma/d\Omega(180°)$	6.9 ± 0.6		3.4 ± 0.8	5.2	5.1
a	6.30 ± 0.45		4.7 ± 0.5	6.2	6.0
c	-0.60 ± 0.45		1.3 ± 0.5	1.0	0.9

[a]Ref. 1.
[b]Ref. 9.
[c]Ref. 2.
[d]Ref. 3.

[1]R. J. Huges, A. Zieger, H. Wäffler, and B. Ziegler, Nucl. Phys. A267, 329 (1976). 7½ Hμ -
[2]F. Partovi, Ann. Phys. (N.Y.) 27, 79 (1964).
[3]E. L. Lomon, Phys. Lett. 68B, 419 (1977).
[4]M. L. Rustgi, T. S. Sandhu, and O. P. Rustgi, Phys. Lett. 70B, 145 (1977).
[5]H. Arenhövel and W. Fabian, Nucl. Phys. A282, 397 (1977).
[6]E. Hadjimichaël, Phys. Lett. 85B, 27 (1979); E. Hadjimichaël and D. P. Saylor, Phys. Rev. Lett. 45, 1776 (1980).
[7]H. Baier, Fortschr. Phys. 27, 209 (1979).
[8]B. Weissman and H. L. Schultz, Nucl. Phys. A147, 129 (1971).
[9]J. F. Gilot *et al.*, Nucl. Instrum. 171, 607 (1980).
[10]M. Bosman *et al.*, Phys. Lett. 82B, 212 (1979).
[11]L. Allen, Phys. Rev. 98, 705 (1955).

REF. J. Uegaki, L.O. Dallin, Y.M. Shin, C.Y. Kim
Nucl. Inst. Meth. 179, 55 (1981)

ELEM. SYM.	A	Z
H	2	1

METHOD

REF. NO. 81 Ue 1 hg

REACTION	RESULT	EXCITATION ENERGY	SOURCE		DETECTOR		ANGLE
			TYPE	RANGE	TYPE	RANGE	
G,P	RLX	2-160	C	160	TEL-D		90

High resolution telescope counters which employ thick germanium and silicon surface barrier detectors have been constructed and used for experiments with bremsstrahlung beams at high energies. The system has been tested with ≤160 MeV bremsstrahlung beams and Li targets. All charged particles up to $E \simeq 100$ MeV are clearly separated, and there is little background in the measured spectra except at very low energies. Data have been acquired for the $^2D(\gamma, p)$ n reaction at 90° and for the $^4He(\gamma, \gamma')$ reaction angular distributions. The system may be constructed at about 1% of the cost of a magnetic spectrometer with a comparable energy resolution and analyzing capability.

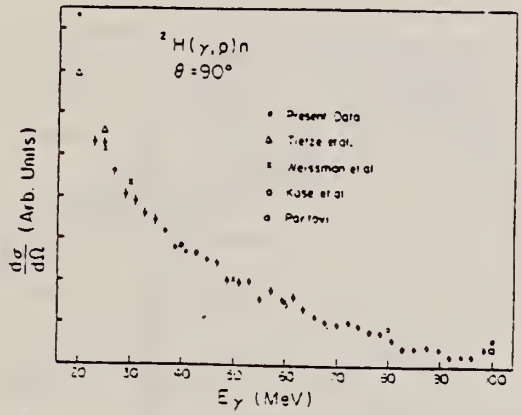

Fig. 7. Differential cross sections at $\theta_{LAB} = 90°$ for the $^2H(\gamma, p)n$ reaction. The experimental data are taken from Tietze et al. [9], Weissman et al. [10] and Kose et al. [11], and the theoretical results from Partovi [8].

REF. K. Baba, I. Endo, H. Fukuma, K. Inoue, T. Kawamoto, T. Ohsugi, Y. Sumi, T. Takeshita, S. Uehara, Y. Yano, T. Maki
Phys. Rev. Lett. 48, 729 (1982)

EL.EM. SYM.	A	Z
H	2	1

METHOD

REF. NO.: 82 Ba 1 egf

REACTION	RESULT	EXCITATION ENERGY	SOURCE		DETECTOR		ANGLE
			TYPE	RANGE	TYPE	RANGE	
G,P	ABX	180-600	D	180-600	MAG-D		DST

The differential cross section for $\gamma d \rightarrow pn$ has been measured in the energy range between 180 and 600 MeV at c.m. angles 15°, 30°, 42°, and 72°, by using tagged photons. The results, in particular at smaller angles, are in disagreement with theoretical calculations which take into account the effect of dibaryon resonances.

PACS numbers: 25.20.+y, 25.10.+s, 13.75.Cs

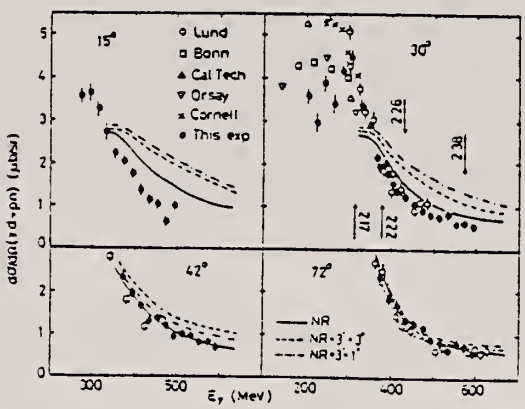

FIG. 1. The differential cross section for the process $\gamma d \rightarrow pn$ as a function of E_γ at fixed angles. The errors are statistical only. The curves are from Ref. 2; the dashed and dot-dashed ones are NR + DB's of $J^P = 3^- + 3^-$, and NR + $3^- + 1^-$, respectively, while the solid one is NR only. The arrows indicate the position of possible DB's.

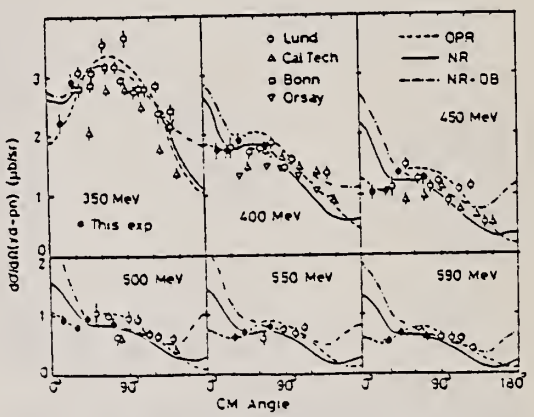

FIG. 2. The differential cross section for $\gamma d \rightarrow pn$ as a function of c.m. angle of proton. The dot-dashed and solid curves are the same as in Fig. 1, and the dashed one is the OPR contribution.

REF. M.P. DePascale, L. Federici, G. Giordano, G. Matone, P. Picozza, L. Azario, R. Caloi, L. Casano, M. Mattioli, E. Poldi, D. Prosperi, C. Schaerf
Phys. Lett. B114, 11 (1982)

ELEM. SYM.	A	Z
H	2	1

METHOD

REF. NO. 82 De 1 egf

REACTION	RESULT	EXCITATION ENERGY	SOURCE		DETECTOR		ANGLE
			TYPE	RANGE	TYPE	RANGE	
$ G,N	ASM	19	D	19	TOF		DST

$ G,19=19.8 MEV

The symmetry $\Sigma(\theta)$ for the reaction $^2H(\gamma, n)p$ has been measured at nine angles for E_γ = 19.8 MeV. The source of monochromatic and linearly polarized γ-rays was the Frascati Ladon facility, obtained by Compton scattering of laser light against high-energy electrons. The experimental results are compared with theoretical calculations based on the Reid-soft-core and with the De Tourreil–Sprung (version B) interactions.

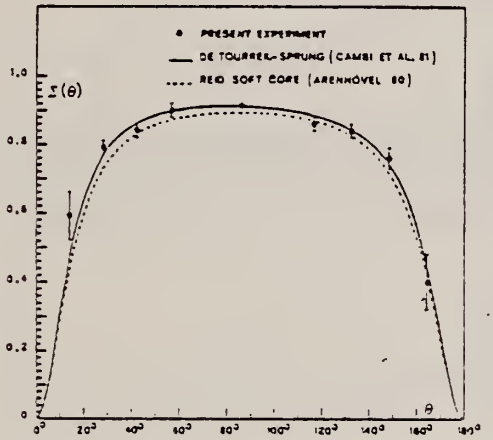

Fig. 2. Plot of $\Sigma(\theta)$ versus θ (c.m. proton angle) for the reaction $^2H(\gamma, n)p$ at E_γ = 19.8 MeV. Dotted and full curves are the theoretical calculation of refs. [9] and [11] with the RSC and DTS potentials, respectively.

Table 2
Comparison between our values for the ratios a/b, f/b, g/b at E_γ = 19.8 MeV and the corresponding theoretical predictions as given by refs. [10] (RSC), [14] (DTS), [12] (HJ) and [13] (Paris). Our best estimates of the other coefficients appearing in eq. (5) are: b = (65.7 ± 1.2) μb/sr, c = (0.47 ± 0.27) μb/sr, d = (20.6 ± 1.2) μb/sr, e = (−4.75 ± 0.57) μb/sr.

Ratio	Fitted values	Theoretical values			
		DTS	RSC	HJ	Paris
a/b	0.0622 ± 0.0041	0.0711	0.0821	0.0845	0.0844
f/b	0.9706 ± 0.0061	0.984	0.980	0.978	0.979
g/b	0.319 ± 0.013	0.275	0.273	0.275	0.276

REF. V.G. Gorbenko, Yu.V. Zhebrovskij, L.Ya. Kolesnikov, A.L. Rubashkin, P.V. Sorokin
Nucl. Phys. A381, 330 (1982)

ELEM. SYM.	A	Z
H	2	1

METHOD

REF. NO. 82 Go 1 egf

REACTION	RESULT	EXCITATION ENERGY	SOURCE		DETECTOR		ANGLE
			TYPE	RANGE	TYPE	RANGE	
$ G,P	ASM	80-600	D	600-999	MAG-D		DST

$ G,999=1.6 GEV

Abstract: The asymmetry of cross sections for the photodisintegration of the deuteron has been measured in the linearly polarized photon energy range 80–600 MeV at c.m. proton emission angles 75°–150°. The obtained data are not found to be in agreement with theoretical predictions.

E NUCLEAR REACTIONS ^{2}H(polarized γ, p), E = 80–600 MeV; measured $\sigma(\theta)$ asymmetry. Linearly polarized beam.

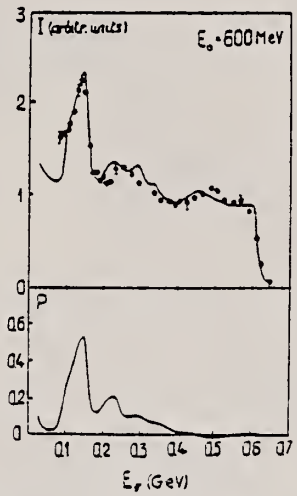

Fig. 2. Intensity and polarization spectra of bremsstrahlung from a 2 mm diamond single crystal at orientation angles ϑ = 75.3 mrad and α = 84.7° (ϑ is the polar angle between the electron momentum p_0 and the crystal axis b_1 = [110], α is the azimuthal angle between the planes (p_0, b_1) and (b_2, b_3)). The curve represents the calculation with the following experimental parameters: the energy resolution of the spectrometer $\Delta E_\gamma / E_\gamma$ = 3%, the angles of photon collimation $\theta_c = 5 \times 10^{-4}$ rad, electron beam divergence $\omega_0 = 10^{-4}$ rad and multiple scattering in the target $\omega_t = 3 \times 10^{-3}$ rad.

(continued)

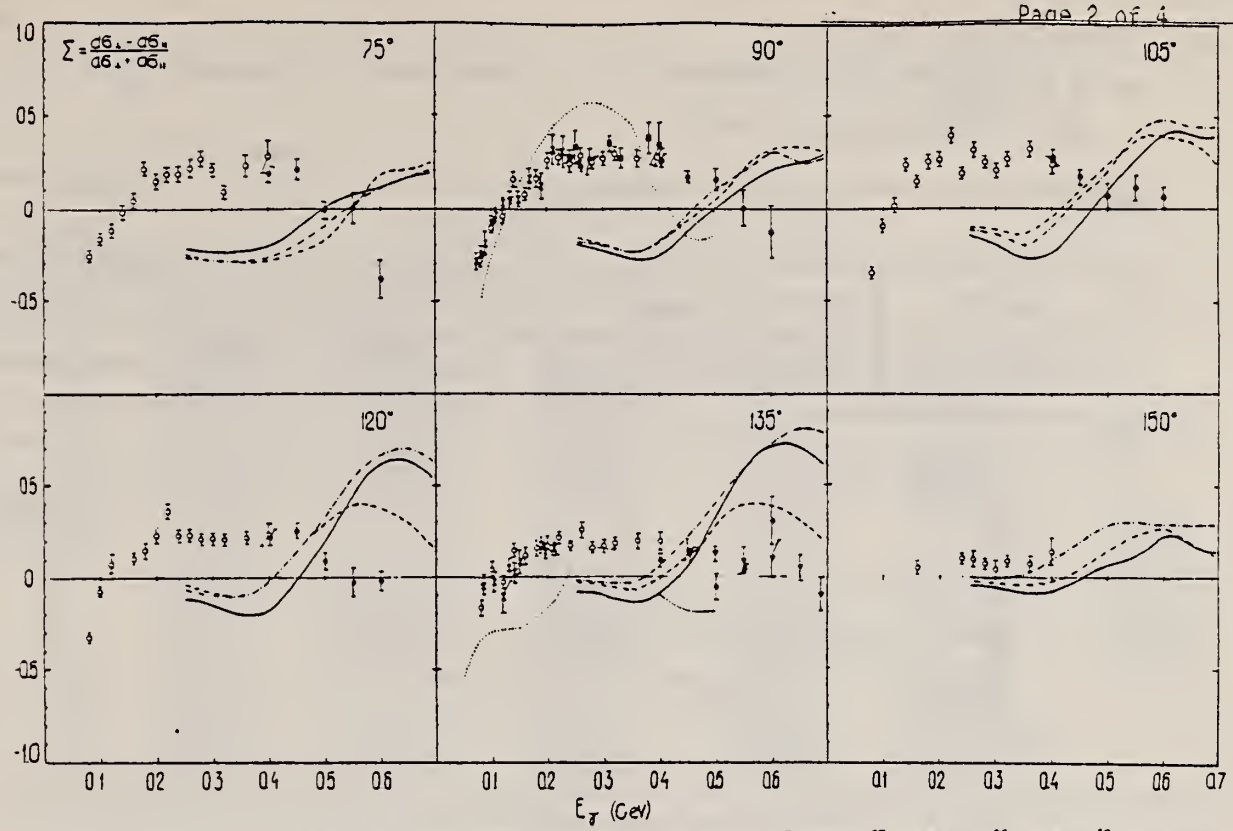

Fig. 3. Energy distributions of the cross section asymmetry. Points are: ●, ○ our present data; ⌶ Stanford [27]); ■ Frascati [28]); ▼ Bonn [29]). The dotted curve represents the calculation by Laget [31]); the solid, dashed and dash-dotted curves show the results of the analysis by the Japanese group [9]).

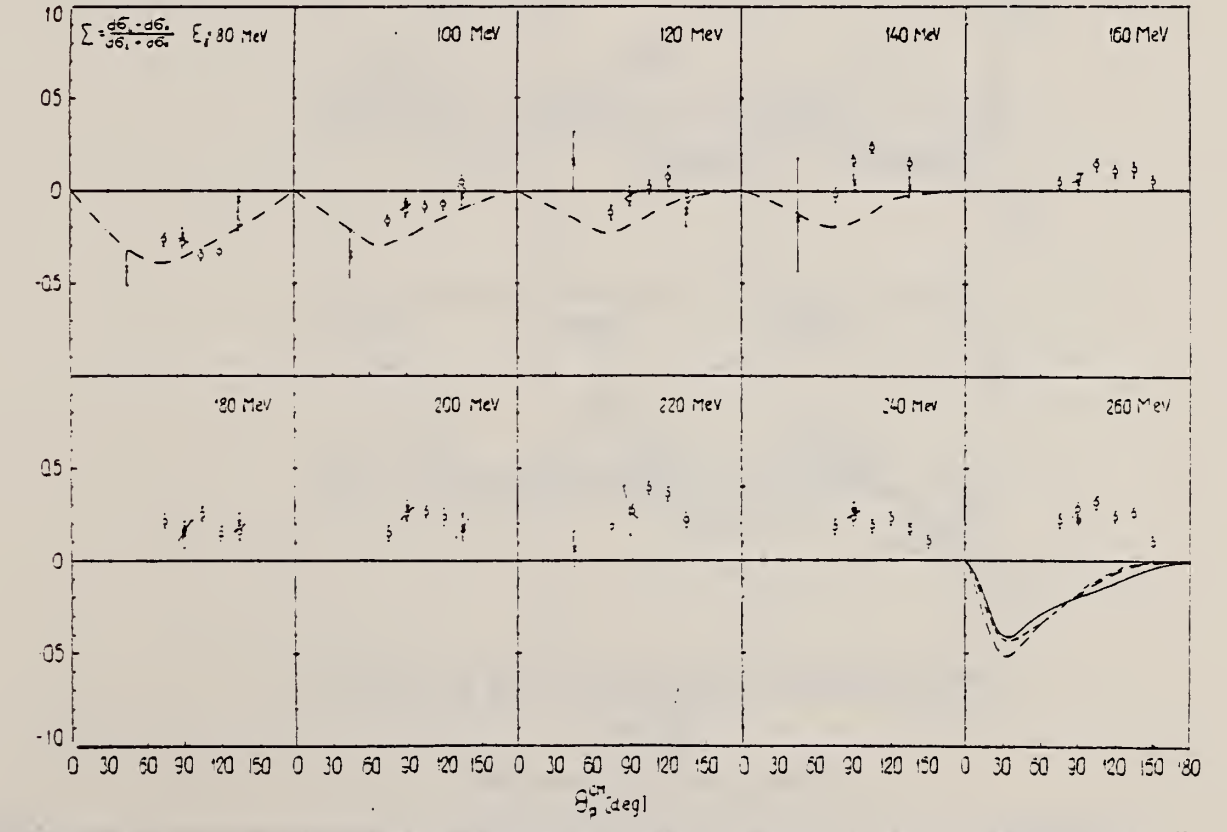

Fig. 4. Angular distributions of the cross-section asymmetry for E_γ = 80–260 MeV. A double dash-dotted line representing Partovi's calculation [30]) is added to the notation of fig. 3.

(continued)

ELEM. SYM.	A	Z
H	2	1

METHOD

REF. NO.: 82 Go 1 egf

REACTION	RESULT	EXCITATION ENERGY	SOURCE TYPE	SOURCE RANGE	DETECTOR TYPE	DETECTOR RANGE	ANGLE
$ G,P	ASM	80-600	D	600-999	MAG-D		DST

$ G,999=1.6 GEV

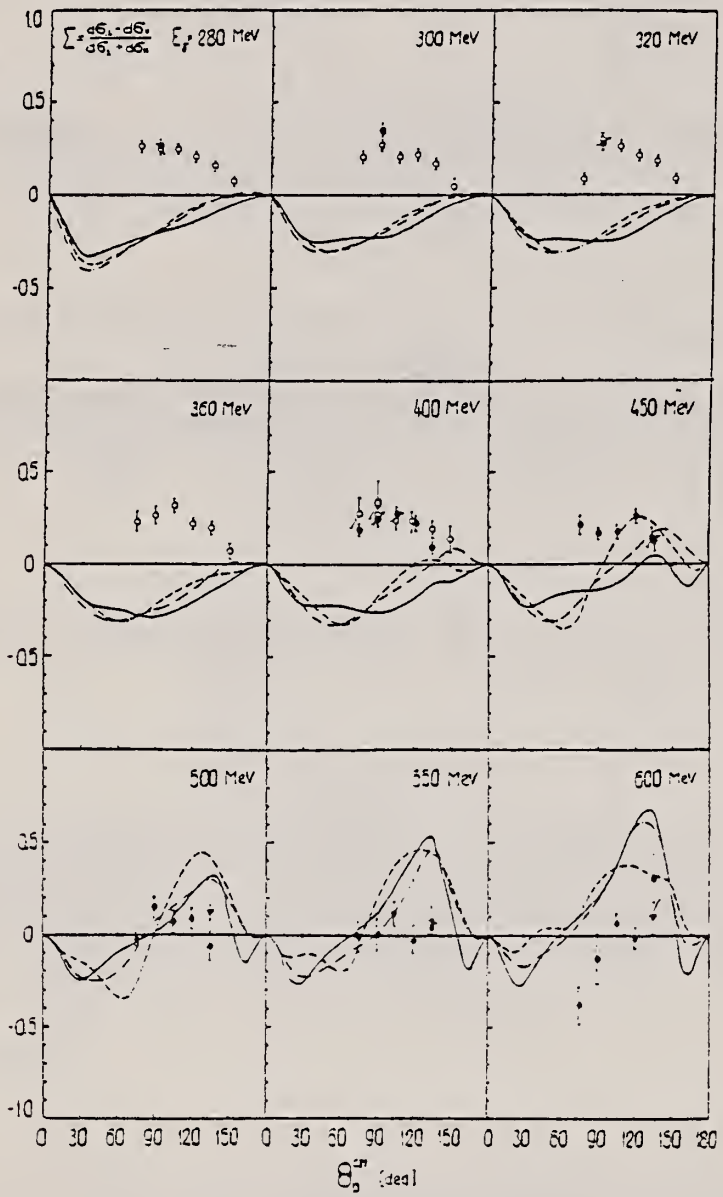

Fig. 5. Same as in Fig. 4 for E_γ = 280–600 MeV.

(continued)

TABLE 2

Cross-section asymmetry values in the $\gamma d \rightarrow np$ reaction

E_γ (MeV)	$\vartheta_p^* = 75°$	90°	105°	120°	135°	150°
80	−0.260 ± 0.016	−0.280 ± 0.026	−0.345 ± 0.025	−0.328 ± 0.025	−0.169 ± 0.045	
100	−0.165 ± 0.028	−0.105 ± 0.015	−0.091 ± 0.034	−0.074 ± 0.026	0.043 ± 0.042	
120	−0.120 ± 0.040	−0.043 ± 0.035	0.019 ± 0.044	0.078 ± 0.057	−0.029 ± 0.029	
140	−0.020 ± 0.040	0.159 ± 0.031	0.237 ± 0.030		0.147 ± 0.035	
160	0.042 ± 0.037	0.076 ± 0.026	0.144 ± 0.032	0.104 ± 0.029	0.119 ± 0.044	0.050 ± 0.033
180	0.213 ± 0.030	0.159 ± 0.044	0.252 ± 0.036	0.147 ± 0.043	0.160 ± 0.040	
200	0.145 ± 0.041	0.258 ± 0.035	0.261 ± 0.031	0.231 ± 0.045	0.171 ± 0.052	
220	0.187 ± 0.042	0.277 ± 0.037	0.390 ± 0.038	0.361 ± 0.034	0.217 ± 0.024	
240	0.185 ± 0.043	0.233 ± 0.044	0.188 ± 0.030	0.229 ± 0.032	0.170 ± 0.024	0.100 ± 0.032
260	0.216 ± 0.047	0.280 ± 0.045	0.314 ± 0.039	0.237 ± 0.030	0.256 ± 0.038	0.098 ± 0.044
280	0.265 ± 0.036	0.248 ± 0.029	0.248 ± 0.025	0.210 ± 0.024	0.160 ± 0.022	0.073 ± 0.024
300	0.203 ± 0.034	0.267 ± 0.032	0.204 ± 0.036	0.217 ± 0.029	0.171 ± 0.027	0.046 ± 0.050
320	0.088 ± 0.032	0.292 ± 0.040	0.263 ± 0.033	0.212 ± 0.033	0.187 ± 0.029	0.088 ± 0.027
360	0.228 ± 0.058	0.267 ± 0.043	0.319 ± 0.039	0.220 ± 0.030	0.195 ± 0.038	0.074 ± 0.042
400	0.277 ± 0.086	0.267 ± 0.061	0.237 ± 0.061	0.235 ± 0.058	0.191 ± 0.049	0.140 ± 0.073
400*	0.184 ± 0.043	0.257 ± 0.033	0.274 ± 0.040	0.225 ± 0.050	0.191 ± 0.037	
450*	0.209 ± 0.053	0.164 ± 0.028	0.171 ± 0.042	0.258 ± 0.039	0.147 ± 0.057	
500*	−0.017 ± 0.042	0.150 ± 0.057	0.070 ± 0.067	0.092 ± 0.047	−0.060 ± 0.072	
550*	−0.006 ± 0.081	0.000 ± 0.094	0.116 ± 0.066	−0.026 ± 0.083	0.039 ± 0.015	
600*	−0.380 ± 0.107	−0.126 ± 0.142	0.068 ± 0.053	−0.017 ± 0.013	0.304 ± 0.128	

* Results published earlier in ref. [12]).

REF. T. Ishii, S. Kato, H. Okuno, K. Ukai, Y. Ohashi, N. Awaji, H. Hayashii, N. Horikawa, K. Kimura, A. Miyamoto, T. Nakanishi, S. Okumi, H. Ozaki, A. Sugiyama, R. Suzaki, T. Tauchi, K. Mori, Y. Takeuchi
Phys. Lett. 110B, 441 (1982)

ELEM. SYM.	A	Z
H	2	1

METHOD

REF. NO. 82 Is 1 egf

REACTION	RESULT	EXCITATION ENERGY	SOURCE TYPE	SOURCE RANGE	DETECTOR TYPE	DETECTOR RANGE	ANGLE
$ G,P	ASM	300-700	C	1*	MAG-D		DST

$D 1*=1.3GEV, P-N COIN

The target asymmetry in $\gamma d \to pn$ has been measured at proton c.m. angles of 70°, 100° and 130° in the photon energies between 0.3 and 0.7 GeV. Results show relatively small asymmetry values in contrast to large proton polarizations. A phenomenological analysis by Ikeda et al. does not reproduce the present data, especially in the lower energy region.

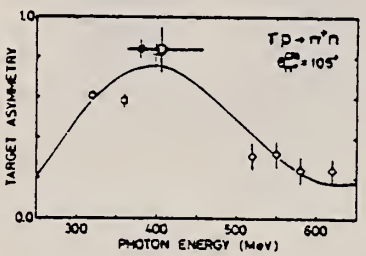

Fig. 3. The polarized target asymmetry in $\gamma d \to \pi^+ n(n)$ at a π^+ c.m. angle of 105°. Data points are from ref. [5] (squares), ref. [6] (rhomboids) and the present experiment (circle), and the curve is from ref. [9].

Table 1
Results of the polarized target asymmetry in $\gamma d \to pn$. The errors are statistical.

Photon energy E_γ (GeV)	Proton c.m. angle 70°	100°	130°
0.30–0.35	−0.08 ± 0.12	−0.02 ± 0.10	0.02 ± 0.23
0.35–0.40	−0.14 ± 0.11	−0.05 ± 0.14	0.34 ± 0.14
0.40–0.45	−0.19 ± 0.11	−0.04 ± 0.26	0.14 ± 0.16
0.45–0.50	0.18 ± 0.14	−0.04 ± 0.18	0.36 ± 0.09
0.50–0.55	0.15 ± 0.10	−0.02 ± 0.16	0.21 ± 0.11
0.55–0.60	−0.14 ± 0.12	0.11 ± 0.18	−0.12 ± 0.13
0.60–0.65	−0.12 ± 0.14	−0.04 ± 0.22	0.12 ± 0.17
0.65–0.70	0.43 ± 0.22	−0.16 ± 0.53	−0.18 ± 0.30

The polarized target asymmetry $T(\theta)$ in $\gamma d \to pn$ is obtained by

$$T(\theta) = \{(D_+ - D_-)/[P_-(D_+ - N) + P_+(D_- - N)]\},$$

where $P_\pm$ represents the vector polarization of deuterons. $D_\pm$ and N represent the normalized yields from the polarized deuterated butanol target and dummy target, respectively. The subscript '+' denotes the direction of $k \times p$, where k is the incident photon momentum and p is the proton momentum.

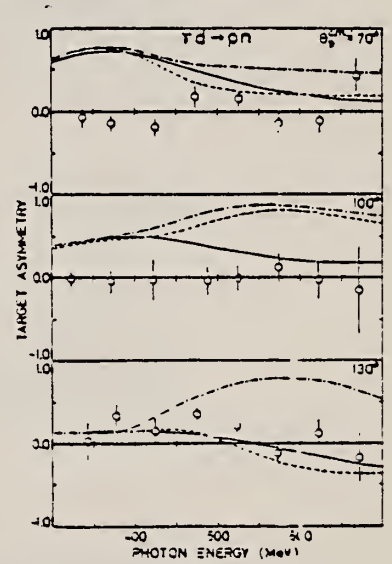

Fig. 4. Energy dependences of the polarized target asymmetry $T(\theta)$ for $\gamma d \to pn$ at θ_p(c.m.) = 70°, 100° and 130°. Curves are the predictions by Ikeda et al. [2]; solid curves: without dibaryon resonances, dashed–dotted curves: solution A (with $I = 1, J^P = 3^-$ and $I = 0, J^P = 1^-$), dashed curves: solution B (with $I = 1, J^P = 3^-$ and $I = 0, J^P = 3^-$).

H
A=3

H
A=3

H
A=3

REF.

M. Cerineo, K. Ilakovac, I. Slaus, and P. Tomaš
Phys. Rev. 124, 1947 (1961)

ELEM. SYM.	A	Z
H	3	1

METHOD

$D(n,H^3)\gamma$

REF. NO.: 61 Ce 2 JOC

REACTION	RESULT	EXCITATION ENERGY	SOURCE		DETECTOR		ANGLE
			TYPE	RANGE	TYPE	RANGE	
N,G	ABX	16	D	14	TEL-D		4PI

$\sigma_{capture}$(14.4 MeV neutrons on deuterium) = 29.4 ± 5.8 μb

by DT balance $\sigma_{dis}(E_\gamma$ = 15.9 MeV) = 2.1 ± .4 μb

Ref. H.Collard, R.Hofstadter, A.Johansson, R.Parks, M.Ryneveld, A.Walker, M.R.Yearian, R.B.Day, R.T.Wagner

Phys.Rev.Letters 11, 132 (1963)

Elem. Sym.	A	Z
H	3	1

Method

Ref. No.	
63Co2	BG

Reaction	E or ΔE	E_0	Γ	$\int \sigma dE$	Jπ	Notes
(e,e)	up to 661					Study of mirror nuclei H^3 and He^3. rms charge radius = 1.68×10^{-13} cm. rms magnetic moment radius equals 1.63×10^{-13} cm. Electromagnetic size of H^3 is smaller than that of He^3. The three form factors $F_{charge}(H^3)$, $F_{mag}(H^3)$, and $F_{mag}(He^3)$ are similar but not exactly equal. $F_{charge}(He^3)$ is different from others. Indicates charge structure in He^3 larger in size than the other three density distributions. H^3 cross section falls off less rapidly with q^2(mom.transfer) than the He^3 cross section.

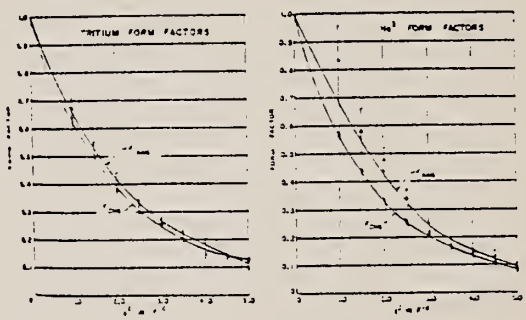

FIG. 2. The four form-factor determinations made in this experiment. On the left are shown F_{ch} and F_{mag} for H^3 and on the right the similar quantities for He^3 are shown. F_{ch} and F_{mag} are defined as in Eqs. (5) and (6) of reference 1. In a subsequent account of this work, graphs of the corresponding Dirac and Pauli form factors will be given.

Ref. L.I. Schiff, H. Collard, R. Hofstadter, A. Johansson, M.R. Yearian
Phys. Rev. Letters 11, 387 (1963)

Elem. Sym.	A	Z
H	3	1

Method: (Linac); more detailed analysis of earlier experimental data*

Ref. No.: 63 Sc 2 JHH

Reaction	E or ΔE	E_o	Γ	$\int \sigma dE$	Jπ	Notes
$H^3(e,e)$						*Refer to "63 Co 2" and "63 Co 4"

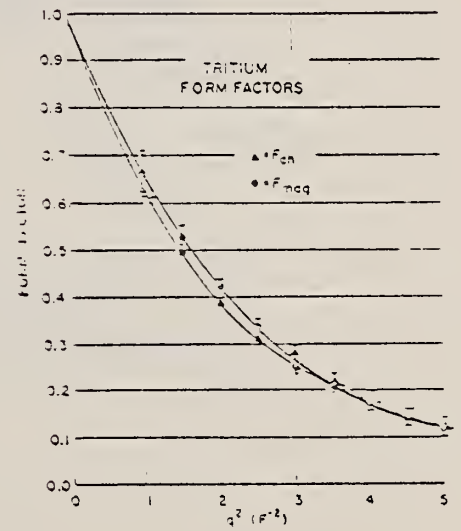

FIG. 1. New values of H^3 form factors

REF.

R. Bösch, J. Lang, R. Müller and W. Wölfli
Phys. Letters 8, 120 (1964)

ELEM. SYM.	A	Z
H	3	1

METHOD

(n,γ) Monoenergetic source
$H^2(\gamma,n)$ comparison

REF. NO.: 64 Bo 2 | JOC

REACTION	RESULT	EXCITATION ENERGY	SOURCE		DETECTOR		ANGLE
			TYPE	RANGE	TYPE	RANGE	
G,N	ABX	7 - 9	D	7 - 9	BF3-I		4 PI
		(6.7 - 9.)					

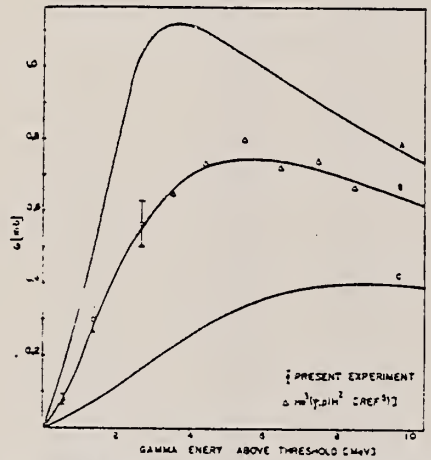

Fig. 1. The total cross section for the $H^3(\gamma,n)H^2$ photodisintegration. The curves have been taken from ref. 9).
Curve A: μ^{-1} = 3.0 fm. Curve B: μ^{-1} = 2.6 fm.
Curve C: μ^{-1} = 2.0 fm.

REF.

A. Johansson
Phys. Rev. 136, B1030 (1964)

ELEM. SYM.	A	Z
H	3	1

METHOD

REF. NO.	
64 Jo 1	JOC

REACTION	RESULT	EXCITATION ENERGY	SOURCE		DETECTOR		ANGLE
			TYPE	RANGE	TYPE	RANGE	
E,E/P	ABX	0-16	D	550	MAG-D		DST

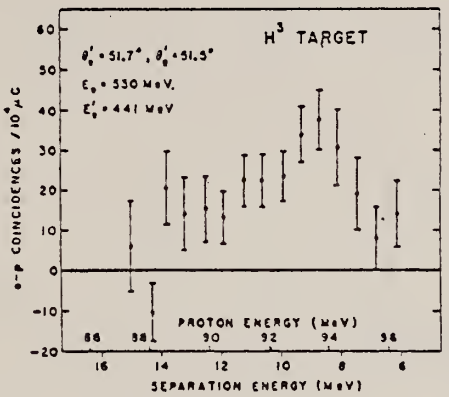

FIG. 2. The energy spectrum of protons at 51.5° in coincidence with 441-MeV electrons at 51.7° from H^3 $(e,e'p)$.

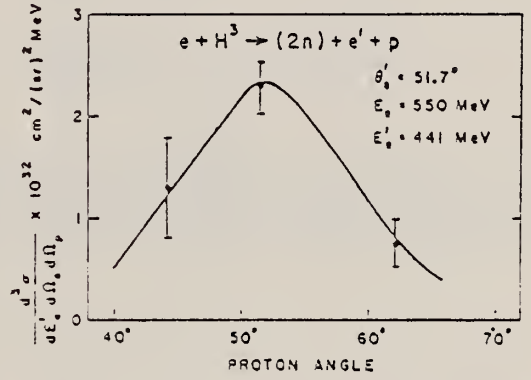

FIG. 4. The coincidence cross section of reaction (C) as a function of proton angle. The curve is explained in Sec. VI of the text.

REF.

R. Bösch, J. Lang, R. Müller and W. Wölfli
Helv. Phys. Acta 38, 753 (1965)

ELEM. SYM.	A	Z
H	3	1

METHOD

(n,γ) sources

REF. NO. 65 Bo 2 JDM

REACTION	RESULT	EXCITATION ENERGY	SOURCE TYPE	SOURCE RANGE	DETECTOR TYPE	DETECTOR RANGE	ANGLE

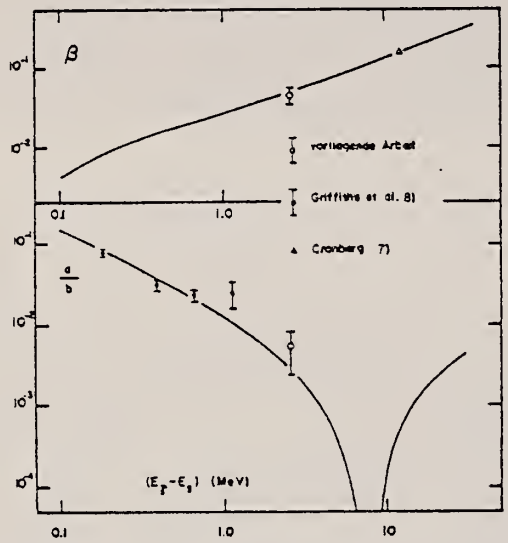

Figur 7

Vergleich der experimentellen und theoretischen Werte von a/b und β. Die durchgezogene Kurve wurde auf Grund der Gunn-Irvingschen Wellenfunktion ($\mu^{-1} = 2{,}5\ F$, $\delta = 0{,}07$) berechnet (vergleiche 3.3.1).

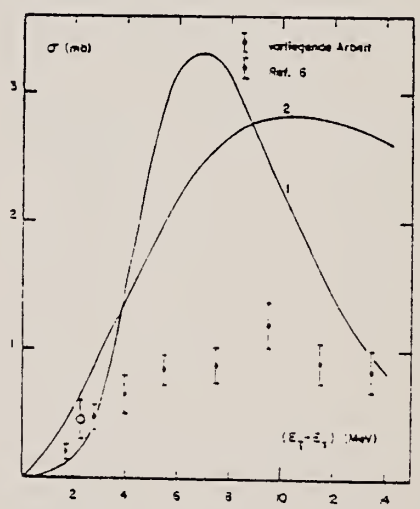

Figur 8

Experimentelle und theoretische Werte für den totalen Wirkungsquerschnitt des 3-Körperzerfalles.
Kurve 1: Theoretische Werte (durch einen Faktor + dividiert) von DELVES[5]) unter Berücksichtigung einer Wechselwirkung der auslaufenden Teilchen.
Kurve 2: Theoretische Werte von GUNN und IRVING[6]) für eine Wellenfunktion der Form (1.2) mit $\mu^{-1} = 2{,}5\ F$. Beschreibung des Endzustandes durch 3 ebene Wellen.

(continued)

REF.

R. Bösch, J. Lang, R. Müller and W. Wölfli
Helv. Phys. Acta 38, 753 (1965)

ELEM. SYM.	A	Z
H	3	1

METHOD

(n,γ) sources

REF. NO. 65 Bo 2 JDM

REACTION	RESULT	EXCITATION ENERGY	SOURCE TYPE	SOURCE RANGE	DETECTOR TYPE	DETECTOR RANGE	ANGLE
G,N	ABX	6 - 11	D	6 - 11	BF3		DST

$f(\theta) = a + b \sin^2\theta\,(1 - \beta\cos\theta)$

$\sigma_3(E^* = 2.3\ \text{MeV}) = .45\ I.15\ \text{mb}$

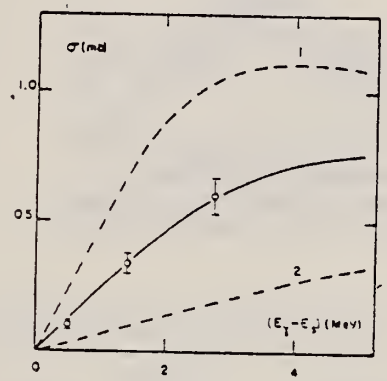

Figur 5

Experimentelle Werte des totalen Wirkungsquerschnittes der Reaktion $H^3(\gamma, n)H^2$. Die ausgezogene Kurve wurde auf Grund der Gunn-Irvingschen Wellenfunktion ($\mu^{-1} = 2.5\ F$, $\delta = 0.07$) berechnet (vgl. 3.3.1). Die übrigen Kurven entsprechen demselben Ansatz für die Wellenfunktion, mit $\mu^{-1} = 3.0\ F$, $\delta = 0$ (Kurve 1) und $\mu^{-1} = 2.0\ F$, $\delta = 0$ (Kurve 2).

REF.

E. B. Hughes, M. R. Yearian, and R. Hofstadter
Phys. Rev. 151, 841 (1966)

ELEM. SYM.	A	Z
H	3	1

METHOD
Linac

REF. NO.
66 Hu 2

JDM

REACTION	RESULT	EXCITATION ENERGY	SOURCE		DETECTOR		ANGLE
			TYPE	RANGE	TYPE	RANGE	
E,E/	FMF	0-160	D	250-370	MAG-D	130-360	DST

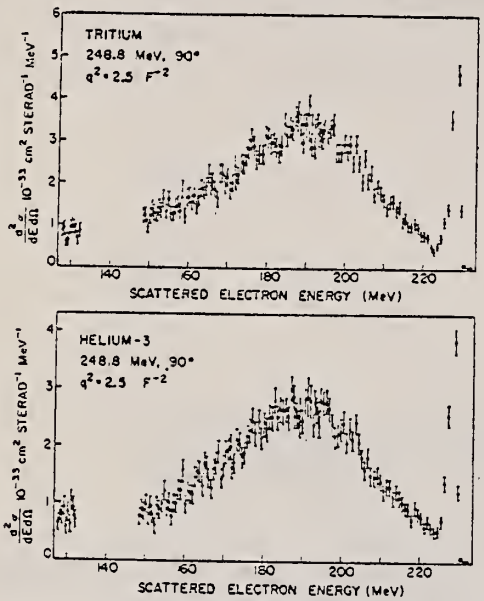

FIG. 3. The absolute inelastic electron-tritium and electron-helium-3 cross sections as a function of scattered electron momentum for $q^2=2.5$ F^{-1}.

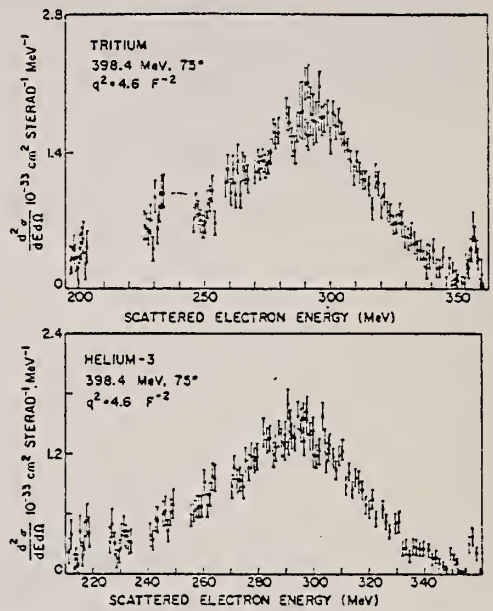

FIG. 4. The absolute inelastic electron-tritium and electron-helium-3 cross sections as a function of scattered electron momentum for $q^2=4.6$ F^{-1}.

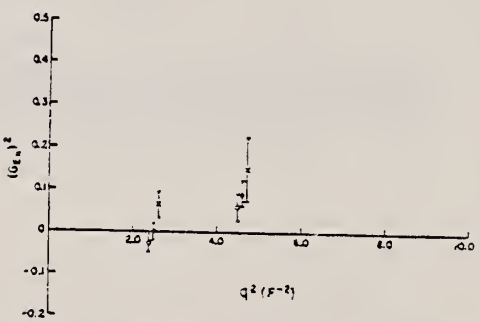

FIG. 5. The values of the square of the neutron electric form factor $(G_{En})^2$ as a function of q^2. The full circle points were obtained using Eq. (7), the crosses using Eq. (8) and the open circles using Eq. (9). The crosses and open circles have been shifted slightly in the q^2 direction for purposes of clarity.

(continued)

REF.

E. B. Hughes, M. R. Yearian, and R. Hofstadter
Phys. Rev. 151, 841 (1966)

ELEM. SYM.	A	Z
H	3	1

METHOD

Linac

REF. NO.	
66 Hu 2	JDM

REACTION	RESULT	EXCITATION ENERGY	SOURCE		DETECTOR		ANGLE
			TYPE	RANGE	TYPE	RANGE	

TABLE I. The experimental ratios of the electron-tritium and electron–helium-3 quasi-elastic cross sections as a function of q^2 and scattering angle. Also shown are the ratios of the elastic electron-neutron and electron-proton cross sections which follow from the experimental ratios by means of Eq. (3). The errors attached are purely statistical.

q^2 (F^{-2})	E (MeV)	Angle (degrees)	$\frac{(d^2\sigma/dEd\Omega)_{H^3}}{(d^2\sigma/dEd\Omega)_{He^3}}$	$\frac{(d\sigma/d\Omega)_n}{(d\sigma/d\Omega)_p}$
2.5	248.8	90	0.619±0.018	0.173±0.028
4.6	667.5	40	0.579±0.017	0.111±0.025
			0.581±0.017	0.114±0.025
			0.582±0.017	0.116±0.025
4.6	398.4	75	0.655±0.019	0.230±0.032
			0.632±0.018	0.193±0.030
			0.604±0.017	0.150±0.027
4.6	296.4	120	0.675±0.020	0.264±0.035
			0.666±0.017	0.249±0.030

TABLE II. The neutron form factors as a function of q^2. The expected form factors are taken from Eq. (14) of Ref. 5.

q^2 (F^{-2})	Measured values		Expected values	
	$(G_{En})^2$	$-G_{Mn}/\mu_n$	$(G_{En})^2$	$-G_{Mn}/\mu_n$
2.5	0.006±0.038		0.0	0.71
4.6	0.003±0.007	0.537±0.028	0.0	0.59

TABLE III. The total inelastic cross sections for tritium and helium-3 as a function of q^2 and scattering angle. Column 6 shows the correction factors applied to the measured cross sections, due to the experimental low-momentum cutoff.

q^2 (F^{-2})	Angle (degrees)	Target	$\sigma_{observed}$ (cm²/Sr)	% cutoff	Correction factor	$\sigma_{corrected}$ (cm²/Sr)
2.5	90	H^3	$(1.64\pm0.05)\times10^{-31}$	30.0	1.043	$(1.71\pm0.09)\times10^{-31}$
		He^3	$(2.68\pm0.08)\times10^{-31}$	30.0	1.043	$(2.79\pm0.15)\times10^{-31}$
4.6	75	H^3	$(1.32\pm0.04)\times10^{-31}$	30.0	1.032	$(1.36\pm0.06)\times10^{-31}$
		He^3	$(1.32\pm0.05)\times10^{-31}$	25.0	1.058	$(1.92\pm0.13)\times10^{-31}$

REF.

R. Kosiek, D. Muller and R. Pfeiffer and O. Merwitz
Phys. Letters 21, 199 (1966)

ELEM. SYM.	A	Z
H	3	1

METHOD

REF. NO.	
66 Ko 2	EGF

REACTION	RESULT	EXCITATION ENERGY	SOURCE		DETECTOR		ANGLE
			TYPE	RANGE	TYPE	RANGE	
G,P	SPC	THR - 33	C	33	TEL-D	4 - 14	90
G,D	ABX	THR - 33	C	33	TEL-D	4 - 9	90

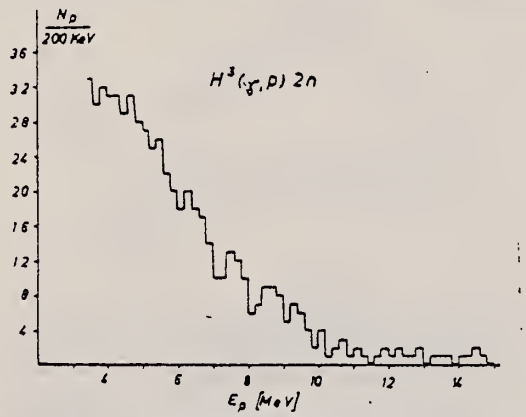

Fig. 1. Energiespektrum der Protonen aus der Reaktion $^3T(\gamma,p)2n$.

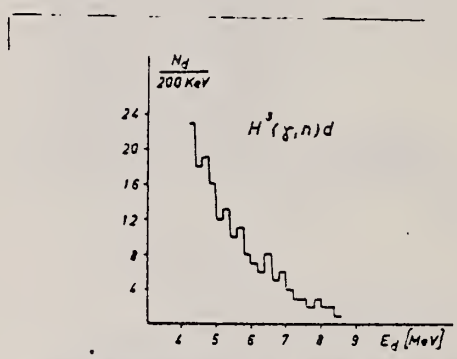

Fig. 2. Energiespektrum der Deuteronen aus der Reaktion $^3T(\gamma,n)d$.

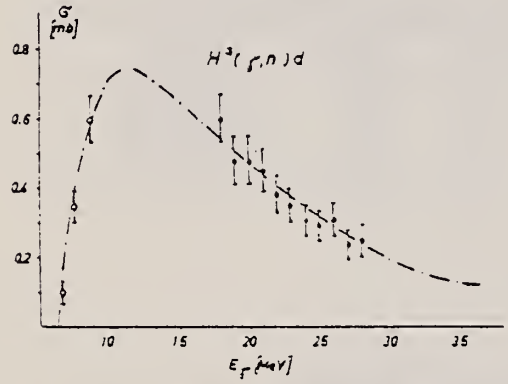

Fig. 3. Wirkungsquerschnitt für den Prozess $^3T(\gamma,n)d$; ● berechnet aus dem Spektrum der Fig. 2 unter der Annahme einer $\sin^2\vartheta$-Winkelverteilung; ○ Messpunkte nach Bösch et al. [16]; Kurve: Theorie nach Bösch et al. [5] mit $\mu^{-1} = 2.5$ fm und $\delta = 0.07$.

REF. R. Pfeiffer
Z. Physik 208, 129 (1968)

ELEM. SYM.	A	Z
H	3	1

METHOD

REF. NO. 68 Pf 1 EGF

REACTION	RESULT	EXCITATION ENERGY	SOURCE		DETECTOR		ANGLE
			TYPE	RANGE	TYPE	RANGE	
G,D	ABX	18-31	C	33	TEL-D	4-8	90
G,P	ABX	11-33	C	33	TEL-D	3-15	90
				(32.5)			

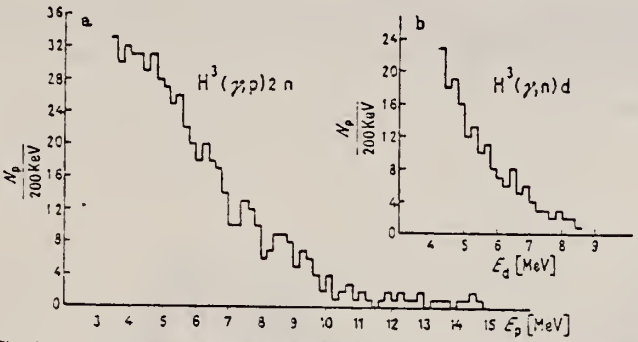

Fig. 6a u. b. Gemessene Energieverteilung; a der Protonen; b der Deuteronen

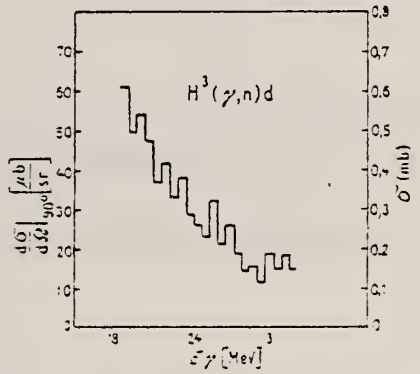

Fig. 7. Aus Fig. 6b bestimmter Wirkungsquerschnitt der Reaktion $^3H(\gamma,n)d$. *Linke Ordinate:* Differentieller Wirkungsquerschnitt $d^2\sigma/d\Omega\,dE_\gamma$. *Rechte Ordinate:* Über die Winkel integrierter Wirkungsquerschnitt

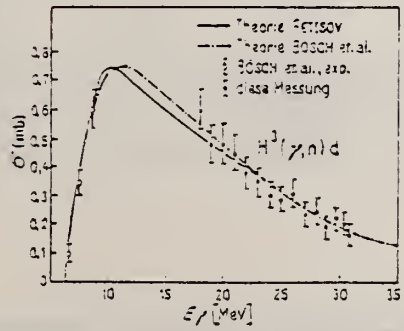

Fig. 8. Experimenteller bestimmter Wirkungsquerschnitt der Reaktion $^3H(\gamma,n)d$ im Vergleich zur Theorie

(continued)

REF.

R. Pfeiffer
Z. Physik 208, 129 (1968)

ELEM. SYM.	A	Z
H	3	1

METHOD

REF. NO. 68 Pf 1 EGF

REACTION	RESULT	EXCITATION ENERGY	SOURCE		DETECTOR		ANGLE
			TYPE	RANGE	TYPE	RANGE	

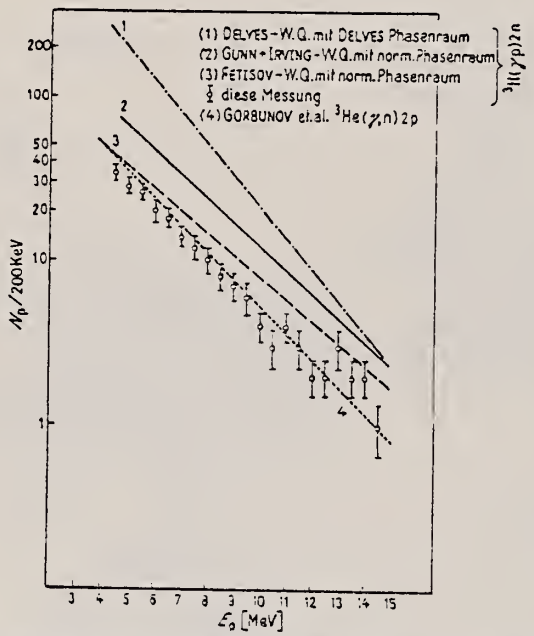

Fig. 10. Berechnete Protonenspektren der Dreikörperreaktion am ^{3}H (Kurve *1 – 3*). Experimentelles Protonenspektrum der Dreikörperreaktion am ^{3}He (4) und am ^{3}H (‡)

Tabelle. *Von der Schwelle bis 32,5 MeV integrierte Wirkungsquerschnitte der Zweikörperreaktion*

Autor	Target	σ_0 MeVmb	σ_{-1} mb
STEWART et al.[4]	^{3}He	11,6 ± 1,2	0,95 ± 0,10
GORBUNOV et al.[5]	^{3}He	17,3 ± 1,5	1,20 ± 0,10
BERMAN et al.[3]	^{3}He	12,0 ± 1,3	0,34 ± 0,08
SIEBERT et al.[7]	^{3}He	11,7 ± 2,0	0,31 ± 0,12
diese Arbeit	^{3}H	11,3 ± 1,4	0,78 ± 0,10

REF. D.D. Faul, B.L. Berman, P. Meyer, D.L. Olson
Phys. Rev. Lett. 44, 129 (1980)

ELEM. SYM.	A	Z
H	3	1

METHOD

REF. NO. 80 Fa 2 hg

REACTION	RESULT	EXCITATION ENERGY	SOURCE		DETECTOR		ANGLE
			TYPE	RANGE	TYPE	RANGE	
G,N	ABX	6-20	D	6-20	3F3-I		4PI
G,2N	ABX	8-26		8-26	BF3-I		4PI

Measurements of the two-body and three-body photodisintegration cross sections for tritium are reported. The measurements were done with monoenergetic photons, high-pressure gas samples, and neutron-multiplicity detection. Presently available theoretical calculations are not adequate to explain the results.

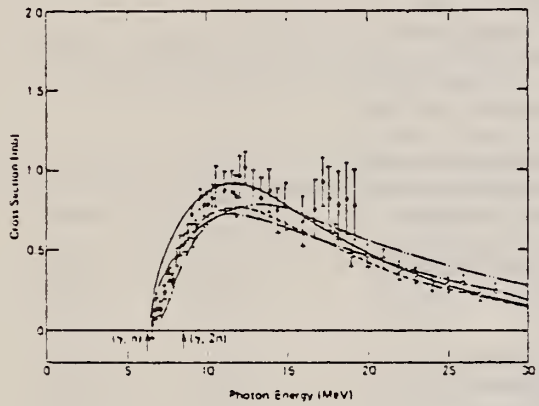

FIG. 1. Two-body photodisintegration cross section, for $^3H(\gamma,n)^2H$: filled circles, present data; triangles, data of Ref. 1; open circles, data of Ref. 2; solid curve and dashed curve, Ref. 4; dash-dot-dash curve, Ref. 1; dash-dot-dot-dash curve, Ref. 5. The error flags indicate statistical uncertainties only. The arrows indicate the reaction thresholds.

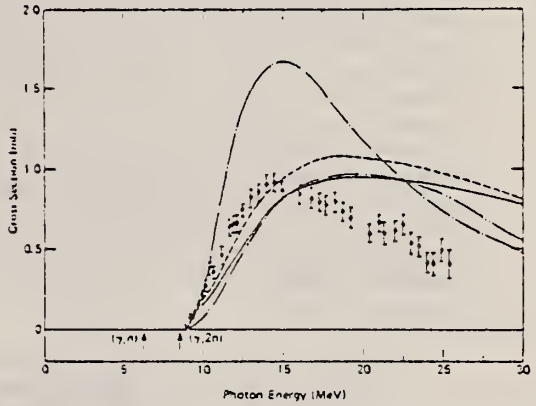

FIG. 2. Three-body photodisintegration cross section, for $^3H(\gamma,2n)^1H$: filled circles, present data; solid curve and dashed curve, Ref. 6; dash-dot-dash curve and dash-dot-dot-dash curve, Ref. 7.

TABLE I. Integrated cross sections and moments.

Nucleus, reaction	E_{max} [a] (MeV)	I_{int} (MeV mb)	σ_{-1} (mb)	I_{-2} (mb MeV^{-1})
$^3H(\gamma,n)$ [b]	19.2	9.2	0.73	0.062
$^3H(\gamma,2n)$ [c]	19.2	6.9	0.48	0.035
$^3H(\gamma,2n)$ [c]	25.4	10.4	0.64	0.042

[a] The energy up to which the integrations are carried out.
[b] The statistical uncertainties are less than 4%; systematic uncertainties might be as large as 15%.
[c] The statistical uncertainties are less than 2%; systematic uncertainties might be as large as 10%.

REF. D.D. Faul, B.L. Berman, P. Meyer, D.L. Olson
Phys. Rev. C24, 849 (1981)

ELEM. SYM.	A	Z
H	3	1

METHOD

REF. NO. 81 Fa 1 hg

REACTION	RESULT	EXCITATION ENERGY	SOURCE		DETECTOR		ANGLE
			TYPE	RANGE	TYPE	RANGE	
G,N	ABX	6-24	D	6-24	BF3-I		4PI
G,2N	ABX	8-28	D	8-28	BF3-I		4PI

The photoneutron cross sections for ^{3}H and ^{3}He have been measured from threshold to ~25 MeV with monoenergetic photons from the annihilation in flight of fast positrons. These reactions include the two-body breakup of ^{3}H and the three-body breakup of both ^{3}H and ^{3}He; these measurements for ^{3}H are the first to span the energy region across the peaks of the cross sections. An efficient BF_3-tube-and-paraffin neutron detector and high-pressure gaseous samples were employed in these measurements. The results, when compared with each other and with results for the two-body breakup cross section for ^{3}He from the literature, show that: (a) the two-body breakup cross sections for ^{3}H and ^{3}He have nearly the same shape, but the one for ^{3}He lies lower in magnitude; (b) the three-body breakup cross section for ^{3}He lies higher in magnitude, broader in the peak region, and also rises less sharply from threshold than that for ^{3}H; and (c) these differences between the cross sections for the breakup modes largely compensate in their sum, so that the total photon absorption cross sections for ^{3}H and ^{3}He are nearly the same in both size and shape at energies near and above their peaks. Theoretical results from the literature disagree with the experimental results to a certain extent over the entire photon-energy region for which the photoneutron cross sections were measured. Sum rule predictions also fail to reproduce the experimental results. These discrepancies constitute a challenge to the principle of charge symmetry of the nuclear force, but more complete theoretical calculations are needed to ascertain whether these discrepancies can be ascribed entirely to electromagnetic effects.

[NUCLEAR REACTIONS ^{3}H(γ,n), ^{3}H(γ,2n), ^{3}He(γ,n); measured $\sigma(E_\gamma)$, threshold to ~25 MeV; monoenergetic photons, high-pressure gas samples; two-body breakup, three-body breakup, charge asymmetry.]

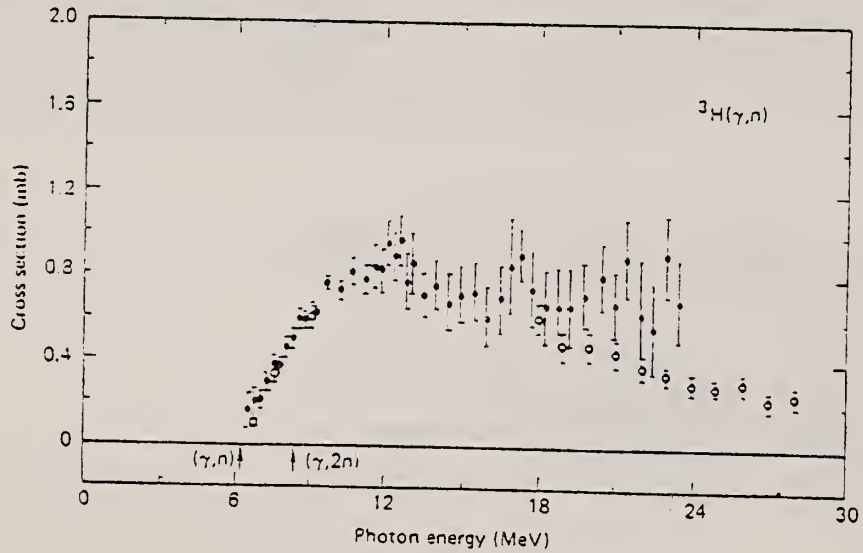

FIG. 10. Two-body photodisintegration cross section for ^{3}H: filled circles, present data; open squares, data of Ref. 33; open circles, Ref. 34. The error flags indicate statistical uncertainties only.

(continued)

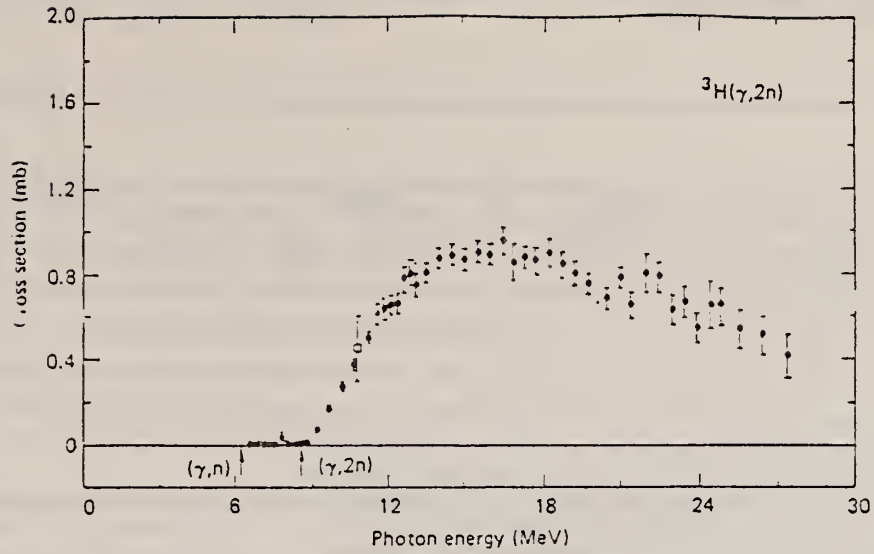

FIG. 11. Three-body photodisintegration cross section for ^{3}H: filled circles, present data; open square, datum of Ref. 33. The error flags indicate statistical uncertainties only.

TABLE III. Integrated cross sections and moments.

Reaction	$E_{\gamma_{max}}$ (MeV)	σ_{int} (MeV mb)[a]	σ_{-1} (mb)[b]	σ_{-2} (mb MeV^{-1})[c]
^{3}He(γ,n)	23.4	12.3 ± 1.2	0.760 ± 0.061	0.050 ± 0.004
^{3}H(γ,n)	23.4	11.7 ± 1.2	0.840 ± 0.067	0.067 ± 0.005
^{3}H(γ,2n)	23.4	10.2 ± 1.0	0.638 ± 0.051	0.042 ± 0.003
^{3}He(γ,n)	25.8	14.1 ± 1.4	0.833 ± 0.067	0.053 ± 0.004
^{3}H(γ,n)[d]	25.8	13.2 ± 1.3	0.896 ± 0.072	0.069 ± 0.006
^{3}H(γ,2n)	25.8	11.5 ± 1.2	0.691 ± 0.055	0.044 ± 0.003
^{3}He(γ,n)[d]	26.4	14.4 ± 1.4	0.850 ± 0.068	0.053 ± 0.004
^{3}H(γ,n)[d]	26.4	13.6 ± 1.3	0.900 ± 0.072	0.070 ± 0.006
^{3}H(γ,2n)	26.4	12.0 ± 1.2	0.709 ± 0.057	0.045 ± 0.004
^{3}He(γ,n)[d]	30.0	16.4 ± 2.0	0.917 ± 0.092	0.056 ± 0.004
^{3}H(γ,n)[d]	30.0	15.4 ± 1.8	0.986 ± 0.099	0.072 ± 0.006
^{3}H(γ,2n)[d]	30.0	13.6 ± 1.6	0.767 ± 0.077	0.047 ± 0.004

[a] $\sigma_{int} = \int_0^{E_{\gamma_{max}}} \sigma(E_\gamma) dE_\gamma$

[b] $\sigma_{-1} = \int_0^{E_{\gamma_{max}}} \sigma(E_\gamma) E_\gamma^{-1} dE_\gamma$

[c] $\sigma_{-2} = \int_0^{E_{\gamma_{max}}} \sigma(E_\gamma) E_\gamma^{-2} dE_\gamma$

[d] Extrapolated (from the present data only).

REF. D.M. Skopik, D.H. Beck, J. Asai, J.J. Murphy II
Phys. Rev. C24, 1791 (1981)

ELEM. SYM.	A	Z
H	3	1

METHOD

REF. NO. 81 Sk 4 hg

REACTION	RESULT	EXCITATION ENERGY	SOURCE		DETECTOR		ANGLE
			TYPE	RANGE	TYPE	RANGE	
G,D	ABX	15-36	C	100	MAG-D		DST

The angular asymmetry and the total cross section for the $^3H(\gamma,d)$ reaction have been measured. The total cross section measurement agrees with the most recent Faddeev-type calculation but the angular asymmetry departs from the prediction of a simple plane wave calculation that fits the $^3He(\gamma,d)$ data. In the absence of final state interactions the ^3He and ^3H asymmetries should be related by $-1/5$ (i.e., the isospin dependence). These data would appear to indicate that the $E2$ final state interaction in the $^3H(\gamma,d)$ reaction has to be carefully treated.

[NUCLEAR REACTIONS $^3H(\gamma,d)$, $E=15-36$ MeV. Measured $\sigma(\theta,E)$.]

[6] J. L. Matthews *et al.*, Nucl. Phys. A223, 221 (1974). 74 Mat 6
[11] D. M. Skopik *et al.*, Phys. Rev. C 11, 693 (1975). 75 Sk
[12] N. M. O'Fallon, L. J. Koester, Jr., and J. H. Smith, Phys. Rev. C 5, 1926 (1972). 72 OF 2
[13] A. van der Woude *et al.*, Phys. Rev. Lett. 26, 909 (1971). 71 Va 1
[14] B. D. Belt *et al.*, Phys. Rev. Lett. 24, 1120 (1970). 70 Bel 4
[15] W. Wolfli *et al.*, Helv. Phys. Acta 40, 946 (1967). 67 Wol

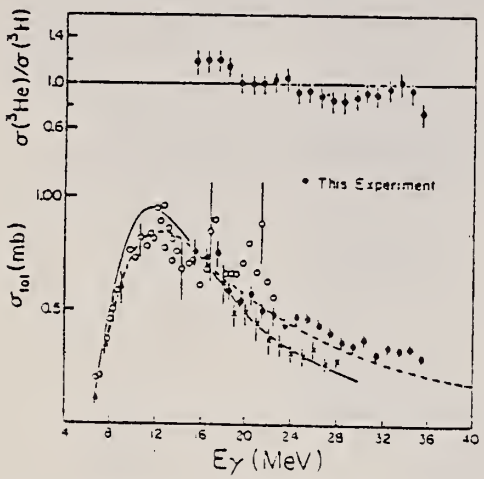

FIG. 2. Total cross sections for the two-body disintegration of ^3H. The data are Ref. 3 —○, Ref. 4 —▲, Ref 5 —×, and this work — ●. Only statistical errors are shown for the previous data. Using Eq. (2), the total cross section for our data is determined from the relation $\sigma=2\pi[\sigma(\theta_f)-\sigma(\theta_b)]$. We have folded into the data, in percent quadrature, the systematic error for our experiment. Thus our error bars represent the total uncertainty for our experiment. The statistical errors were typically 2%. The curves give the theory of Ref. 9 — solid line, and Ref. 10 —dashed line.

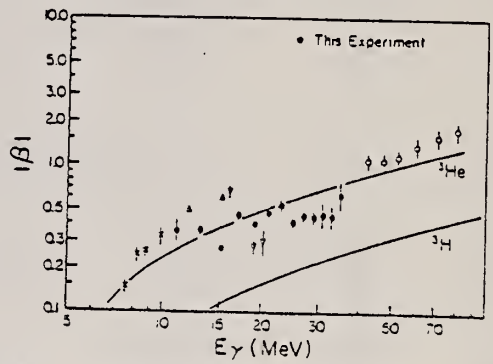

FIG. 3. Angular asymmetry data for ^3He and ^3H. The ^3He data are from Ref. 12 —○, Ref. 13 —▽, Ref. 6 —▼, Ref. 14 —△, and Ref. 15 —×. Shown are the plane wave asymmetry calculations for the $^3He(\gamma,d)$ and $^3H(\gamma,d)$ reactions. The ^3He data are fit reasonably well (perhaps surprisingly) up to 70 MeV by this model. The ^3H data are not well described by this model, which may indicate that the effects of final state interactions are markedly different for ^3H.

$$\beta=\frac{1}{P_1(\cos\theta_f)}\left[\frac{\sigma(\theta_f)-\sigma(\theta_b)}{\sigma(\theta_f)-\sigma(\theta_b)}\right], \qquad (1)$$

where

$$\sigma(\theta)=\sum_l A_l P_l(\cos\theta) \text{ and } A_4 << 1 . \qquad (2)$$

REF. E.T. Jurney, P.J. Bendt, J.C. Browne
Phys. Rev. C25, 2810 (1982)

ELEM. SYM.	A	Z
H	3	1

METHOD

REF. NO. 82 Ju 1 egf

REACTION	RESULT	EXCITATION ENERGY	SOURCE		DETECTOR		ANGLE
			TYPE	RANGE	TYPE	RANGE	
N,G	ABX	6	D	0	NAI-D		4PI

Capture cross section is 0.508±0.015 mb

THERMAL N CAPTURE

We have measured the thermal neutron capture cross section of deuterium by direct observation of the prompt gamma ray.

[NUCLEAR REACTIONS $^{2}H(n,\gamma)^{3}H$ and $^{12}C(n,\gamma)^{13}C$, E_n=th, measured $\sigma(n,\gamma)$.]

H
A=4

H
A=4

H
A=4

REF.
W. L. Imhof, F. J. Vaughn, L. F. Chase, Jr., H. A. Grench and M. Walt
Nucl. Phys. 59, 81-88 (1964)

ELEM. SYM.	A	Z
H	4	1

METHOD
$H^3(n,\gamma)H^4$; Van de Graaff, neutrons from $Li^7(p,n)Be^7$ reaction.

REF. NO. 64 Im 1 JOC

REACTION	RESULT	EXCITATION ENERGY	SOURCE TYPE	SOURCE RANGE	DETECTOR TYPE	DETECTOR RANGE	ANGLE
N,G	ABY		D	0-1	ACT-I		4 PI
				(0 - 1.2)			

NO H4 FOUND

TABLE I
Upper limits to the cross sections

Reaction	Bombarding energy (MeV)	Half-life interval (sec)	Upper limit to cross section (cm^2)
$H^3(n,\gamma)H^4$	thermal	3×10^{-3}–10^2	6×10^{-30}
$H^3(n,\gamma)H^4$	thermal	10^2 –10^3	1×10^{-30}
$H^3(n,\gamma)H^4$	0.030–1.2	3×10^{-3}–10^2	6×10^{-32}
$H^3(n,\gamma)H^4$	0.030–1.2	10^2 –10^3	1×10^{-32}
$H^3(d,p)H^4$	2.5	10^{-3}–10^2	3×10^{-32}
$He^3(p,\gamma)Li^4$	0.5	3×10^{-4}–4×10^{-3}	9×10^{-34}
$He^3(p,\gamma)Li^4$	1.3	3×10^{-3}–10^{-1}	2×10^{-34}
$He^3(p,\gamma)Li^4$	1.3	10^{-1}–10^2	6×10^{-34}
$He^3(p,\gamma)Li^4$	2.4	10^{-1}–10^2	8×10^{-34}
$He^3(p,\gamma)Li^4$	2.6	3×10^{-4}–10^{-1}	2×10^{-33}
$He^3(d,a)Li^4$	0.5	3×10^{-4}–4×10^{-3}	3×10^{-33}
$He^3(d,n)Li^4$	0.7	4×10^{-3}–10^3	4×10^{-33}
$He^3(d,n)Li^4$	2.3	10^{-4}–10^{-1}	4×10^{-33}
$He^3(d,n)Li^4$	2.3	10^{-1}–10^3	8×10^{-33}

REF. V. Ajdacic, M. Cerineo, B. Lalovic, G. Paic, I. Slaus, and P. Tomas
Phys. Rev. Letters 14, 444 (1965)

ELEM. SYM.	A	Z
H	4	1

METHOD
$H^3(n,H^4)\gamma$ E_n = 14.4 MeV, H^4 detected

REF. NO. 65 Aj 1 JOC

REACTION	RESULT	EXCITATION ENERGY	SOURCE		DETECTOR		ANGLE
			TYPE	RANGE	TYPE	RANGE	
N,G	ABX	11	D	14	SCD-D		0

UPPER LIMIT ON ABX

$\sigma_{n,\gamma} < 0.2$ μb/sr

See Errata PRL 14, 730 (1965)

HELIUM
Z=2

Helium, discovered in 1868, was first found in the gaseous atmosphere surrounding the sun. J. Norman Lockyer, a brilliant English astrophysicist, and P. Jansen, a prominent French astronomer, are credited with the discovery of the gaseous solar envelope (composed of the yet undiscovered helium). Lockyer's findings were reported to the Royal Society and Jansen's finding were reported to the French Academy of Sciences. Strangely enough, these independent announcements were reported on the same day only a few minutes apart. Thus a problem of proper apportionment of credit for the discovery of the gaseous nature of the prominences was presented. The coincidence of their separate investigations served to cement a close friendship between the two scientists however, and a medallion bearing the profiles and names of both Jansen and Lockyer was struck by the French Academy of Sciences. Further work by Lockyer showed this gaseous envelope was caused by a substance then unknown on earth. He called the substance helium, deriving the word from *helios*, the Greek name for the sun.

HE
A=3

HE
A=3

REF. G. M. Griffiths and J. B. Warren
Proc. Phys. Soc. A68, 781 (1955)

ELEM. SYM.	A	Z
He	3	2

METHOD
$D(p,\gamma)He^3$

REF. NO. 55 Gr 1 JOC

REACTION	RESULT	EXCITATION ENERGY	SOURCE		DETECTOR		ANGLE
			TYPE	RANGE	TYPE	RANGE	
P,G	ABX	5-8	D	0-2	NAI-D	4-8	DST

Measured Q = 5.50 ± .03 MeV

$\sigma(E_p = 1.0) = 4 \times 10^{-30} cm^2 \pm 50\%$

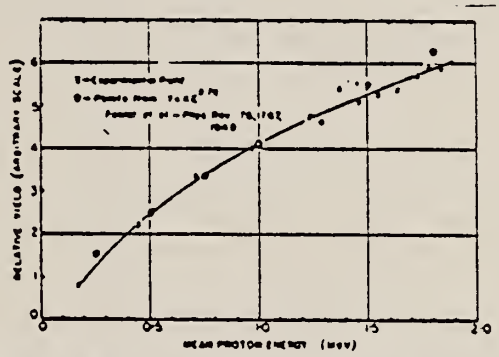

Figure 10. Relative yield of radiation from the reaction $D(p,\gamma)^3He$ for proton bombarding energies from 0·25 to 1·8 MeV.

Table 3. Angular Distributions of Gamma Rays from the Reaction $D(p,\gamma)^3He$ at Different Energies

E_p (MeV)	Distribution	% Isotropic Component in total yield
1·75	$\sin^2\theta$ · 0·025 ± 0·006	3·6 ± 0·8%
1·0	$\sin^2\theta$ · 0·046 ± 0·005	6·5 ± 0·7%
0·8	$\sin^2\theta$ · 0·04 ± 0·015	5·7 ± 2·0%
0·6	$\sin^2\theta$ · 0·026 ± 0·010	3·8 ± 1·5%

REF.

G.M. Griffiths, E.A. Larson and L.P. Robertson
Can. J. Phys. 40, 402 (1962)

EL EM. SYM.	A	Z
He	3	2

METHOD

$D(p,\gamma)He^3$

REF. NO.	
62 Gr 1	JOC

REACTION	RESULT	EXCITATION ENERGY	SOURCE		DETECTOR		ANGLE
			TYPE	RANGE	TYPE	RANGE	
P,G	ABX	5-7	D	0-2	NAI-D	2-7	DST

$Y(\theta) = A(b + \sin^2\theta)$

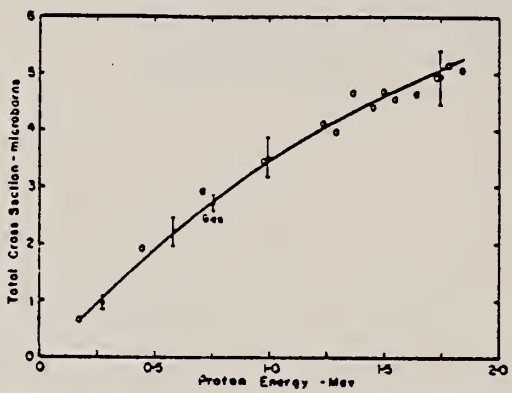

FIG. 6. The total cross section for the reaction $D(p,\gamma)He^3$. The experimental points with the errors shown by vertical bars are the results of the present measurements; the circles are the previous measurements of Griffiths and Warren (1955), normalized to the present results at 1.0 Mev.

TABLE I

$D(p,\gamma)He^3$ cross section and angular distributions

E_p (kev)	Target	σ_T (10^{-30} cm²)	b	σ_γ (10^{-30} cm²)	σ_1 (10^{-30} cm²)
275	ice	0.97±0.11	0.08±0.01	0.87	0.10
580	ice	(2.20±0.25)	0.032±0.005	(2.1)	(0.10)
735	gas	2.71±0.13	—	—	—
985	ice	3.50±0.38	0.024±0.003	3.38	0.12
1750	ice	(4.92±0.50)	0.025±0.010	(4.74)	(0.18)

Ref.	Elem. Sym.	A	Z
B.L.Berman, L.J.Koester, Jr., J.H.Smith Phys.Rev.Letters 10, 527 (1963)	He	3	2

Method	Ref. No.	
Betatron - CsI	63Be1	B G

Reaction	E or ΔE	E_o	Γ	$\int \sigma dE$	Jπ	Notes
(γ,d)	8.5-22					Concludes that the photodisintegration cross section is very sensitive to nuclear size.

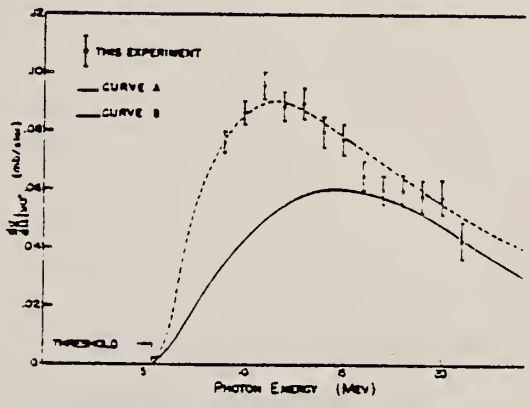

FIG. 3. The 90° differential cross sections for the $He^3(\gamma,p)d$ photodisintegration. Curve *A* is taken from reference 6. Curve *B* is computed from reference 7. No normalization has been performed.

Ref. E. Finckh, R. Kosiek, K.H. Lindenberger, U. Meyer-Berkhout, N. Nücker, K. Schlüpmann
Phys. Letters 7, 271 (1963)

Elem. Sym.	A	Z
He	3	2

Method Betatron; CsI

Ref. No. 63 Fi 2 JHH

Reaction	E or ΔE	E_0	Γ	$\int \sigma dE$	Jπ	Notes
$He^3(\gamma, d)$	Bremss. 31					Histogram in Figure 1 calculated from measured proton energy distribution.

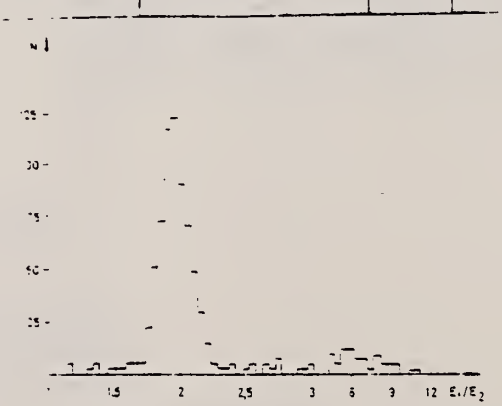

Fig. 1. Distribution of the energy ratio from coincident particles in the interval [illegible] MeV.

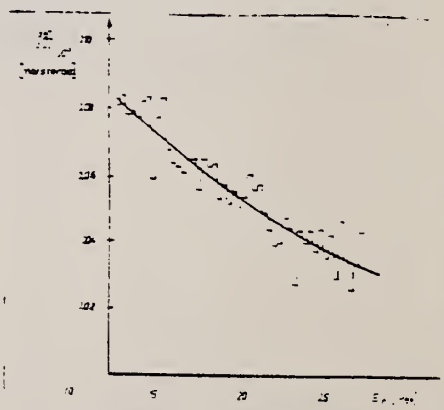

Fig. 2. Differential cross section for the reaction [illegible]. Estimated uncertainty in absolute [illegible].

Ref. A.N. Gorbunov, A.T. Varfolomeev
Phys. Letters 5, 149 (1963)

Elem. Sym.	A	Z
He	3	2

Method
170 MeV Synchrotron - cloud chamber

Ref. No. 63Go2

BG

Reaction	E or ΔE	E_o	Γ	$\int \sigma dE$	Jπ	Notes
$He^3(\gamma,p)He^2$	0-170	18		30 ± 3 $)_0^{170}$		Yields of (γ,p) and (γ,n) same within statistical error. $Y_i = \int_0^{170} \sigma_i(w)\,\eta(w)dw = 1.6\pm0.08$mb. $\eta(w)$ = Bethe-Heitler spectrum of bremsstrahlung corrected for the absorption in target. σ_i is cross section for ith reaction. $(\sigma_{-1})_{\gamma p} = \int_0^{170} \sigma_{\gamma p}(w)\frac{dw}{w}$ $= 1.5\pm0.15$ mb. Thus $\sigma_{-1} = 3\pm0.3$ mb. R_c = r.m.s. radius of charge distribution $= 1.93\pm0.11\times10^{-13}$cm.

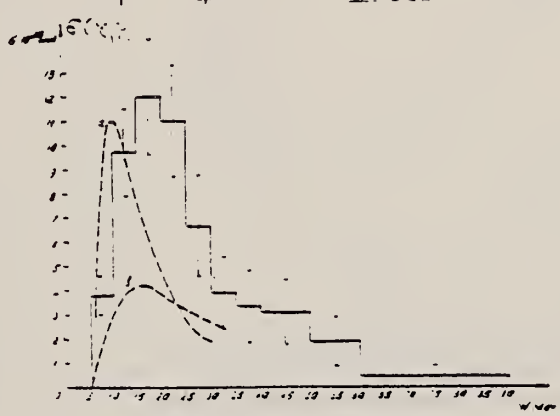

Fig. 1. The dotted lines are the theoretical curves [1].
a. $1/a = 3.0 \times 10^{-13}$ cm.
b. $1/a = 2.0 \times 10^{-13}$ cm.

REF.

G.M. Griffiths, M. Lal, C.D. Scarfe
Can. J. Phys. 41, 724 (1963)

EL EM. SYM.	A	Z
He	3	2

METHOD: Cockcroft-Walton; inverse; NaI spectrometer

REF. NO.: 63 Gr 1 NVB

REACTION	RESULT	EXCITATION ENERGY	SOURCE TYPE	SOURCE RANGE	DETECTOR TYPE	DETECTOR RANGE	ANGLE
P,G	ABX	5	D	0-1	NAI-D		DST
		5	(24-48 keV)				

Most measurements at 0° and 90°, some at 45° to improve $(\sin^2\theta + b)$ relation. Breaks σ up into s and p wave components.

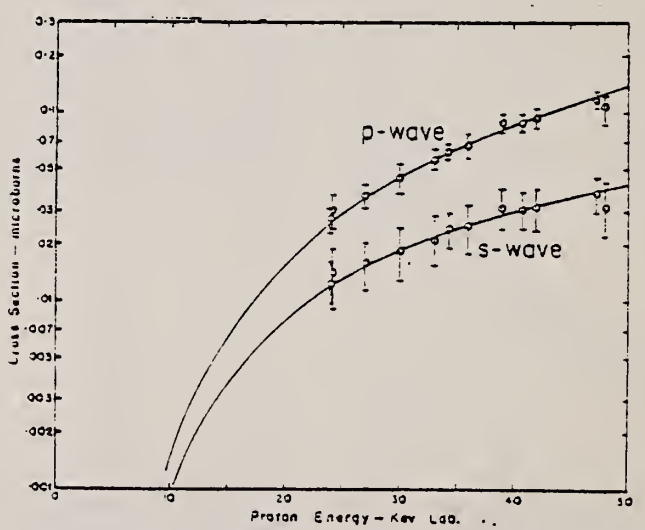

FIG. 5. The total cross sections for p-wave and s-wave capture obtained from unfolding the thick target yield curve. The solid lines show the energy dependence assumed in the analysis normalized to the experimental data.

Ref. J.B. Warren, K.L. Erdman, L.P. Robertson, D.A. Axen, J.R. MacDonald
Phys. Rev. 132, 1691 (1963)

Elem. Sym.	A	Z
He	3	2

Method $F^{19}(p,\alpha\gamma)O^{16}$; proton yield; ionization chamber

Ref. No. 63 Wa 1 JHH

Reaction	E or ΔE	E_o	Γ	$\int \sigma dE$	Jπ	Notes
(γ,p)	6.14					σ = 0.109 mb (873 kev res., E_p) = 0.102 mb (935 kev res., E_p)
	6.97					σ = 0.298 mb (E_γ weighted average of 6.92 and 7.12 MeV)
	7.08					σ = 0.307 mb
						Comparison of these data with G.M. Griffiths detailed balance analysis of $H^2(p,\gamma)He^3$ data in Figure 2.

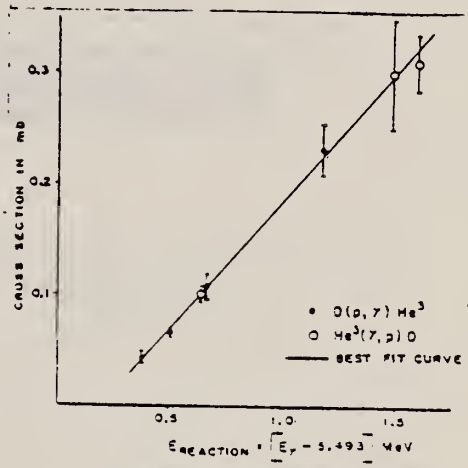

FIG. 2. Comparison of cross sections for the inverse reactions $He^3(\gamma,p)D$ and $D(p,\gamma)He^3$.

TABLE II. Cross section for the reaction $He^3(\gamma,p)D$.

E_γ (MeV)	σ (mb)	Experimental error	Total probable error including uncertainties in relative gamma-ray yields
6.14 (873-keV resonance)	0.109	9%	14%
(935-keV resonance)	0.102	6%	7%
6.97	0.298	5%	16%
7.08	0.307	5%	8%

REF.

C. Becchi, G.E. Manuzio, L. Meneghetti and S. Vitale
Phys. Letters 8, 322 (1964)

ELEM. SYM.	A	Z
He	3	2

METHOD

Betatron

REF. NO. 64 Be 2 JOC

REACTION	RESULT	EXCITATION ENERGY	SOURCE		DETECTOR		ANGLE
			TYPE	RANGE	TYPE	RANGE	
G, D	ABX	THR - 30	C	34	SCD - D	3-10	90

SPECTRUM

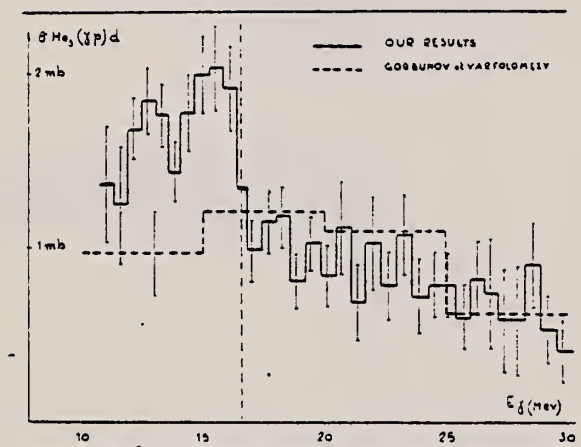

Fig. 2. He^3(γ,p)d cross section. The dashed vertical line indicates the energy at which the results obtained with the coincidence p-d method are adjusted to those obtained with the telescope.

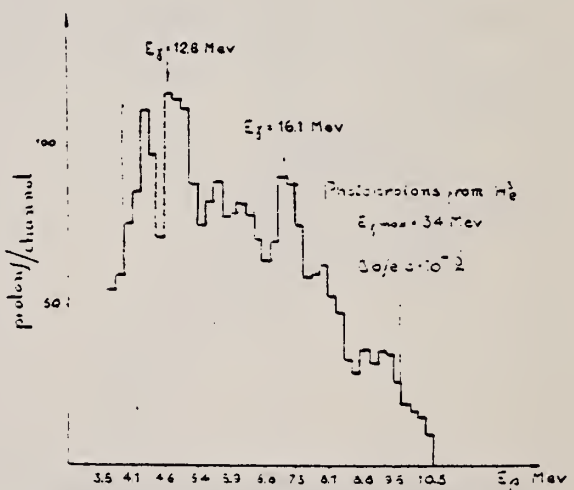

Fig. 3. Photoproton spectrum obtained with the telescope. The result at 4.6 MeV channel is not reported as it was affected by an instrumental failure.

REF.	EL EM. SYM.	A	Z
B.L. Berman, L J. Koester, Jr., and J. H. Smith Phys. Rev. 133, B117-129 (1964	He	3	2

METHOD	REF. NO.	
Betatron; CsI(T1) detectors; NBS chamber	64 Be 5	NVB

REACTION	RESULT	EXCITATION ENERGY	SOURCE		DETECTOR		ANGLE
			TYPE	RANGE	TYPE	RANGE	
G,P	ABX	8-22	C	8-22	SCI-D		90
G,2P	ABX	8-22	C	8-22	SCI-D		90

RMS radius = 1.94 f FØRM FACTØR
Charge radius = 2.1 f - using modified exponential wave function of Gunn and Irving.

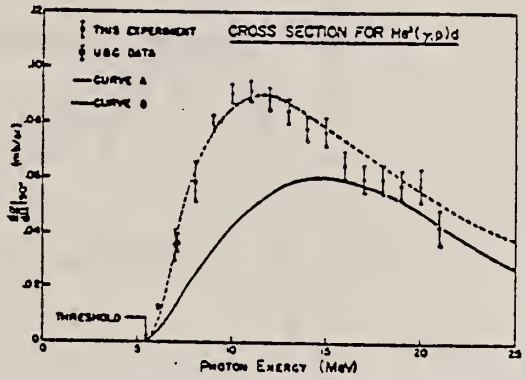

FIG. 12. Experimental and theoretical 90° differential cross sections for $He^3(\gamma,p)d$. Curve A results from the Gaussian ground-state wave function for He^3 of Verde (Ref. 1); curve B, from the modified exponential wave function of Gunn and Irving (Ref. 2), with $1/\mu = 2.6$ F. The square points represent the data from recent experiments at the University of British Columbia (Ref. 20). No normalization has been performed.

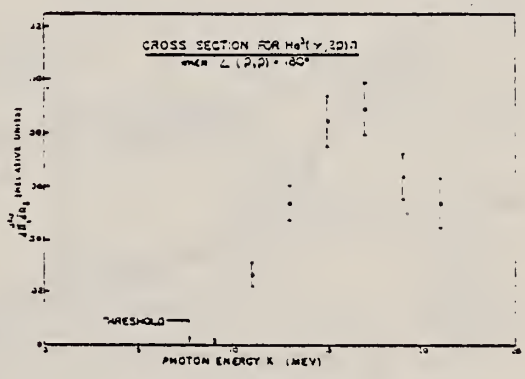

FIG. 13. Experimental double differential cross sections for $He^3(\gamma,2p)n$ when the two outgoing protons are emitted back-to-back.

REF.

A.N. Gorbunov and A.T. Varfolomeev
Phys. Letters 11, 137 (1964)

EL.EM. SYM.	A	Z
He	3	2

METHOD

Cloud chamber in magnetic field

REF. NO. 64 Go 1 JOC

REACTION	RESULT	EXCITATION ENERGY	SOURCE		DETECTOR		ANGLE
			TYPE	RANGE	TYPE	RANGE	
G, P	ABX	THR - 120	C	175	CCH		DST
G,2P	ABX	THR - 120	C	175	CCH		DST

$$Y_{\gamma p} = Y_{\gamma n} = \int_0^{170} \sigma\eta_\gamma dE_\gamma = 1.47 \pm 0.03 \text{ mb}$$

γ,d; $\int \sigma dE_\gamma$ = 26.5 ± 1.3 MeV-mb

γ,n; $\int \sigma dE_\gamma$ = 43.6 ± 2.7 MeV-mb

Total 70. ± 3 MeV-mb

E2 contributions estimated as 11 ± 4%

γ,d $\int \frac{\sigma}{E_\gamma} dE_\gamma$ = 1.34 ± 0.05 mb

γ,n $\int \frac{\sigma}{E_\gamma} dE_\gamma$ = 1.42 ± 0.07 mb

Total 2.76 ± 0.08 mb

E2 ~ 8.5 ± 2%

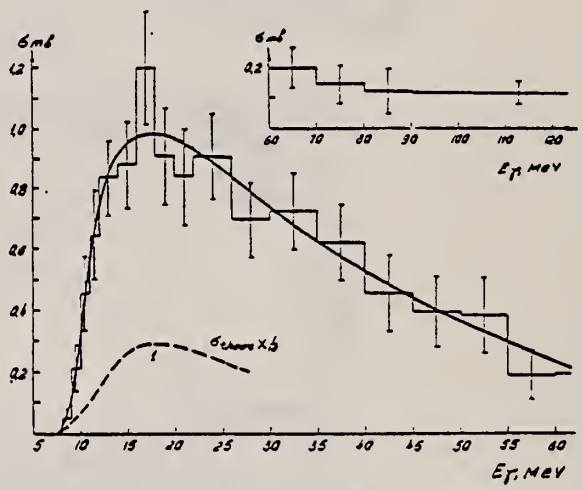

Fig. 2. The cross section of the $He^3(\gamma,n)2p$ reaction.

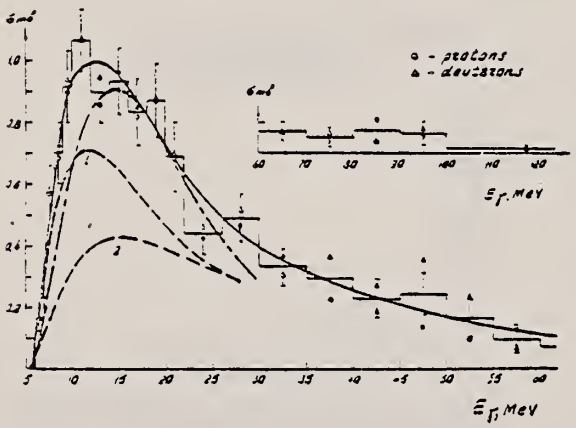

Fig. 1. The cross section of the $He^3(\gamma,p)D^2$ reaction.
o calculated on proton tracks; Δ on deuteron tracks.

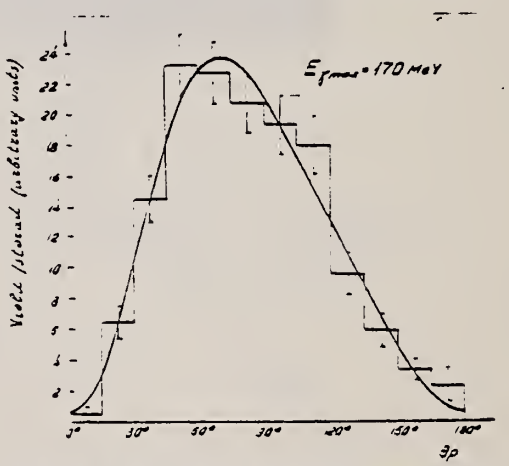

Fig. 3. The centre-of-mass angular distribution of protons emitted in the $He^3(\gamma,p)D^2$ reaction. The full line is calculated in the form

$\sin^2\vartheta + (0.66 \pm 0.10)\sin^2\vartheta\cos\vartheta + (0.46 \pm 0.10)\sin^2\vartheta\cos^2\vartheta + (0.03 \pm 0.01)$.

REF.

A. N. Gorbunov and A. T. Varfolomeev
Proc. Paris Conf. 1071 (1964)

ELEM. SYM.	A	Z
He	3	2

METHOD

REF. NO.	
64 Go 4	JDM

REACTION	RESULT	EXCITATION ENERGY	SOURCE		DETECTOR		ANGLE
			TYPE	RANGE	TYPE	RANGE	
G,P	ABX	5-170	C	170	CCH-D		DST
G,N	ABX	5-170	C	170	CCH-D		

$(\sigma_0)\gamma,p = 26.5 \pm 1.3$ MeV mb.

$(\sigma_0)\gamma,n = 43.6 \pm 2.7$ MeV mb.

So Total$(\sigma_0) = 70 \pm 3.2$ MeV mb.

$(\sigma_{-1})\gamma,p = 1.34 \pm 0.05$ mb.

$(\sigma_{-1})\gamma,n = 1.42 \pm 0.07$ mb.

So Total$(\sigma_{-1}) = 2.76 \pm 0.08$ mb.

Charge rms radium $R_c = 1.81 \pm 0.06$ fm.

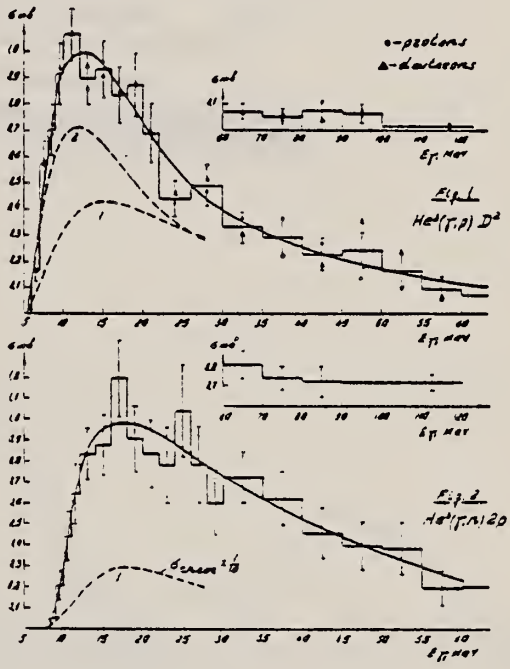

REF.

A. Johansson
Phys. Rev. 136, B1030 (1964)

ELEM. SYM.	A	Z
He	3	2

METHOD

REF. NO.	
64 Jo 1	JOC

REACTION	RESULT	EXCITATION ENERGY	SOURCE		DETECTOR		ANGLE
			TYPE	RANGE	TYPE	RANGE	
E,E/P	ABX	0-12	D	550	MAG-D		DST

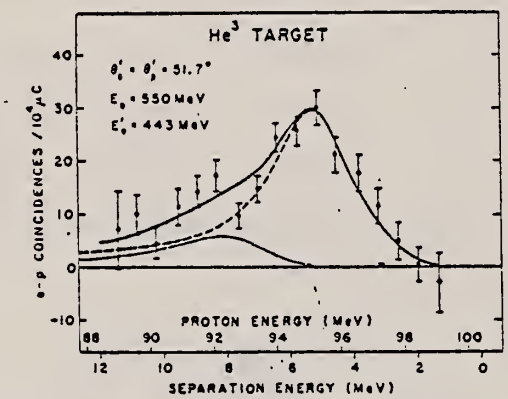

FIG. 1. The energy spectrum of protons at 51.7° in coincidence with 443-MeV electrons at 51.7° from He^3 $(e,e'p)$. The curves are discussed in Sec. VI of the text.

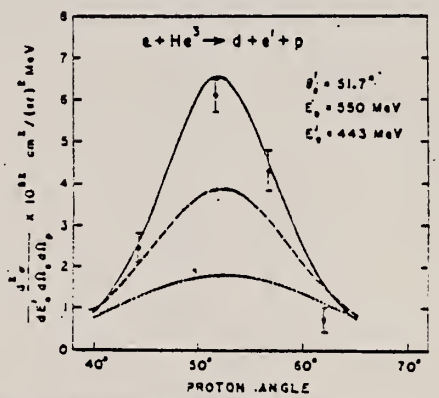

FIG. 3. The coincidence cross section of reaction (A) as a function of proton angle. The curves correspond to calculations using different wave functions and are explained in Sec. VI of the text.

REF.

V. N. Fetisov, A. N. Gorbunov and A. T. Varfolomeev
Nuclear Phys. 71, 305 (1965)

ELEM. SYM.	A	Z
He	3	2

METHOD

REF. NO.	
65 Fe 1	EGF

REACTION	RESULT	EXCITATION ENERGY	SOURCE		DETECTOR		ANGLE
			TYPE	RANGE	TYPE	RANGE	
G.P	ABX	THR - 170	C	170	CCH		DST
G,N	ABX	THR - 170	C	170	CCH		DST

TOT
65T

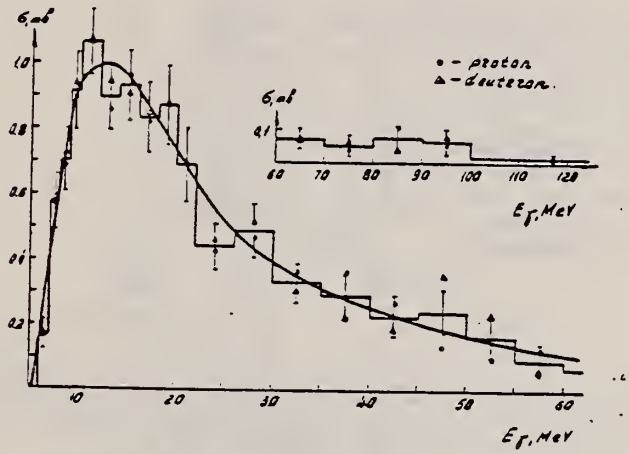

Fig. 2. Effective cross section of the $He^3(\gamma, p)D^3$ reaction.

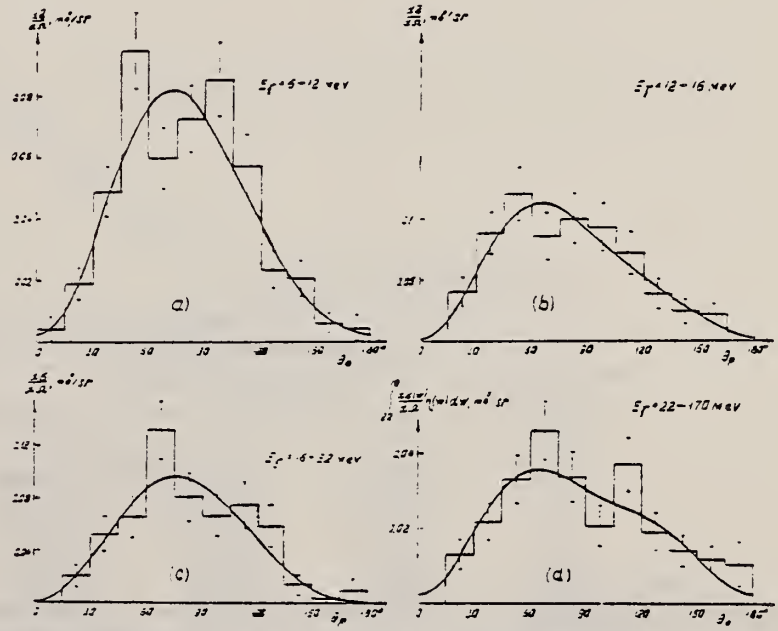

Fig. 3. Angular distributions of protons in the $He^3(\gamma, p)D^3$ reaction in the c.m. system.

(continued)

REACTION	RESULT	EXCITATION ENERGY	SOURCE		DETECTOR		ANGLE
			TYPE	RANGE	TYPE	RANGE	

TABLE 1

Coefficients A, β, γ and δ characterizing the angular distribution of protons in the $He^3(\gamma, p)D^2$ reaction

Energy interval ΔE_γ (MeV)	6-12	12-16	16-22	22-170	6-22	6-170
A (mb/sr)	0.072±0.065	0.086±0.013	0.091±0.011	0.028±0.004	0.123±0.008	0.153±0.006
β	0.69 ±0.14	0.95 ±0.25	0.57 ±0.18	0.57 ±0.24	0.7 ±0.1	0.66 ±0.1
γ	0.1 ±0.3	0.9 ±0.6	0.1 ±0.4	1.1 ±0.6	0.4 ±0.2	0.5 ±0.2
δ	0.03 ±0.04	0.02 ±0.08	0.02 ±0.06	0.09 ±0.11	0.01 ±0.02	0.03 ±0.02
$\varepsilon = \sigma/\frac{8}{3}\pi A$	1.06 ±0.09	1.21 ±0.17	1.05 ±0.12	1.35 ±0.20	1.09 ±0.05	1.14 ±0.05

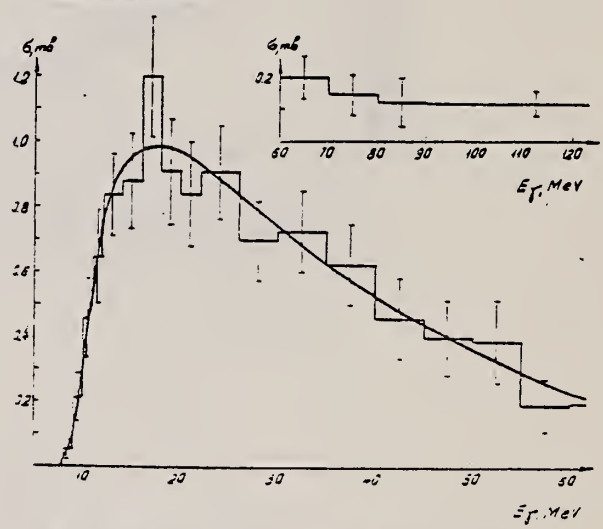

Fig. 4. Effective cross section of the $He^3(\gamma, n)2p$ reaction.

TABLE 2

Partial integral cross sections

The energy interval ΔE_γ (MeV)	σ_0 (MeV · mb)		σ_{-1} (mb)	
	γ, p	γ, n	γ, p	γ, n
0-22	12.9±0.6	10.7±0.7	1.00 ±0.04	0.69±0.05
0-30	16.6±0.7	17.1±1.0	1.14 ±0.04	0.94±0.05
0-40	19.7±0.8	23.8±1.4	1.23 ±0.05	1.14±0.06
0-100	25.9±1.2	38.0±2.3	1.34 ±0.05	1.37±0.07
0-170	26.5±1.3	43.6±2.7	1.34 ±0.05	1.42±0.07
22-100	13.0±1.1	27.3±2.2	0.34 ±0.03	0.68±0.05
100-170	0.6±0.4	5.6±2.2	0.005±0.003	0.04±0.02

Only statistical errors are given.

(continued)

REACTION	RESULT	EXCITATION ENERGY	SOURCE		DETECTOR		ANGLE
			TYPE	RANGE	TYPE	RANGE	

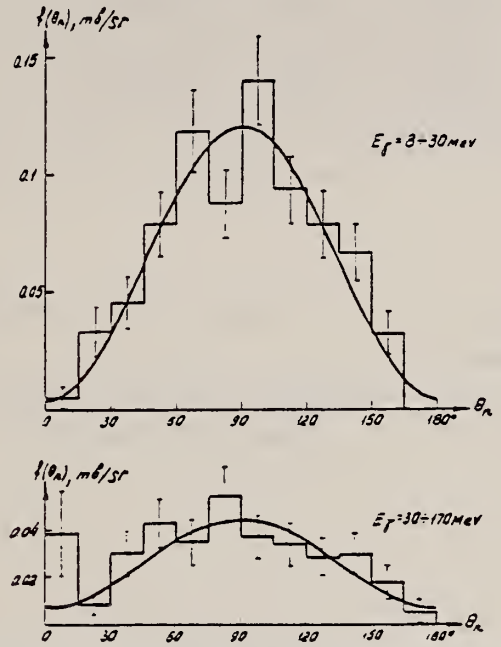

Fig. 5. Angular distribution of neutrons in the $He^3(\gamma, n)2p$ reaction in the c.m. system. Smooth curves are calculated by the least-squares method. (a) $f(\theta_n) = (0.116 \pm 0.009)\ [\sin^2\theta_n + (0.03 \pm 0.03)]$ mb/sr. (b) $f(\theta_n) = (0.038 \pm 0.006)\ [\sin^2\theta_n + (0.18 \pm 0.12)]$ mb/sr.

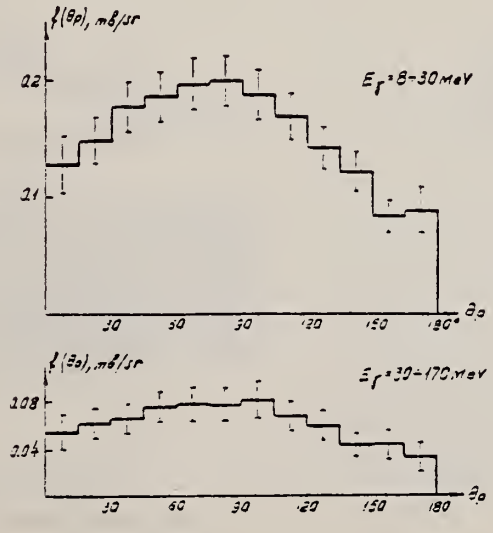

Fig. 6. Angular distribution of protons in the $He^3(\gamma,n)2p$ reaction in the laboratory system.

(continued)

REF.

V. N. Fetisov, A. N. Gorbunov and A. T. Varfolomeev
Nuclear Phys. 71, 305 (1965)

ELEM. SYM.	A	Z
He	3	2

METHOD

REF. NO. 65 Fe 1 EGF

REACTION	RESULT	EXCITATION ENERGY	SOURCE		DETECTOR		ANGLE
			TYPE	RANGE	TYPE	RANGE	

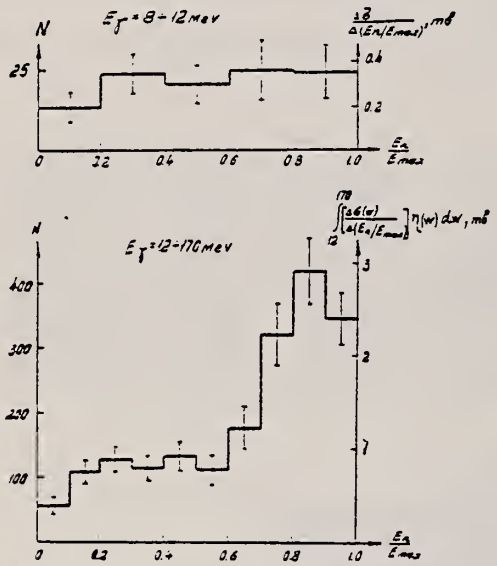

Fig. 7. Energy spectrum of neutrons in the $He^3(\gamma, n)2p$ reaction.

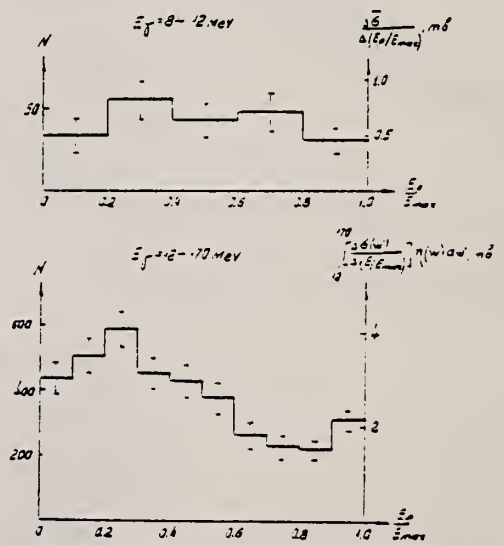

Fig. 8. Energy spectrum of protons in the $He^3(\gamma, n)2p$ reaction.

REF.

J. R. Stewart, R. C. Morrison, and J. S. O'Connell
Phys. Rev., 138, B372-81 (1965)

ELEM. SYM.	A	Z
He	3	2

METHOD

Linac; ion chamber monitor

REF. NO.: 65 St 1 NVB

REACTION	RESULT	EXCITATION ENERGY	SOURCE		DETECTOR		ANGLE
			TYPE	RANGE	TYPE	RANGE	
G,D	ABX	9-46	C	40,55	SCD-D		90
G,2P	SPC	9-40	C	40	SCD-D	1-8	90

$$\int_0^{40\ \mathrm{MeV}} \sigma(\gamma,d)dE_\gamma = 16.5 \pm 10\%\ \mathrm{MeV - mb},$$

$$\int_0^{40\ \mathrm{MeV}} \frac{\sigma(\gamma,d)}{E_\gamma} dE_\gamma = 1.07 \pm 10\%\ \mathrm{mb},$$

assuming Gorbunov angular distribution: $0.03 + \sin^2\theta(1 + 0.66\cos\theta + 0.46\cos^2\theta)$.

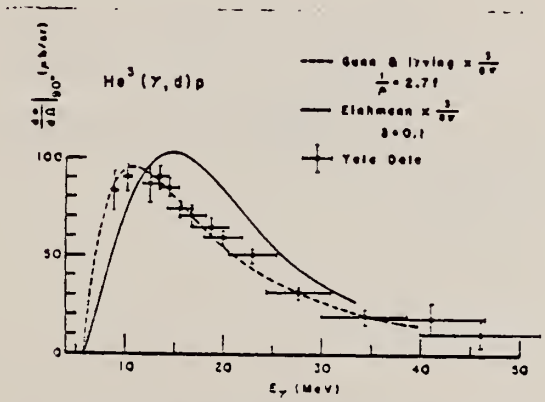

FIG. 3. Final experimental $He^3(\gamma,d)p$ data is compared with two theoretical predictions. The vertical error bars are combined from statistical errors and estimates of systematic errors for each point. The horizontal error bars are the full width at half-maximum for each point. This width includes about 70% of the data used for each point. The dashed curve is from Gunn and Irving (Ref. 18) with $1/\mu = 2.7$ F assuming a pure $\sin^2\theta$ distribution, $(d\sigma/d\Omega)_{90°} = \sigma_{total}3/8\pi$. The solid curve is from Eichmann (Ref. 20) with mixing parameter $\delta = 0.1$, and again the total cross section is multiplied by $3/8\pi$ to compare with the data.

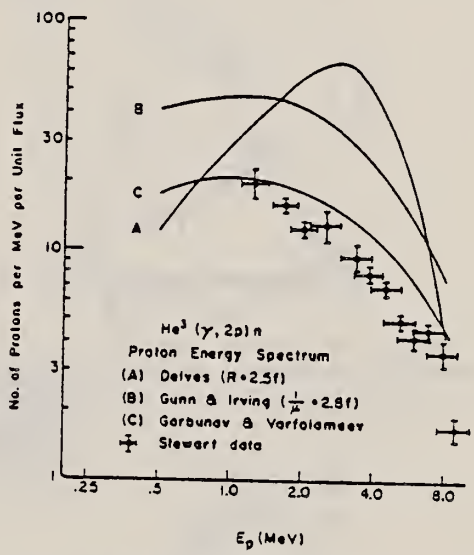

FIG. 4. The proton spectrum from three-body breakup produced by 40-MeV bremsstrahlung. The three curves shown are calculations made with different three-body breakup cross sections: theories by Deives (Ref. 21) and by Gunn and Irving (Ref. 18); and an experiment by Gorbunov and Varfolomeev (Ref. 13).

(continued)

REF.

J. R. Stewart, R. C. Morrison, and J. S. O'Connell
Phys. Rev., 138, B372-81 (1965)

EL EM. SYM.	A	Z
He	3	2

METHOD

Linac; ion chamber monitor

REF. NO.

65 St 1 NVB

REACTION	RESULT	EXCITATION ENERGY	SOURCE		DETECTOR		ANGLE
			TYPE	RANGE	TYPE	RANGE	

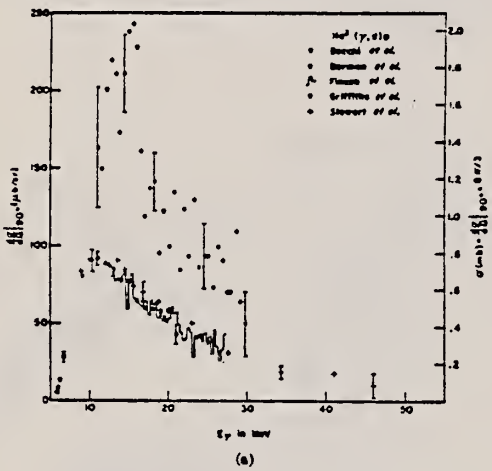

(a)

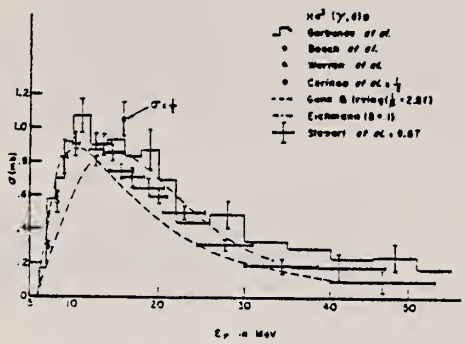

(b)

FIG. 5. (a) Comparison of experimental 90° differential two-body breakup cross sections. The right-hand ordinate shows the total cross section assuming a $\sin^2\theta$ angular distribution. Shown with some representative error bars are two-body photodisintegration data from Becchi *et al.* (Ref. 6) (data as published is divided by $3/8\pi$ to compare with the rest of 90° data), Berman *et al.* (Ref. 4), Finckh *et al.* (Ref. 5), and the present experiment as well as low-energy capture data from Griffiths *et al.* (Refs. 7–9) (transformed by detailed balance). (b) Comparison of experimental total two-body breakup cross sections. Shown with some representative error bars are He^3 photodisintegration data from Bösch *et al.* (Ref. 12) and $D(n,\gamma)T$ capture from Cerineo *et al.* (Ref. 14) both corrected for different thresholds of H^3 and He^3, and He^3 photodisintegration data from Gorbunov *et al.* (Ref. 13) and Warren *et al.* (Ref. 11). The data of the present experiment are multiplied by a factor of 9.97 in accordance with the angular distribution of Gorbunov *et al.* (Ref. 13). The curves are theoretical predictions of Gunn and Irving (Ref. 18), $\mu^{-1}=2.3$ F, and Eichmann (Ref. 20).

REF. A.T. Varfolomeev and A.N. Gorbunov
J. Expl. Theoret. Phys.(USSR) 47, 30 (1964)
Soviet Phys. JETP 20, 20 (1965)

ELEM. SYM.	A	Z
He	3	2

METHOD Cloud chamber in magnetic field; monitor quantameter and $C^{12}(\gamma,n)C^{11}$

REF. NO. 65 Va 1 JOC

REACTION	RESULT	EXCITATION ENERGY	SOURCE		DETECTOR		ANGLE
			TYPE	RANGE	TYPE	RANGE	
G,PD	ABX	THR-170	C	170	CCH-D		DST
G,2P	ABX	THR-170	C	170	CCH-D		DST

$$f(\theta) \sim \sin^2\theta + \beta \sin^2\theta \cos\theta + \gamma \sin^2\theta \cos^2\theta + \delta$$

$\sigma_{-1}(\gamma,d) = 1.34 \pm 0.05$ mb

$\sigma_{-1}(\gamma,2p) = 1.42 \pm 0.07$

$\sigma_{-1}(\text{total}) = 2.76 \pm 0.08$ mb

(E2 contribution subtracted)

rms charge radius = 1.81 ± 0.06 F

$\sigma_{int}(\gamma,d) = 26.5 \pm 1.3$ MeV - mb.

$\sigma_{int}(\gamma,2p) = 43.6 \pm 2.7$ MeV - mb.

$\sigma_{int}(\text{total}) = 70 \pm 3$ MeV - mb.

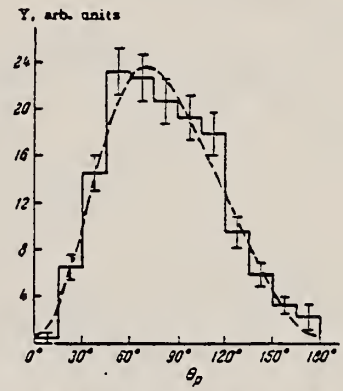

FIG. 5. Angular distribution of protons from the reaction $He^3(\gamma, p)D^2$ in the c.m. system. Dashed curve – distribution according to (5) with $\beta = 0.66 \pm 0.10$, $\gamma = 0.46 \pm 0.10$, and $\delta = 0.03 \pm 0.01$. Y is the yield per unit solid angle; E_γ = 6–170 MeV.

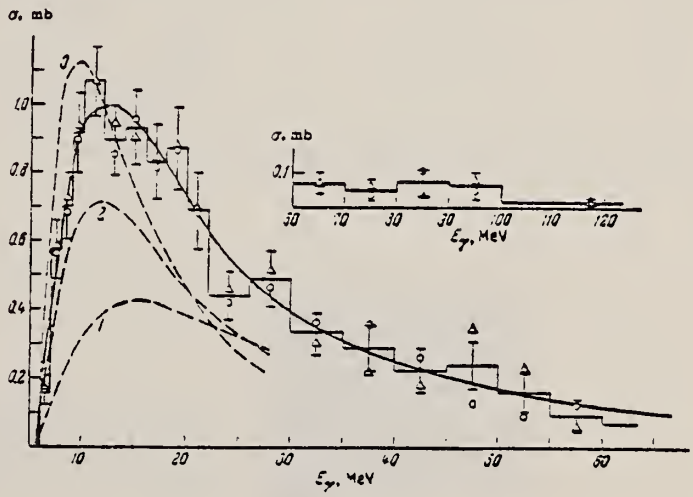

FIG. 4. Cross section for $He^3(\gamma, p)D^2$.
o – from proton tracks; Δ – from deuteron tracks.

REF. D. Bachelier, M. Bernas, I. Brissaud, C. Detraz, J.P. Didelez, H. Langevin-Joliot, J. Lee and P. Radvanyi
Phys. Letters 21, 697 (1966)

ELEM. SYM.	A	Z
He	3	2

METHOD: Synchrocyclotron

REF. NO.: 66 Ba 2 JDM

REACTION	RESULT	EXCITATION ENERGY	SOURCE TYPE	SOURCE RANGE	DETECTOR TYPE	DETECTOR RANGE	ANGLE
P,G	ABX	110	D	156	SCI-D	83 - 122	DST

$\sigma = 1.4 \pm 0.3$ µb

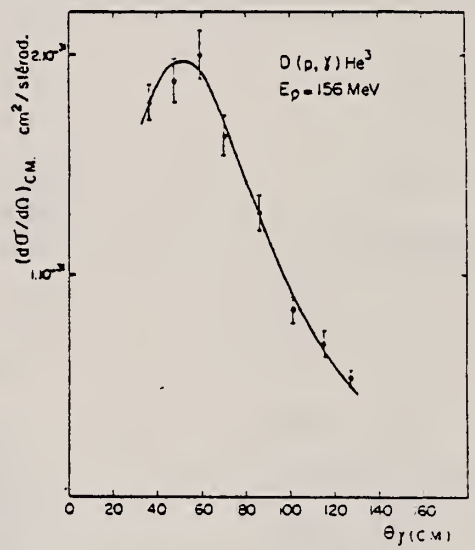

Fig. 2. Section efficace différentielle de la réaction $D(p,\gamma)^3He$ à E_p = 156 MeV, dans le système du centre de masse.

REF.

H. M. Gerstenberg and J. S. O'Connell
Phys. Rev. 144, B834 (1966)

ELEM. SYM.	A	Z
He	3	2

METHOD

Betatron

REF. NO. 66 Ge 1 JDM

REACTION	RESULT	EXCITATION ENERGY	SOURCE TYPE	SOURCE RANGE	DETECTOR TYPE	DETECTOR RANGE	ANGLE
G,N	ABX	THR - 30	C	THR - 30	BF3-I		4PI

$$\int_0^{28\,\mathrm{MeV}} \sigma dE_\gamma = 12.1\ \mathrm{MeV\ mb} \pm 1\%$$

$$\int_0^{28\,\mathrm{MeV}} \frac{\sigma}{E\gamma}\, dE\gamma = 0.68\ \mathrm{mb} \pm 10\%$$

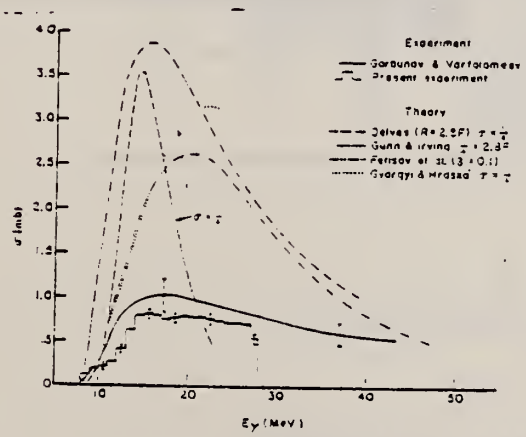

FIG. 4. Total cross section of the reaction $He^3(\gamma,n)2p$ compared to another measurement (Ref. 14) and to four theoretical calculations (Refs. 16–20). Note that two of the cross sections are reduced by a factor of 4 for presentation. The number following the names of the theoretical papers identify a particular parameter of the theory.

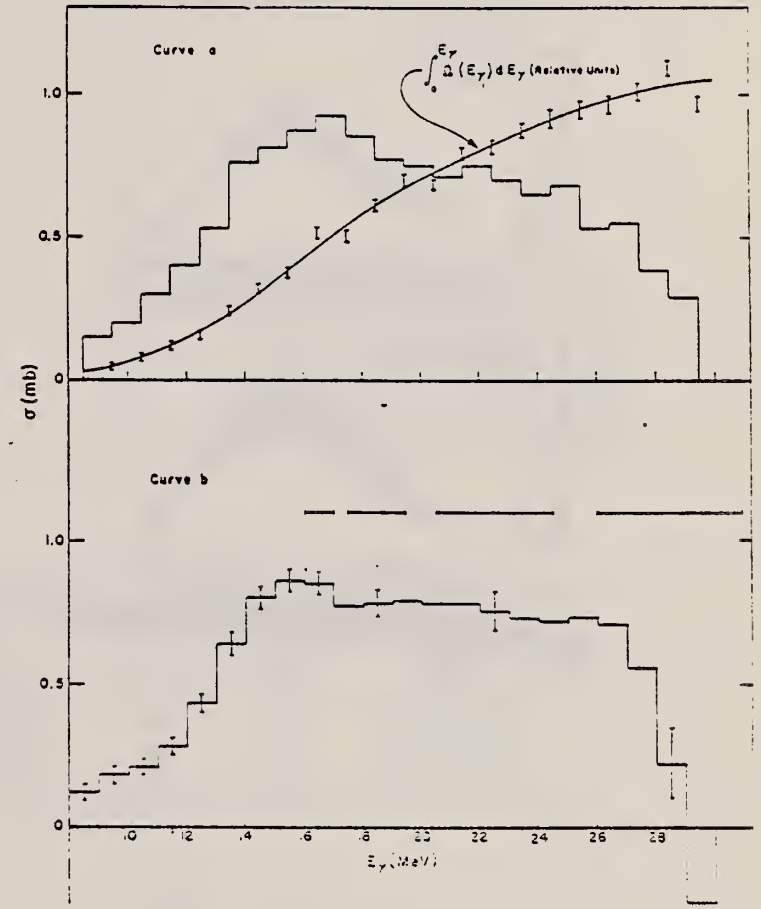

FIG. 3. Total cross section of the reaction $He^3(\gamma,n)2p$ as obtained by an analysis of the neutron yield curve. Figure 3(a) was obtained by smoothing the running integral of the reduced cross section and using first differences to obtain the cross section. Figure 3(b) was obtained using the "least-structure analysis" of Cook. The horizontal error bars indicate the energy interval over which the data are smoothed.

REF.

E. B. Hughes, M. R. Yearian, and R. Hofstadter
Phys. Rev. 151, 841 (1966)

ELEM. SYM.	A	Z
He	3	2

METHOD

Linac

REF. NO.	
66 Hu 2	JDM

REACTION	RESULT	EXCITATION ENERGY	SOURCE		DETECTOR		ANGLE
			TYPE	RANGE	TYPE	RANGE	
E,E/	ABX	0-150	D	250-670	SCI-D	130-360	DST

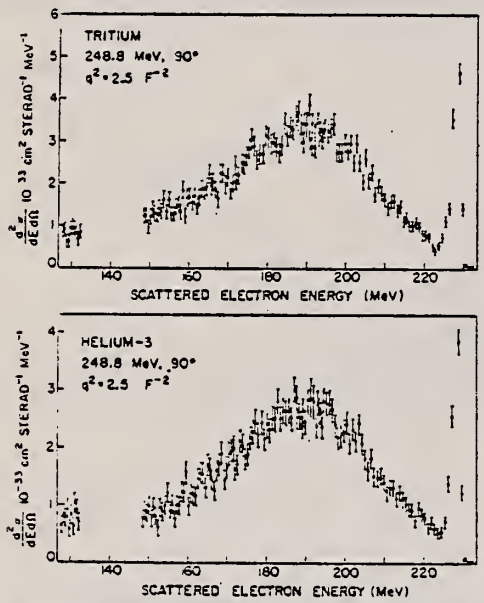

FIG. 3. The absolute inelastic electron-tritium and electron-helium-3 cross sections as a function of scattered electron momentum for $q^2=2.5$ F^{-2}.

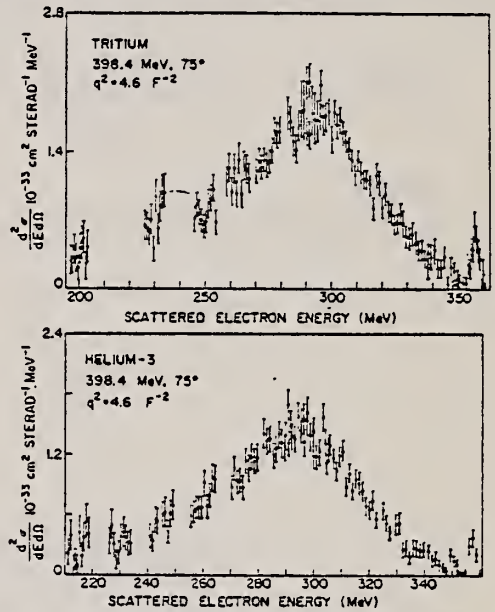

FIG. 4. The absolute inelastic electron-tritium and electron-helium-3 cross sections as a function of scattered electron momentum for $q^2=4.6$ F^{-2}.

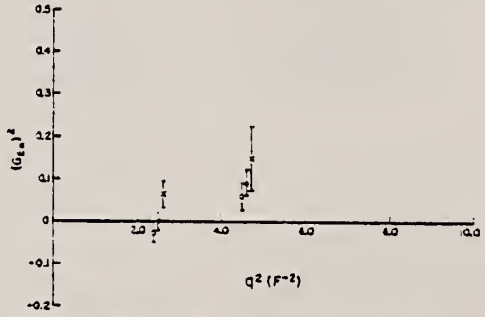

FIG. 5. The values of the square of the neutron electric form factor $(G_{En})^2$ as a function of q^2. The full circle points were obtained using Eq. (7), the crosses using Eq. (8) and the open circles using Eq. (9). The crosses and open circles have been shifted slightly in the q^2 direction for purposes of clarity.

(continued)

REACTION	RESULT	EXCITATION ENERGY	SOURCE TYPE	SOURCE RANGE	DETECTOR TYPE	DETECTOR RANGE	ANGLE

TABLE I. The experimental ratios of the electron-tritium and electron-helium-3 quasi-elastic cross sections as a function of q^2 and scattering angle. Also shown are the ratios of the elastic electron-neutron and electron-proton cross sections which follow from the experimental ratios by means of Eq. (3). The errors attached are purely statistical.

q^2 (F^{-2})	E (MeV)	Angle (degrees)	$\frac{(d^2\sigma/dEd\Omega)_{H^3}}{(d^2\sigma/dEd\Omega)_{He^3}}$	$\frac{(d\sigma/d\Omega)_n}{(d\sigma/d\Omega)_p}$
2.5	248.8	90	0.619±0.018	0.173±0.028
4.6	667.5	40	0.579±0.017	0.111±0.025
			0.581±0.017	0.114±0.025
			0.582±0.017	0.116±0.025
4.6	398.4	75	0.655±0.019	0.230±0.032
			0.632±0.018	0.193±0.030
			0.604±0.017	0.150±0.027
4.6	296.4	120	0.675±0.020	0.264±0.035
			0.666±0.017	0.249±0.030

TABLE II. The neutron form factors as a function of q^2. The expected form factors are taken from Eq. (14) of Ref. 5.

q^2 (F^{-2})	$(G_{En})^2$ Measured values	$-G_{Mn}/\mu_n$ Measured values	$(G_{En})^2$ Expected values	$-G_{Mn}/\mu_n$ Expected values
2.5	0.006±0.038		0.0	0.71
4.6	0.003±0.007	0.537±0.028	0.0	0.59

TABLE III. The total inelastic cross sections for tritium and helium-3 as a function of q^2 and scattering angle. Column 6 shows the correction factors applied to the measured cross sections, due to the experimental low-momentum cutoff.

q^2 (F^{-2})	Angle (degrees)	Target	$\sigma_{observed}$ (cm^2/Sr)	% cutoff	Correction factor	$\sigma_{corrected}$ (cm^2/Sr)
2.5	90	H^3	$(1.64\pm0.05)\times10^{-31}$	30.0	1.043	$(1.71\pm0.09)\times10^{-31}$
		He^3	$(2.68\pm0.08)\times10^{-31}$	30.0	1.043	$(2.79\pm0.15)\times10^{-31}$
4.6	75	H^3	$(1.32\pm0.04)\times10^{-31}$	30.0	1.032	$(1.36\pm0.06)\times10^{-31}$
		He^3	$(1.32\pm0.05)\times10^{-31}$	25.0	1.058	$(1.92\pm0.13)\times10^{-31}$

REF. A.T. Varfolomeev, A.N. Gorbunov and G.G. Taran
J. Nucl. Phys. (USSR) 3, 647 (1966)
Sov. J. Nucl. Phys. 3, 473 (1966)

ELEM. SYM.	A	Z
He	3	2

METHOD

REF. NO.	
66 Va 3	JDM

REACTION	RESULT	EXCITATION ENERGY	SOURCE		DETECTOR		ANGLE
			TYPE	RANGE	TYPE	RANGE	
G,P	ABX	THR - 170	C	170	CCH-D		4PI
G,N	ABX	THR - 170	C	170	CCH-D		4PI

Determined $\int[\sigma(\gamma,n) + \sigma(\gamma,p)]dE$ in terms of $\int\sigma(\gamma,n)d$ for deuteron by comparing yields of protons for two reactions using same cloud chamber. Result obtained was consistent with previous measurement of cross sections for $^3He(\gamma,p)$ and $^3He(\gamma,n)$.[1,2]

[1]A.N. Gorbunov and A.T. Varfolomeev, Phys. Letters 11, 137 (1964).
[2]A.T. Varfolomeev and A.N. Gorbunov, JETP 47, 30 (1964), Soviet Phys. JETP 20, 20 (1965).

REF.

W. Wölfli, R. Bösch, J. Lang, R. Müller and P. Marmier
Phys. Letters 22, 75 (1966)

ELEM. SYM.	A	Z
He	3	2

METHOD

REF. NO.	
66 Wö 1	JDM

REACTION	RESULT	EXCITATION ENERGY	SOURCE		DETECTOR		ANGLE
			TYPE	RANGE	TYPE	RANGE	
P,G	ABX	7 - 14	D	2 - 12	NAI-D	5 - 20	DST

$$\frac{d\sigma}{d\Omega} = a + b \sin^2\theta \,(1 + \beta \cos\theta)$$

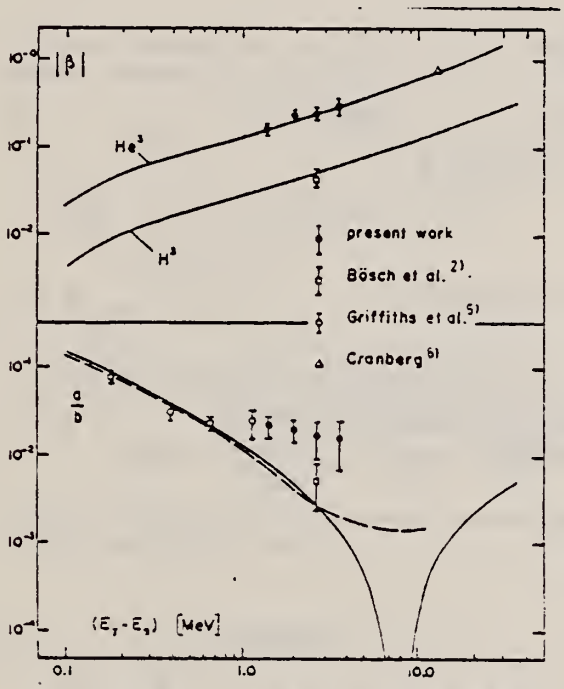

Fig. 2. Comparison of the experimental with the theoretical values of the angular distribution coefficients a/b and β. The solid curves have again been evaluated with the Gunn-Irving wave function, using the parameters $\mu^{-1} = 2.5$ fm and $\delta = 0.07$. The dashed curve shows the influence of the proton-deuteron interaction associated with nuclear and Coulomb forces.

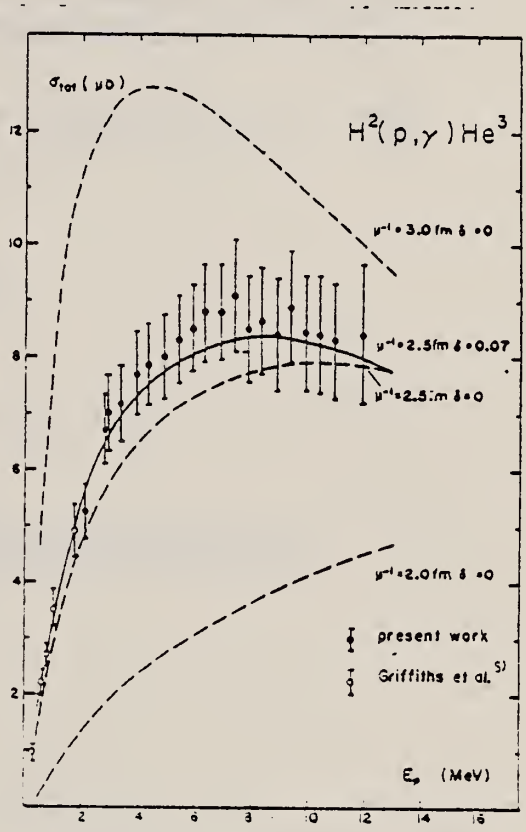

Fig. 1. Compilation of the experimental values of the total cross section for the $^2H(p,\gamma)^3He$ reaction. The various curves have been calculated with the aid of the Gunn-Irving wave function for the ground state of the three-body nuclei. The effect of the Coulomb interaction between proton and deuteron has been taken into account.

REF.

R.F. Frosch, H.L. Crannell, J.S. McCarthy, R.E. Rand, R.S. Safrata, L.R. Suelzle and M.R. Yearian
Phys. Letters 24B, 54 (1967)

ELEM. SYM.	A	Z
He	3	2

METHOD

REF. NO.	
67 Fr 1	JDM

REACTION	RESULT	EXCITATION ENERGY	SOURCE		DETECTOR		ANGLE
			TYPE	RANGE	TYPE	RANGE	
E,E/	ABX	0-17	D	200	MAG-D		60

There exists no evidence for narrow states excited with cross section > 3×10^{-33} cm^2/sr for excitation energies up to 17 MeV.

$$\frac{d\sigma_{el}}{d\Omega} = (1.91 \pm 0.10) \times 10^{-30} \text{ cm}^2/\text{sr}.$$

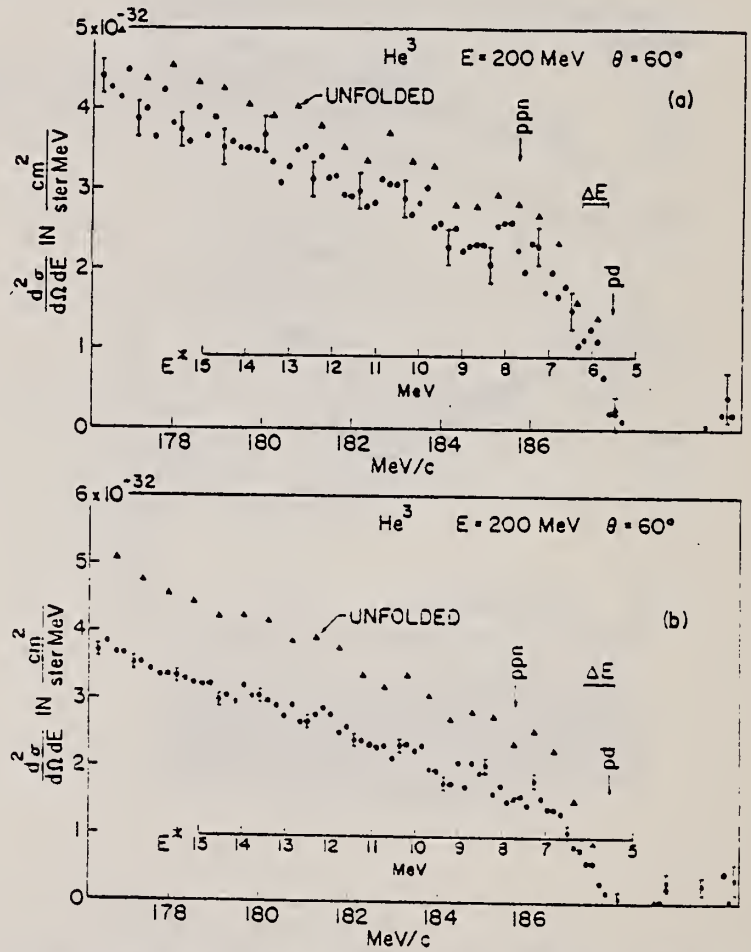

Fig. 1. Two spectra of electrons scattered inelastically on ^{3}He. The inserted horizontal scale gives the mass difference E^* between the recoiling 3-nucleon-system and the ^{3}He ground state. The length ΔE indicates the experimental resolution (FWHM). The result of a radiation unfolding procedure, and the pd and ppn breakup thresholds are shown. Spectrum (a) was obtained with a liquid ^{3}He target, spectrum (b) with a high pressure gas target. In both spectra the radiative tail of the elastic peak has been subtracted. The spectra show no consistent evidence for narrow excited states of the ^{3}He nucleus.

FORM NBS-418
(REV. 7-14-64)
USCOMM-DC 26010-P64

REF. K. N. Geller, E. G. Muirhead and L. D. Cohen
Nucl. Phys. A96, 397 (1967)

ELEM. SYM.	A	Z
He	3	2

METHOD

REF. NO.	
67 Ge 1	EGF

REACTION	RESULT	EXCITATION ENERGY	SOURCE		DETECTOR		ANGLE
			TYPE	RANGE	TYPE	RANGE	
P,G	ABX	7-9	D	2-4	NAI-D		90

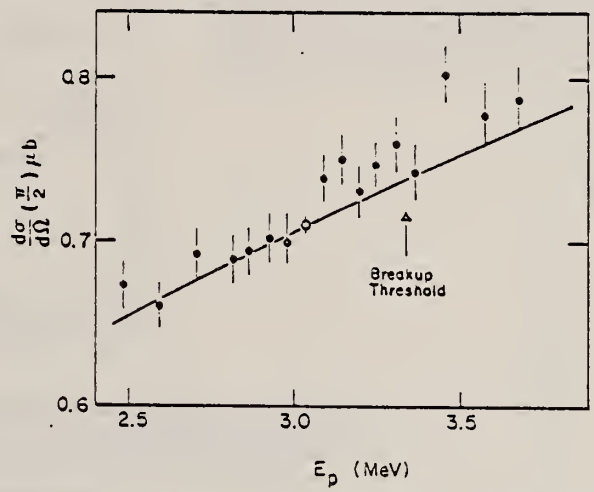

Fig. 2. Yield function of $^3H(p,\gamma)$ capture gamma rays in the region of the breakup threshold. Experimental yields are normalized to the Gunn-Irving cross section (solid curve) at the standard energy point, E_p = 3.07 MeV (open circle).

REF.

W. Wölfli, R. Bösch, J. Lang, R. Müller and P. Marmier
Helv. Phys. Acta 40, 946 (1967)

ELEM. SYM.	A	Z
He	3	2

METHOD

REF. NO.	
67 Wö 1	egf

REACTION	RESULT	EXCITATION ENERGY	SOURCE		DETECTOR		ANGLE
			TYPE	RANGE	TYPE	RANGE	
P,G	ABX	7-14	D	2-12	NAI-D	2-14	DST

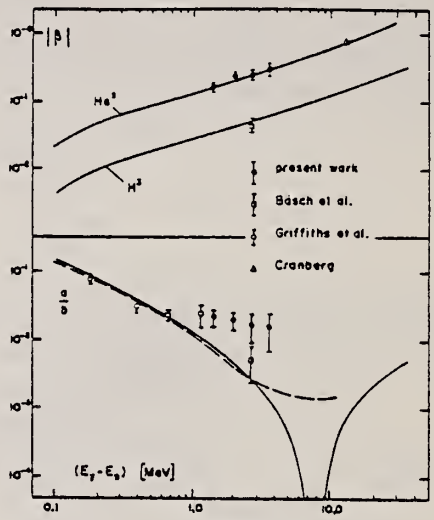

Fig. 7

Vergleich der experimentellen und theoretischen Werte für die Koeffizienten der Winkelverteilung β und a/b. Die ausgezogenen Kurven wurden mit dem Gunn-Irvingschen Ansatz und den Parameterwerten $\mu^{-1} = 2{,}5$ F, $\delta = 0{,}07$ ohne Berücksichtigung der Wechselwirkung im Kontinuumszustand berechnet. Die gestrichelte Kurve zeigt den Einfluss der zwischen dem Proton und dem Deuteron wirkenden Coulomb- und Kernkräften.

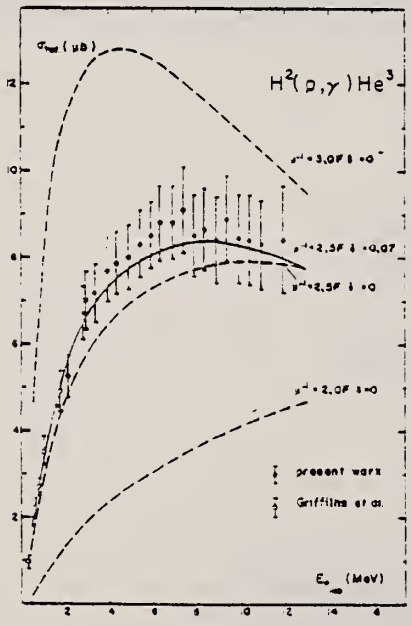

Fig. 5

Zusammenstellung der experimentellen Werte für den Gesamtwirkungsquerschnitt der Reaktion $H^2(p,\gamma)He^3$. Die verschiedenen Kurven wurden unter Berücksichtigung des Gunn-Irvingschen Ansatzes für die Wellenfunktion des Grundzustandes und der Coulombwechselwirkung zwischen dem Proton und dem Deuteron im Kontinuumszustand berechnet.

REF.

P. Picozza, C. Schaerf, R. Scrimaglio, G. Goggi,
A. Piazzoli, D. Scannicchio
Nuovo Cimento 55A, 206 (1968)

ELEM. SYM.	A	Z
He	3	2

METHOD

REF. NO.: 68 Pi 1 egf

REACTION	RESULT	EXCITATION ENERGY	SOURCE		DETECTOR		ANGLE
			TYPE	RANGE	TYPE	RANGE	
G,D	ABX	180-550	C	800	TEL-D		90

[1]Fetisov et al., Nucl. Phys. 71, 305 (1965).

[3]Berman et al., Phys. Rev. 133, B117 (1964).

[4]Bosch et al., Phys. Lett. 8, 120 (1964).

[6]Stewart et al., Phys. Rev. 138, B372 (1965).

[10]Gunn et al., Phil. Mag. 42, 1353 (1951).

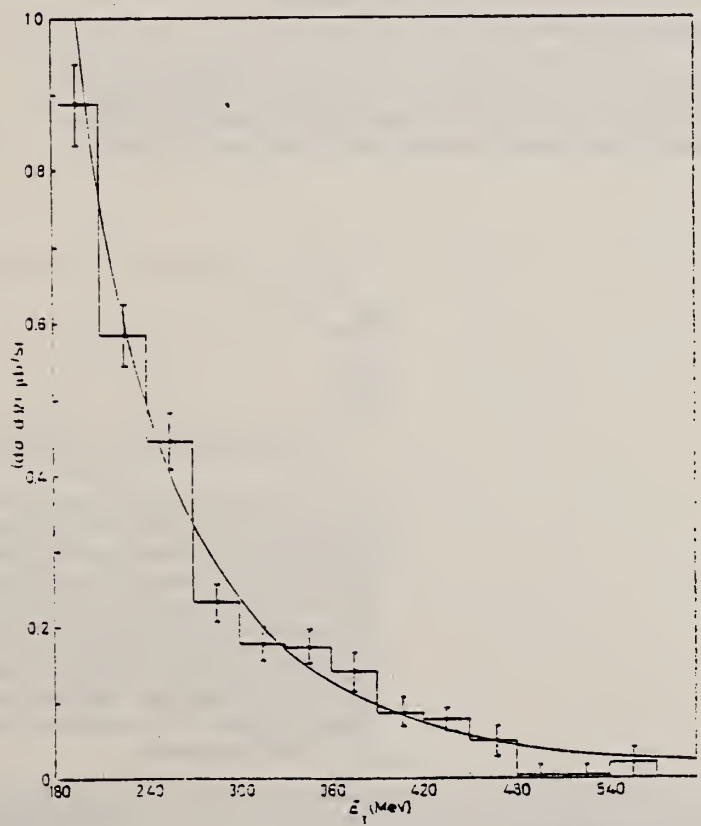

Fig. 2. – Experimental differential cross-section (c.m.s. angle = 90°) for the reaction $\gamma + {}^3He \rightarrow p + d$.

Fig. 3. – Comparison of the experimental 90° c.m.s. differential two-body photodisintegration cross-sections. Assuming a $\sin^2\vartheta$ angular distribution in the whole energy range, the data by FETISOV *et al.* and by BÖSCH *et al.* have been multiplied by $3/8\pi$ to compare them with the other data. The dashed curve is the Gunn and Irving theoretical calculation with $\mu^{-1} = 2.6$ fm. o, FETISOV *et al.*, $\times 3/8\pi$ (ref. [1]); ▼, BERMAN *et al.* (ref. [3]); ■, BÖSCH *et al.*, $\times 3/8\pi$ (ref. [4]); ×, STEWART *et al.* (ref. [6]); ●, this experiment; – – –, GUNN and IRVING, $1/\mu = 2.6$ fm (ref. [10]).

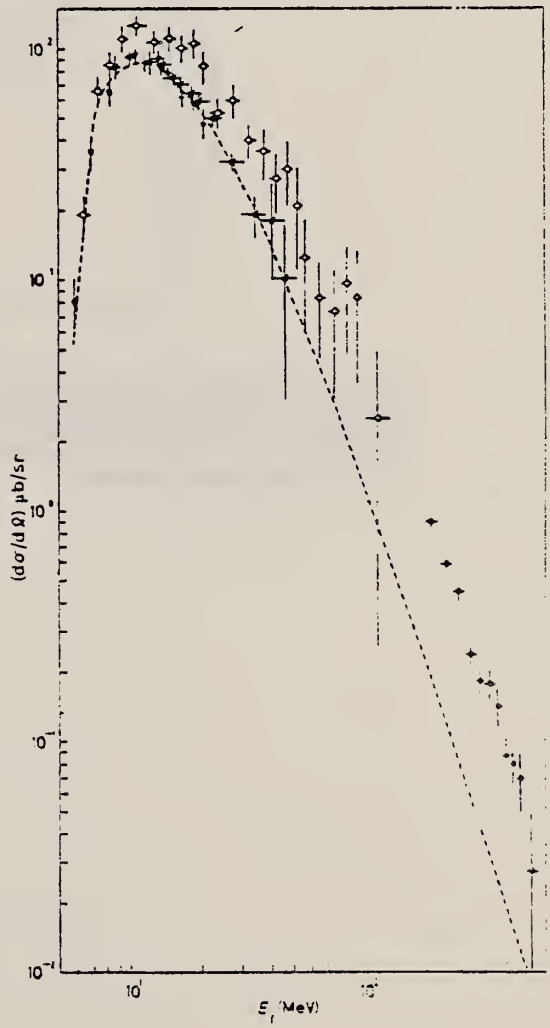

REF.

B. T. Chertok, E. C. Jones, W. L. Bendel and L. W. Fagg
Phys. Rev. Letters 23, 34 (1969)

ELEM. SYM.	A	Z
He	3	2

METHOD

REF. NO.	
69 Ch 1	egf

REACTION	RESULT	EXCITATION ENERGY	SOURCE		DETECTOR		ANGLE
			TYPE	RANGE	TYPE	RANGE	
E,E/	ABX	5-20	D	57	MAG-D	28-56	180

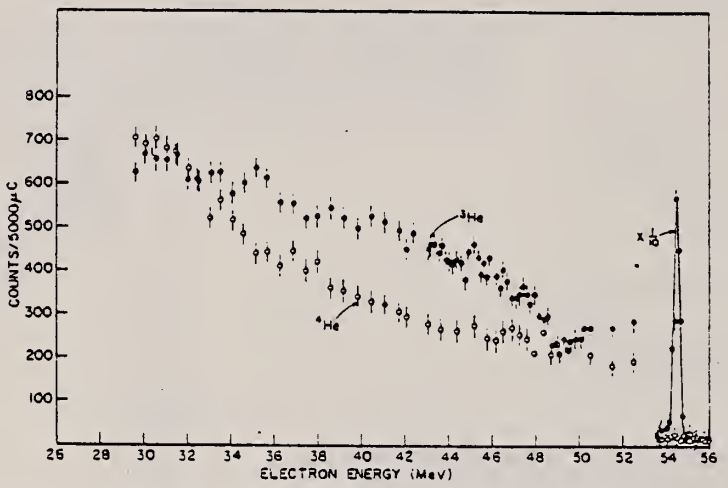

FIG. 1. The electron-scattering spectra of ^{3}He and ^{4}He at $E_0 = 56.6$ MeV, $\theta = 178.9°$, and a resolution $\Delta p/p = 0.5\%$. The data are from three overlapping runs which have been normalized to 5000 μC per point, 4.4-atm gas-target pressure, and equal elastic-peak areas. The variation of the solid angle and efficiency of the plastic scintillators with energy, which would tend to reduce the number of lower energy electrons, has not been folded in. The error bars are from counting statistics.

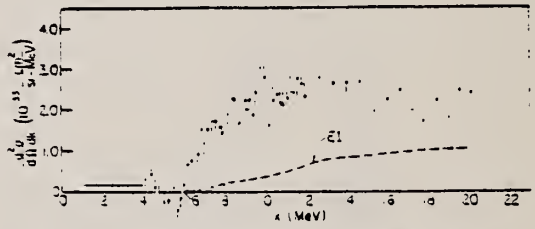

FIG. 2. The $M1$ electroexcitation of ^{3}He plotted versus nuclear excitation energy k. The radiative tail from both the elastic peak and the $M1$ continuum is unfolded from Fig. 1 after first removing the background, i.e., ^{3}He−^{4}He, and correcting for the solid angle and efficiency dependency on E. Next the magnetic bremsstrahlung and $E1$ electroexcitation are removed. The magnitude of the latter is computed from Eq. (3) and shown by the dashed line. The error bars are from counting statistics. We estimate the overall uncertainty to be ±25% per point.

REF. B. T. Chertok, E. C. Jones, W. L. Bendel, L. W. Fagg, H. F. Kaiser and S. K. Numrich
PICNS-69 Proceedings of the Third International Conference on High Energy Physics and Nuclear Structure. New York City, September 8-12, 1969, p.60.

ELEM. SYM.	A	Z
He	3	2

METHOD

REF. NO. 69 Ch 2 egf

REACTION	RESULT	EXCITATION ENERGY	SOURCE		DETECTOR		ANGLE
			TYPE	RANGE	TYPE	RANGE	
E,E/	SPC	0-14	D	56	MAG-D	40-56	180

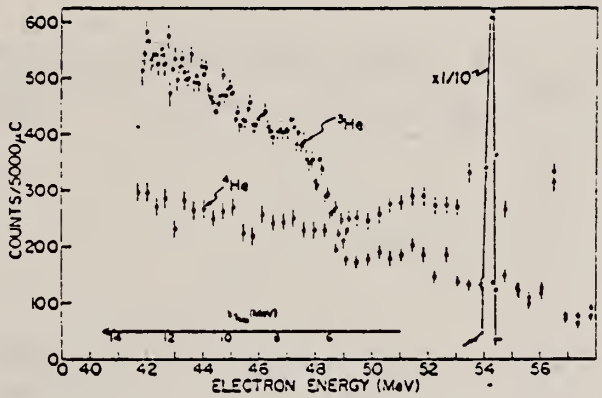

The electron scattering spectra are presented for ^{3}He and ^{4}He at 56.5 MeV, $\theta = 178.9°$ and a resolution $\Delta p/p = 0.5\%$.

REF. P. Picozza, C. Schaerf, R. Scrimaglio, G. Goggi, A. Piazzoli, and D. Scannicchio
PICNS-69 Proceedings of the Third International Conference on High Energy Physics and Nuclear Structure, Columbia University New York City, Sept. 8-12, 1969.

ELEM. SYM.	A	Z
He	3	2

METHOD

REF. NO. 69 Pi 3 egf

REACTION	RESULT	EXCITATION ENERGY	SOURCE		DETECTOR		ANGLE
			TYPE	RANGE	TYPE	RANGE	
G,P	ABX	200-500	C	999	TEL-D		90

999 = 1 GEV

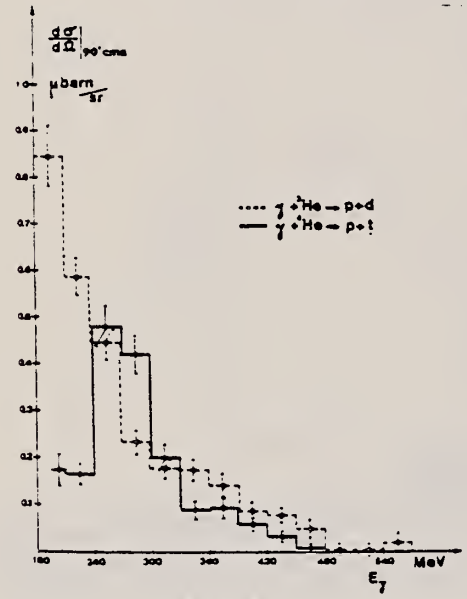

Fig. 1

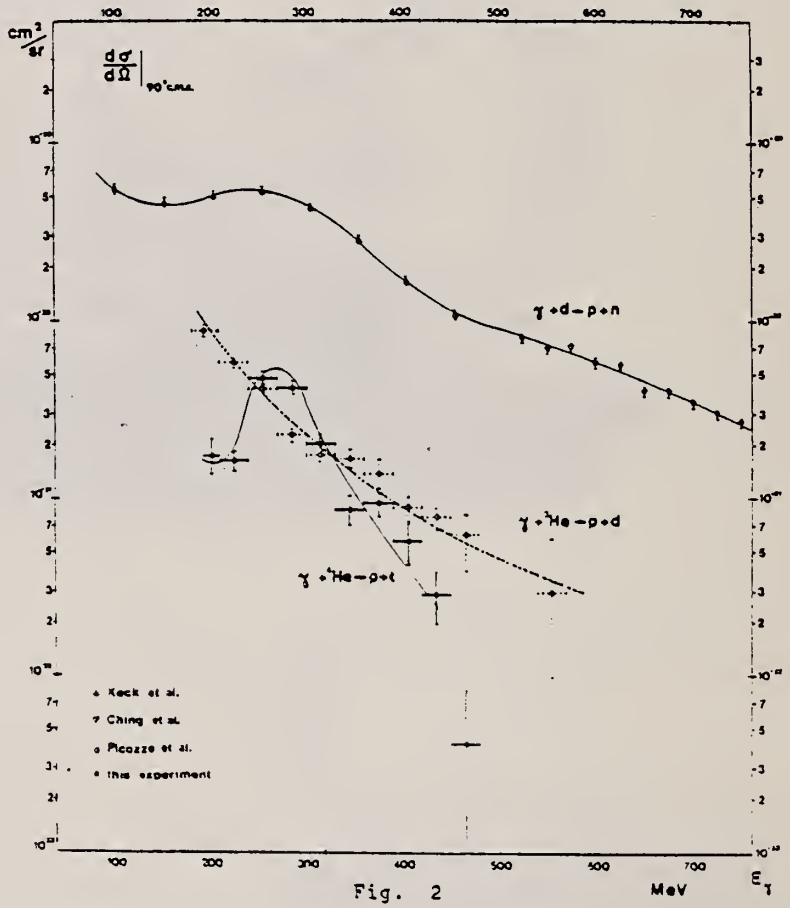

Fig. 2

REF.

G. M. Bailey, G. M. Griffiths, M. A. Olivo and R. L. Helmer
Can. J. Phys. 48, 3059 (1970)

ELEM. SYM.	A	Z
He	3	2

METHOD

REF. NO.	
70 Ba 2	hmg

REACTION	RESULT	EXCITATION ENERGY	SOURCE		DETECTOR		ANGLE
			TYPE	RANGE	TYPE	RANGE	
P,G	ABX	5-7	D	0-2	NAI-D		DST
				(0-1.1)			

Assume $\frac{d\sigma}{d\Omega} = a + b \sin^2\theta(1 + \beta \cos\theta)$

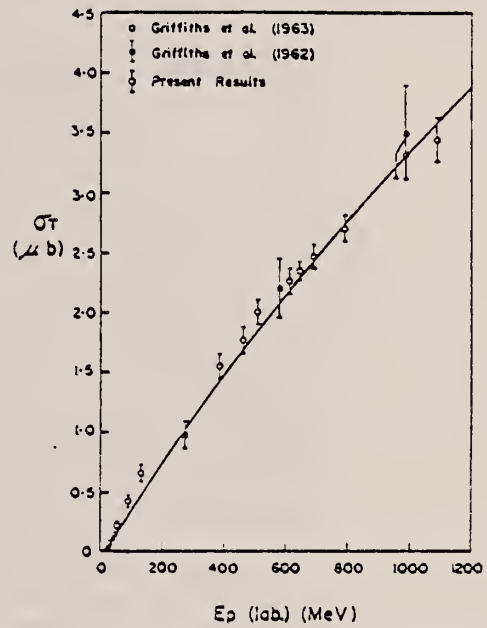

FIG. 1. Total cross section (σ_T) for the nonresonant reaction $D(p,\gamma)^3He$ below 1.2 MeV. The solid curve corresponds to the theoretical calculations of Wölfli *et al.* (1967) which assume a Gunn-Irving wave function for ^3He with parameters μ^{-1} = 2.5 fm, δ = 0.07.

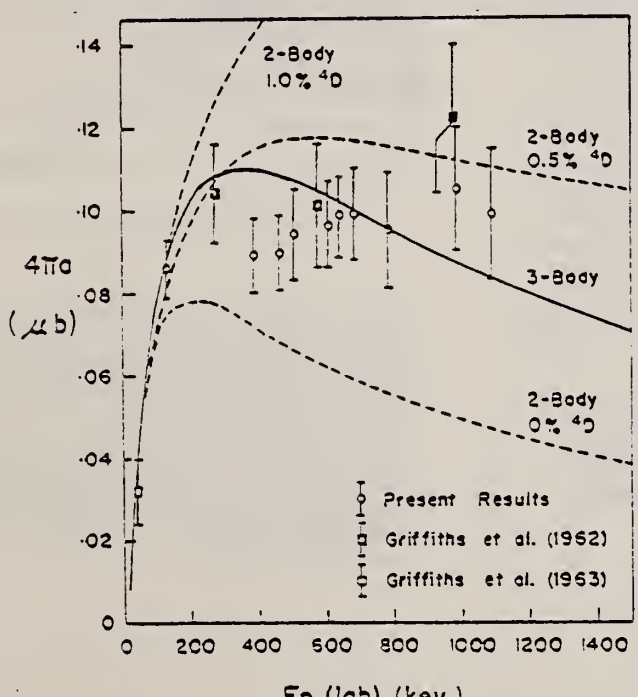

FIG. 2. The energy dependence of the isotropic component of the total cross section ($4\pi a$) for the $D(p,\gamma)^3He$ reaction below 1.5 MeV. The solid curve corresponds to the three-body calculations of Wölfli cited in Fig. 1. The dotted curves correspond to approximate two-body calculations by Bailey *et al.* (1967) and serve to illustrate the sensitivity of this cross section to inclusion of small ^4D-state probabilities in the ^3He ground state.

REF. B. D. Belt, C. R. Bingham, M. L. Halbert, A. van der Woude
Phys. Rev. Letters 24, 1120 (1970)

ELEM. SYM.	A	Z
He	3	2

METHOD

REF. NO. 70 Be 4 hmg

REACTION	RESULT	EXCITATION ENERGY	SOURCE TYPE	SOURCE RANGE	DETECTOR TYPE	DETECTOR RANGE	ANGLE
D,G	ABX	12.15	D	19,29	MAG-D		DST
		(12.1),15.3)	(19.8,29.6)				

DEUT. BEAM

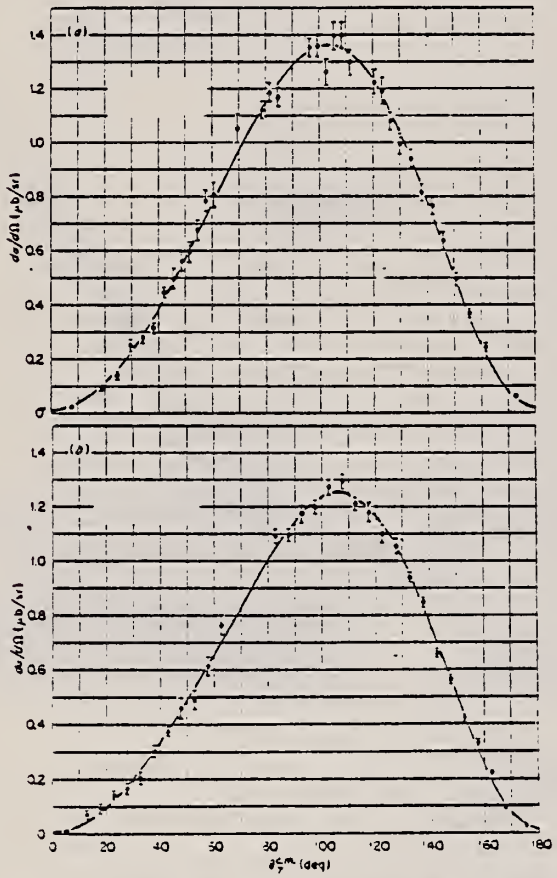

FIG. 1. Center-of-mass cross sections for $H(d,{}^3He)\gamma$ as a function of the c.m. angle between the γ ray and the deuteron. The deuteron bombarding energy was 19.8 MeV for (a) and 29.6 MeV for (b). The errors shown do not include the uncertainty in the absolute cross section.

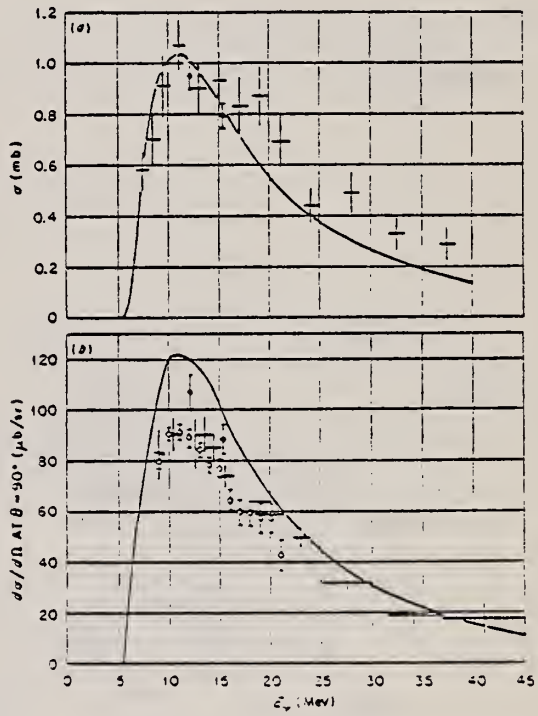

FIG. 2. Comparison of cross sections for photodisintegration of ^3He as a function of γ-ray energy. The full points are from the present experiment and were obtained by using detailed balance. The curves are theoretical calculations from Ref. 1. (a) Total cross sections. The crosses are from Ref. 3. (b) 90° lab cross sections. The crosses are from Ref. 4 and the open points from Ref. 6. The curve is for 90° proton angle. The present results are given for 90° lab proton angle with respect to the γ ray, i.e., ~88° c.m. between the deuteron and gamma.

REF. B. L. Berman, S. C. Fultz, and P. F. Yergin
Phys. Rev. Letters 24, 1494 (1970)

ELEM. SYM.	A	Z
He	3	2

METHOD

REF. NO. 70 Be 6 hmg

REACTION	RESULT	EXCITATION ENERGY	SOURCE		DETECTOR		ANGLE
			TYPE	RANGE	TYPE	RANGE	
G,N	ABX	8-30	D	8-30	MOD-I		4PI

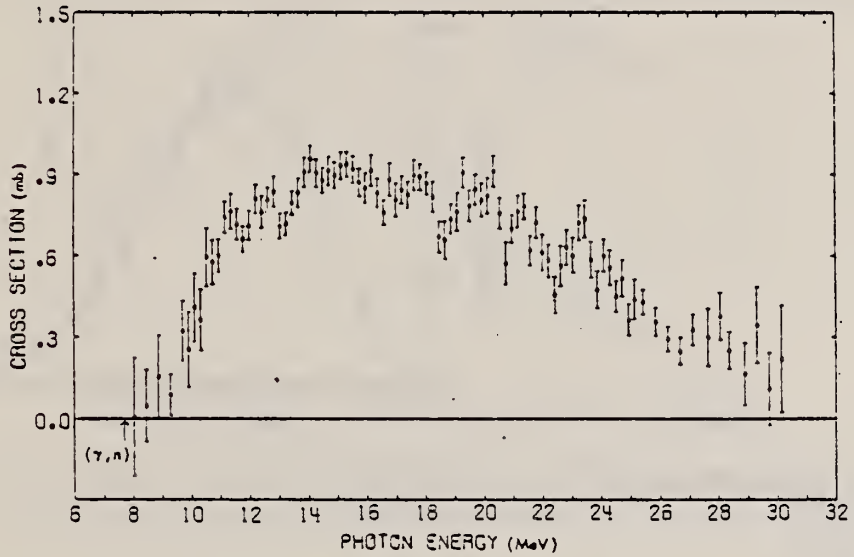

FIG. 1. Photoneutron cross section for He^3.

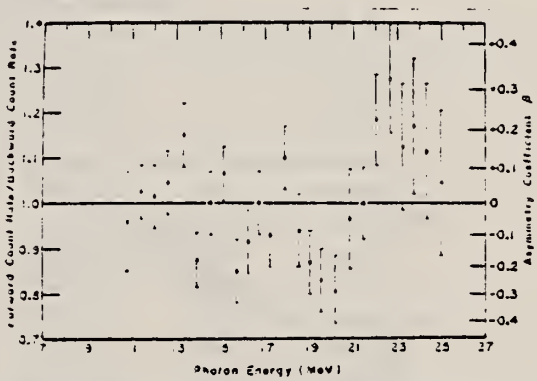

FIG. 2. Fore-aft asymmetry of the photoneutrons. The asymmetry coefficient β is computed on the assumption that the angular distribution is given by $\sin^2\vartheta(1+\beta\cos\vartheta)$.

REF. H. Bock and H. Walenta
Z. Physik 238, 56 (1970)

ELEM. SYM.	A	Z
He	3	2

METHOD

REF. NO.	
70 Bo 3	egf

REACTION	RESULT	EXCITATION ENERGY	SOURCE		DETECTOR		ANGLE
			TYPE	RANGE	TYPE	RANGE	
G,P	NOX	16-26	C	33	SPK-I		DST

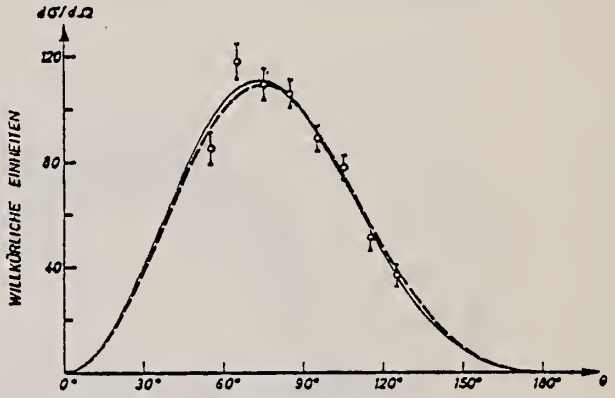

Fig. 6. Winkelverteilung

Tabelle 2. *Koeffizienten der Winkelverteilung (für E_x = 16 bis 27 MeV)*

a/b	$0{,}00 \pm 0{,}14$
β	$0{,}77^{+0{,}14}_{-0{,}07}$
γ	$0{,}00 \pm 0{,}30$

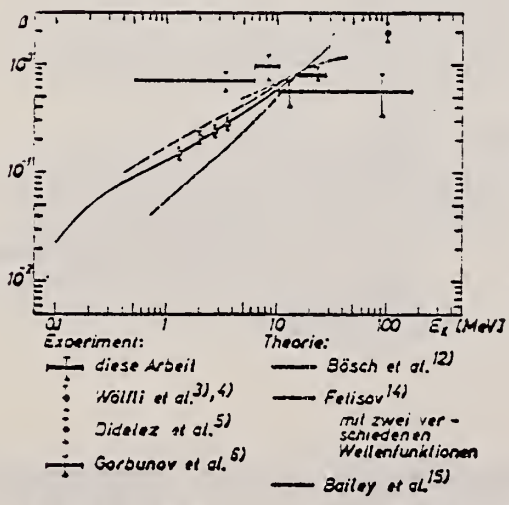

Fig. 7. Experimentelle und theoretische Werte von β

[3] Wölfli, W., Bösch, R., Lang, J., Marmier, P.: Phys. Letters 22, 75 (1966).

[4] Wölfli, W., Bösch, R., Lang, J., Marmier, P.: Helv. Phys. Acta 40, 946 (1967).

[5] Didelez, J.P., Langevin-Joliot, H., Maric, Z., Radojevic, V.: Eingesandt fur Nuclear Physics.

[6] Gorbunov, A.N., Varfolomeev, A.T.: Phys. Letters 11, 137 (1964) - Fetisov, V.N., Gorbunov, A.N., Varfolomeev, A.T.: Nucl. Phys. 71, 305 (1965).

[12] Bösch, R., Lang, J., Müller, R., Wölfli, W.: Helv. Phys. Acta 38, 753 (1965).

[14] Fetisov, V.N.: Nucl. Phys. 98, 437 (1967).

[15] Bailey, G.M. Griffiths, G.M., Donnelly, T.W.: Phys. Letters 24B, 222 (1967); Nucl. Phys. A94, 502 (1967).

REF.

J. P. Didelez, H. Langevin-Joliot, Z. Maric and V. Radojevic
Nucl. Phys. A143, 602 (1970)

ELEM. SYM.	A	Z
He	3	2

METHOD

REF. NO.: 70 Di 1 | egf

REACTION	RESULT	EXCITATION ENERGY	SOURCE		DETECTOR		ANGLE
			TYPE	RANGE	TYPE	RANGE	
P,G	ABX	106	D	156	MAG-D	33-74	DST

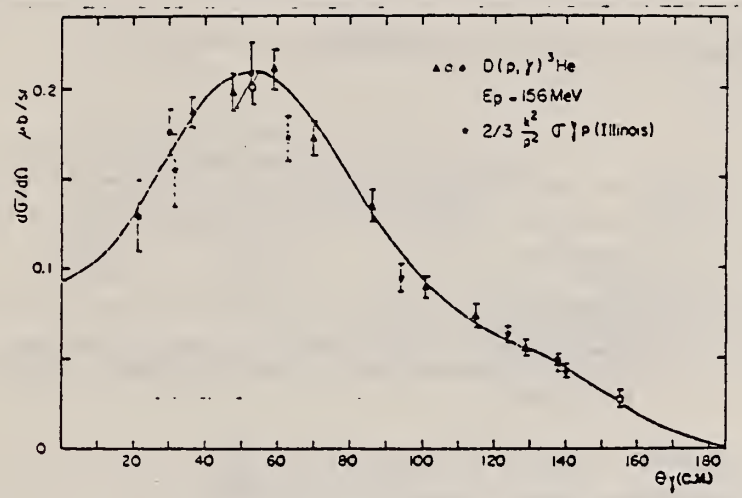

Fig. 4. Differential cross section for the $D(p,\gamma)^3He$ reaction at 156 MeV. Square, triangle and circle points correspond to three different targets. Dashed points are deduced by detailed balance procedure from the experimental data of ref. [13]). The solid curve corresponds to the least-square fit eq. (5).

TABLE I

Differential cross sections in lab and c.m. for the $D(p,\gamma)^3He$ reaction at 156 MeV

θ_γ (lab)	$(d\sigma/d\Omega)$ (lab) 10^{-1} (μb/sr)	θ_γ (c.m.)	$(d\sigma/d\Omega)$ (c.m.) 10^{-1} (μb/sr)
17.5	1.86 ± 0.25	21.1	1.29 ± 0.2
25	2.46 ± 0.2	30.0	1.76 ± 0.15
30	2.46 ± 0.1	36.0	1.87 ± 0.08
40	2.46 ± 0.15	47.6	1.98 ± 0.1
45	2.62 ± 0.12	53.3	2.04 ± 0.1
50	2.48 ± 0.14	58.9	2.11 ± 0.11
60	1.9 ± 0.1	69.9	1.72 ± 0.09
75	1.37 ± 0.09	85.8	1.35 ± 0.08
90	0.81 ± 0.05	100.9	0.89 ± 0.06
105	0.61 ± 0.05	115.2	0.73 ± 0.06
120	0.42 ± 0.04	129.0	0.55 ± 0.04
130	0.36 ± 0.04	138.0	0.47 ± 0.05
150	0.19 ± 0.04	155.0	0.27 ± 0.05

REF.

S. K. Kundu, Y. M. Shin and G. D. Wait
Nucl. Phys. A171, 384 (1971)

ELEM. SYM.	A	Z
He	3	2

METHOD

REF. NO.: 71 Ku 3 — egf

REACTION	RESULT	EXCITATION ENERGY	SOURCE		DETECTOR		ANGLE
			TYPE	RANGE	TYPE	RANGE	
E,D	ABX	13-45	D	86	MAG-D		DST

$$\left(\frac{d\sigma}{d\Omega}\right)_{el} = \bar{a} + \bar{b}\,\sin^2\theta + \bar{c}\,\cos\theta\,\sin^2\theta + \bar{d}\,\sin^2\theta\,\cos^2\theta + \bar{e}\,\cos\theta$$

TABLE 1
Comparison of the integrated cross sections up to $E_\gamma = 40$ MeV

	Ref. [2] [a]	Ref. [3] [b]	Ref. [5]	Present work
[c] σ_{int} (MeV · mb)	13.0	14.0 ±1.4	19.7 ±1.4	17.6 ±1.5
[c] σ_{-1} (mb)	0.87	10.1±0.1	1.23±0.09	1.22±0.12

[a]) Results extrapolated to 40 MeV.
[b]) Quoted from ref. [3]). The authors of ref. [3]) gave a value 16.5 MeV · mb. assuming an angular distribution $W(\theta) = 0.03 + \sin^2\theta(1 + 0.66\cos\theta + 0.46\cos^2\theta]$.
[c]) Up to 40 MeV.

[3] J. Stewart, R. Morrison and J. O'Connell, Phys. Rev. 138, B372 (1964).
[5] V. Fetisov, A. Gorbunov and A. Varfolomeev, Nucl. Phys. 71 (1965) 305.
[13] B. D. Belt, C. R. Bingham, M. L. Halbert and A. Van der Woude, Phys. Rev. Lett. 24, 1120 (1970).

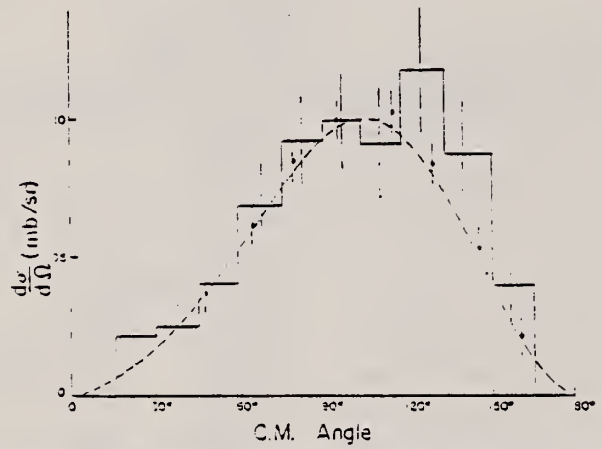

Fig. 5. Comparison of angular distribution of deuterons from the reaction ^{3}He(γ, d)^{1}H with other experimental results. Symbols used are: ⎯⎯ for ref. [5]) at 12-16 MeV, --- for ref. [13]) at 15.3 MeV and | for the present experiment at 15 MeV.

[2] B. Berman, L. Koester, Jr. and J. Smith, Phys. Rev. 133 (1963) B117.

(continued)

16
B. F. Gibson, Nucl. Phys. B2 (1967) 501.
17
U. Eichmann, Z. Phys. 175 (1963) 115.
19
L. M. Delves, Nucl. Phys. 29 (1962) 268.

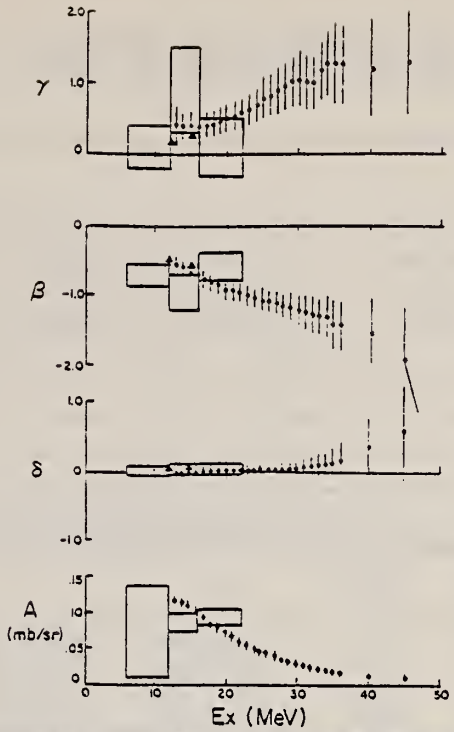

Fig. 3. Energy dependence of the coefficients in the angular distribution of deuterons from the reaction $^3He(\gamma, d)^1H$. Results from refs. [5]) and [13]) are also plotted. Symbols used are: □ for ref. [5]), ↑ for ref. [13]) and ¦ for the present experiment. $A = b$, $\delta = a/b$, $\beta = c/b$, $\gamma = d/b$ in the text.

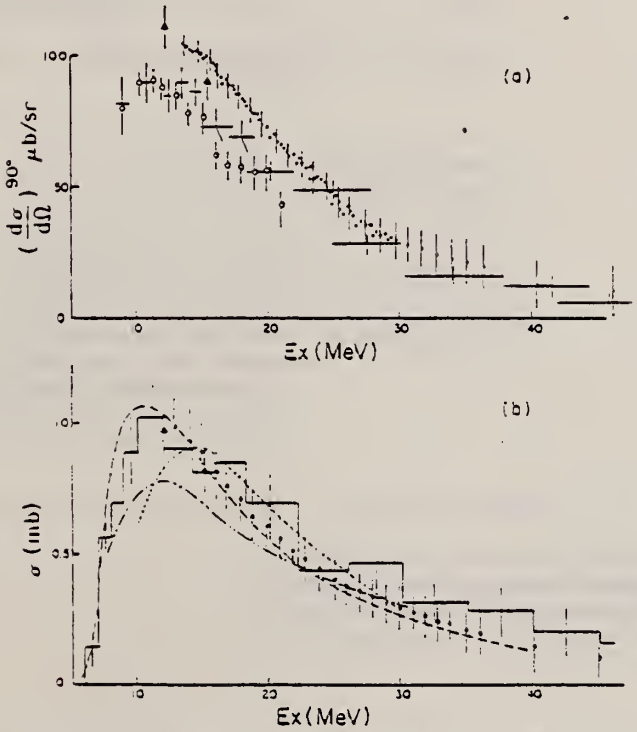

Fig. 4a. Comparison of 90° differential cross section of the reaction $^3He(\gamma, d)^1H$ with other experimental results. Symbols used are: › for ref. [2]), — for ref. [3]), ↑ for ref. [12]) and ¦ for the present experiment.

Fig. 4b. Comparison of the total cross section of the reaction $^3He(\gamma, d)^1H$ with other experimental and theoretical results. Symbols used are: ⊓ for ref. [5]), ¦ for ref. [13]), --- for ref. [19]), -.-.- for ref. [16]) (dipole and quadrupole), ... for ref. [17]) ($\delta = .1$) and ¦ for the present experiment.

REF. A. Van der Woude, M.L. Halbert, C.R. Bingham, B.D. Belt
Phys. Rev. Letters 26, 909 (1971)

ELEM. SYM.	A	Z
He	3	2

METHOD

REF. NO. 71 Va 1 hmg

REACTION	RESULT	EXCITATION ENERGY	SOURCE		DETECTOR		ANGLE
			TYPE	RANGE	TYPE	RANGE	
D,G	ABX	12-21	D	20-45	MAG-D		DST

SEE 72HA2

Table I. Results of the angular-distribution measurements for $d+p \rightarrow {}^3\mathrm{He}+\gamma$.

E_d (MeV)	E_{exc} (MeV)	a/b	β	γ	b (μb/sr)	$\sigma_{capture}$ (μb)
19.8	12.1	0.013 ± 0.007	−0.49 ± 0.03	0.16 ± 0.05	1.27 ± 0.09	11.18 ± 0.77
29.6	15.3	0.008 ± 0.003	−0.59 ± 0.02	0.25 ± 0.04	1.14 ± 0.08	10.17 ± 0.67
41.1	19.2	0.08 ± 0.02	−0.27 ± 0.03	0.39 ± 0.06	1.10 ± 0.09	11.04 ± 0.80
45.2	20.6	0.11 ± 0.03	−0.30 ± 0.06	$0.44^{+0.1}_{-0.2}$	1.30 ± 0.11	13.55 ± 1.00

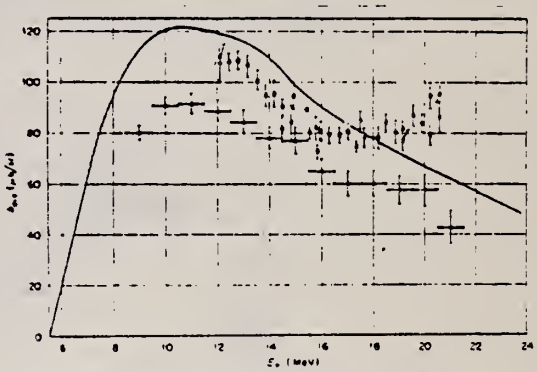

FIG. 1. Variation of b with excitation energy. Our results (closed square, open circle, open square) are given in terms of the two-body photodisintegration. The energy spread associated with each of these points is ≈0.015 MeV, while the uncertainty of the abscissa is about ≈0.03 MeV. The photodisintegration data of Ref. 11 are shown by closed triangles. The curve is a theoretical calculation from Ref. 10.

[10] I. M. Barbour and A. C. Phillips, Phys. Rev. C 1, 165 (1970).

Evidence for a broad resonance in the ^{3}He system has been found in the excitation function for the radiative capture of deuterons by protons. Supporting evidence is provided by the behavior of the angular distributions. The resonance is centered at (19.5 ± 0.5)-MeV excitation, has a width of about 2 MeV, and is most likely characterized by $(L^\pi, S, T) = (1^-, \frac{1}{2}, \frac{1}{2})$.

(continued)

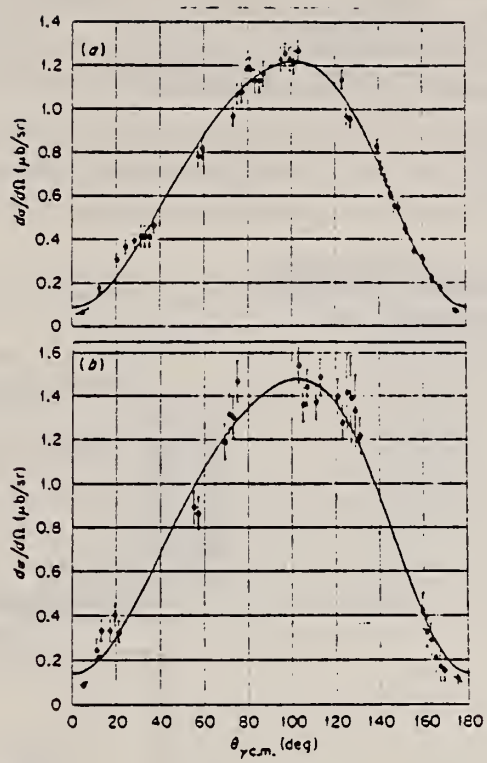

FIG. 2. Center-of-mass cross sections for H(d, ^{3}He)γ as a function of the c.m. angle between the γ ray and the deuteron. The deuteron bombarding energies were 41.1 MeV for (a) and 45.2 MeV for (b), corresponding to excitation energies of 19.2 and 20.6 MeV, respectively. The errors shown do not include the uncertainty (±8%) in the absolute cross section. The curves were calculated from Eq. (1) with the parameters of Table I. The effect of the finite bin size and energy resolution is shown near 0° and 180° by the short line segments.

REF. C. C. Chang, E. M. Diener, and E. Ventura
Phys. Rev. Letters 29, 307 (1972)

ELEM. SYM.	A	Z
He	3	2

METHOD

REF. NO. 72 Ch 3 hmg

REACTION	RESULT	EXCITATION ENERGY	SOURCE		DETECTOR		ANGLE
			TYPE	RANGE	TYPE	RANGE	
P,G	RLX	12 - 18	D	10 - 18	NAI-D		90

616

The excitation function of the capture reaction $^2H(p,\gamma)^3He$ has been measured in the range $E_p = 10-17.5$ MeV. An anomaly was observed and is interpreted as a broad resonance in ^3He at an excitation energy of 14.5 ± 0.5 MeV with a width of about 2 MeV.

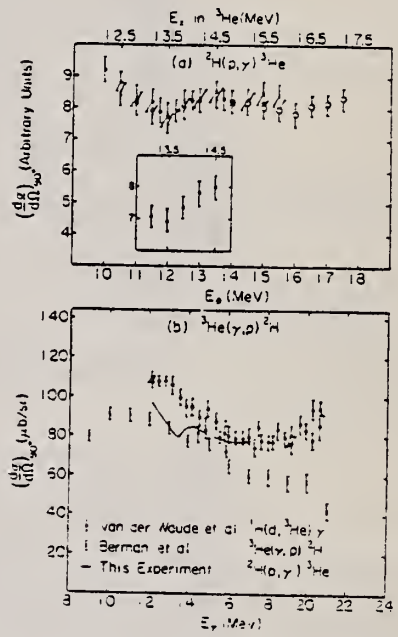

FIG. 2. (a) 90° yield curve for $^2H(p,\gamma)^3He$ obtained by fitting an appropriate line shape to each γ spectrum gated by the "γ window." Different symbols correspond to different runs. Inset, results when the gas-out runs were subtracted from the gas-in runs for $E_p = 11.5$ to 13.5 MeV; (b) Comparison of the present results, converted to photodisintegration data, with those of Refs. 9 and 13.

REF.

F. L. Fabbri, P. Picozza & C. Schaerf
Lettere al Nuovo Cimento 3, 63 (1972)

ELEM. SYM.	A	Z
He	3	2

METHOD

REF. NO.: 72 Fa 3 egf

REACTION	RESULT	EXCITATION ENERGY	SOURCE		DETECTOR		ANGLE
			TYPE	RANGE	TYPE	RANGE	
$G,P	NOX	170-290	D	170-290	TEL-D		90

POL ASYM PARAM G

TABLE I. – *Experimentally measured values of the asymmetry parameter and the calculated polarization of the gamma-ray beams.*

E_γ (MeV)	A/90° c.m.s.	Photon polarizatiou	
		First run	Second run
170÷190	-0.41 ± 0.10	0.24 ± 0.01	—
190÷210	-0.40 ± 0.08	0.32 ± 0.01	0.20 ± 0.01
210÷230	-0.35 ± 0.05	0.40 ± 0.01	0.25 ± 0.01
230÷250	-0.28 ± 0.05	0.46 ± 0.01	0.31 ± 0.01
250÷270	-0.31 ± 0.07	—	0.38 ± 0.01
270÷290	-0.28 ± 0.07	—	0.44 ± 0.01

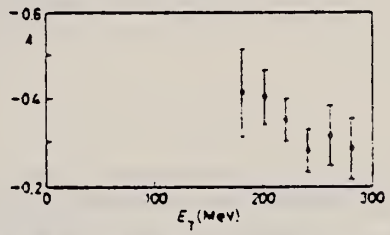

Fig. 1. – The asymmetry parameter A from Table I: $A = (d\sigma_\perp - d\sigma_\parallel)/(d\sigma_\perp + d\sigma_\parallel)$. $\gamma + {}^3He \to p + d$. $\vartheta^* = 90°$ c.m.s.

$$A = \frac{d\sigma_\perp - d\sigma_\parallel}{d\sigma_\perp + d\sigma_\parallel} = -\frac{b_1}{a_{-1} - b_1} = -\frac{1}{1 - a_{-1}/b_1}.$$

where

$d\sigma_\parallel$ is the differential cross-section at 90° in the c.m.s. measured in the plane of linear polarization of the gamma-ray beam.

$d\sigma_\perp$ is the differential cross-section at 90° in the c.m.s. measured in the plane perpendicular to the plane of polarization of the gamma-ray beam.

b_1 is the contribution to the cross-section from the E_1 transition.

a_{-1} is the contribution to the cross-section from the M_1 transition.

REF.

M.L. Halbert and E.K. Warburton
PICNS-72 - Proceedings of International Conference on Few Particle Problems in the Nuclear Interaction, UCLA (Aug. 28-Sept. 1, 1972)

ELEM. SYM.	A	Z
He	3	2

METHOD

REF. NO.	
72 Ha 2	egf

REACTION	RESULT	EXCITATION ENERGY	SOURCE		DETECTOR		ANGLE
			TYPE	RANGE	TYPE	RANGE	
P,G	RLX	14-23	D	14-26	NAI-D		DST

CORRECTS 71VA1

ABSTRACT

An experimental study of the reaction p + d → ^{3}He + γ between E_p = 14.0 and 25.5 MeV gave no indication of a resonance in ^{3}He in the excitation energy range from 14.9 to 22.5 MeV.

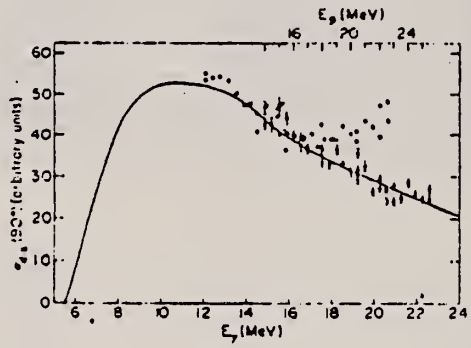

Fig. 1. Excitation function for ^{3}He(γ,d) at 90°. Data from this experiment (•) and Ref. 1 (o) were converted to photodisintegration by detailed balance. The curve is from Ref. 8. Normalizations were adjusted for best overlap in the 14-16 MeV region.

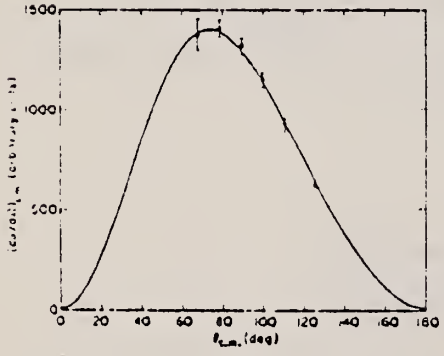

Fig. 2. Angular distributions for D(p,γ) near 15 MeV. The points are the present results. The curve is from Ref. 12.

[1] A. van der Woude, M.L. Halbert, C.R. Bingham, B.D. Belt, Phys. Rev. Lett. 26, 909 (1971).

[8] I.M. Barbour and A.C. Phillips, Phys. Rev. C1, 165 (1970).

[12] B.D. Belt, C.R. Bingham, M.L. Halbert, and A. van der Woude, Phys. Rev. Lett. 24, 1120 (1970).

REF.

N.M. O'Fallon, L.J. Koester,Jr., and J.H. Smith
Phys. Rev. C5, 1926 (1972)

ELEM. SYM.	A	Z
He	3	2

METHOD

REF. NO.: 72 O'Fa 2 hmg

REACTION	RESULT	EXCITATION ENERGY	SOURCE		DETECTOR		ANGLE
			TYPE	RANGE	TYPE	RANGE	
G,P	ABX	40-150	C	250	TEL-D		DST

P AND D COINC

TABLE III. Angular-distribution coefficients and total cross sections.

Incident photon energy (MeV)	Expression (2), "traditional" A (μb/sr)	B	C	Expression (3) with retardation a (μb/sr)	b	c	σ_T (μb)
42.4	14.6 ± 0.4	1.11 ± 0.13	1.13 ± 0.22	14.2 ± 0.4	0.51 ± 0.11	0.90 ± 0.22	153 ± 8
47.4	12.5 ± 0.4	1.11 ± 0.14	1.14 ± 0.24	12.2 ± 0.4	0.46 ± 0.11	0.86 ± 0.23	130 ± 7
52.5	10.5 ± 0.4	1.18 ± 0.17	1.23 ± 0.29	10.2 ± 0.4	0.48 ± 0.14	0.92 ± 0.28	110 ± 6
60	7.45 ± 0.31	1.41 ± 0.20	1.65 ± 0.33	7.19 ± 0.32	0.60 ± 0.16	1.30 ± 0.32	84 ± 4
70	5.07 ± 0.21	1.64 ± 0.23	2.05 ± 0.37	4.83 ± 0.22	0.72 ± 0.19	1.66 ± 0.36	61 ± 4
80	3.56 ± 0.16	1.81 ± 0.27	2.38 ± 0.44	3.37 ± 0.16	0.76 ± 0.22	1.94 ± 0.44	45 ± 3
100	2.09 ± 0.13	1.81 ± 0.32	2.41 ± 0.57	1.98 ± 0.13	0.67 ± 0.25	1.95 ± 0.57	27 ± 2
109	1.75 ± 0.13	1.86 ± 0.40	2.60 ± 0.72	1.65 ± 0.13	0.62 ± 0.30	2.08 ± 0.70	23 ± 2
120	1.44 ± 0.13	1.63 ± 0.46	2.04 ± 0.84	1.37 ± 0.13	0.49 ± 0.34	1.51 ± 0.78	18 ± 2
140	1.06 ± 0.12	1.31 ± 0.56	1.16 ± 0.90	1.04 ± 0.12	0.27 ± 0.38	0.62 ± 0.76	11 ± 2

TABLE II. Differential cross sections in the c.m. system. The two angles at the head of each column are mean values at 40 and 150 MeV, respectively. The actual mean proton angle in each photon energy interval may be obtained to sufficient accuracy by a linear interpolation against photon energy.

Incident photon energy (lab system) (MeV)	dσ/dΩ (c.m. system) in μb/sr at c.m. proton angle specified 33.5–29.6°	57.2–51.3°	95.0–92.3°	127.1–122.7°	141.1–137.7°
42.4	15.5 ± 1.2	10.22 ± 0.38	12.06 ± 0.46	7.29 ± 0.47	4.42 ± 0.37
47.4	10.4 ± 1.1	14.52 ± 0.52	11.63 ± 0.42	5.56 ± 0.36	3.04 ± 0.31
52.4	9.4 ± 1.1	14.22 ± 0.46	8.75 ± 0.40	5.37 ± 0.47	3.32 ± 0.31
57.1		12.53 ± 0.39	7.40 ± 0.28	4.16 ± 0.45	
59.6	10.4 ± 0.9				3.31 ± 0.23
64.5		8.78 ± 0.57		3.04 ± 0.28	
69.5	7.07 ± 0.79		4.77 ± 0.24		1.33 ± 0.16
74.7		6.02 ± 0.34		1.53 ± 0.26	
81.5	5.30 ± 0.72		2.17 ± 0.15		1.37 ± 0.15
84.7		5.06 ± 0.32		1.98 ± 0.26	
99.0	3.88 ± 0.46	3.47 ± 0.24	1.63 ± 0.13	1.40 ± 0.16	0.88 ± 0.11
119.2	1.60 ± 0.53	2.41 ± 0.22	1.10 ± 0.13	0.73 ± 0.12	0.77 ± 0.12
139.3	1.56 ± 0.53	1.49 ± 0.28	0.99 ± 0.12	0.66 ± 0.14	0.27 ± 0.07

(2) $d\sigma/d\Omega = A \sin^2\theta(1 + B\cos\theta + C\cos^2\theta)$

(3) $d\sigma/d\Omega = a \sin^2/(1 - \beta\cos\theta)^2 \ (1 + b\cos\theta + c\cos^2\theta)$

(continued)

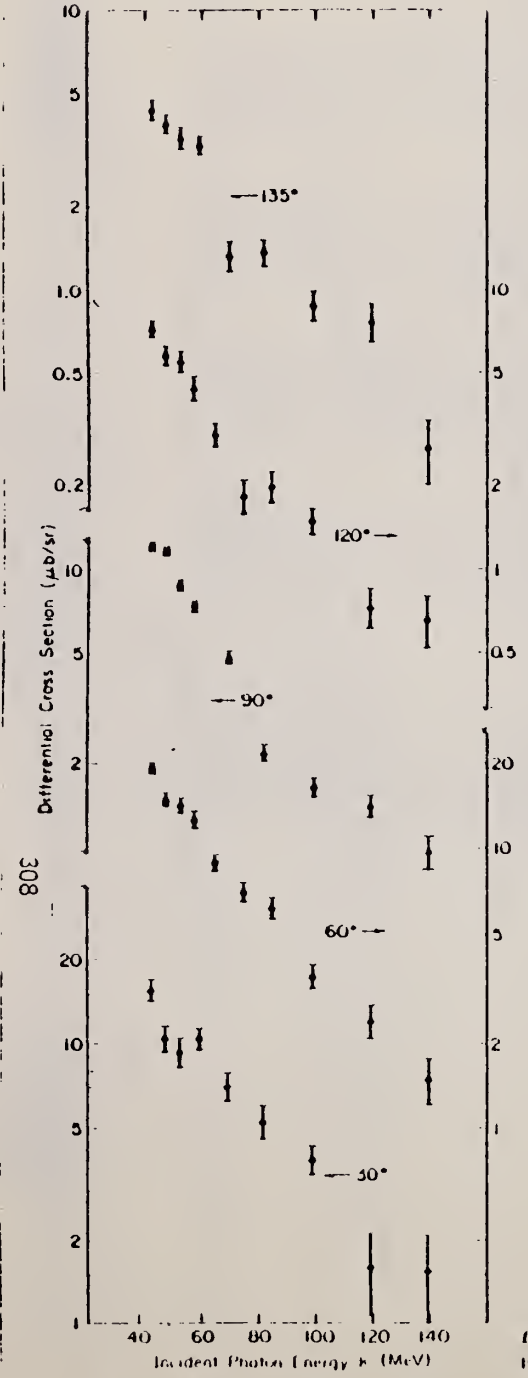

FIG. 10. Differential cross sections measured at the five proton angles of this experiment versus incident photon energy.

FIG. 11. Angular distributions for seven incident photon energy intervals centered at the energies indicated in MeV. The points are obtained by interpolation of Fig. 9. The curves are least-squares fits with Eq. (2) (dotted) and Eq. (3) (solid).

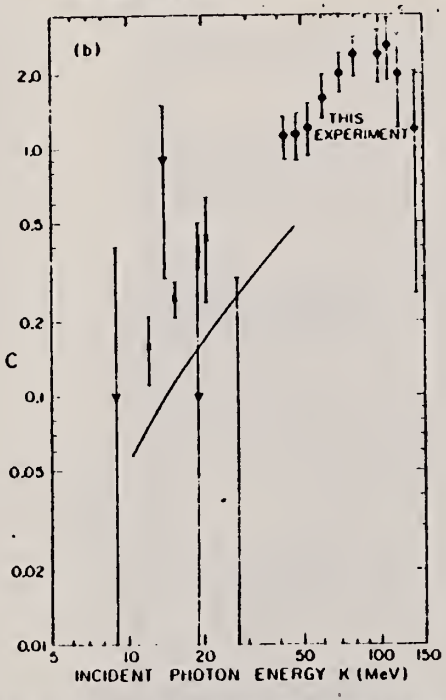

FIG. 15. Angular-distribution coefficients B (a) and C (b) in Eq. (2). Symbols are as follows: ●, this experiment; ▲, Ref. 8; ▼, Ref. 6; ×, Ref. 11; ■, Ref. 9; †, Ref. 1. Curves are theoretical, Ref. 12.

[1] L. Cranberg, Bull. Am. Phys. Soc. 3, 173 (1958).

[6] V. N. Fetisov et al., Nucl. Phys. 71, 305 (1965).

[8] W. Wolfli et al., Phys. Letters 22, 75 (1966).

[9] H. Bock et al., Z. Physik 238, 56 (1970).

[11] A. van der Woude et al., Phys. Rev. Letters 26, 909 (1971).

[12] G. M. Bailey et al., Nucl. Phys. A94, 502 (1967).

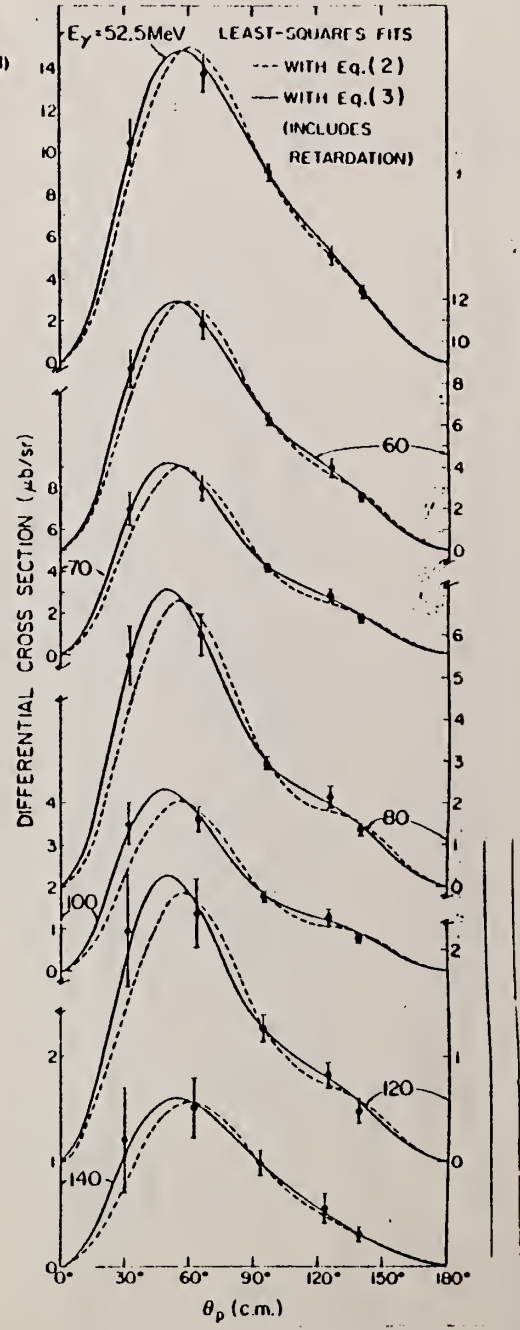

REF. Y.M. Shin, D.M. Skopik and C. Pla
PICNS-72, 481 (1972) Sendai

ELEM. SYM.	A	Z
He	3	2

METHOD

REF. NO. 72 Sh 8 hvm

REACTION	RESULT	EXCITATION ENERGY	SOURCE		DETECTOR		ANGLE
			TYPE	RANGE	TYPE	RANGE	
E,PD	RLX	19- 30	D	100	MAG-D		DST

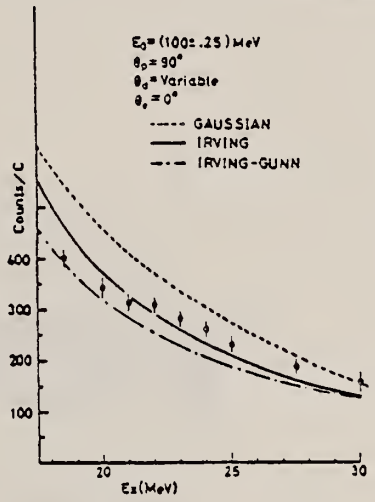

Fig. 2.
Coincidence cross sections for the reaction ^{3}He(e, pd)e' at θ_1=0° E_e=100 MeV are compared with theories.

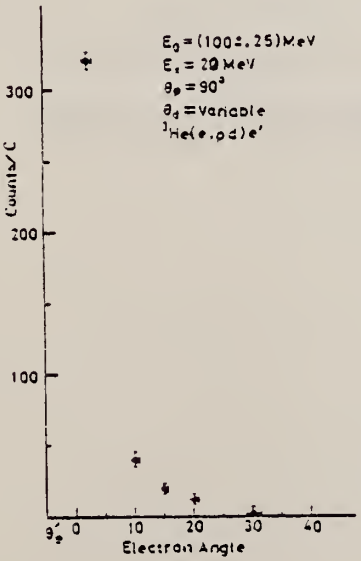

Fig. 3.
Electron angle dependence of the coincidence cross section at E_x=20 MeV.

Fig. 4.
Comparison of the experimental squared matrix elements with theories.

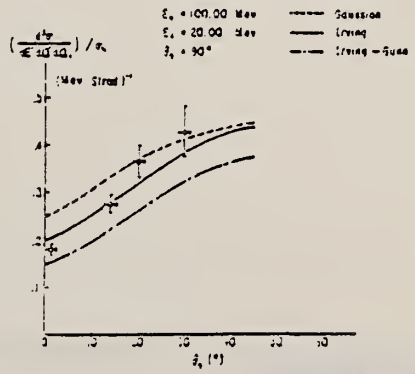

REF.

D. M. Skopik and Y. M. Shin
Can. J. Phys. 50, 392 (1972)

ELEM. SYM.	A	Z
He	3	2

METHOD

REF. NO.	
72 Sk 1	hmg

REACTION	RESULT	EXCITATION ENERGY	SOURCE		DETECTOR		ANGLE
			TYPE	RANGE	TYPE	RANGE	
E,D	RLX	16-27	D	43,87	MAG-D		DST

DETECTED D AND P

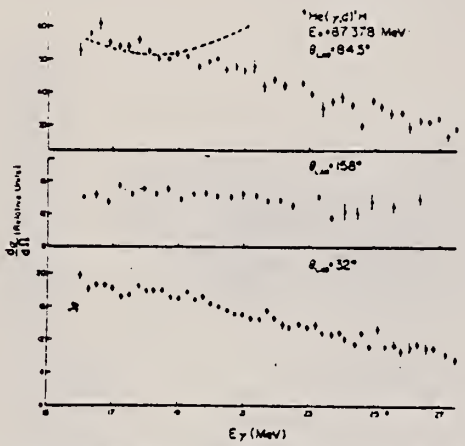

FIG. 2. Differential cross sections of the reaction ^{3}He(e,e'd)^{1}H, at an initial energy of 87.34 MeV. The dashed curve is from van der Woude *et al.* (1971).

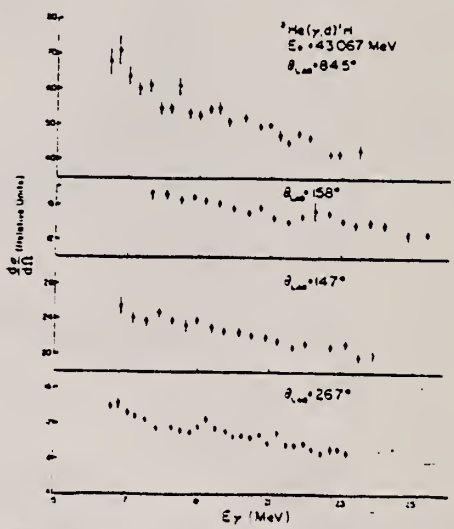

FIG. 3. Differential cross sections of the reaction ^{3}He(e,e'd)^{1}H at an initial electron energy of 43.07 MeV.

REF. Y.M. Shin, D.M. Skopik, and E.L. Tomusyak
Izv. Akad. Nauk SSSR Ser. Fiz. 37, 1863 (1973)
Bull. Acad. Sci. USSR Phys. Ser. 37, 60 (1973)

ELEM. SYM.	A	Z
He	3	2

METHOD

REF. NO.	
73 Sh 18	hmg

REACTION	RESULT	EXCITATION ENERGY	SOURCE		DETECTOR		ANGLE
			TYPE	RANGE	TYPE	RANGE	
E,E/P	SPC	18- 30	D	100	MAG-D		DST

COINC E,P

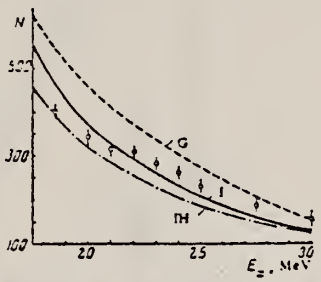

Fig. 2. Experimental and calculated heavy-particle coincidence rates from the ^{3}He(e,pd)e' reaction at E_e = 100.00 ± 0.25 MeV, θ_p = 90°, and θ_e = 0°.

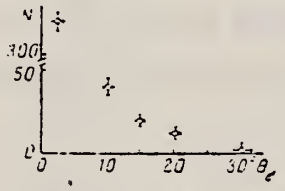

Fig. 3. Dependence of the heavy-particle coincidence rate from the ^{3}He(e,pd)e' reaction on the momentum transfer at E_x = 20 MeV (θ_p = 90°).

REF.

G. Ticcioni, S.N. Gardiner, J.L. Matthews, and R.O. Owens
Phys. Letters 46B, 369 (1973)

ELEM. SYM.	A	Z
He	3	2

METHOD

REF. NO.: 73 Ti 4 egf

REACTION	RESULT	EXCITATION ENERGY	SOURCE		DETECTOR		ANGLE
			TYPE	RANGE	TYPE	RANGE	
G,D	ABX	11- 65	C	67	MAG-D		DST

2 J.A. Hendry et al., to be published

4 G.M. Griffiths, et al., Can. J. Phys. 40, (1962) 402.

5 J.B. Warren et al., Phys. Rev. 132, 1691 (1963).

6 W. Wolfli et al., Helv. Phys. Acta 40 (1967) 946.

7 A. Van Der Woude et al., Phys. Rev. Lett. 24, Phys. Rev. Lett. 24 (1970) 1120 and 26 (1971) 909.

9 S.K. Kundu et al., Nucl. Phys. A171 (1971) 384.

10 V.N. Fetisov, Nucl. Phys. 71 (1965) 305.

11 N.M. O'Fallon et al., Phys. Rev. C5 (1972) 1926.

12 J.L. Matthews et al., Bull. Am. Phys. Soc. 18, (1973) 19.

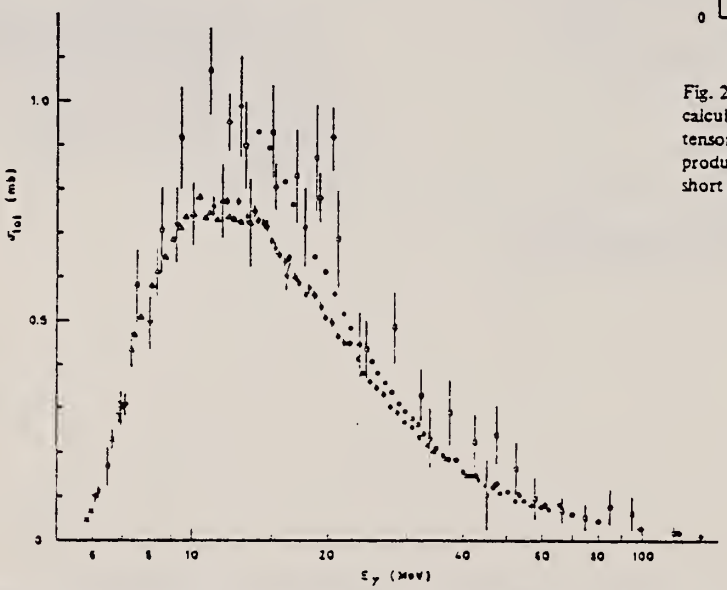

Fig. 1. The total cross section for the reaction $^3He(\gamma,d)^1H$. The data are: • this experiment, ◇ Van Der Woude et al. [7], ▫ Fetisov et al. [10], ▫ Kundu et al. [9], △ Wölfli et al. [6], ♦ O'Fallon et al. [11], × Griffiths et al. [4], ▽ Warren et al. [5], and ▪ Matthes et al. [12]. In addition to the displayed errors the results of refs. [9–11] contain additional systematic errors of ± 15%, 6% and 7% respectively. Only statistical errors in the present data are shown.

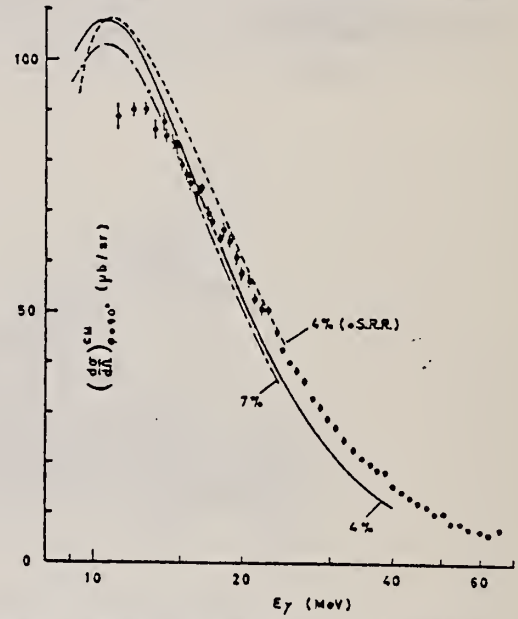

Fig. 2. The $^3He(\gamma,d)^1H$ cross section at 90° is compared with calculations by Hendry and Phillips [2]. The strength of the tensor force is indicated by the deuteron D-state probabilities produced. The dotted curve shows a modification to simulate short range repulsion between nucleon pairs.

REF. C. Tzara
PICNS-73, Vol. I, p. 573 Asilomar

EL EM. SYM.	A	Z
He	3	2

METHOD

REF. NO. 73 Tz 2 hmg

REACTION	RESULT	EXCITATION ENERGY	SOURCE		DETECTOR		ANGLE
			TYPE	RANGE	TYPE	RANGE	
G,DP	ABX	160-370	C		MAG-D		DST

DP DETECTED IN COIN

Fig. 1a

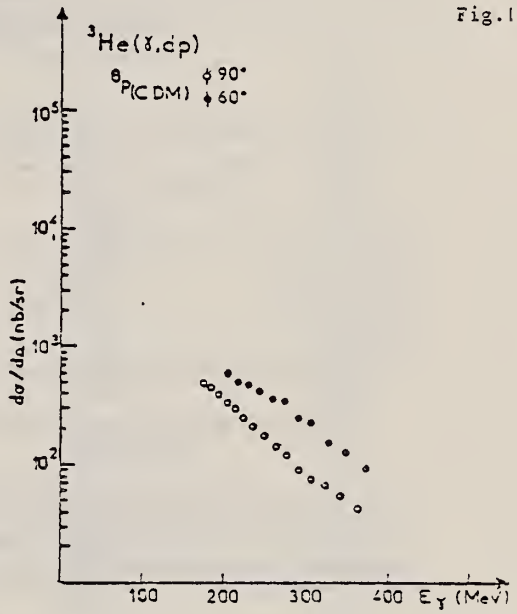

Fig. 1c

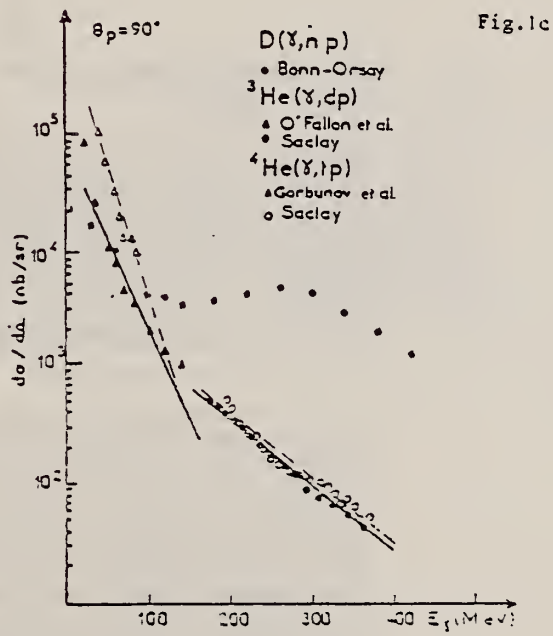

Fig. 1a, b, c.

Two-body photodisintegration cross-sections for d, ^{3}He, ^{4}He, at 60° and 90°. The cross-sections for $\gamma + {}^4\text{He} \rightarrow n + {}^3\text{He}$ at θ_n = 90° and 120° are also given.

REF.

B.L. Berman, S.C. Fultz, and P.F. Yergin
Phys. Rev. C10, 2221 (1974)

ELEM. SYM.	A	Z
He	3	2

METHOD

REF. NO. 74 Be 8 hmg

REACTION	RESULT	EXCITATION ENERGY	SOURCE		DETECTOR		ANGLE
			TYPE	RANGE	TYPE	RANGE	
G,N	ABX	7- 31	D	7- 31	BF3-I		4PI

The photoneutron cross section for ^{3}He has been measured from threshold to 30 MeV using monochromatic photons from positron annihilation in flight. The cross section reaches its maximum of about 0.95 mb at about 15 MeV. Several distinct structures are apparent, some correlated with observed fore-aft asymmetry of the photoneutrons. The integrated cross section is 13.0 MeV mb, and the $1/E$ integrated cross section is 0.77 mb. With reasonable extrapolations to higher energies this is consistent with sum-rule predictions, well within experimental uncertainties. Current theoretical calculations are capable of accounting for the over-all size and shape of the cross section, but not for the fine details of the present measurement.

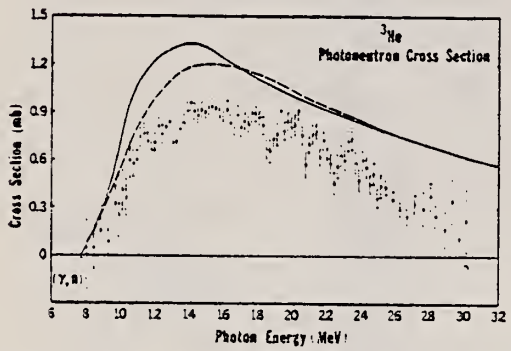

FIG. 14. ^{3}He$(\gamma,n)2p$ cross section. The points with error bars are the experimental results (as in Fig. 11). The solid curve is taken from the paper of Barbour and Phillips (Ref. 22), and the dashed curve is the result of a recent calculation by Gibson and Lehman (Ref. 28).

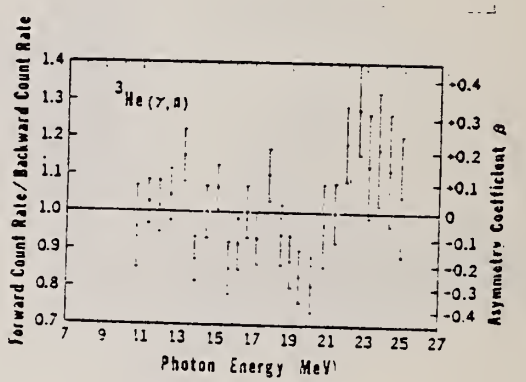

FIG. 13. Fore-aft asymmetry in neutron counting rates for the ^{3}He$(\gamma,n)2p$ reaction. The points with error bars are the ratios of counting rates in the front two quadrants to those in the back two quadrants of the neutron detector, as a function of photon energy. Backgrounds have been subtracted, so that the ratios of net neutron yields from monochromatic photons are given. The asymmetry coefficient β also is shown (right scale) on the assumption of identical angular dependence of detection efficiency of the detector halves, with zero half-to-half scattering, and that the angular distribution is given by $\sin^2\vartheta\,(1+\beta\cos\vartheta)$, so that $\beta = 3(F-B)/(F+B)$, where F is the forward count rate and B is the backward count rate.

[11] C.C. Chang, E.M. Diener, and E. Ventura, Phys. Rev. Lett. 29, 307 (1972).

[22] I.M. Barbour, A.C. Phillips, Phys. Rev. C1, 165 (1970).

[28] B.F. Gibson, private communication.

REF.

C.C. Chang, W.R. Dodge, and J.J. Murphy,II
Phys. Rev. C9, 1300 (1974)

ELEM. SYM.	A	Z
He	3	2

METHOD

REF. NO. 74 Ch 3 — hmg

REACTION	RESULT	EXCITATION ENERGY	SOURCE		DETECTOR		ANGLE
			TYPE	RANGE	TYPE	RANGE	
E,D	ABX	10- 21	D	21, 23	MAG-D		90

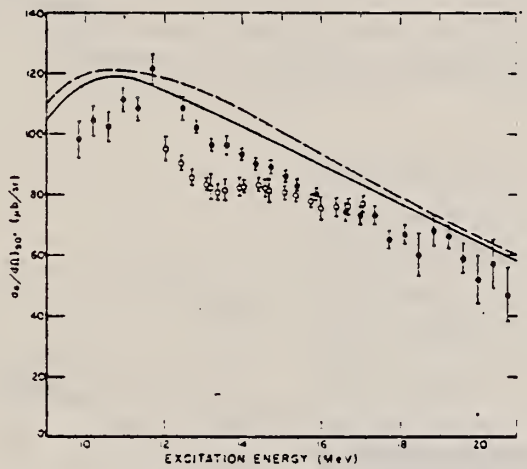

FIG. 4. The $^3He(e,d)^1H$ cross section as a function of excitation energy. The • are the results of the current work; ○ the $^3He(\gamma,d)^1H$ results of Chang, Diener, and Ventura (Ref. 2) converted to the $^3He(e,d)^1H$ reaction as explained in the text. The solid curve is the calculation of Lehman and Gibson (Ref. 5), the dashed curve that of Barbour and Phillips (Ref. 4). All cross sections are absolute. The indicated uncertainties on our results include only counting statistics.

TABLE I. Data from this experiment. All data are given in the center-of-mass system. Uncertainties are only counting statistics.

Excitation energy (MeV)	$(d\sigma/d\Omega)_{90°}$ [a] (μb/sr)
9.891	98 ± 6
10.266	104 ± 5
10.641	102 ± 4
11.016	111 ± 3
11.391	108 ± 4
11.766	120 ± 5
12.516	108 ± 4
12.891	102 ± 2
13.266	96 ± 2
13.641	96 ± 3
14.016	93 ± 2
14.391	90 ± 2
14.766	89 ± 2
15.141	86 ± 2
15.516	83 ± 2
15.891	80 ± 2
16.641	74 ± 3
17.016	73 ± 3
17.391	73 ± 3
17.766	65 ± 3
18.141	67 ± 3
18.516	60 ± 7
18.891	68 ± 5
19.266	66 ± 4
19.641	59 ± 5
20.016	52 ± 3
20.391	57 ± 8
20.766	47 ± 9

[a] The data were taken at a laboratory angle of 90° and were converted to 90° in the center-of-mass system by assuming $(d\sigma/d\Omega)_{c.m.} = \frac{5}{4}\sin^2\vartheta(1-\frac{1}{2}\beta\cos\vartheta)$. Values of β were taken from Ref. 11. See also Ref. 1.

[1] A. van der Woude, M.L. Halbert, C.R. Bingham, and B.D. Belt, Phys.Rev.Lett. 26, 909 (1971).

[2] C.C. Chang, E.M. Diener, F. Ventura, Phys.Rev. Lett. 29, 307 (1972).

[4] I.M. Barbour and A.C. Phillips, Phys. Rev. C1, 165 (1970).

[5] D.R. Lehman and B.F. Gibson, private communication.

[11] I.M. Barbour and J.A. Hendry, Phys.Lett. 38B, 151(1972).

REF.

J.L. Matthews, T. Kruse, M.E. Williams, R.O. Owens, and W. Savin
Nucl. Phys. A223, 221 (1974)

ELEM. SYM.	A	Z
He	3	2

METHOD

REF. NO.	
74 Ma 6	egf

REACTION	RESULT	EXCITATION ENERGY	SOURCE		DETECTOR		ANGLE
			TYPE	RANGE	TYPE	RANGE	
P,G	ABX	16	D	16	MAG-D		DST

$d\sigma/d\Omega = b \sin^2\theta(1 + \beta \cos\theta + \gamma \cos^2\theta)$

DETECTED RECOIL

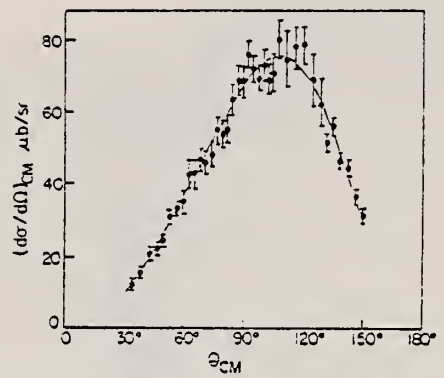

Fig. 4. Angular distribution of the $^2H(p, ^3He)\gamma$ reaction. The cross section has been converted to that for photo disintegration using detailed balance. The error bars represent statistical uncertainties only; an additional systematic uncertainty of ±5% is estimated. The curve is a least squares fit to the data using the expression $b \sin^2\theta (1+\beta \cos\theta+\gamma \cos^2\theta)$ as discussed in the text.

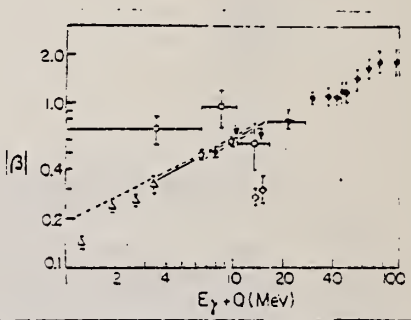

Fig. 5. Values of the parameter β as a function of $(E_\gamma + Q)$, where E_γ is the photon energy and $Q = -5.493$ MeV. The solid square (■) is the present measurement, and the other data are as follows: △ – Wölfli *et al.* [14]); □ – Fetisov *et al.* [8]); ● – Owens *et al.* [12]); ○ – Belt *et al.* [17]); ◇ – Van der Woude *et al.* [18]); ▼ – Bock and Walenta [9]); ♦ – O'Fallon *et al.* [10]). The theoretical curves are due to Fetisov using the Dalitz-Thacker wave function [25]) (dashed line), Gibson and O'Connell [26]) (dot-dash line), and Barbour and Hendry [22]) using a wave function with 2.1% S' state (solid line).

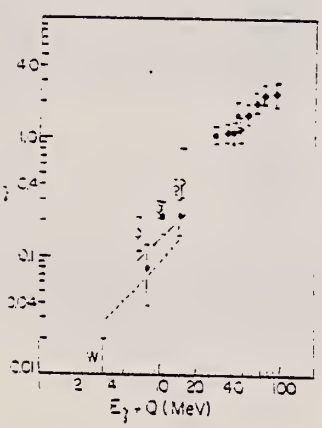

Fig. 6. Values of the parameter γ as a function of $(E_\gamma + Q)$. The solid square (■) is the present measurement and the other data are as follows: W – Wölfli *et al.* [14]); ● – Owens *et al.* [12]); ○ – Belt *et al.* [17]); ◇ – Van der Woude *et al.* [18]); ♦ – O'Fallon *et al.* [10]). The dotted curve was obtained from the results of Barbour and Hendry (see fig. 5) using the relation $\gamma = \frac{1}{2}\beta^2$. The dot-dash curve was calculated by Gibson and O'Connell [26]).

(continued)

TABLE 1
Cross section for $^3He(\gamma, d)^1H$ at $E_\gamma = 16$ MeV

Reaction	Ref.	$\sigma_{tot}(\mu b)$ [a]	$(d\sigma/d\Omega)_{c.m.}$ at $\theta_{c.m.} = 90°$ ($\mu b/sr$) [a]
$^2H(p, ^3He)\gamma$	present data	591 ± 12 (±28)	67.5 ± 1.4 (±3.2)
$^3He(\gamma, d)^1H$	[5]		67 ± 9 (±8)
	[6]		64 ± 5 (≦ ±4)
	[7]		69 ± 5 (±7)
	[8]	881 ± 107 (±53)	89 ± 12 (±5)
	[11]	642 ± 11 (±32)	74.4 ± 1.3 (±3.7)
$^3He(e, d)^1H$	[2]	816 ± 97 (≦ ±122)	90 ± 5 (≦ ±13)
	[3]		85 ± 3 (±5)
$^1H(d, ^3He)\gamma$	[18]		82 ± 7 (±5)
theory	[22]	730	82

[a]) The numbers in parentheses represent additional systematic uncertainties in the data.

[2] S.K. Kundu et al., Nucl.Phys. A171 (1971) 384.

[3] C.C. Chang et al. preprint.

[5] E. Finckh et al., Phys. Lett. 7 (1963) 271.

[6] B.L. Berman et al., Phys. Rev. 133 (1964) B117.

[7] J.R. Stewart et al., Phys. Rev. 138 (1965) B372.

[8] V.N. Fetisov et al., Nucl. Phys. 71 (1965) 305.

[9] H. Bock et al, Z. Phys. 238 (1970) 56.

[10] N.M. O'Fallon et al., Phys. Rev. C5 (1972) 1926.

[11] G. Ticcioni et al, Phys. Lett 46B (1973) 369.

[12] R.O. Owens et al., to be published

[14] W. Wolfli et al., Helv. Phys. Acta 40 (1967) 946.

[17] B.D. Belt et al., Phys. Rev. Lett 24 (1970) 1120.

[18] A. van der Woude et al., Phys. Rev. Lett. 26 (1971) 909.

[22] J.A. Hendry and al, Nucl. Phys. A211 (1973) 533.

[38] B.F. Gibson et al., quoted in Ref. 16, B.D. Belt, thesis, University of Tennessee, 1970.

REF. P.E. Argan, G. Audit, N. De Botton, J.-L. Faure, J.-M. Laget, J. Martin, C.G. Schuhl, and G. Tamas
Nucl. Phys. A237, 447 (1975)

EL EM. SYM.	A	Z
He	3	2

METHOD

REF. NO.	
75 Ar 1	egf

REACTION	RESULT	EXCITATION ENERGY	SOURCE		DETECTOR		ANGLE
			TYPE	RANGE	TYPE	RANGE	
G,P	ABX	175-370	C	405	MAG-D		DST

2-BODY COINC

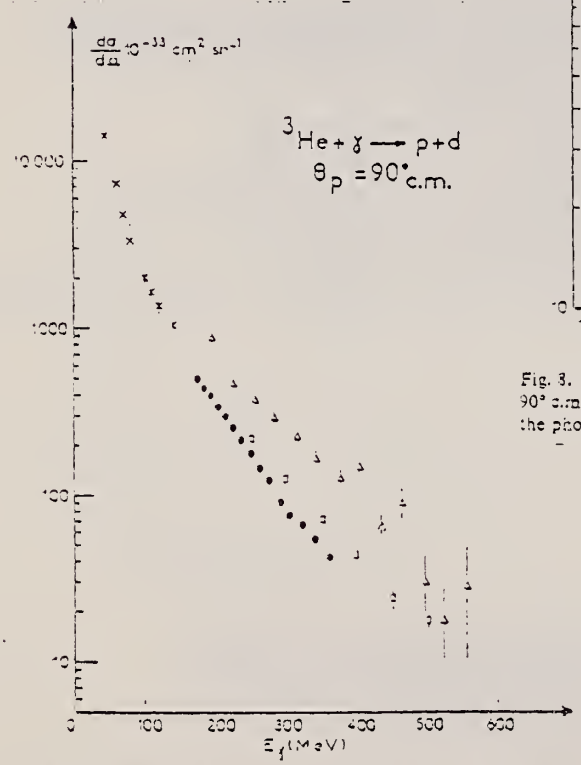

Fig. 9. The $\gamma + {}^3$He → p + d (c.m.) differential cross section at θ_p = 90° c.m.; E_γ is the photon lab energy. Dots: this work; crosses: ref. [14]); stars: ref. [15]); squares: ref. [16]); triangles: ref. [17]).

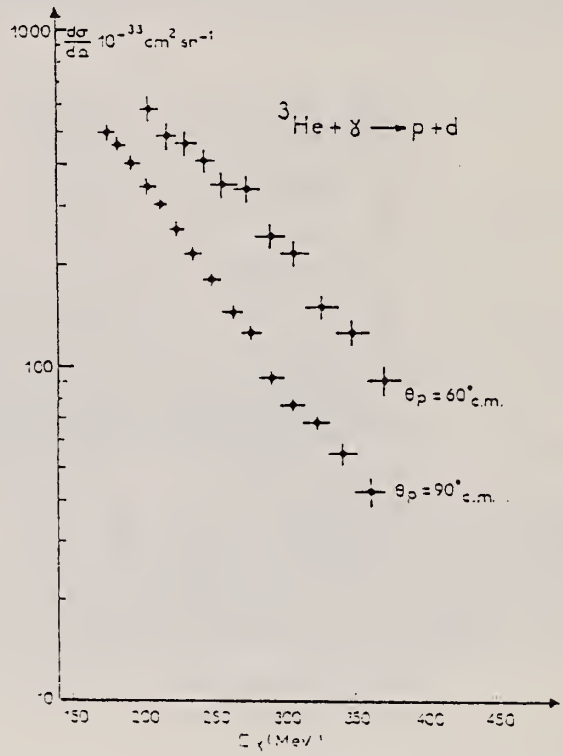

Fig. 8. The $\gamma + {}^3$He → p + d (c.m.) differential cross sections at θ_p = 60°, 90° c.m. (this work); E_γ is the photon lab energy. Horizontal error bars give the photon energy resolution; vertical error bars represent statistical errors.

[15] N.M. O'Fallon et al., Phys. Rev. C5, 1926 (1972).

[16] C.A. Heusch et al., CALT 68-319 (Presented at the Int. Symp. on electron and photon interactions at high energy, Cornell Univ. Aug. 23-37, 1971).

[17] P. Picozza et al., Nucl. Phys. A157, 190 (1970).

[18] S.K. Kundu et al., Nucl. Phys. A171, 384 (1971).

(continued)

TABLE 4

Differential cross section for the reaction $\gamma + {}^3\mathrm{He} \rightarrow \mathrm{d} + \mathrm{p}$ at 60° and 90° proton angle (c.m.)

Photon lab energy (MeV)	$\left.\frac{d\sigma}{d\Omega}\right\|_{60° \text{ c.m.}}$ (10^{-33} cm²/sr)	Photon lab energy (MeV)	$\left.\frac{d\sigma}{d\Omega}\right\|_{90° \text{ c.m.}}$ (10^{-33} cm²/sr)
204.4 ± 6.7	582.2 ± 36.5	173.6 ± 5.1	502.0 ± 18.2
217.1 ± 7.2	488.3 ± 33.0	182.6 ± 5.3	448.0 ± 12.1
229.8 ± 7.7	461.5 ± 23.4	192.6 ± 5.6	397.5 ± 11.4
243.8 ± 8.2	407.3 ± 18.5	202.8 ± 5.8	340.5 ± 14.9
257.8 ± 8.7	348.5 ± 12.8	213.1 ± 6.1	301.8 ± 10.0
274.0 ± 9.3	338.8 ± 12.8	223.7 ± 6.4	254.6 ± 10.5
290.4 ± 9.9	240.9 ± 9.7	236.0 ± 6.7	215.9 ± 7.1
307.4 ± 10.5	217.5 ± 8.0	249.0 ± 7.1	180.3 ± 5.6
327.1 ± 11.2	149.3 ± 7.5	262.7 ± 7.4	145.4 ± 5.0
348.5 ± 12.0	125.7 ± 8.0	276.4 ± 7.8	125.0 ± 4.6
371.7 ± 12.9	91.0 ± 8.0	290.7 ± 8.2	92.0 ± 3.7
		305.6 ± 8.6	77.3 ± 3.2
		323.3 ± 9.1	68.1 ± 3.3
		341.4 ± 9.8	54.9 ± 3.4
		360.6 ± 10.5	42.5 ± 4.2

The photon energy uncertainty is the FWHM of the photon energy resolution function. The cross-section uncertainty is due only to counting statistics.

REF. D Bachelier, M. Bernas, J. L. Boyard, J. C. Jourdain and P. Radvanyi
Nucl. Phys. A251, 433 (1975)

ELEM. SYM.	A	Z
He	3	2

METHOD

REF. NO.: 75 Ba 7 egf

REACTION	RESULT	EXCITATION ENERGY	SOURCE TYPE	SOURCE RANGE	DETECTOR TYPE	DETECTOR RANGE	ANGLE
G,PI+	ABX	227-453	C	600	MAG-D		DST

PI+T IN COINC

TABLE 2

Experimental results

q^2 (fm^{-2})	E_γ(lab) (MeV)	$\Delta(q^2)$ (fm^{-2})	ΔE_γ (MeV)	θ_π(lab) (deg)	θ_π(lab) (deg)	θ_π(c.m.) (deg)	$(d\sigma/d\Omega_\pi)_{lab}$ (μb/sr)	$(d\sigma/d\Omega)_{c.m.}$ (μb/sr)
3.1	228.2	0.34	9.05	19	131.7	135.9	1.11 ±0.17	1.27 ±0.19
3.1	253.6	0.40	11.6	31	104.0	109.7	1.41 ±0.14	1.50 ±0.15
3.1	282.0	0.44	14.2	39	87.0	93.2	1.55 ±0.13	1.55 ±0.13
3.1	306.8	0.48	16.3	44	76.9	83.3	1.17 ±0.17	1.13 ±0.16
3.9	244.9	0.43	10.7	15	142.6	146.1	0.88 ±0.06	1.04 ±0.07
3.9	252.3	0.46	11.5	20	130.7	135.0	0.91 ±0.04	1.05 ±0.05
3.9	262.4	0.48	12.5	25	119.0	124.2	0.84 ±0.04	0.94 ±0.04
3.9	275.7	0.51	13.7	30	107.8	113.6	0.75 ±0.03	0.80 ±0.03
3.9	292.9	0.55	15.3	35	96.9	103.2	0.63 ±0.03	0.66 ±0.03
3.9	315.3	0.58	17.2	40	86.3	93.0	0.363 ±0.018	0.361 ±0.018
3.9	435.9	0.72	26.6	55	56.5	63.7	0.191 ±0.037	0.166 ±0.032
4.55	318.6	0.66	17.8	36.2	95.0	101.6	0.20 ±0.02	0.20 ±0.02
4.9	280.1	0.61	14.2	20.7	130.0	134.6	0.394 ±0.025	0.456 ±0.029
4.9	296.1	0.65	15.7	27.2	115.0	120.6	0.289 ±0.025	0.321 ±0.027
4.9	355.5	0.76	20.9	41.1	85.0	92.1	0.072 ±0.006	0.071 ±0.006
3.1	227.5			18.5	132.9	137	1.10 ±0.17 [a]	1.27 ±0.20
3.9	250.8			19.1	132.7	137	0.91 ±0.04 [a]	1.05 ±0.05
4.9	277.9			19.6	132.6	137	0.41 ±0.03 [a]	0.48 ±0.04
6	305.6	0.64	16.0	19.9	132.3	137	0.15 ±0.03	0.18 ±0.04
8	352.0	0.96	20.4	20.3	131.9	137	0.051 ±0.027	0.061 ±0.032
10.5	404.5	1.30	25.4	20.5	131.3	137	0.048 ±0.01	0.053 ±0.012
11.5	424.3	1.45	27.3	20.6	131.1	137	0.039 ±0.003	0.048 ±0.009
13	452.8	1.62	30.1	20.7	130.8	137	0.028 ±0.007	0.035 ±0.008

[a]) Slightly extrapolated values from our fixed q^2 measurements.

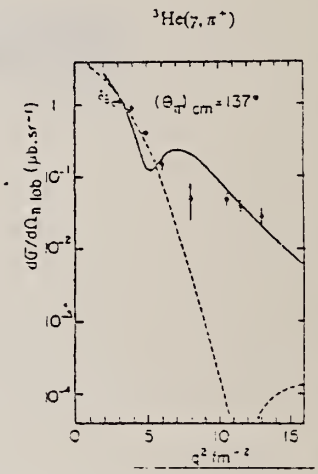

Fig. 5. Experimental results at variable q^2 for a fixed value of θ_π(c.m.) = 137°. The curves are calculations from ref. [16]) with a CGLN elementary amplitude and a Bijedić *et al.* wave function (ρ_S = 100%); dashed curve, without rescattering term; solid curve with a rescattering term.

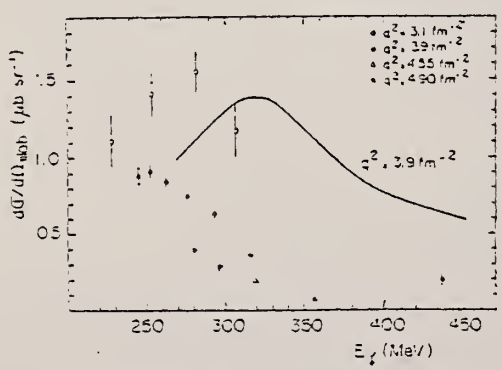

Fig. 4. Experimental results at fixed values of q^2. The solid curve is a calculation with a CGLN elementary amplitude, a Ballot *et al.* [22]) wave function (ρ_S = 100%) and assuming $\langle k_3 \rangle = 0$ in the lab system (see text) [16]).

[16] C. Lazard et al., Nuovo Cim. 16A (1973) 605.

[22] J.L. Ballot et al. Proc. Symp. on recent status and novel development in the many-body problem, Rome, 1972.

REF. J. M. Hendry and A. M. Macleod
J. Phys. (London) G1, 528 (1975)

ELEM. SYM.	A	Z
He	3	2

METHOD

REF. NO. 75 He 7 egf

REACTION	RESULT	EXCITATION ENERGY	SOURCE		DETECTOR		ANGLE
			TYPE	RANGE	TYPE	RANGE	
G,N	RLY	8- 23	C	23	CCH-D		4PI *
G,D	RLY	6- 23	C	23	CCH-D		4PI

* DALITZ PLOTS

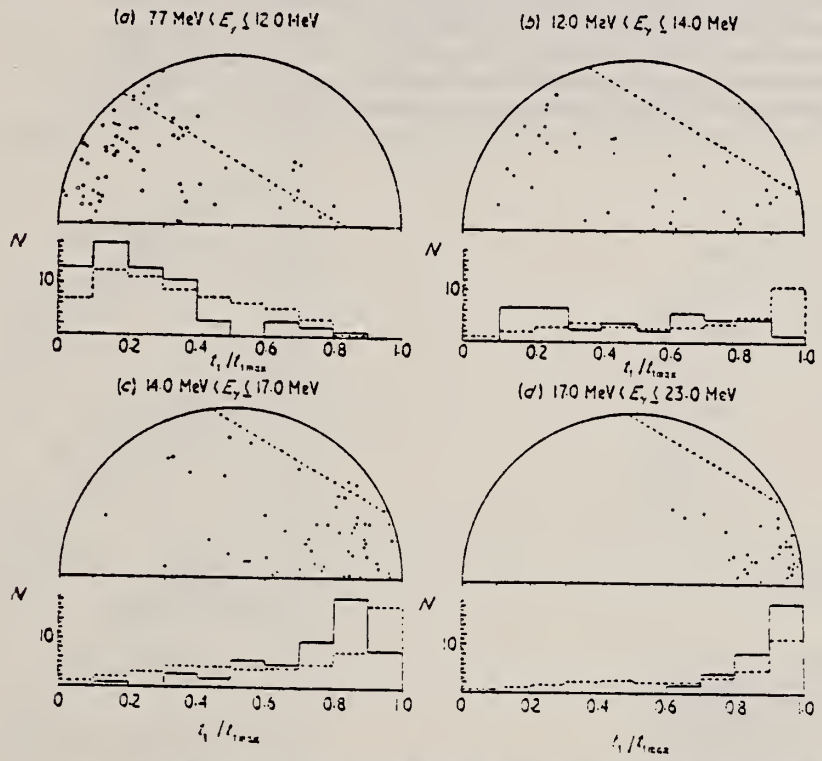

Figure 1. Dalitz plots and corresponding neutron spectra for defined events. Dalitz plot phase space cuts due to ionization losses shown by broken line. Experimental neutron spectra shown as solid histograms with theoretical predictions of Barbour and Phillips as broken-line histograms.

(continued)

5.1. *Yields*

From 7500 expansions photographed, 663 events were analysed as photodisintegrations of ^{3}He. Of these, 371 were assigned to the two-body channel and 292 to the three-body channel.

As no measure was made of the photon spectrum due to the 23 MeV electrons used in this experiment, the formula of Schiff (1951) has been used in the comparison of the yields of this work and other data. The total cross sections of Fetisov *et al* and Barbour and Phillips have been modified by this calculated spectrum. Ignoring two-body events below 7·5 MeV γ-ray energy the total cross sections of Barbour and Phillips allocate 47% of the events to the three body channel; in the case of the data of Fetisov *et al* this figure is 42%; while in the present experiment the figure is (44 ± 2%) allowing for random errors and a small contribution from uncertain assignment of events.

5.2. *The* $\gamma(^3He, n)2p$ *reaction*

Figures 1(*a*)–(*d*) show the Dalitz plots of completely defined events for the γ-ray energies shown. Beneath each Dalitz plot is its projection onto the neutron axis. The neutron spectra are compared with the predicted neutron spectra of the theory of Barbour and Phillips (broken line histograms) normalized to the number of events in each plot. These theoretical spectra are for γ-ray energies of 10·0, 12·5, 15·0 and 17·5 MeV and are modified to allow for the lost events discussed above. The dashed line on each Dalitz plot is the locus of $t_2 = 0{\cdot}5$ MeV for the same γ-ray energies.

REF. P. T. Kan, G. A. Peterson, D. V. Webb, Z. M. Szalata, S. P. Fivozinsky, J. W. Lightbody, Jr., and S. Penner
Phys. Rev. Lett. 34, 899 (1975)

ELEM. SYM.	A	Z
He	3	2

METHOD

REF. NO. 75 Ka 6 hmg

REACTION	RESULT	EXCITATION ENERGY	SOURCE TYPE	SOURCE RANGE	DETECTOR TYPE	DETECTOR RANGE	ANGLE
E,E/	ABX	5- 12	D	60-120	MAG-D		DST

BROAD PEAK AT 6.4 MEV

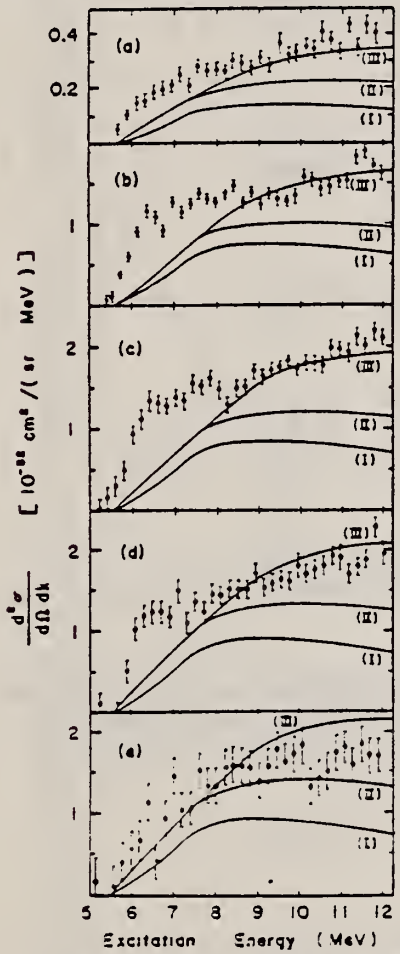

FIG. 2. Measured cross sections in the region of breakup thresholds. In (a), $E_0 = 120$ MeV and $\vartheta = 127.7°$; in (b)–(d), $E_0 = 110$, 90, 75, and 60 MeV, respectively, for a fixed $\vartheta = 92.6°$. Curve (I) is the $E1$ contribution converted from two-body photodisintegration cross sections by virtual-photon theory, curve (II) is the sum of (I) and the $M1$ contribution from a 180° electron-scattering experiment, and curve (III) is the sum of (II) and the $E1$ contribution from the three-body photodisintegration calculation of Gibson and Lehman, converted by virtual-photon theory.

A broad electric monopole excitation peaking at 6.4 MeV has been observed in the breakup of ^{3}He induced by inelastic electron scattering. The monopole cross section was obtained from the observed cross section by subtracting the electric-dipole contributions converted from photodisintegration cross sections by using the virtual photon theory, and also subtracting the magnetic multipole contributions obtained from a 180° electron-scattering experiment. The extracted monopole matrix element is 2.4± 0.5 fm^2.

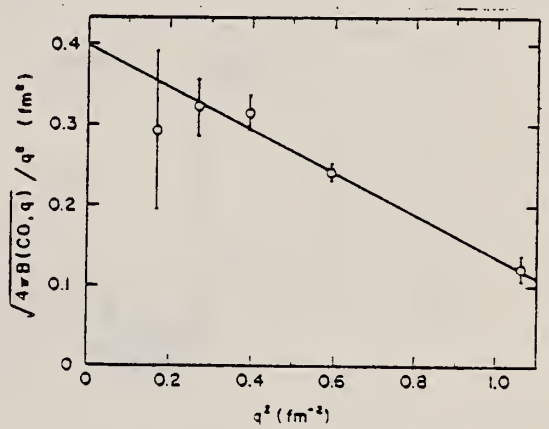

FIG. 3. The square root of the reduced transition probability as a function of momentum transfer for the monopole excitations above curve (III) in Fig. 2, integrated between 5.5 and 9.5 MeV. Errors indicated on the data points are statistical only. An additional 10% uncertainty should be included to account for systematic errors and uncertainties in the analysis. The solid line is a least-squares fit to the data.

REF. P. T. Kan, G. A. Peterson, D. V. Webb, Z. M. Szalata, J. S. O'Connell, S. P. Fivozinsky, J. W. Lightbody, Jr. and S. Penner
Phys. Rev. C12, 1118 (1975)

ELEM. SYM.	A	Z
He	3	2

METHOD

REF. NO.	
75 Ka 7	hmg

REACTION	RESULT	EXCITATION ENERGY	SOURCE		DETECTOR		ANGLE
			TYPE	RANGE	TYPE	RANGE	
E,E/	ABX	0- 40	D	60-120	MAG-D		DST

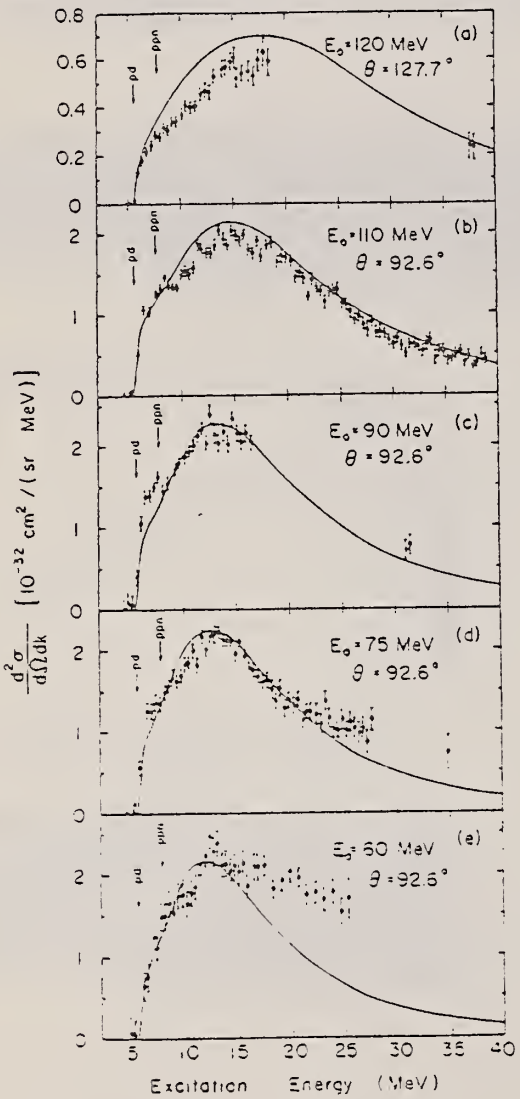

FIG. 3. Radiatively unfolded cross sections. The notations *pd* and *ppn* indicate the two- and three-body breakup thresholds, respectively. In each graph, the solid curve is the calculated result in the zero-range approximation (see Sec. V).

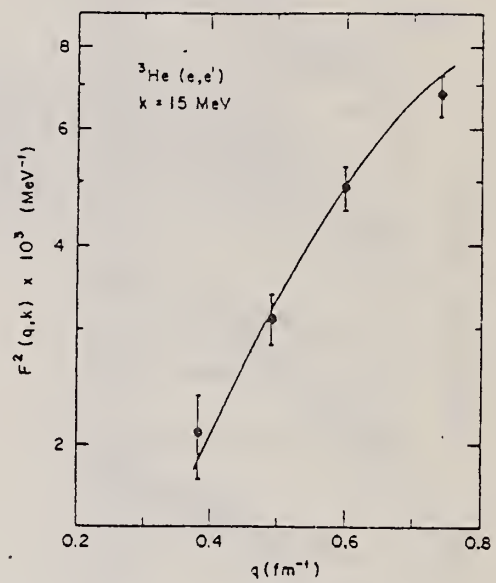

FIG. 4. Form factor $F^2(q, k)$ at an excitation energy of 15 MeV. Systematic uncertainties of ±5% have been included in all of the data points except the point at $q = 0.382$ fm^{-1}, where a systematic error of ±10% has been estimated. The solid curve is the zero-range model form factor.

(continued)

TABLE I. Measured continuum form factors $F^2(q,k)$ averaged over 1 MeV intervals. The numbers in parentheses are the percentage standard deviations which include 5% systematic uncertainties for all spectra except for the $E_0 = 60$ MeV spectrum, in which 5–30% systematic errors have been included.

	$E_0 = 120$ MeV		$E_0 = 110$ MeV		$E_0 = 90$ MeV		$E_0 = 75$ MeV		$E_0 = 60$ MeV	
k (MeV)	q^2 (fm^{-2})	$F^2(q,k)$ (10^{-3} MeV^{-1})	q^2 (fm^{-2})	$F^2(q,k)$ (10^{-3} MeV^{-1})	q^2 (fm^{-2})	$F^2(q,k)$ (10^{-3} MeV^{-1})	q^2 (fm^{-2})	$F^2(q,k)$ (10^{-3} MeV^{-1})	q^2 (fm^{-2})	$F^2(q,k)$ (10^{-3} MeV^{-1})
6.0	1.058	3.12(12.2)	0.695	2.23 (6.3)	0.395	1.96(11.3)	0.271	1.20(12.9)	0.170	0.56(25.1)
7.0	1.048	5.68 (9.4)	0.690	4.02 (7.6)	0.390	3.23 (8.2)	0.268	1.93 (9.8)	0.167	1.03(14.3)
8.0	1.039	6.86 (9.0)	0.584	4.78 (7.1)	0.386	3.47 (8.0)	0.264	2.16 (9.0)	0.165	1.53(11.4)
9.1	1.029	7.66 (9.1)	0.578	4.64 (7.4)	0.381	3.89 (7.2)	0.260	2.43 (8.3)	0.162	1.64(10.9)
10.1	1.020	9.01 (8.0)	0.573	5.05 (7.6)	0.377	4.18 (7.1)	0.257	2.66 (8.2)	0.159	1.65(10.8)
11.2	1.010	9.68 (8.6)	0.568	5.74 (7.3)	0.373	4.68 (7.3)	0.253	2.84 (8.0)	0.156	2.01(10.7)
12.2	1.001	11.24 (9.3)	0.562	6.09 (7.2)	0.368	5.00 (7.5)	0.250	3.20 (7.7)	0.154	2.30(10.3)
13.2	0.992	13.26 (8.6)	0.557	6.37 (7.1)	0.364	4.82 (8.0)	0.246	3.23 (7.6)	0.151	2.28(10.9)
14.2	0.983	13.69(10.3)	0.552	6.58 (7.0)	0.360	4.84 (7.9)	0.243	3.15 (7.7)	0.149	2.08(12.7)
15.3	0.974	13.35(11.0)	0.547	0.76 (7.0)	0.356	4.90 (7.9)	0.240	3.09 (8.0)	0.146	2.08(14.6)
16.4	0.965	12.79(11.6)	0.542	6.49 (7.0)	0.352	4.79 (8.0)	0.237	2.57 (8.1)	0.144	2.02(15.8)
17.5	0.956	14.37(13.2)	0.537	6.21 (7.1)			0.234	2.41 (8.6)	0.142	2.07(19.5)
18.3			0.532	0.26 (7.2)			0.230	2.22 (9.3)	0.139	1.83(21.5)
19.3			0.527	5.74 (7.1)			0.228	2.10 (9.6)	0.137	2.08(25.5)
20.3			0.522	5.44 (7.0)			0.224	1.98 (9.9)	0.135	1.94(29.8)
21.4			0.517	4.91 (7.9)			0.222	1.84(10.5)	0.133	1.70(36.0)
22.4			0.513	4.52 (8.8)			0.219	1.64(11.5)	0.130	1.82(46.1)
23.4			0.508	4.20 (8.9)			0.216	1.83(10.9)		
24.4			0.503	4.37 (9.0)			0.213	1.52(12.4)		
25.5			0.499	3.68 (8.9)			0.210	1.54(11.9)		
26.6			0.494	3.35(10.0)			0.208	1.50(12.5)		
27.6			0.490	2.86(10.8)			0.205	1.30(15.3)		
28.7			0.485	2.73(10.8)						
29.7			0.481	2.35(11.4)						
30.8			0.477	2.15(11.1)						

REF.

D.M. Skopik, J.J. Murphy,II, Y.M. Shin, K.F. Chong, and E.L. Tomusiak
Phys. Rev. C11, 693 (1975)

ELEM. SYM.	A	Z
He	3	2

METHOD

REF. NO.	
75 Sk 1	hmg

REACTION	RESULT	EXCITATION ENERGY	SOURCE		DETECTOR		ANGLE
			TYPE	RANGE	TYPE	RANGE	
E,D	ABX	11- 40	D	43-103	MAG-D		DST

Tables of cross section data given.

An experimental study of the reaction $^3He(e,d)e'p$ was carried out by measuring differential cross sections of deuterons as a function of deuteron energy and angle for three incident electron energies. The electrodisintegration cross section was also calculated using an Irving-Gunn wave function for the ground state with a plane wave for the final state. As in the case of photodisintegration calculations the result indicates the need for including complete final state rescattering effects.

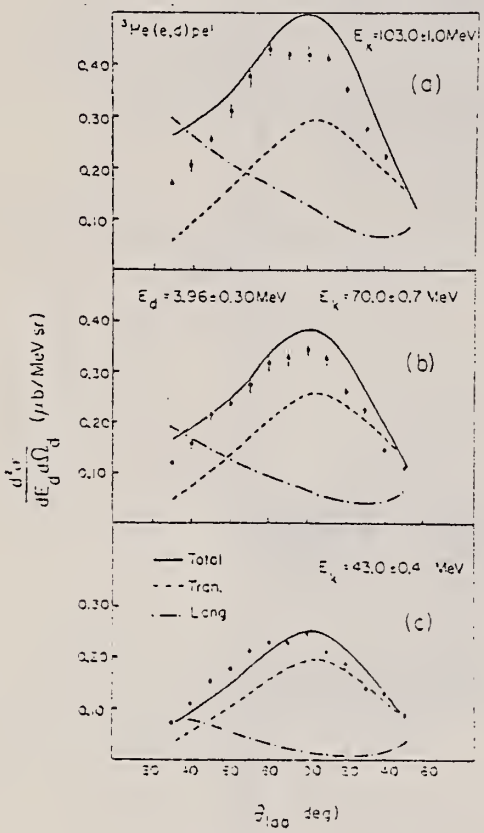

FIG. 3. (a)–(c) Angular distributions for 3.96 MeV deuterons at three different incident electron energies. The errors shown are statistical only. The solid curve is the calculation described in the text.

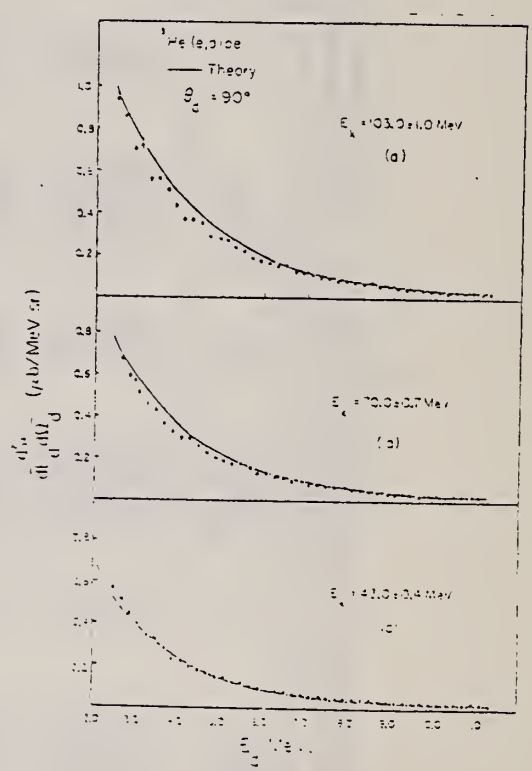

FIG. 4. (a)–(c) Deuteron energy distributions at 90° in the laboratory for three different incident electron energies. The errors shown are statistical only. The solid curve is the calculation described in the text.

(continued)

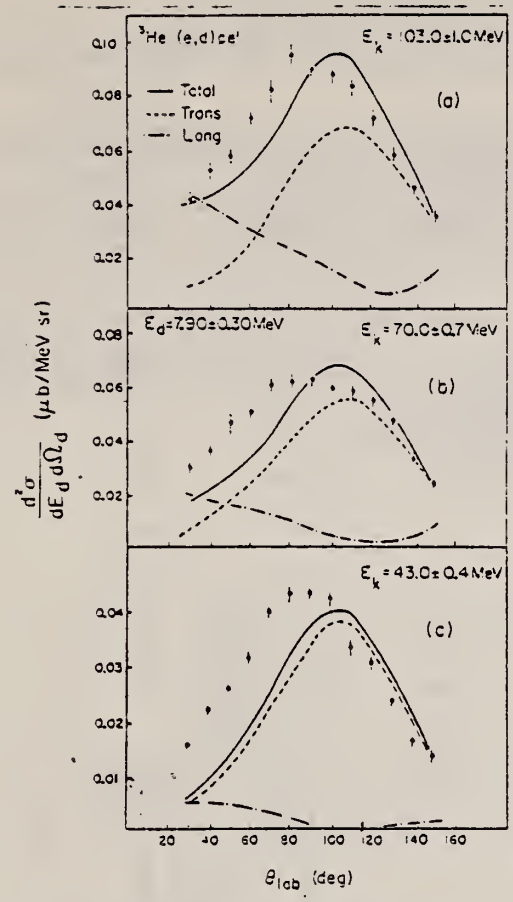

FIG. 3. (a)–(c) Angular distributions for 7.90 MeV deuterons at three different incident electron energies. The errors shown are statistical only. The solid curve is the calculation described in the text.

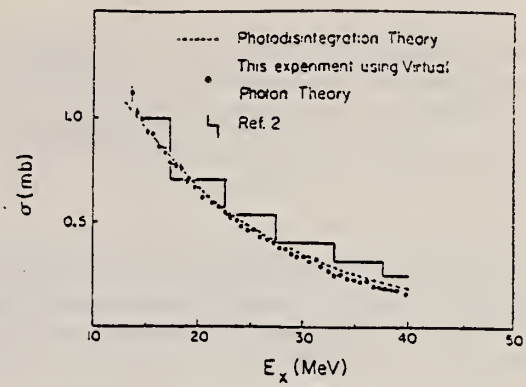

FIG. 5. Total two-body photodisintegration cross section given by Eq. (A1). The data of Ref. 3 are essentially identical with the virtual photon analyzed data of this experiment.

[3] S.K. Kundu, Y.M. Shin, G.D. Wait, Nucl. Phys. A171, 384 (1971).

REF. C. A. Heusch, R. V. Kline, K. T. McDonald, C. Y. Prescott
Phys. Rev. Lett. 37, 405 (1976)

ELEM. SYM.	A	Z
He	3	2

METHOD

REF. NO. 76 He 2 hmg

REACTION	RESULT	EXCITATION ENERGY	SOURCE TYPE	SOURCE RANGE	DETECTOR TYPE	DETECTOR RANGE	ANGLE
G,HE	ABX	200-600	C	700	MAG-D		DST

TIME REVERSAL TEST

We have measured the two-body photodisintegration process γ^3He$\rightarrow pd$ in the energy region sensitive to intermediate photoexcitation of one nucleon to the isobar $\Delta(1238)$. We present angular distributions at center-of-mass angles from 30° to 150° for incoming photon energies 200–600 MeV. Magnetic dipole excitation appears to be suppressed.

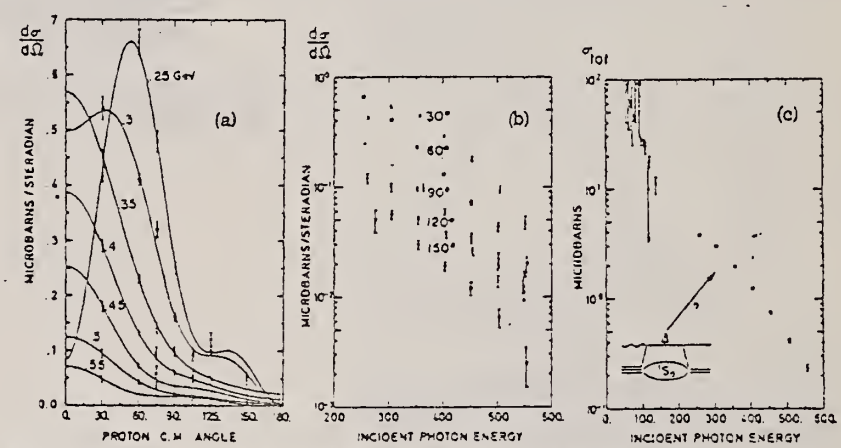

FIG. 3. (a) Angular distributions for the process γ^3He$\rightarrow pd$ at photon energies from 250 to 550 MeV, between 30 and 150° c.m. Solid lines denote fits as described in the text. Note that secondary maxima at ~140° are due to the specific form of our fits at lower energy. They are not seen in these data. (b) Energy dependence of the differential cross section at fixed angles between 30 and 150°. (c) Total cross section for the process γ^3He$\rightarrow pd$ versus photon energy, obtained from polynomial fits to our data. Also shown are previous results at lower energies (Ref. 9). Note that the 250-MeV point could be raised if the forward dip were not as pronounced as emerging from the fit. At $\Delta(1236)$ excitation energy (see inset), at best a hint is visible.

[9] N. O'Fallon, L.J. Koester, J.H. Smith, Phys. Rev. C5, 1926 (1972).

REF.		EL EM. SYM.	A	Z
	C.A. Heusch, R.V. Kline, K. T. McDonald, J. B. Carroll, D. H. Fredrickson, M. Goitein, B. Macdonald, V. Perez-Mendez, and A.W. Stetz Phys. Rev. Lett. 37, 409 (1976) (See erratum: Phys.Rev. Lett. 37, 960 (1976))	He	3	2
METHOD		REF. NO.		
		76 He 3		hmg

REACTION	RESULT	EXCITATION ENERGY	SOURCE		DETECTOR		ANGLE
			TYPE	RANGE	TYPE	RANGE	
P,G	ABX	256-390	D	377-576	SPK-D		DST

We report on the measurement of the formation of $^3He^{++}$ in the collision of protons and deuterons, with the emission of a single photon. Energies and angles as chosen allow a comparison with the inverse process $\gamma^3He - pd$. These data restrict possible T-invariance-violation effects in the electromagnetic interaction.

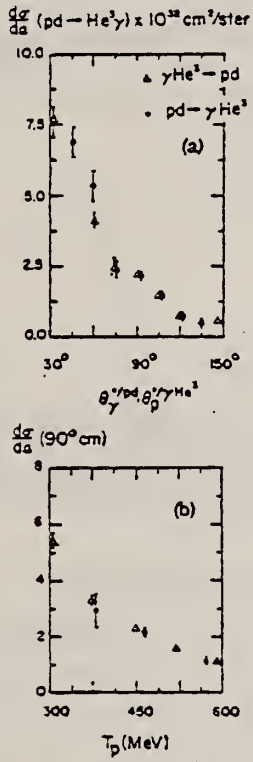

FIG. 3. (a) Angular distributions for $pd \rightarrow {}^3He\gamma$ at $T_p = 465$ MeV and $E_\gamma = 320$ MeV; (b) energy dependence at 90° (c.m.) for $pd \rightarrow {}^3He\gamma$.

TABLE I. Quantitative comparison of cross-section data for $pd \rightarrow {}^3He\gamma$ and inverse. The $\gamma^3He \rightarrow pd$ data are inverted assuming T invariance to be valid. $\Delta = \sigma(pd) - \sigma(\gamma^3He)$.

$\theta_{^3He}^{c.m.}$	T_p (GeV)	$\sigma(\gamma^3He)$ (10^{-32} cm^2)	$\sigma(pd)$ (10^{-32} cm)	$\Delta/\sigma(pd)$	χ^2
60	0.462	0.64 ± 0.15	0.77 ± 0.11	−0.17 ± 0.24	0.46
75	0.462	1.43 ± 0.23	1.48 ± 0.10	0.04 ± 0.17	0.04
90	0.462	2.16 ± 0.17	2.16 ± 0.12	0.00 ± 0.10	0.00
105	0.462	2.63 ± 0.35	2.50 ± 0.17	−0.05 ± 0.16	0.19
120	0.462	4.04 ± 0.21	5.27 ± 0.60	−0.23 ± 0.12	3.81
			average	0.03 ± 0.07	sum 4.50

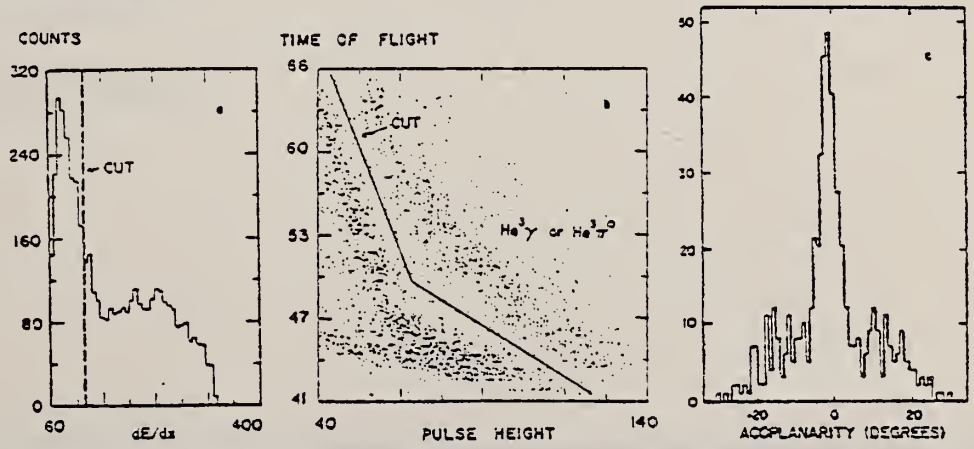

FIG. 2. (a) Pulse height distribution in ^3He differential counter; (b) time of flight versus pulse height in ^3He total-absorption counter; (c) ^3He–γ coplanarity.

REF.

J. S. McCarthy, I. Sick, R. R. Whitney, M. R. Yearian
Phys. Rev. C13, 712 (1976)

ELEM. SYM.	A	Z
He	3	2

METHOD

REF. NO.	
76 Mc 2	hmg

REACTION	RESULT	EXCITATION ENERGY	SOURCE		DETECTOR		ANGLE
			TYPE	RANGE	TYPE	RANGE	
E,E/	ABI	23-263	D	500	MAG-D		60

QUASIELAST SCAT

TABLE I. Quasielastic cross sections at $E_0 = 500$ MeV and $\theta = 60°$ integrated up to 200 MeV energy loss. The values used for the nucleon elastic cross sections were 1.14×10^{-31} cm^2/sr for the proton and 0.21×10^{-31} cm^2/sr for the neutron (Ref. 4).

	^{3}He ($\times 10^{-31}$ cm^2/sr)		^{4}He ($\times 10^{-31}$ cm^2/sr)
Static-impulse model	2.50		2.7
"Fermi-gas" fit to data	2.62		2.86
Lehman model	2.96		...
Experiment	2.59 ± 0.07 [a]		3.00 ± 0.08 [a]
^{4}He-^{3}He difference		0.41 ± 0.11	

[a] Error bars do not include the ± 3% uncertainty in the proton elastic cross section (Ref. 4).

[4] T. Janssens, R. Hofstadter, E.B. Hughes, and M.R. Yearian, Phys. Rev. 142, 922 (1966).

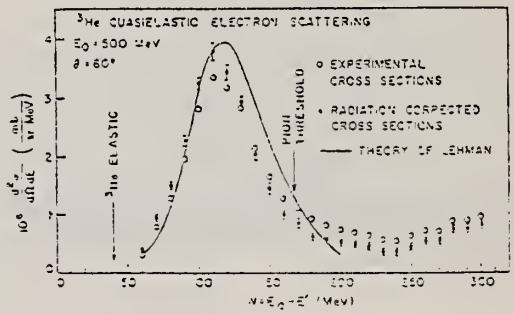

FIG. 1. ^{3}He quasielastic electron scattering spectrum as a function of electron energy loss.

REF. V. A. Gold'shtein, É. L. Kuplennikov, V. V. Lubyanyi, E. V. Pegushin, V. I. Startsev, V. B. Shostak, N. G. Afanas'ev
Yad. Fiz. 27, 1565 (1978)
Sov. J. Nucl. Phys. 27, 824 (1978)

ELEM. SYM.	A	Z
He	3	2

METHOD

REF. NO.	
78Go6	hg

REACTION	RESULT	EXCITATION ENERGY	SOURCE		DETECTOR		ANGLE
			TYPE	RANGE	TYPE	RANGE	
E,E/P	ABX	150*	D	999	MAG-D		30

The angular distribution of knock-out protons and the momentum distribution of recoil nuclei have been measured for the $^3He(e, e'p)$ reaction at an incident electron energy of 1200 MeV.

*P MEV/C,999=1.2 GEV

PACS numbers: 78. -XN, 27.10. + h

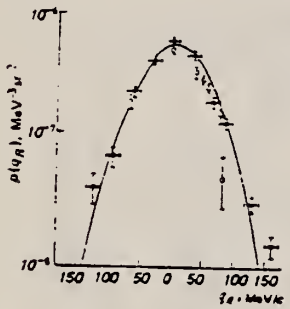

FIG. 1. Recoil-nucleus momentum distribution for the reactions $^3He(e, e'p)$ (●—Khar'kov, ○—Ref. 1) and $^3He(p, 2p)$ (△—Ref. 4).

TABLE I.

θ_p, deg	q_R, MeV/c	$\frac{d^6\sigma}{dE'_p d\Omega_e d\Omega_p} \cdot 10^{30}$, cm²/MeV · sr⁻²	$\rho(q_R) \cdot 10^{27}$, MeV⁻³sr⁻²	θ_p, deg	q_R, MeV/c	$\frac{d^6\sigma}{dE'_p d\Omega_e d\Omega_p} \cdot 10^{30}$, cm²/MeV · sr⁻²	$\rho(q_R) \cdot 10^{27}$, MeV⁻³sr⁻²
45.5	125.4	0.91±0.24	0.29±0.10	60.5	253	10.18±0.56	3.54±0.21
48.5	95.1	1.62±0.30	0.67±0.12	63.5	60.7	4.69±0.38	1.72±0.14
51.5	64.8	4.86±0.43	2.03±0.18	66.5	82.7	3.33±0.20	1.19±0.11
54.5	34.4	8.08±0.57	3.51±0.23	69.5	125.5	0.88±0.11	0.301±0.039
57.75	2.00	12.92±0.43	4.99±0.17	72.5	159.7	0.45±0.08	0.149±0.027

REF. É.L. Kuplennikov, V.A. Gol'dshtein, V.B. Shostak & E.V. Pegushin
Yad. Fiz. 28, 283 (1978)
Sov. J. Nucl. Phys. 28, 142 (1978)

ELEM. SYM.	A	Z
He	3	2

METHOD

REF. NO.: 78 Ku 9 hmg

REACTION	RESULT	EXCITATION ENERGY	SOURCE		DETECTOR		ANGLE
			TYPE	RANGE	TYPE	RANGE	
E,E/	ABX	0-300	C	999	MAG-D		DST

999=1211 MEV

The absolute differential cross section for quasielastic scattering of electrons in the reaction $^3He(e,e')$ has been measured as a function of the scattered electron energy in the range of scattering angles 15–29° for an incident electron energy 1211 MeV.

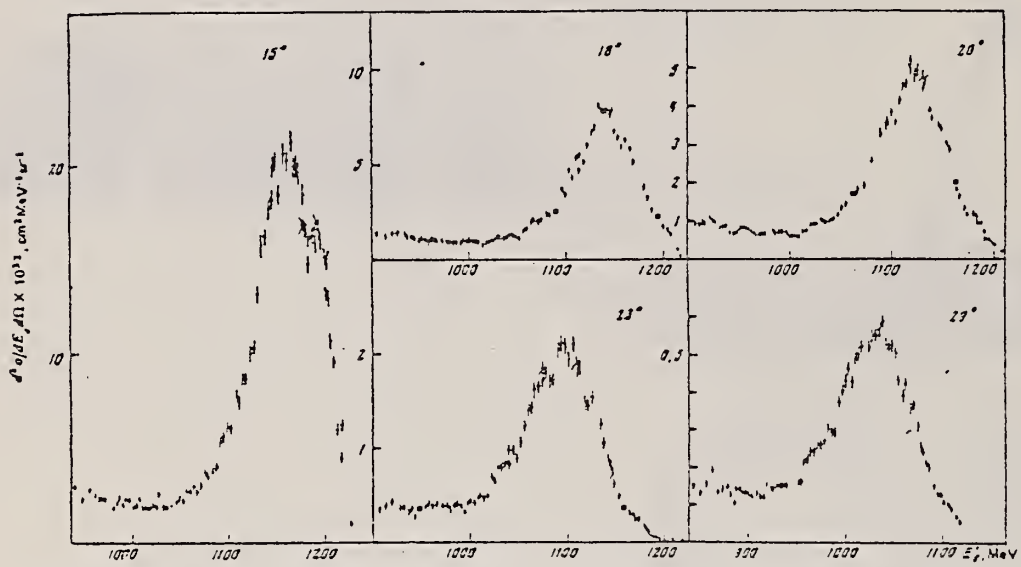

FIG. 2. Differential cross section for scattering of 1211-MeV electrons by the ^3He nucleus as a function of the energy of the detected electron.

REF. D.M. Skopik, E.L. Tomusiak, J. Asai and J.J. Murphy, II
Phys. Rev. C 18, 2219 (1978)

ELEM. SYM.	A	Z
He	3	2

METHOD

REF. NO. 78 Sk 6 hg

REACTION	RESULT	EXCITATION ENERGY	SOURCE TYPE	SOURCE RANGE	DETECTOR TYPE	DETECTOR RANGE	ANGLE
E,PI+	ABX	170-190	D	170-190	MAG-D		DST

The $^3He(e,t)\pi^+,e'$ cross section has been measured as a function of incident electron energy, triton recoil energy, and angle. The experiment corresponds to excitation energies near 20 MeV above pion threshold. Comparison is made with a theory including all partial waves using Gaussian and Irving-Gunn ground states for ^3He. The forward peaking approximation is also discussed.

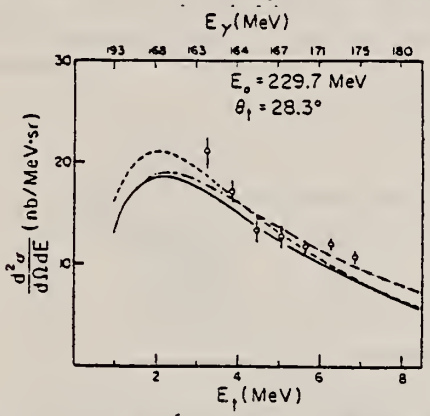

FIG. 2. Triton recoil cross section for an incident electron energy of 229.7 MeV. The curves are calculated as explained in Ref. 12 with a dashed line corresponding to Gaussian (FPA), a straight line corresponding to Gaussian (exact), and a dash-dot line corresponding to Irving-Gunn (exact). The effective photon energy shown on the upper horizontal scale is calculated assuming the electron scatters forward. The "double-valuedness" of this scale corresponds to the fact that a photon of a given energy can produce at a particular triton angle either a lower energy recoil triton and a pion in the forward direction or a higher energy recoil triton and a pion in the backward direction.

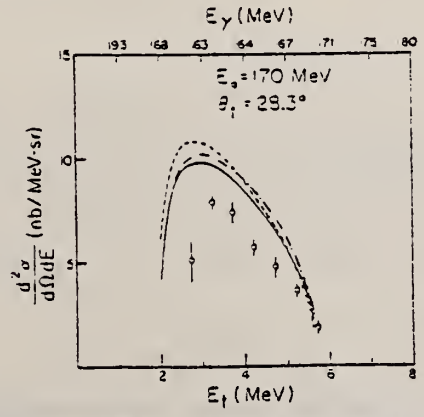

FIG. 4. Same as Fig. 2 except $E_0 = 170$ MeV.

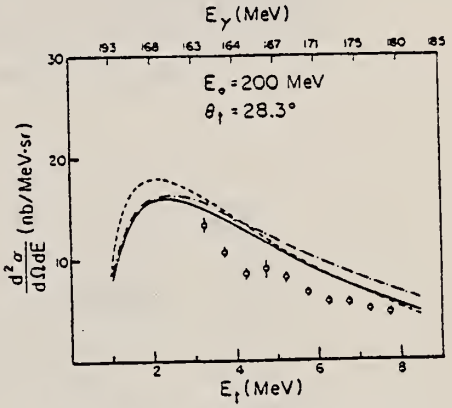

FIG. 3. Same as Fig. 2 except $E_0 = 200$ MeV.

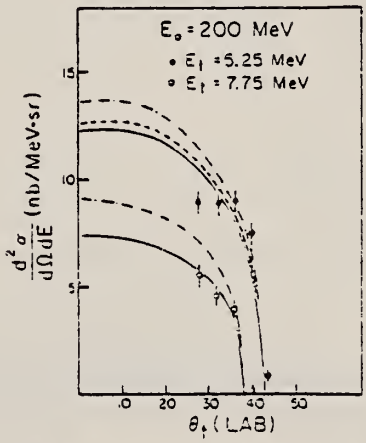

FIG. 5. Angular distribution of the recoil tritons at $E_t = 5.25$ and 7.75 MeV for $E_0 = 200$ MeV. It should be noted that these angular distribution data were taken in different runs from the data shown in Fig. 3. The small difference in the cross sections (~10%) between the two figures is consistent with the statistical errors shown. The curves have the same meaning as in Fig. 2 except that the difference between the exact and the FPA Gaussian wave function calculation for $E_t = 7.75$ MeV is too small for both curves to be separately plotted.

12 J. Asai and E.L. Tomusiak, Can. J. Phys. 55, 2066 (1977)

REF. P. Argan, G. Audit, A. Bloch, N. de Botton, J.L. Faure, C.Schuhl, G. Tamas, C. Tzara, E. Vincent, J. Deutsch, D. Favart, R. Prieels, B. Van Oystaeyen
Phys. Rev. C20, 242 (1979)

ELEM. SYM.	A	Z
He	3	2

METHOD

REF. NO. 79 Ar 1 hg

REACTION	RESULT	EXCITATION ENERGY	SOURCE		DETECTOR		ANGLE
			TYPE	RANGE	TYPE	RANGE	
G,PI+	ABX	150-156	C	152-156	ACT-I		90

The positive-pion photoproduction yield on ^{3}He was measured near threshold. The transition matrix element of this process is extracted with a $\pm 1.5\%$ accuracy. We discuss the relation of our result, firstly, with magnetic electron scattering on ^{3}He and ^{3}H, secondly, with the properties of pionic ^{3}He atom.

[NUCLEAR REACTION ^{3}He(γ, π^+)^{3}H, measured σ, E = 1–5 MeV.]

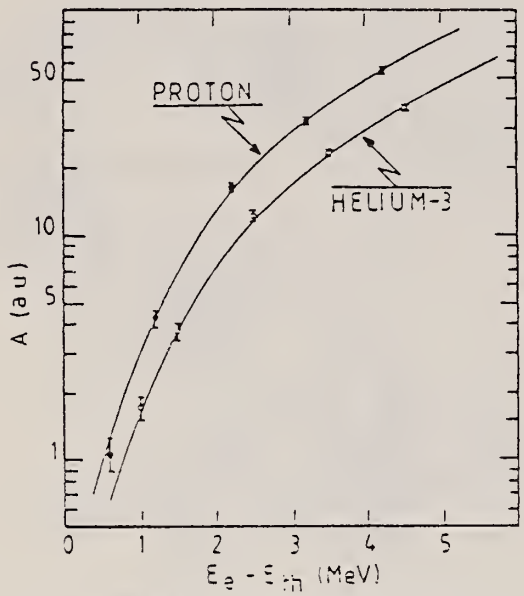

FIG. 1. Measured π^+ photoproduction yields per nucleus as a function of the excess energy above threshold in the laboratory system for hydrogen and ^{3}He. Solid lines are the calculated yields giving the best fit to the experimental data.

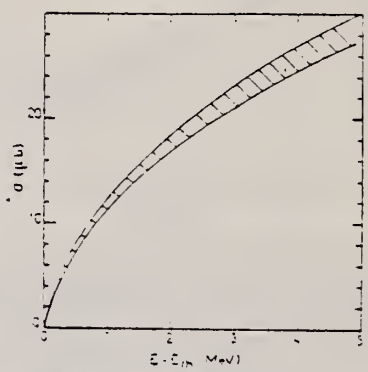

FIG. 2. Cross section of the ($\gamma\pi^+$) reaction on ^{3}He deduced from this experiment as a function of the excess energy above threshold in the laboratory system. The shaded area represents the experimental error taking into account the uncertainty both of this experiment and that of $\sigma_\gamma = 4\pi/(E_{\gamma,cm}k^*)$[2].

REF. V.A. Goldstein, E.L. Kuplennikov, E.M. Malyarzh, V.K. Tartakovsky, V.B. Shostak
Ukr. Fiz. Zh. 24, 1835 (1979)

ELEM. SYM.	A	Z
He	3	2

METHOD

REF. NO. 79 Go 9 hg

REACTION	RESULT	EXCITATION ENERGY	SOURCE TYPE	SOURCE RANGE	DETECTOR TYPE	DETECTOR RANGE	ANGLE
E,E/P	ABX	UKN	C	999	MAG-D		DST

999 = 1200 MeV

Summary

Angular dependence of the ^{3}He(e, e'p) cross-section is measured using the electron linac for the incident energy 1200 MeV in the proton angle range $45.5 \leqslant O_p \leqslant 72.5°$. Cross-sections for two- and three-particle disintegration of ^{3}He were calculated with account for the final-state interaction. The calculated results are compared with the experimental measurements.

θ_p°	$\frac{d^3\sigma}{dE_p d\Omega_e d\Omega_p} \cdot 10^{32}$, см²/(МэВ·ср²)	θ_p°	$\frac{d^3\sigma}{dE_p d\Omega_e d\Omega_p} \cdot 10^{32}$, см²/(МэВ·ср²)
45,5	0,91±0,24	60,5	10,18±0,56
48,5	1,62±0,30	63,5	4,69±0,38
51,5	4,86±0,43	66,5	3,33±0,30
54,5	8,68±0,57	69,5	0,88±0,11
57,75	12,82±0,43	72,5	0,45±0,08

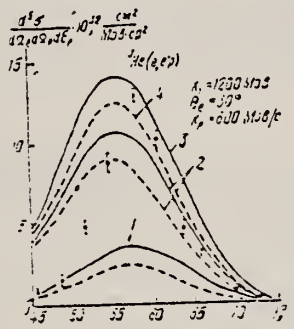

Угловые зависимости дифференциального сечения электрорасщепления ядра ^{3}He: *1* — вклад двухчастичного расщепления (сплошная кривая соответствует выбору функции $\psi_p(p)$ в виде плоской волны, штриховая — учету взаимодействия выбитого протона и дейтрона в дифракционном приближении); *2* — вклад трехчастичного расщепления (сплошная кривая соответствует выбору функции $\Phi_\varepsilon(r)$ в виде плоской волны, штриховая — учету взаимодействия между вторым и третьим нуклонами в дифракционном приближении); *3* и *4* — суммарное сечение реакции без учета и с учетом взаимодействия в конечном состоянии; точки — экспериментальные значения.

ЛИТЕРАТУРА

1. *Johansson A.* Quasifree electron-proton scattering in ^{2}H and ^{3}He.— Phys. Rev., 1964, 136B, N 4, p. 1030—1035.
2. *Griffy T. A., Oakes R. J.* Electron-proton coincidence cross section for ^{3}He and ^{3}H.— Phys. Rev., 1964, 133B, N 5, p. 1161—1167; Structure of ^{3}He and ^{3}H from high-energy electron scattering.— Rev. Mod. Phys., 1965, 37, N 3, p. 402—405.
3. *Lehman D. R.* Electrodisintegration of ^{3}H and ^{3}He.— Phys. Rev. Lett., 1969, 23, N 23, p. 1339—1343; Quasielastic electron scattering from ^{3}He and ^{3}H.— Phys. Rev., 1971, C3, N 5, p. 1827—1840.
4. *Тартаковский В. К., Козловский И. В.* Вычисление сечения реакции ^{3}He(e, e'p)^{3}H с применением метода K-гармоник. Сравнение с другими расчетами.— ЯФ, 1973, 17, № 2, с. 278—285.

Ref. 4. V.K. Tartakovskii and I.V. Kozlovskii, Sov. J. Nucl. Phys. 17, 142 (1973) - Theory

REF. E.C. Jones, Jr., W.L. Bendel, L.W. Fagg, R.A. Lindgren
Phys. Rev. C19, 610 (1979)

ELEM. SYM.	A	Z
He	3	2

METHOD

REF. NO. 79 Jo 4 hg

REACTION	RESULT	EXCITATION ENERGY	SOURCE		DETECTOR		ANGLE
			TYPE	RANGE	TYPE	RANGE	
E,E/	ABX	0-30	D	40-61	MAG-D		180

Elastic and inelastic cross sections for 180° electron scattering from ^{3}He were measured at incident electron energies of 40.44, 50.53, and 60.63 MeV. Our radiatively corrected cross section measurements are in good agreement with theoretical calculations of the behavior near the two-body breakup threshold at 5.5 MeV. The measurements were also compared to cross sections calculated in the zero-range approximation and to sum rules. At $q = 0.602$ fm^{-1} the measured magnetic radius was $r = 1.79 \pm 0.14$ fm. The possibility of the existence of a state at about 10 MeV excitation is also discussed.

[NUCLEAR REACTIONS ^{3}He(e,e'); $\theta = 180°$, $E_0 = 40, 51, 61$ MeV; measured σ for $E_x = 0$ to $E_0/2$. Deduced magnetic radius.]

TABLE I. The ^{2}H and ^{3}He measurements are integrated by comparing the sum rule $J-M$ deduced from experiment with that from theory (Ref. 5). The elastic and inelastic experimental terms are presented separately and then totaled. Error shown on the $J-M$ total are chiefly due to the inelastic term. The ^{2}H cross section was measured up to 19 MeV excitation energy.

	^{3}He	^{2}H
E_0 (MeV)	60.63	56.6
σ	132×10^{-32}	152×10^{-32}
Experiment		
$J-M$ elastic	0.0238	0.0042
$J-M$ inelastic	0.0432	0.0535
$J-M$ total	0.0670 ± 0.0014	0.0577 ± 0.0033
Theory		
$J-M$ total	0.104	0.078

(continued)

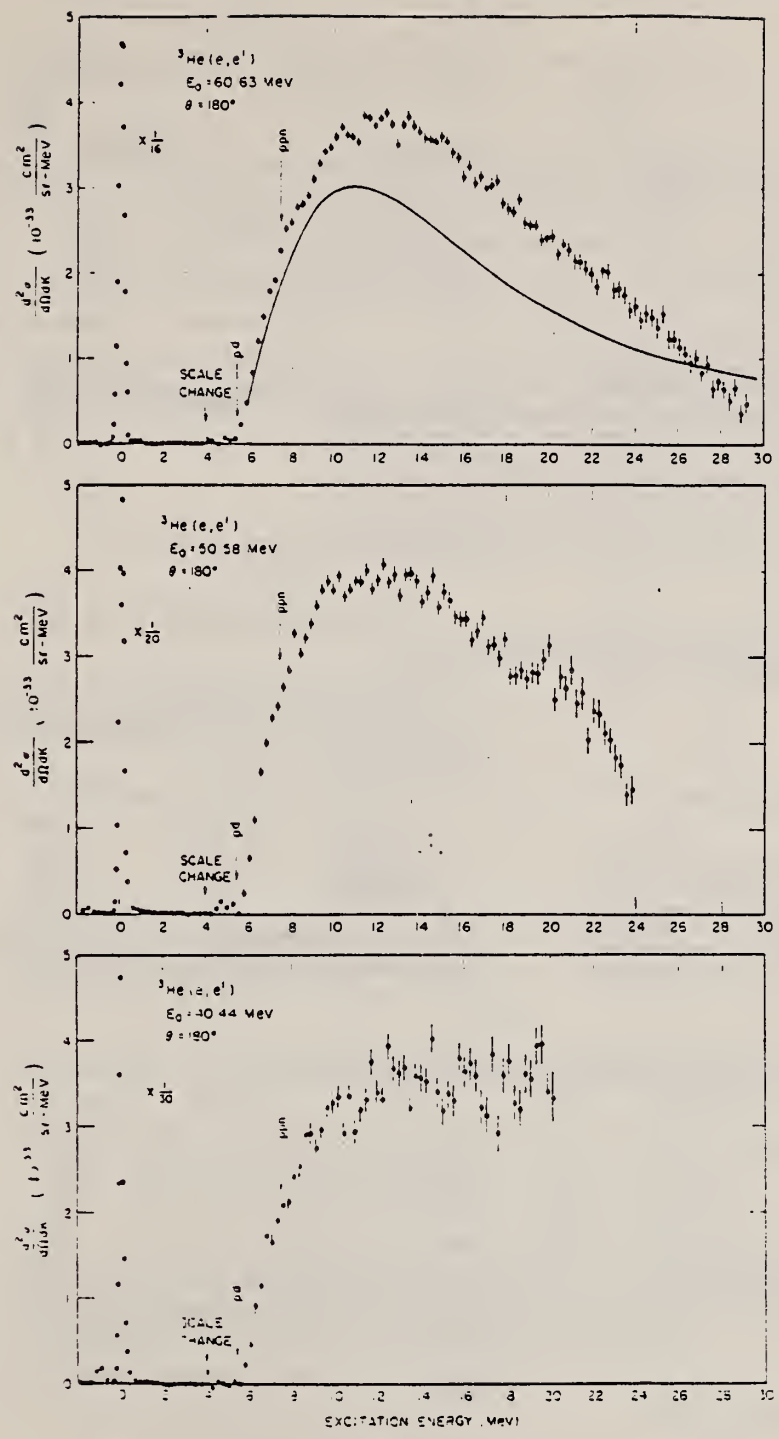

FIG. 3. The radiative unfolded spectra of ^{3}He with background removed is shown for three different incident beam energies, 40.44, 50.58, and 60.63 MeV. The solid line in the upper graph is the zero range calculation.

REF. D. M. Skopik, H. R. Weller, N. R. Roberson, S. A. Wender
Phys. Rev. C19, 601 (1979)

ELEM. SYM.	A	Z
He	3	2

METHOD

REF. NO. 79Sk4 hg

REACTION	RESULT	EXCITATION ENERGY	SOURCE		DETECTOR		ANGLE
			TYPE	RANGE	TYPE	RANGE	
$ P,G	ABX	7-15	D	3-15	NAI-D		DST
				(3.0-14.8)			

The 90° yield curve for the $^2H(p,\gamma)^3He$ reaction has been studied over the excitation region in ^3He of approximately 7 to 15 MeV. Both polarized and unpolarized proton beams were used to measure the angular distributions of cross section and analyzing power at E_x = 8.83, 9.83, and 10.83 MeV. If only the four non-spin-flip $E1$ and $E2$ T-matrix elements are considered, their amplitudes and relative phases can be extracted. The $E2$ cross section obtained from this analysis is found to be $(12 \pm 5)\%$ of the total cross section. The detailed balanced differential ($\theta_{c.m.} = 90°$) and total cross sections at E_x = 10.83 MeV are found to be (117 ± 11) μb/sr and (1.07 ± 0.11) mb, respectively; the quoted errors represent the total uncertainties in the cross sections obtained in this experiment. The results are also compared with recent $E1$ and $E2$ calculations.

POLARIZED PROTONS

[NUCLEAR REACTIONS $^2H(p,\gamma)^3He$; measured σ(90°), $E_x \cong 7$–15 MeV; $\sigma(\theta)$, $A(\theta)$, and σ(tot), E_x = 8.83, 9.83, and 10.83 MeV; deduced $E1$ and $E2$ T-matrix amplitudes and phases.]

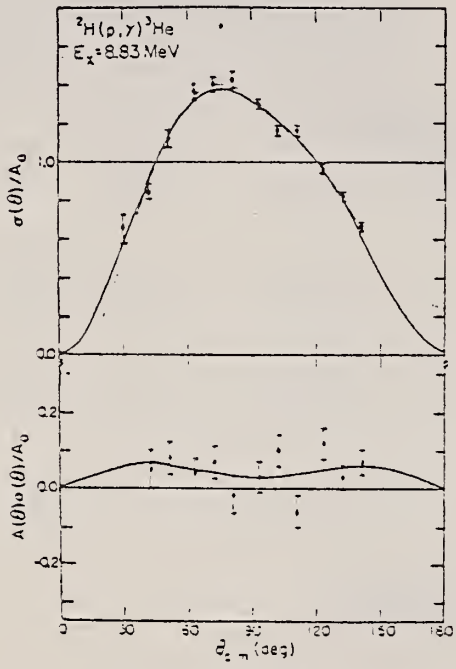

FIG. 4. Cross section and asymmetry data at E_x = 8.83 MeV. The dotted line represents the curve generated by fitting the data to a Legendre polynomial expansion. The solid line corresponds to the fit constrained (see text) at $\theta = 0°$ and 180°. The asymmetry data are unaffected by this constraint.

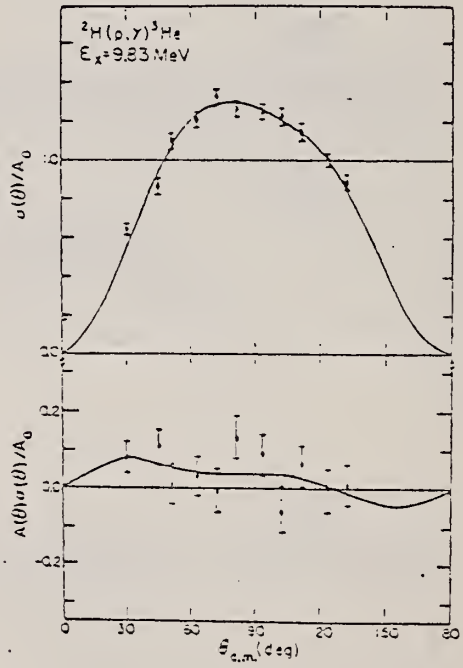

FIG. 5. Cross section and asymmetry data at E_x = 9.83 MeV. Curves are the same as Fig. 4.

(continued)

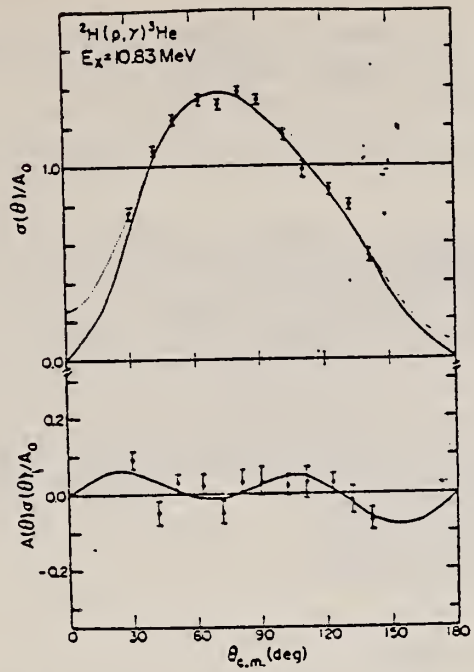

FIG. 6. Cross section and asymmetry data at E_x = 10.83 MeV: Curves are the same as Fig. 4.

TABLE III. Comparison of $E2$ strength near the maximum γ-ray energy measured in this experiment.

Reference	E_γ (MeV)	$E2$ cross sections (% of total)
Ref. 1 [a]	12–16	15 ±10
Ref. 2 [a]	12.1	3.2 ± 1.0
Ref. 2 [a]	15.3	5.0 ± 0.8
Ref. 3 [a]	15.0	7.9 ± 2.8
Present work	10.8	12 ±5

[a] The $E2$ strength was estimated from these experiments using Eqs. (6) and (7).

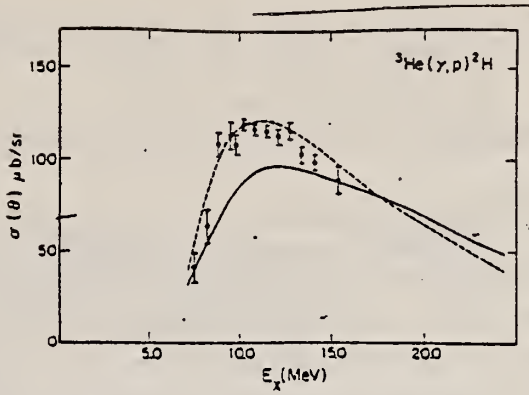

FIG. 8. Differential cross section for the reaction $^3He(\gamma,d)^1H$ at $\theta = 90°$. Curve (— — —) is from Ref. 13, curve (——) is from Ref. 12. These data should be compared with those given in Fig. 1.

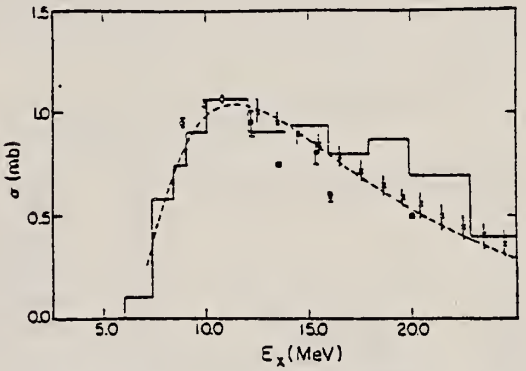

FIG. 9. Total cross section for the reaction $^3He(\gamma,d)$. Open circles are the present results found from $\sigma(\text{tot}) = 4\pi A_0$, ⌐⌙—Ref. 1, ●—Ref. 2, ×—Ref. 3, ■—Ref. 4, and ▼—Ref. 10. Note that only total cross sections are shown. The dashed line is from Barbour and Phillips (Ref. 13).

TABLE I. Angular distribution coefficients at the three energies of this experiment. [a]

E_γ (MeV)	χ^2	A_0 (μb) [c]	a_1	a_2	a_3	a_4	χ^2	b_1	b_2	b_3	b_4
8.83	1.42	76.8 ± 1.5	0.09 ± 0.03	−0.79 ± 0.07	−0.27 ± 0.06	−0.16 ± 0.08	1.36	0.05 ± 0.02	0 ±0.01	0.02 ± 0.01	0 ±0.01
8.83 [b]	1.93	82.5 ± 0.8	0.14 ± 0.02	−0.80 ± 0.03	−0.15 ± 0.02	−0.20 ± 0.03			(as above) [d]		
9.82	0.49	85.2 ± 2.5	0.04 ± 0.07	−0.83 ± 0.12	−0.13 ± 0.09	−0.11 ± 0.09	1.11	0.04 ± 0.02	0.02 ± 0.02	0 ±0.02	0.01 ± 0.01
9.83 [b]	0.71	86.4 ± 1.1	0.08 ± 0.02	−0.77 ± 0.02	−0.09 ± 0.02	−0.24 ± 0.03			(as above) [d]		
10.83	2.76	86.7 ± 1.4	0.25 ± 0.03	−0.69 ± 0.06	−0.19 ± 0.05	−0.15 ± 0.07	1.5	0.01 ± 0.01	0.01 ± 0.01	0 ±0.01	0.02 ± 0.01
10.83 [b]	4.26	96.1 ± 0.6	0.24 ± 0.02	−0.75 ± 0.03	−0.24 ± 0.02	−0.25 ± 0.03			(as above) [d]		

[a] The errors reported here were obtained by multiplying the standard deviations by the value of χ.
[b] Results obtained when data sets were constrained at 0° and 180° (see text).
[c] $\sigma_T(\gamma,p) = 4\pi A_0$.
[d] Results were unchanged by the use of the constraint.

$$\sigma(\theta) = A_0\left[1 + \sum_{i=1}^{4} a_i Q_i P_i(\cos\theta)\right] \qquad (1)$$

$$A(\theta)\sigma(\theta)/A_0 = \sum_i b_i Q_i P_i^1(\cos\theta)\,, \qquad (2)$$

where the Q_i's arise from geometrical effects due to the finite angular acceptance of the crystal. $A(\theta)$, the analyzing power, is defined as

$$A(\theta) = \left(\frac{N_+ - N_-}{N_+ + N_-}\right)\frac{1}{P}\,, \qquad (3)$$

REF. P. Argan, G. Audit, A. Bloch, N. de Botton, J.L. Faure, C. Schuhl, G. Tamas, C. Tzara, E. Vincent, J. Deutsch, D. Favart, R. Prieels, B. Van Oystaeyen
Phys. Rev. C21, 1416 (1980)

ELEM. SYM.	A	Z
He	3	2

METHOD

REF. NO.	
80 Ar 2	hg

REACTION	RESULT	EXCITATION ENERGY	SOURCE TYPE	SOURCE RANGE	DETECTOR TYPE	DETECTOR RANGE	ANGLE
G,PIØ	ABY	138-148	C	140-148	CKV-D		0

Relative measurements of π^0 photoproduction yields have been performed on hydrogen, deuterium, ^{3}He, and ^{4}He, in the region of 1 to 10 MeV above threshold. A simplified distorted-wave impulse approximation model of the four reactions is described; it leads to an overall understanding of the results. Large rescattering effects are brought to evidence in deuterium and ^{3}He, making the extraction of precise values for the dipole photoproduction amplitudes E_{0+} on nucleons strongly dependent on the theoretical description of the processes.

THRESHOLD MEASUREMENT

Final data in 81Ar2.

[NUCLEAR REACTIONS (γ,π^0), ^{1}H, ^{2}H, ^{3}He, and ^{4}He targets; measured reaction yields, E_γ = 1–10 MeV.]

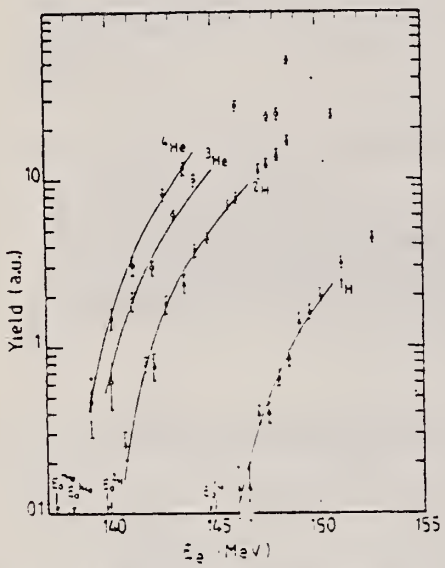

FIG. 5. The measured π^0 photoproduction yields as a function of the end-point bremsstrahlung energy E_γ. The curves are the theoretical yields computed with DWIA cross sections, and adjusted to the data up to 6 MeV above threshold as explained in the text.

TABLE III. Experimental yields $Y_A(E_\gamma) = C\int_{E_0}^{E_\gamma}\int_{\Omega_M} B(E,E_\gamma)\epsilon_A(E,\Omega)(d\sigma_A/d\Omega)d\Omega\,dE$ in microbarns, normalized to one target nucleus and one equivalent quantum, for different values of the bremsstrahlung end-point energy E_γ above threshold E_0. *Note:* The measurements with empty targets gave $Y_{empty} = 0.00 \pm 0.02$. The average yields measured below threshold amounted to $Y_H = 0.02 \pm 0.02$, $Y_D = 0.07 \pm 0.04$, $Y_{^3He} = 0.01 \pm 0.12$, and $Y_{^4He} = 0.01 \pm 0.15$. All have been taken into account in the table.

Hydrogen $E_\gamma - E_0$ (MeV)	Hydrogen $10^3 Y_H$	Deuterium $E_\gamma - E_0$ (MeV)	Deuterium $10^3 Y_D$	^{3}He $E_\gamma - E_0$ (MeV)	^{3}He $10^3 Y_{^3He}$	^{4}He $E_\gamma - E_0$ (MeV)	^{4}He $10^3 Y_{^4He}$
1.41	0.14 ± 0.05	0.88	0.26 ± 0.05	1.87	0.61 ± 0.19	1.72	0.47 ± 0.19
1.91	0.14 ± 0.06	1.38	0.79 ± 0.08	2.37	1.38 ± 0.24	2.72	1.43 ± 0.22
2.41	0.39 ± 0.05	2.26	0.77 ± 0.14	3.37	2.34 ± 0.28	3.72	3.02 ± 0.39
2.91	0.40 ± 0.06	2.88	1.79 ± 0.21	4.37	6.08 ± 0.47	5.22	8.12 ± 0.63
3.41	0.65 ± 0.07	3.76	2.38 ± 0.29	5.37	9.86 ± 0.83	6.22	11.52 ± 0.89
3.91	0.85 ± 0.10	4.26	3.75 ± 0.32	9.37	23.7 ± 1.2	8.72	27.3 ± 1.7
4.41	1.39 ± 0.17	4.88	4.47 ± 0.31	9.87	24.4 ± 1.3	11.22	51.1 ± 3.2
4.91	1.60 ± 0.15	5.38	7.07 ± 0.47				
5.41	2.00 ± 0.16	6.26	7.75 ± 0.55				
6.41	3.15 ± 0.25	7.38	11.10 ± 1.12				
7.91	4.40 ± 0.28	7.76	12.40 ± 0.72				
		8.26	13.9 ± 1.1				
		8.76	16.9 ± 1.1				
		10.38	24.3 ± 1.1				

TABLE VII. The deuterium and ^{3}He threshold amplitudes in units of $10^{-3} m_{\pi^+}^{-1}$.

	Experiment	PWIA [a]	Rescattering amplitudes computed in FSA
D	−7.38 ± 0.36	$E_{0+}^{\pi^0} - E_{0+}^{\pi^+} = -1.5 \pm 0.5$	−6.3
^{3}He	−4.55 ± 0.48	$E_{0+}^{\pi^0} = 0.5 \pm 0.5$	−5.4

[a] The E_{0+} values from Sec. V A.

REF. Yu.T. Grin
Yad. Fiz. 31, 1390 (1980)
Sov. J. Nucl. Phys. 31, 717 (1980)

ELEM. SYM.	A	Z
He	3	2

METHOD

REF. NO.	
80 Go 3	hg

REACTION	RESULT	EXCITATION ENERGY	SOURCE		DETECTOR		ANGLE
			TYPE	RANGE	TYPE	RANGE	
E,E/P	SPC	0*100	C	643,806	MAG-D		UKN

* NUCL. RECOIL MEV/C

(continued)

Study of the two-particle electrodisintegration of ^{3}He

V. A. Gol'dshteĭn, V. L. Kuplennikov, V. V. Lubyanyĭ, V. I. Startsev, V. B. Shostak, and N. G. Afanas'ev

Khar'kov Physico-technical Institute, Ukrainian Academy of Sciences
(Submitted 23 August 1979)
Yad. Fiz. 31, 1388–1389 (May 1980)

PACS numbers: 25.30. – c, 25.10. + s

Study of the ^{3}He$(e, e'p)$ reaction is a valuable source of information not only on the structure of this nucleus but also on the nature of the nucleon-nucleon interaction. A single article by Johansson[1] has been devoted to the experimental study of this reaction. In spite of the more intensive investigation[2–5] of the reaction ^{3}He$(p, 2p)$, obtaining information on the nucleon-nucleon interaction in this case involves fundamental difficulties. Calculations which have appeared recently for the cross section of two-particle electrodisintegration of ^{3}He by Dieperink *et al.*[6] and Heimbach *et al.*[7] with use of the Faddeev technique and various types of nucleon-nucleon interactions permit a comparison to be made between the results of these calculations and experiment for the purpose of choosing a more realistic type of internucleon interaction.

We have carried out a study of the reaction ^{3}He$(e, e'p)$ for two momentum-transfer values 416 and 303 MeV/c with respective energy resolutions 4 and 2.6 MeV. The measurements were made in the linear electron accelerator at the Khar'kov Physico-technical Institute.

Beams of electrons with energies 306 and 643 MeV were scattered by a target of liquid ^{3}He, and electrons with momentum k'_e and protons with momentum p'_p after magnetic analysis were recorded by a multichannel telescope of scintillation counters. Selection of (e, p) coincidences was carried out by amplitude-to-digital converters working in conjunction with an M-6000 computer. Monitoring of the primary energy, and calibration of the scale of missing energy E_s and the reaction cross section $d^5\sigma/d\Omega_e d\Omega_p dE_p$, were carried out on the basis of electron scattering in hydrogen. Separation of the reaction channels corresponding to two-particle and three-particle disintegration of ^{3}He was accomplished by fitting the experimental spectrum with two Gaussians with a width at half-height equal to the experimental energy resolution and with a fixed distance between maxima equal to 2.2 MeV. The value of the distorted spectral function $S(E_s, q_R)$ was determined in accordance with Ref. 8:

$$S(E_s, q_R) = \frac{d^5\sigma/d\Omega_e\, d\Omega_p\, dE_p}{K\Lambda(k_e, k'_e, p'_p)Z},$$

where q_R is the momentum of the recoil nucleus, K is a kinematic factor, $\Lambda(k_e, k'_e, p'_p)$ is the cross section for elastic scattering of an electron by a moving proton, and Z is the number of protons in the nucleus. The experimental results and also the data of Ref. 1 with the analysis of Ref. 9 are shown in the figure. The data for $p'_p = 303$ MeV/c have been multiplied by a factor of 3.2. Curves 1 and 2 were obtained in accordance with Refs. 6 and 7 and correspond to calculations with use of a Reid soft-core potential and a separable potential of the Yamaguchi type with the parameters of Tabakin. Curves 3 and 4 were obtained in terms of the shell model with an oscillator potential, for which the parameter $p_0 = 104$ MeV/c was obtained from data on elastic scattering of electrons by ^{3}He with inclusion of a correction for the motion of the center of mass (curve 3), and the parameter $p_0 = 90$ MeV/c was taken for comparison from Ref. 6. Curve 5 is the result of a calculation[10] in the plane-wave approximation with use of a Gaussian-like wave function of the bound state of ^{3}He.

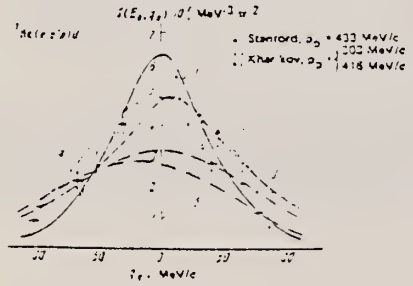

FIG. 1.

[1] A. Johansson, Phys. Rev. 136, B1030 (1964).
[2] I. Slaus, M. B. Epstein, *et al.*, Phys. Rev. Lett. 27, 731 (1971).
[3] P. Kitching *et al.*, Phys. Rev. C6, 769 (1972).
[4] R. Frascaria *et al.*, Nucl. Phys. A178, 307 (1971).
[5] H. G. Pugh *et al.*, Phys. Lett. 46B, 192 (1973).
[6] A. E. L. Dieperink *et al.*, Phys. Lett. 63B, 261 (1976).
[7] C. R. Heimbach *et al.*, Phys. Lett. 66B, 1 (1977).
[8] J. Potter, Nucl. Phys. 45, 33 (1963).
[9] B. F. Gibson and G. B. West, Nucl. Phys. B1, 349 (1967).
[10] V. A. Gol'dshteĭn, É. L. Kuplennikov, *et al.*, Ukr. Fiz. Zh. 24, 1335 (1979).

REF. James S. McCarthy
Nucl. Phys. A335, 27 (1980)

ELEM. SYM.	A	Z
He	3	2

METHOD

REF. NO. 80 Mc 3 hg

REACTION	RESULT	EXCITATION ENERGY	SOURCE		DETECTOR		ANGLE
			TYPE	RANGE	TYPE	RANGE	
E,E/	NOX	2@7	D	3*11	MAG-D		UKN

Abstract: Inclusive electron scattering from the nuclei ^{56}Fe and ^{3}He has been measured over a wide range of incident energy and momentum transfer. The data is used to separate the longitudinal and transverse response functions. The two-nucleon correlation function and the momentum distribution of the internal nucleons is compared to the data.

*GEV, @FM-1

NUCLEAR REACTIONS: (e,e') on ^{56}Fe, ^{3}He Incident Energies E = 0.1 to 14 GeV; measured scattered electron at energy loss ω = E-E' of 0-.2 GeV. Deduced momentum distribution.

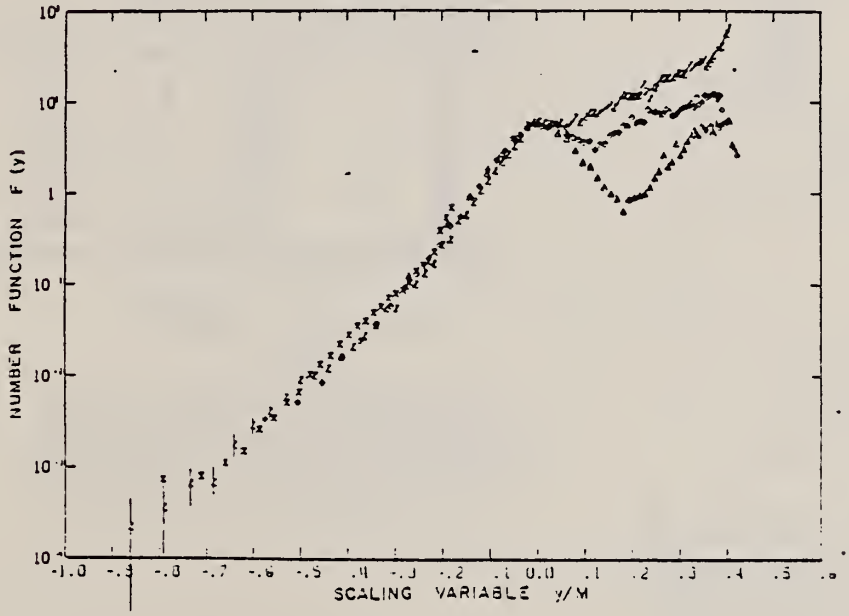

Fig. 5 The scaling variable y for ^{3}He has been divided by the nucleon mass in this plot. (Δ) represent data at incident energy of 1.26 GeV, (Φ) at 7.25 GeV, (X) at 3.61 GeV, and (Z) at 10.95 GeV. The momentum transfer q^2 extends to 2.25(GeV/c)^2.

REF. B.M.K. Nefkens, Th.S. Bauer, K. Baba, A. Boudard, W.J. Briscoe, G. Bruge, J.L. Faure, J. Gosset, A. Hegerath, J.C. Lugol, B.H. Silverman, Y. Terrien
Phys. Rev. Lett. 45, 168 (1980)

ELEM. SYM.	A	Z
He	3	2

METHOD

REF. NO. 80 Ne 2 hg

REACTION	RESULT	EXCITATION ENERGY	SOURCE		DETECTOR		ANGLE
			TYPE	RANGE	TYPE	RANGE	
P,G	ABX.	308,375	D	450,550	MAG-D		DST

GAMMA-HE3 COINC

Seven differential cross sections of the reaction $p + d \rightarrow {}^3\mathrm{He} + \gamma$ have been measured at T_p = 450 and 550 MeV between 52° and 92° (θ_γ c.m.). ^{3}He's were analyzed by the SPES I spectrometer in coincidence with photons detected by Cherenkov counters. The results are about twice the cross sections of the inverse reaction measured recently by Hegerath *et al.* and by Argan *et al.* The data are consistent, however, with the $\gamma + {}^3\mathrm{He} \rightleftharpoons p + d$ data of Heusch *et al.*

PACS numbers: 25.40.Lw, 11.30.Er, 25.10.+s

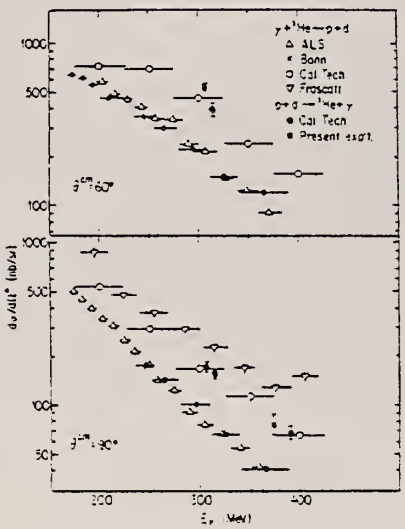

FIG. 1. Existing controversy in $\gamma + {}^3\mathrm{He} \rightarrow p + d$. The $\gamma + {}^3\mathrm{He} \rightarrow p + d$ measurements are those of Heusch *et al.* (Ref. 1, open circles), Argan *et al.* (Ref. 3, triangles), Picozza *et al.* (Ref. 4, inverted triangles), and Hegerath *et al.* (Ref. 5, crosses). The $p + d \rightarrow {}^3\mathrm{He} + \gamma$ data of Heusch *et al.* (Ref. 2, closed circles) and the present experiment (squares) have been multiplied by the appropriate detailed-balance factors, and the data of the present experiment have been interpolated to θ = 60° and 90° from slightly different angles.

TABLE I. Differential cross sections in center of mass for $p + d \rightarrow {}^3\mathrm{He} + \gamma$. Errors quoted do not include an overall systematic uncertainty of 10%.

T_p (lab) (MeV)	θ_γ (c.m.)	$d\sigma/d\Omega$ (nb/sr)
450	51.6	81 ± 10
450	59.6	71.5 ± 4.3
450	69.2	48.9 ± 3.4
450	78.9	32.6 ± 2.3
450	91.8	21.3 ± 1.8
550	71.0	27.7 ± 3.3
550	93.3	9.9 ± 1.4

REF. P. Argan, G. Audit, A. Bloch, N. de Botton, J.L. Faure, C. Schuhl, G. Tamas, C. Tzara, E. Vincent, J. Deutsch, D. Favart, R. Prieels, B. Van Oystaeyen
Phys. Rev. C24, 300 (1981)

ELEM. SYM.	A	Z
He	3	2

METHOD

REF. NO.: 81 Ar 2 | egf

REACTION	RESULT	EXCITATION ENERGY	SOURCE		DETECTOR		ANGLE
			TYPE	RANGE	TYPE	RANGE	
G,PIØ	ABY	140-147	C	140-147	CKV-D		Ø

Our recently published π^0 photoproduction data at threshold have been reanalyzed with the use of a more refined detection efficiency calculation. The high energy points appear to be consistent with the threshold measurements; the effective threshold amplitudes remain unchanged, and are now supported by the complete set of experimental data.

REANALYSIS OF 80AR2

[NUCLEAR REACTIONS (γ,π^0), ^{1}H, ^{2}H, ^{3}He, and ^{4}He targets; measured reaction yields, E_{π^0}=1-10 MeV.]

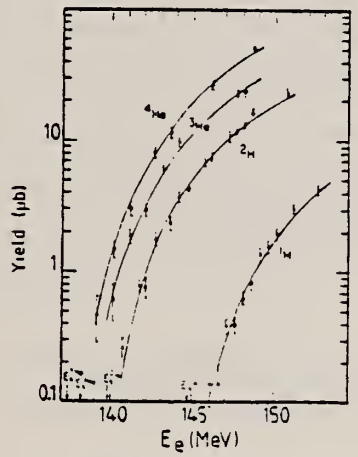

FIG. 2. The measured π^0 photoproduction yields in microbarns, normalized to one target nucleus and one equivalent quantum, as functions of the Bremsstrahlung end-point energy E_e. The curves are the theoretical yields computed with DWIA cross sections, and adjusted to the complete set of data as explained in the text.

REF. B. Bellinghausen, A. Christ, H.J. Gassen, G. Goerigk, R. Müller, G. Nöldeke, T. Reichelt, H. Stanek, P. Stipp
Nucl. Phys. A358, 373c (1981)

ELEM. SYM.	A	Z
He	3	2

METHOD

REF. NO.	
81 Be 3	HG

REACTION	RESULT	EXCITATION ENERGY	SOURCE		DETECTOR		ANGLE
			TYPE	RANGE	TYPE	RANGE	
G,PIO	ABX	280-386	C	300-450	MGP-D		0

Abstract: π^0 photoproduction on ^{3}He, Li(nat) and ^{9}Be has been measured under small angles in the P_{33} resonance region.

Table 1
Cross sections as function of energy and momentum transfer

K_{max}	K	q	$d\sigma/d\Omega^*$ in ub/sterad		
MeV	MeV	fm^{-1}	^{3}He	Li(nat)	^{9}Be
300	280	0.27	12.4 ± 1.5	21.0 ± 2.4	23.6 ± 2.7
320	296	0.27	14.6 ± 1.5	26.9 ± 2.1	34.4 ± 2.7
370	334	0.26	14.3 ± 1.5	24.9 ± 2.0	31.0 ± 2.6
390	361	0.23	10.0 ± 1.1	21.1 ± 1.6	24.5 ± 1.8
450	386	0.27	7.7 ± 1.1	22.7 ± 2.3	22.8 ± 2.3

REF. D.D. Faul, B.L. Berman, P. Meyer, D.L. Olson
Phys. Rev. C24, 849 (1981)

EL EM. SYM.	A	Z
He	3	2

METHOD

REF. NO. 81 Fa 1 hg

REACTION	RESULT	EXCITATION ENERGY	SOURCE		DETECTOR		ANGLE
			TYPE	RANGE	TYPE	RANGE	
G,N	ABX	7-25	D	7-25	BF3-I		4PI

The photoneutron cross sections for ^{3}H and ^{3}He have been measured from threshold to ~25 MeV with monoenergetic photons from the annihilation in flight of fast positrons. These reactions include the two-body breakup of ^{3}H and the three-body breakup of both ^{3}H and ^{3}He; these measurements for ^{3}H are the first to span the energy region across the peaks of the cross sections. An efficient BF_3-tube-and-paraffin neutron detector and high-pressure gaseous samples were employed in these measurements. The results, when compared with each other and with results for the two-body breakup cross section for ^{3}He from the literature, show that: (a) the two-body breakup cross sections for ^{3}H and ^{3}He have nearly the same shape, but the one for ^{3}He lies lower in magnitude; (b) the three-body breakup cross section for ^{3}He lies higher in magnitude, broader in the peak region, and also rises less sharply from threshold than that for ^{3}H; and (c) these differences between the cross sections for the breakup modes largely compensate in their sum, so that the total photon absorption cross sections for ^{3}H and ^{3}He are nearly the same in both size and shape at energies near and above their peaks. Theoretical results from the literature disagree with the experimental results to a certain extent over the entire photon-energy region for which the photoneutron cross sections were measured. Sum rule predictions also fail to reproduce the experimental results. These discrepancies constitute a challenge to the principle of charge symmetry of the nuclear force, but more complete theoretical calculations are needed to ascertain whether these discrepancies can be ascribed entirely to electromagnetic effects.

[NUCLEAR REACTIONS ^{3}H(γ,n), ^{3}H(γ,2n), ^{3}He(γ,n); measured $\sigma(E_\gamma)$, threshold to ~25 MeV; monoenergetic photons, high-pressure gas samples; two-body breakup, three-body breakup, charge asymmetry.]

(continued)

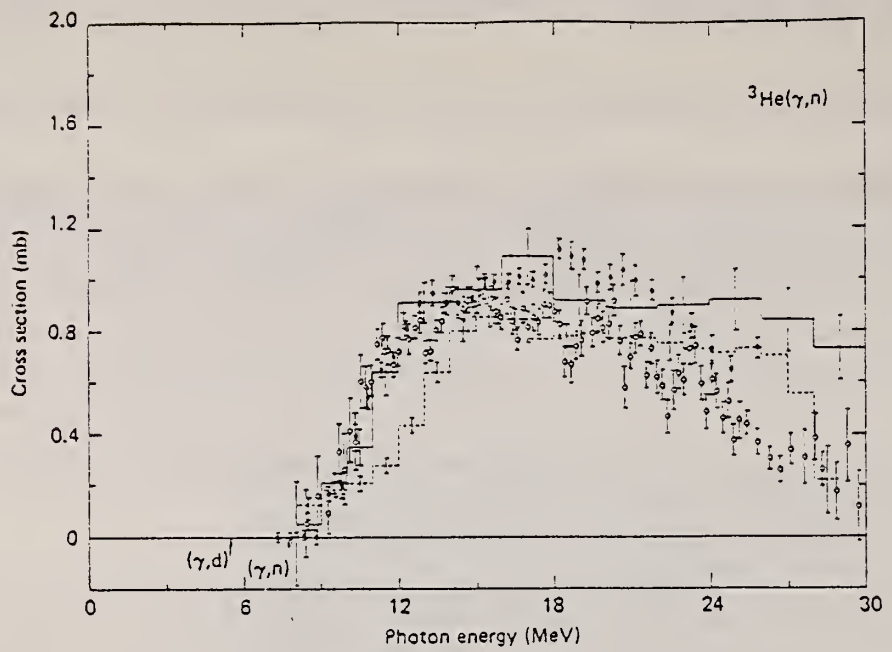

FIG. 9. Three-body photodisintegration cross section for ^{3}He: filled circles, present data; open circles, data of Ref. 31; solid histogram, Ref. 12; dashed histogram, Ref. 30. The error flags indicate statistical uncertainties only. The arrows in this and the following figures indicate the reaction thresholds, as labeled.

TABLE III. Integrated cross sections and moments.

Reaction	$E_{\gamma_{max}}$ (MeV)	σ_{int} (MeV mb)[a]	σ_{-1} (mb)[b]	σ_{-2} (mb MeV^{-1})[c]
^{3}He(γ,n)	23.4	12.3 ± 1.2	0.760 ± 0.061	0.050 ± 0.004
^{3}H(γ,n)	23.4	11.7 ± 1.2	0.840 ± 0.067	0.067 ± 0.005
^{3}H(γ,2n)	23.4	10.2 ± 1.0	0.638 ± 0.051	0.042 ± 0.003
^{3}He(γ,n)	25.8	14.1 ± 1.4	0.833 ± 0.067	0.053 ± 0.004
^{3}H(γ,n)[d]	25.8	13.2 ± 1.3	0.896 ± 0.072	0.069 ± 0.006
^{3}H(γ,2n)	25.8	11.5 ± 1.2	0.691 ± 0.055	0.044 ± 0.003
^{3}He(γ,n)[d]	26.4	14.4 ± 1.4	0.850 ± 0.068	0.053 ± 0.004
^{3}H(γ,n)[d]	26.4	13.6 ± 1.3	0.900 ± 0.072	0.070 ± 0.006
^{3}H(γ,2n)	26.4	12.0 ± 1.2	0.709 ± 0.057	0.045 ± 0.004
^{3}He(γ,n)[d]	30.0	16.4 ± 2.0	0.917 ± 0.092	0.056 ± 0.004
^{3}H(γ,n)[d]	30.0	15.4 ± 1.8	0.986 ± 0.099	0.072 ± 0.006
^{3}H(γ,2n)[d]	30.0	13.6 ± 1.6	0.767 ± 0.077	0.047 ± 0.004

[a] $\sigma_{int} = \int_0^{E_{\gamma_{max}}} \sigma(E_\gamma) dE_\gamma$

[b] $\sigma_{-1} = \int_0^{E_{\gamma_{max}}} \sigma(E_\gamma) E_\gamma^{-1} dE_\gamma$

[c] $\sigma_{-2} = \int_0^{E_{\gamma_{max}}} \sigma(E_\gamma) E_\gamma^{-2} dE_\gamma$

[d] Extrapolated (from the present data only).

REF. H.J. Gassen, A. Hegerath, W. Loers, B. Mecking, G. Nöldeke
T. Reichelt, H. Stanek
Z. Phys. A303, 35 (1981)

ELEM. SYM.	A	Z
He	3	2

METHOD

REF. NO. 81 Ga 5 egf

REACTION	RESULT	EXCITATION ENERGY	SOURCE TYPE	SOURCE RANGE	DETECTOR TYPE	DETECTOR RANGE	ANGLE
G,P	ABX	200-450	C	500	TOF-D		DST

The $^3He(\gamma, p)d$ reaction has been measured in the photon energy region between 200 MeV and 450 MeV at proton c.m. angles between 20° and 150°.
Protons and deuterons were detected in coincidence with two time-of-flight spectrometers consisting of scintillation counters; both particles were identified and their energies and angles were measured.
The angular distributions show a strong forward peak. The differential cross sections fall off with increasing photon energy without showing a significant influence of the Δ resonance.

P - D COINC

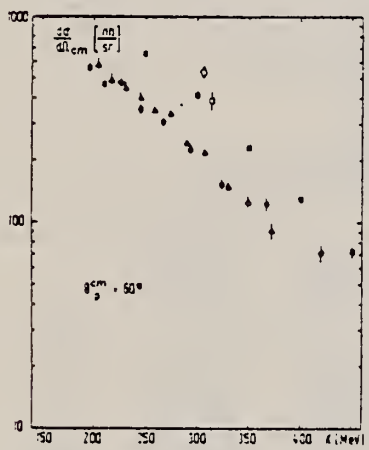

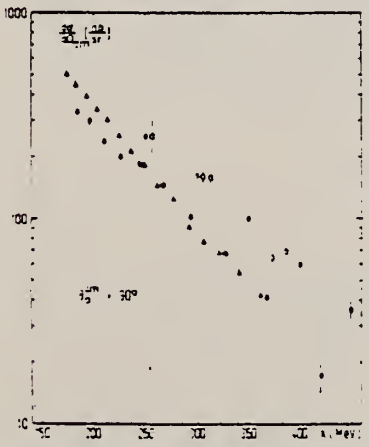

Fig. 2. Differential cross sections as a function of photon energy k for $\vartheta_p^{cm} = 60°$ and 90°; our results (●) are compared to the photodisintegration data of Argan et al. (▲) [6] and Heusch et al. (■) [7] and, after using the detailed balance factor, to the radiative capture data of Heusch et al. (□) [8] and Neikens et al. (○) [17]

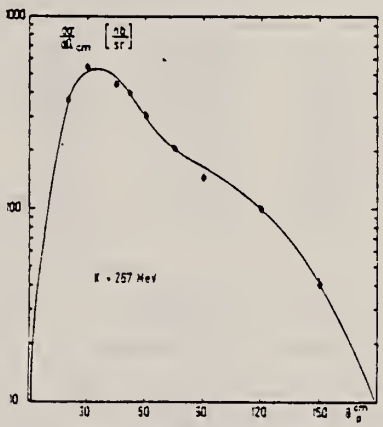

Fig. 3. Angular distribution at $k = 267$ MeV; the full curve represents the fit in $\cos \vartheta_p^{cm}$ to the data

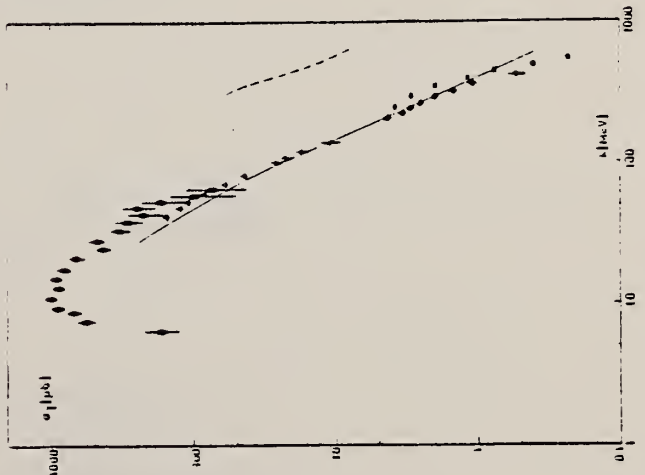

Fig. 4. The total cross section as a function of photon energy. Our results (●) are shown together with those of Heusch et al (■) [7], O'Fallon et al (▲) [16] and Gurbunov (●) [19]. The full curve has been calculated using the scaling behaviour of the measured differential cross sections.
Dashed line, total cross section for the deuteron disintegration

continued)

Table 1. Differential cross sections (nb/sr); the errors are due to counting statistics only

k(MeV)	Proton c.m. angle (deg)									
	20°	30°	45° (1. series)	45° (2. series)	52°	60°	75°	90°	120°	150°
154									326 ± 10	105 ± 6
163									302 ± 9	98 ± 5
173							603 ± 17		270 ± 9	82 ± 5
184							513 ± 15	337 ± 17	243 ± 8	66 ± 4
196						573 ± 29	434 ± 13	304 ± 15	209 ± 7	57 ± 4
210			707 ± 31	691 ± 26	556 ± 12	472 ± 23	359 ± 11	242 ± 12	193 ± 6	42 ± 3
226		618 ± 27	606 ± 24	557 ± 21	467 ± 10	487 ± 24	320 ± 10	204 ± 11	166 ± 6	35 ± 3
245		635 ± 27	522 ± 26	529 ± 20	425 ± 9	362 ± 21	254 ± 9	187 ± 11	139 ± 5	30 ± 3
267	376 ± 27	557 ± 23	443 ± 22	451 ± 18	399 ± 9	311 ± 13	207 ± 7	147 ± 9	100 ± 4	31 ± 3
294	352 ± 24	477 ± 20	377 ± 19	369 ± 15	359 ± 8	228 ± 13	147 ± 7	104 ± 7	67 ± 3	26 ± 3
326	343 ± 24	414 ± 17	296 ± 15	240 ± 11	259 ± 8	155 ± 11	107 ± 6	68 ± 5	43 ± 3	24 ± 3
367	279 ± 19	360 ± 16	223 ± 13	189 ± 9	189 ± 4	125 ± 10	74 ± 5	42 ± 4	23 ± 2	20 ± 2
420	230 ± 16	196 ± 15	75 ± 7	93 ± 6	104 ± 3	72 ± 7	27 ± 3	17 ± 3	10 ± 2	12 ± 2

Table 2. Coefficients of the polynomial fits and total cross sections

k (MeV)	A (nb/sr)	B	C	D	E	σ_T (μb)
210	372.5 ± 23.0	−0.77 ± 0.09	−0.64 ± 0.44	2.53 ± 0.25	2.42 ± 0.62	4.34 ± 0.42
226	250.1 ± 8.5	−0.57 ± 0.09	0.95 ± 0.28	2.05 ± 0.20	0.60 ± 0.38	3.38 ± 0.18
245	221.6 ± 8.1	−0.8. ± 0.09	0.40 ± 0.28	2.76 ± 0.20	1.60 ± 0.38	3.04 ± 0.16
267	166.6 ± 6.4	−0.48 ± 0.10	0.61 ± 0.30	2.26 ± 0.22	2.12 ± 0.38	2.57 ± 0.14
294	109.3 ± 5.4	−0.31 ± 0.13	1.16 ± 0.39	2.46 ± 0.30	2.71 ± 0.48	2.03 ± 0.13
326	75.8 ± 4.1	−0.12 ± 0.18	0.10 ± 0.41	1.94 ± 0.42	5.42 ± 0.63	1.50 ± 0.10
367	48.5 ± 3.2	0.32 ± 0.21	−0.66 ± 0.45	1.51 ± 0.49	8.18 ± 0.74	1.11 ± 0.09
420	16.9 ± 2.3	1.16 ± 0.56	−0.03 ± 1.09	−0.44 ± 1.18	12.34 ± 2.05	0.54 ± 0.08

6. Argan, P.E., Audit, G., De Botton, N., Faure, J.-L., Laget, J.-M., Martin, J., Schuhl, C.G., Tamas, G.: Nucl. Phys. A 237, 447 (1975)
7. Heusch, C.A., Kline, R.V., McDonald, K.T., Prescott, C.Y.: Phys. Rev. Lett. 37, 405 (1976)
8. Heusch, C.A., Kline R.V., McDonald, K.T., Carroll, J.B., Fredrickson, D.H., Gottein, M., Macdonald, B., Perez-Mendez, V., Stetz, A.W.: Phys. Rev. Lett. 37, 409 (1976)
17. Neifens, B.M.K., Bauer, Th.S., Baba, K., Boudard, A., Briscoe, W.J., Bruge, G., Faure, J.L., Gosset, J., Hegerath, A., Lugol, J.C., Silverman, B.H., Terrien, Y.: Phys. Rev. Lett. 45, 168 (1980)

REF. I.V. Kozlovsky, V.A. Goldshtein, E.L. Kuplennikov, E.M. Malyarzh, V.K. Tartakovsky, V.B. Shostak
Nucl. Phys. A368, 493 (1981)

ELEM. SYM.	A	Z
He	3	2

METHOD

REF. NO. 81 Ko 2 hg

REACTION	RESULT	EXCITATION ENERGY	SOURCE		DETECTOR		ANGLE
			TYPE	RANGE	TYPE	RANGE	
E,E/P	ABX	THR-806	D	643,806	MAG-D		DST

Abstract: The differential cross sections of the ^{3}Hele, e'p) reaction are measured, the channels associated with the two- and three-particle electrodisintegration being separated. Angular distributions of the outgoing protons for the reaction ^{3}Hele, e'p) and energy spectra of scattered electrons for the process ^{3}Hele, e') are calculated. The influence of the nuclear structure and the interaction in the final state on the magnitudes and shapes of these distributions is analysed in detail.

E NUCLEAR REACTIONS ^{3}Hele, e'p), $E = 806$, 643 MeV; measured $\sigma(\theta_p, E_p, \theta_e)$. Calculation, structure effects, final state interactions.

2,3 BODY BRKUP, COINC

TABLE 2

Angular dependence of the ^{3}Hele, e'p) cross section

$k_p = 416$ MeV/c			$k_p = 303$ MeV/c		
θ_p (deg)	$\frac{d^3\sigma_2}{dE_e\, d\Omega_e\, d\Omega_f}$	$\frac{d^3\sigma_3}{dE_e\, d\Omega_e\, d\Omega_f}$	θ_p (deg)	$\frac{d^3\sigma_2}{dE_e\, d\Omega_e\, d\Omega_f}$	$\frac{d^3\sigma_3}{dE_e\, d\Omega_e\, d\Omega_f}$
	$(10^{-32}\,cm^2 \cdot MeV^{-1} \cdot sr^{-2})$			$(10^{-32}\,cm^2 \cdot MeV^{-1} \cdot sr^{-2})$	
47.5	2.32 ± 0.27	0.80 ± 0.31	54	7.27 ± 2.78	9.00 ± 2.21
52.5	5.76 ± 0.78	4.40 ± 0.83	60	19.29 ± 2.91	31.59 ± 2.88
57.5	11.40 ± 0.89	10.26 ± 0.89	67.2	24.37 ± 1.86	31.84 ± 2.02
62.25	11.98 ± 0.87	13.95 ± 0.89	72	18.87 ± 3.71	31.08 ± 4.58
67.5	8.32 ± 0.64	7.41 ± 0.64	78	13.35 ± 2.78	3.85 ± 1.34
72.5	3.57 ± 0.48	3.26 ± 0.49			

$d\sigma_2$ and $d\sigma_3$ are the two- and three-particle disintegration cross sections, respectively.

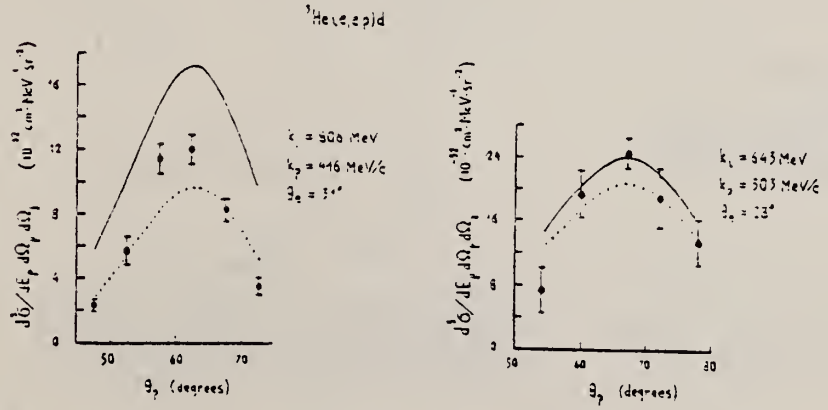

Fig. 2. Outgoing proton angular distributions calculated with the use of the interpolation model wave functions (see the text). Solid lines – FSI, dotted lines – PWA.

REF. W.J. Briscoe, D.H. Fitzgerald, B.M.K. Nefkens, H. Crannell, D.I. Sober, R. Goloskie, W.W. Sapp, Jr.
Phys. Rev. Lett. 49, 187 (1982)

EL EM. SYM.	A	Z
He	3	2

METHOD

REF. NO.	
82 Br 9	egf

REACTION	RESULT	EXCITATION ENERGY	SOURCE		DETECTOR		ANGLE
			TYPE	RANGE	TYPE	RANGE	
G,D	ABX	150-350	C	275-360	MAG-D		DST

Differential cross sections for ^{3}He(γ, d)p have been measured at θ_c(c.m.) ~60° and ~90° for photon energies between 150 and 350 MeV. The data have an absolute normalization uncertainty of 6% and provide absolute differential cross sections suitable for a test of time-reversal invariance when used in conjunction with comparable data on the inverse reaction.

PACS numbers: 25.20.+y, 11.30.Er, 25.10.+s

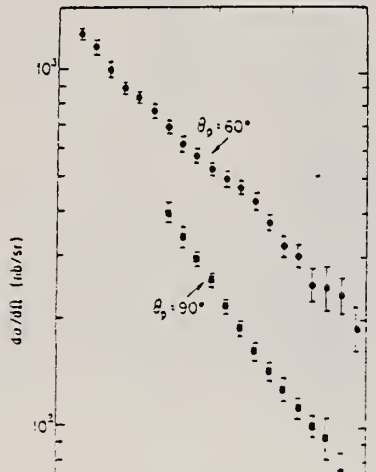

FIG. 2. The differential cross sections obtained in this experiment interpolated to θ_c(c.m.) = 60° and 90°. The errors shown are statistical only.

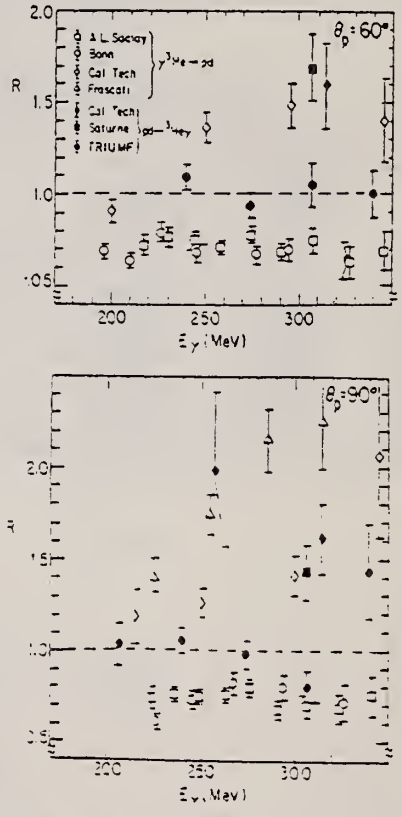

FIG. 3. The ratios (R) of the $d\sigma/d\Omega$'s obtained in measurements of ^{3}He(γ,p)d, open symbols (Refs. 4, 3, 6, 5, respectively), and d(p,γ)^{3}He, solid symbols (Refs. 9, 7, 8, respectively), to our results.

Fig. 3 Refs.:
4) 75Ar1
3) 81Ga5
6) 76He2
[5]P. Picozza *et al.*, Nucl. Phys. A157, 190 (1970).
9) 76He3
7) 80Ne2
[8]J. M. Cameron *et al.*, in Abstracts of the Proceedings of the Ninth International Conference on High Energy Physics and Nuclear Structure, Versailles, France, 1981 (unpublished), p. 473; A. W. Stetz, private communication.

REF. V.A. Gol'dshtein
Yad. Fiz. 35, 801 (1982)
Sov. J. Nucl. Phys. 35, 465 (1982)

ELEM. SYM.	A	Z
He	3	2

METHOD

REF. NO.	
82 Go 3	egf

REACTION	RESULT	EXCITATION ENERGY	SOURCE		DETECTOR		ANGLE
			TYPE	RANGE	TYPE	RANGE	
E,E/P	ABX	1*12	D	643,806	TEL-D		DST

We describe the technique and present the results of a study of the reaction ^{3}He$(e,e'p)$ for primary energies E_i = 806 and 643 MeV and electron scattering angles θ_e = 31 and 28° with energy resolution 4 and 2.6 MeV, respectively. The angular distributions (θ_p = 47.5–72.5° and 54–72°) and momentum distributions (q_R = ±100 MeV/c) of protons for two-particle and three-particle disintegration of ^{3}He are compared with model and exact calculations with use of various wave functions of the ^{3}He ground state. It is shown that the angular and momentum distributions obtained are best described by a model calculation with use of the Irving wave function and the exact calculation with the Yamaguchi potential and the Tabakin parameters.

PACS numbers: 25.30.Cg, 25.10. + s, 27.10. + h

*MISSING ENERGY

TABLE I. Cross sections for the reactions ^{3}He$(e,e'p)d$ and ^{3}He$(e,e'p)np$.

Kinematics 1				Kinematics 2			
θ_p, deg	Reaction cross section* ^{3}He$(e,e'p)d$	Reaction cross section* ^{3}He$(e,e'p)np$	χ^2	θ_p, deg	Reaction cross section* ^{3}He$(e,e'p)d$	Reaction cross section* ^{3}He$(e,e'p)np$	χ^2
47.5	2.3±0.3	0.8±0.3	0.3	54	7.2±2.0	8.9±1.7	0.2
52.5	5.8±0.8	4.4±0.8	1.1	60	19.1±2.2	31.2±2.1	0.4
57.5	11.4±0.9	10.3±0.9	1.0	67.2	24.1±1.4	31.5±1.5	1.5
62.25	12.0±0.9	14.0±0.9	2.8	72	18.6±2.8	30.7±3.4	0.4
67.5	8.3±0.8	7.4±0.8	4.9	78	13.1±2.0	3.8±1.0	0.1
72.5	3.8±0.5	3.3±0.5	1.5				

*Here for the cross sections we have given values of $(d^6\sigma/d\Omega_e d\Omega_p dE_p) \cdot 10^{32}$ in cm^2 MeV^{-1} sr^{-2}.

Measurement of the ^{3}He$(e,e'p)$ cross sections was carried out under two kinematic conditions: kinematics 1—

E_i=806 MeV, ϑ_e=31°, p_e=416 MeV/c, ϑ_p=47.5° −72.5°, ΔE=4 MeV, Δq_R=±7 MeV/c,

and kinematics 2—

E_i=643 MeV, ϑ_e=28°, p_e=303 MeV/c, ϑ_p=54° −72°, ΔE=2.6 MeV, Δq_R=±13.6 MeV/c

(here ΔE and Δq_R are the resolutions in energy and momentum).

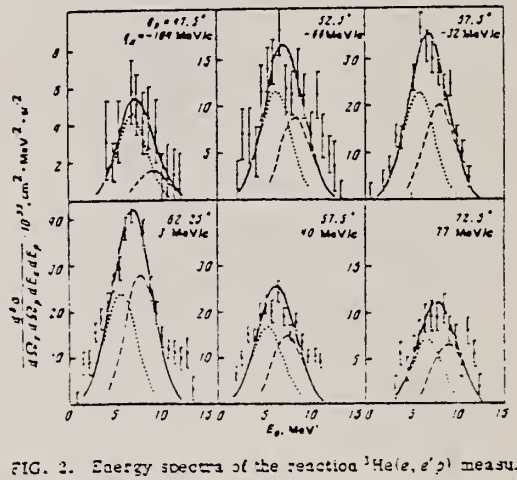

FIG. 2. Energy spectra of the reaction ^{3}He$(e,e'p)$ measured under the conditions of kinematics 1 for various values of the angle ϑ_p and momentum q_R. The dotted and dashed curves are the result of fitting the cross sections for two-particle and three particle disintegration, and the solid curve is their sum.

REF. E. Jans, P. Barreau, M. Bernheim, J.M. Finn, J. Morgenstern, J. Mougey, D. Tarnowski, S. Turck-Chieze, S. Frullani, F. Garibaldi, G.P. Capitani, E. de Sanctis, M.K. Brussel, I. Sick
Phys. Rev. Lett. 49, 974 (1982)

ELEM. SYM.	A	Z
He	3	2

METHOD

REF. NO.: 82 Ja 3 egf

REACTION	RESULT	EXCITATION ENERGY	SOURCE		DETECTOR		ANGLE
			TYPE	RANGE	TYPE	RANGE	
E,E/P	DST	5*305	D	509,528	MAG-D		DST

*MEV/C P MOMENTUM DST

The proton momentum distribution of ^{3}He has been determined up to momenta of 310 MeV/c by use of the reaction ^{3}He(e,$e'p$). The experimental missing-energy resolution, δE_m = 1.2 MeV, was sufficient to separate the two- and three-body breakup channels. Results for the three-body disintegration have been obtained up to missing-energy values of 80 MeV. The resulting spectral function is compared to the predictions of Faddeev and variational calculations.

PACS numbers: 25.30.Cg, 24.10.-k, 21.40.+d, 25.10.+s

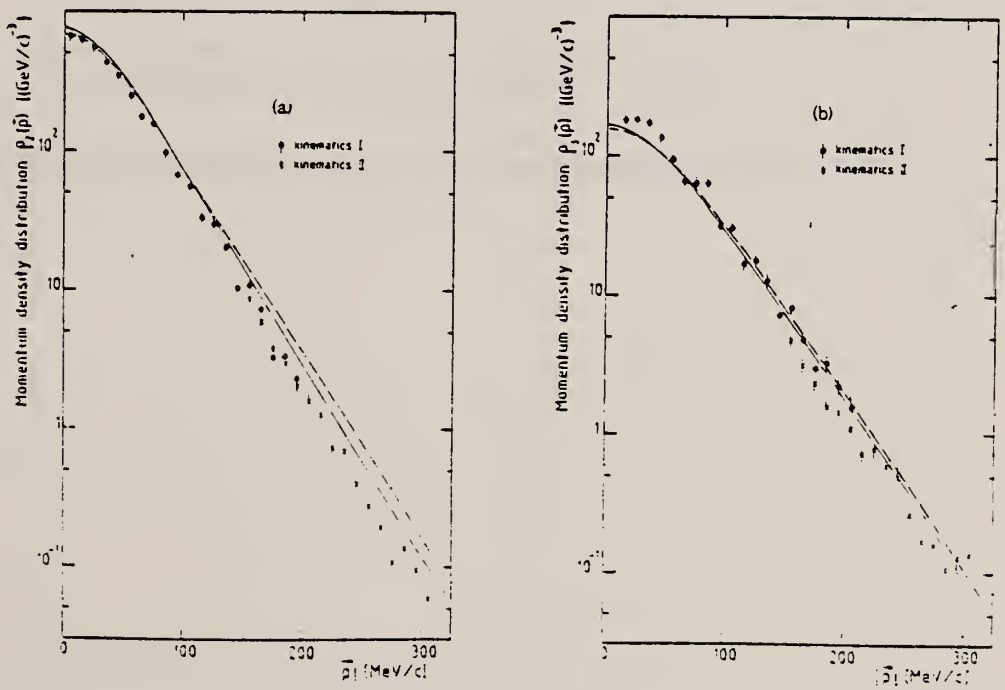

FIG. 1. Proton momentum distribution of ^{3}He for (a) two-body and (b) three-body breakup. The three-body breakup contribution has been obtained by integration up to a missing energy of 20 MeV. Dots and crosses correspond to measurements in kinematics I and II, respectively. The solid curves represent the calculation of Dieperink *et al.* (Ref. 11), the dashed lines that of Cioffi degli Atti, Pace, and Salmè (Ref. 1). The error bars include both the statistical error and an 8% error due to the estimated uncertainty in the absolute normalization.

(continued)

TABLE II. Proton momentum distributions, ρ_2 and ρ_3, for the two- and three-body disintegrations, respectively. ρ_3 has been obtained by integration of the three-body breakup contribution up to 20 MeV. The errors represent the statistical error only.

$\vec{p}$ (MeV/c)	ρ_2 Kin.I $(GeV/c)^{-3}$	ρ_3 Kin.I $(GeV/c)^{-3}$	$\vec{P}$ (MeV/c)	ρ_2 Kin.II $(GeV/c)^{-3}$	ρ_3 Kin.II $(GeV/c)^{-3}$
5	659 ± 37		155	8.66 ± 0.45	4.76 ± 0.39
15	608 ± 18	180 ±10	165	5.81 ± 0.29	3.14 ± 0.26
25	543 ± 16	182 ± 8	175	3.77 ± 0.20	2.35 ± 0.23
35	427 ± 10	173 ± 8	185	3.00 ± 0.14	1.59 ± 0.15
45	345 ± 8	135 ± 4	195	2.01 ± 0.12	1.47 ± 0.13
55	242 ± 8	94.9 ± 4.2	205	1.58 ± 0.10	1.10 ± 0.11
65	174 ± 4	66.3 ± 2.7	215	1.24 ± 0.11	0.733 ± 0.096
75	156 ± 4	63.6 ± 2.1	225	0.716 ± 0.059	0.787 ± 0.083
85	96.0 ± 3.3	63.4 ± 2.5	235	0.678 ± 0.072	0.598 ± 0.083
95	67.6 ± 1.5	31.5 ± 1.4	245	0.397 ± 0.031	0.492 ± 0.081
105	55.2 ± 1.5	30.7 ± 1.2	255	0.276 ± 0.026	0.260 ± 0.040
115	32.5 ± 1.1	16.9 ± 1.1	265	0.192 ± 0.023	0.167 ± 0.029
125	29.6 ± 0.7	17.9 ± 0.8	275	0.107 ± 0.014	0.160 ± 0.027
135	20.1 ± 0.6	12.8 ± 0.5	285	0.138 ± 0.023	0.108 ± 0.022
145	10.1 ± 0.5	7.25 ± 0.58	295	0.095 ± 0.018	0.130 ± 0.025
155	10.8 ± 0.4	8.25 ± 0.58	305	0.059 ± 0.015	0.134 ± 0.028
165	7.10± 0.33	4.93 ± 0.33			
175	3.14± 0.33	2.97 ± 0.38			
185	3.31± 0.23	3.23 ± 0.37			
195	2.25± 0.23	2.21 ± 0.26			
205		1.56 ± 0.37			

REF. S. Rock, R.G. Arnold, B.T. Chertok, Z.M. Szalata, D. Day, J.S. McCarthy, F. Martin, B.A. Mecking, I. Sick, G. Tamas
Phys. Rev. C26, 1592 (1982)

EL EM. SYM.	A	Z
He	3	2

METHOD

REF. NO. 82 Ro 2 egf

REACTION	RESULT	EXCITATION ENERGY	SOURCE TYPE	SOURCE RANGE	DETECTOR TYPE	DETECTOR RANGE	ANGLE
E,E/	RLX	1*5	D	6@17	MAG-D		8

Tabular Data given .8*5(GEV/C)SQR,@GEV

The cross section for inclusive inelastic electron scattering from the helium isotopes has been measured at momentum transfers squared of $0.8 \le Q^2 \le 5.0$ (GeV/c)^2 for ^{3}He and $0.8 \le Q^2 \le 2.4$ (GeV/c)^2 for ^{4}He. The data were taken at 8° and cover the range $0.6 < x < 1$, where $x = Q^2/2M_{He}\nu$, which includes the elastic peak, nuclear breakup threshold, the high momentum tail of the quasielastic scattering, and pion production. The structure function, νW_2, derived from the data, is approaching a scaling limit at high Q^2. It can be factored into a product of functions of Q^2 and of x as predicted by some models.

[NUCLEAR REACTIONS ^{3}He, ^{4}He$(e,e')X$; $E = 6.4-16.5$ GeV; $\theta_e = 8°$; measured $d\sigma/d\Omega\, dE'$; deduced νW_2 at threshold.]

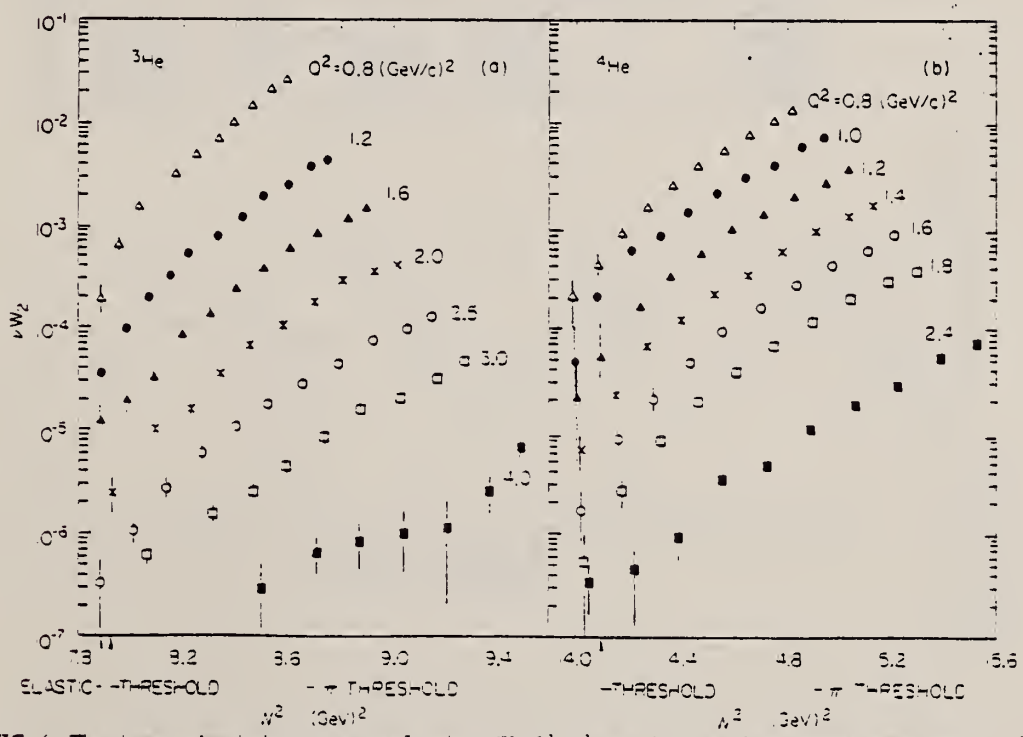

FIG. 6. The dimensionless inelastic structure function $\nu W_2(Q^2, W^2)$ as a function of the missing mass squared (W^2) for several values of the momentum transfer squared (Q^2), (a) ^{3}He and (b) ^{4}He.

(continued)

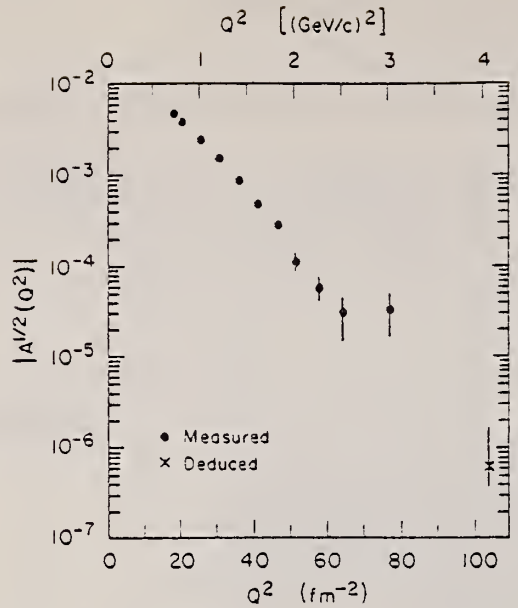

FIG. 14. The elastic structure function $A(Q^2)$ for ^{3}He as a function of Q^2 showing previously directly measured values (Ref. 1) and the highest Q^2 value derived from the elastic-inelastic connection.

REF. R.M. Sealock, H.S. Caplan, B.W. Zulkoskey, A. Szyjewicz, E.L. Tomusiak
Can. J. Phys. 60, 1257 (1982)

ELEM. SYM.	A	Z
He	3	2

METHOD

REF. NO.: 82 Se 1 | egf

REACTION	RESULT	EXCITATION ENERGY	SOURCE		DETECTOR		ANGLE
			TYPE	RANGE	TYPE	RANGE	
E,PI+	ABX	7*12	D	200	TEL-D		DST

*PION ENERGY

Differential cross sections were measured for the electro-pion production from H and ^{3}He at an incident energy of 200 MeV and pion energies from 7.3 to 12.1 MeV. Pion-angular distributions are presented and compared with theory. For hydrogen there is good agreement. A simple three-channel calculation performed for the pion production from ^{3}He was found to overestimate the cross section at forward pion angles.

On a mesuré les sections efficaces différentielles d'électroproduction de pions à partir de H et ^{3}He, pour une énergie incidente de 200 MeV et des énergies des pions allant de 7,3 à 12,1 MeV. Les distributions angulaires des pions sont présentées et comparées avec la théorie. Dans le cas de l'hydrogène, l'accord est bon. Un calcul simple, à trois voies, a été effectué pour la production de pions à partir de ^{3}He, et l'on a trouvé qu'il surestime la section efficace pour la production de pions dirigés vers l'avant.

TABLE 2. ^{3}He(e,π^+) $d^2\sigma/dE_{\pi}d\Omega_{\pi}$ nb/(MeV sr) for T_e = 200 MeV

E_{π}/θ_{π}	45°	60°	90°	120°	128°	145°
7.3	1.02±0.11	0.97±0.10	0.85±0.12	0.78±0.10	0.61±0.14	0.67±0.08
8.2	0.92±0.10	0.91±0.10	0.87±0.11	0.89±0.10	—	0.64±0.07
10.1	0.88±0.08	0.94±0.09	0.89±0.09	0.67±0.07	—	0.63±0.06
12.1	0.86±0.07	—	0.83±0.08	0.57±0.06	—	0.60±0.05

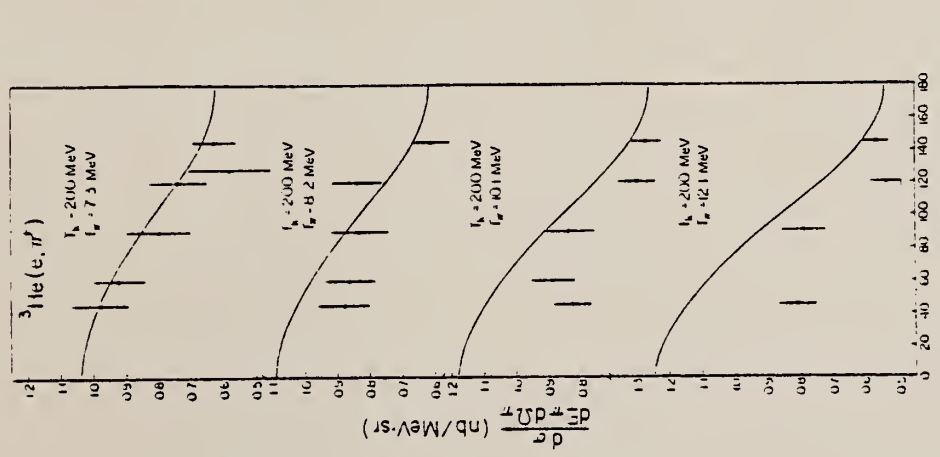

FIG. 3. Pion angular distributions for the reaction ^{3}He(e,π$^+$)^{3}H. The solid curve is our model prediction based on the impulse approximation.

HE
A=4

HE
A=4

HE
A=4

REF.
J.E. Perry, Jr., S.J. Bame, Jr.
Phys. Rev. 99, 1368 (1955)

ELEM. SYM.	A	Z
He	4	2

METHOD
Van de Graaff; inverse; NaI

REF. NO.	
55 Pe 2	NVB

REACTION	RESULT	EXCITATION ENERGY	SOURCE		DETECTOR		ANGLE
			TYPE	RANGE	TYPE	RANGE	
P,G	ABX	20-36	D	0-6	NAI-D		DST

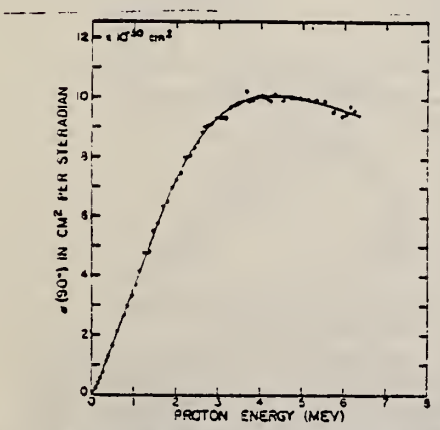

FIG. 3. 90° excitation function of $T(p,\gamma)He^4$. This is a composite of the sets of data mentioned in Table III.

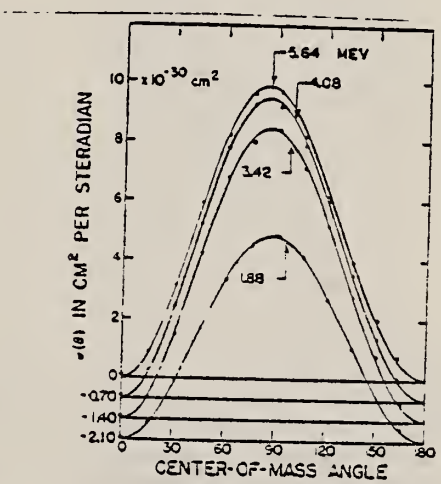

FIG. 6. Angular distributions of $T(p,\gamma)He^4$ in the center-of-mass system. The abscissa has been dropped 0.70×10^{-30} cm²/steradian for each successive energy to prevent overlapping of data. The curves drawn through the experimental points are of the form $K(\sin\theta+a\sin\theta\cos\theta)^2$, where K is 9.77×10^{-30}, 10.1×10^{-30}, 9.79×10^{-30}, and 6.93×10^{-30}, and a is 0.110, 0.098, 0.082, and 0.051 for the respective energies 5.64, 4.08, 3.42, and 1.88 Mev.

(continued)

REACTION	RESULT	EXCITATION ENERGY	SOURCE		DETECTOR		ANGLE
			TYPE	RANGE	TYPE	RANGE	

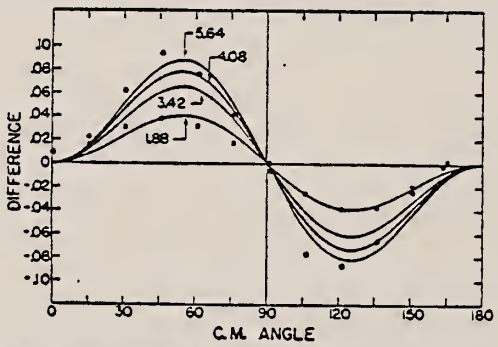

FIG. 7. Difference curves showing how the angular distributions deviate from a $\sin^2\theta$ distribution. The four angular distributions of Fig. 6 were normalized to unity at 90°, and $\sin^2\theta$ was subtracted to yield the difference values. The smooth curves have the form $2a\sin^2\theta\cos\theta+a^2\sin^2\theta\cos^2\theta$, with the values of a listed for Fig. 6. The round and square experimental points are for the 5.64- and 1.88-Mev distributions, respectively. Points for the 4.08- and 3.42-Mev distributions show similar deviations from their smooth curves.

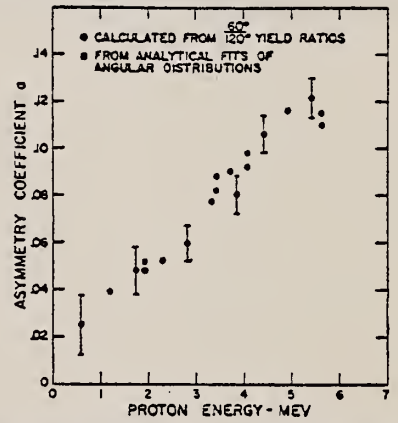

FIG. 8. Asymmetry coefficient a as a function of proton energy, where angular distributions are assumed to have the form $(\sin\theta+a\sin\theta\cos\theta)^2$. The rms statistical uncertainties in a shown for several points do not include the possibility of a small isotropic component in the angular distributions.

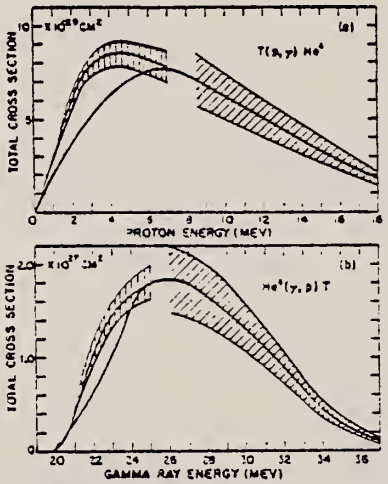

FIG. 11. Cross sections for the inverse reactions $T(p,\gamma)He^4$ and $He^4(\gamma,p)T$, based on detailed balance calculations of Fuller's data (reference 10) and the results of this experiment. The vertical shading represents the absolute error of this experiment, while the slanted shading is the error associated with Fuller's experiment. Fuller's experiment has quite large errors in the unshaded region (below 3.5-Mev proton energy or 26-Mev gamma-ray energy).

Ref. A.N. Gorbunov, V.M. Spiridonov
Zhur. Eksp. i Teoret. Fiz. 33, 21 (1957)
Soviet Phys. JETP 6, 16 (1958)

Elem. Sym.	A	Z
He	4	2

Method: Cloud Chamber

Ref. No.: 57 Go 1 F/H

Reaction	E or ΔE	E_o	Γ	$\int \sigma dE$	Jπ	Notes
He(γ,p)		27-28	15 Mev	$\int_{19.8}^{170} = 37.8 \pm 2.8$		E threshold - 19.8 σmax - $1.8 \cdot 10^{-27}$
He (γ,pn)				$\int^{170} 10 \pm 1.4$ Mev mb		Assuming $\sigma(\gamma,n) = \sigma(\gamma,p)$ 88 ±7 Mev 84 MeV mb is given by the Levinger and Bethe (LB) sum rule with 50% exchange. Angular distributions indicate that this absorption is all E1 below 30 MeV. Above this energy E2 contributes about 10%. This means that it represents about 6% of He total integrated cross section.

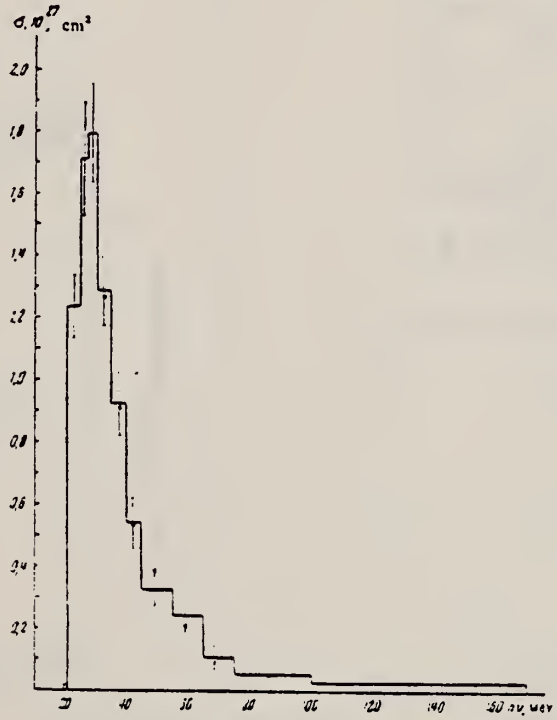

FIG. 5. Energy dependence of the cross section for the reaction $He^4(\gamma, p)H^3$ as determined from proton tracks. Only the statistical uncertainties are indicated. The threshold (19.8 Mev) is indicated by the arrow. The cross sections obtained from triton tracks are indicated by the full circles.

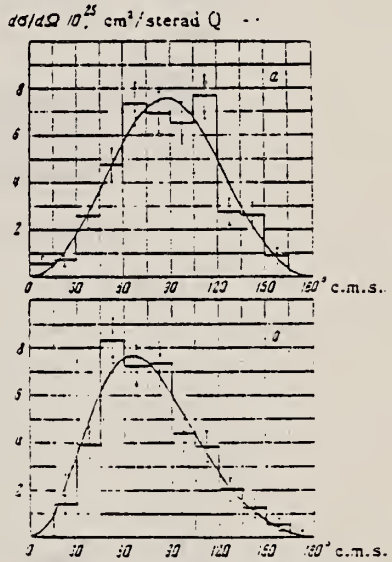

FIG. 6. Angular distributions of the protons from the reaction $He^4(\gamma, p)H^3$ in the c.m.s. (a) proton energy 21 — 30 Mev; (b) 30 — 170 Mev. In (b) the full circles indicate the proton angular distribution inferred from the measurements on triton tracks. The full curves represent Eq. (9).

REF.

M. O. Barton, J. H. Smith
Phys. Rev. 110, 1143 (1958)

EL EM. SYM.	A	Z
He	4	2

METHOD: Betatron; ion chamber monitor; plastic scintillator proton telescope; liquid scintillator neutron detector

REF. NO.: 58 Ba 3 NVB

REACTION	RESULT	EXCITATION ENERGY	SOURCE TYPE	SOURCE RANGE	DETECTOR TYPE	DETECTOR RANGE	ANGLE
G,NP	RLX	150-280	C	280	TEL-D	60-180	DST

NP COINC., PSPC

rms radius
$= (1.40 \pm 0.12) \times 10^{-13}$ cm.

Found Gaussian momentum spectrum.

$$\left(\frac{d\sigma}{d\Omega}\right)_{np} = (6.3 \pm 1.0)\left(\frac{d\sigma}{d\Omega}\right)_{\text{deuterium}}$$

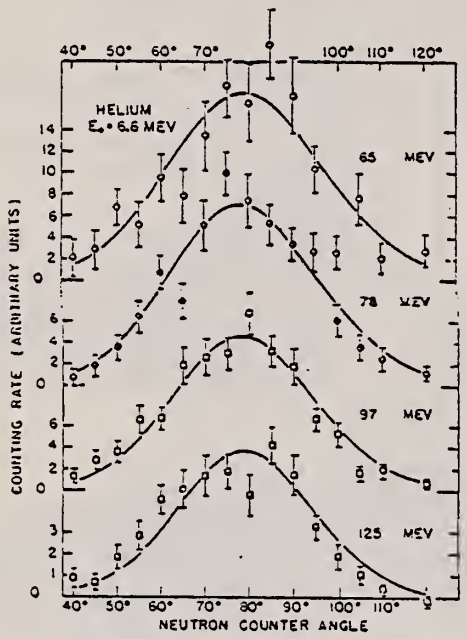

FIG. 9. Helium coincidence counting rate vs angle of the neutron counter.

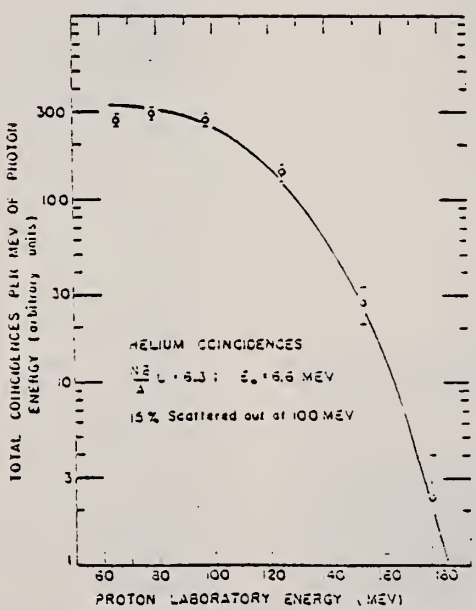

FIG. 11. Total coincident counts per Mev of proton energy from helium vs the proton laboratory energy.

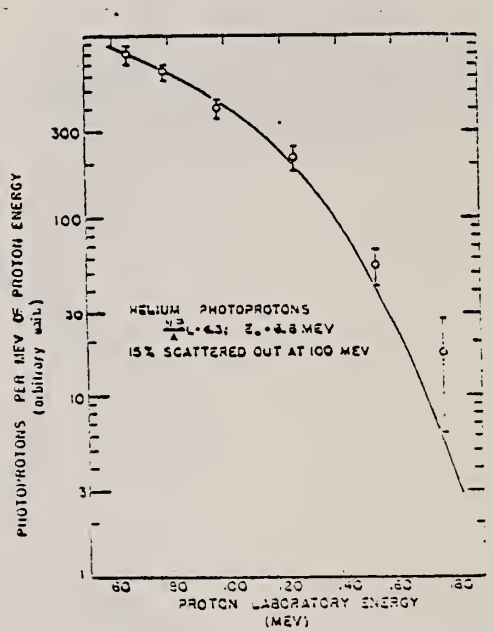

FIG. 13. Total proton counts per Mev of proton energy from helium vs the proton laboratory energy.

Ref. A.N. Gorbonov, V.M. Spiridonov
Zhur. Eksp. i Theoret Fiz. 34, 862 (1958)
Soviet Phys. JETP 7, 596 (1958)

Elem. Sym.	A	Z
He	4	2

Method: Cloud Chamber

Ref. No.: 58 Go 1 — F/H

Reaction	E or ΔE	E_o	Γ	$\int \sigma dE$	Jπ	Notes
(γ,n)		27-28 MeV		$\int_{20.6}^{40} = 21.6 \pm 0.9$ Mev mb $\int_{20.6}^{100} = 41.3 \pm 1.7$ $\int_{20.6}^{170} = 43.8 \pm 1.8$		$\int \frac{\sigma dE}{E} = 1.09 \pm 0.08$ mb At all photon averages the angular distribution approximately $(a + b \sin^2\vartheta)$.

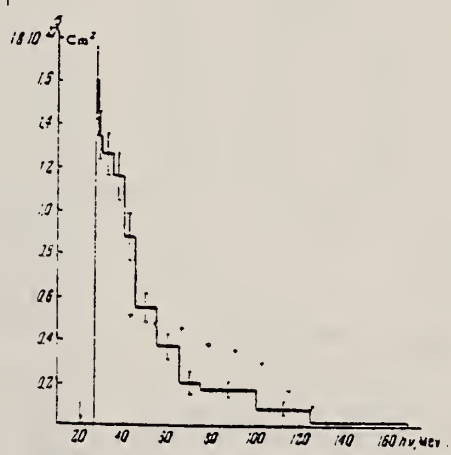

FIG. 2. Dependence of the cross section for the $He^4(\gamma, n)He^3$ reaction on photon energy. Only statistical errors are shown on the figure. The reaction threshold (20.6 Mev) is indicated by the arrow. The points marked with a + are the data of Ref. 2.

Ref. A.N. Gorbunov, V.M. Spiridonov
Zhur. Eksp. i Teoret. Fiz. 34, 866 (1958)
Soviet Phys. JETP 7, 600 (1958)

Elem. Sym.	A	Z
He	4	2

Method: Cloud Chamber

Ref. No.: 58 Go 2 F/H

Reaction	E or ΔE	E_o	Γ	$\int \sigma dE$	Jπ	Notes
$H^4(\gamma,pn)$		~ 50 MeV				σ max = 2.10^{-28} $\int \frac{\sigma\, dE}{E} = 1.810^{-28}$ mb

Photon E	$\int \sigma dE$ γ, pn	MeV mb γ, n+γ, p
< 75	$\int_{25.7}^{75}$ 7.2±0.9	71.6±2.2
75-170	$\int_{75}^{170}$ 4.6±1.2	10.0±1.9
<170	$\int_{170}^{260}$ 11.8±1.5	81.6±2.9

Angular distribution shows that this is a psuedo-deutron proton.

$\int \sigma_{tot} dE$ = 95 ± 7 MeV mb

Levinger and Rustgi give 89.

$\int \frac{\sigma\, dE}{E}$ = 2.4± 0.15 mb which gives for the mean square radious Ag He:

1.57 ± 0.06 10^{-B}cm.

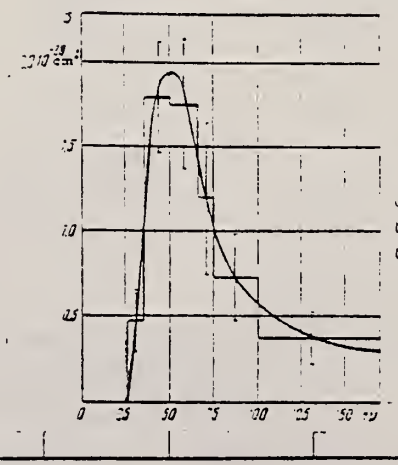

FIG. 1 Dependence of the cross section for the He^4 (γ, pn) D reaction on photon energy.

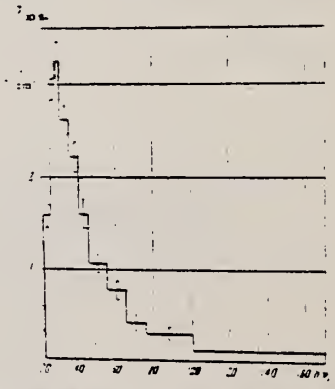

FIG. 8. Dependence of total cross section for absorption of photons by He^4 on photon energy. Only statistical errors are shown on the graph. Errors in absolute values are ~ 5%.

Ref. D.L. Livesey, I.G. Main
Nuovo Cimento 10, 590 (1958)

Elem. Sym.	A	Z
He	4	2

Method: Emulsion to detect He^3

Ref. No.: 58 Li 1 | FH

Reaction	E or ΔE	E_0	Γ	$\int \sigma dE$	Jπ	Notes
He(γ,n)	Bremss. 70			$\int_{40}^{60}$ = 7.5 MeV-mb		$He^4(\gamma,n)He^3$

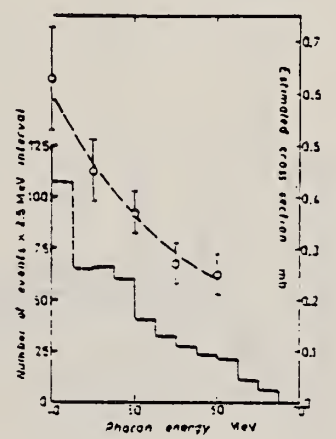

Fig. 1. – Lower: number of (γ, n) events plotted against photon energy. Upper: estimated (γ, n) cross-section as a function of photon energy; the smooth curve has been fitted to give the best agreement with the integrated cross-sections shown in Table I.

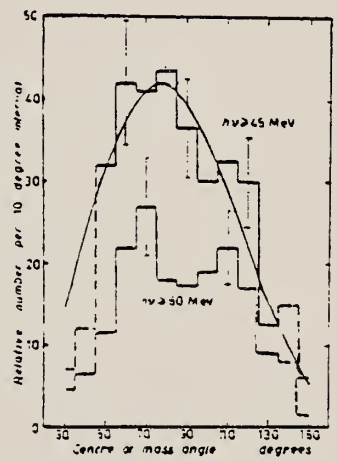

Fig. 2. – Angular distribution of ^3He particles emitted in the C.M. co-ordinates, after correction for the variation of solid angle of collection with angle in the laboratory system. Lower: all events above 30 MeV. Upper: all events above 45 MeV, the curve representing the function $f(\theta) = B \sin^2\theta (1 - 0.5 \cos\theta)$.

Ref. C. Milone
Phys. Rev. 120, 1302 (1960)

Elem. Sym.	A	Z
He	4	2

Method
Betatron; emulsions

Ref. No. 60 Mi 1 F/H

Reaction	E or ΔE	E_o	Γ	$\int \sigma dE$	Jπ	Notes
(γ,p)	32 MeV	...				Peaks in $\sigma(\gamma,p)$ at E_γ = 24.7 ± 0.2, 26.1 ± 0.1, 26.9, and 27.8 MeV (see Figure 4) for range $70° < \theta_p < 110°$. These data were derived from E_p spectrum in Figure 3.

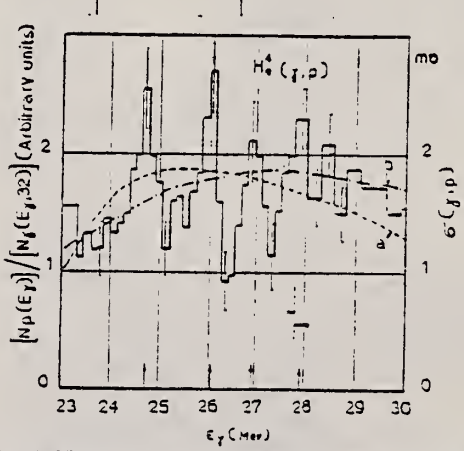

FIG. 4. Histogram: $He(\gamma,p)$ differential cross section derived from the 90°±20° spectrum of Fig. 3 (present work) in arbitrary units. Curve (a): $He(\gamma,p)$ cross section in millibarns according to Fuller.[2] Curve (b): $He(\gamma,p)$ cross section in millibarns according to Gorbunov and Spiridonov.[4]

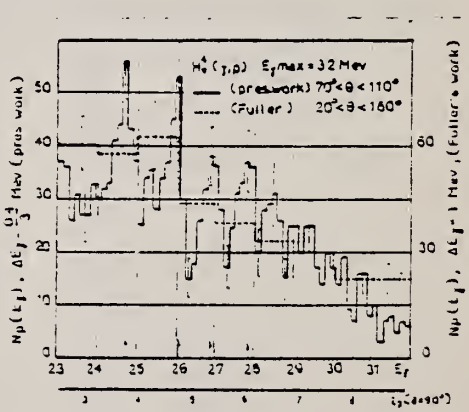

FIG. 3. Photoproton spectrum from He in ΔE_γ steps of 0.133 Mev; 70°<θ<110° (plates parallel to the γ beam). The correspondence between E_p and E_γ for θ=90° is reported. The statistical root mean square errors are indicated. The legend on the left-hand side of the figure should read 0.133, rather than 0.3.

REF.

J. M. Reid and B. Lalovic
Proc. Phys. Soc. (London) 76, 65 (1960)

ELEM. SYM.	A	Z
He	4	2

METHOD

REF. NO.	
60 Re 2	EGF

REACTION	RESULT	EXCITATION ENERGY	SOURCE		DETECTOR		ANGLE
			TYPE	RANGE	TYPE	RANGE	
G,XP			C	330	CCH		

Recorded only events where photon with 20≤ E ≤120 MeV was emitted.

28 events saw evidence for $^{4}He(\gamma,p)T$
$(\gamma,pn)D$
$(\gamma,p2n)p$

REF. G.R. Burleson
Phys. Rev. 121, 624 (1961)

ELEM. SYM.	A	Z
He	4	2

METHOD
Linac; inelastic electron scattering; magnetic spectrometer; Faraday cup or SEM

REF. NO. 61 Bu 2 NVB

REACTION	RESULT	EXCITATION ENERGY	SOURCE		DETECTOR		ANGLE
			TYPE	RANGE	TYPE	RANGE	
E,E/	ABX	0-325	D	400,500	MAG-D		DST
E,E	ABX	0	D	400,500	MAG-D		DST

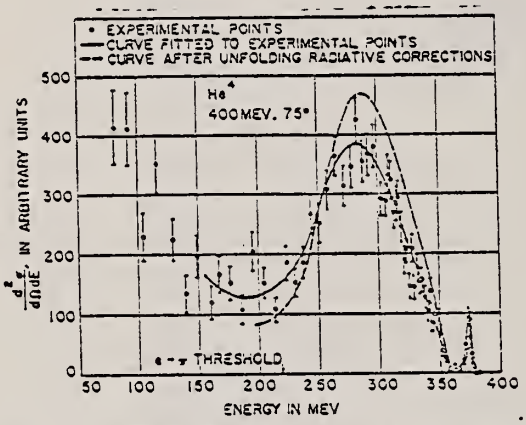

FIG. 3. The corrected inelastic curve found at 400 Mev, 75°.

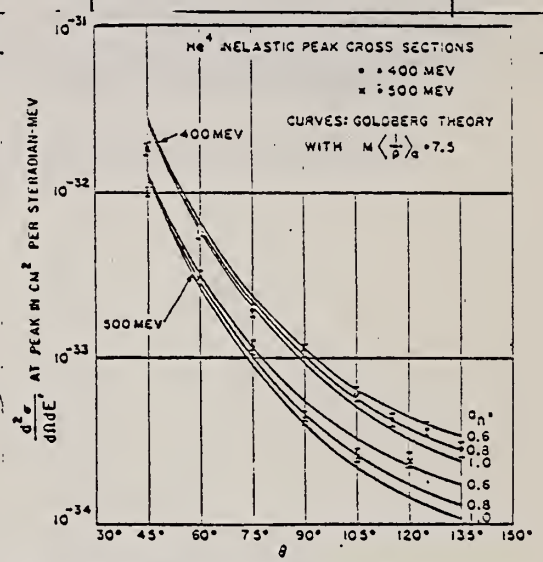

FIG. 6. Experimental inelastic peak cross sections. The errors shown are the statistical standard deviations. The curves are predictions of the Goldberg theory, as adapted for He⁴, for values of a_n for the neutron of 0.6, 0.8, and 1.0 f and for a value of $M\langle 1/\rho\rangle_a$ of 7.5.

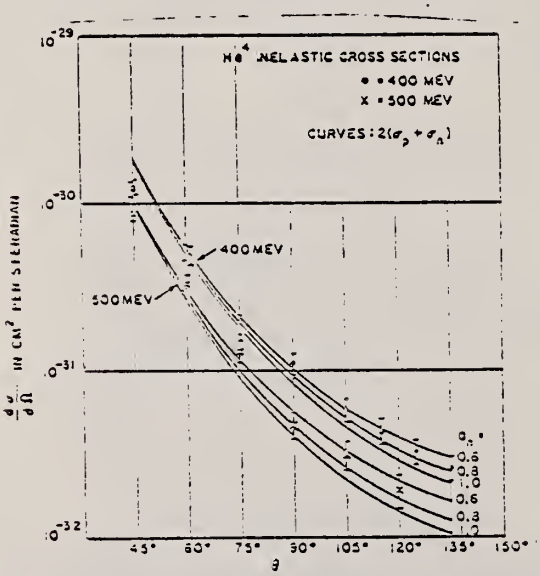

FIG. 7. Experimental inelastic cross sections. The errors shown represent uncertainties due to counting statistics and to the measurement of the areas of the curves below the pion-production threshold. The curves shown are $2(d\sigma_p/d\Omega + d\sigma_n/d\Omega)$ for values of a_n for the neutron of 0.6, 0.8, and 1.0 f.

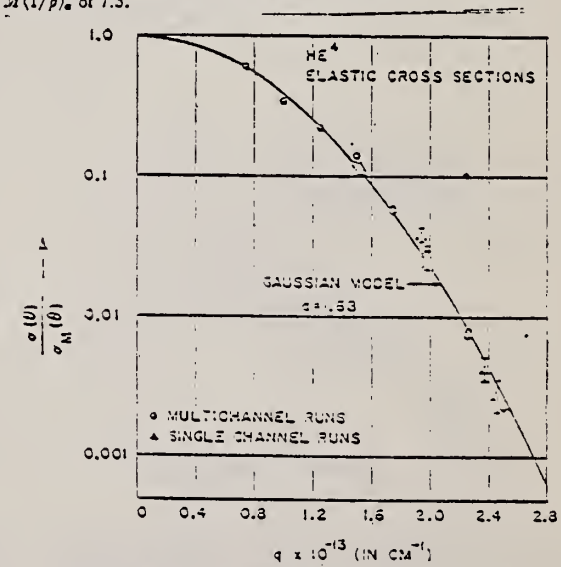

FIG. 8. Experimental values of $(d\sigma/d\Omega)/(d\sigma_M/d\Omega)$ plotted as a function of the four-momentum transfer q. The errors shown are the statistical standard deviations. Also shown are data found in an earlier measurement with a multichannel detector.

Ref. C.C. Gardner, J.D. Anderson
Phys. Rev. 125, 626 (1962)

Elem. Sym.	A	Z
He	4	2

Method 90-inch variable energy cyclotron; NaI

Ref. No. 62 Ga 1 JHH

Reaction	E or ΔE	E_o	Γ	$\int \sigma dE$	Jπ	Notes
(p,γ)	5.8-9.2					$W(\theta) = (\sin\theta + \underline{a}\sin\theta\cos\theta)^2$, where $\underline{a}$ is plotted versus E_p in Figure 5. Excitation function at $\theta_{lab.} = 90^\circ$ (Figure 4) is consistent with Perry and Bame [Phys. Rev. 99, 1368 (1955)].

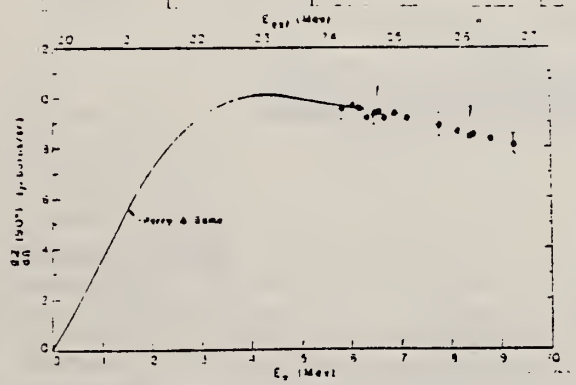

FIG. 4. $T(p,\gamma)He^4$ excitation function.

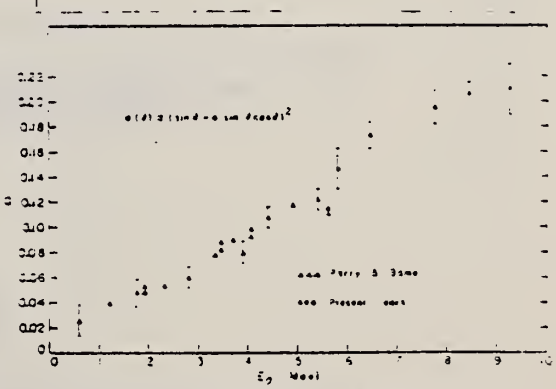

FIG. 5. Asymmetry coefficient.

Ref. D.S. Gemmell, G.A. Jones
Nuclear Phys. 33, 102 (1962)

Elem. Sym.	A	Z
He	4	2

Method: Tandem generator; NaI

Ref. No.: 62 Ge 1 JHH

Reaction	E or ΔE	E_o	Γ	$\int \sigma dE$	Jπ	Notes
$H^3(p,\gamma)He^4$	4-11					No significant structure in $\sigma(p,\gamma)$ observed. $W(\theta) = A + B\sin^2\theta + C\sin^2\theta\cos\theta + D\sin^2\theta\cos^2\theta$; where A/B < 0.01, C/B and D/B given in Figure 4. Calculations from measured $\sigma(p,\gamma)$ give: $\int_{th}^{28\ MeV} \sigma_{E1}(\gamma,p)dE_\gamma = 10.2\pm1.2$ MeV-mb and $\int_{th}^{28\ MeV} \sigma_{E1}(total)dE_\gamma = 20.4\pm2.4$ MeV-mb using assumptions: $\Gamma_n = \Gamma_p$; $\Gamma_d = 0$.

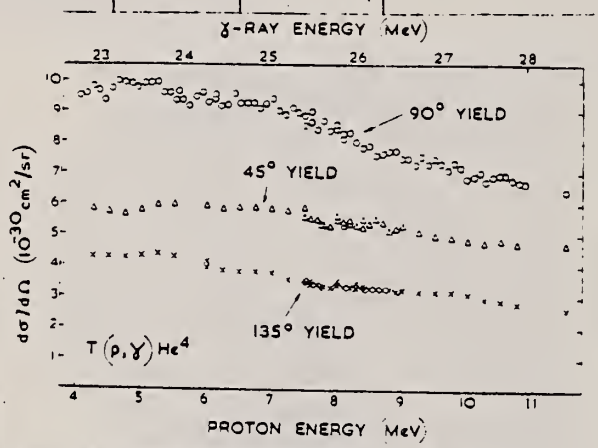

Fig. 2. Yield curves for T(p, γ)He⁴ measured at 45°, 90° and 135°.

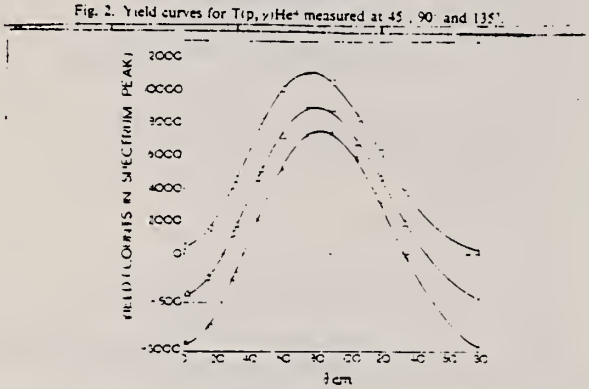

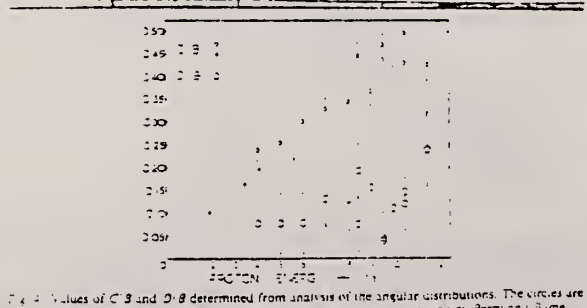

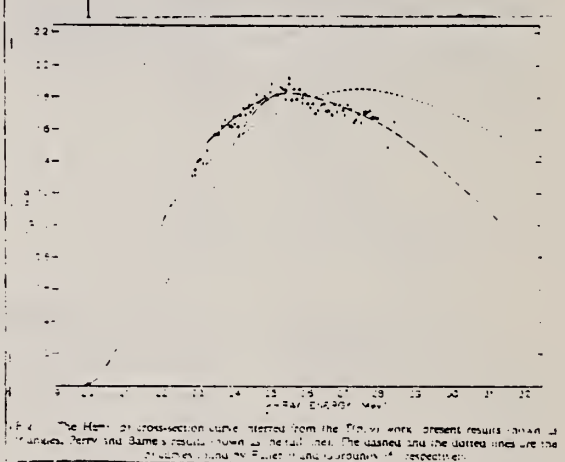

Ref 5: Fuller - Phys. Rev. 96, 1306 (1954)

Ref 16: Gorbunov - Lebedev Physical Institute Report (USSR) 13, 174 (1960).

Ref. I.G. Main

Nuovo Cimento 26, 884 (1962)

Elem. Sym.	A	Z
He	4	2

Method

70 MeV Betasynchrotron- emulsions

Ref. No. 62Mal

BG

Reaction	E or ΔE	E_0	Γ	$\int \sigma dE$	Jπ	Notes
(γ, p)	23-32					Angular distributions of protons obtained. Least squares fit for $f(\theta) = B(1 + C\cos\theta + D\cos^2\theta)\sin^2\theta$ was made.

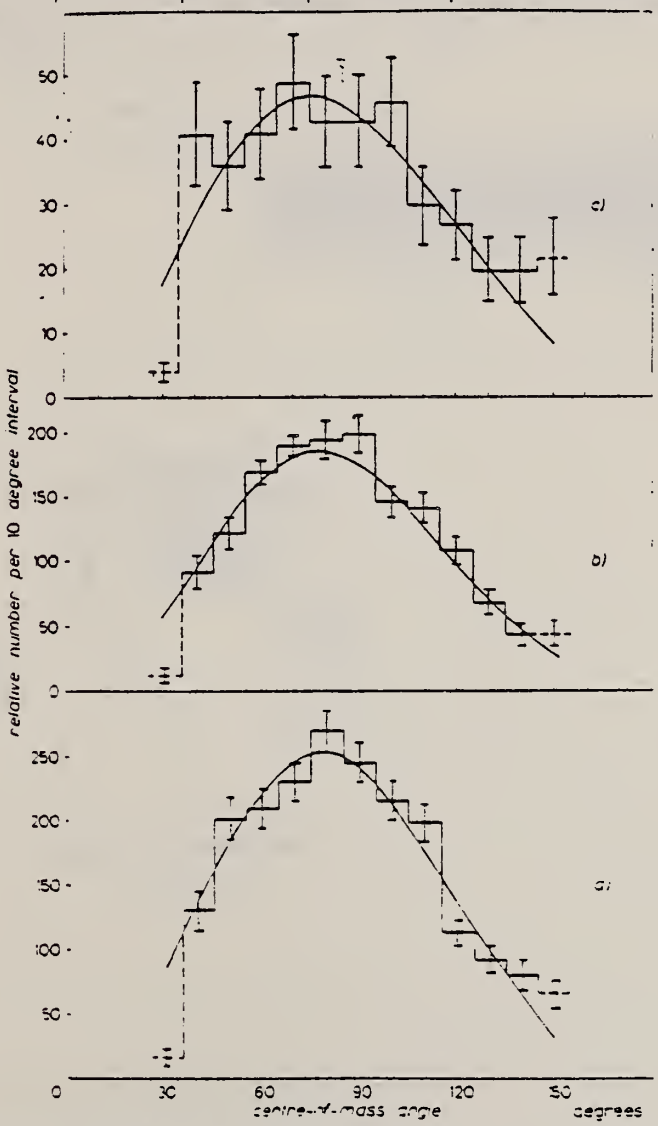

Fig. 2. – Centre-of-mass angular distributions of protons from (γ, p) reactions in ^{4}He in photon energy ranges a) (23÷26) MeV (1777 tracks), b) (26÷29) MeV (1330 tracks), c) (29÷32) MeV (351 tracks); smooth curves represent the functions: a) $f(\theta) = B(1 - 0.46\cos\theta)\sin^2\theta$. b) $f(\theta) = B(1 - 0.48\cos\theta)\sin^2\theta$. c) $f(\theta) = B(1 + 0.47\cos\theta - 0.25\cos^2\theta)\sin^2\theta$.

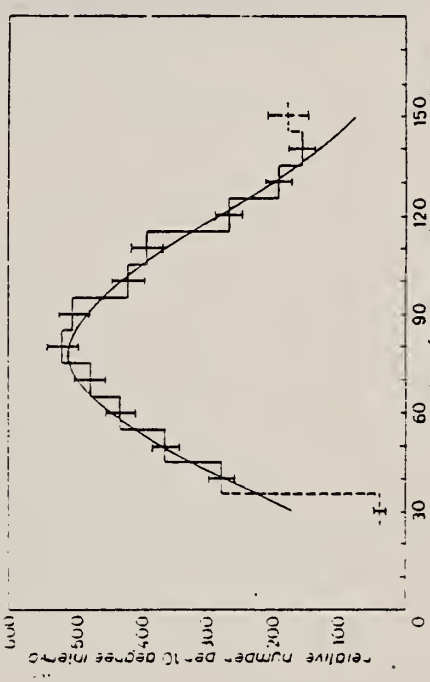

Fig. 1. – Centre-of-mass angular distribution of 3500 proton tracks from (γ, p) reactions in ^{4}He above 23 MeV photon energy; the smooth curve represents the function $f(\theta) = A(1 + 0.46\cos\theta + 0.01\cos^2\theta)\sin^2\theta$.

REF.

R. W. Zurmühle, W. E. Stephens and H. H. Staub
Phys. Rev. 132, 751 (1963)

ELEM. SYM.	A	Z
He	4	2

METHOD

REF. NO.	
63 Zu 1	HMG

REACTION	RESULT	EXCITATION ENERGY	SOURCE		DETECTOR		ANGLE
			TYPE	RANGE	TYPE	RANGE	
N,G	ABX	24	D	4	NAI		DST(90,45)
D,G	ABX	24	D	1	NAI		45
				(1.35)			

[D,G] 1=1.35

The gamma rays from the $He^3(n,\gamma)He^4$ and the $D(d,\gamma)He^4$ reaction have been observed. The gamma detector, a 3-in.×4-in. NaI crystal, was surrounded by a plastic scintillator to eliminate the cosmic-ray background. A pileup rejection circuit was used to reduce the background from neutron induced reactions in the NaI. The cross section of the $He^3(n,\gamma)He^4$ reaction at 4 MeV is $\sigma = 5\,\mu b/sr$ at 90°. The intensity ratio, $I(90°)/I(45°) \approx 2$, agrees with that expected for electric dipole radiation ($\Delta M = 0$). The $D(d,\gamma)He^4$ reaction at 1.35 MeV has a cross section $\sigma = 2\times10^{-33}$ cm²/sr at 45°.

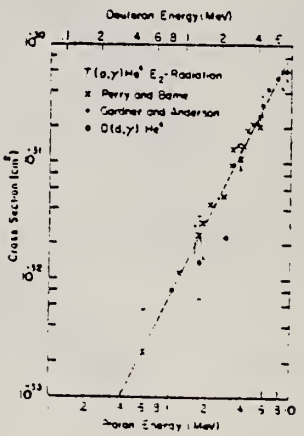

FIG. 6. Cross sections of the $D(d,\gamma)He^4$ reaction and the quadrupole component of the $T(p,\gamma)He^4$ reaction.

REF.

P. E. Argan, G. Mantovani, and A. Piazzoli
Il Nuovo Cimento 37, 376 (1965)

EL EM. SYM.	A	Z
He	4	2

METHOD

REF. NO.	
65 Ar 1	JOC

REACTION	RESULT	EXCITATION ENERGY	SOURCE		DETECTOR		ANGLE
			TYPE	RANGE	TYPE	RANGE	
G,P	ABX	THR - 999	C	999	CCH-D		4PI
G,D	ABY	THR - 999	C	999	CCH-D		4PI

999= 1 GEV

$\bar{\sigma}(\gamma,p)$/avg 20-40 MeV = 1.85 ± .46 mb

Yield | $^4He(\gamma,D)D \sim 15\%$ Y (γ,p)
20 - 40 MeV

REF. J. G. Asbury and F. J. Loeffler
Phys. Rev. 137, B1214-20 (1965)

EL EM. SYM.	A	Z
He	4	2

METHOD: Synchrotron; ion chamber monitor

REF. NO.: 65 As 1 | NVB

	REACTION	RESULT	EXCITATION ENERGY	SOURCE TYPE	SOURCE RANGE	DETECTOR TYPE	DETECTOR RANGE	ANGLE
(1)	G,2D	ABX	24-300	C	250,300	TEL-D		DST
	G,XP	ABX	78-300	C	250,300	TEL-D	58-128	DST

(1) COINCIDENCE

TABLE II. Differential and total cross sections for the process $\gamma+He \rightarrow d+d$ for two different mean photon energies. The angles for the differential cross sections are center-of-mass angles. The total cross sections were calculated under the assumption that the angular form for the differential cross section is $\sin^2\theta\cos^2\theta$.

Photon energy	Cross sections
$k=220.5$ MeV	$\sigma_{tot}=22.3\pm7.9\times10^{-32}$ cm^2
	$d\sigma/d\Omega(\theta=52.4°)=(6.3\pm2.2)\times10^{-32}$ cm^2/sr
$k=265.3$ MeV	$\sigma_{tot}=5.4\pm3.8\times10^{-32}$ cm^2
	$d\sigma/d\Omega(\theta=53.2°)=(1.5\pm1.1)\times10^{-32}$ cm^2/sr

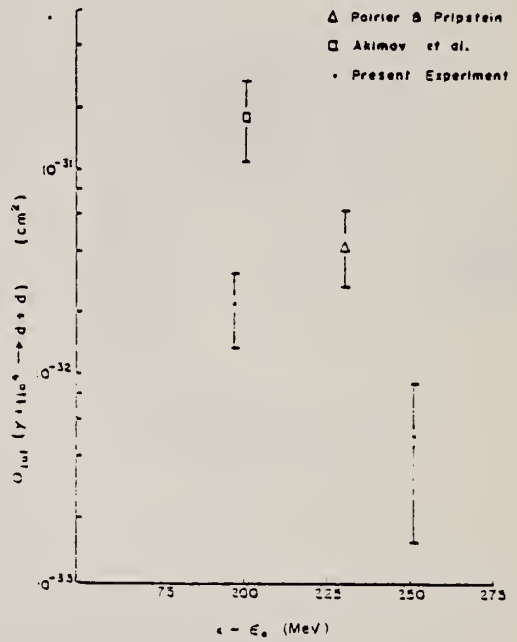

FIG. 5. The high-energy experimental cross sections for $\gamma+He^4 \rightarrow d+d$. The cross section due to Akimov *et al.* and the upper limit of Poirier and Pripstein were inferred from their measurements of the inverse cross section $\sigma(d+d \rightarrow He^4+\gamma)$. Threshold energy $\epsilon_0=23.9$ MeV.

(continued)

REACTION	RESULT	EXCITATION ENERGY	SOURCE		DETECTOR		ANGLE
			TYPE	RANGE	TYPE	RANGE	

TABLE III. Differential photoproton cross sections for the reaction $\gamma+He^4 \rightarrow p+X$.

Proton angle	Proton energy (MeV)	Differential cross section $d^2\sigma/d\Omega dT_p Q$ $\mu b/\text{sr MeV}Q$
45°	87.5	0.215 ±0.020
45°	115.4	0.170 ±0.015
45°	127.8	0.114 ±0.010
118°	58.2	0.187 ±0.017
118°	87.5	0.0710±0.0070

[16] K. Grieder, Phys. Rev. 122, 1919 (1961).

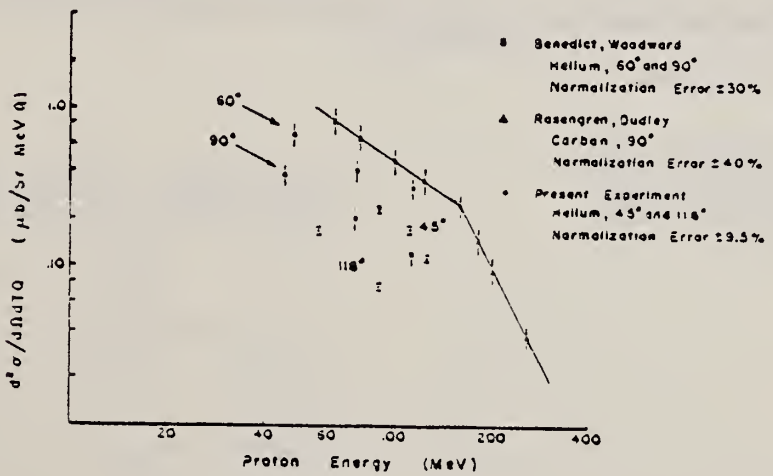

FIG. 7. Photoproton spectra.

REF.

H. G. Clerc, R. J. Stewart, and R. C. Morrison
Phys. Letters 18, 316 (1965)

ELEM. SYM.	A	Z
He	4	2

METHOD

Bremsstrahlung Yale Linac.

REF. NO.: 65 C1 1 EGF

REACTION	RESULT	EXCITATION ENERGY	SOURCE		DETECTOR		ANGLE
			TYPE	RANGE	TYPE	RANGE	
G,P	ABX	24 - 56	C	40 - 60?	SCD-D	3 - 10	90

Magnetic quadrupole triplet used to determine momentum.

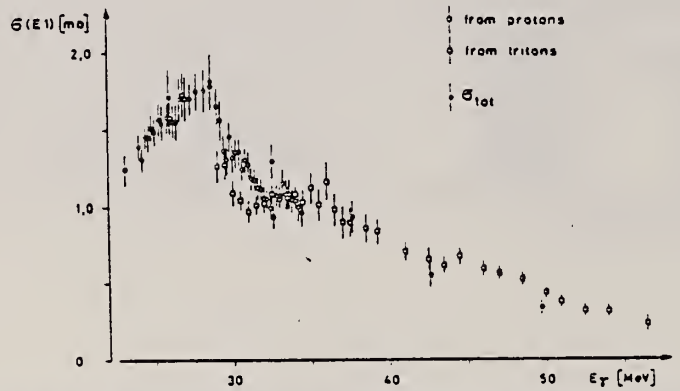

Fig. 1. Electric dipole cross section σ(E1) for the reaction $^{4}He(\gamma,p)^{3}H$ as a function of incident gamma ray energy. The error bars represent one standard deviation; σ_{tot} is the total cross section (including E2) measured by Gorbunov and Spiridonov [1].

REF. R. Frosch, R.E. Rand, M.R. Yearian, H.L. Crannell and L.R. Suelzle
Phys. Letters 19, 155 (1965)

EL EM. SYM.	A	Z
He	4	2

METHOD: Linac

REF. NO.: 65 Fr 1 JDM

REACTION	RESULT	EXCITATION ENERGY	SOURCE		DETECTOR		ANGLE
			TYPE	RANGE	TYPE	RANGE	
E,E/	ABX	0-30	D	200	MAG-D	160-175	DST

For (20.5±0.1) MeV level Γ = (0.4±0.1) MeV.

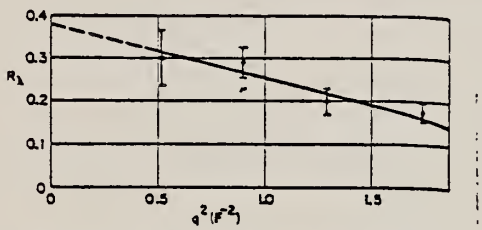

Fig. 2. Experimental values of the ratio $R_\lambda(q^2) = F_{inel.}(q^2)/\{1 - F_{el.}(q^2)\}$ for the 20.5 MeV level. We also show the best straight line fit to the four points. The large error of the point at 0.52 fm^{-2} is mainly due to the uncertainty of the elastic form factor measurement.

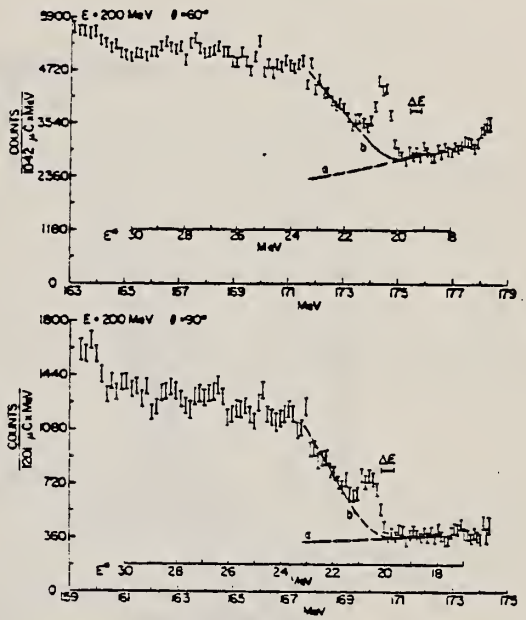

Fig. 1. Two spectra of inelastically scattered electrons. The vertical scale refers to a standard solid angle of 1 msr. The inserted horizontal scale gives the mass difference E* between the recoiling 4-nucleon-system and the ^{4}He ground state. The length ΔE shows the experimental resolution.

Table 1
Results for the 20.5 MeV level. Note that q^2, the square of the 4-momentum transfer, is calculated for the inelastic scattering event. $R_\lambda(q^2)$ is defined in the text.

E_0 (MeV)	ϑ	$q^2(fm^{-2})$	$\frac{d\sigma_{inel}}{d\Omega}$ (10^{-33} cm^2/ster)	$R_\lambda(q^2)$
198	45°	0.52	22 ± 5	0.20 ± 0.07
200	60°	0.90	15 ± 3	0.29 ± 0.04
198	75°	1.29	4.8 ± 1.2	0.20 ± 0.03
200	90°	1.75	2.4 ± 0.6	0.175 ± 0.023

REF. R. Schrack, D. Kohler, N. G. Puttaswamy and W.E. Meyerhof
Phys. Letters 18, 327 (1965)

ELEM. SYM.	A	Z
He	4	2

METHOD

Stanford Van de Graaff, NAI

REF. NO.	
65 Sc 1	EGF

REACTION	RESULT	EXCITATION ENERGY	SOURCE		DETECTOR		ANGLE
			TYPE	RANGE	TYPE	RANGE	
P,G	ABX	20 - 23	D	0 - 4	NAI-D	20 - 24	0

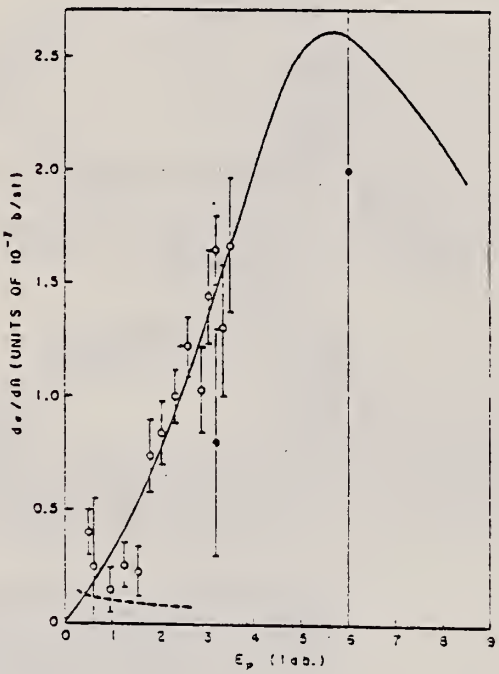

Fig. 2. Differential cross section in the lab. system for the T(p,γ) reaction at 0° as a function of proton lab. energy. Effects of the singlet contribution have been subtracted. A ± 20% uncertainty in the cross section calibration has not been included in the error bars. Coulomb scattering of the protons in the target material gives the estimated effects at low energies shown in dashed lines. The solid dots are taken from Perry and Bame [1]. The solid curve assumes that the cross section is due to a 1⁻, S = 1, T = 1 resonance in ⁴He with a resonance energy at 26 MeV (but peaking at approximately 24 MeV). The resonance parameters were chosen in accord with Tombrello's analysis of the analog states in ⁴H and ⁴Li [10]. See text for the values used.

REF.

F. Ferrero, C. Manfredotti, L. Pasqualini, G. Piragino and P. G. Rama
Il Nuovo Cimento 45B, 273 (1966)

EL EM. SYM.	A	Z
He	4	2

METHOD

REF. NO.	
66 Fe 1	JDM

REACTION	RESULT	EXCITATION ENERGY	SOURCE		DETECTOR		ANGLE
			TYPE	RANGE	TYPE	RANGE	
G,N	ABX	20-80	C	20-80	BF3-I		4PI

603

$$\int_{20.6}^{80} \sigma dE = (40.5 \pm 3)\ \text{mb.MeV}.$$

The rms $< R_c >$ from bremsstrahlung-weighted σ is (1.54±0.06) fermi.

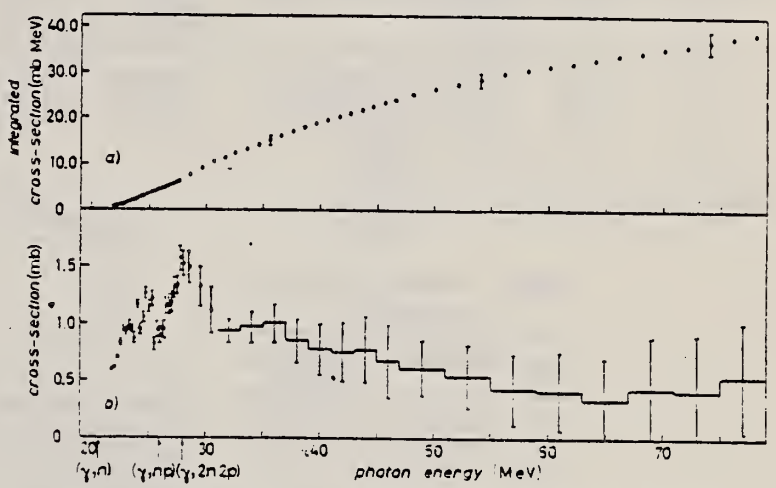

Fig. 1. – a) Integrated cross-section; b) cross-section for the $^4He(\gamma, Tn)$ reaction.

REF. H. v. Buttlar, F. Freund und G. Gammel
Z. Physik 200, 1 (1967)

ELEM. SYM.	A	Z
He	4	2

METHOD: Linac

REF. NO.: 67 Bu 1 JDM

REACTION	RESULT	EXCITATION ENERGY	SOURCE TYPE	SOURCE RANGE	DETECTOR TYPE	DETECTOR RANGE	ANGLE
G,P	RLY	THR-54	C	44,54	ACT-I		4PI

Normalized with $^{12}C(\gamma,n)^{11}C$ yield assume average σ is proportioned from yields.

Tabelle 2. *Vergleich der gemessenen reduzierten Ausbeute $(\sigma_y)_3$ mit Literaturwerten*

E_m [MeV]	$(\sigma_y)_{11}$ [mbarn]		$(\sigma_y)_3$, eigene Messung [mbarn]			$(\sigma_y)_3$, andere Messungen [mbarn]		
	nach BARBER et al.[9]	nach COOK et al.[10]	ausgewertet nach[9], ohne Fehler von $(\sigma_y)_{11}$	ausgewertet nach[9], mit Fehler von $(\sigma_y)_{11}$	ausgewertet nach[10], mit Fehler von $(\sigma_y)_{11}$	GORBUNOV und SPIRIDONOV[2]	CLERC et al.[3]	FULLER[1]
44,3	2,14 ± 0,11	2,33 ± 0,20	0,70 ± 0,07	0,70 ± 0,08	0,76 ± 0,10	0,80 ± 0,06	0,75 ± 0,08	0,60 ± 0,19
54,3	2,36 ± 0,13	2,60 ± 0,22	0,84 ± 0,06	0,84 ± 0,08	0,92 ± 0,11	0,94 ± 0,07	0,90 ± 0,09	0,65 ± 0,20

Tabelle 1. *Meßresultate für das Ausbeuteverhältnis*

E_m [MeV]	Y_3/Y_{11} (ohne Eichfehler)	Y_3/Y_{11} (Eichfehler berücksichtigt)
44,3	0,328 ± 0,011	0,328 ± 0,031
54,3	0,354 ± 0,006	0,354 ± 0,027

REF. V. P. Denisov and L. A. Kul'chitskii
J. Nucl. Phys. (USSR) 6, 437 (1967)
Sov. J. Nucl. Phys. 6, 318 (1968)

ELEM. SYM.	A	Z
He	4	2

METHOD

REF. NO.	
67 De 3	HMG

REACTION	RESULT	EXCITATION ENERGY	SOURCE		DETECTOR		ANGLE
			TYPE	RANGE	TYPE	RANGE	
G.P	ABX	24-50	C	52	TEL-D	3-13	90

Angular distribution of p and t assumed to be $\sin^2\Theta$.

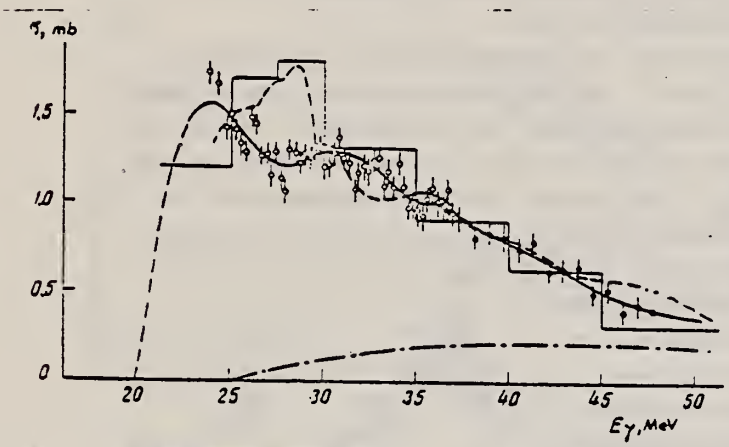

Fig. 1. The cross section curve for the reaction $He^4(\gamma, p)H^3$: ○—cross section obtained from the photoproton spectrum; ●—cross section obtained from the photo-triton spectrum; the solid curve (with a dotted extension) is the curve for the cross section drawn through the experimental points with an arbitrary extrapolation to the reaction threshold; histogram is the cross section for the (γ, p) reaction according to the data of [1]; the dotted curve is the cross section for the (γ, p) reaction according to the data of [4]; the dash-dotted curve is the cross section for the (γ, pn) reaction according to the data of [1].

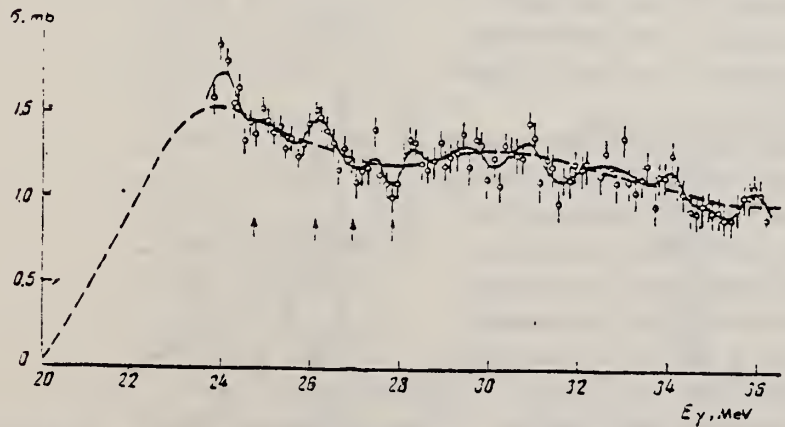

Fig. 2. The cross section curve for the reaction $He^4(\gamma, p)H^3$ obtained by utilizing the intervals $\Delta E_\gamma = 100$ keV. Solid curve—approximation to the points by the method of reference[11]; dotted curve—the same as the solid curve of Fig. 1. Arrows indicate positions of the peaks according to the data of [3].

Integral cross sections for individual intervals of the γ-quantum energy E_γ.

$E_{\gamma_1} - E_{\gamma_2}$, MeV	$\sigma_{int} = \int_{E_{\gamma_1}}^{E_{\gamma_2}} \sigma(\gamma, p) dE_\gamma$, MeV·mb		
	According to the data of this paper	According to the data of [1]	According to the data of [4]
20—25	(5.8)*	(5.4)	(4.6)
25—30	6.3	8.7	8.1
30—40	10.4	11.8	10.1
40—50	5.5	4.7	6.0
20—50	28.0±2.0	30.6	28.8

*In brackets—values taking extrapolation into account.

REF.

A. N. Gorbunov
PICNS-67 Contributions, International Conference on Nuclear Structure, Tokyo, Japan, 1967 (Institute for Nuclear Study, University of Tokyo, Tanashi-shi, Tokyo, Japan) 10.12, p.376

ELEM. SYM.	A	Z
He	4	2

METHOD

REF. NO.	
67 Go 5	EGF

REACTION	RESULT	EXCITATION ENERGY	SOURCE		DETECTOR		ANGLE
			TYPE	RANGE	TYPE	RANGE	
G,P	ABX	20-170	C	170	CCH-D	1-150	DST

Photodisintegration of He^4

A.N. Gorbunov

P.N.Lebedev Physical Institute, Academy ofSciencee

Leninsky Prospect, Moscow, USSR

The photodisintegration of He^4 was investigated with a cloud chamber at E_{max} = 170 Mev. The $He^4(\gamma,p)H^3$ cross section (histogram in fig.1) was found to be in a good agreement with Perry, Bame [1] and Gemmell,Jones [2] results below 28 Mev (dashed line), obtained from the inverse reaction measurements and with Clero et al. [3] $\left(\frac{d\sigma}{d\Omega}\right)_{90°}$ cross section for the energy range 25÷55 Mev multiplied by the factor $8\pi/3$ to estimate a total cross section (solid line).

Bransden et al. [4] has shown theoretically that it is not possible to describe simultaneously the radius of He^4 nucleus,its binding energy (which demands a smaller radius),position of the γ,p cross section maximum and its absolute value (which demands a larger radius), when one uses a simple wave function of He^4. Curve "a" was calculated by Braneden et al with the exponentional type variational wave function. This curve is in a sharp contradiction with the experiment. Curve "b" better agrees with the experimental data, but it corresponds to too large He^4 radius ($\langle R^2\rangle^{1/2}$ = 2,35 F).

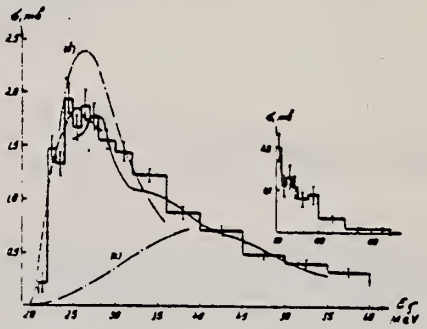

Fig.1 $He^4(\gamma,p)H^3$ total cross section

In fig.2 we give the angular distributions of proton from the γ,p reaction.The solid curves are a least squares fit of the functional form $Sin^2\theta + \beta Sin^2\theta Cos\theta + \gamma Sin^2\theta Cos^2\theta + \delta$ .Parameters γ and δ are found to be equal to zero within the errors at least up to 65 Mev. The asymmetry parameter β shown in the fig.2 rapidly increases with the photon energy.

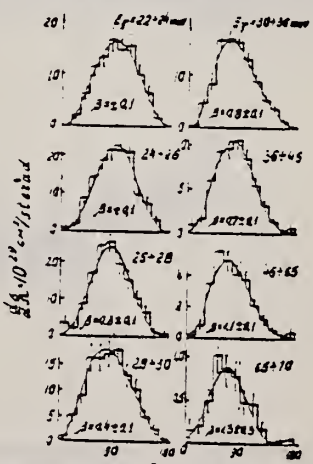

Proton angle θ_p (deg).

Fig.2 Angular distributions of protons.

References : 1) J.E.Perry,S.Bame : Phys.Rev. 99(1955) 1368
2) D.S.Gemmell, G.A.Jones : Nucl.Phys. 33 (1962) 102.
3) H.G.Clero, R.C.Morrison, R.J.Stewart : Phys.Lett.18 (1965) 316
4) B.H. Bransden, A.C.Douglas, H.H.Robertson : Phil.Mag.2(1957) 1211.

REF. R. F. Frosch, R. E. Rand, Hall Crannell, J. S. McCarthy, L. R. Zuelzle and M. R. Yearian
Nucl. Phys. A110, 657 (1968)

ELEM. SYM.	A	Z
He	4	2

METHOD

REF. NO. 68 Fr 1 EGF

REACTION	RESULT	EXCITATION ENERGY	SOURCE		DETECTOR		ANGLE
			TYPE	RANGE	TYPE	RANGE	
E,E/	ABX	20-30	D	150-400	MAG-D	162-270	DST

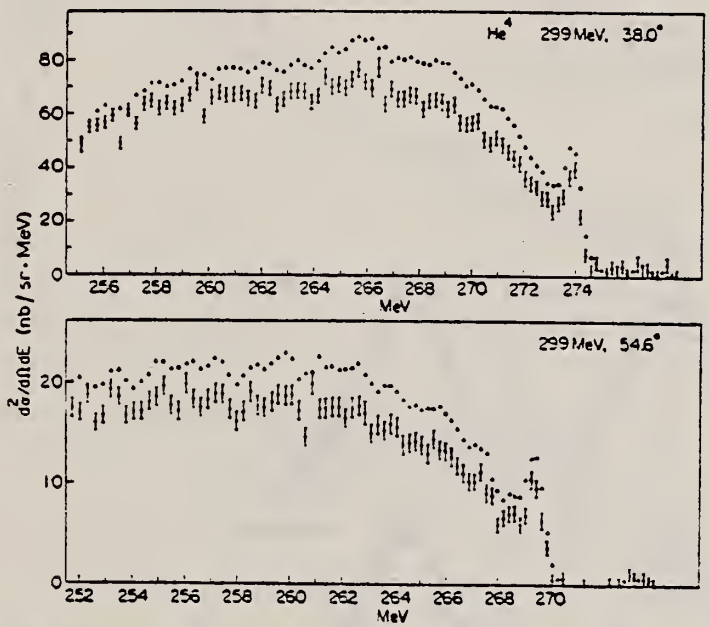

Fig. 7. Experimental data for ^{4}He showing the excited 20 MeV peak and a large portion of the inelastic continuum. The points represented by the triangles have been corrected for radiative losses.

(Similar data given for other E_o)

TABLE 2

Experimental results for the 20 MeV level inelastic form factor

q_1^2 (fm^{-2})	F_{inel}
0.29	0.094 ± 0.019
0.53	0.114 ± 0.018
0.89	0.153 ± 0.019
1.30	0.160 ± 0.026
1.74	0.162 ± 0.020
2.20	0.155 ± 0.023
2.66	0.132 ± 0.019
3.67	0.114 ± 0.022

The error quoted for these values again includes the systematic uncertainty for the asymmetric peak correction.

REF. A. N. Gorbunov
ZhETF Pis. Red. 8, 148 (1968)
JETP Letters 8, 88 (1968)

ELEM. SYM.	A	Z
He	4	2

METHOD

REF. NO. 68 Go 2 hmg

REACTION	RESULT	EXCITATION ENERGY	SOURCE		DETECTOR		ANGLE
			TYPE	RANGE	TYPE	RANGE	
G,P	ABX	THR-260	C	260	CCH-D		DST
G,N							

G,P

σ_0 (170 MeV) = 40.1 ± .9 MeV-mb

σ_{-1} (170 MeV) = 1.13 ± .02 mb

G,N

σ_0 (170 MeV) = 42.5 ± 1.1 MeV-mb

σ_{-1} (170 MeV) = 1.09 ± .03 mb

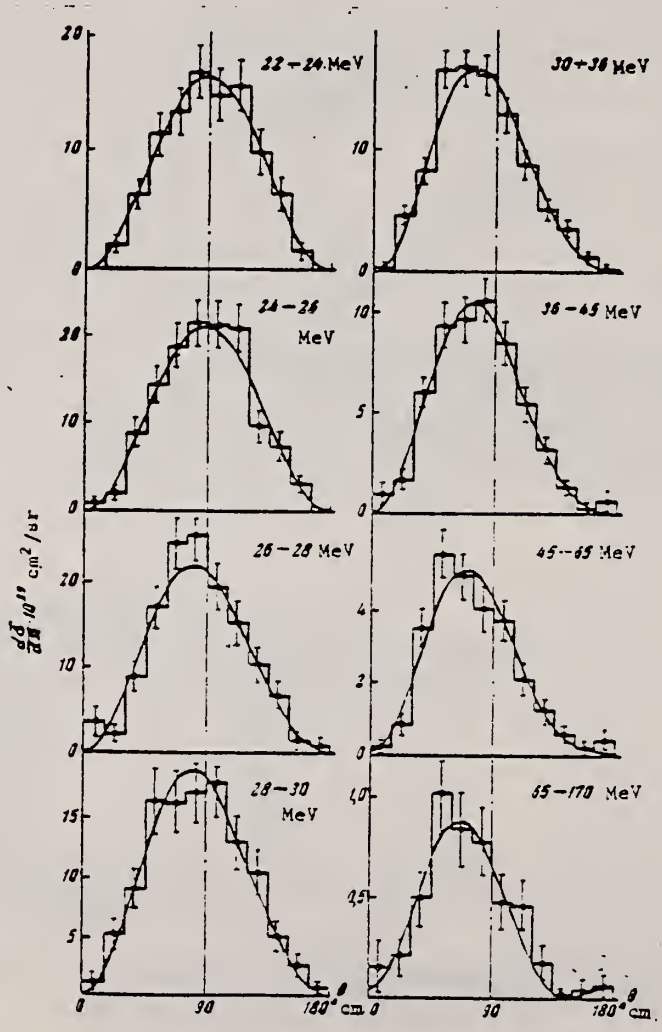

Fig. 2. Angular distributions of the protons in the reaction $He^4(\gamma, p)H^3$.

(continued)

FORM NBS-418
(REV. 7-1-64)
USCOMM-DC 28010-P64

REF.

A. N. Gorbunov
ZhETF Pis. Red. 8, 148 (1968)
JETP Letters 8, 88 (1968)

ELEM. SYM.	A	Z
He	4	2

METHOD

REF. NO. 68 Go 2 hmg

ECTOR	
RANGE	ANGLE

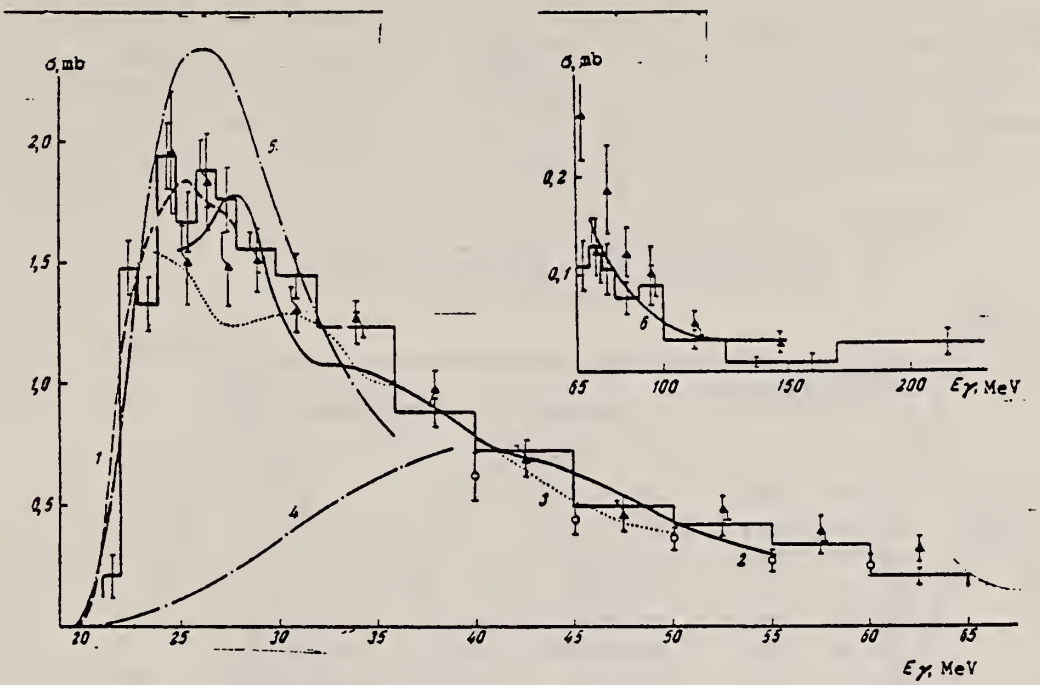

Fig. 1. Effective cross sections of the reactions $He^4(\gamma, p)H^3$ (histogram) and $He^4(\gamma, n)He^3$ (triangles)

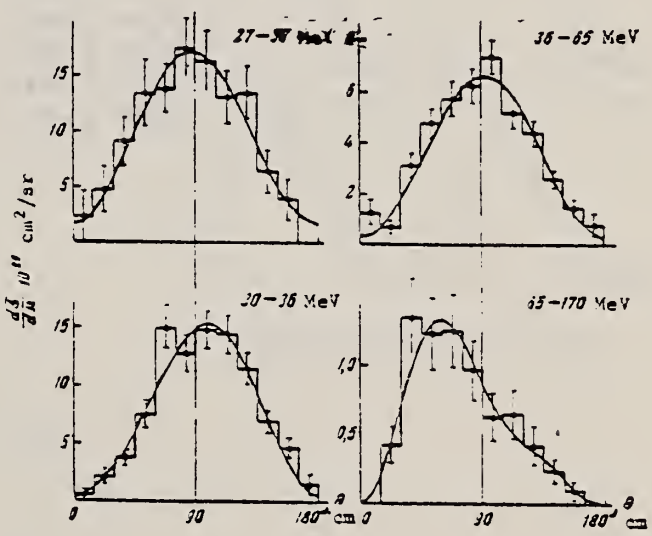

Fig. 3. Angular distributions of the neutrons in the reaction $He^4(\gamma, n)He^3$.

(continued)

Angular distributions of protons and neutrons in the reactions $He^4(\gamma, p)H^3$ and $He^4(\gamma, n)He^3$ (in the c.m.s.)

E_γ MeV	A_1 μb/sr	B	γ	δ	P,%
		Protons			
22 – 24	165 ± 9	0.04 ± 0.11	–	–	93
24 – 26	210 ± 11	0.07 ± 0.10	–	–	47
26 – 28	213 ± 11	0.33 ± 0.10	–	–	10
28 – 30	184 ± 11	0.34 ± 0.11	–	–	79
30 – 36	155 ± 6	0.66 ± 0.07	–	–	14
36 – 45	93 ± 4	0.79 ± 0.07	–	–	55
45 – 65	43 ± 3	0.98 ± 0.10	–	0.03 ± 0.02	22
65 – 170	6.1 ± 0.9	1.48 ± 0.22	–	0.08 ± 0.06	75
		Neutrons			
27 – 30	152 ± 19	0.10 ± 0.18	–	0.12 ± 0.08	89
30 – 36	142 ± 9	−0.36 ± 0.09	–	0.04 ± 0.03	30
36 – 65	68 ± 4	−0.03 ± 0.08	–	0.04 ± 0.03	4
65 – 170	8.7 ± 1.2	1.43 ± 0.32	1.5 ± 0.6	–	87
30 – 170	44 ± 2	0.05 ± 0.07	–	0.13 ± 0.02	81

REF.

A. N. Gorbunov
Phys. Letters 27B, 436 (1968)

ELEM. SYM.	A	Z
He	4	2

METHOD

REF. NO.	
68 Go 5	egf

REACTION	RESULT	EXCITATION ENERGY	SOURCE		DETECTOR		ANGLE
			TYPE	RANGE	TYPE	RANGE	
G,P	ABX	20-200	C	170,260	CCH	2-240	DST
G,N	ABX	26-150	C	170,260	CCH	5-130	DST

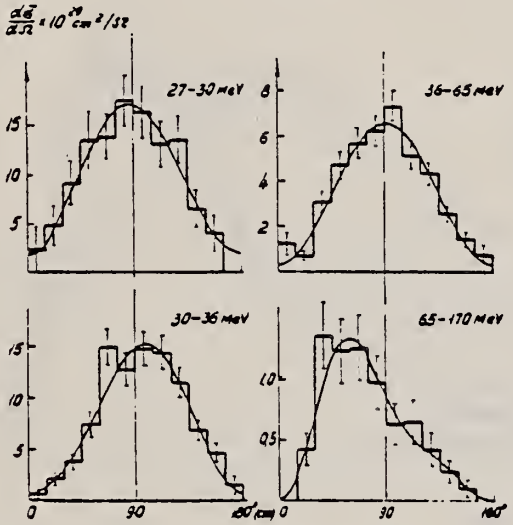

Fig. 3. Angular distribution of neutrons from the $^4He(\gamma, n)^3He$ reaction in the c.m. system.

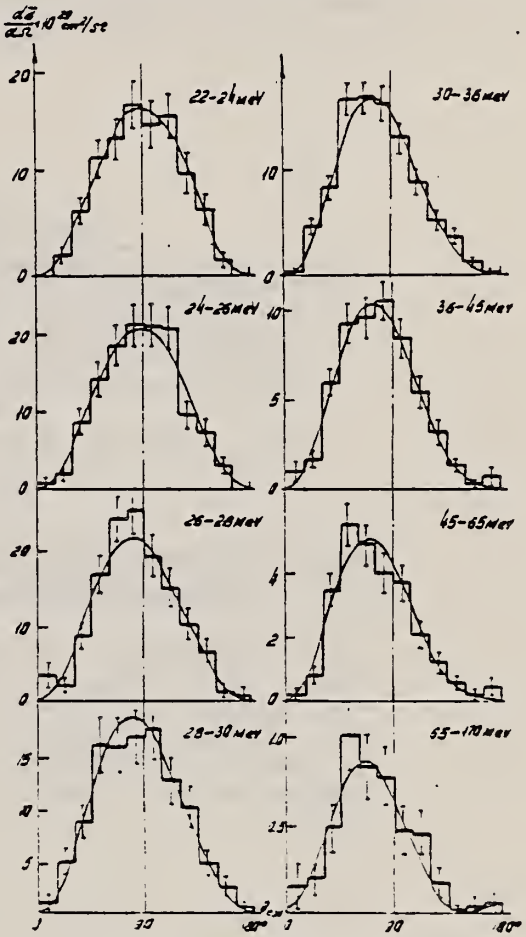

Fig. 2. Angular distribution of protons from the $^4He(\gamma, p)^3H$ reaction in the c.m. system.

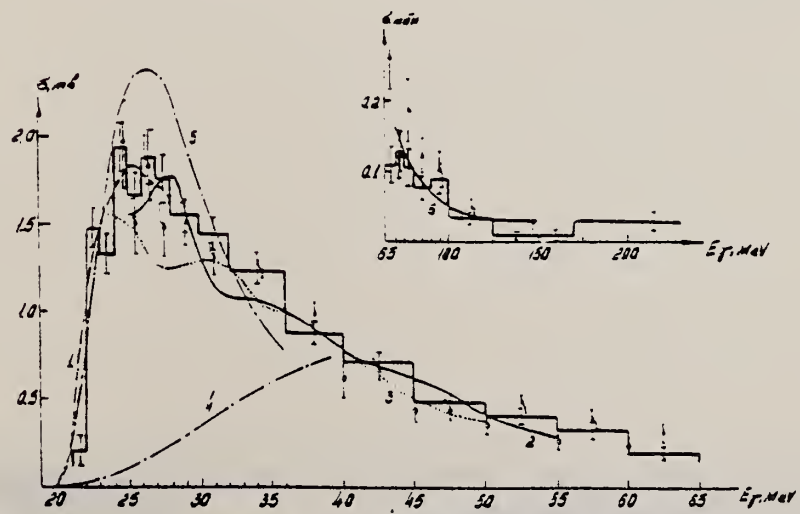

Fig. 1. Cross sections for the $^4He(\gamma, p)^3H$ and $^4He(\gamma, n)^3He$ reactions.

REF. R. Mundhenke, R. Kosiek and G. Kraft
Z. Physik 216, 232 (1968)

ELEM. SYM.	A	Z
He	4	2

METHOD

REF. NO. 68 Mu 1 egf

REACTION	RESULT	EXCITATION ENERGY	SOURCE		DETECTOR		ANGLE
			TYPE	RANGE	TYPE	RANGE	
G,P	ABX	23-32	C	28,33	SCI-D	3-10	90

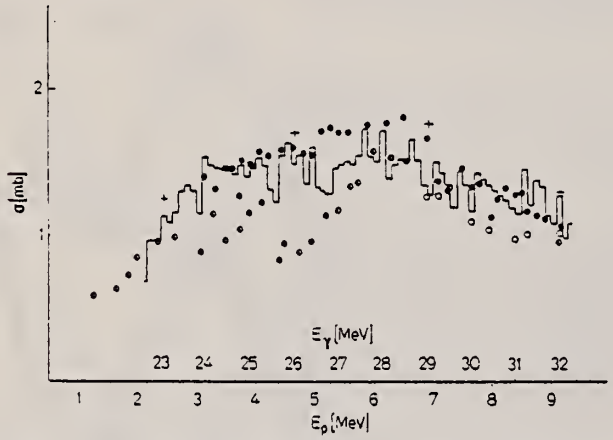

Fig. 3a—c. Wirkungsquerschnitt der Reaktion $^4He(\gamma, p)^3T$: a) + GORBUNOV et al.[11]; b) • bzw. ○ CLERC et al.[13]; c) Histogramm: diese Arbeit; d) ◐ Wirkungsquerschnitt der Reaktion $^4He(\gamma, n)^3He$ nach FERRERO et al.[14]

[11] A. N. Gorbunov and V. M. Spiridonov; J. Exp. Theoret. Phys. USSR 6, 16 (1958).
[13] H. G. Clerc, R. J. Stewart and R. C. Morrison, Phys. Let. 18, 316 (1965).
[14] F. Ferrero, C. Manfredotti, L. Pasqualini, G. Piragino and P. G. Rama; Nuovo Cimento B45, 273 (1966).

REF.

Yu. M. Arkatov, A. V. Bazaeva, P. I. Vatset, V. I. Voloshchuk, A. P. Klyucharev, and A. F. Khodyachikh
ZhETF Pis. Red. 9, 462 (1969)
JETP Letters 9, 278 (1969)

ELEM. SYM.	A	Z
He	4	2

METHOD

REF. NO.	
69 Ar 1	HMG

REACTION	RESULT	EXCITATION ENERGY	SOURCE		DETECTOR		ANGLE
			TYPE	RANGE	TYPE	RANGE	
G,PN	ABX	26-120	C	120	CCH-D		4PI

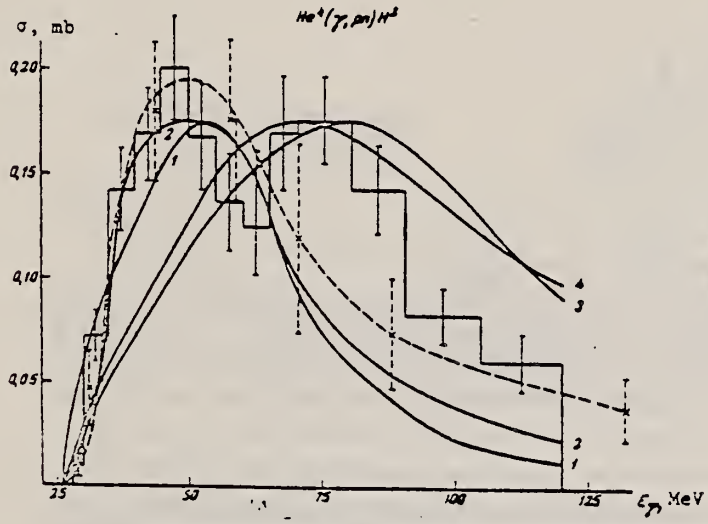

Total cross section of the reaction $He^4(\gamma, pn)H^2$ vs. gamma-quantum energy. Histogram - our results; dahsed curve - data of Gorbunov et al. [3]; solid curves - results of theoretical calculations [4, 5].

REF. Yu. M. Arkatov, P. I. Vatset, V. I. Voloshchuk, V. V. Kirichenko, I. M. Prokhorets, and A. F. Khodyachikh
ZhETF Pis. Red. 9, 574 (1969)
JETP Letters 9, 350 (1969)

ELEM. SYM.	A	Z
He	4	2

METHOD

REF. NO.	
69 Ar 2	HMG

REACTION	RESULT	EXCITATION ENERGY	SOURCE		DETECTOR		ANGLE
			TYPE	RANGE	TYPE	RANGE	
G,P	ABX	23-32	C	300	CCH-D		4PI

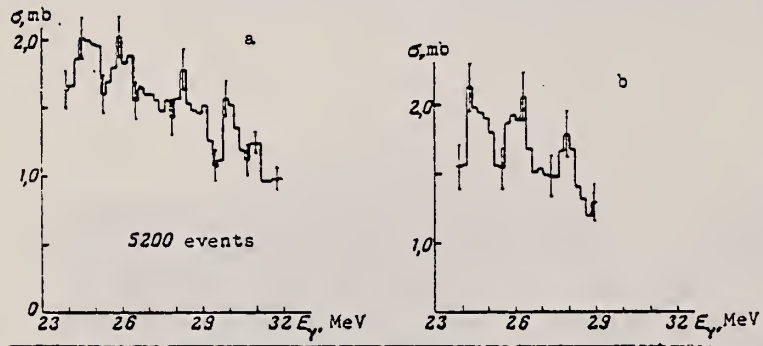

Energy dependence of the cross section of the reaction $He^4(\gamma, p)H^3$.

The dependence of the cross section σ on the energy E_γ is shown in Fig. a in the form of a histogram with energy spacing 0.2 MeV. This distribution was constructed from 5200 events. The statistical errors are indicated. At gamma-quantum energies 24.8, 26.0, 28.0, and 30 MeV one can clearly see the peaks. The distribution shown in Fig. b includes events in which the tritium emergence angle relative to the direction of the gamma quantum does not exceed 110°, thus improving the energy resolution. The normalization was against the angular distribution of all the events. It is seen that the peaks at 24.8, 26.0, and 28.0 MeV are more pronounced.

REF.

Yu. M. Arkatov, P. I. Vatset, V. I. Voloshchuk, V. L. Marchenko, A. F. Khodyachikh and V. I. Chmil
ZhETF Pis. Red. 9, 626 (1969)
JETP Letters 9, 384 (1969)

ELEM. SYM.	A	Z
He	4	2

METHOD

REF. NO.	
69 Ar 3	HMG

REACTION	RESULT	EXCITATION ENERGY	SOURCE		DETECTOR		ANGLE
			TYPE	RANGE	TYPE	RANGE	
$ G,P	NOX	22-64	C	300	CCH-D		DST
$ G,N	NOX	22-64	C	300	CCH-D		DST

W= reliability of sign of polarization

[P] POL OF P AND T
[N] POL OF HE3

Table I

Particle and E_γ, MeV / θ c.m.s. deg	p 25 – 40	^{3}H 22 – 60	^{3}He 27 – 64
10 – 90°	0.185 ± 0.172	– 0.228 ± 0.236	– 0.151 ± 0.215
90. – 170°	0.333 ± 0.245	–0.06 ± 0.245	–0.139 ± 0.295

Table II

Particle	θ c.m.s. deg. E_γ, MeV	10 – 90°	W	90 – 170°	W	10 – 170°
p	23 – 40	0.02 ± 0.05	—	– 0.23 ± 0.14	—	—
	23 – 27	—	—	—	—	– 0.05±0.07
	27 – 40	—	—	—	—	0.10 ±0.08
^{3}H	22 – 40	0.79 ± 3.3	50.5%	– 0.9 ± 2.7	63%	—
^{3}He	31 – 45	– 0.33 ±1.46	60.3%	–0.68 ± 1.74	65.2%	—

Note: E_γ – γ-quantum energy,
θ – polar angle

REF.

Yu. M. Arkatov, P. I. Vatset, V. I. Voloshchuk, A. P. Klyucharev, V. L. Marchenko, and A. F. Khodyachikh
Yad. Fiz. 9, 473 (1969)
Sov. J. Nucl. Phys. 9, 271 (1969)

ELEM. SYM.	A	Z
He	4	2

METHOD

REF. NO.	
69 Ar 4	hmg

REACTION	RESULT	EXCITATION ENERGY	SOURCE		DETECTOR		ANGLE
			TYPE	RANGE	TYPE	RANGE	
G,N	ABX	21-120	C	120	CCH-D		DST
							263 T

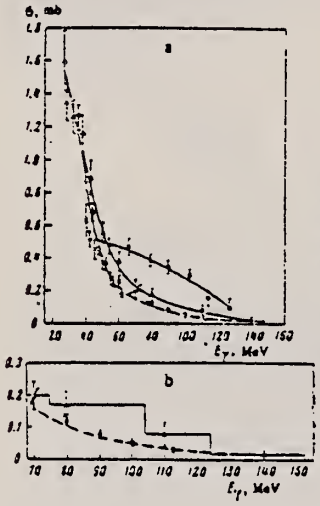

FIG. 1. Total cross section for the reaction $He^4(\gamma, n)He^3$ as a function of γ-ray energy: a—for the energy interval 30–120 MeV, b—for the energy interval 70–120 MeV. Points: ▲—ref. 1, X—ref. 2, ■—ref. 7, O—our data; dashed curve, theory. [8]

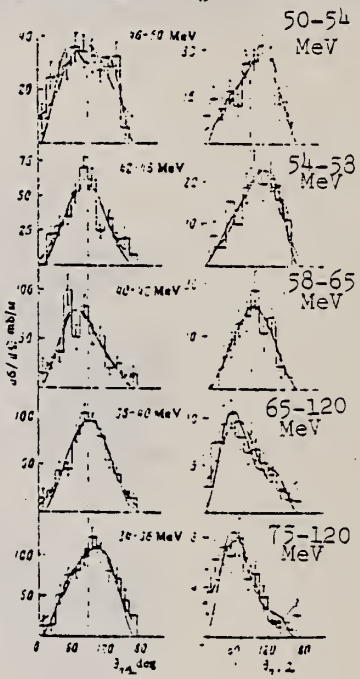

FIG. 3. Neutron angular distributions in the c.m.s. for the reaction $He^4(\gamma, n)He^3$ for $E_{\gamma max}$ = 120 MeV. Solid curve—theory according to formula (2); dot dash curve—according to formula (3).

$$\frac{d\sigma}{d\Omega} = F(\sin^2\theta + \beta\sin^2\theta\cos\theta + \varepsilon). \qquad (2)$$

$$\frac{d\sigma}{d\Omega} = F(\sin^2\theta + \beta\sin^2\theta\cos\theta + \gamma\sin^2\theta\cos^2\theta + \varepsilon). \qquad (3)$$

E_γ, MeV	Shape of angular distribution	F, mb/sr	β	γ	ε
24–30	2	10.5±1.3	−1.330±1.127		0.22±0.06
	3	10.7±1.1	−0.29±1.12	0.85±1.27	−0.040±0.015
30–34	2	8.5±1.5	−1.02±0.11		0.11±0.05
	3	9.9±1.1	−1.02±0.09	0.13±0.22	−0.140±0.014
34–40	2	5.9±0.9	0.92±0.38		0.23±0.15
	3	8.2±1.3	0.75±0.32	0.91±0.51	−0.04±0.03
40–42	2	8.0±1.0	0.37±0.23		0.13±0.10
	3	10.1±1.7	0.21±0.19	0.63±0.37	−0.05±0.035
42–46	2	9.8±1.2	0.20±0.33		0.30±0.17
	3	11.2±1.5	0.15±0.19	2.12±0.63	−0.04±0.03
46–50	2	12.20±0.43	−0.83±0.20		0.22±0.12
	3	14.3±1.7	−0.58±0.18	1.17±0.42	−0.03±0.03
50–54	2	17.7±0.3	−0.79±0.20		0.18±0.11
	3	18.9±2.5	−0.75±0.17	1.09±0.39	−0.02±0.03
54–58	2	16.3±1.9	−0.15±0.16		−0.007±0.048
	3	15.7±1.5	−0.17±0.12	−0.15±0.27	−0.013±0.04
58–120	2	4.24±1.45	1.05±0.84		0.81±0.27
	3	5.3±1.1	1.20±0.52	3.04±0.71	−0.30±0.035
70–120	2	2.35±1.14	1.50±1.46		1.21±0.53
	3	3.2±1.5	1.56±0.58	3.04±1.47	0.11±0.05

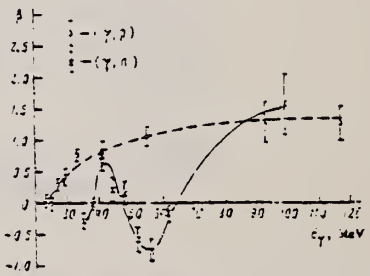

FIG. 4. Asymmetry coefficient β as a function of γ-ray energy for (γ,n) and (γ,p) reactions. Points: O—ref. 9, X—our data.

REF. Yu. M. Arkatov, A.V. Bazaeva, P.I. Vatset, V.I. Voloshchuk, A.P. Klyucharev, and A.F. Khodyachikh
Yad. Fiz. 10, 1123 (1969)
Sov. J. Nucl. Phys. 10, 639 (1970)

ELEM. SYM.	A	Z
He	4	2

METHOD

REF. NO.	
69 Ar 5	hmg

REACTION	RESULT	EXCITATION ENERGY	SOURCE		DETECTOR		ANGLE
			TYPE	RANGE	TYPE	RANGE	
G,PN	ABX	26-120	C	120	EMU-D		DST
G,2P2N	ABX	28-120	C	120	EMU-D		4PI

233
282

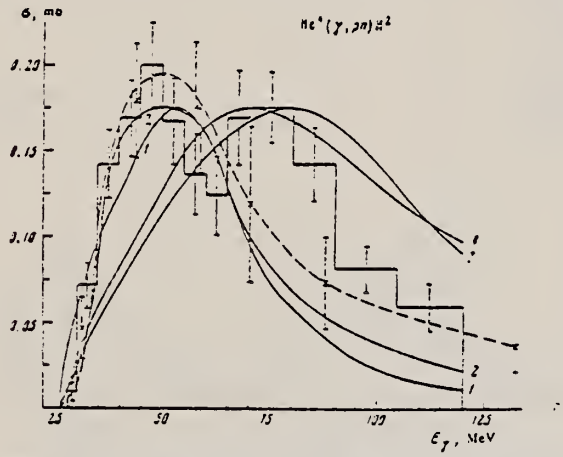

FIG. 1. Total cross section for the (γ, pn) reaction as a function of γ-ray energy. The histogram shows our result. The dashed curve is the data of Gorbunov et al. [3]. Solid curve 1 is that calculated by Dzhibuti et al. [6]. Curves 2–4 are those of Kopaleĭshvili et al. [7].

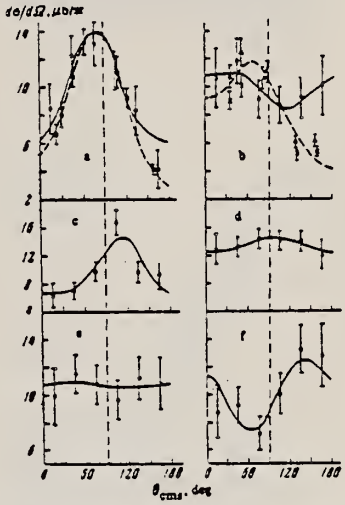

FIG. 3. Angular distributions of protons (a, b), neutrons (c, d), and deuterons (e, f) in the c.m.s.; a, c, e – for the energy interval 28 – 60 MeV; b, d, f – for the energy interval 60 – 120 MeV. Points: ○ – our data. ■ – Allen's data [13], x, ▲ – data of Whalin et al. [13].

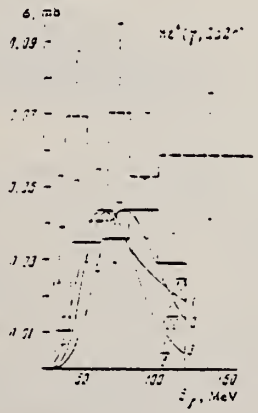

FIG. 2. Total cross section for the reaction (γ, 2p2n) as a function of γ-ray energy. The solid-line histogram shows our results, and the dashed histogram the data of Gorbunov [4]. Solid curve 1 is that calculated by Gunn and Irving [5], and curves 2 and 3 by Dzhibuti et al. [6].

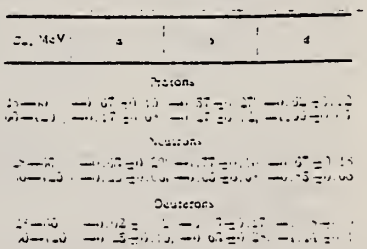

(continued)

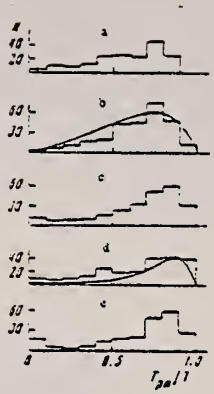

FIG. 4. Distribution of number of events in relative energy of neutron-proton pairs in units of their maximum possible energy, for γ-ray energies of: a–28–38 MeV; b–38–50 MeV; c–50–65 MeV; d–65–80 MeV; e–80–120 MeV. The solid curves are theoretical values from the work of Kopaleĭshvili et al [10].

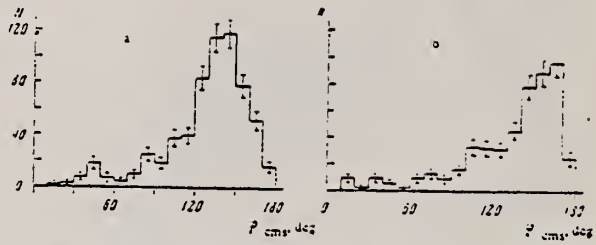

FIG. 5. Distribution of number of neutron-proton pair events as a function of the opening angle between them in the c.m.s.: a – γ-ray energy 28 – 60 MeV; b – γ-ray energy 60 – 120 MeV.

[3]A.N. Gorbunov and V.M. Spiridonov, Zh. Eksp. Teor. Fiz. 34, 866 (1958)[Sov. Phys. JETP 7, 600 (1958)].
[4]A.N. Gorbunov, Preprint T-00103, FIAN, 1969.
[5]J.C. Gunn and J. Irving, Phil. Mag. 42, 1353 (1951).
[6]R.I. Dzhibuti, N.B. Krupennikova, and V.I. Mamasakhlisov, Yad. Fiz. 7, 803 (1968)[Sov. J. Nucl. Phys. 7, 489 (1968)].
[7]T.I. Kopaleishvili and I.Z. Machabeli, Izv. AN SSSR, ser.fiz.30, 511 (1966)[Bull. USSR Acad. Sci., Phys. Ser. p.520].
[8]R.I. Dzhibuti, V.I. Mamasakhlisov, and T.S. Macharadze, Izv. AN SSSR, ser.fiz.29, 1141 (1965) [Bull.USSR Acad.Sci., Phys. Ser. p.1147].
[9]G.M. Shklyarevskii, Zh. Eksp. Teor.Fiz. 41, 294 (1961)[Sov. Phys. JETP 14, 170 (1962)].
[10]T.I. Kopaleishvili and R.I. Dzhibuti, Zh. Eksp. Teor. Fiz. 42, 467 (1962)[Sov. Phys. JETP 15, 327 (1962)].
[11]E.A. Whalin, B.D. Schriever, and A.O. Hanson, Phys. Rev. 101, 377 (1956).

REF.

W. Del Bianco and J. M. Poutissou
Phys. Letters 29B, 299 (1969)

ELEM. SYM.	A	Z
He	4	2

METHOD

REF. NO.	
69 De 3	EGF

REACTION	RESULT	EXCITATION ENERGY	SOURCE		DETECTOR		ANGLE
			TYPE	RANGE	TYPE	RANGE	
D,G	ABX	26-30	D	4-10	NAI-D	10-30	130

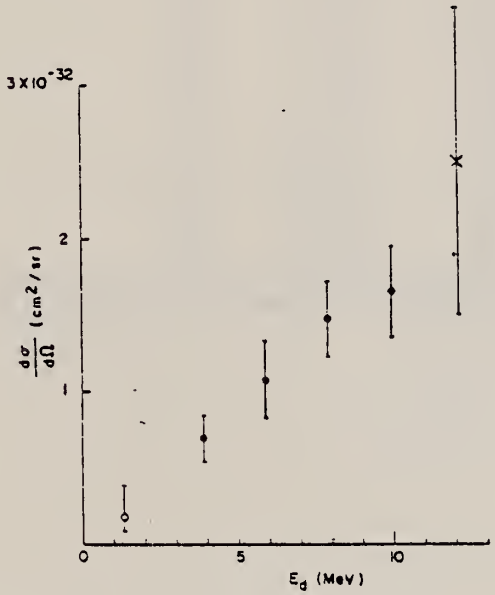

Fig. 1. The 130° differential cross section of the D(d,γ)⁴He reaction. Dots represent the results of this experiment. Points at E_d = 1.35 MeV and E_d = 12.1 MeV are those of Zurmuehle [5] et al. and Meyernof et al. [6].

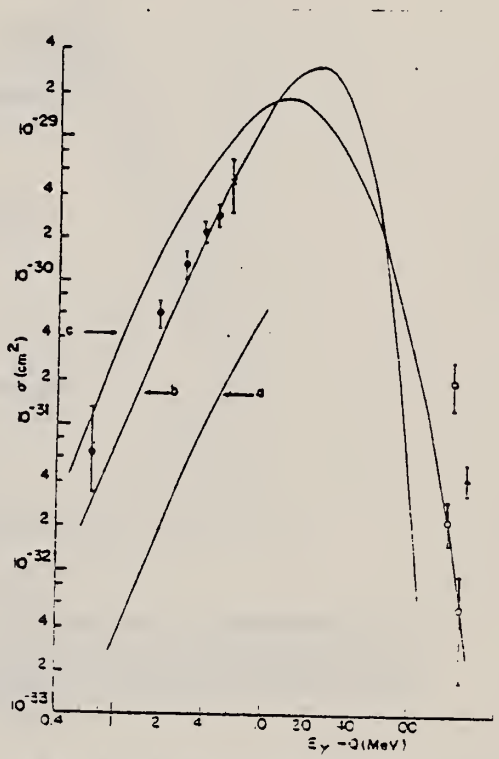

Fig. 2. Total cross sections for ⁴He(γ,d)D. Comparison of experimental results and theoretical curves. ⊙ - Zurmuehle et al. ● - present experiment. × - Meyernof et al. ○ - Asbury and Loeffler. □ - Akimov et al. △ - Poirier and Pripstein. Curve a - Delves. Curve b - Flowers and Mandl. Curve c - Asbury and Loeffler.

References

1. W. E. Meyerhof and T. A. Tombrello, Nucl. Phys. A109 (1968) 1.
2. W. Del Bianco and F. Lemire, Nucl. Instr. and Meth. 61 (1968) 229.
3. J. M. Poutissou, Master's Thesis (unpublished) Université de Montréal (1968).
4. W. Del Bianco and W. E. Stephens, Phys. Rev. 126 (1962) 709.
5. R. W. Zurmuehle, W. E. Stephens and H. H. Staub, Phys. Rev. 132 (1963) 751.
6. W. E. Meyerhof, W. Feldman and S. Gilbert, Bull. Am. Phys. Soc. 13 (1968) 564.
7. L. M. Delves, Australian J. Phys. 15 (1962) 59.
8. B. H. Flowers and F. Mandl, Proc. Roy. Soc. 206 (1951) 131.
9. J. C. Asbury and F. J. Loeffler, Phys. Rev. 137B (1965) 1214.
10. K. Akimov, O. V. Savchenko and L. M. Soroko, Zh. Eksp. Teor. Fiz. 41 (1961) 708; JETP 14 (1962) 512.
11. J. A. Poirier and M. Pripstein, Phys. Rev. 130 (1963) 1171.
12. B. H. Bransden, A. C. Douglas and H. H. Robertson, Phil. Mag. 2 (1957) 1211.

REF.

W. E. Meyerhof, W. Feldman, S. Gilbert, W. O'Connell
Nucl. Phys. A131, 489 (1969)

ELEM. SYM.	A	Z
He	4	2

METHOD

REF. NO.: 69 Me 1 egf

REACTION	RESULT	EXCITATION ENERGY	SOURCE		DETECTOR		ANGLE
			TYPE	RANGE	TYPE	RANGE	
D,G	ABX	26-34	D	6-19	NAI-D	20-36	135

ANG DIST AT 10 MEV

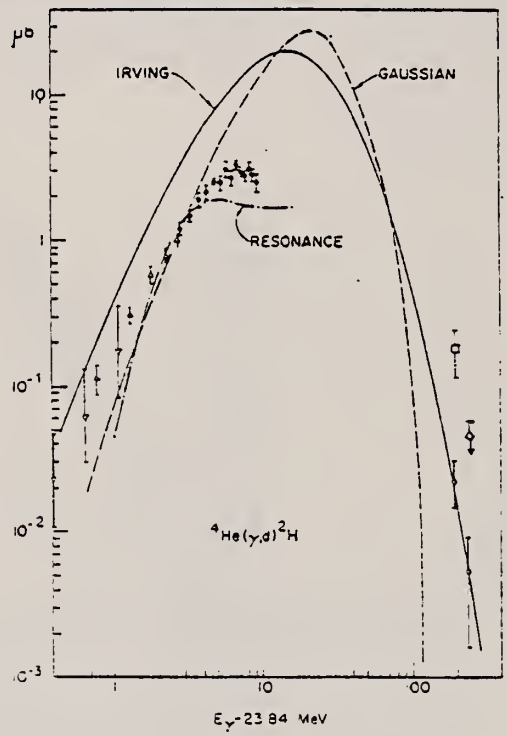

Fig. 3. Experimental and theoretical total cross section for $^4He(\gamma, d)^2H$ reaction. The symbols have the following meaning: ⊤ - ref. [12]), ⊥ - ref. [13]), ● - present results, ○ - ref. [5]), ⊐ - ref. [30]), △ - ref. [31]). Solid curve assumes Irving wave function for ^4He [ref. [5])]. Dashed curve is computed with Gaussian wave function for ^4He [ref. [4])]. Dot-and-dash curve is based on 2^- resonance in ^4He at 29 MeV [ref. [2])].

TABLE 2

Experimental and theoretical cross-section moments

Reaction	E_γ(max) (MeV)	Σ_1 ($\mu\bar{b}$ · MeV²)	Σ_0 ($\mu\bar{b}$ · MeV)	Σ_{-1} (μb)	Σ_{-2} (μb · MeV)	Σ_1/Σ_0 (MeV)	Σ_0/Σ_{-1} (MeV)	Σ_{-1}/Σ_{-2} (MeV)
$^4He(\gamma, d)^2H$	34 [a])	570	19	0.65	0.032			
$^4He(\gamma, d)^2H$	325 [b])	0.05×10^5	0.08×10^3	1.8	0.044	≈ 61	46	39
$^4He(\gamma, p)^3H$	260 [c])	1.7×10^5	1.7×10^3	27	0.60	≈100	≈ 63	≈ 45
Sum rule [d])		1.5×10^5	3.0×10^3	60 [e])	1.2			

[a]) Absolute cross section values accurate to ±25 %.
[b]) Smooth extrapolation of data of fig. 3 to high energies.
[c]) Lower limits estimated from eq. (12) and ref. [19]). Σ_1 is quite uncertain.
[d]) Assumes $E_\gamma = 50$ MeV.
[e]) The quadrupole sum rule estimate of ref. [23]) gives a similar value for Σ_{-1} assuming uncorrelated protons.

(continued)

TABLE 1

Measured $^2H(d,\gamma)^4He$ differential cross section at 135° lab and computed total $^4He(\gamma,d)^2H$ cross section assuming a $\sin^2\theta\cos^2\theta$ c.m. angular distribution

E_d(lab) (MeV)	$\left[\frac{d\sigma(d,\gamma)}{d\Omega}\right]_{lab}$ (nb/sr)	E_γ(c.m.) (MeV)	$\sigma(\gamma,d)$ (μb)
5.82	9.9±1.0	26.75	1.18±0.12
6.83	10.7±0.9	27.26	1.45±0.12
7.85	12.5±1.4	27.76	1.90±0.21
8.86	12.5±1.3	28.27	2.06±0.22
9.87	14.3±0.7	28.78	2.54±0.12
10.88	13.1±1.5	29.28	2.48±0.29
11.89	15.1±1.9	29.78	3.04±0.38
12.89	12.5±1.5	30.29	2.66±0.32
13.90	14.8±1.1	30.79	3.29±0.24
14.91	12.7±1.0	31.29	2.94±0.23
15.91	11.8±1.1	31.80	2.82±0.26
16.91	12.5±1.4	32.30	3.08±0.34
17.92	11.0±1.2	32.80	2.80±0.32
18.92	9.4±1.5	33.30	2.48±0.39

Possible systematic errors in gamma-detector efficiency up to ±25 % have not been included in the quoted errors.

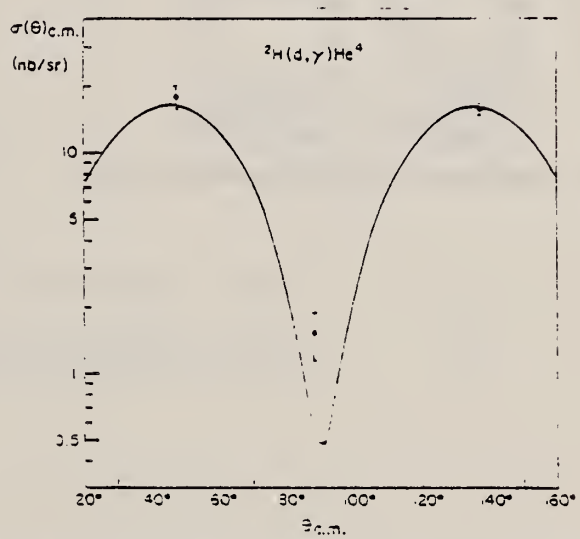

Fig. 2. The c.m. differential cross section of the $^2H(d,\gamma)$ reaction at 10 MeV deuteron energy. The solid curve represents a $\sin^2\theta\cos^2\theta$ angular distribution folded with the detector geometry. The normalization of the curve to the data is arbitrary.

REF. A. N. Gorbunov
Yad. Fiz. 10, 469 (1969)
Sov. J. Nucl. Phys. 10, 268 (1969)

ELEM. SYM.	A	Z
He	4	2

METHOD

REF. NO.: 69 Go 1 egf

REACTION	RESULT	EXCITATION ENERGY	SOURCE		DETECTOR		ANGLE
			TYPE	RANGE	TYPE	RANGE	
G,2P2N	ABX	28-160	C	170	CCH-D		4PI

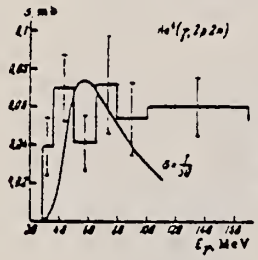

FIG. 1. Total cross section for the reaction $He^4(\gamma, 2p2n)$—histogram. Solid curve—theoretical cross section, reduced by a factor of 50, calculated by Gunn and Irving.

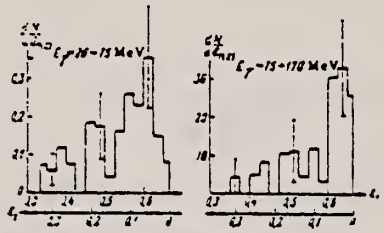

FIG. 2. Energy spectrum of protons in the reaction $He^4(\gamma, 2p2n)$.

Yield of photonuclear reactions in He^4

Type of reaction	Number of observed cases	Yield Y, mb	$Y Y_{(\gamma, p)}$	$Y \sum_i Y_i$
$He^4(\gamma, p) H^3$	7351 ± 83	1.17 ± 0.04	1	0.460 ± 0.007
$He^4(\gamma, n) He^3$	7474 ± 137	1.12 ± 0.04	0.95 ± 0.02	0.440 ± 0.009
$He^4(\gamma, pn) H^3$	1114 ± 107	0.17 ± 0.02	0.14 ± 0.01	0.066 ± 0.008
$He^4(\gamma, 2p2n)$	561 ± 114	0.08 ± 0.02	0.06 ± 0.015	0.029 ± 0.007
$He^4(\gamma, pn) H^3$ + $He^4(\gamma, 2p2n)$	1615 ± 51	0.24 ± 0.01	0.21 ± 0.006	0.095 ± 0.003
$He^4(\gamma, 2np)$	73 ± 100	0.011 ± 0.015	0.01 ± 0.012	0.004 ± 0.006

Note. Only statistical errors are shown. Errors associated with measurement of the absolute intensity of the radiation from the synchrotron do not exceed 6%.

REF.

P. Picozza, C. Schaerf, R. Scrimaglio, G. Goggi, A. Piazzoli and D. Scannicchio
Lettere al Nuovo Cimento II, 9, 445 (1969)

ELEM. SYM.	A	Z
He	4	2

METHOD

REF. NO.	
69 Pi 2	egf

REACTION	RESULT	EXCITATION ENERGY	SOURCE		DETECTOR		ANGLE
			TYPE	RANGE	TYPE	RANGE	
G,P	ABX	180-480	C		TEL-D	160-500	90

P AND T COINC

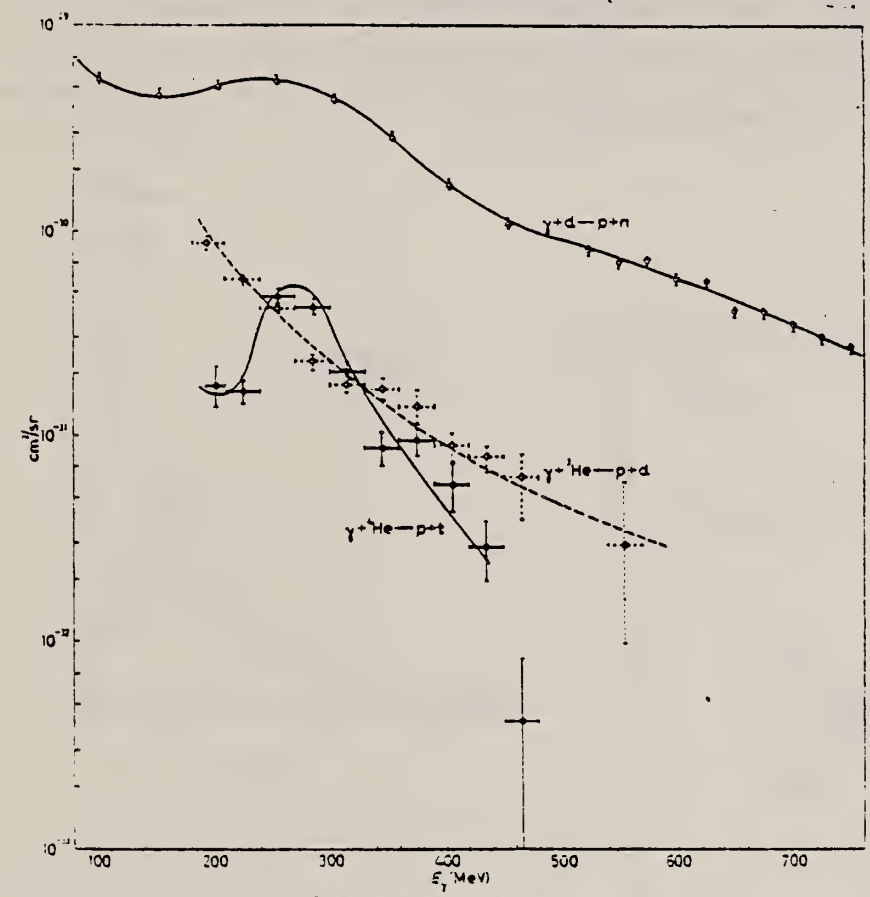

Fig. 3. – Comparison of the experimental 90° c.m.s. differential photodisintegration cross-section in two modes for d, ³He, ³He. ○ PICOZZA *et al.* (ref. (¹)); ▲ KEECK *et al.* (ref. (⁶)); ▽ CHENG *et al.* (ref. (⁷)); ● this experiment.

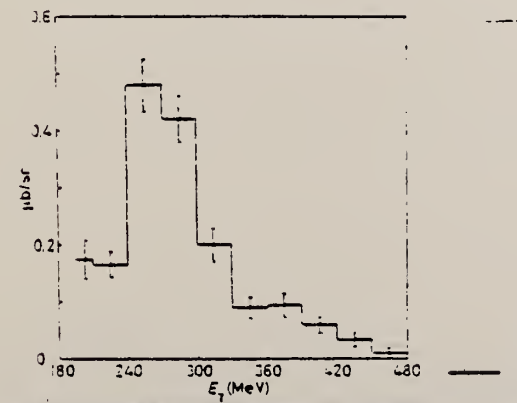

Fig. 1. – Experimental differential cross-section (c.m.s. angle = 90°) for the reaction γ+³He → p+t.

(continued)

Fig. 2. – Comparison of the experimental 90° c.m.s. differential two-body ³He photodisintegration cross-section. Assuming a $\sin^2\vartheta$ angular distribution in the whole energy range, the data by GORBUNOV (○, ref. (⁵)), CLERC *et al.* (×, ref. (⁸)), GEMMELL *et al.* (▲, ref. (⁴)) have been multiplied by 3/8π to compare them with our data (●).

[1]P. Picozz, C. Schaerf, R. Scrimaglio, G. Goggi, A. Piazzoli and D. Scannicchio: Nuovo Cimento 55A, 206, (1968).

[2]A. N. Gorbunov: Phys. Lett. 27B, 436 (.968).

[3]H. G. Clerc, R. J. Stewart and R. C. Morrison: Phys. Lett. 18, 316 (.965).

[4]D. S. Gemmell and G. A. Jones: Nucl. Phys. 33, 102 (1962).

[5]J. C. Keck and A. V. Tollestrup: Phys. Rev. 101, 360 (.956).

[6]R. Ching and C. Schaerf: Phys. Rev. 141, 1320 (1966).

REF. P. Picozza, C. Schaerf, R. Scrimaglio, G. Goggi, A. Piazzoli, and D. Scannicchio
PICNS-69 Proceedings of the Third International Conference on High Energy Physics and Nuclear Structure, Columbia University, New York City, Sept. 8-12, 1969.

ELEM. SYM.	A	Z
He	4	2

METHOD

REF. NO.: 69 Pi 3 egf

REACTION	RESULT	EXCITATION ENERGY	SOURCE		DETECTOR		ANGLE
			TYPE	RANGE	TYPE	RANGE	
G,P	ABX	200-500	C	999	TEL-D		90

999 = 1 GEV

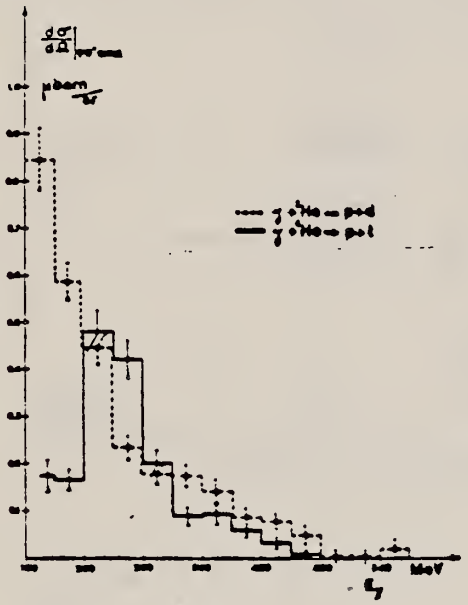

Fig. 1

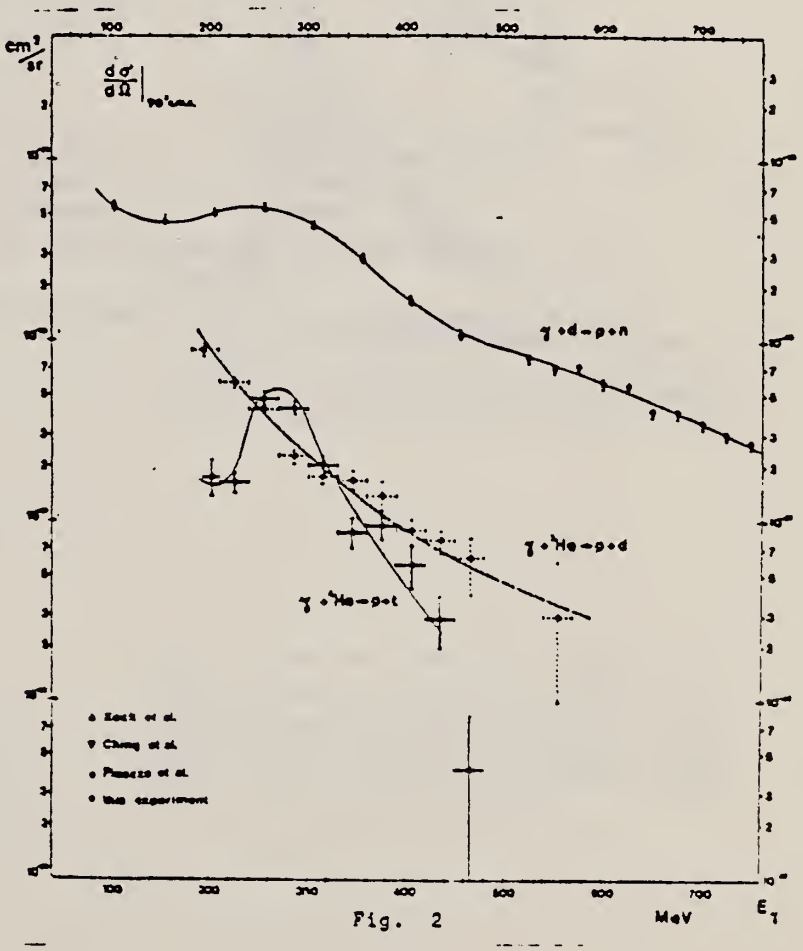

Fig. 2

REF.

J. Sanada, M. Yamanouchi, N. Sakai and S. Seki
J. Phys. Soc. Japan 26, 850 (1969)

ELEM. SYM.	A	Z
He	4	2

METHOD

REF. NO.	
69 Sa 1	egf

REACTION	RESULT	EXCITATION ENERGY	SOURCE		DETECTOR		ANGLE
			TYPE	RANGE	TYPE	RANGE	
G,P	ABX	22-30	C	32	EMU-D	2-8	DST

$d\sigma/d\Omega$ almost pure $\sin^2\theta$.

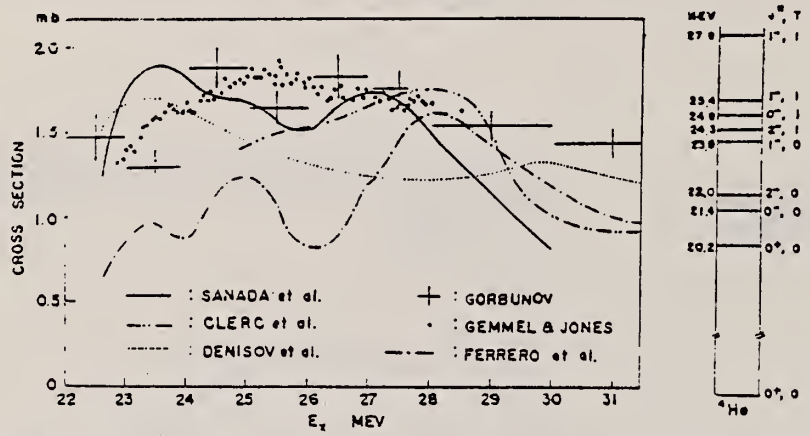

Fig. 1. Excitation curves of $^4He(\gamma, p)^3H$, $^4He(\gamma, n)^3He$ and $^3H(p, \gamma)^4He$ reactions, and a recently proposed ... level scheme of ^4He.[3]

REF. Yu. M. Arkatov, P.I. Vatset, V.I. Volshchuk, V.V. Kirichenko, I.M. Prokhorets, and A.F. Khodyachikh
Yad. Fiz. 12, 227 (1970)
Sov. J. Nucl. Phys. 12, 123 (1971)

ELEM. SYM.	A	Z
He	4	2

METHOD

REF. NO. 70 Ar 2 hmg

REACTION	RESULT	EXCITATION ENERGY	SOURCE TYPE	SOURCE RANGE	DETECTOR TYPE	DETECTOR RANGE	ANGLE
G,P	ABX	20-120	C	20-120	CCH-D		DST
		(19.8 - 120)		(19.8-120)			

SEE 71AR1

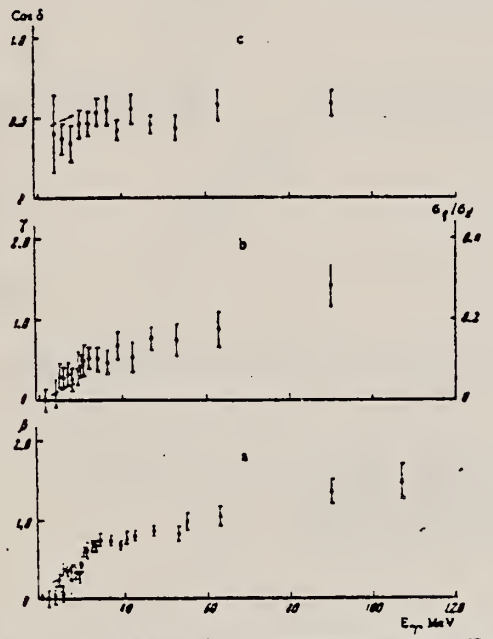

FIG. 2. γ-ray dependence of: a—the coefficient β, b—the coefficient γ, c—the phase factor cos δ. Points: ●, ○—our data, X—data of ref. 3. Dashed curve—data of ref. 3.

$$\beta = b/a, \quad \gamma = c/a, \quad \cos\delta = \beta/2\sqrt{\gamma}$$

$$\frac{d\sigma}{d\Omega} = a\sin^2\theta + b\sin^2\theta\cos\theta + c\sin^2\theta\cos^2\theta + d, \qquad (2)$$

where a and c characterize the contributions of E1 and E2 photon absorption, b the interference between them, and d all transitions in which the angular distribution is isotropic.

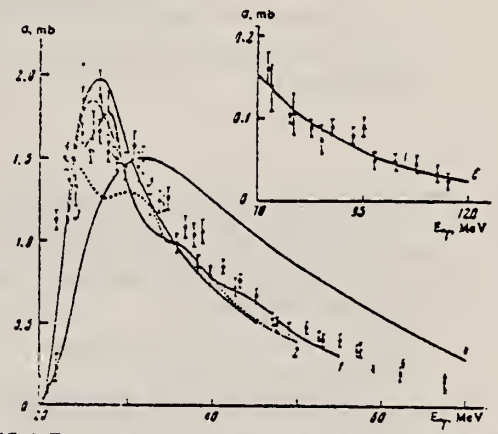

FIG. 1. Total cross section for the reaction $He^4(\gamma, p)H^3$ as a function of energy. Points: ●—our data, X—data of ref. 3. Curves: 1—experiment, ref. 4; 2—ref. 5; 3—ref. 8; 4—theory, ref. 11; 5—ref. 12; and 6—ref. 13.

Type of absorption	σ_{int}, mb·MeV	σ_{γ}, mb	σ_{γ}, mb·MeV^{-1}	σ_{γ^2}, mb·MeV^{-1}	E_{th}, MeV
E1 absorption	37.15±0.51	1.08±0.01	1501.6±27.4	(2.16±0.04)·10^{-3}	40.0±0.9
E2 absorption	2.81±0.21	0.100±0.007	176.3±9.6	(22.7±2.1)·10^{-4}	44.8±3.5
Combined absorption	41.25±0.54	1.185±0.012	1671.9±20.0	(2.59±0.05)·10^{-3}	40.5±0.9

(continued)

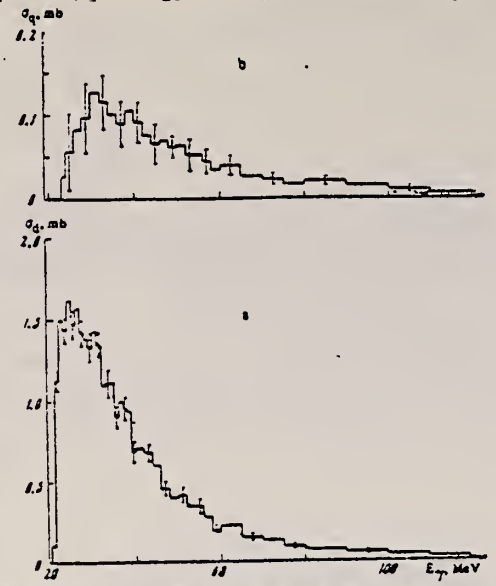

FIG. 3. γ-ray dependence of the cross sections: a—E1 absorption, b—E2 absorption.

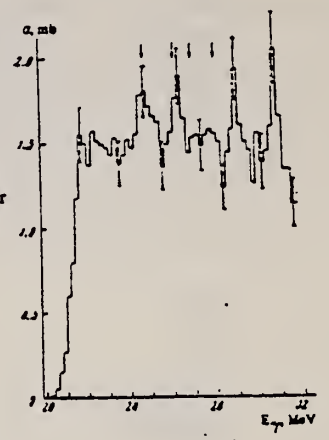

FIG. 4. Total cross section for the reaction $He^4(\gamma, p)H^3$ in the region of the giant resonance, with a step of 0.2 MeV.

[1] E. G. Fuller, Phys. Rev. 96, 1306 (1954).
[2] A. N. Gorbunov and V. M. Spiridonov, Zh. Eksp. Teor. Fiz. 33, 21 (1957) [Sov. Phys.-JETP 6, 16 (1958)].
[3] A. N. Gorbunov, ZhETF Pis. Red. 8, 148 (1968) [JETP Lett. 8, 38 (1968)].
[4] H. G. Clerc, J. R. Stewart, and R. C. Morrison, Phys. Letters 18, 316 (1965).
[5] V. P. Denisov and L. A. Kul'chitskiĭ, Yad. Fiz. 6, 437 (1967) [Sov. J. Nucl. Phys. 6, 318 (1968)].
[6] R. Mundhenke, R. Kosiek, and G. Kraft, Z. Physik 216, 232 (1968).
[7] C. Milone, Phys. Rev. 120, 1302 (1960).
[8] D. S. Gemmell and G. A. Jones, Nucl. Phys. 30, 102 (1962).
[9] Yu. M. Arkatov, P. I. Vatset, V. I. Voloshchuk, et al., ZhETF Pis. Red. 9, 574 (1969) [JETP Lett. 9, 350 (1969)].
[10] Yu. M. Arkatov, P. I. Vatset, V. I. Voloshchuk, et al., Prib. Tech. Eksp., 4, 208 (1969).
[11] R. I. Dzhibuti, N. B. Krupennikova, and V. I. Mamasakhlisov, Yad. Fiz. 7, 900 (1968) [Sov. J. Nucl. Phys. 7, 489 (1968)].
[12] F. Beck and A. Muller-Arnke, Phys. Letters 27B, 343 (1968).
[13] R. I. Dzhibuti and A. V. Tsagvlashvili, Zh. Eksp. Teor. Fiz. 39, 1756 (1960) [Sov. Phys.-JETP 12, 1223 (1961)].
[14] A. N. Gorbunov, Trudy FIAN 13, 174 (1960).
[15] P. Quarati, Nucl. Phys. A115, 651 (1968).
[16] A. N. Gorbunov, Doctoral Dissertation, FIAN, 1969.

REF. B.L. Berman, S.C. Fultz, M.A. Kelly
Phys. Rev. Letters 25, 938 (1970)

ELEM. SYM.	A	Z
He	4	2

METHOD

REF. NO. 70 Be 9 hmg

REACTION	RESULT	EXCITATION ENERGY	SOURCE		DETECTOR		ANGLE
			TYPE	RANGE	TYPE	RANGE	
G,XN	ABX	21-32	D	20-32	BF3-I		4PI

333

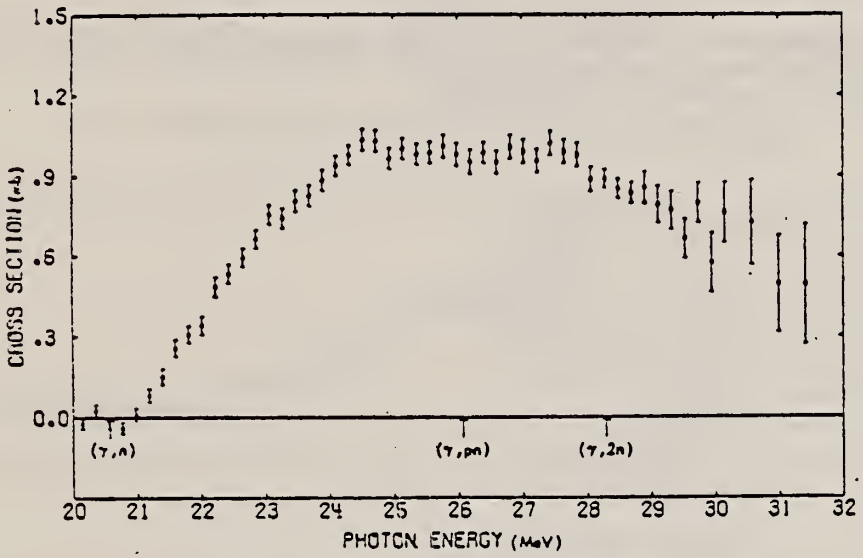

FIG. 1. Photoneutron cross section for He^4.

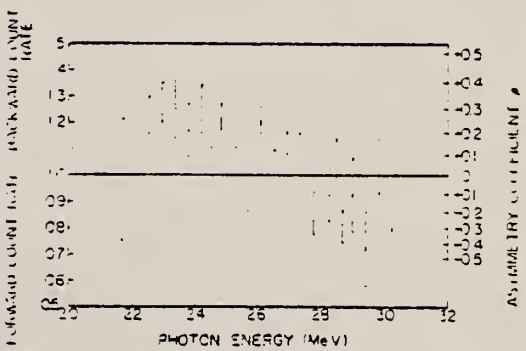

FIG. 2. Fore-aft asymmetry of the photoneutrons. The asymmetry coefficient β is computed on the assumption that the angular distribution is given by $\sin^2\theta(1+\beta\cos\theta)$.

REF. L. Busso, S. Costa, L. Ferrero, R. Garfagnini, L. Pasqualini, G. Piragino, S. Rochi della Rocca, and A. Zanini
Lettere al Nuovo Cimento III, 423 (1970)

ELEM. SYM.	A	Z
He	4	2

METHOD

REF. NO.	
70 Bu 1	egf

REACTION	RESULT	EXCITATION ENERGY	SOURCE		DETECTOR		ANGLE
			TYPE	RANGE	TYPE	RANGE	
G,N	ABX	25-60	C	THR- 60	CCH-D		DST

Fit with 236

$\sigma(\theta) = F(\sin^2\theta + \beta \sin^2\theta \cos\theta + \gamma \sin^2\theta \cos^2\theta + \varepsilon)$ for energy intervals given in 69Ar4 resulted in poor fit due to low number of events per interval. Statistics about same as in 69Ar4 but parameters were not in agreement within errors.

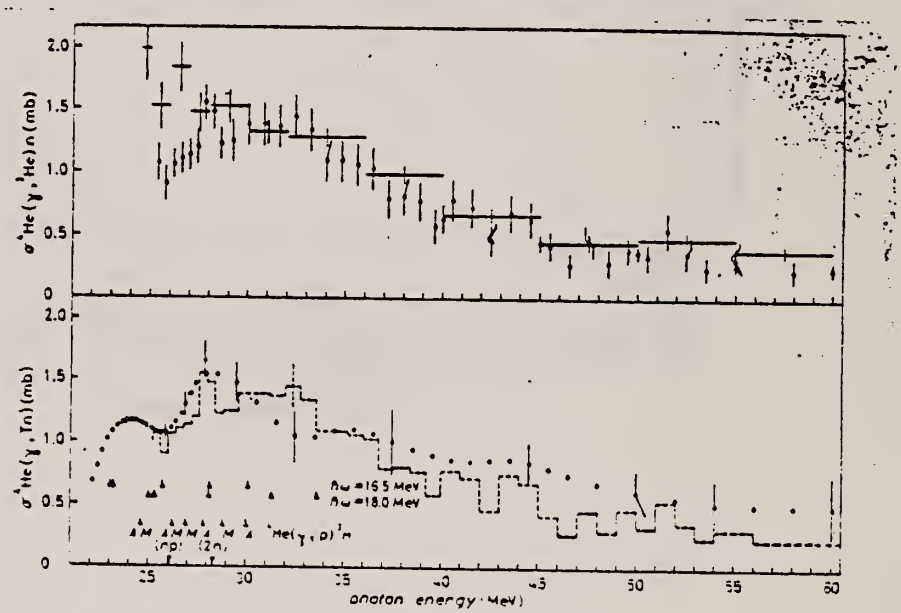

Fig. 3. – Upper part: cross-section of the ⁴He(γ, ³He)n reaction compared with the data of ref. (⁸) (crosses), ref. (⁹) (open circles), ref. (¹⁰) (triangles). Lower part: cross-section of the ⁴He(γ, Tn) reaction compared with the cross-section of the ⁴He(γ, ³He)n reaction we have obtained (dashed-line histogram). The arrows indicate levels experimentally deduced in ref. (⁸) (M), in ref. (¹⁰) (Z) and theoretically deduced in ref. (¹¹) for E_γ = 16.5 MeV and E_γ = 18 MeV.

[3] A. N. Gorbunov: Phys. Lett., 27B, 436 (1968).
[7] D. L. Livesey and I. G. Main: Nuovo Cimento, 10, 590 (1958).
[8] G. De Saussure and L. S. Osborne: Phys. Rev., 99, 843 (1955).
[9] C. Milone: Phys. Rev. 120, 1302 (1960).
[10] Yu. M. Arkatov, P. I. Vatset, V. I. Voloshchuk, I. M. Prokhorets and A. F. Khodyachikh: Sov. Phys. JETP Lett. 9, 350 (1969).
[11] G. Sh. Gogsadze and T. I. Kopaleishvile: Sov. Journ. Nucl. Phys. 8, 509 (1969).

(continued)

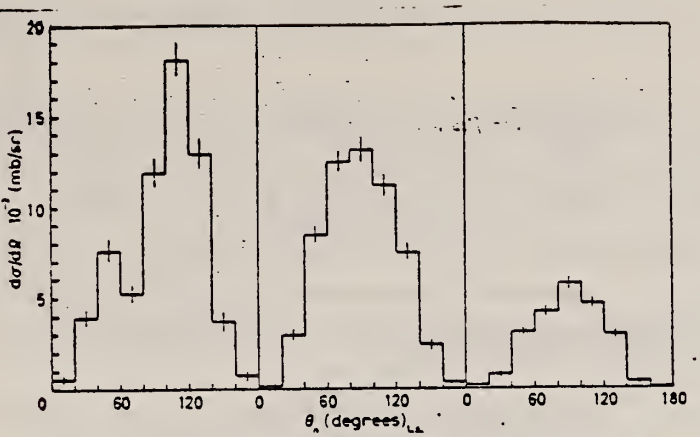

Fig. 4. – Angular distribution of the photoneutrons emitted in the c.m. system (from the left side) for (25 ÷ 30) MeV, (30 ÷ 40) MeV and (40 ÷ 50) MeV photon energy intervals.

TABLE I. – *Angular distribution of neutrons from the* ^{4}He(γ, ^{3}He)n *reaction.*

ΔE_γ (MeV)	a_0	a_1	a_2	a_3	a_4	$\chi^2(8)$
27 ÷ 36	29.85 ± 0.87	− 2.43 ± 1.03	− 31.38 ± 1.59	2.46 ± 1.16	1.49 ± 1.33	16
30 ÷ 40	9.09 ± 2.28	0.54 ± 0.32	− 9.95 ± 0.51	− 0.68 ± 0.35	0.74 ± 0.41	2
	8.98 ± 0.27	− 0.04 ± 0.08	− 9.19 ± 0.30	—	—	9 (*)
40 ÷ 60	3.39 ± 0.13	0.21 ± 0.14	− 4.23 ± 0.23	− 0.13 ± 0.16	0.92 ± 0.17	12

(*) Fit with $d\sigma/d\Omega = \sum_0^3 a_n P_n$.

REF. W. E. Meyerhof, M. Suffert and W. Feldman
Nucl. Phys. A148, 211 (1970)

ELEM. SYM.	A	Z
He	4	2

METHOD

REF. NO. 70 Me 2 egf

REACTION	RESULT	EXCITATION ENERGY	SOURCE		DETECTOR		ANGLE
			TYPE	RANGE	TYPE	RANGE	
P,G	RLX	22-33	D	3-18	NAI-D	15-33	DST

$\sigma(\theta) = A + B \sin^2\theta + C \sin^2\theta \cos\theta + D \sin^2\theta \cos^2\theta$ →40

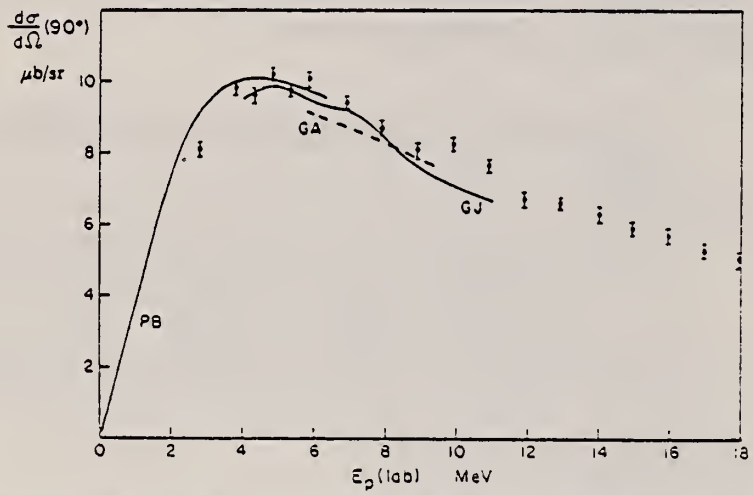

Fig. 2. Differential cross section for $^3H(p,\gamma)^4He$ reaction at 90° lab. Solid dots – present results, normalized to absolute cross section measurements of Perry and Bame (PB), ref. [5]). The measurements of ref. [4]) (GJ) and of ref. [12]) (GA) are also indicated.

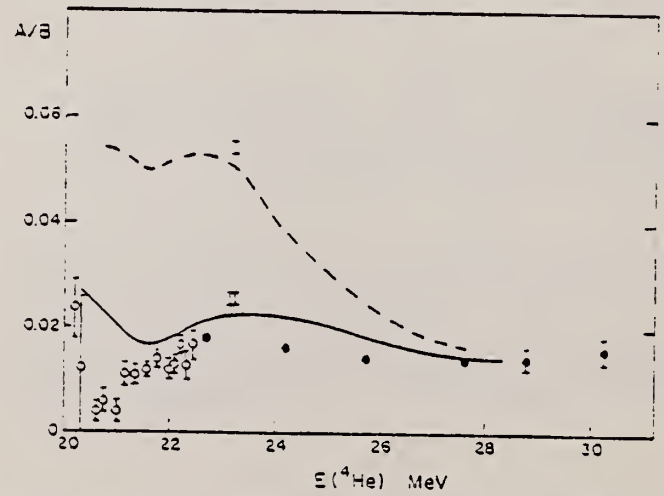

Fig. 3. Ratio A/B in $^3H(p,\gamma)^4He$ differential cross section. Solid dots – present results. Open circles – ref. [5]). The curves marked I and II are theoretical estimates of ref. [9]), discussed in the text.

(continued)

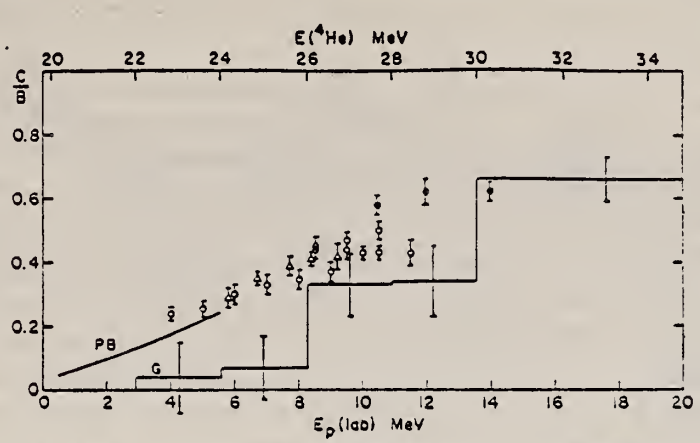

Fig. 4. Ratio C/B in $^3H(p,\gamma)^4He$ differential cross section. Solid dots – present results. Open circles – ref. [4]). Triangles – ref. [12]). (PB) – ref. [6]). (G) – ref. [13]).

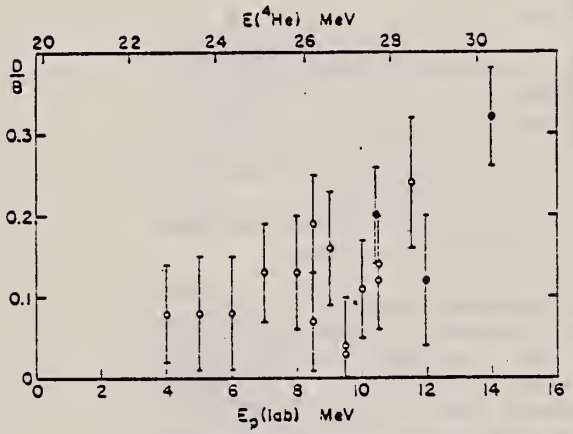

Fig. 5. Ratio D/B in $^3H(p,\gamma)^4He$ differential cross section. Solid dots – present results. Open circles – ref. [4]).

4) D. S. Gemmel and G. A. Jones, Nucl. Phys. 33 (1962) 102
5) R. Schrack, D. Kohler, N. G. Puttaswamy and W. E. Meyerhof, Phys. Lett. 18 (1965) 327
6) J. E. Perry and S. J. Bame, Phys. Rev. 90 (1953) 316
7) J. P. Didelez, H. Langevin-Joliot, N. Bejedic and Z. Maric, Nuovo Cim., to be published
8) D. Dixon in Nuclear forces and the few-nucleon problem (Pergamon Press, London, 1960) p. 295
9) L. Crone and C. Werntz, Nucl. Phys. A154 (1969) 161
10) J. Hüfner and C. M. Shakin, Phys. Rev. 175 (1968) 1350;
F. Beck and A. Müller-Arnke, Phys. Lett. 27B (1968) 343
11) M. Suffert, W. Feldman, J. Mahieux and S. S. Hanna, Nucl. Instr. 63 (1968) 1;
S. L. Blatt, J. Mahieux and D. Kohler, Nucl. Instr. 60 (1968) 221
12) C. C. Gardner and J. D. Anderson, Phys. Rev. 125 (1962) 626
13) A. N. Gorbunov, Phys. Lett. 27B (1963) 436; JETP Lett. 8 (1968) 38

REF.

J. Sanada, M. Yamanouchi, N. Sakai and S. Seki
J. Phys. Soc. Japan 28, 537 (1970)

ELEM. SYM.	A	Z
He	4	2

METHOD

REF. NO.: 70 Sa 1 egf

REACTION	RESULT	EXCITATION ENERGY	SOURCE		DETECTOR		ANGLE
			TYPE	RANGE	TYPE	RANGE	
G,P	ABX	23-32	C	32	EMU-D	3-9	DST
							(45,90,135)

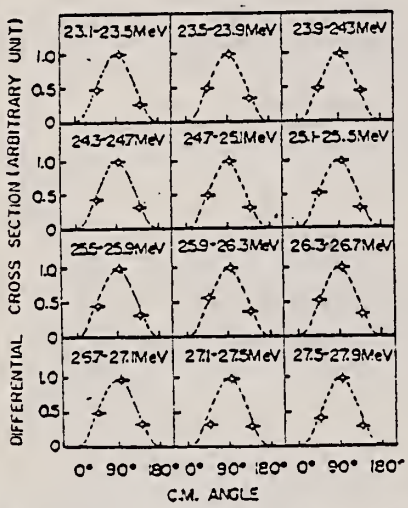

Fig. 4. Angular distributions in the c.m. system. Dotted lines are $\sin^2\theta$ distributions.

^{4}He(γ, p) reaction in successive steps of 400 keV intervals between the excitation energies 23.3 and 27.9 MeV. The angular distributions are almost proportional to $\sin^2\theta$ with no distinct isotropic component. Some of the previous experiments

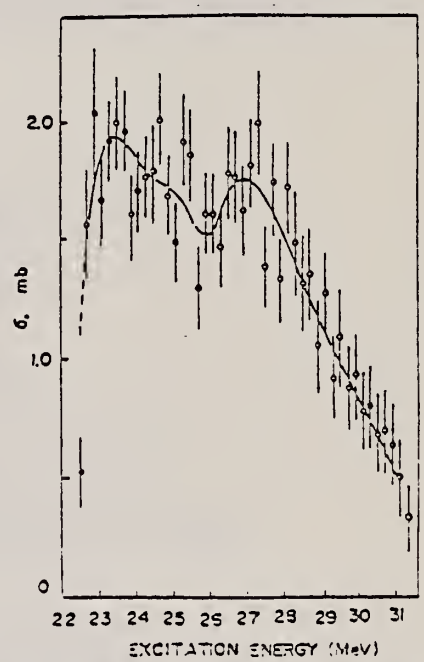

Fig. 5. Cross section of ^{4}He(γ, p)^{3}H reaction. The solid curve is a least-squares fit to the measured values.

REF. G. D. Wait, S. K. Kundu, Y. M. Shin and W. F. Stubbins
Phys. Letters 33B, 163 (1970)

ELEM. SYM.	A	Z
He	4	2

METHOD

REF. NO. 70 Wa 2 egf

REACTION	RESULT	EXCITATION ENERGY	SOURCE		DETECTOR		ANGLE
			TYPE	RANGE	TYPE	RANGE	
G,P	ABX	22-70	D	91	MAG-D		DST
G,N	ABX	50-85	D	91	MAG-D		DST

For low excitation energy no corrections made for multiparticle final states.

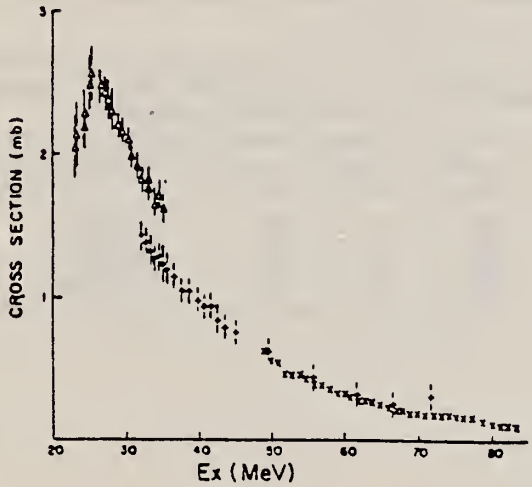

Fig. 1. Total cross section for the reactions $^4He(\gamma,p)^3H$ and $^4He(\gamma,n)^3He$. Triangles are obtained from proton data and crosses from triton data. The total cross section for the reaction $^4He(\gamma,n)^3He$ is obtained from the ^3He data (x's).

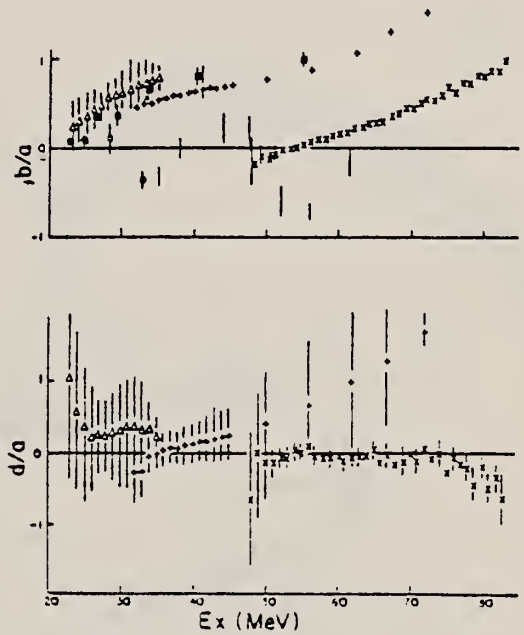

Fig. 2. Energy dependence of coefficients in the angular distributions obtained from the least-squares fits to the form $W(\theta) = a[\sin^2\theta + (b/a)\sin^2\theta\cos\theta + (d/a) \times \sin^2\theta\cos^2\theta + c/a)]$. Triangles are obtained from proton data, crosses from triton data and x's from ^3He data of the present experiment. Squares are from the results of the (γ,p) reaction and circles from the (γ,n) reaction of Gorbunov et al. Solid bars are from the results of Arkatov et al. for the (γ,n) reaction. a) The coefficient b/a. b) The coefficient d/a.

REF. Th. Walcher
Z. Physik 237, 368 (1970)

ELEM. SYM.	A	Z
He	4	2

METHOD

REF. NO. 70 Wa 4 hmg

REACTION	RESULT	EXCITATION ENERGY	SOURCE		DETECTOR		ANGLE
			TYPE	RANGE	TYPE	RANGE	
E,E/	LFT	19-31	D	56-65	MAG-D		DST

Inelastic Electron Scattering from ^{4}He at Low Momentum Transfer

20.1 MEV LEVEL

Using a liquid helium target, inelastic electron scattering from ^{4}He was investigated at momentum transfers below 0.5 fm^{-1} with improved resolution. The assignment 0^+ for the state at (20.10 ± 0.05) MeV (measured excitation energy) has been confirmed, and new values for the monopole matrix element (1.10 ± 0.16) fm^2 and the total width (270 ± 50) keV were derived. The giant resonance region shows evidence for the $M2$-resonance at 24 MeV.

Tabelle 3. Das Verhältnis des differentiellen elastischen (σ_E) und unelastischen (σ_I) Wirkungsquerschnittes und die Wurzel aus den reduzierten Matrixelementen des 20,1 MeV-Zustandes für verschiedene q

q^2/fm^{-2}	Θ/Grad	$(\sigma_I/\sigma_E)\cdot 10^{-4}$	$(\sqrt{4\pi B(CO,q)}/q^2)$/fm^2
0,199	117	2,69	0,152 ± 0,013
0,215	117	4,17	0,175 ± 0,012
0,224	117	4,33	0,172 ± 0,012
0,296	165	9,9	0,179 ± 0,045

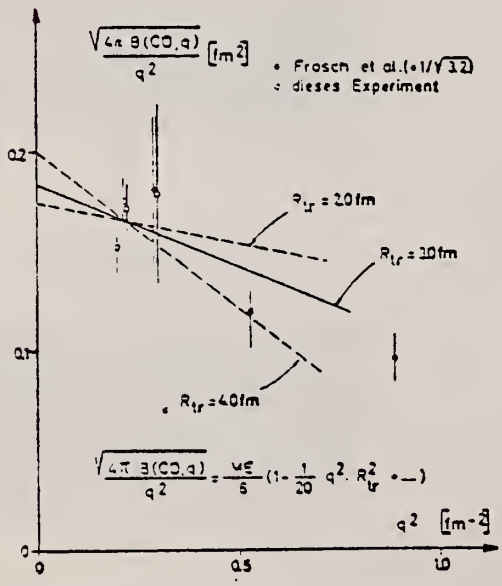

Fig. 5. Die Wurzel der reduzierten Matrixelemente als Funktion von q^2 für den 20.1 MeV-Zustand. Die ausgezogene Gerade zeigt die Extrapolation zur Bestimmung des Monopolmatrixelementes, die gestrichelten Geraden illustrieren die Unempfindlichkeit der Extrapolation auf große Änderungen in R_{tr}

(continued)

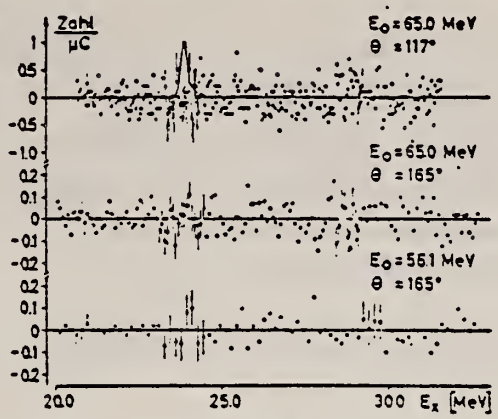

Fig. 4. Differenz zwischen drei Spektren und den glatten Kurven, die durch Tabelle 1 gegeben sind

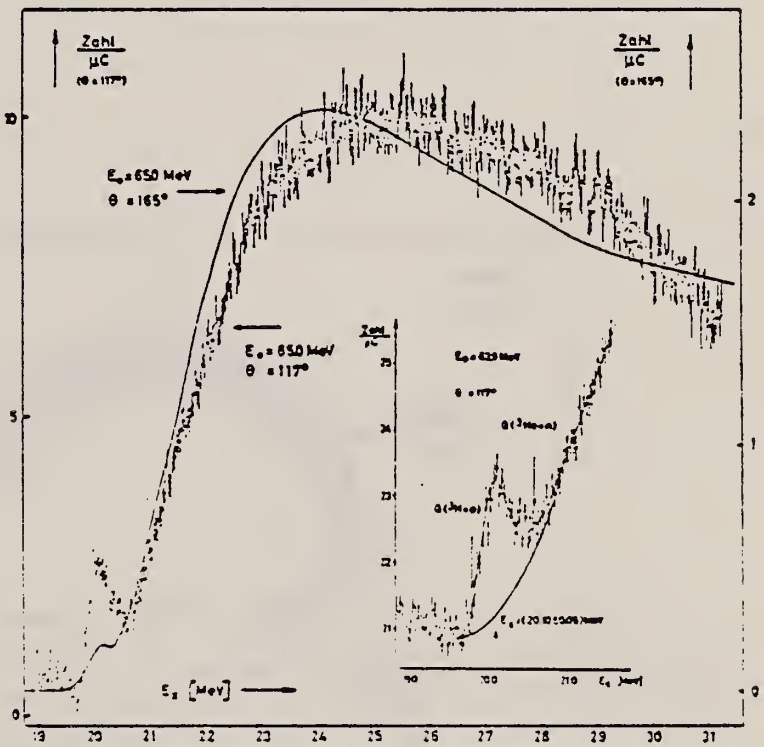

Fig. 3. Zwei Spektren unelastisch gestreuter Elektronen nach Abzug des elastischen Strahlungsschwanzes und der Untergründe. Das Spektrum bei $\theta = 165°$ ist durch eine glatte Kurve dargestellt, wie sie zur Bestimmung der Wirkungsquerschnitte der Tabelle 1 benutzt wurde. Der Einschub zeigt ein weiteres Spektrum ohne Abzug des Strahlungsschwanzes und des Untergrundes

REF.

Th. Walcher
Phys. Letters 31B, 442 (1970)

ELEM. SYM.	A	Z
He	4	2

METHOD

REF. NO.	
70 Wa 5	egf

REACTION	RESULT	EXCITATION ENERGY	SOURCE		DETECTOR		ANGLE
			TYPE	RANGE	TYPE	RANGE	
E,E/	FMF	19-31	D	65	MAG-D		DST

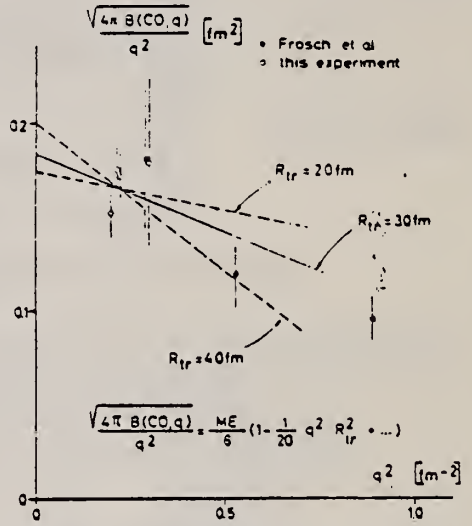

Fig. 2. Square root of reduced transition probabilities as function of momentum transfer squared. The dashed lines showing extreme R_{tr} illustrate that the extrapolation is uncritical.

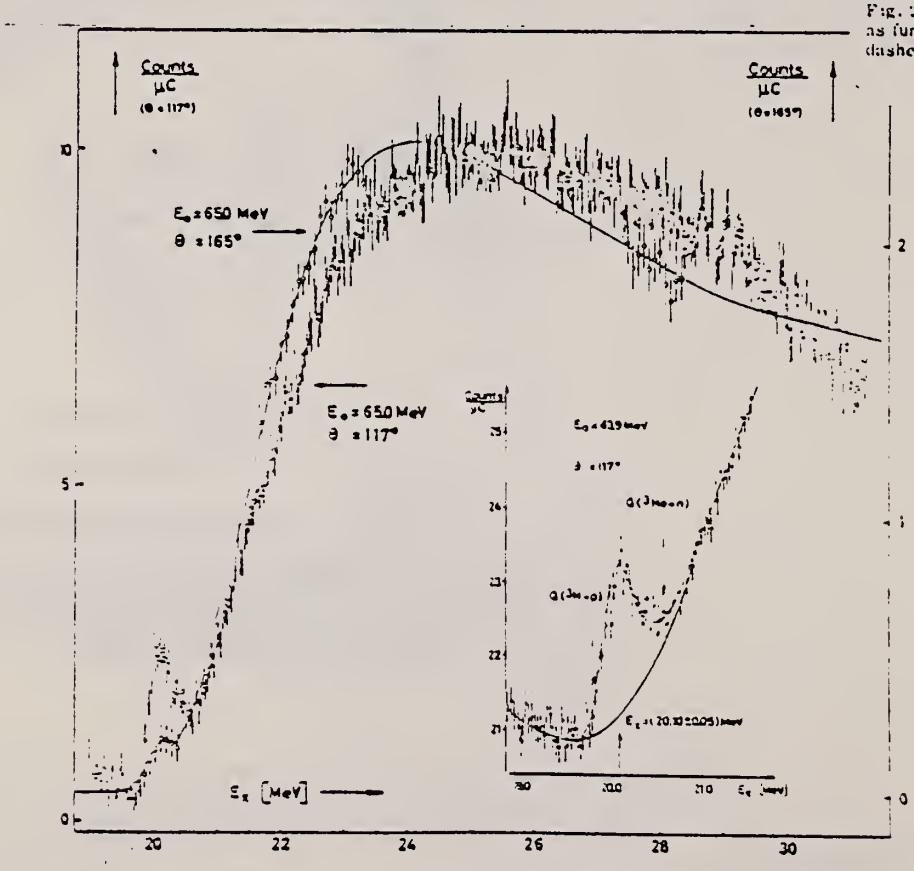

Fig. 1. Three spectra of electrons scattered inelastically from ^{4}He. energies and angles as indicated. The background of the empty target and the elastic radiative tail have been subtracted from the 65 MeV spectra.

REF.	ELEM. SYM.	A	Z
Yu. M. Arkatov, P. I. Vatset, V. I. Voloshchuk, V. V. Kirichenko, I. M. Prokhorets, and A. G. Khodyachikh Yad. Fiz. 13, 256 (1971) Sov. J. Nucl. Phys. 13, 142 (1971)	He	4	2

METHOD	REF. NO.	
	71 Ar 1	hmg

REACTION	RESULT	EXCITATION ENERGY	SOURCE		DETECTOR		ANGLE
			TYPE	RANGE	TYPE	RANGE	
G,XP	NOX	20-50	C	20-50	CCH-D		DST

New study of previously published data: see 70 AR2

NEW ANAL OF 70AR2

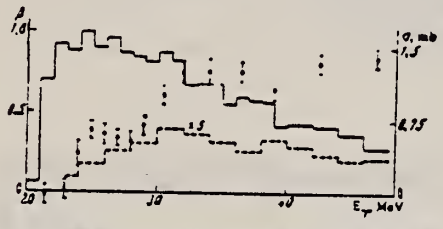

FIG. 1. Asymmetry coefficient (points), $\sigma_{\parallel}$ (solid histogram) and $\sigma_{\perp}$ (dashed histogram) as a function of γ-ray energy. The data on $\sigma_{\parallel}$ and $\sigma_{\perp}$ were taken from ref. 7.

$$\frac{d\sigma}{d\Omega} = a \sin^2\theta(1 + \beta\cos\theta + \gamma\cos^2\theta), \quad (1)$$

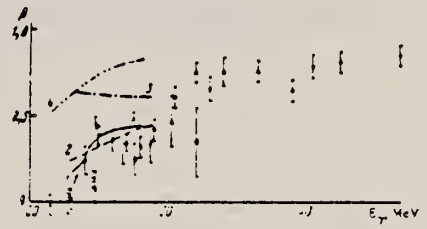

FIG. 2. Comparison of data on the asymmetry coefficient. Points. ●—present experiment, ○—ref. 3, △—ref. 4, □—ref. 1. Curves: 1—ref. 5, 2—ref. 6, 3 and 4—calculated from Eq. (2) with data of refs. 10–12.

[1] E. G. Fuller, Phys. Rev. 96, 1306 (1954).
[2] A. N. Gorbunov and V. M. Spiridonov, Zh. Éksp. Teor. Fiz. 33, 21 (1957) [Sov. Phys. JETP 6, 16 (1958)].
[3] A. N. Gorbunov, ZhETF Pis. Red. 8, 140 (1968) [JETP Letters 8, 88 (1968)].
[4] I. G. Main, Nuovo Cimento 23, 884 (1962).
[5] D. S. Gemmell and G. A. Jones, Nucl. Phys. 33, 102 (1962).
[6] C. C. Gardner and J. D. Anderson, Phys. Rev. 125, 626 (1962).
[7] Yu. M. Arkatov, P. I. Vatset, V. I. Voloshchuk, et al., Yad. Fiz. 12, 227 (1970) [Sov. J. Nucl. Phys. 12, 123 (1971)].
[8] A. N. Gorbunov, Dissertation, FIAN, 1969.
[9] W. E. Meyerhof and T. A. Tombrello, Nucl. Phys. A109, 1 (1968).
[10] T. A. Tombrello, Phys. Rev. 138, B40 (1965).
[11] T. A. Tombrello, Phys. Rev. 143, 772 (1966).
[12] T. B. Clegg, A. C. L. Barnard, J. B. Swint, and J. L. Weil, Nucl. Phys. 50, 621 (1964).

REF.

B. L. Berman, S. C. Fultz, and M. A. Kelly
Phys. Rev. C4, 723 (1971)

ELEM. SYM.	A	Z
He	4	2

METHOD

REF. NO.: 71 Be 3 hmg

REACTION	RESULT	EXCITATION ENERGY	SOURCE		DETECTOR		ANGLE
			TYPE	RANGE	TYPE	RANGE	
G,XN	ABX	20-31	D	20-31	BF3-I		DST

233

The photoneutron cross section for ^{4}He has been measured with monoenergetic photons from threshold to 31 MeV. The cross section reaches its maximum value of 1.0 mb from 24.3 to 27.3 MeV and appears to be split into two broad peaks. The integrated cross section is 7.9 MeV mb. The fore-aft asymmetry of the photoneutrons also was measured. This quantity, which is a measure of the interference between the $E1$ amplitude and the underlying positive-parity contribution, changes from forward to backward peaking at about 27 MeV. The $E2$-to-$E1$ amplitude ratio deduced from these data is of the order of 0.04. A comparison of the cross-section results with the considerably larger values for the ^{4}He(γ, p) reaction measured elsewhere shows appreciable ($\gtrsim$15%) isospin mixing throughout the energy region studied, with indications that this mixing might be increasing with energy above 28 MeV.

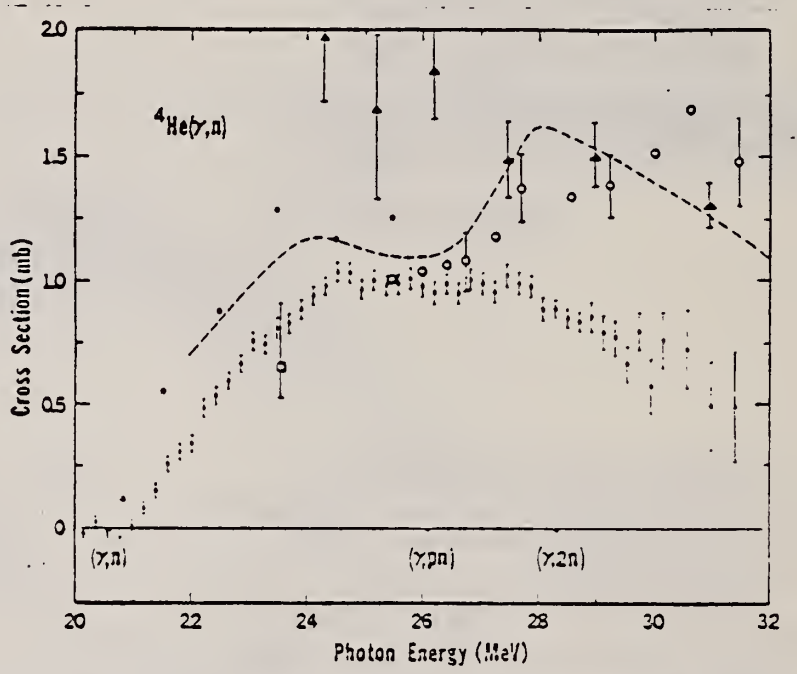

FIG. 6. The ^{4}He(γ,n) cross section as a function of incident photon energy (closed squares). The arrows indicate threshold energies, as given in J. H. E. Mattauch, W. Thiele, and A. H. Wapstra, Nucl. Phys. 67, 32 (1965). The ^{4}He-(γ,n) data of Refs. 1 and 2 are shown as the closed circles and the dashed line, respectively; the ^{4}He$(\gamma, ^3$He) data of Refs. 3 and 4 are shown as the triangles and the open circles, respectively; and the ^{3}He(n,γ) datum of Ref. 12 is shown as the open square.

(continued)

[1]G. A. Ferguson, J. Halpern, R. Nathans, and P. F. Yergin, Phys. Rev. 95, 776 (1954).
[2]F. Ferrero, C. Manfredotti, L. Pasqualini, G. Piragino, and P. G. Rama, Nuovo Cimento 45B, 273 (1966).
[3]A. N. Gorbunov, Phys. Letters 27B, 436 (1968).
[4]L. Busso, S. Costa, L. Ferrero, R. Garfagnini, L. Pasqualini, G. Piragino, S. Ronchi della Rocca, and A. Zanini, Lettere Nuovo Cimento 3, 423 (1970); L. Busso, R. Garfagnini, G. Piragino, S. Ronchi della Rocca, and A. Zanini, private communication.
[12]R. W. Zurmuhle, W. E. Stephens, and H. H. Staub, Phys. Rev. 132, 751 (1963). An error was made in the detailed-balance calculation in Phys. Rev. Letters 25, 938 (1970); The (n,γ) result yields a (γ,n) cross section of $0.64^{+0.26}_{-0.13}$ mb at 23.6 MeV, compared with the present result of 0.82 mb at that energy.
[17]D. S. Gemmell and G. A. Jones, Nucl. Phys. 33, 102 (1962).
[18]W. E. Meyerhof, M. Suffert, and W. Feldman, Nucl. Phys. A148, 211 (1970).
[22]H. A. Medicus, E. M. Bowey, D. B. Gayther, B. H. Patrick, and E. J. Winhold, Nucl. Phys. A156, 257 (1970).

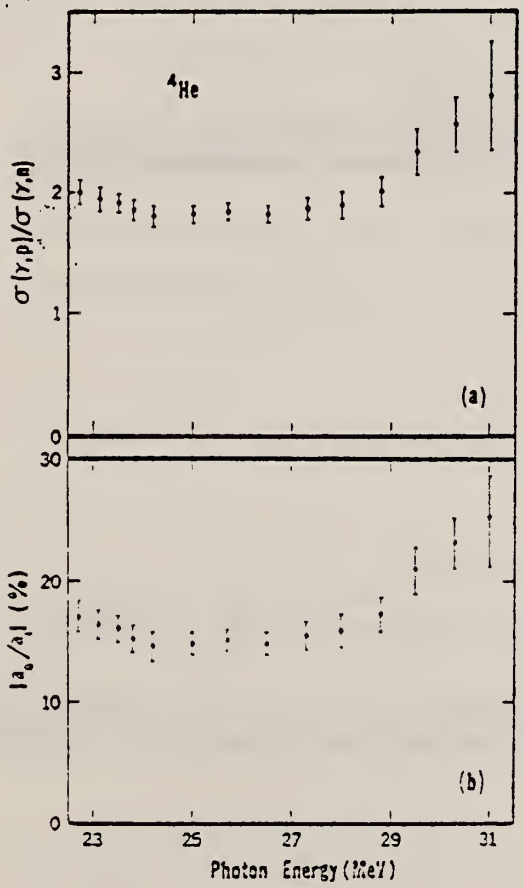

FIG. 10. (a) The ratio of the ^{4}He(γ,p) to the ^{4}He(γ,n) cross sections. The (γ,p) cross section used is a weighted average of the (p,γ) data of Refs. 17, 18, and 22. (b) The isospin-mixing ratio $|a_0/a_1|$ obtained from the cross-section-ratio data of (a).

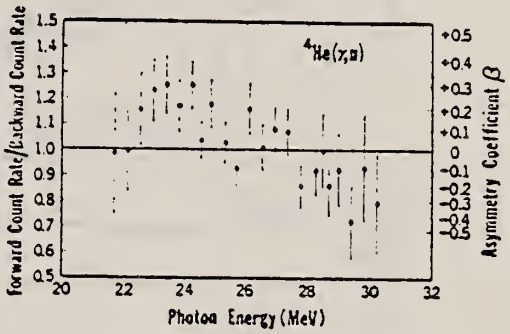

FIG. 8. The fore-aft asymmetry of the photoneutrons from ^{4}He as a function of photon energy. The asymmetry coefficient β is computed on the assumption that the angular distribution is given by $\sin^2\vartheta(1+\beta\cos\vartheta)$.

REF. L. Busso, R. Garfagnini, G. Piragino, S. Ronchi della Rocca, A. Zanini
Lettere al Nuovo Cimento 1, 941 (1971)

ELEM. SYM.	A	Z
He	4	2

METHOD

REF. NO. 71 Bu 1 egf

REACTION	RESULT	EXCITATION ENERGY	SOURCE		DETECTOR		ANGLE
			TYPE	RANGE	TYPE	RANGE	
G,N	ABX	25-80	C	80	CCH-D		DST
G,P	ABX	24-80	C	80	CCH-D		DST

346
337

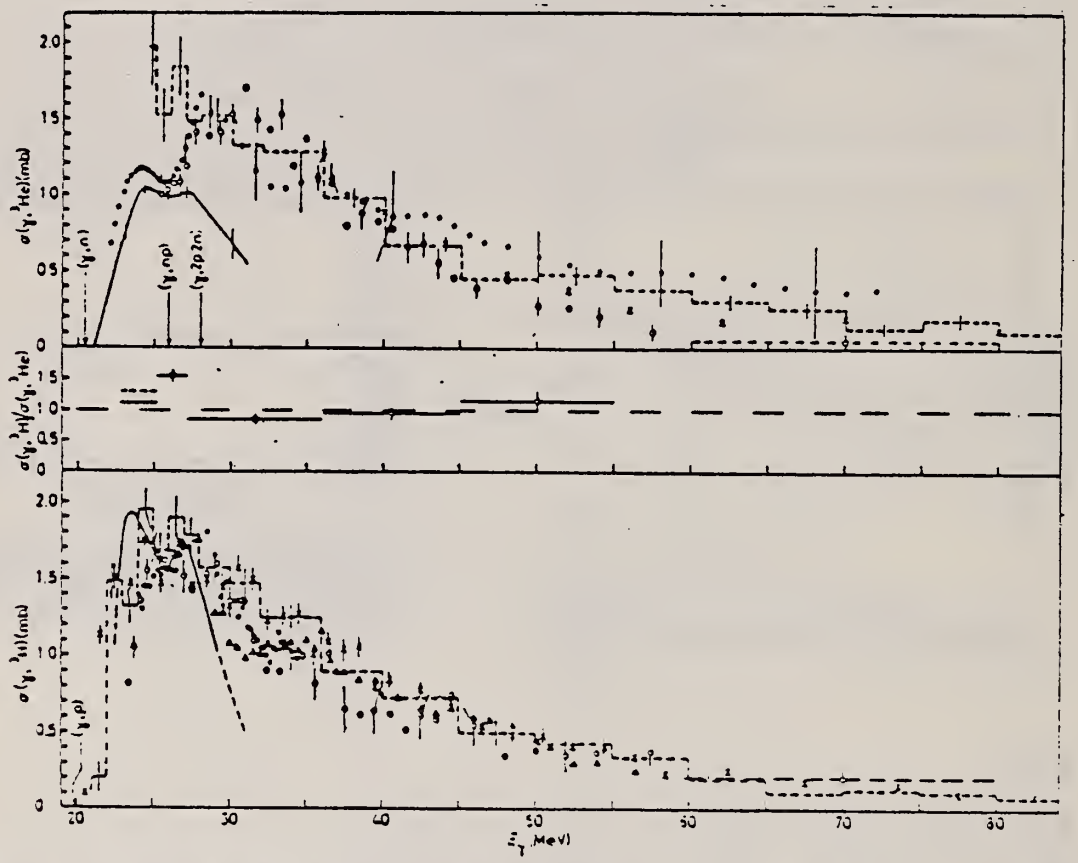

Fig. 1. – Upper part: cross-section of the $^3He(\gamma,{}^3He)n$ reaction; o, present experiment; •, ref. (14); ×, ref. (15); full line, ref. (11); dashed line, ref. (5). Lower part: cross-section of the $^3He(\gamma,{}^3H)p$ reaction; o, present experiment; x, ref. (15); • and ▲, ref. (5); full line, ref. (16); dashed line, ref. (5). Middle part: $\sigma(\gamma,{}^3H)/\sigma(\gamma,{}^3He)$; for $22.3 < E_\gamma < 33.1$ MeV the ratio was deduced using the $\sigma(\gamma,{}^3He)$ values of ref. (14) (full line) and of ref. (11) (dashed line).

(continued)

[8]A. N. Gorbunov: Phys. Lett., 27B, 436 (1968).
[6]H. G. Clerc, R. J. Steward, R. C. Morrison: Phys. Lett., 18, 316 (1965).
[11]Yu. M. Arkatov, P. I. Vatset, V. I. Voloshchuk, V. V. Kirichenko, I. M. Prokhorets and A. F. Khodyachikh: Sov. Journ. Nucl. Phys., 12, 123 (1971).
[12]J. Sanada, M. Yamanouchi, N. Sakai and S. Seki: Journ. Phys. Soc. Jap., 28, 537 (1970).
[15]F. Ferrero, C. Manfredotti, L. Pasqualini, G. Piragino and P. G. Rama: Nuovo Cimento 45B, 273 (1966).
[16]Yu. M. Arkatov, P. I. Vatset, V. I. Voloshchuk, A. P. Klyucharev, V. L. Marchenko and A. F. Khodyachikh: Sov. Journ. Nucl. Phys. 9, 271 (1969).

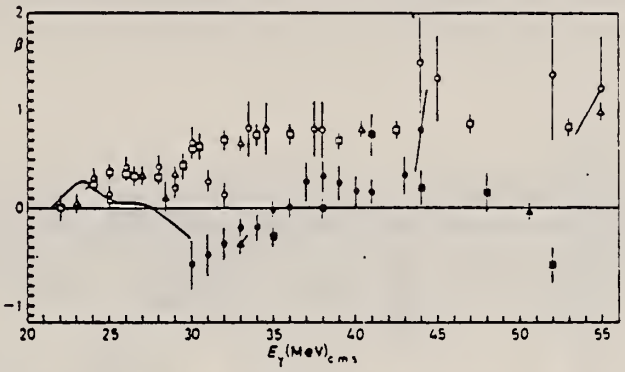

Fig. 3. – Behaviour of the asymmetry coefficient β of the proton (open symbols) and neutron (full symbols) angular distributions (c.m.s.). Only the values consistent with the χ^2 test are reported in our case (circles); ▲ and △, ref. (6); ■ and □, ref. (11); full line, relative β neutron behaviour deduced in ref. (11) (l.s.).

REF.

A. Degre, M. Schaeffer, and M. Suffert
J. de Physique 32, C5B-221 (1971)

ELEM. SYM.	A	Z
He	4	2

METHOD

REF. NO.	
71 De 1	egf

REACTION	RESULT	EXCITATION ENERGY	SOURCE		DETECTOR		ANGLE
			TYPE	RANGE	TYPE	RANGE	
D,G	ABx	24- 30	D	1- 6	NAI-D		DST

Fig. 2

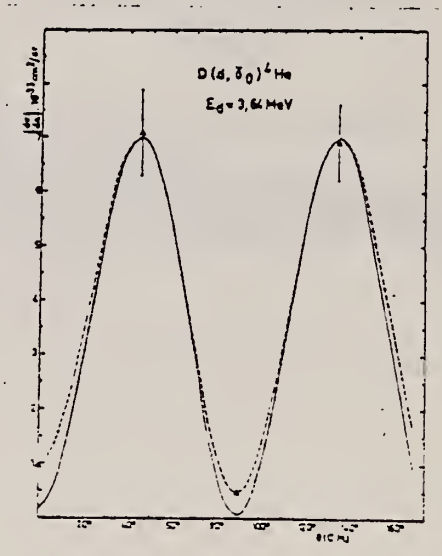

Fig. 3

REF. N.V. Goncharov, A.I. Derebchinskii, O.P. Konovalov, S.G. Tonapetyan, and V.M. Khvorostyan
Yad. Fiz. 14, 31 (1971)
Sov. J. Nucl. Phys. 14, 18 (1972)

ELEM. SYM.	A	Z
He	4	2

METHOD

REF. NO.	
71 Go 2	hmg

REACTION	RESULT	EXCITATION ENERGY	SOURCE		DETECTOR		ANGLE
			TYPE	RANGE	TYPE	RANGE	
G,PI+	RLY	150-500	C	500	CCH-D		DST

PI-/PI+ YIELD RATIO

Measurements are reported of the relative yield of π^+ mesons and the π^-/π^+ yield ratio for mesons with energy 40 ± 10 MeV emitted in the angular range θ_{lab} = 50—160° in photon-induced reactions with E_γ^{max} = 500 MeV with light and medium nuclei. The charged π-meson detector was a 34-cm Freon bubble chamber with a tube for the beam. The π^-/π^+ yield ratio for He^4, Li^7, C^{12}, Si^{28}, S^{32}, Ca^{40}, and Nb^{93} was found to be respectively 0.94 ± 0.14, 2.15 ± 0.31, 1.22 ± 0.21, 1.25 ± 0.15, 1.0 ± 0.13, 1.11 ± 0.13, and 1.53 ± 0.25. It was established that the π^+-meson yield follows a $ZA^{-1/3}$ law.

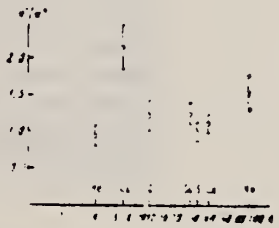

FIG. 3. π^-/π^+ yield ratio as a function of mass number A.

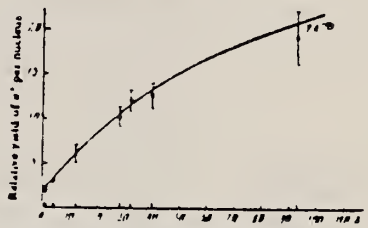

FIG. 2. Relative yield of π^+ mesons per nucleus as a function of mass number A.

REF.

P.E. Argan, G. Audit, N. De Botton, J.M. Laget, J. Martin, C. Schuhl, and G. Tamas
Phys. Rev. Letters 29, 1191 (1972)

ELEM. SYM.	A	Z
He	4	2

METHOD

REF. NO.	
72 Ar 5	hmg

REACTION	RESULT	EXCITATION ENERGY	SOURCE		DETECTOR		ANGLE
			TYPE	RANGE	TYPE	RANGE	
G,P PI-	ABX	THR-575	C	346-575	TEL-D		DST

TABLE I. The experimental conditions and the measured cross sections.

P_R MeV/c	θ_R	Q (MeV)	$Q_{NN\pi}-2m$ (MeV) a	E_{γ_0} (MeV) b	$\frac{d\sigma(Q,\omega,P_R,\theta_R)}{d\Omega_\omega d\Omega_R P_R^2 dP_R}$ (μb fm^2 sr^{-2}) c
50	90	1136	212	246	15.5 ± 2.3
		1147	223	259	19.3 ± 2.7
		1156	233	271	18.6 ± 2.6
		1171	250	290	17.6 ± 2.9
		1176	256	297	25.4 ± 2.9
		1186	267	309	20.6 ± 2.8
		1206	289	335	20.6 ± 1.9
		1236	324	376	16.1 ± 1.2
		1256	346	403	12.3 ± 1.7
		1285	380	449	12.5 ± 0.7
		1306	404	473	6.7 ± 0.9
125	90	1206	302	346	7.4 ± 1.5
200	90	1146	260	288	1.4 ± 0.7
		1156	270	300	3.8 ± 1.9
		1161	276	306	3.2 ± 0.7
		1169	285	317	3.1 ± 0.6
		1176	292	326	3.5 ± 0.5
		1191	309	346	2.1 ± 0.5
		1206	325	365	2.1 ± 0.4
		1226	342	392	1.9 ± 0.4
		1246	370	419	1.8 ± 0.3
		1266	393	447	0.7 ± 0.3
		1286	416	475	0.6 ± 0.3
275	90	1206	360	394	0.4 ± 0.5
300	90	1186	299	334	1 ± 0.5
		1206	318	336	0.2 ± 0.2
		1246	357	383	0.2 ± 0.4

[a] $Q_{NN\pi}$ is the invariant mass of the three-particle system: the pion, the proton, and an unobserved nucleon with a momentum equal to $\vec{P}_R$ (m is the nucleon mass).
[b] E_{γ_0} is the energy of the photon inducing the reaction when $E_R = 0$. The end-point energy of the bremsstrahlung spectrum was chosen about 100 MeV above E_{γ_0}.
[c] Experimental cross sections.

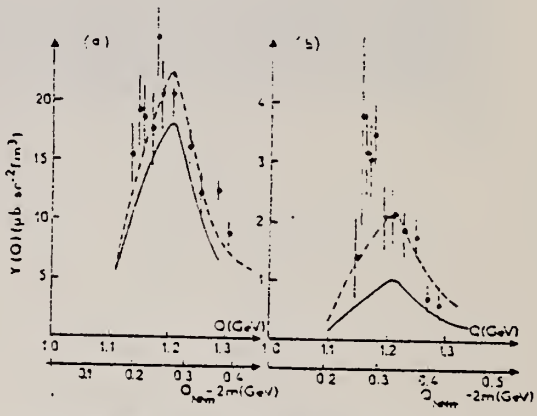

FIG. 3. The differential cross-section values $Y(Q) = d\sigma/d\Omega_R d\Omega_\omega P_R^2 dP_R$ of the reaction ^{4}He($\gamma, p\pi^-$) for $\theta_R = 90°$ and $\omega = 90°$. (This means that the recoil $\vec{P}_R$ vector occurs on the same side of the photon beam as the emitted pion.) The solid lines correspond to the calculation outlined in Sect. 3.1 of Ref. 1 (a realistic single-particle wave function and optical-parameter set III were used). The dashed curves are obtained by multiplying by the normalization factors 1.25 for $P_R = 50$ MeV/c in (a), and 2.1 for $P_R = 200$ MeV/c in (b).

REF. Yu. M. Arkatov, P.I. Vatset, V.I. Voloshchuk, I.M. Prokhorets, A.F. Khodyachikh, and V.I. Chmil
Yad. Fiz. 16, 12 (1972)
Sov. J. Nucl. Phys. 16, 6 (1973)

ELEM. SYM.	A	Z
He	4	2

METHOD

REF. NO. 72 Ar 6 hmg

REACTION	RESULT	EXCITATION ENERGY	SOURCE		DETECTOR		ANGLE
			TYPE	RANGE	TYPE	RANGE	
G,D	ABX	28- 75	C	150	CCH-D		DST

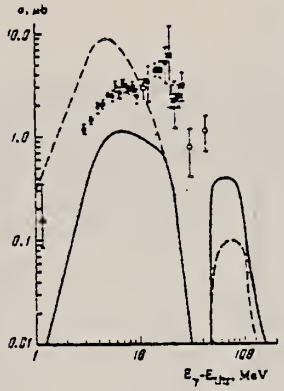

FIG. 1. Total cross section for the $He^4(\gamma, d)H^2$ reaction. Experimental points: ▲–Zurmühle et al., [5] ●–Meyerhof et al., [6] ■–Skopik et al., [3] O–present experiment. Theoretical curves [6]: Solid curve–calculated with a Gaussian wave function; dashed curve–with an Irving function.

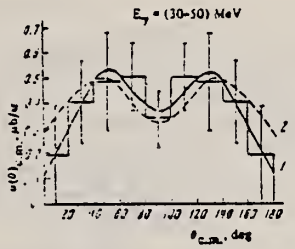

FIG. 3. Angular distributions (c.m.s.) of deuterons from the He^4 $(\gamma, d)H^2$ reaction. Curve 1–fitted by Eq. (2); curve 2–by Eq. (3).

$$\frac{d\sigma}{d\Omega} = a\sin^2\theta + b\sin^2\theta\cos\theta + c\sin^2\theta\cos^2\theta + d, \qquad (2)$$

$$\frac{d\sigma}{d\Omega} = c\sin^2\theta\cos^2\theta + d, \qquad (3)$$

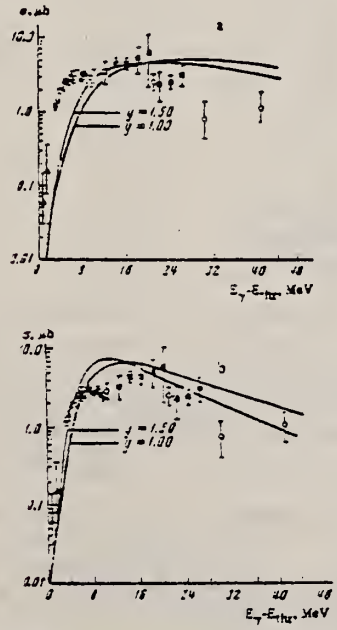

FIG. 2. Total cross section for the $He^4(\gamma, d)H^2$ reaction. The experimental points are the same as in Fig. 1. Theoretical curves [6]: a–for a Gaussian wave function. b–for an Irving function.

Table I

ΔE_γ, MeV	σ, μb
30—40	2.94 ± 0.65
40—50	2.17 ± 0.64
50—60	0.79 ± 0.39
60—73	1.14 ± 0.43

Remark: E_{thr} = 23.8 MeV.

REF.

B. L. Berman, F. W. K. Firk and C. P. Wu
Nucl. Phys. A179, 791 (1972)

EL.EM. SYM.	A	Z
He	4	2

METHOD

REF. NO.	
72 Be 2	egf

REACTION	RESULT	EXCITATION ENERGY	SOURCE		DETECTOR		ANGLE
			TYPE	RANGE	TYPE	RANGE	
G,N	ABX	22-32	C	35	TOF-D		90

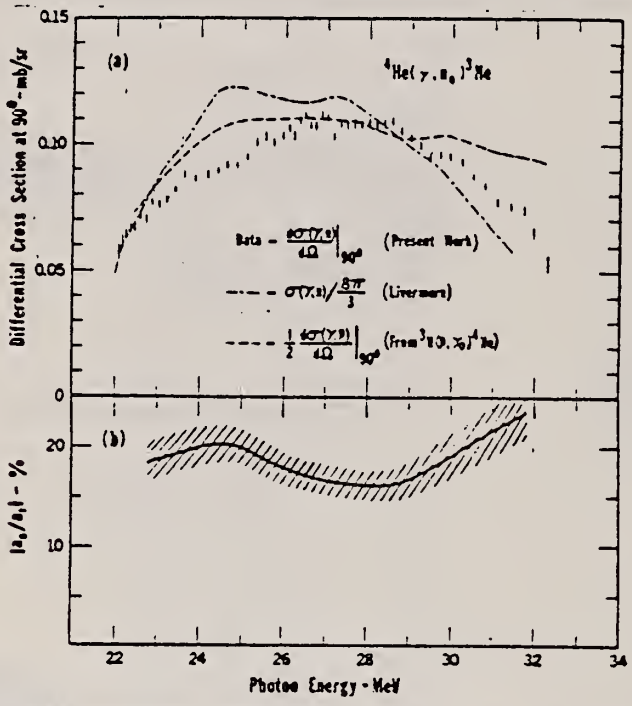

Fig. 2 (a) The 90° (lab) differential photoneutron cross section for ^4He (data points). The dot-dash curve is the total $^4He(\gamma,n)$ cross section of ref. [8] divided by $\frac{8}{3}\pi$; the dashed curve is half the $^4He(\gamma,p_0)$ 90° differential cross section obtained from the $^3H(p,\gamma_0)$ measurements of refs. [9-11]. (b) The isospin mixing ratio $|a_0/a_1|$ obtained from the differential cross-section data of (a).

[8] B.L. Berman, S.C. Fultz & M.A. Kelly, Phys. Lett. 25 (1970) 938; Univ. of California Lawrence Radiation Laboratory Report UCRL-73186, 1971; Phys. Rev. C4 (1971) 723.

[9] J.E. Perry & S.J. Bame, Phys. Rev. 99 (1955) 1368.

[10] D.S. Gemmell & G.A. Jones, Nucl. Phys. 33 (1962) 102.

[11] W.E. Meyerhof, M. Suffert & W. Feldman, Nucl. Phys A148 (1970) 211.

REF.

W. R. Dodge and J. J. Murphy, II
Phys. Rev. Letters 28, 839 (1972)

ELEM. SYM.	A	Z
He	4	2

METHOD

REF. NO.	
72 Do 1	hmg

REACTION	RESULT	EXCITATION ENERGY	SOURCE		DETECTOR		ANGLE
			TYPE	RANGE	TYPE	RANGE	
E,T*	ABX	30-52	D	90	MAG-D		90
E,HE	ABX	30-52	D	90	MAG-D		90

HE=HE3, RATIO G,P/G,N
* RATIO G,P/G,N

TABLE I. Summary of the results of this experiment and the data for calculating $\sigma(\gamma,p)/\sigma(\gamma,n)$. The angular-distribution coefficients $A(k_\gamma)$, $B(k_\gamma)$, and $C(k_\gamma)$ are from Meyerhof, Suffert, and Feldman,[a] Perry and Bame,[b] Berman, Fultz, and Kelly,[c] and Gorbunov.[d] In those columns in which there are two entries, the upper entry refers to the $^4He(\gamma,p)$ reaction and the lower to the $^4He(\gamma,n)$ reaction. The uncertainties of σ include only the errors in the angular-distribution coefficients and uncertainties due to counting statistics. T' and T are the particle kinetic energies before and after correction for energy loss in the ^4He gas and the target cell wall.

k (MeV)	$A(k_\gamma)/B(k_\gamma)$[e]	$C(k_\gamma)/B(k_\gamma)$[e]	R_e/R_γ	T (MeV)	T' (MeV)	Relative Counting Efficiency	θ Degrees	$(d\sigma_\nu/d\Omega)_{c.m.}$ $\mu b/sr$	σ_ν mb	$\frac{\sigma(\gamma,p)}{\sigma(\gamma,n)}$
29.8[f]	.016±.005 .12 ±.08	-.53±.11 .22±.15	1.017	2.392 2.202	2.213 1.355	1.00 .83	100.1 101.6	202.± 4. 159.±25.	1.61±.06 1.54±.34	1.07±.24
31.7[f]	.016±.005 .038±.028	-.60±.05 .30±.13	1.005	2.856 2.665	2.631 1.594	1.00 .90	100.6 101.0	173.± 4. 127.±17.	1.40±.04 1.19±.17	1.18±.16
31.7[g]	.016±.005 .038±.028	-.60±.05 .30±.13	1.005	2.856 2.665	2.631 1.594	1.00 .90	100.6 101.0	192.± 9. 159.±16.	1.54±.14 1.48±.15	1.04±.12
33.9[g]	.0 .04 ±.03	-.66±.07 .34±.10	1.020	3.294 3.104	3.092 2.181	1.00 .96	100.4 100.7	168.± 8. 131.±13.	1.30±.10 1.24±.17	1.05±.17
31.7[h]	.016±.005 .038±.028	-.60±.05 .30±.13	1.005	2.856 2.665	2.558 1.165	1.00 .80	100.6 101.0	192.±11. 164.±45.	1.51±.12 1.53±.51	.98±.33
33.5[h]	.0 .04 ±.03	-.67±.07 .35±.10	1.037	3.292 3.201	3.131 1.975	1.00 .93	100.4 100.7	150.± 6. 117.± 6.	1.16±.10 1.10±.14	1.05±.16
35.2[h]	.0 .04 ±.03	-.70±.07 .46±.13	1.039	3.708 3.517	3.464 2.400	1.00 1.00	100.3 100.6	137.± 5. 104.± 5.	1.05±.04 1.00±.08	1.05±.09
37.1[h]	.0 .04 ±.03	-.75±.09 .47±.07	1.022	4.170 3.980	3.947 2.985	1.00 1.00	100.3 100.5	105.± 3. 81.± 3.	.80±.03 .78±.05	1.03±.08
44.3[h]	.0 .04 ±.03	-.84±.07 .34±.04	1.020	5.916 5.726	5.746 5.000	1.00 1.00	100.3 100.4	74.± 1. 54.± 2.	.36±.02 .55±.03	1.01±.07
51.3[i]	.0 .0	-.96±.10 .06±.03	1.022	7.680 7.539	7.541 6.961	1.00 1.00	100.3 100.3	51.± 1. 43.± 1.3	.36±.02 .36±.01	1.00±.08

[a] See Ref. 7.
[b] See Ref. 14.
[c] See Ref. 6.
[d] See Ref. 4.
[e] Angular-distribution coefficients for the $^4He(\gamma,^1H)$ and $^4He(\gamma,^1He)$ reactions.
[f] 0.000 26-g·cm^{-2} Mylar window 0.31 cm long and 1.27 cm wide.
[g] 0.000 26-g cm^{-2} Mylar window 1.587 cm in diameter with a 0.953-cm collimator.
[h] 0.0006-g/cm^2 Mylar window 1.587 cm in diameter with a 0.953-cm collimator.

[4] A. N. Gorbunov, Phys. Lett. 27B, 436 (1968).
[5] L. G. Main, Nuovo Cimento 26, 584 (1962).
[6] B. L. Berman, S. C. Fultz, and M. A. Kelly, Phys. Rev. C 4, 723 (1971), and Phys. Rev. Lett. 25, 938 (1970).
[7] W. E. Meyerhof, M. Suffert, and W. Feldman, Nucl. Phys. A148, 211 (1970).
[14] J.E. Perry & S.J. Bame, Jr., Phys. Rev. 99, 1368 (1955).

(continued)

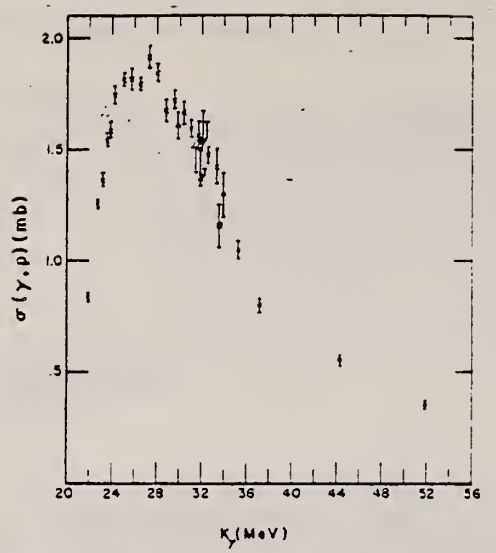

FIG. 2. The $^4He(\gamma,p)^3H$ total cross section as a function of k. Crosses, results of Meyerhof, Suffert, and Feldman (Ref. 7); circles, our results using a 0.0006-g/cm^2 Mylar window 1.587 cm in diameter; squares, our results using a 0.000 36-g/cm^2 Mylar window 1.587 cm in diameter; triangles, our results using a 0.000 36-g/cm^2 Mylar window 3.81 cm long and 1.27 cm wide.

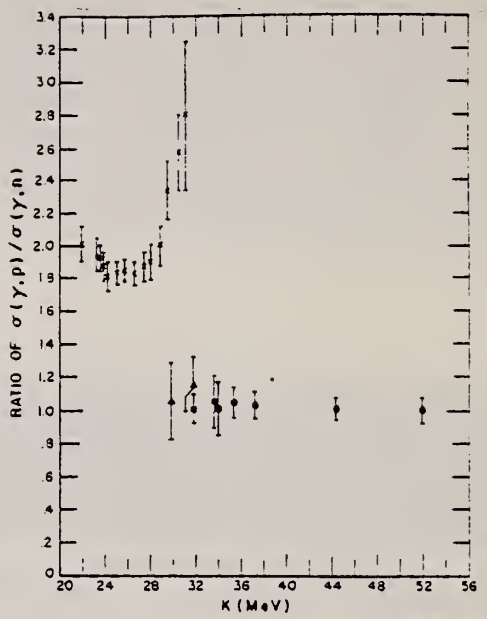

FIG. 3. The ratio $\sigma(\gamma,p)/\sigma(\gamma,n)$. The crosses are the results calculated by Berman, Fultz, and Kelly (Ref. 6) using the $\sigma(\gamma,p)$ values of Meyerhof, Suffert, and Feldman (Ref. 7). The other symbols are defined in Fig. 2.

REF. Stanley S. Hanna
PICNS-72, p.453 Sendai

ELEM. SYM.	A	Z
He	4	2

METHOD

REF. NO. 72 Ha 9 hvm

REACTION	RESULT	EXCITATION ENERGY	SOURCE TYPE	SOURCE RANGE	DETECTOR TYPE	DETECTOR RANGE	ANGLE
$ P,G	NOX	24- 70	D	6- 14	NAI-D		DST

POLARIZED PROTONS

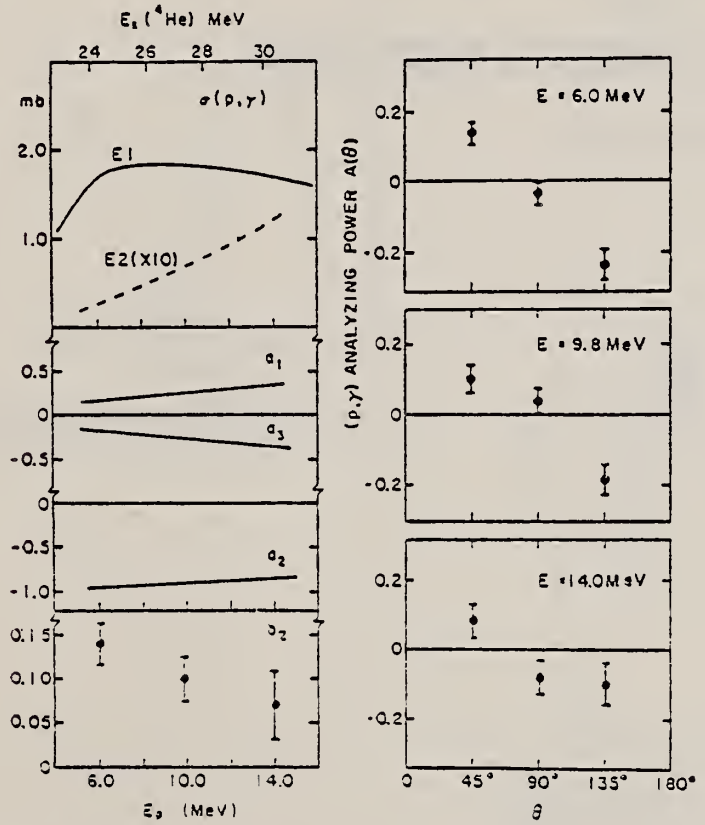

Fig. 8.
Right: measured analyzing powers for $^3H(p,\gamma_0)^4He$.
Left : summary of the existing information on $^3H(p,\gamma_0)^4He$. The E2(X10) curve shows the E2 component of the yield as determined from the coefficients a_1 and a_3.

(continued)

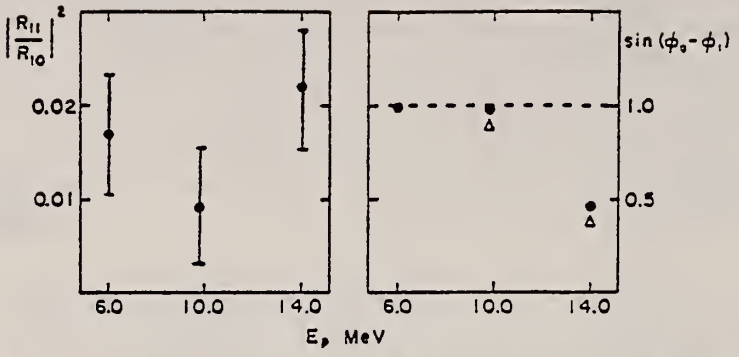

Fig. 9. Solutions obtained for the proton channel in $^3H(p,\gamma_0)^4He$. The triplet to singlet ratio is designated R_{11}/R_{10}.

REF.

D. M. Skopik and W. R. Dodge
Phys. Rev. C6, 43 (1972)

ELEM. SYM.	A	Z
He	4	2

METHOD

REF. NO.	
72 Sk 3	hmg

REACTION	RESULT	EXCITATION ENERGY	SOURCE		DETECTOR		ANGLE
			TYPE	RANGE	TYPE	RANGE	
E,D	ABX	35-50	D	35-50	MAG-D		DST
		(35.7-49.4)		(35.7-49.4)			

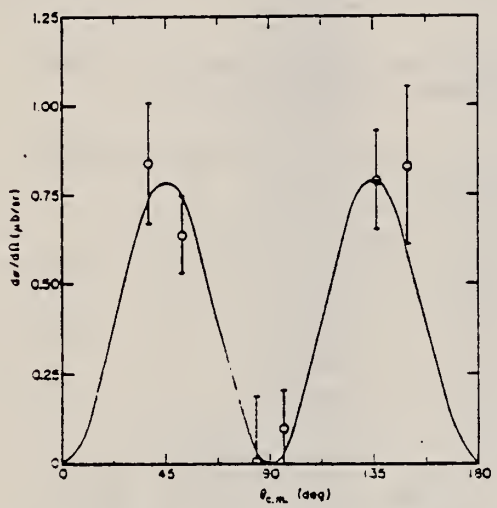

FIG. 4. The $^4He(e,d)e'^2H$ angular distribution in the 40 ± 1-MeV energy interval. The solid curve is $0.92 \sin^2 2\theta$ μb/sr.

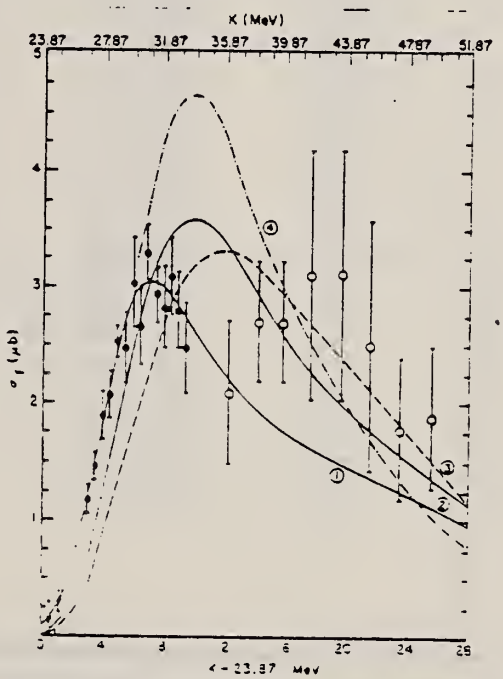

FIG. 6. The $^4He(\gamma,d)^2H$ total cross section with the same notation as Fig. 5. Curve 1 is from Erdas *et al.* (Ref. 4) with resonance parameters E_{ex} = 33 MeV and a reduced width of 5 MeV. Curve 2 is from Erdas *et al.* (Ref. 4) with E_{ex} = 30 MeV and a reduced width of 3.2 MeV. Curves 3 and 4 are from Gibson (Ref. 26) with V_1 = 210 and 230 MeV.

(continued)

TABLE II. All $^4He+\gamma \rightleftarrows {}^2H+{}^2H$ data published up to August 1971 plus the unpublished data of Degré. Uncertainties are those quoted by the original authors. All data are referred to the absorption experiment $^4He+\gamma \rightarrow {}^2H+{}^2H$ in the center-of-mass system. The production experiment $d\sigma/d\Omega$ and σ_T has been converted to the absorption experiment by

$$\frac{d\sigma}{d\Omega}(\gamma,d)=\frac{9}{2}\left(\frac{P_d}{K_\gamma}\right)^2\frac{d\sigma}{d\Omega}(d,\gamma) \quad \text{and} \quad \sigma(\gamma,d)=\frac{9}{4}\left(\frac{P_d}{K_\gamma}\right)^2\sigma(d,\gamma)\,.$$

$E_\gamma - Q$ (MeV)	$\theta_{c.m.}$ (deg)	$d\sigma/d\Omega$ (μb/sr)	σ_T (μb)	Experiment
190.7	41.5	0.119 ±0.044	0.202 ±0.076	Production [a]
215.7	65	≤0.0078 ±0.002	≤0.044 ±0.012	Production [b]
184.6	52.4	0.0063 ±0.0022	0.022 ±0.008	Absorption [c]
224.4	53.2	0.0015 ±0.0011	0.0054 ±0.0038	Absorption [c]
0.32	45.6	...	0.023	Production [d]
0.60	45.8	0.018 $^{+0.036}_{-0.030}$	0.061 $^{-0.122}_{-0.030}$	Production [d]
1.04	46	...	0.17	Production [d]
1.91	131.3	0.175 ±0.079	0.59 ±0.27	Production [e]
2.90	131.6	0.378 ±0.095	1.32 ±0.33	Production [e]
3.89	131.9	0.644 ±0.071	2.26 ±0.25	Production [e]
4.88	132.2	0.842 ±0.035	2.83 ±0.12	Production [e]
2.88	136.6	0.351 ±0.036	1.18 ±0.12	Production [f]
3.39	136.8	0.432 ±0.036	1.45 ±0.12	Production [f]
3.89	136.9	0.566 ±0.063	1.90 ±0.21	Production [f]
4.40	137	0.608 ±0.064	2.06 ±0.22	Production [f]
4.91	137.1	0.628 ±0.030	2.54 ±0.12	Production [f]
5.41	137.3	0.729 ±0.085	2.48 ±0.29	Production [f]
5.91	137.4	0.894 ±0.112	3.04 ±0.38	Production [f]
6.42	137.5	0.782 ±0.094	2.66 ±0.32	Production [f]
6.92	137.6	0.966 ±0.070	3.29 ±0.24	Production [f]
7.42	137.7	0.863 ±0.068	2.94 ±0.23	Production [f]
7.92	137.8	0.827 ±0.076	2.82 ±0.26	Production [f]
8.43	137.8	0.903 ±0.100	3.08 ±0.34	Production [f]
8.92	137.9	0.820 ±0.094	2.80 ±0.32	Production [f]
9.43	138	0.726 ±0.114	2.48 ±0.39	Production [f]
15.9	38	0.84 ±0.18	3.0 ±0.6	$^4He+e \rightarrow {}^2H+{}^2H+e'\gamma$
15.9	53	0.65 ±0.15	2.4 ±0.5	$^4He+e \rightarrow {}^2H+{}^2H+e'\gamma$
15.9	83	0.01 ±0.10	...	$^4He+e \rightarrow {}^2H+{}^2H+e'\gamma$
15.9	97	0.10 ±0.10	...	$^4He+e \rightarrow {}^2H+{}^2H+e'\gamma$
15.9	137	0.80 ±0.14	2.7 ±0.5	$^4He+e \rightarrow {}^2H+{}^2H+e'\gamma$
15.9	152	0.83 ±0.22	4.2 ±1.1	$^4He+e \rightarrow {}^2H+{}^2H+e'\gamma$
11.8	37	0.58 ±0.16	2.1 ±0.6	$^4He+e \rightarrow {}^2H+{}^2H+e'\gamma$
13.7	38	0.63 ±0.11	2.7 ±0.5	$^4He+e \rightarrow {}^2H+{}^2H+e'\gamma$
17.6	152	0.60 ±0.20	3.1 ±1.1	$^4He+e \rightarrow {}^2H+{}^2H+e'\gamma$
19.6	152	0.60 ±0.20	3.1 ±1.1	$^4He+e \rightarrow {}^2H+{}^2H+e'\gamma$
21.5	153	0.46 ±0.20	2.5 ±1.1	$^4He+e \rightarrow {}^2H+{}^2H+e'\gamma$
23.5	154	0.32 ±0.10	1.8 ±0.6	$^4He+e \rightarrow {}^2H+{}^2H+e'\gamma$
25.5	154	0.33 ±0.10	1.9 ±0.6	$^4He+e \rightarrow {}^2H+{}^2H+e'\gamma$
0.80	...	...	0.112 ±0.026	Production [i]
1.30	...	...	0.303 ±0.044	Production [i]
1.80	...	...	0.577 ±0.084	Production [i]
2.30	...	...	0.766 ±0.111	Production [i]
2.80	...	...	1.005 ±0.093	Production [i]

[a] Yu. K. Akimov, O. V. Savchenko, and M. L. Soroko, Zh. Eksperim. i Teor. Fiz. 41, 709 (1961) [transl.: Soviet Phys.-JETP 14, 512 (1962)].
[b] J. A. Poirier and M. Priostem, Phys. Rev 130, 1171 (1963).
[c] See Ref. 23.
[d] See Ref. 22.
[e] W. Del Bianco and J. M. Poumissou, Phys. Letters 29B, 299 (1969).
[f] See Ref. 3.
[g] This experiment. Uncertainties are due to counting statistics only.
[h] A. Degré, M. Schaeffer, and M. Suffert, private communication to W. E. Meyerhof (Ref. 3).

3. W. E. Meyerhof, et al., Nucl. Phys. A131, 489 (1969).
22. R. W. Zurmuhle, et al., Phys. Rev. 132, 751 (1963).
23. J. Asbury, et al., Phys. Rev. 137, B124 (1965).

REF. Stanley S. Hanna
PICNS-73, Vol. I, p.417 (1973) Asilomar

ELEM. SYM.	A	Z
He	4	2

METHOD

REF. NO. 73 Ha 15 egf

REACTION	RESULT	EXCITATION ENERGY	SOURCE		DETECTOR		ANGLE
			TYPE	RANGE	TYPE	RANGE	
P,G	ABX	26 (26.0)	D	8 (8.34)	NAI-D		90

Table IV. Summary of cross section measurements for (γ,p_o) and (γ,n_o) reactions on ^4He, ^{12}C, and ^{16}O. Underlined values are essentially the consensus of several values.

	E_x (MeV)	$\sigma(\gamma,p_o)$ in mb		$\sigma(\gamma,n_o)$ in mb	
		New[a]	Old	New	Old
^4He	26.0	1.95 ± 0.13	<u>1.84</u>[b]	<u>2.0</u>[c]	1.0[d]
^{12}C	22.5	12.2 ± 1.2	13.4[e], 8.0[f]	<u>6.0</u>[g]	6.0[h]
^{16}O	22.2	9.6 ± 1.5	8.8[i], 12.2[j]	~ 7.2[k]	9.1[h], 7.2[l]

a) Ref. 25
b) Refs. 30-32
c) Refs. 22-24
d) Ref. 33
e) Ref. 34
f) Ref. 35
g) Ref. 36,37
h) Ref. 38
i) Ref. 39
j) Ref. 40
k) Ref. 41
l) Ref. 42

(continued)

[22] W. R. Dodge and J. J. Murphy, II, Phys. Rev. Letters 28, 839 (1972).

[23] J. D. Irish, R. G. Johnson, B. J. Thomas, B. L. Berman, K. G. McNeill, and J. W. Jury, contribution to this conference.

[24] D. V. Webb, C. K. Malcolm, Y. M. Smith, and D. M. Skopik, contribution to this conference.

[25] J. R. Calarco, G. A. Fisher, E. M. Diener, C. C. Chang, and S. S. Hanna, to be published.

[26] J. E. Brolley, Jr., T. M. Putman, and Louis Rosen, Phys. Rev. 107, 820 (1957).

[27] J. L. Detch, Jr., R. L. Hutson, N. Jarmie, and J. H. Jett, Phys. Rev. C4, 52 (1971).

[28] M. Suffert, W. Feldman, J. Mahieux, and S. S. Hanna, Nucl. Instr. and Meth. 63, 1 (1968).

[29] B. L. Berman, private communication.

[30] M. Suffert, private communication.

[31] J. E. Perry, Jr. and S. J. Bame, Jr., Phys. Rev. 99, 1368 (1955).

[32] W. E. Meyerhof, M. Suffert, and W. Feldman, Nucl. Phys. A148, 211 (1970); the cross sections in this paper are based on Ref. 31.

[33] B. L. Berman, S. C. Fultz, and M. A. Kelly, Phys. Rev. C4, 723 (1971); B. L. Berman, F. W. K. Firk, and C. P. Wu, Nucl. Phys. A179, 791 (1972).

[34] R. G. Allas, S. S. Hanna, L. Meyer-Schützmeister, and R. E. Segel, Nucl. Phys. 58, 122 (1964).

[35] C. Brassard, H. D. Shay, J. P. Coffin, W. Scholz, and D. A. Bromley, Phys. Rev. C6, 53 (1972).

[36] J. W. Jury, J. S. Hewitt, and K. G. McNeill, contribution to this conference.

[37] B. L. Berman et al., contribution to this conference.

[38] C. P. Wu, F. W. K. Firk, and T. W. Phillips, Phys. Rev. Letters 20, 1182 (1968).

[39] E. D. Earle and N. W. Tanner, Nucl. Phys. A95, 241 (1967).

[40] J. E. E. Baglin and M. N. Thompson, Nucl. Phys. A138, 73 (1969).

[41] D. B. C. B. Syme and G. I. Crawford, contribution to this conference.

[42] J. T. Caldwell, R. L. Bramblett, B. L. Berman, R. R. Harvey, and S. C. Fultz, Phys. Rev. Letters 15, 976 (1965).

REF. J.D. Irish, R.G. Johnson, B.J. Thomas, B.L. Berman, K.G. McNeill and J.W. Jury
PICNS-73, Vol.I, p.147 Asilomar

ELEM. SYM.	A	Z
He	4	2

METHOD

REF. NO.	
73 Ir 2	hmg

REACTION	RESULT	EXCITATION ENERGY	SOURCE		DETECTOR		ANGLE
			TYPE	RANGE	TYPE	RANGE	
G,N	ABX	21- 31	D	21- 31	TOF-D		DST

$$d\sigma/d\Omega = a_o(1 + \sum^{4} a_i P_i(\cos\theta))$$

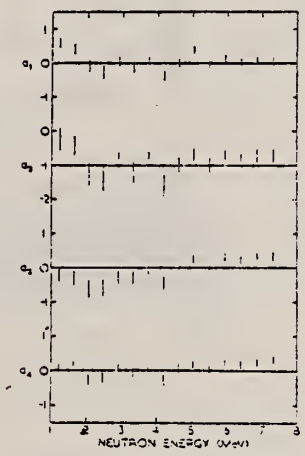

Fig. 1. Angular Distribution Coefficients for ^4He (γ,n) ^3He

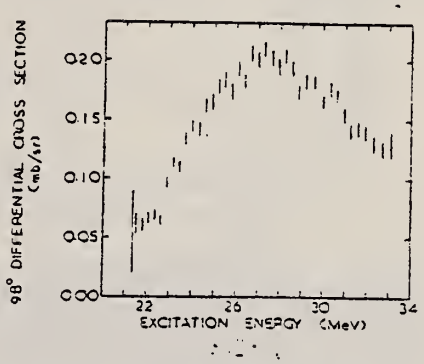

Fig. 2. 90° Differential Cross-section for ^4He (γ,n) ^3He

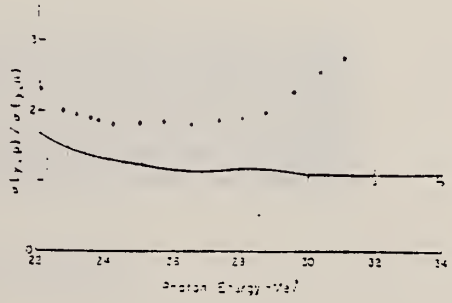

Fig. 3. $\sigma(\gamma,p)/\sigma(\gamma,n)$ for ^4He

REF.

J.D. Irish, R.G. Johnson, B.L. Berman, B.J. Thomas, K.G. McNeill, and J.W. Jury
Phys. Rev. C8, 1211 (1973)

EL.EM. SYM.	A	Z
He	4	2

METHOD

REF. NO.	
73 Ir 4	hmg

REACTION	RESULT	EXCITATION ENERGY	SOURCE		DETECTOR		ANGLE
			TYPE	RANGE	TYPE	RANGE	
G,N	ABX	21- 37	C	35, 39	TOF-D		98

Two measurements: (1) liquid target
(2) gas target

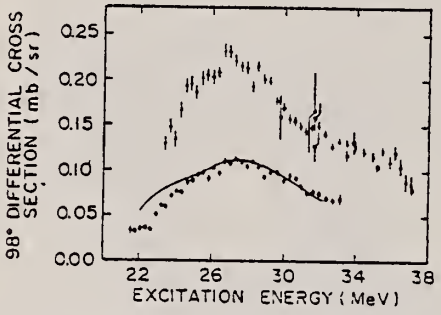

FIG. 3. $^4He(\gamma, n)^3He$ differential cross section as a function of excitation energy. Present results: Circles (lower curve) denote liquid target; triangles denote gas target. The squares are the results of Dodge and Murphy obtained at a center-of-mass angle of 101° (see Ref. 3). The solid line was obtained by drawing a line by eye through the Yale results obtained at 90° using a liquid target (see Ref. 2).

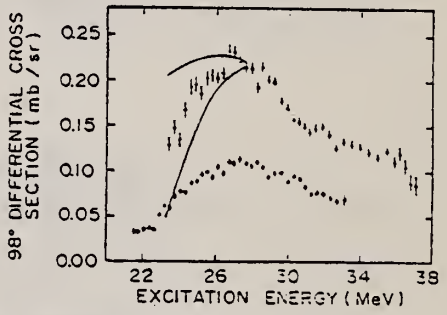

FIG. 2. 98° $^4He(\gamma, n)^3He$ differential cross section. Circles (lower curve) denote results obtained with the liquid target. Triangles (upper curve) denote results obtained with the gas target. The solid lines indicate the limits of the uncertainty in the gas target cross section due to the correction for scattered neutrons.

The 98° differential photoneutron cross section for ^4He has been measured for excitation energies between 22 and 33 MeV with a liquid ^4He target at its normal boiling point and for excitation energies between 23 and 37 MeV with a ^4He gas target at a pressure of 51.6 bars. The cross-section values obtained with the gas target were approximately a factor of 1.9 greater than those obtained with the liquid target. This apparent dependence of the cross section upon the physical state of the ^4He target may explain the large values for the ratio $\sigma(\gamma, p)/\sigma(\gamma, n)$ obtained by comparing photoneutron and photoproton cross sections obtained with targets in different physical states.

REF. S. E. Kiergan, A. O. Hanson, and L. J. Koester, Jr.
Phys. Rev. C8, 431 (1973)

ELEM. SYM.	A	Z
He	4	2

METHOD

REF. NO. 73 Ki 2 hmg

REACTION	RESULT	EXCITATION ENERGY	SOURCE		DETECTOR		ANGLE
			TYPE	RANGE	TYPE	RANGE	
G,P	ABX	180-320	C	320	SPK-D		DST

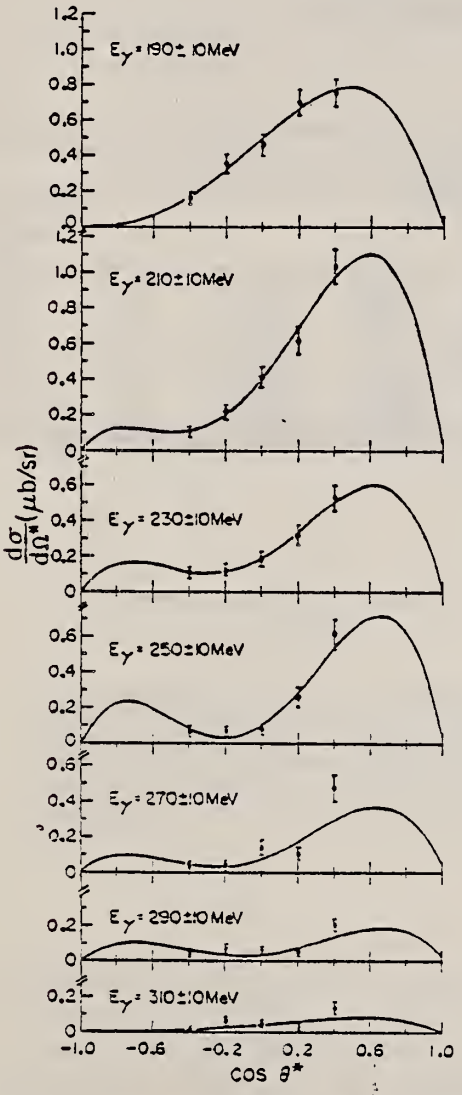

FIG. 5. Experimental differential cross sections and fitted angular distributions for various energies. The curves are least-squares fits of $d\sigma/d\Omega^* = A \sin^2\theta^* [1 + \beta \cos\theta^* + \gamma \cos^2\theta^*]$ to the data. The cross sections and angles are in the c.m. system.

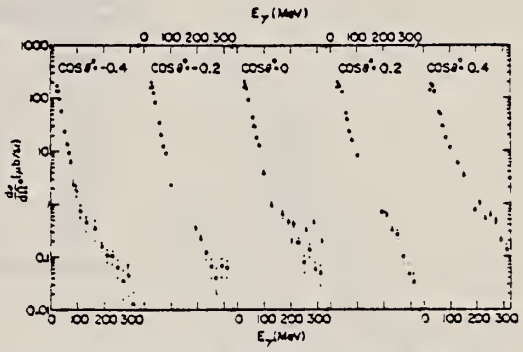

FIG. 4. Experimental differential cross sections. The closed circles are data of Gorbunov, closed triangles are from Stenberg, closed squares are from this experiment, and open diamonds are from Picozza *et al.* The cross sections and angles are in the c.m. system.

(continued)

TABLE I. Differential cross sections in the center-of-mass system for $^4He(\gamma,p)^3H$ in units of $10^{-32}cm^2/sr$. The errors shown are based on counting statistics only.

Energy (MeV)	$\cos\theta^*$ −0.4	−0.2	0.	0.2	0.4
190	16.1 ± 3.4	35.4 ± 5.1	45.7 ± 5.8	70.2 ± 7.2	75.6 ± 7.7
210	10.8 ± 3.0	21.9 ± 4.3	41.7 ± 6.0	62.0 ± 7.3	103.6 ± 9.5
230	10.5 ± 3.2	12.8 ± 3.5	18.6 ± 4.3	31.8 ± 5.8	52.4 ± 7.3
250	6.5 ± 2.8	6.6 ± 2.7	7.8 ± 2.9	26.0 ± 5.4	61.4 ± 8.4
270	3.6 ± 2.1	4.1 ± 2.1	13.5 ± 3.9	10.2 ± 3.2	47.2 ± 7.7
290	4.6 ± 2.7	6.8 ± 2.8	5.9 ± 2.1	4.7 ± 1.7	20.0 ± 3.5
310	1.3 ± 0.9	6.3 ± 2.2	4.8 ± 2.0	3.3 ± 1.6	13.5 ± 3.4

TABLE II. Total cross section, χ^2, and parameters calculated for fits to the angular distribution $d\sigma/d\Omega^* = A \sin^2\theta^*[1 + \beta\cos\theta^* + \gamma\cos^2\theta^*]$. The errors are calculated from the statistical errors of the experimental data.

Energy (MeV)	A (cm^2/sr)	β	γ	χ^2	Calculated total cross section (μb)
190	$(5.0 \pm 0.9) \times 10^{-31}$	1.8 ± 0.45	0.8 ± 1.9	1.28	4.8 ± 1.7
210	$(4.0 \pm 0.9) \times 10^{-31}$	3.1 ± 0.9	3.7 ± 2.7	1.67	5.9 ± 1.9
230	$(1.9 \pm 0.8) \times 10^{-31}$	3.0 ± 1.2	5.8 ± 4.0	0.378	3.4 ± 1.2
250	$(1.0 \pm 0.4) \times 10^{-31}$	6.7 ± 3.1	16.3 ± 9.0	3.87	3.6 ± 1.1
270	$(7.8 \pm 4.3) \times 10^{-32}$	4.7 ± 3.1	10.0 ± 10.0	12.94	1.9 ± 1.1
290	$(4.0 \pm 2.8) \times 10^{-32}$	2.7 ± 2.3	12.0 ± 13.0	9.52	1.1 ± 0.7
310	$(4.1 \pm 3.7) \times 10^{-32}$	2.1 ± 1.9	2.0 ± 12.0	8.75	0.5 ± 0.8

REF.

C.K. Malcom, D.V. Webb, Y.M. Shin, and D.M. Skopik
Physics Letters 47B, 433 (1973)

EL.EM. SYM.	A	Z
He	4	2

METHOD

REF. NO. 73 Ma 11 egf

REACTION	RESULT	EXCITATION ENERGY	SOURCE		DETECTOR		ANGLE
			TYPE	RANGE	TYPE	RANGE	
G,N	ABX	20-110	C	110	TOF-D		DST

The $^4He(\gamma, n)^3He$ differential cross section has been simultaneously measured at five laboratory angles between 30° and 142°, from threshold to 110 MeV. The asymmetry in the angular distribution from 24 to 70 MeV has been extracted and found to have sign changes at energies which are in accord with previous experiments. The total photoneutron cross section has been observed to be close to the known (γ, p) cross section. From the energy dependence of the asymmetry coefficient a 2^+ state in ^4He at ≈ 35 MeV has been confirmed.

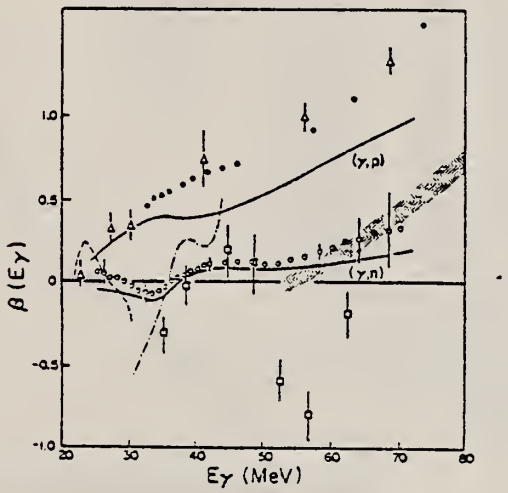

Fig. 2. Comparison of the (γ, n) and (γ, p) angular distribution asymmetry coefficients. The (γ, n) data shown are: o, present experiment; ———, Berman et al. [2]; –·–, Busso et al. [5]; ▫, Arkatov et al., [6]; dashed curve. Wait et al., [7]. The (γ, p) data shown are: •, Wait et al. [7]; Δ, Gorbunov [4]. The solid curves were calculated by introducing a broad 2^+ state near 35 MeV.

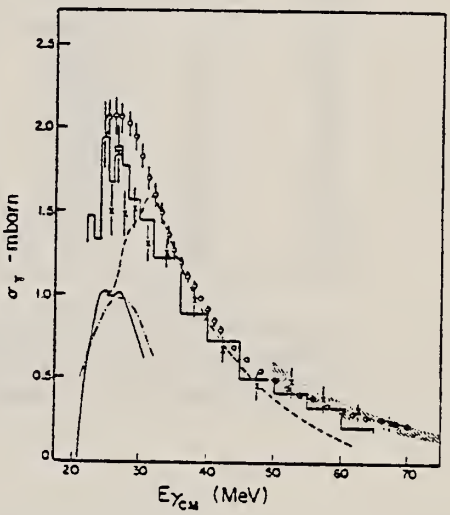

Fig. 1. The $^4He(\gamma, n)^3He$ total cross section. The data are: o, present measurement; x, Gorbunov [4]; –, Berman et al. [2]; –·–, Berman et al. [3]; ——— Busso et al. [5]; dashed curve. Wait et al. [7]. Also shown as the histogram is the $^4He(\gamma, p)^3H$ total cross section of Gorbunov [4].

[2] B.L. Berman, S.C. Fultz, M.A. Kelly; Phys. Rev. Lett. 25 (1970) 938; Phys. Rev. C4 (1971) 723.

[3] B.L. Berman, F.W.K. Firk, C.P. Wu; Nucl. Phys. A179 (1972) 791.

[4] A.N. Gorbunov, ZhETF Pis. Red. 8 (1968) 148; JETP Lett. 8 (1968) 88.

[5] L. Busso et al., Nuovo Cimento Lett. 1 (1971) 941.

[6] Z.M. Arkatov et al., Yad. Fiz. 13 (1971) 256; Sov. J. Nucl. Phys. 13 (1971) 142.

[7] G.D. Wait et al., Phys. Lett. 33B (1970) 163; G.D. Wait, Saskatchewan Accelerator Laboratory report SAL-20 (1972), unpublished.

REF. J. M. Poutissou and W. Del Bianco
Nucl. Phys. A199, 517 (1973)

ELEM. SYM.	A	Z
He	4	2

METHOD

REF. NO. 73 Po 2 egf

REACTION	RESULT	EXCITATION ENERGY	SOURCE		DETECTOR		ANGLE
			TYPE	RANGE	TYPE	RANGE	
D,G	ABX	25- 28	D	6- 12	NAI-D		DST

TABLE 2
Differential cross section of the $^2H(d,\gamma)^4He$ reaction

θ_L (deg.)	$\theta_{c.m.}$ (deg.)	$d\sigma/d\Omega$ (nb/sr)	$\theta_{c.m.}$ (deg.)	$d\sigma/d\Omega$ (nb/sr)	$\theta_{c.m.}$ (deg.)	$d\sigma/d\Omega$ (nb/sr)
0	0	0.0 ±0.32	0	0.0 ±0.52	0	0.0 ±0.65
40	41.5	1.24±0.17	41.8	1.68±0.22	42.1	1.56±0.19
50	51.8	1.08±0.15	52.2	1.71±0.24	52.5	1.64±0.16
60	62	0.80±0.13	62.4	1.04±0.17	62.8	0.73±0.13
70	72.2	0.33±0.12	72.6	0.74±0.22	73.0	0.51±0.13
80	82.3	0.08±0.12	82.8	0.23±0.20	83.2	0.20±0.11
90	92.3	0.04±0.10	92.8	−0.02±0.18	93.2	0.12±0.11
100	102.3	0.13±0.11	102.7	0.36±0.20	103.1	0.35±0.12
110	112.1	0.55±0.13	112.6	0.86±0.21	113.0	0.89±0.12
120	122.0	0.81±0.14	122.4	1.30±0.15	122.7	1.08±0.14
130	131.7	1.12±0.14	132.1	1.66±0.14	132.4	1.61±0.16
	E_d = 6.05 MeV		E_d = 8.96 MeV		E_d = 11.87 MeV	

* The errors quoted in Table 1 are larger than those reported in a previous publication [7] on the γ-ray yield of the $^2H(d,\gamma)^4He$ reaction at θ_L = 130°. The difference is partly due to a revaluation of the errors and partly to difficult experimental conditions at small angles.

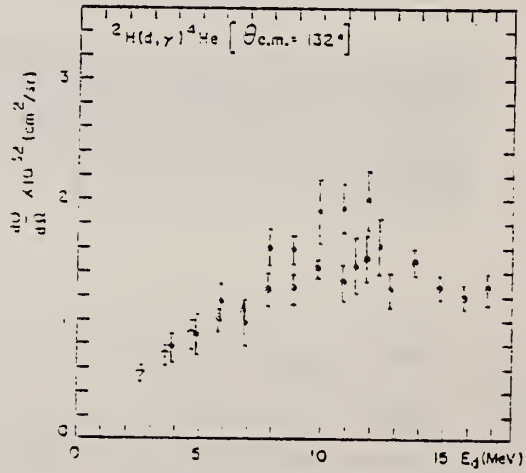

Fig. 3. Differential cross section for the $^2H(d,\gamma)^4He$ reaction at $\theta_{c.m.}$ = 132°. The symbols have the following meaning: ● present results; ○ ref. [7]); ▽ ref. [4]).

[4] A. Degre, Masther's thesis, Universite de Strasbourg, 1969, unpublished.

[7] W. E. Meyerhof et al., Nucl. Phys. A131 (1969) 489.

REF. C. Tzara
PIGNS-73, Vol.I, p.573 Asilomar

ELEM. SYM.	A	Z
He	4	2

METHOD

REF. NO. 73 Tz 2 hmg

REACTION	RESULT	EXCITATION ENERGY	SOURCE TYPE	SOURCE RANGE	DETECTOR TYPE	DETECTOR RANGE	ANGLE
G,TP (1)	ABX	190-415	C		MAG-D		DST
G,HE (2)	ABX	275-430	C		MAG-D		DST
G,PI-P (3)	ABX	150-950	C		MAG-D		DST

(1) TP DETECTED IN COIN
(2) N AND HE3 IN COIN
(3) PI- AND P IN COIN

Fig.1c

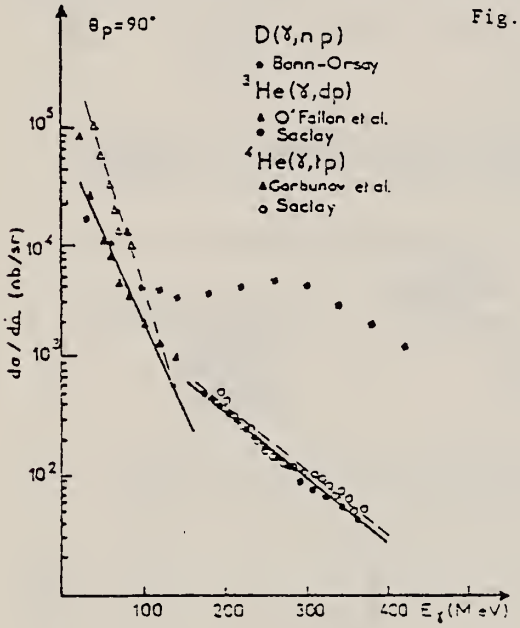

Fig.1b

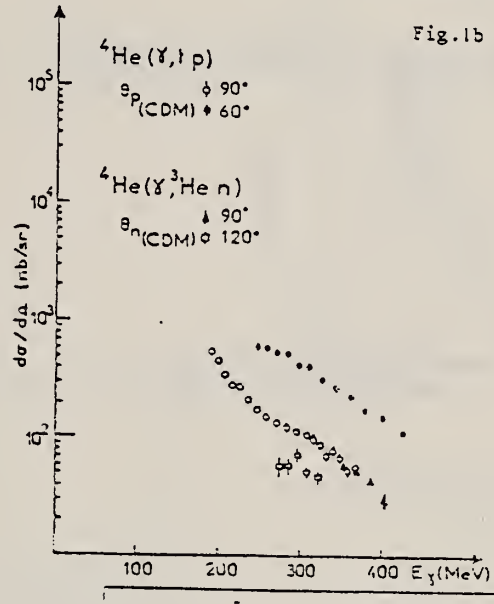

Fig. 1a, b, c.

Two-body photodisintegration cross-sections for d, ^{3}He, ^{4}He, at 60° and 90°. The cross-sections for $\gamma + {}^4He \rightarrow n + {}^3He$ at θ_n = 90° and 120° are also given.

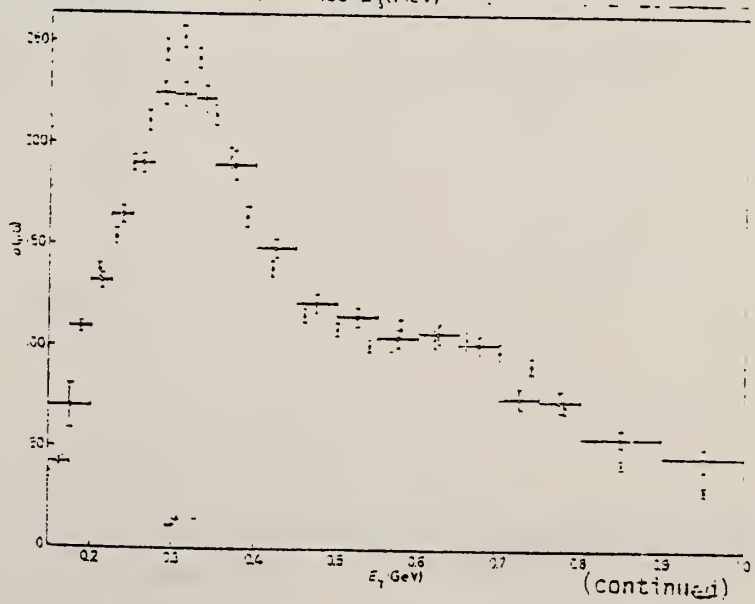

Fig. 3

Total cross-section for the π^- photoproduction on deuteron. Results from Frascati and Bonn.

(continued)

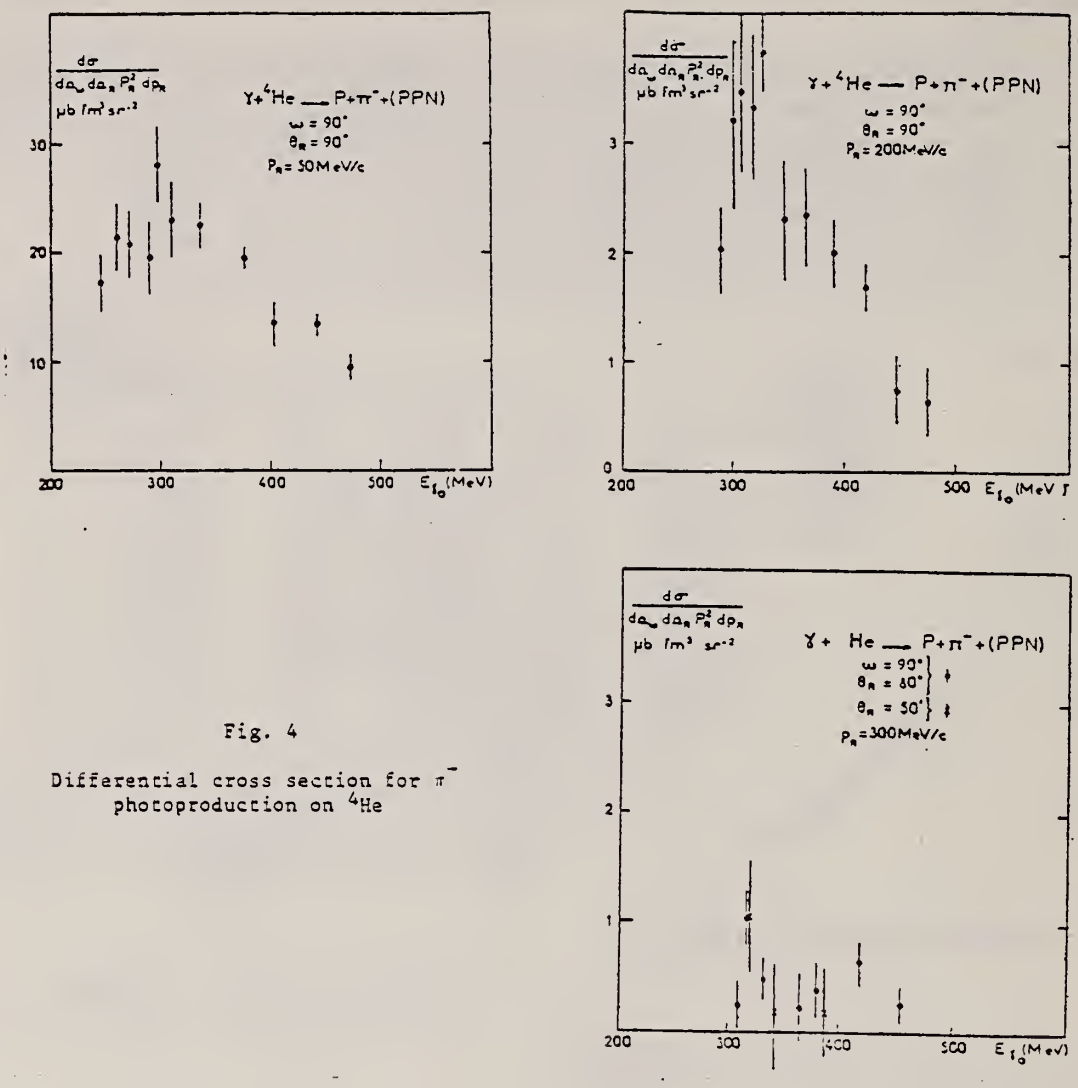

Fig. 4

Differential cross section for π^- photoproduction on ^4He

REF. D. V. Webb, C. K. Malcolm, Y.M. Shin, D. M. Skopik
PICNS-73, Vol.I, p.149 Asilomar

ELEM. SYM.	A	Z
He	4	2

METHOD

REF. NO.	
73 We 5	hmg

REACTION	RESULT	EXCITATION ENERGY	SOURCE		DETECTOR		ANGLE
			TYPE	RANGE	TYPE	RANGE	
G,N	ABX	25- 75	G	25- 75	TOF-D		DST

$$\frac{d\sigma}{d\Omega} = A + B \sin^2\theta + C \sin^2\theta \cos\theta$$

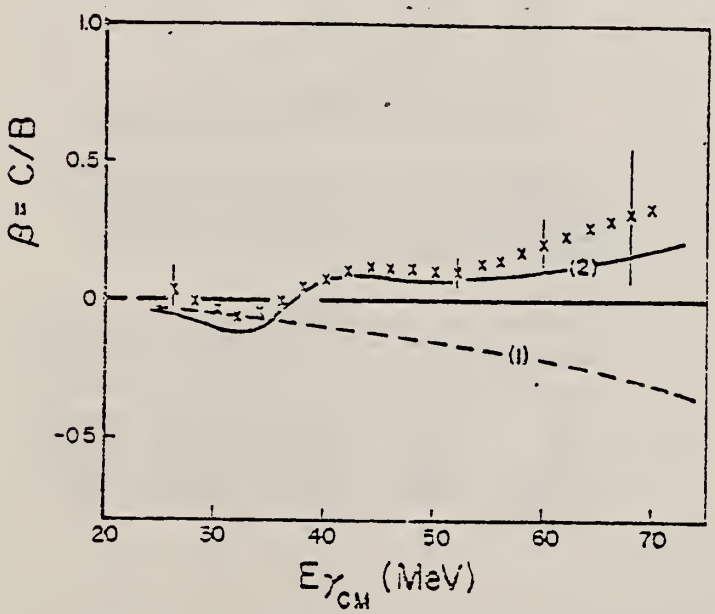

Fig. 1 Asymmetry coefficient B/C as a function of photon energy. Curve 1 shows the direct reaction; curve 2 shows the effect of introducing a broad 2⁺ state at 35 MeV.

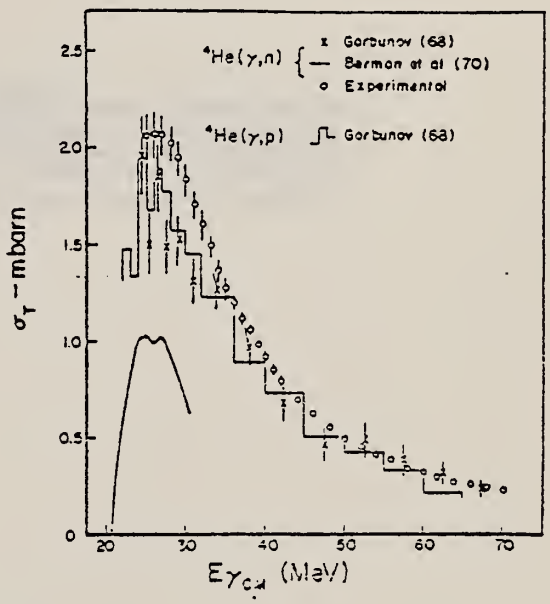

Fig. 2 Total cross section.

REF. Yu.M. Arkatov, P.I. Vatset, V.I. Voloshchuk, V.A. Zolenko, I.M. Prokhorets, and V.I. Chmil
Yad. Fiz. 19, 1172 (1974)
Sov. J. Nucl. Phys. 19, 598 (1974)

ELEM. SYM.	A	Z
He	4	2

METHOD

REF. NO. 74 Ar 6 hmg

REACTION	RESULT	EXCITATION ENERGY	SOURCE		DETECTOR		ANGLE
			TYPE	RANGE	TYPE	RANGE	
G,P	ABI	26-120	C	120	CCH-D		4PI
G,N	ABI	26-120	C	120	CCH-D		4PI
G,2D	ABI	26-120	C	120	CCH-D		4PI
G,PN	ABI	26-120	C	120	CCH-D		4PI
G,2P2N	ABI	26-120	C	120	CCH-D		4PI

ENERGY MOMENTS

The energy moments of the cross section for total absorption of γ rays by ^{4}He have been determined. The method of sum rules has been used to calculate the mean energies of dipole and quadrupole transitions, the contribution of $E2$ transitions to the total cross sections, and the mean square radius of ^{4}He. It is concluded that the contribution of quadrupole absorption to the total cross section of the reaction ^{4}He$(\gamma, pn)^3$H can be as high as 50%.

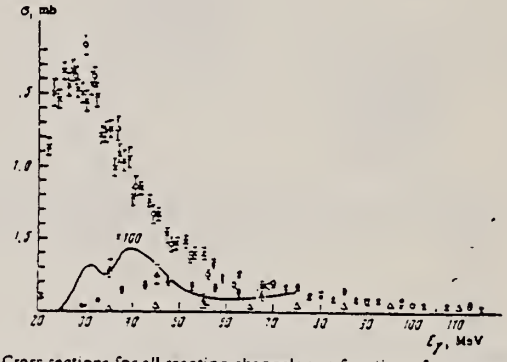

Cross sections for all reaction channels as a function of γ-ray energy. Points: ×—(γ, p) reaction, ○—(γ, n) reaction, ▲—(γ, 2d) reaction, ●—(γ, pn) reaction, △—(γ, 2p2n) reaction. The solid curve is the cross section for the (γ, 2d) reaction with inclusion of the data of other authors, [12] multiplied by a factor of 100.

TABLE I

Reaction channel	Energy moments			
	m_{-1}, F^2·MeV^2	m_0, F^2·MeV	m_1, 10^4, F^2	m_{-1}/m_0, 10^4, F^2/MeV
(γ, p)	177.3±11.9	4.16±0.25	11.70±0.70	26.92±2.20
(γ, n)	197.3±12.5	3.87±0.25	10.16±0.77	31.52±3.20
(γ, 2d)	0.45±0.06	0.01±0.001	0.025±0.002	0.062±0.016
(γ, pn)	52.1±5.3	1.15±0.13	1.56±0.21	3.43±1.02
(γ, 2p2n)	30.2±5.1	0.23±0.04	0.76±0.06	0.65±0.19
Total absorption	458.5±30.8	9.50±0.61	24.50±1.52	72.4±4.4

[12] R.W. Zurmühle, W.E. Stephens, Phys. Rev. 132, 751 (1963); W. Del Bianco, J.M. Poutissou, Phys. Lett. 29B, 299 (1969).

REF.

V.A. Gol'dshtein, V.B. Shostak, N.G. Afanas'ev, V.G. Vlasenko, E.L. Kuplennikov, and V.I. Startsev
Yad. Fiz. 19, 727 (1974)
Sov. J. Nucl. Phys. 19, 369 (1974)

EL EM. SYM.	A	Z
He	4	2

METHOD

REF. NO.	
74 Go 5	hmg

REACTION	RESULT	EXCITATION ENERGY	SOURCE		DETECTOR		ANGLE
			TYPE	RANGE	TYPE	RANGE	
E,E/P	ABX	0* 30	D	999	MAG-D		20

Electron scattering angle is 20°.

*SEP E, 999=1.1 GEV

The cross section for the reaction $^4He(e,e'p)^3H$ has been measured as a function of the separation energy of the protons. The experiment was performed in the beam of the LUÉ-2000 electron accelerator at an energy of 1187 MeV. The proton binding energy is found to be 17±1 MeV. The suppression coefficient is 0.87.

REF. V. A. Gol'dshtein, V. B. Shostak, N. G. Afanas'ev, V. G. Vlasenko, E. L. Kuplennikov, V. I. Startsev
Yad. Fiz. 20, 447 (1974)
Sov. J. Nucl. Phys. 20, 241 (1975)

ELEM. SYM.	A	Z
He	4	2

METHOD

REF. NO.	
74 Go 8	hmg

REACTION	RESULT	EXCITATION ENERGY	SOURCE		DETECTOR		ANGLE
			TYPE	RANGE	TYPE	RANGE	
E,E/P	ABX	* 17	D	999	MAG-D		DST

*SEP E, 999=1.2 GEV

The angular distribution of protons from the reaction $^4He(e,e'p)^3H$ has been measured in the electron beam of the LUÉ–2000 accelerator at an energy of 1187 MeV. Values have been obtained for the oscillator-potential parameter and the reduction factor for 1S protons emitted from the ^4He nucleus.

Angular distribution of protons in the reaction $^4He(e,e'p)^3H$, B = 17 MeV.

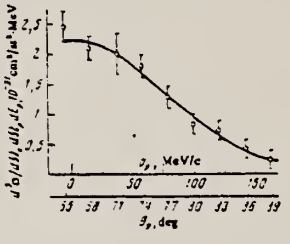

REF.

J.D. Irish, R.G. Johnson, K.G. McNeill, and J.W. Jury
Phys. Rev. C9, 2060 (1974)

ELEM. SYM.	A	Z
He	4	2

METHOD

REF. NO.	
74 Ir 1	hmg

REACTION	RESULT	EXCITATION ENERGY	SOURCE		DETECTOR		ANGLE
			TYPE	RANGE	TYPE	RANGE	
G,XN	RLY	20- 35	C	35	TOF-I		98

N YLD VS BEAM CURR.

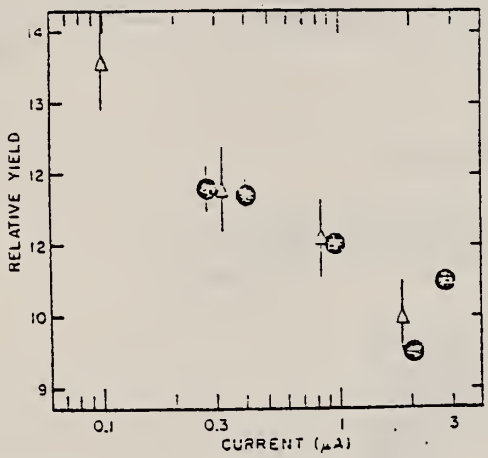

FIG. 1. Relative yield of photoneutrons from a liquid ^{4}He target as a function of average beam current: circles indicate points obtained using an aluminum Dewar and triangles indicate points obtained using a glass Dewar. The points obtained using the glass Dewar have been normalized to the points obtained using the aluminum Dewar at an average current of 0.3 μA. All points were obtained using an electron energy of 35 MeV.

Experiments to measure the photoneutron yield from a liquid ^{4}He target as a function of beam intensity have been carried out. They show that the most recent measurements of the photoneutron cross section with liquid helium targets can be made consistent with each other, and that the results are then not inconsistent with measurements of the ^{4}He(γ,n)^{3}He cross section using gaseous targets.

[NUCLEAR REACTIONS ^{4}He(γ,n), E = 35 MeV; measured σ (beam current).]

REF. P.E. Argan, G. Audit, N. De Botton, J.-L. Faure, J.-M. Laget, J. Martin, C.G. Schuhl, and G. Tamas
Nucl. Phys. A237, 447 (1975)

ELEM. SYM.	A	Z
He	4	2

METHOD

REF. NO. 75 Ar 1 egf

REACTION	RESULT	EXCITATION ENERGY	SOURCE TYPE	SOURCE RANGE	DETECTOR TYPE	DETECTOR RANGE	ANGLE
G,P	ABX	175-370	C	405	MAG-D		DST
G,N	ABX	274-403	C	405	MAG-D		DST

2-BODY COINC

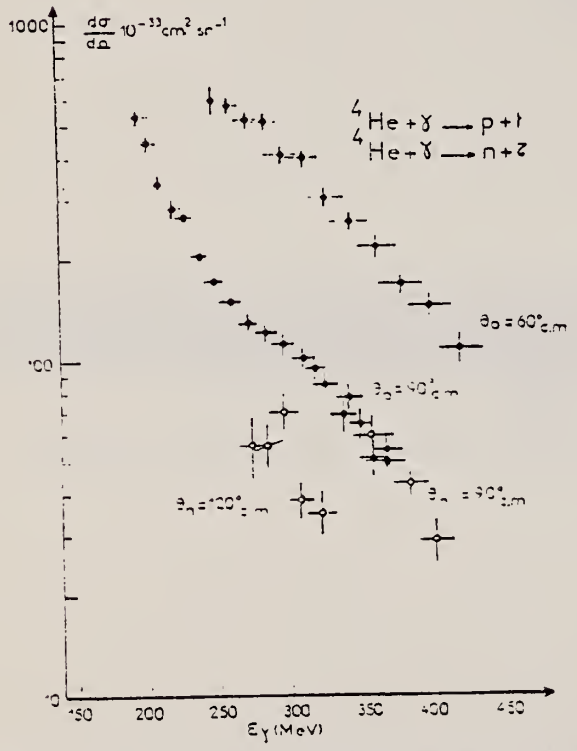

Fig. 10. The $\gamma + {}^4\mathrm{He} \to p + t$ (c.m.) differential cross sections at $\theta_p = 60°$, 90° c.m. and the $\gamma + {}^4\mathrm{He} \to n + {}^3\mathrm{He}$ (c.m.) differential cross sections at $\theta_n = 90°$, 120° c.m. (this work); E_γ is the photon lab energy. Horizontal error bars give photon energy resolution; vertical error bars represent statistical error.

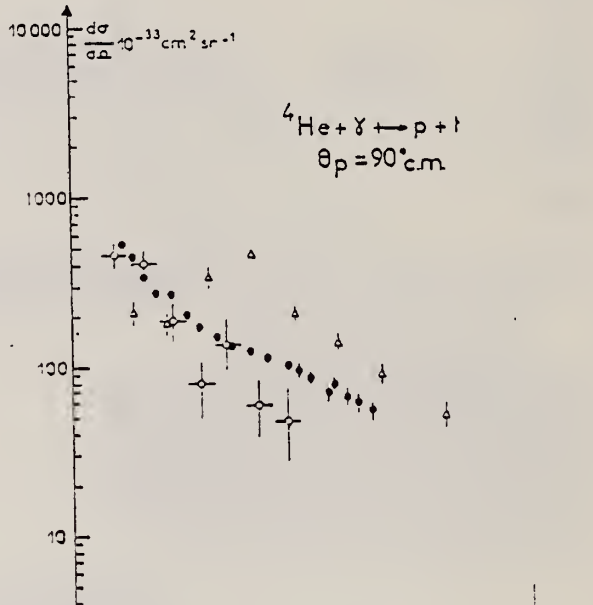

Fig. 11. The $\gamma + {}^4\mathrm{He} \to p + t$ (c.m.) differential cross section at $\theta_p = 90°$ c.m.; E_γ is the photon lab energy. Dots: this work; circles: ref. [19]); triangles: ref. [17]).

[17] P. Picozza et al., Nucl. Phys. A157, 190 (1970).

[19] S.E. Kiergan et al., Phys. Rev. C8, 431 (1973).

(continued)

TABLE 5

Differential cross section for the reaction $\gamma + {}^4\mathrm{He} \rightarrow t + p$ at 60° and 90° proton angle (c.m.)

Photon lab energy (MeV)	$\frac{d\sigma}{d\Omega}\Big\|_{60° \text{ c.m.}}$ (10^{-33} cm²/sr)	Photon lab energy (MeV)	$\frac{d\sigma}{d\Omega}\Big\|_{90° \text{ c.m.}}$ (10^{-33} cm²/sr)
248.0±10.1	585.8±44.2	194.5± 6.9	532.3±22.9
259.4±10.3	572.8±19.6	202.4± 6.6	446.8±17.6
271.4±10.5	519.6±14.8	210.4± 6.5	336.8±13.6
284.1±10.8	508.7±14.8	219.4± 6.4	278.4±11.5
296.9±11.2	409.0±12.8	228.2± 6.4	267.2±12.4
311.4±11.7	398.3±12.4	237.9± 6.4	204.9±10.7
327.2±12.3	302.7±11.6	248.8± 6.6	170.7± 9.2
343.8±12.7	255.9±11.2	260.2± 6.9	149.3± 9.4
361.7±13.5	218.0±12.6	271.6± 7.3	131.4± 8.9
379.1±14.1	166.7± 8.4	284.3± 7.6	121.9±10.4
399.6±14.9	144.7± 9.7	296.2± 8.0	111.4± 8.0
422.7±15.6	108.0± 9.9	310.2± 8.3	102.5± 5.8
		317.7± 8.5	94.6± 8.7
		325.3± 8.7	85.5± 5.8
		338.8± 9.0	69.3± 7.4
		342.0± 9.3	77.5± 5.5
		351.0± 9.5	65.5± 7.1
		358.8± 9.7	51.0± 6.3
		369.2±10.0	53.6± 6.4

The photon energy uncertainty is the FWHM of the photon energy resolution function. The cross-section uncertainty is due only to counting statistics.

TABLE 6

Differential cross section for the reaction $\gamma + {}^4\mathrm{He} \rightarrow {}^3\mathrm{He} + n$ at 90° and 120° neutron angle (c.m.)

Photon lab energy (MeV)	$\frac{d\sigma}{d\Omega}\Big\|_{90° \text{ c.m.}}$ (10^{-33} cm²/sr)	Photon lab energy (MeV)	$\frac{d\sigma}{d\Omega}\Big\|_{120° \text{ c.m.}}$ (10^{-33} cm²/sr)
357.8±14.3	59.4±3.1	274.1±10.9	56.1±11.0
369.1±13.8	49.8±3.6	284.8±10.4	55.9± 7.8
385.2±13.3	43.0±3.2	296.1± 9.9	70.2± 7.7
403.0±12.6	28.8±4.4	308.4± 9.3	48.6± 4.4
		321.5± 8.9	45.4± 5.3

REF.	ELEM. SYM.	A	Z
Yu. M. Arkatov, P.I. Vatset, V.I. Voloshchuk, V.N. Gur'ev, V.A. Zolenko, I.M. Prokhorets, and V.I. Chmil Yad. Fiz. 21, 925 (1975) Sov. J. Nucl. Phys. 21, 475 (1976)	He	4	2

METHOD	REF. NO.	
	75 Ar 10	hmg

REACTION	RESULT	EXCITATION ENERGY	SOURCE		DETECTOR		ANGLE
			TYPE	RANGE	TYPE	RANGE	
G,N	ABX	27- 30	C	UKN	CCH-D		DST

$$d\sigma/d\Omega = A(\sin^2\Theta) + \beta_n \sin^2\Theta\cos\Theta + \gamma\sin^2\Theta\cos^2\Theta + \delta)$$

Experimental values of the total cross sections and of the angular distributions of the photoneutrons of the reaction $^4He(\gamma, n)^3He$ were obtained in the photon energy region 27–30 MeV. The electric dipole and quadrupole cross sections and the phase shifts of the $E1$ and $E2$ amplitudes are obtained from an analysis of the angular distributions. The results are compared with analogous values for the (γ, p) reactions.
PACS numbers: 25.10.

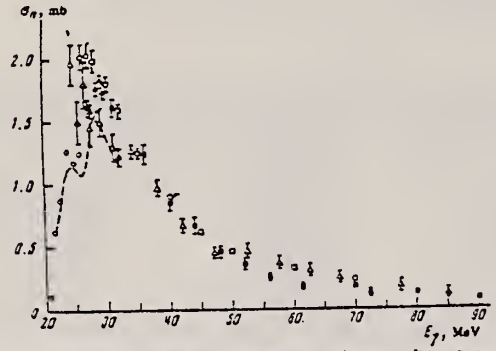

FIG. 1. Total cross section of the reaction $^4He(\gamma, n)^3He$. Points: ▲—our data, △—data of [3], □—data of [7], ○—data of [15], •—data of [17]; dashed curve—data of [16].

TABLE I

E_γ, MeV	A, mb/sr	β_n	γ	σ_n, mb
27—28	0.175±0.013	−0.133±0.032	0.242±0.124	1.50±0.05
28—29	0.194±0.015	−0.133±0.037	0.148±0.078	1.77±0.05
29—30	0.178±0.009	−0.165±0.038	0.291±0.103	1.75±0.06
27—30	0.188±0.024	−0.143±0.034	0.261±0.084	1.70±0.03

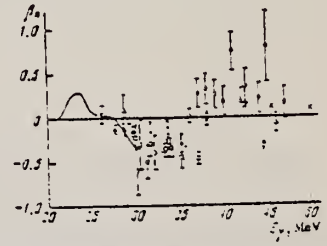

FIG. 2. Energy dependence of the photoneutron angular-asymmetry coefficient. Points: ▲—our data, •—data of [17], △—[3], □—[7], ○—[21], X—[7]; solid curve—data of [6].

TABLE II

E_γ, MeV	(γ, n) reaction			(γ, p) reaction		
	$\sigma_{\gamma n}$, mb	$\sigma_{\gamma n}$, mb	cos η	$\sigma_{\gamma p}$, mb	$\sigma_{\gamma p}$, mb	cos η
27—28	1.52±0.04	0.07±0.04	−0.14±0.07	1.46±0.06	0.070±0.020 [4] 0.070±0.020 [6]	
28—29	1.72±0.05	0.05±0.03	−0.17±0.10	1.42±0.07	0.073±0.013 [4] 0.031±0.020 [6]	0.299±0.09
29—30	1.66±0.06	0.09±0.03	−0.16±0.06	1.27±0.07	0.074±0.017 [4] 0.087±0.030 [6]	
27—30	1.62±0.04	0.08±0.02	−0.15±0.04	1.42±0.07	0.072±0.010 [4] 0.031±0.030 [6]	

Note. The data on the (γ, p) reaction are taken from [4,6].

(continued)

[3] A.N. Gorbunov, ZhETF Pis. Red. 8, 148 (68); JETP Lett. 8, 88 (68).
[4] Yu.M. Arkatov et al., ZhETF Pis Red. 9, 574 (69); JETP Lett. 9, 350 (69); Yad. Fiz. 12, 227 (70); Sov.J.Nucl.Phys. 12, 123 (71).
[6] J.D. Irish et al., Proc. Intern.Conf.Phot.React.,California 1973, p.2B3-1.
[7] D.N. Webb et al., cm. 6, p.2B3-1.
[8] W.R. Dodge et al., Phys. Rev. Lett. 28, 839 (1972).
[9] W.E. Meyerhof et al., 2nd Top.Symp.Nucl.Phys. Novsibirsk, 1971.
[15] J.A. Ferguson et al., Phys. Rev. 95, 776 (1954).
[16] F. Ferrero et al., Nuovo Cim. 45B, 273 (1966).
[17] Yu.M. Arkatov et al., ZhETF Pis. Red. 17, 356 (73); JETP Lett. 17, 253 (73).
[21] L. Busso et al., Nuovo Cim. Lett. 1, 941 (71).

REF.		EL EM. SYM.	A	Z
	S.V. Dementii, V.I. Ogurtsov, A.V. Shebeko, and N.G. Afanas'ev Yad. Fiz. 22, 13 (1975) Sov. J. Nucl. Phys. 22, 6 (1976)	He	4	2

METHOD	REF. NO.
	75 De 6 hmg

REACTION	RESULT	EXCITATION ENERGY	SOURCE		DETECTOR		ANGLE
			TYPE	RANGE	TYPE	RANGE	
E,E/	ABX	0-300	D	800-999	MAG-D		DST

999= 1.18 GEV

Results are presented of an experimental investigation of inelastic scattering of electrons with energies 800–1200 MeV in the angle interval 16–40° by the ^{4}He nucleus. It is shown that the experimental cross sections measured in the region of the quasielastic maximum can be reconciled with the results of elastic scattering by ^{4}He within the framework of the shell model only when account is taken of the correction for the motion of the mass center. An analysis of the results leads to the conclusion that the effect of motion of the mass center leads to a narrowing (in comparison with the predictions of the shell model) of both the nuclear density distribution and the momentum distribution of the internal electrons.

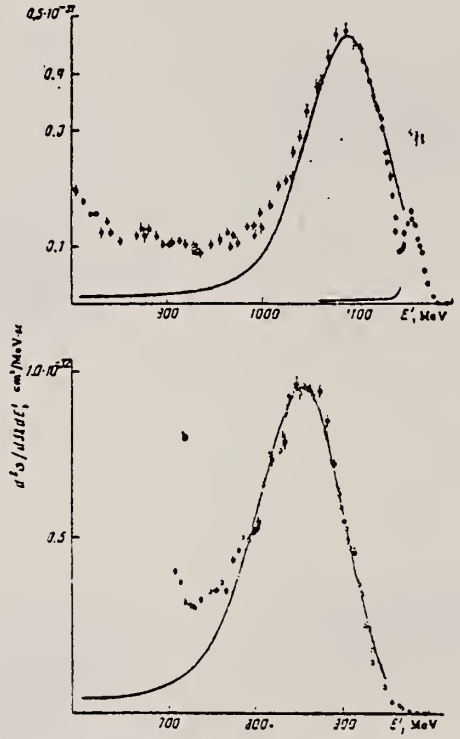

FIG. 1. Dependence of the cross section for electron scattering by ^{4}He on the energy of the scattered electron: a) E = 1180 MeV, θ = 20°; b) E = 988 MeV, θ = 30°; curves—calculated from formulas (2) and (24) with p_0 = 150 MeV/c.

REF. J. D. Irish, R. G. Johnson, B. L. Berman, B. J. Thomas, K. G. McNeill, and J. W. Jury
Can. J. Phys. 53, 802 (1975)

ELEM. SYM.	A	Z
He	4	2

METHOD

REF. NO.	
75 Ir 1	hmg

REACTION	RESULT	EXCITATION ENERGY	SOURCE		DETECTOR		ANGLE
			TYPE	RANGE	TYPE	RANGE	
G,N	ABX	22- 32	C	22- 33	TOF-D		DST

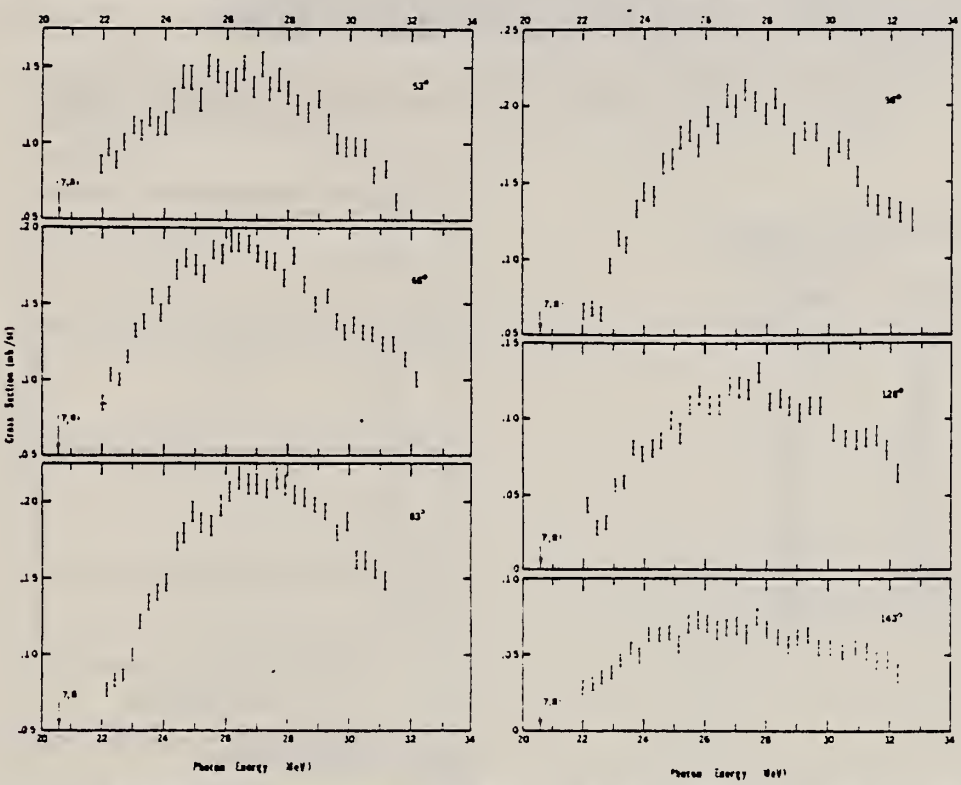

FIG. 5. The measured differential photoneutron cross sections for the reaction $^4He(\gamma,n)^3He$, normalized to the gas sample cross section data of Irish *et al.* (1973*b*).

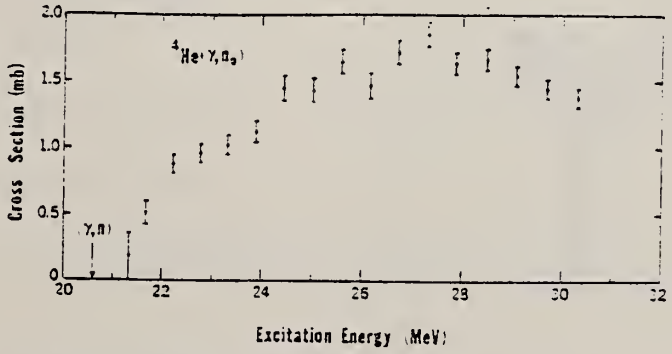

FIG. 7. Total cross section for the reaction $^4He(\gamma,n)^3He$, normalized to the gas sample cross section data of Irish *et al.* (1973*b*).

(continued)

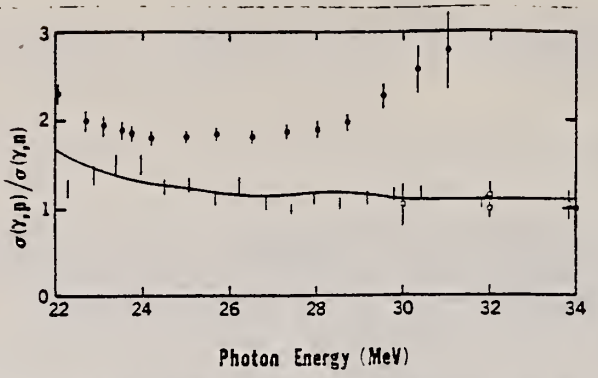

FIG. 9. Ratio $\sigma(\gamma,p)/\sigma(\gamma,n)$ for ^{4}He adapted from Fig. 4 of Londergan and Shakin (1972): bars — values inferred from the present normalized results and the ^{4}He(γ,p) cross section data of Meyerhof *et al.* (1970); closed circles — values inferred from the ^{4}He(γ,n) data of Berman *et al.* (1971) and the ^{4}He(γ,p) data of Meyerhof *et al.* (1970); open circles — values measured by Dodge and Murphy (1972); solid curve — coupled channel reaction theory calculation of Londergan and Shakin (1972).

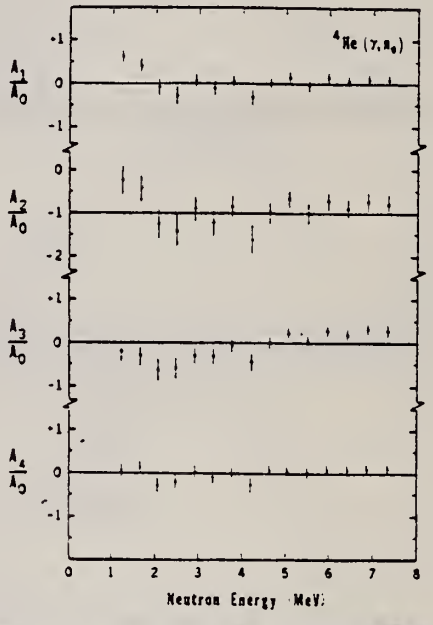

FIG. 6. Photoneutron angular distribution coefficients obtained by fitting the relation

REF.

J. Arends, J. Eyink, T. Hegerath, H. Hartmann, B. Mecking, G. Noldeke, H. Rost
Phys. Lett. 62B, 411 (1976)

ELEM. SYM.	A	Z
He	4	2

METHOD

REF. NO.: 76 Ar 5 egf

REACTION	RESULT	EXCITATION ENERGY	SOURCE		DETECTOR		ANGLE
			TYPE	RANGE	TYPE	RANGE	
G,D	ABX	201-359	C	UKN	TEL-D		DST

D,D COINC

High-energy differential cross-section measurements of the ^{4}He(γ, d)d reaction are presented. The cross sections are considerable smaller than previously published results and are not consistent with a predicted E2 transition.

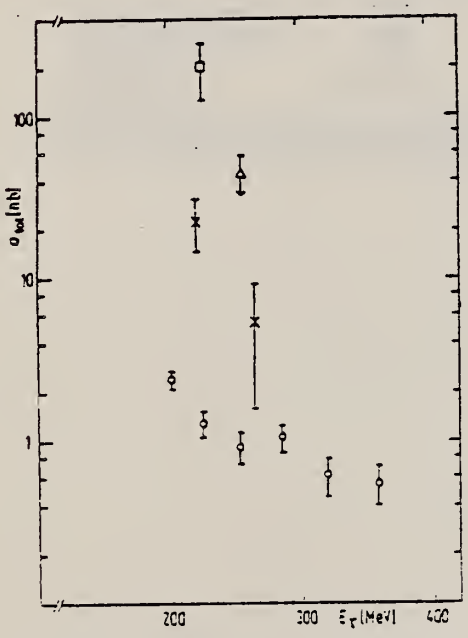

Fig. 2. Total cross section σ_{tot} for the ^{4}He(γ, d)d reaction; ▫ shows the data of Akimov et al. [4], △ the data of Poirier et al. [3], × of Asbury et al. [5], ○ are our data.

Table 1
Differential cross sections for the ^{4}He(γ, d)d reaction with statistical errors only.

$\bar{E}_\gamma$ (MeV)	$\bar{\theta}_{CMS}$ (deg)	dσ/dΩ (nb/sr)
213	46	0.22 ± 0.04
213	61	0.35 ± 0.09
213	73	0.41 ± 0.09
213	87	0.54 ± 0.10
258	46	0.08 ± 0.03
258	61	0.23 ± 0.08
258	73	0.16 ± 0.07
258	87	0.25 ± 0.07
330	46	0.14 ± 0.03
330	61	0.16 ± 0.05
330	73	0.07 ± 0.05
330	87	0.19 ± 0.05

[3] J.A. Poirier et al., Phys. Rev. 130 (1963) 1171.
[4] Y. K. Akimov et al., Phys. JETP 14 (1962) 512.
[5] J. G. Asbury et al., Phys. Rev. 137 (1965) B1214.

Table 2
The ^{4}He(γ, p)d total cross section and number of collected waves.

$\bar{E}_\gamma$ (MeV)	σ (nb)	Counts
201	2.41 ± 0.32	104 ± 12
225	1.29 ± 0.23	54 ± 9
253	0.92 ± 0.20	40 ± 8
285	1.04 ± 0.20	44 ± 8
320	0.61 ± 0.16	32 ± 7
359	0.55 ± 0.15	22 ± 6

REF. Yu. M. Arkatov, P. I. Vatset, V. I. Voloshchuk, V. N. Gur'ev, V. A. Zolenko, and I. M. Prokhorets
JETP Lett. 24, 439 (1976)
Pis'ma Zh. Eksp. Teor. Fiz. 24, 478 (1976)

ELEM. SYM.	A	Z
He	4	2

METHOD

REF. NO. 76 Ar 8 hmg

REACTION	RESULT	EXCITATION ENERGY	SOURCE		DETECTOR		ANGLE
			TYPE	RANGE	TYPE	RANGE	
G,N	ABX	21-150	C	UKN	CCH-D		4PI

The electric dipole and quadrupole cross sections are determined for the reaction $^4He(\gamma,n)^3He$ from the threshold to 150 MeV. The quadrupole cross sections of the reactions $^4He(\gamma,n)^3He$ and $^4He(\gamma,p)^3H$ agree within the limits of the experimental errors. A structure is observed in the dipole cross section.

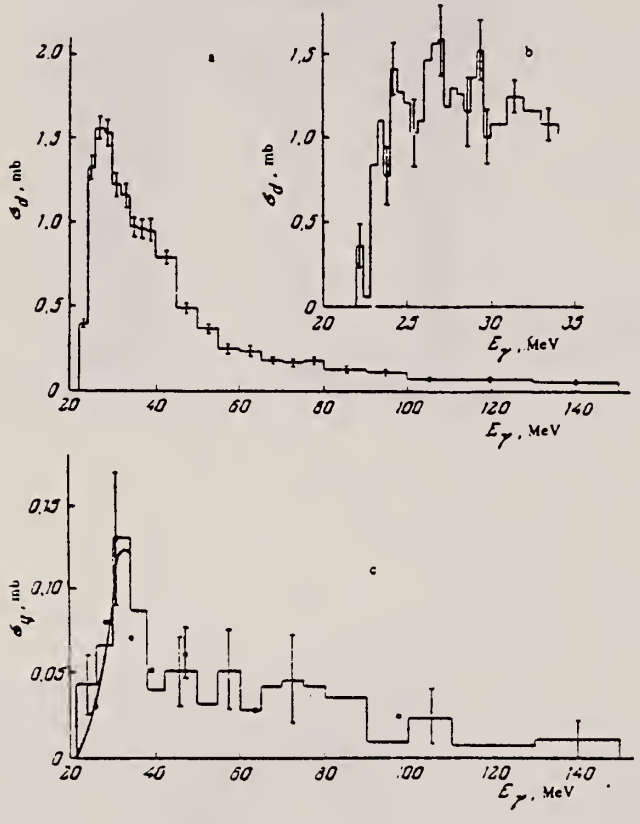

FIG. 1. a) Electric dipole cross section of the reaction $^4He(\gamma,n)^3He$, b) structure in the electric dipole cross sections, c) quadrupole electric cross section. Histogram—our data for the (γ,n) reaction, points—our data for the (γ,p) reaction,[6] curve—data of Meyerhof[10] for the (γ,p) reaction.

[6] P.I. Vatset, Doctoral Dissertation, Khar'kov, 1974

[10] W.E. Meyerhof, M. Suffert, and W. Feldman, Nucl. Phys. A148, 211 (1970)

REF. J. S. McCarthy, I. Sick, R. R. Whitney, M. R. Yearian
Phys. Rev. C13, 712 (1976)

EL EM. SYM.	A	Z
He	4	2

METHOD

REF. NO. 76 Mc 2 hmg

REACTION	RESULT	EXCITATION ENERGY	SOURCE		DETECTOR		ANGLE
			TYPE	RANGE	TYPE	RANGE	
E,E/	ABI	32-272	D	500	MAG-D		60

QUASIELAST SCAT

TABLE I. Quasielastic cross sections at $E_0 = 500$ MeV and $\theta = 60°$ integrated up to 200 MeV energy loss. The values used for the nucleon elastic cross sections were 1.14×10^{-31} cm^2/sr for the proton and 0.21×10^{-31} cm^2/sr for the neutron (Ref. 4).

	^{3}He ($\times 10^{-31}$ cm^2/sr)		^{4}He ($\times 10^{-31}$ cm^2/sr)
Static-impulse model	2.50		2.7
"Fermi-gas" fit to data	2.62		2.86
Lehman model	2.86		...
Experiment	2.59 ± 0.07 [a]		3.00 ± 0.03 [a]
^{4}He-^{3}He difference	-	0.41 ± 0.11	

[a] Error bars do not include the ±3% uncertainty in the proton elastic cross section (Ref. 4).

[4] T. Janssens, R. Hofstadter, E.B. Hughes, and M.R. Yearian, Phys. Rev. 142, 922 (1966).

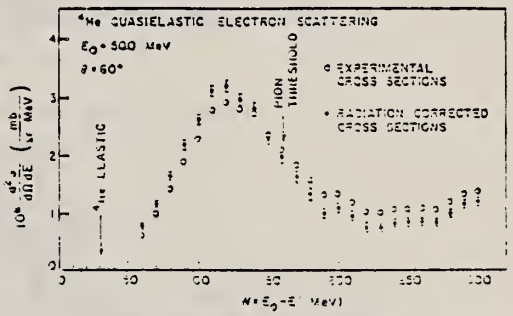

FIG. 2. ^{4}He quasielastic electron scattering spectrum as a function of energy electron loss.

REF.

F. Balestra, E. Bollini, L. Busso, R. Garfagnini,
C. Guaraldo, G. Piragino, R. Scrimaglio and A. Zanini
Il Nuovo Cimento 38A, 145 (1977)

ELEM. SYM.	A	Z
He	4	2

Uses: $\frac{d\sigma}{d\Omega} = A(\sin^2\theta + \beta\sin^2\theta\cos\theta + \gamma\sin^2\theta\cos^2\theta + \epsilon)$

REF. NO. 77 Ba 14

REACTION	RESULT	EXCITATION ENERGY	SOURCE		DETECTOR		ANGLE
			TYPE	RANGE	TYPE	RANGE	
G,P	ABX	20- 46	C	85	CCH-D		DST
G,N	ABX	20- 46	C	85	CCH-D		DST
G,PN	ABX	28- 75	C	85	CCH-D		DST
G,2P2N	ABX	28- 70	C	85	CCH-D		4π

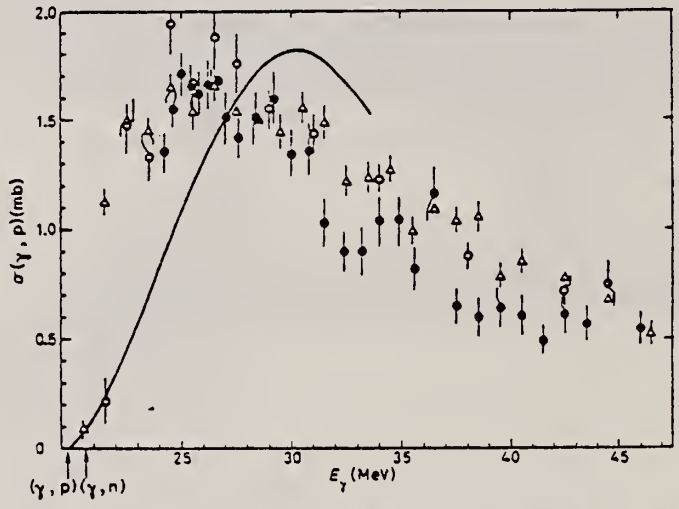

Fig. 2. – $^4He(\gamma, p)^3H$ reaction cross-section. Full points: present work; open circles: ref. [11]; triangles: ref. [8]; full-line curve: ref. [21].

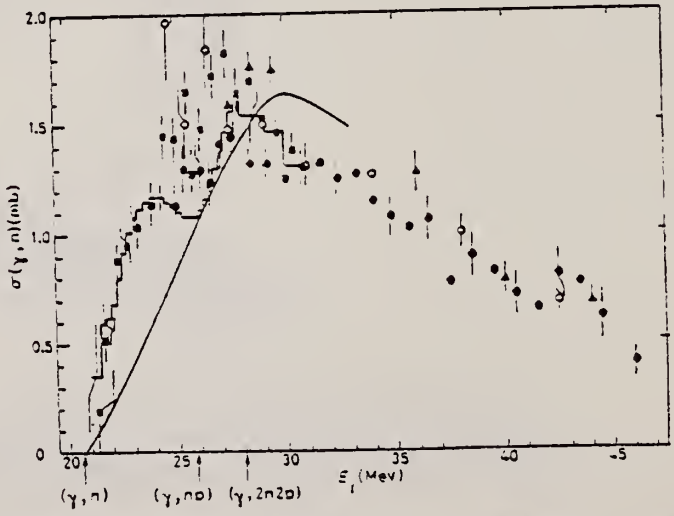

Fig. 3. – $^4He(\gamma, n)^3H$ reaction cross-section. Full points: present work; open circles: ref. [11]; triangles: ref. [4,12]; squares: ref. [19]; histogram: ref. [7,8]; full-line curve: ref. [21].

(continued)

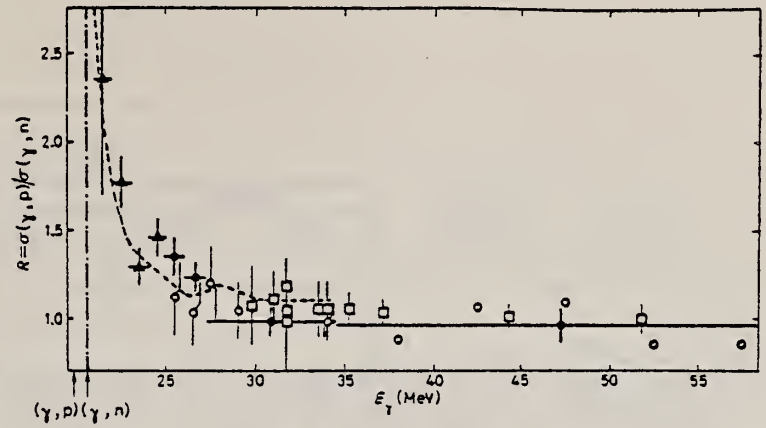

Fig. 4. – $R(E_\gamma)=\sigma(\gamma, p)/\sigma(\gamma, n)$. Full points: present work; open circles: deduced from the data of ref. [11]; squares: ref. [12]; triangles: deduced from the data of ref. [8] and ref. [7,8]; dashed-line curve: ref. [11].

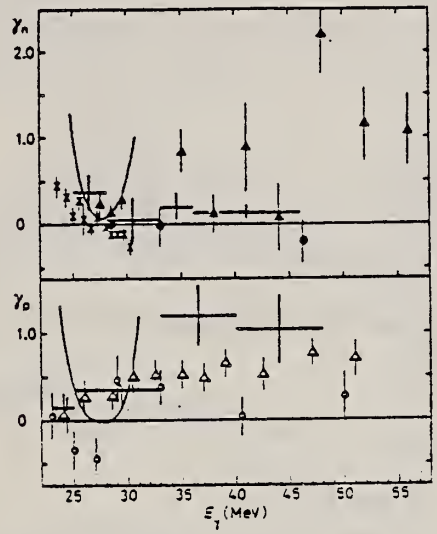

Fig. 5. – Coefficient γ_n and γ_p values as a function of E_γ. Full-line crosses: present work; full triangles: ref. [4,12]; full points: ref. [11]; × crosses: ref. [13]; open circles: ref. [11]; open triangles: ref. [3]. The full-line curves represent the $5\sigma_\gamma/\sigma_d=\gamma(E_\gamma)$ values deduced from the data of table I (see the text).

(continued)

REACTION	RESULT	EXCITATION ENERGY	SOURCE		DETECTOR		ANGLE
			TYPE	RANGE	TYPE	RANGE	

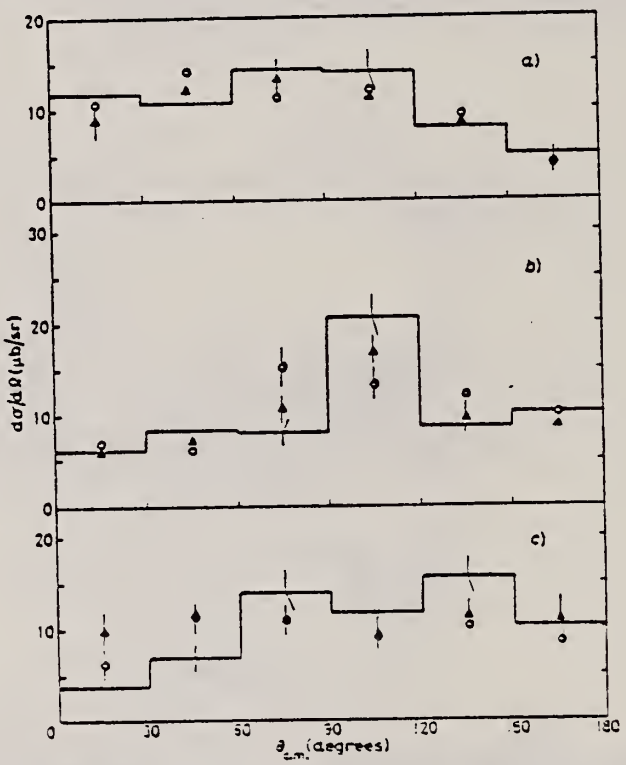

Fig. 15. – Angular distribution of p, n and d from the $^4He(\gamma, np)^2H$ reaction (respectively *a*), *b*), *c*)). Full-line histograms: present work ($28 < E_\gamma < 60$ MeV); triangles: ref. (*) ($28 < E_\gamma < 60$ MeV); open circles: ref. (3) ($25.9 < E_\gamma < 75$ MeV; data normalized in area to ours).

(continued)

[3]A.N. Gorbunov and V.M. Spiridonov: Sov. Phys. JETP, 7, 600 (1958).

[4]Yu.M. Arkatov, P.I. Vatset, V.I. Voloschuk, A.P. Klyucharev, V.L. Marchenko and A.F. Khodyachikh: Sov. Journ. Nucl. Phys., 9, 271 (1969).

[5]Yu. Arkatov, P.I. Vatset, V.I. Voloschuk, V.V. Kirichenko, I.M. Prokhorets and A.F. Khodyachikh: Sov. Journ. Nucl. Phys., 12, 123 (1971).

[6]Yu.M. Arkatov, A.V. Bazaeva, P.I. Vatset, V.I. Voloshchuk, A.P. Klyucharev and A.F. Khodyachikh: Sov. Journ. Nucl. Phys., 10, 639 (1970).

[7]F. Ferrero, C. Manfredotti, L. Pasqualini, G. Piragino and P.G. Rama: Nuovo Cimento 458, 273 (1966).

[11]A.N. Gorbunov: Proc. of P. N. Lebedev Phys. Inst., 71, 1 (1974).

[19]J.D. Irish, R.G. Johnson, B.L. Berman, B.J. Thomas and K.G. McNeill: Can. Journ. Phys. 53, 802 (1975).

[21]J.T. Londergan and C.M. Shakin: Phys. Rev. Lett., 28, 1729 (1972).

[22]W.R. Dodge and J.J. Murphy: Phys. Rev. Lett., 28, 839 (1972).

REF. A.S. Alexanian, T.L. Asatiani, A.O. Gasparian, L.A. Jirova, L.A. Genina, V.A. Ivanov, G.K. Megrabian, G.G. Mkrtchian, R.N. Pikhtelev, M.I. Dayon, A.D. Kamenski, F.F. Kayumov, V.A. Kramarenko, G.L. Melkumov & M.N.Khachaturian

METHOD Nucl. Inst. & Methods 148, 251 (1978)

EL.EM. SYM.	A	Z
He	4	2

REF. NO. 78 A1 10 hmg

REACTION	RESULT	EXCITATION ENERGY	SOURCE		DETECTOR		ANGLE
			TYPE	RANGE	TYPE	RANGE	
G,PIO	ABI	1*5	C	1*5	TEL-D		DST

ENERGY IN GEV

An experimental arrangement designed for the study of π^0-photoproduction on the nuclei of helium gas at small momentum transfers (the kinetic energy of the recoil nuclei $T_A^{lim} = 1$–20 MeV) is described. The arrangement consists of a recoil nucleus detector which is a self-triggering helium spark chamber and a π^0-meson detector which is a combination of total absorption Cherenkov spectrometers, wide gap spark chambers and scintillation counters. By this arrangement the reaction $\gamma + {}^4He \to {}^4He + \pi^0$ has been investigated and for the energy interval $E_\gamma = 1.5$–4.5 GeV a value of the cross section has been obtained integrated over the angular interval $\theta_{\pi^0}^{lab} = 2°$–$8°$ equal to $(0.28 \pm 0.02)\,\mu b$ (statistical errors).

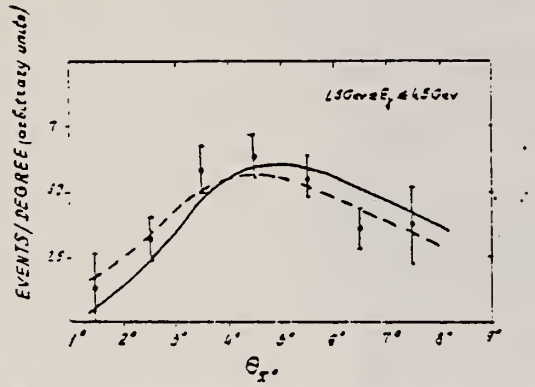

Fig. 6. Dependence of the yield of the reaction $\gamma + {}^4He \to {}^4He + \pi^0$ on photon energy E_γ in the angular interval $\theta_{\pi^0}^{lab} = 1°$–$10°$. The curve is the theoretical cross section normalized to the total number of events according to ref. 3.

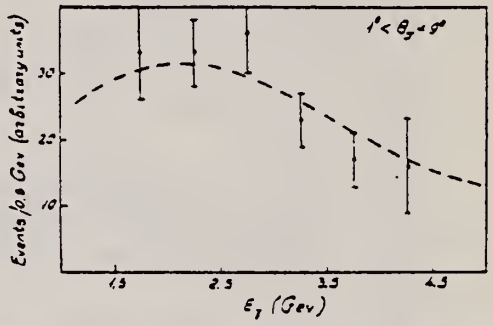

Fig. 7. Dependence of the yield of the reaction $\gamma + {}^4He \to {}^4He + \pi^0$ on the angle $\theta_{\pi^0}^{lab}$ for the photon energy interval $E_\gamma = 1.5$–4.5 GeV. The curve is the theoretical cross section normalized to the total number of events according to ref. 3.

REF. V.P. Alfimenkov, S.B. Borzakov, J. Wierzbicki, O.N. Ovchinnikov, L.B. Pikel'ner, E.I. Sharapov
JETP Lett. 29, 91 (1979)

ELEM. SYM.	A	Z
He	4	2

METHOD

REF. NO. 79 A1 6 hg

REACTION	RESULT	EXCITATION ENERGY	SOURCE TYPE	SOURCE RANGE	DETECTOR TYPE	DETECTOR RANGE	ANGLE
N,G	ABX	20-22	D	0-1	NAI-D		DST
		(20.6-20.653)		(.001-.070)			

SIGMA AT THRESHOLD

First measurements are reported of the effective cross section of radiative capture of He^3 neutrons in the energy interval 1–70 keV. The resultant energy dependence of the cross section is compared with theoretical predictions.

PACS numbers: 25.10. + s, 25.40.Lw

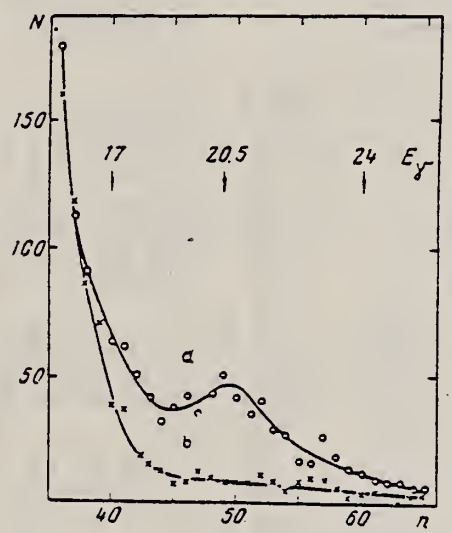

FIG. 1. a—γ-ray spectrum in the reaction $He^3(n,\gamma)$ obtained by means of NaI(Tl) crystal at an angle of 90° with the beam: N—number of readouts per channel during 48-hour period of measurements; n—amplitude analyzer channels. b—background spectrum after He^3 substitution with graphite sample, indentical to He^3 with respect to scattering. Numbers indicate energy in MeV.

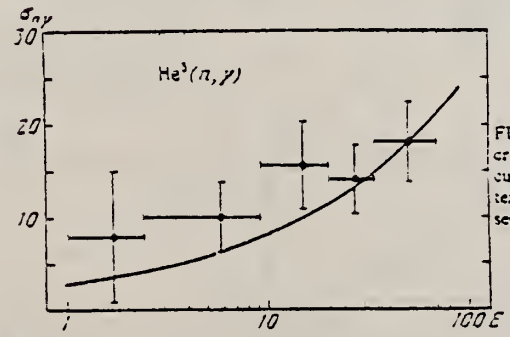

FIG. 2. Energy dependence of the effective cross section $\sigma_{n\gamma}(He^3)$: points—experiment, curve—theoretical prediction discussed in the text. E—neutron energy in keV, $\sigma_{n\gamma}$—cross section in μbarn.

REF. J. Arends, J. Eyink, A. Hegerath, H. Hartmann, B. Mecking, G. Nöldeke, and H. Rost
Nucl. Phys. A322, 253 (1979)

ELEM. SYM.	A	Z
He	4	2

METHOD

REF. NO.: 79 Ar 3 | hg

REACTION	RESULT	EXCITATION ENERGY	SOURCE		DETECTOR		ANGLE
			TYPE	RANGE	TYPE	RANGE	
G,P	ABX	197-420	C	500	TOF-D		DST

Abstract: The $^4He(\gamma, p)^3H$ reaction was investigated in the photon energy region between 200 and 450 MeV and at proton c.m. angles between 30° and 150°. The outgoing particles were detected in coincidence in two time-of-flight spectrometers consisting of scintillation counters; energies and angles of both particles were determined. The measured angular distributions show a strong forward peak. The differential cross sections and the total cross section fall off smoothly with increasing photon energy. However, the slope is not as steep as in the low energy region.

E NUCLEAR REACTIONS $^4He(\gamma, p)^3H$, $E = 200$–450 MeV, $\theta = 30°$–$150°$; measured $\sigma(E, \theta)$

TABLE 2

Differential cross sections in units of nb/sr; the errors are due to counting statistics only

Photon energy (MeV)	Proton c.m.s. angle (deg)								
	30	45	60	75	90	105	120	135	150
197						154.4 ±5.4			
209					426.1 ±14.7	143.1 ±5.0			13.9 ±1.2
223			784.3 ±47.2	483.8 ±24.8	348.9 ±13.0	130.6 ±4.6	35.0 ±1.8	25.9 ±2.1	13.0 ±1.2
239			641.6 ±39.5	411.8 ±20.1	242.6 ±10.5	102.0 ±4.0	26.6 ±1.3	25.1 ±2.1	12.5 ±1.2
257			568.6 ±35.0	293.7 ±18.0	194.4 ±9.1	64.4 ±3.1	27.1 ±1.5	21.1 ±2.0	12.3 ±1.3
278		401.4 ±22.7	481.5 ±30.6	246.6 ±15.8	125.0 ±7.0	52.6 ±2.6	23.0 ±1.4	18.9 ±2.2	10.8 ±1.2
303	238.2 ±23.9	394.6 ±19.1	395.2 ±26.3	176.5 ±12.8	92.3 ±5.8	43.2 ±2.3	20.6 ±1.4	16.7 ±2.1	11.6 ±1.4
334	166.3 ±15.6	339.7 ±16.7	329.1 ±22.7	142.1 ±10.9	69.9 ±5.2	30.8 ±1.8	20.6 ±1.5	11.1 ±2.0	9.3 ±1.4
371	180.9 ±14.0	246.0 ±13.2	196.7 ±16.4	105.1 ±8.8	48.4 ±3.7	23.5 ±1.5	13.4 ±1.4	9.4 ±2.1	6.2 ±1.5
420	163.1 ±12.9	181.9 ±10.8	154.1 ±13.8	67.6 ±6.9	23.3 ±2.6	13.6 ±1.1	8.9 ±1.3	5.1 ±1.3	5.1 ±1.4

$$\frac{d\sigma}{d\Omega} = a \sin^2\theta(1 + b\cos\theta + c\cos^2\theta + d\cos^3\theta + e\cos^4\theta),$$

TABLE 3

Parameters and χ^2 of the least square fits to the data and the calculated total cross section

k (MeV)	a (nb/sr)	b	c	d	e	χ^2	σ_{tot} (μb)
223	332.4±9.6	2.90±0.09	2.00±0.31	−1.55±0.74	−1.47±0.59	15.6	3.52±0.24
239	249.5±7.9	3.02±0.10	2.58±0.35	−0.58±0.87	−0.84±0.68	13.9	3.01±0.22
257	173.9±6.9	3.27±0.12	4.15±0.48	1.58±1.19	0.09±0.92	9.3	2.66±0.20
278	128.7±5.1	3.27±0.15	4.58±0.35	2.37±0.73	0.49±0.70	3.9	2.06±0.13
303	94.2±4.1	3.09±0.18	5.16±0.44	4.81±0.78	2.54±0.78	3.8	1.77±0.12
334	71.6±3.5	3.46±0.19	6.35±0.52	4.45±0.82	1.00±0.82	7.9	1.41±0.10
371	48.5±2.7	3.10±0.23	6.41±0.66	7.36±1.10	3.86±1.11	0.1	1.06±0.09
420	24.9±2.0	3.14±0.36	9.23±1.18	15.10±2.20	9.27±2.02	1.5	0.76±0.09

(continued)

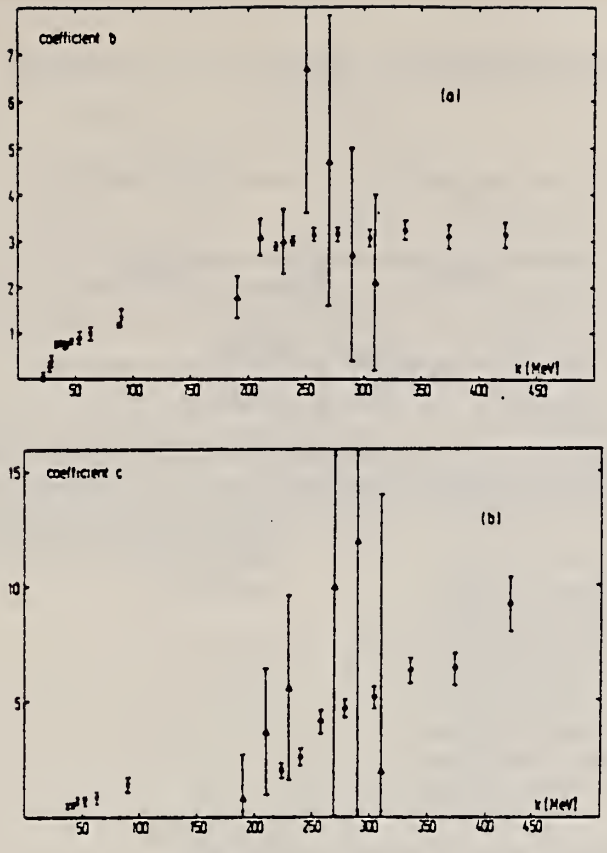

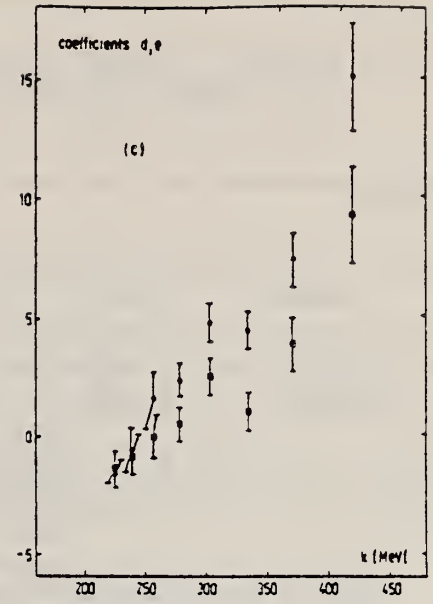

Fig. 8. Photon energy dependence of the fit parameters; the coefficient b is shown in (a), coefficient c is plotted in (b); closed circles: this experiment, triangles: ref. [4]), crosses: ref.[9]), points: ref. [10]). The parameters d (closed points) and e (closed squares) are shown in (c).

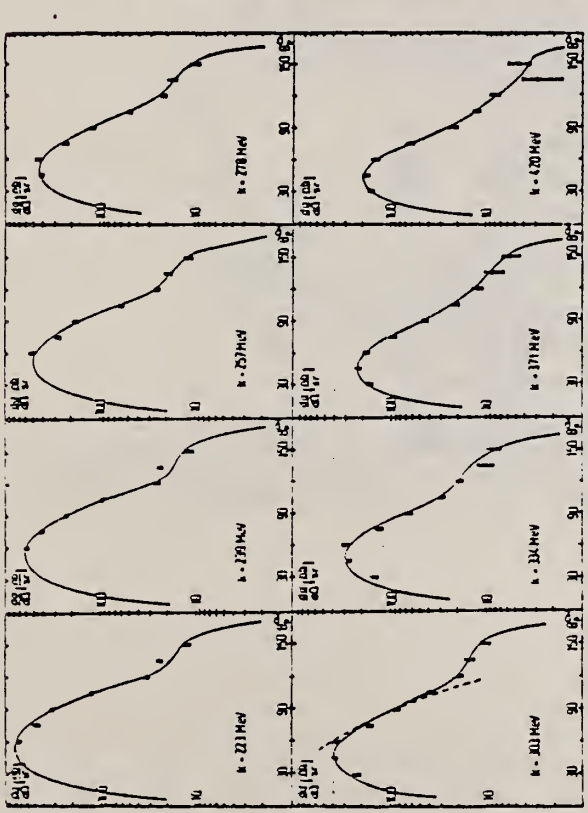

Fig. 7. The angular distributions; the full curves represent the best fits to the data; the dashed curve at $k = 303$ MeV is from ref. [13]).

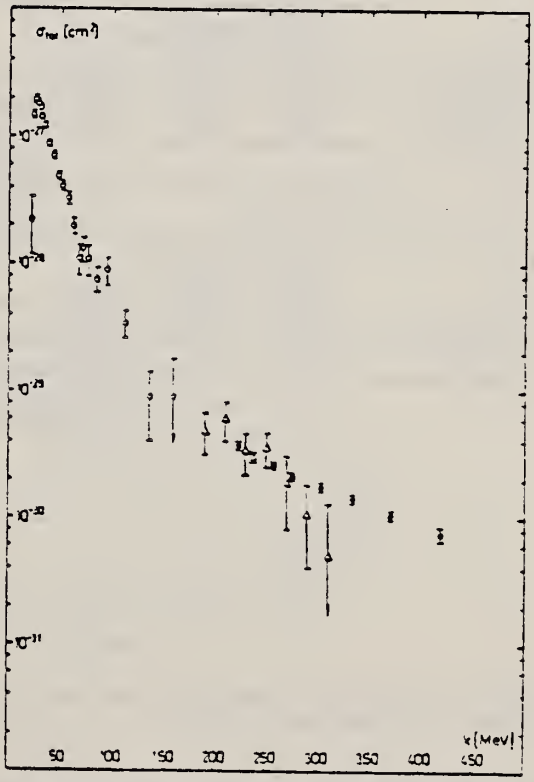

Fig. 9. The total cross section as a function of the photon energy (closed circles); the open circles are the results of ref. [10]), the triangles are from ref. [4]).

REF. F. Balestra, L. Busso, R. Garfagnini, G. Piragino & A. Zanini
Il Nuovo Cimento 49A, 575 (1979)

ELEM. SYM.	A	Z
He	4	2

METHOD

REF. NO. 79 Ba 5 hg

REACTION	RESULT	EXCITATION ENERGY	SOURCE		DETECTOR		ANGLE
			TYPE	RANGE	TYPE	RANGE	
G,NP	ABX	26-60	C	120	CCH-D		DST
G,2N2P	ABX	28-60	C	120	CCH-D		DST

Summary. — The total and the differential cross-sections, the angular and the energy correlations for the three- and four-body ^{4}He photodisintegration have been investigated, with a diffusion cloud chamber placed in a magnetic field and exposed to the 100 MeV electrosynchrotron of Torino University. The analysis seems to indicate that, in about 71% of the (γ, pn) events the photons are absorbed by a n-p pair, in about 15% of the events by a n-d pair and in about 14% of tho events the particles photoemitted are not correlated. For the (γ, 2n2p) reaction, the results seem to suggest, as main reaction mechanism, the photoabsorption from a quasi-deuteron correlated to another quasi-deuteron, which are decomposed too.

Data also given as function of opening angle of p-n,p-d,n-d and p,p pairs.

TABLE I. – *Average values of the opening angles* (c.m.s.) *between* p-n, p-d *and* n-d *pairs.*

θ_{pn}	$28 < E_\gamma < 40$ MeV			$40 < E_\gamma < 60$ MeV		
(c.m.s.)	θ_{pn}	θ_{pd}	θ_{nd}	θ_{pn}	θ_{pd}	θ_{nd}
$0° \div 90°$	63°	145°	125°	40°	145°	166°
$90° \div 180°$	125°	115°	85°	142°	116°	73°

TABLE II. – *Average values of the relative energy of the* p-n, p-d *and* n-d *pairs, related to the energy of the third particle.*

θ_{pn}	$28 < E_\gamma < 40$ MeV			$40 < E_\gamma < 60$ MeV		
(c.m.s.)	E_{pn}/E	E_{pd}/E	E_{nd}/E	E_{pn}/E	E_{pd}/E	E_{nd}/E
$0° \div 90°$	0.40	0.58	0.59	0.15	0.37	0.32
$90° \div 180°$	0.69	0.44	0.47	0.32	0.43	0.37

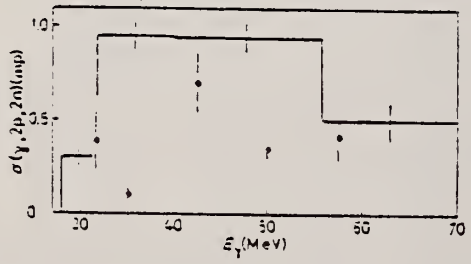

Fig. 7. – ^{4}He(γ, 2p, 2n) reaction cross-section; full-line hystogram: present data; full points: ref. (1); open circles: ref. (14).

(continued)

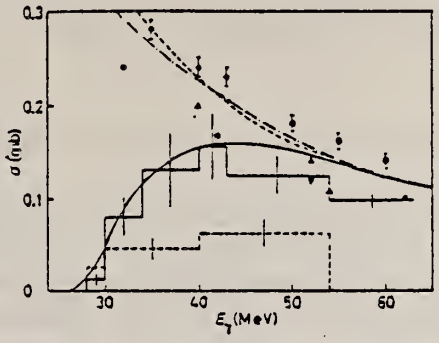

Fig. 4. – $^4He(\gamma, pn)^2H$ reaction cross-section; full-line hystogram, deduced for the events with $\vartheta_{pn} > 90°$; dashed-line hystogram, deduced for $\vartheta_{pn} < 90°$; full-line curve: ref. (4); dot-dashed–line curve: deuterium photodisintegration cross-section from ref. (11); dashed-line curve: deuterium photodisintegration cross-section from ref. (12); open circles: data from ref. (9); full points: ref. (10); open triangles: ref. (14,15); full triangles ref. (13); diamonds: ref. (8).

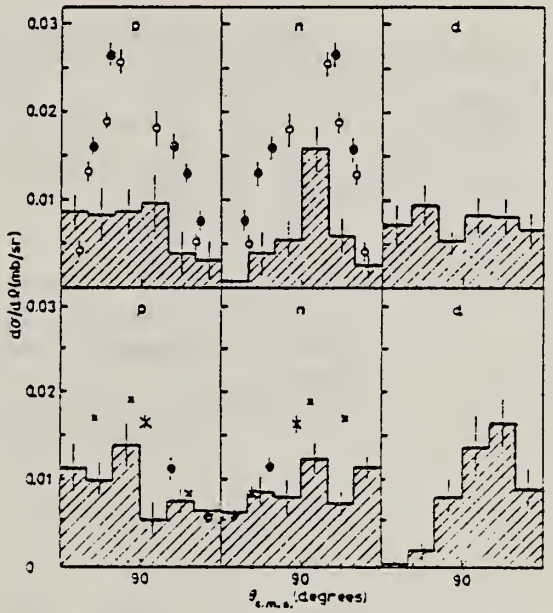

Fig. 5. – Angular distributions of p, n and d from the $^4He(\gamma, pn)^2H$ reaction, for the events with $\vartheta_{pn} > 90°$; upper part: $E_\gamma < 40$ MeV, lower part: $E_\gamma > 40$ MeV. Full-line hystograms: present data. Open circles: ref. (9); full points: ref. (5); the crosses (ref. (10)) are the angular distributions of p and n in the deuterium photodisintegration.

REF. T.W. Phillips, B.L. Berman, D.D. Faul, J.R. Calarco, J.R. Hall
Phys. Rev. C19, 2091 (1979)

EL EM. SYM.	A	Z
He	4	2

METHOD

REF. NO. 79 Ph 3 hg

REACTION	RESULT	EXCITATION ENERGY	SOURCE TYPE	SOURCE RANGE	DETECTOR TYPE	DETECTOR RANGE	ANGLE
G,T	RLX	31-51	D	31-51	TEL-D		90
G,HE3	RLX	31-51	D	31-51	TEL-D		90

We have measured the cross-section ratio $\sigma(\gamma,^3H)/\sigma(\gamma,^3He)$ for ^4He from 31 to 51 MeV with an incident bremsstrahlung beam and a collimated solid-state telescope at 90° laboratory angle. The results obtained from these data for the total cross-section ratio are consistent with unity for most of the energy range covered, but deviate from this value in the energy region near 44 MeV.

SIGMA RATIO G,P/G,N

[NUCLEAR REACTIONS $^4He(\gamma,^3H,^3He)$, $E_\gamma = 31-51$ MeV; measured differential cross-section ratio at 90° (laboratory); deduced total (γ,p)-to-(γ,n) cross-section ratio.]

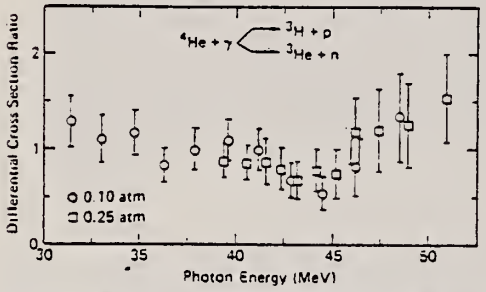

FIG. 6. $^4He(\gamma,p)$-to-(γ,n) differential cross-section ratio at 90° in the laboratory for the detected trinucleons. The data obtained with a ^4He gas pressure at 0.10 atm were normalized to those taken with a pressure of 0.25 atm in the overlap region between 39 and 45 MeV.

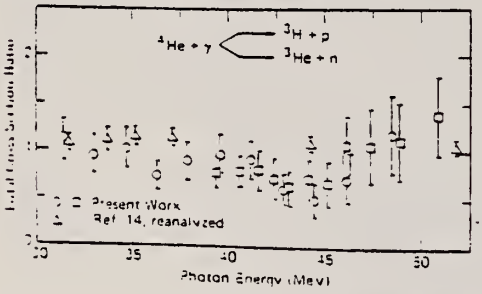

FIG. 7. $^4He(\gamma,p)$-to-(γ,n) total cross-section ratio. The circles and squares are computed from the measured results shown in Figs. 5 and the angular-distribution parameters given in the tables, under the assumption that Eq. (2) holds. The triangles are data of Ref. 14, reanalyzed under the same conditions; the data points shown at 31.7 and 35.7 MeV represent weighted averages of three and two points, respectively.

$$\frac{d\sigma}{d\Omega} = A + B\sin^2\theta + C\sin^2\theta\cos\theta - D\sin^2\theta\cos^2\theta, \quad (1)$$

$$\frac{d\sigma}{d\Omega} = \alpha\sin^2\theta(1 - \beta\cos\theta). \quad (2)$$

TABLE I. Values for the asymmetry coefficient β.

Energy (MeV)	For the $^4He(\gamma,p)$ reaction Ref. 19	Ref. 7	Ref. 4	Ref. 20	Adopted	For the $^4He(\gamma,n)$ reaction Ref. 2	Ref. 11	Ref. 7	Ref. 12	Ref. 22	Adopted
31	0.64		0.58	0.60	0.62	−0.30	−0.25	−0.45	−0.10		−0.25
36		0.80	0.73	0.72	0.73			0	−0.03		−0.02
41			0.82	0.80	0.81			0.20	0.22	−0.36	0.21
46			0.91	0.82	0.88				0.24	−0.24	0.23
51			0.98	0.84	0.93				0.22	−0.12	0.23

TABLE II. Expected differential cross-section ratio.

Energy (MeV)	Reaction	$\cos\theta$	$\beta\cos\theta$ [a]	$\frac{(1+\beta\cos\theta)_p}{(1+\beta\cos\theta)_n}$
31	(γ,p)	0.186	0.112	1.17
	(γ,n)	0.193	−0.048	
36	(γ,p)	0.180	0.131	1.14
	(γ,n)	0.184	−0.004	
41	(γ,p)	0.179	0.135	1.10
	(γ,n)	0.182	0.038	
46	(γ,p)	0.151	0.159	1.11
	(γ,n)	0.183	0.042	
51	(γ,p)	0.184	0.171	1.12
	(γ,n)	0.186	0.043	

[a] Computed with adopted values for β from Table I.

(continued)

References:

2: 71 Be 3
4: 68 Go 5
7: 71 Bu 1
11: 75 Ir 1
12: 73 We 5
19: 70 Me 2
20: 71 Ar 1

REF. P. Argan, G. Audit, A. Bloch, N. de Botton, J.L. Faure, C. Schuhl, G. Tamas, C. Tzara, E. Vincent, J. Deutsch, D. Favart, R. Prieels, B. Van Oystaeyen
Phys. Rev. C21, 1416 (1980)

EL EM. SYM.	A	Z
He	4	2

METHOD

REF. NO. 80 Ar 2 hg

REACTION	RESULT	EXCITATION ENERGY	SOURCE TYPE	SOURCE RANGE	DETECTOR TYPE	DETECTOR RANGE	ANGLE
G,PIØ	ABY	137-148	C	139-148	CKV-D		0

Relative measurements of π^0 photoproduction yields have been performed on hydrogen, deuterium, ^{3}He, and ^{4}He, in the region of 1 to 10 MeV above threshold. A simplified distorted-wave impulse approximation model of the four reactions is described; it leads to an overall understanding of the results. Large rescattering effects are brought to evidence in deuterium and ^{3}He, making the extraction of precise values for the dipole photoproduction amplitudes E_{0+} on nucleons strongly dependent on the theoretical description of the processes.

THRESHOLD MEASUREMENT

Final data in 81Ar2.

[NUCLEAR REACTIONS (γ,π^0), ^{1}H, ^{2}H, ^{3}He, and ^{4}He targets; measured reaction yields, $E_\gamma{}^0 = 1$–10 MeV.]

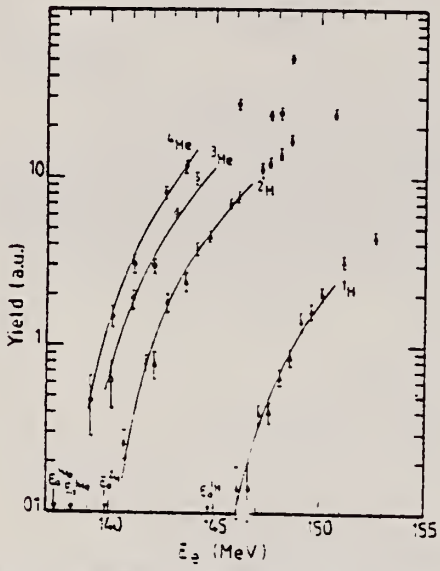

FIG. 5. The measured π^0 photoproduction yields as a function of the end-point bremsstrahlung energy E_e. The curves are the theoretical yields computed with DWIA cross sections, and adjusted to the data up to 6 MeV above threshold as explained in the text.

TABLE III. Experimental yields $Y_A(E_e) = C\int_{E_0}^{E_e}\int_{\Omega_\pi} B(E,E_e)\epsilon_A(E,\Omega)(d\sigma_A/d\Omega)d\Omega\,dE$ in microbarns, normalized to one target nucleus and one equivalent quantum, for different values of the bremsstrahlung end-point energy E_e above threshold E_0. *Note:* The measurements with empty targets gave $Y_{empty} = 0.00 \pm 0.02$. The average yields measured below threshold amounted to $Y_H = 0.02 \pm 0.02$, $Y_D = 0.07 \pm 0.04$, $Y_{^3He} = 0.01 \pm 0.12$, and $Y_{^4He} = 0.01 \pm 0.15$. All have been taken into account in the table.

Hydrogen $E_e - E_0$ (MeV)	Hydrogen $10^6 Y_H$	Deuterium $E_e - E_0$ (MeV)	Deuterium $10^6 Y_D$	^{3}He $E_e - E_0$ (MeV)	^{3}He $10^6 Y_{^3He}$	^{4}He $E_e - E_0$ (MeV)	^{4}He $10^6 Y_{^4He}$
1.41	0.14 ± 0.05	0.88	0.26 ± 0.05	1.37	0.61 ± 0.19	1.72	0.47 ± 0.19
1.91	0.14 ± 0.06	1.38	0.79 ± 0.08	2.37	1.88 ± 0.24	2.72	1.48 ± 0.22
2.41	0.39 ± 0.05	2.26	0.77 ± 0.14	3.87	2.94 ± 0.28	3.72	3.02 ± 0.39
2.91	0.40 ± 0.06	2.88	1.79 ± 0.21	4.87	6.08 ± 0.47	5.22	8.12 ± 0.63
3.41	0.65 ± 0.07	3.76	2.38 ± 0.29	5.87	9.86 ± 0.83	6.22	11.52 ± 0.89
3.91	0.85 ± 0.10	4.26	3.75 ± 0.32	9.37	23.7 ± 1.2	8.72	27.3 ± 1.7
4.41	1.39 ± 0.17	4.88	4.47 ± 0.31	9.87	24.4 ± 1.8	11.22	51.1 ± 3.2
4.91	1.60 ± 0.15	5.38	7.07 ± 0.47				
5.41	2.00 ± 0.16	6.26	7.75 ± 0.55				
6.41	3.15 ± 0.25	7.38	11.13 ± 1.12				
7.91	4.40 ± 0.28	7.76	12.40 ± 0.72				
		8.26	13.9 ± 1.1				
		8.76	16.9 ± 1.1				
		10.38	24.3 ± 1.1				

REF.

Yu.M. Arkatov, P.I. Vatset, V.I. Voloshchuk, V.N. Gur'ev, V.A. Zolenko, I.M. Prokhorets
Sov. J. Nucl. Phys. 32, 2 (1980)
Yad. Fiz. 31, 5 (1980)

EL EM. SYM.	A	Z
He	4	2

METHOD

REF. NO.: 80 Ar 12 hg

REACTION	RESULT	EXCITATION ENERGY	SOURCE		DETECTOR		ANGLE
			TYPE	RANGE	TYPE	RANGE	
G,D	SPC	28-150	C	UKN	CCH-D		DST
G,P	SPC	19-150	C	UKN	CCH-D		DST
G,N	SPC	20-150	C	UKN	CCH-D		DST

ENERGY DST - PN,PD,ND

New experimental results are presented on the reaction $^4He(\gamma, pn)^2H$. In order to carry out comprehensive investigations of the role of the pole mechanism, the distributions obtained have been compared with phase space and with calculations in the pole approximation. It is concluded that the pole mechanism is dominant in this reaction.

PACS numbers: 25.20. + y, 25.10. + s

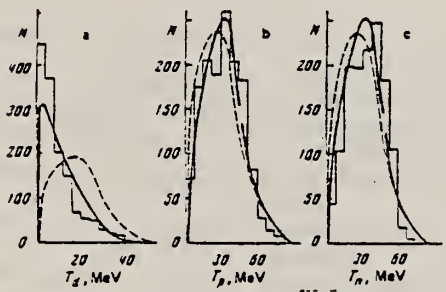

FIG. 2. Distributions in kinetic energies of deuterons (a), protons (b), and neutrons (c). The phase space (dashed curve) and pole-approximation calculations (solid curve) have been normalized to the total number of events.

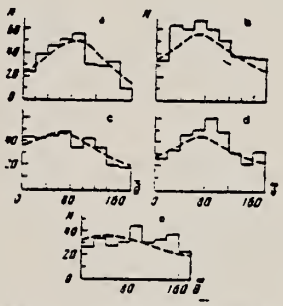

FIG. 4. Distribution (in units of solid angle) in the angle between the γ ray and proton in the rest system of the pn pair for several values of total kinetic energy of the pn pair: (a) 2.2–7.3 MeV, (b) 7.3–17.7 MeV, (c) 17.7–27.7 MeV, (d) 27.7–47.2 MeV, (e) 47.2–95.3 MeV. The dashed curves are the differential cross section (in arbitrary units) for the reaction $\gamma + d \rightarrow p + n$.[7]

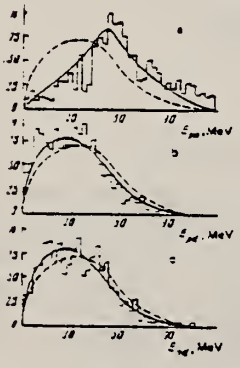

FIG. 3. Distributions in relative energies of the following pairs pn (a), pd (b), and nd (c). The phase-space (dashed curve) and pole-approximation calculations (solid curve) have been normalized to the total number of events.

REF.

Yu. M. Arkatov, P.I. Vatset, V.I. Voloshchuk, V.A. Zolenko, I.M. Prokhorets
Sov. J. Nucl. Phys. 31, 726 (1980)
Yad. Fiz. 31, 1400 (1980)

METHOD

ELEM. SYM.	A	Z
He	4	2

REF. NO.: 80 Ar 13 | hg

REACTION	RESULT	EXCITATION ENERGY	SOURCE		DETECTOR		ANGLE
			TYPE	RANGE	TYPE	RANGE	
G,P	ABI	19 - 150	C	UKN	CCH-D		4PI
G,N	ABI	21 - 150	C	UKN	CCH-D		4PI
G,2D	ABI	23 - 150	C	UKN	CCH-D		4PI
G,NP	ABI	26 - 150	C	UKN	CCH-D		4PI
G,2N2P	ABI	28 - 150	C	UKN	CCH-D		4PI

New experimental data are reported on the photodisintegration of ^{4}He up to the meson-production threshold. The total, dipole, and quadrupole cross sections for absorption of photons by ^{4}He are obtained for the first time. On the basis of the results we have calculated the energy moments of the total, dipole, and quadrupole absorptions of photons and have carried out comparisons with theoretical calculations on the basis of the sum rules.

PACS numbers: 25.20. + y, 25.10. + s

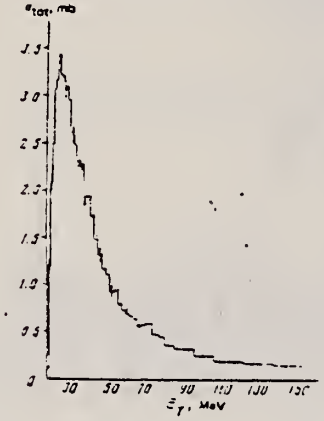

FIG. 1. Energy dependence of the cross section for total absorption of photons by ^{4}He.

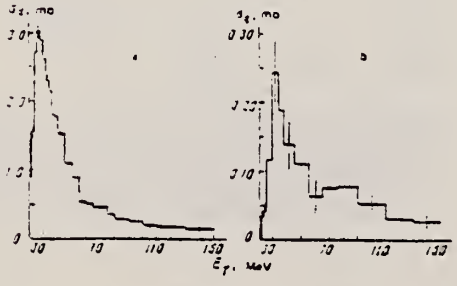

FIG. 2. Energy dependence of the electric-dipole cross section (a) and electric-quadrupole cross section (b) for absorption of photons by ^{4}He.

Total Absorption of Photons

TABLE I.

Reaction	Energy moments				
	σ_0, mb·MeV^1	σ_0, mb·MeV	$\sigma_1 \cdot 10^2$, mb	$\sigma_{-1} \cdot 10^4$, mb·MeV^{-1}	$\sigma_{-3} \cdot 10^4$, mb·MeV^{-3}
(γ, p)	1701.19±25.37	41.250±0.420 (40.1±0.9) * (32.3±0.6) **	1172.10±12.00 (1130±30) *	371.54±4.97	127.770±1.550
(γ, n)	1967.53±36.32	41.810±0.490 (42.5±1.1) * (29.0±0.5) **	1088.25±11.27 (1090±25) *	323.52±3.55	104.510±1.250
$(\gamma, 2d)$	3.08±0.27	0.074±0.004 (0.4) *	1.97±0.11 (10) *	0.563±0.032	0.168±0.010
(γ, pn)	1116.43±48.33	13.460±0.426 (11.5±1.7) * (4.6±0.1) **	194.30±5.20 (190±24) *	33.470±0.970	6.739±0.231
$(\gamma, 2p2n)$	232.5±28.08	2.990±0.317 (8.2±1.2) * (2.3±0.1) **	42.48±4.21 (100±13) *	6.732±0.700	1.192±0.113
Total absorption	5020.30±69.03	99.714±0.551 (103±7) *	2504.40±17.77 (2520±160) *	736.125±5.53	240.370±2.010

*Data of Ref. 4 up to E_γ = 170 MeV.
**Data of Ref. 7 up to E_γ = 60 MeV.

Dipole Absorption

TABLE II.

Reaction	Energy moments			
	σ_0, mb·MeV	σ_1, 10^2, mb	$\sigma_{-1} \cdot 10^4$, mb·MeV^{-1}	$\sigma_{-3} \cdot 10^4$, mb·MeV^{-3}
(γ, p)	28.70±0.58	107.69±[illegible]	342.40±5.20	119.03±1.00
(γ, n)	38.21±0.70	1967.63±15.48	231.06±4.67	89.01±1.39
(γ, pn)	4.21±0.05	95.06±3.73	12.67±0.48	4.47±0.06
$(\gamma, 2p2n)$	1.57±0.20	31.07±2.09	3.80±0.27	0.33±0.04
$\Sigma\sigma$ absorption	48.91±0.99 (101±7) *	2150.86±22.02 (2470±150) *	543.73±7.01	210.24±2.55

*Data of Ref. 4 up to E_γ = 170 MeV.

(continued)

Quadropole Absorption

TABLE III.

Reaction	Energy moments			
	σ_0, mb-MeV	$\sigma_1 \cdot 10^3$, mb	$\sigma_{-1} \cdot 10^3$, mb-MeV^{-1}	$\sigma_{-3} \cdot 10^5$, mb-MeV^{-3}
(γ, p)	3.239±0.500	75.80±11.50	20.711±3.500	6.325±1.200
(γ, n)	3.978±0.634	81.72±12.66	20.555±3.523	5.941±1.135
$(\gamma, 2d)$	0.074±0.004	1.97±0.11	0.563±0.032	0.163±0.010
(γ, pn)	1.048±0.031	18.43±0.59	3.810±0.141	0.845±0.039
$(\gamma, 2p2n)$	0.233±0.025	4.03±0.40	0.787±0.080	0.156±0.019
$E2$ absorption	8.572±0.808 (2) *	181.95±17.12 (50) *	48.412±4.969	13.425±1.652

*Data of Ref. 4 up to $E_\gamma = 170$ MeV.

satisfactorily with the experimental value. Somewhat poorer agreement with our results is given by a calculation taking into account the Rosenfeld mixture of forces ($\sigma_0 = 102$ mb-MeV), and a calculation with a Yukawa potential and an Irving variational wave function for the Serber mixture of forces gives $\sigma_0 = 89$ mb-MeV.

REF. B.L. Berman, D.D. Faul, P. Meyer, D.L. Olson
Phys. Rev. C22, 2273 (1980)

ELEM. SYM.	A	Z
He	4	2

METHOD

REF. NO. 80 Be 1 | hg

REACTION	RESULT	EXCITATION ENERGY	SOURCE TYPE	SOURCE RANGE	DETECTOR TYPE	DETECTOR RANGE	ANGLE
G,1N	ABX	21-47	D	21-47	BF3-I		4PI

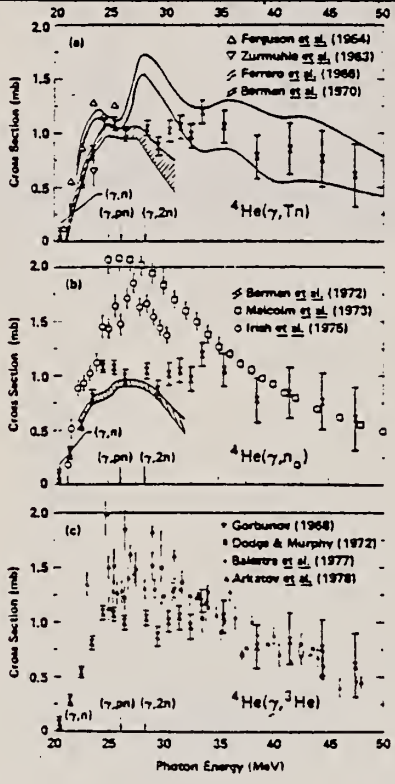

$\sigma_0(\gamma,1n:47.3)=23.1\pm1.6$ MeV-mb

$\sigma_{-1}(\gamma,1n:47.3)=0.71$ mb

$\sigma_{-2}(\gamma,1n:47.3)=.023$ mb/MeV

The photoneutron cross section for ^{4}He has been measured from threshold up to 47 MeV using monoenergetic photons and a high-pressure gas sample. The results agree with earlier monoenergetic-photon and certain photoneutron time-of-flight (liquid-sample) results at the lower energies, and consequently disagree with the results of other measurements at these energies. At the higher energies, however, the present results are essentially in agreement with all previous results.

[NUCLEAR REACTIONS ^{4}He(γ,x); measured $\sigma(E_\gamma)$, 21 to 47 MeV, with monoenergetic photons, 4π neutron detector, high-pressure gas sample; four-nucleon system; isospin mixing; charge asymmetry.]

FIG. 8. Photoneutron cross section for ^{4}He. The present results are indicated as x's in all three parts of the figure. The error flags (except for those for the three highest-energy points; see text) represent statistical uncertainties only. Systematic uncertainties in the 25–28-MeV region could be as large as 15% (see text). (a) Present data compared with the photoneutron-yield results of Ref. 7 (Pennsylvania; open triangles), Ref. 8 (Torino; upper shaded band), Ref. 9 (Livermore; lower shaded band), and with the neutron-capture datum of Ref. 17 (Pennsylvania; open inverted triangle). (b) Present data compared with the photoneutron-time-of-flight data of Ref. 10 (Yale; shaded band), Ref. 11 (Toronto; open circles), and Ref. 12 (Saskatchewan; open squares). The 90° differential cross-section data of Ref. 10 have been converted to total cross sections using the angular-distribution coefficients of Ref. 11. The data of Ref. 11 were obtained with a liquid helium sample and later were renormalized to the results of a 98° measurement obtained with a gaseous sample (see text). (c) Present data compared with the cloud-chamber data of Ref. 13 (Moscow; filled inverted triangles), Ref. 14 (Kharkov; filled triangles), Ref. 15 (Torino; filled circles), and with the magnetic-spectrometer data of Ref. 16 (NBS; filled squares). The data of Ref. 16 were recalculated with the angular-distribution coefficients used in Ref. 6.

U.S. DEPARTMENT OF COMMERCE
NATIONAL BUREAU OF STANDARDS

REF. W. Del Bianco, G. Kajrys
Can. J. Phys. 58, 1496 (1980)

EL EM. SYM.	A	Z
He	4	2

METHOD

REF. NO. 80 De 5 hg

REACTION	RESULT	EXCITATION ENERGY	SOURCE TYPE	SOURCE RANGE	DETECTOR TYPE	DETECTOR RANGE	ANGLE
P,G	SPC	20-21	D	460*930	NAI-D		DST
		(20.145-20.5)					

*ENERGY IN KEV, J-PI

The differential cross section of the $^3H(p,\gamma)^4He$ reaction has been measured at the proton energies E_p = 0.46, 0.50, 0.62, 0.77, and 0.93 MeV. A thin ^3H–Ti target has been used and the γ-rays have been detected by a 12.7 cm diameter × 15.2 cm long NaI(Tl) crystal rotating over the angular range θ_L = 0 to 135°. The $^3H(p,\gamma)^4He$ reaction is found to proceed through E1, M1, and E2 transitions, E1 transitions being predominant. The ratio of the γ-ray flux at θ_L = 0 and 90° is energy dependent and decreases from 0.017 ± 0.003 at E_p = 0.46 MeV to 0.0078 ± 0.006 at E_p = 0.93 MeV.

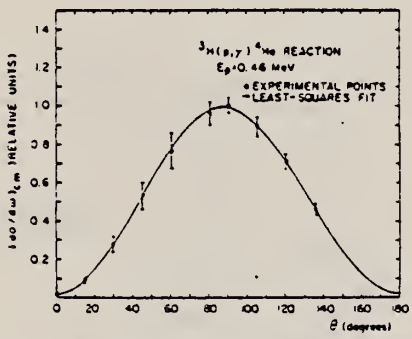

FIG. 4. Angular distribution of the $^3H(p,\gamma)^4He$ reaction at E_p = 0.46 MeV.

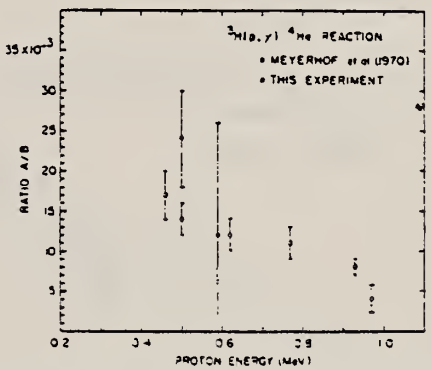

FIG. 5. Plot of the ratio A/B vs. proton energy. The open circles are the results of this experiment and the solid points the data of Meyerhof *et al.* (7).

TABLE 1. Coefficients of the angular distribution of the $^3H(p,\gamma)^4He$ reaction

E_p (MeV)	A	B	C
0.46	0.0165 ± 0.0024	0.97 ± 0.02	0.081 ± 0.033
0.50	0.0135 ± 0.0015	0.98 ± 0.01	0.064 ± 0.018
0.62	0.0120 ± 0.0015	0.99 ± 0.01	0.074 ± 0.024
0.77	0.0109 ± 0.0015	1.01 ± 0.02	0.080 ± 0.036
0.93	0.0078 ± 0.0006	0.99 ± 0.01	0.102 ± 0.015

TABLE 2. $^3H(p,\gamma)^4He$ reaction. Angular distributions and polarization of γ-rays

Entrance channel S	L	J^π	Exit channel J^π	Multipole transition	Angular distribution	Polarization (θ = 90°)
0	1	1^-	0^+	E1	$\sin^2\theta$	100%, parallel
0	2	2^+	0^+	E2	$\sin^2\theta\cos^2\theta$	100%, parallel
1	0	1^+	0^+	M1	Isotropic	Unpolarized
1	1	1^-	0^+	E1	$1+\cos^2\theta$	100%, perpendicular

REF. R.C. McBroom, H.R. Weller, S. Manglos, N.R. Roberson, S.A. Wender
D.R. Tilley, D.M. Skopik, L.G. Arnold, R.G. Seyler
Phys. Rev. Lett. 45, 243 (1980)

EL.EM. SYM.	A	Z
He	4	2

METHOD

REF. NO.	
80 Mc 2	hg

REACTION	RESULT	EXCITATION ENERGY	SOURCE		DETECTOR		ANGLE
			TYPE	RANGE	TYPE	RANGE	
P,G	ABX	26-44	D	8-31	NAI-D	17-31	DST

The fore-aft asymmetry in the angular distribution of the reaction $^3H(p,\gamma_0)^4He$ has been measured as a function of energy for protons from 17 to 31 MeV. The same quantity was also measured using the reaction $^4He(e,^3H)pe'$. These asymmetry data were fitted with an expression which consisted of a term which varied slowly with energy plus a 2^+ resonance having parameters of $\Gamma_{c.m.}=3.5$ MeV and $E_x(\text{res})=40.2$ MeV.

PACS numbers: 25.40.Lw, 25.10.+s

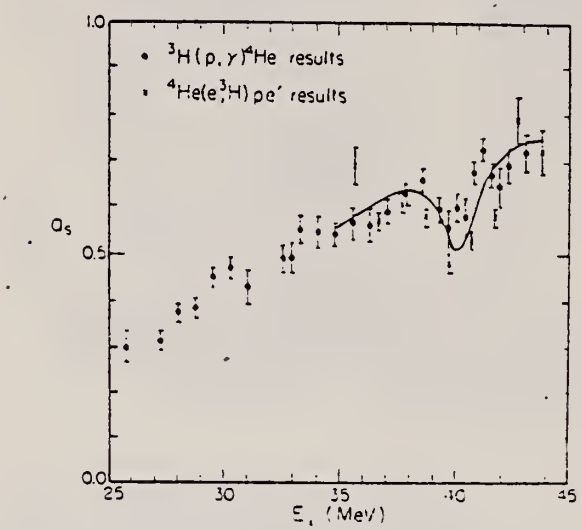

FIG. 1. The measured fore-aft asymmetries in the center-of-mass system are shown as a function of excitation energy in ^4He. The data of both reaction studies are shown. The error bars represent the statistical errors only. The solid curve is the result of a fit described in the text.

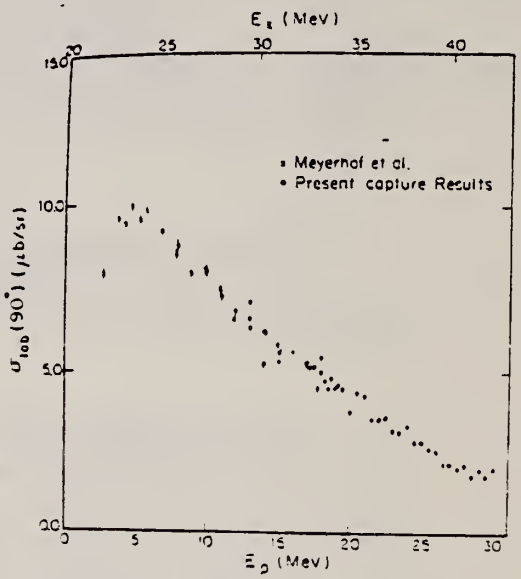

FIG. 2. The experimentally determined cross section for the reaction $^3H(p,\gamma_0)^4He$ at $\theta_{lab}=90^\circ$ as a function of incident proton energy. The data of the present work are shown along with the data of Ref. 10. The error bars represent the statistical uncertainties associated with the data points.

REF. J. Arends, J. Eyink, A. Hegerath, K.G. Hilger, B. Mecking, G. Nöldeke, H. Rost
Phys. Lett. 98B, 423 (1981)

ELEM. SYM.	A	Z
He	4	2

METHOD

REF. NO. 81 Ar 1 hg

REACTION	RESULT	EXCITATION ENERGY	SOURCE TYPE	SOURCE RANGE	DETECTOR TYPE	DETECTOR RANGE	ANGLE
G,MU-T	ABX	215-386	D	215-386	TOF-D		4PI

DATA ALSO IN 81AR3

Double differential cross sections for the photo-emission of protons and charged pion production were investigated for a number of target nuclei (He, Be, C, O, Al, Ti, Cu, Sn, Pb) in the photon energy range k = (215–386) MeV. On the basis of these experimental results the total hadronic cross section was determined.

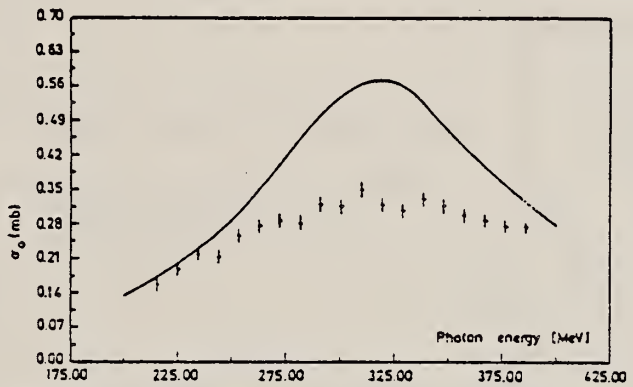

Fig. 7. Parameter σ_0 as a function of photon energy (data points) compared to the mean cross section for a free nucleon (solid line).

The total hadronic cross sections for all measured elements can be parametrized in the form

$$\sigma(k,A) = \sigma_0(k) \cdot A^x ,$$

A being the atomic number, with a constant exponent x = 1.1. The photon energy dependence of σ_0 is shown in fig. 7. Compared to the mean cross section for a free nucleon (the solid line in fig. 7) the excitation of the Δ-resonance is suppressed. Such a suppression is expected in the Δ-hole model [11].

REF. P. Argan, G. Audit, A. Bloch, N. de Botton, J.L. Faure, C. Schuhl, G. Tamas, C. Tzara, E. Vincent, J. Deutsch, D. Favart, R. Prieels, B. Van Oystaeyen
Phys. Rev. C24, 300 (1981)

ELEM. SYM.	A	Z
He	4	2

METHOD

REF. NO.: 81 Ar 2 egf

REACTION	RESULT	EXCITATION ENERGY	SOURCE		DETECTOR		ANGLE
			TYPE	RANGE	TYPE	RANGE	
G,PIØ	ABY	139-148	C	139-148	CKV-D		Ø

REANALYSIS OF 80AR2

Our recently published π^0 photoproduction data at threshold have been reanalyzed with the use of a more refined detection efficiency calculation. The high energy points appear to be consistent with the threshold measurements; the effective threshold amplitudes remain unchanged, and are now supported by the complete set of experimental data.

[NUCLEAR REACTIONS (γ,π^0), ^{1}H, ^{2}H, ^{3}He, and ^{4}He targets; measured reaction yields, $E_{\gamma 0}$=1–10 MeV.]

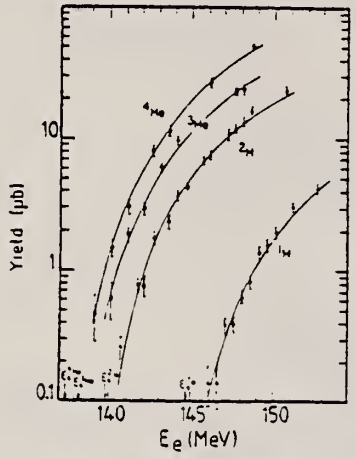

FIG. 2. The measured π^0 photoproduction yields in microbarns, normalized to one target nucleus and one equivalent quantum, as functions of the Bremsstrahlung end-point energy E_e. The curves are the theoretical yields computed with DWIA cross sections, and adjusted to the complete set of data as explained in the text.

REF. J. Arends, J. Eyink, A. Hegerath, K.G. Hilger, B. Mecking, G. Nöldeke, H. Rost
Nucl. Phys. A358, 367c (1981)

ELEM. SYM.	A	Z
He	4	2

METHOD

REF. NO. 81 Ar 3 hg

REACTION	RESULT	EXCITATION ENERGY	SOURCE		DETECTOR		ANGLE
			TYPE	RANGE	TYPE	RANGE	
G,MU-T	ABX	215-386	D	215-386	TOF-D		4PI

Abstract: Double differential cross sections for the photoemission of protons and charged pion photoproduction were investigated for a number of target nuclei (He, Be, C, O, Al, Ti, Cu, Sn, Pb) using the tagged bremsstrahlung beam at the Bonn 500 MeV-Synchrotron in the photon range k = (215-386)MeV. On the basis of these experimental results the total hadronic cross section was determined.

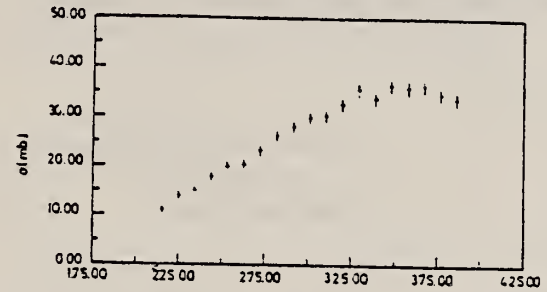

Fig. 2. Cross section for the process: γ + Pb → p + X. The proton threshold is 58 MeV.

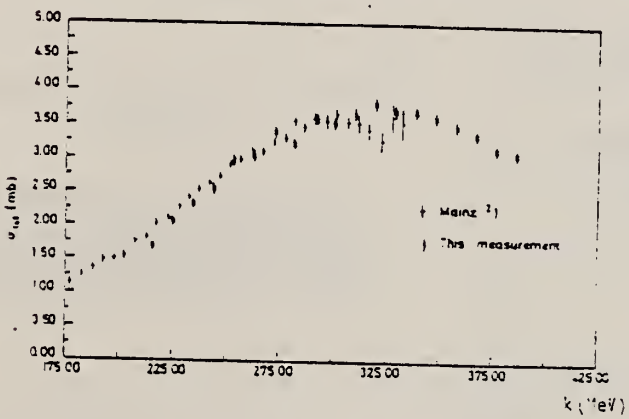

Fig. 3. Total hadronic cross section for Be. The data are compared to the cross section taken from ref.[1]).

The photon energy dependence of the total cross sections for heavier nuclei are similar to the Be results. The complete data set can be parametrized in the form

$$\sigma(k,A) = \sigma_0(k) \cdot A^x.$$

The exponent is constant x = 1.1. The photon energy dependence of σ_0 is shown in fig. 4. Compared to the mean cross section for a free nucleon, the excitation of the Δ-resonance is suppressed.

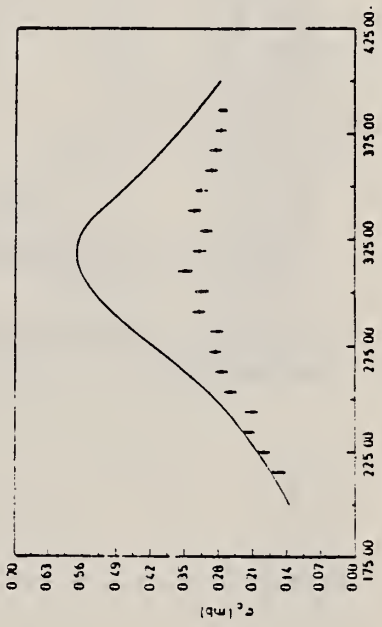

Fig. 4. Parameter σ_0 compared to the cross section for a free nucleon (full line).

REF. J. Uegaki, L.O. Dallin, Y.M. Shin, C.Y. Kim
Nucl. Inst. Meth. 179 179, 55 (1981)

ELEM. SYM.	A	Z
He	4	2

METHOD

REF. NO.	
81 Ue 1	hg

REACTION	RESULT	EXCITATION ENERGY	SOURCE		DETECTOR		ANGLE
			TYPE	RANGE	TYPE	RANGE	
G,T	RLY	5-100	C	100	TEL-D		DST
G,HE3	RLY	21-100	C	100	TEL-D		DST

High resolution telescope counters which employ thick germanium and silicon surface barrier detectors have been constructed nd used for experiments with bremsstrahlung beams at high energies. The system has been tested with ≤160 MeV bremsstrahlung ams and Li targets. All charged particles up to $E \simeq 100$ MeV are clearly separated, and there is little background in the mea- ured spectra except at very low energies. Data have been acquired for the ^{2}D(γ, p) n reaction at 90° and for the ^{4}He(γ, $^3_1$) reac- on angular distributions. The system may be constructed at about 1% of the cost of a magnetic spectrometer with a comparable nergy resolution and analyzing capability.

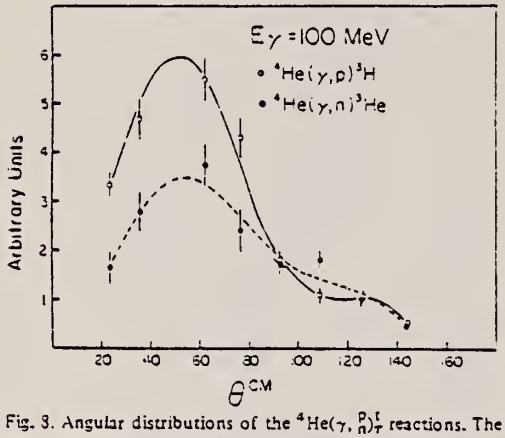

Fig. 3. Angular distributions of the ^{4}He(γ, ^p_n)$^t_3$ reactions. The data are converted to the proton (neutron) angles in the centre-of-mass system.

REF. L. Ward, D.R. Tilley, D.M. Skopik, N.R. Roberson, H.R. Weller
Phys. Rev. C24, 317 (1981)

ELEM. SYM.	A	Z
He	4	2

METHOD

REF. NO. 81 Wa 3 hg

REACTION	RESULT	EXCITATION ENERGY	SOURCE TYPE	SOURCE RANGE	DETECTOR TYPE	DETECTOR RANGE	ANGLE
N,G	ABX	24-34	D	1-17	NAI-D		DST

A recently reported measurement of the photoneutron cross section for ^{4}He indicates a value of about 1.0 mb for E_x of -23 to -33 MeV. This result, when combined with the previously reported (γ,p) cross section in this energy region, implies a (γ,p)-to-(γ,n) cross section ratio of 1.6 to 1.9 in the 26 to 29 MeV region of ^{4}He. We have used the inverse reaction ^{3}He$(n,\gamma)^4$He to measure the photoneutron cross section for ^{4}He. Our detailed balanced results confirm the recently reported measurements.

[NUCLEAR REACTIONS ^{3}He$(n,\gamma)^4$He; measured $\sigma(E;\theta)$, E = 6.0 to 17.0 MeV. Results confirm the most recent ^{4}He$(\gamma,n)^3$He measurements.]

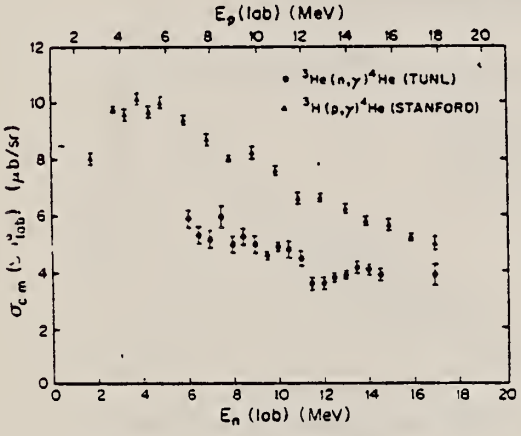

FIG. 2. Differential cross section for the ^{3}He$(n,\gamma)^4$He reaction at 90° (TUNL). The previously reported ^{3}H(p,γ)-^{4}He cross section data at 90° are also shown (Stanford—Ref. 18). The two energy scales are aligned so that the data sets correspond to the same excitation energy in ^{4}He. The error bars are only the statistical errors associated with the data points.

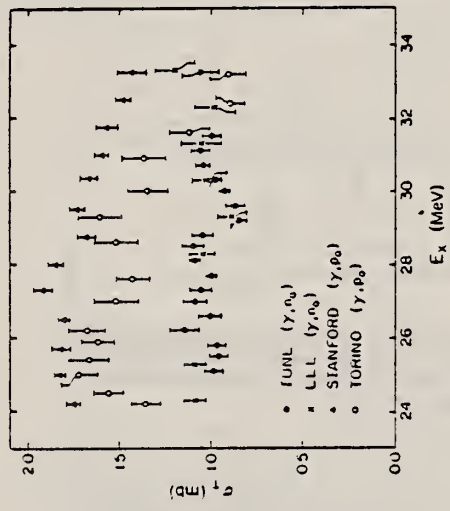

FIG. 4. The angle integrated ^{4}He$(\gamma,n)^3$He data obtained via detailed balance (TUNL) are shown along with the ^{4}He (γ,n) ^{3}He data of Ref. 1 (LLL). The ^{4}He$(\gamma,p)^3$H results of Ref. 19 (Torino) and those obtained from the data of Ref. 18 (Stanford) are also shown. All error bars are statistical.

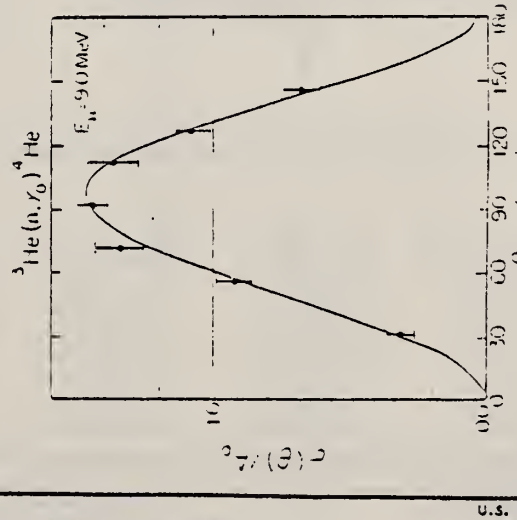

FIG. 3. The measured angular distribution at E_n = 9.0 MeV. The error bars represent statistical errors associated with the data points. The solid curve is the result of a fit to Legendre polynomials and was used to obtain the ratio of $\sigma(90°)$ to σ_T.

[1]B. L. Berman, D. D. Faul, P. Meyer, and D. L. Olson, Phys. Rev. C 22, 2273 (1980). 80Be1

[18]W. E. Meyerhof, M. Suffert, and W. Feldman, Nucl. Phys. A148, 211 (1970). 70Me2

[19]F. Balestra *et al.*, Nuovo Cimento A 38, 145 (1977). 77Ba14

REF. A.S. Aleksanyan, T.L. Asatiani, N.V. Vladimirskiĭ, A.O. Gasparyan, M.I. Daĭon, V.A. Ivanov, S.P. Karavaev, S.N. Karapetyan, F.F. Kayumov, G.K. Megrabyan, N.A. Nalbandyan, É.M. Oganesyan, R.N. Pikhtelev, V.M. Rappoport
Yad. Fiz. 35, 368 (1982)
Sov. J. Nucl. Phys. 35, 210 (1982)

EL EM. SYM.	A	Z
He	4	2

METHOD

REF. NO.	
82 A1 1	egf

REACTION	RESULT	EXCITATION ENERGY	SOURCE		DETECTOR		ANGLE
			TYPE	RANGE	TYPE	RANGE	
G,PIØ	ABX	1*4	C	2*4	TEL-D		DST

1.5*4.5 GEV, 2-8 DEG

Experimental values are reported for the differential cross sections for elastic photoproduction of π^0 mesons from helium nuclei at photon energies 1.5–4.5 GeV in the angle region $\theta_\pi = 2$–8°. The parameters of the ω-meson trajectory are obtained. The work was carried out in the bremsstrahlung beam of the Erevan synchrotron.

PACS numbers: 25.20. + y, 27.10. + h, 25.10. + s

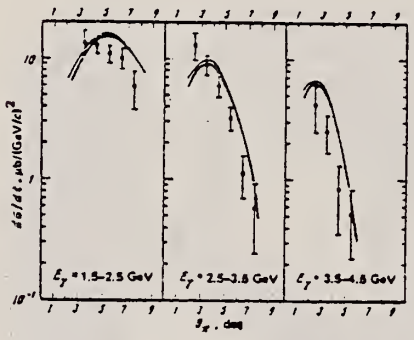

FIG. 4. Differential cross sections for elastic photoproduction of π^0 mesons from ^{4}He as a function of the emission angle of the meson in the laboratory system. The solid lines are the result of calculations from Ref. 7.

TABLE I

E_γ, GeV	ϑ_π, deg	$d\sigma/dt$, $\frac{\mu b}{(GeV/c)^2}$	Statistical errors, $\pm\Delta(d\sigma/dt)$, $(GeV/c)^2$
1.5–2.5	3–4	13.5	±2.9
	4–5	12.9	±2.1
	5–6	10.9	±1.8
	6–7	10.2	±2.0
	7–8	5.8	±2.0
2.5–3.5	2–3	13.1	±3.3
	3–4	8.9	±1.6
	4–5	5.9	±1.1
	5–6	3.2	±0.74
	6–7	1.1	±0.42
	7–8	0.57	±0.33
3.5–4.5	2–3	4.2	±1.7
	3–4	2.5	±0.90
	4–5	0.83	±0.48
	5–6	0.52	±0.30

REF. R.C. McBroom, H.R. Weller, N.R. Roberson, D.R. Tilley
Phys. Rev. C25, 1644 (1982)

ELEM. SYM.	A	Z
He	4	2

METHOD

REF. NO. 82 Mc 1 egf

REACTION	RESULT	EXCITATION ENERGY	SOURCE		DETECTOR		ANGLE
			TYPE	RANGE	TYPE	RANGE	
P,G	ABX	25-44	D	8-30	NAI-D		DST

We have measured the cross section for the $^3H(p,\gamma)^4He$ reaction for incident proton energies from 8–30 MeV. The absolute 90° differential cross section below $E_p = 18$ MeV is in reasonable agreement with previous results. Angular distributions were measured at eight energies between $E_p = 13$ and 30 MeV. The coefficients which result from fitting these data to an expansion in Legendre polynomials are reported.

[NUCLEAR REACTIONS $^3H(p,\gamma)$, measured $\sigma(E,\theta)$ from $E_p = 8-30$ MeV. Obtained Legendre polynomial coefficients.]

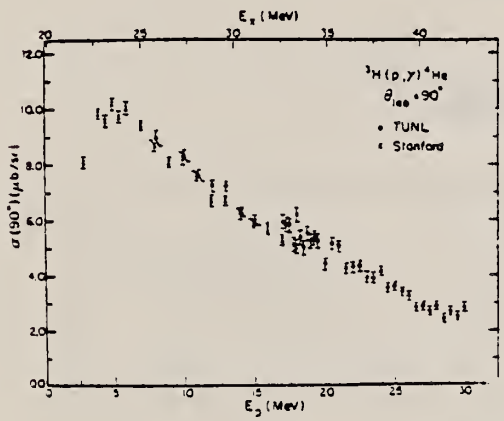

FIG. 3. The laboratory cross sections obtained at $\theta_{lab} = 90°$ are shown along with the data of Ref. 1 (Stanford). The error bars represent only the statistical uncertainties.

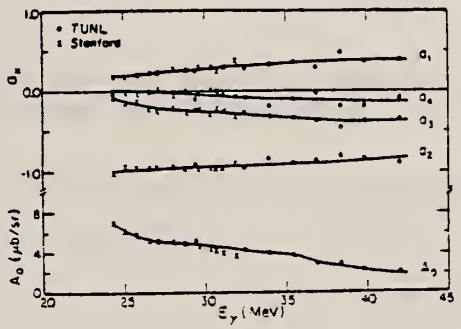

FIG. 5. The A_0 and a_k coefficients of Table II are shown here as a function of the outgoing γ-ray energy. The data of Ref. 1 (Stanford) are also shown. The statistical uncertainties associated with the present results are presented in Table II. The solid lines are smooth curves drawn through the data points.

TABLE II. The A_0 and a_k coefficients obtained for the $^3H(p,\gamma)^4He$ reaction.

E_p MeV	E_γ MeV	A_0 μb/sr	a_1	a_2	a_3	a_4
13	29.4	5.05±0.16	0.243±0.018	−0.908±0.021	−0.247±0.022	−0.106±0.066
17	32.4	4.07±0.12	0.273±0.009	−0.936±0.013	−0.279±0.009	−0.075±0.025
19	33.9	4.03±0.09	0.314±0.009	−0.825±0.012	−0.309±0.009	−0.180±0.013
21	35.4	3.40±0.09	0.348±0.010	−0.893±0.013	−0.337±0.009	−0.104±0.016
23	36.8	2.91±0.05	0.292±0.008	−0.868±0.011	−0.370±0.008	−0.028±0.024
25	38.3	2.83±0.06	0.458±0.009	−0.798±0.011	−0.466±0.009	−0.139±0.010
27	39.8	2.29±0.05	0.353±0.009	−0.841±0.012	−0.359±0.009	−0.174±0.012
30	42.0	2.11±0.14	0.382±0.070	−0.890±0.071	−0.350±0.073	−0.084±0.175

REF. S. Rock, R.G. Arnold, B.T. Chertok, Z.M. Szalata, D. Day, J.S. McCarthy, F. Martin, B.A. Mecking, I. Sick, G. Tamas
Phys. Rev. C26, 1592 (1982)

EL.EM. SYM.	A	Z
He	4	2

METHOD

REF. NO.: 82 Ro 2 egf

REACTION	RESULT	EXCITATION ENERGY	SOURCE TYPE	SOURCE RANGE	DETECTOR TYPE	DETECTOR RANGE	ANGLE
E,E/	RLX	1*5	D	6@17	MAG-D		8

Tabular Data given .8*2.4(GEV/C)SQR,@GEV

The cross section for inclusive inelastic electron scattering from the helium isotopes has been measured at momentum transfers squared of $0.8 \le Q^2 \le 5.0$ (GeV/c)^2 for ^{3}He and $0.8 \le Q^2 \le 2.4$ (GeV/c)^2 for ^{4}He. The data were taken at 8° and cover the range $0.6 < x < 1$, where $x = Q^2/2M_{He}\nu$, which includes the elastic peak, nuclear breakup threshold, the high momentum tail of the quasielastic scattering, and pion production. The structure function, νW_2, derived from the data, is approaching a scaling limit at high Q^2. It can be factored into a product of functions of Q^2 and of x as predicted by some models.

[NUCLEAR REACTIONS ^{3}He, ^{4}He$(e,e')X$; $E = 6.4-16.5$ GeV; $\theta_e = 8°$; measured $d\sigma/d\Omega\, dE'$; deduced νW_2 at threshold.]

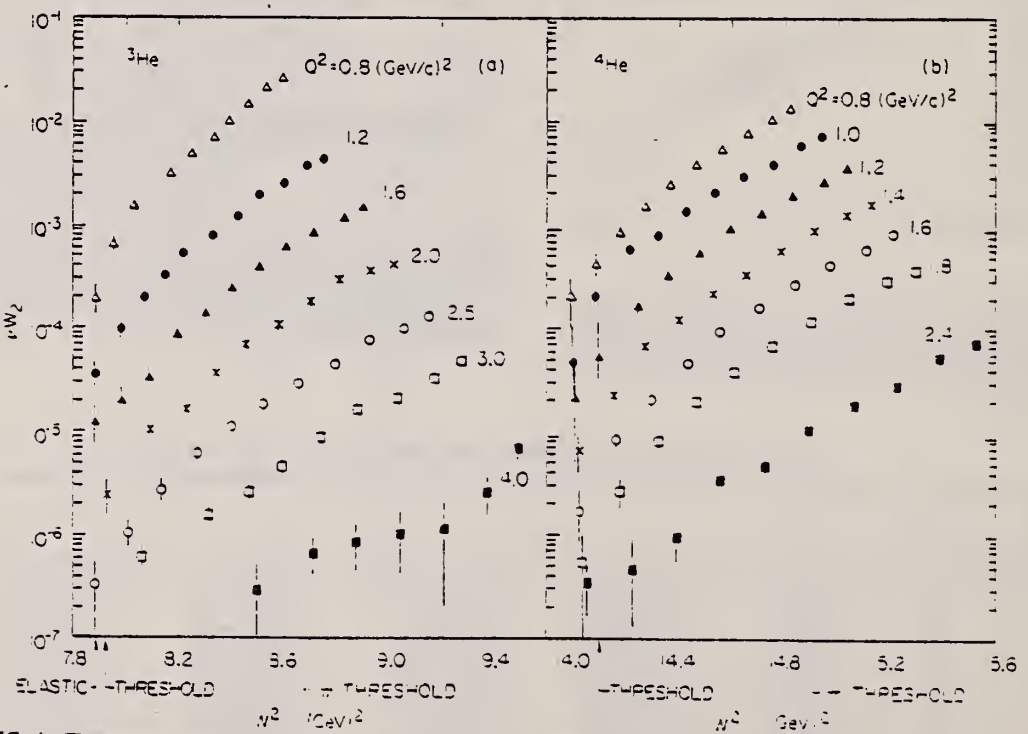

FIG. 6. The dimensionless inelastic structure function $\nu W_2(Q^2, W^2)$ as a function of the missing mass squared (W^2) for several values of the momentum transfer squared (Q^2), (a) ^{3}He and (b) ^{4}He.

(continued)

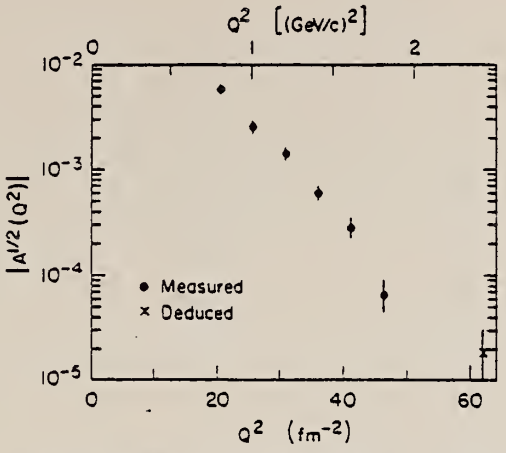

FIG. 15. The elastic structure function $A(Q^2)$ for ^{4}He as a function of Q^2 showing previously directly measured values (Ref. 1) and the highest Q^2 value derived from the elastic-inelastic connection.

HE
A=5

HE
A=5

Ref. J. Buss, H. Waeffler, B. Ziegler
Phys. Letters 4, 198 (1963)

Elem. Sym.	A	Z
He	5	2

Method
(source not given); NaI

Ref. No.
63 Bu 2 JHH

Reaction	E or ΔE	E_o	Γ	$\int \sigma dE$	Jπ	Notes
$H^3(d,\gamma)$	0.150 -1.300	~ 17				At the resonance energy, σ_{max} $H^3(d,\gamma)He^5$ = 60 μb

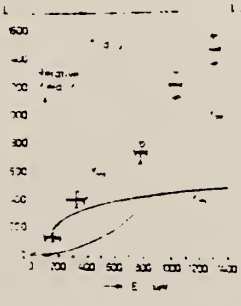

Fig. 1. Thick target excitation curve for Tid, γ reaction
+ Experimental values for the relative yield
Y_{res} Thick target yield, calculated with the cross section (σ_{res}) from fig. 2.
Y_{dir} Thick target yield, calculated with the cross section (σ_{dir}) from fig. 2.
Y_{tot} Y_{res} + Y_{dir}

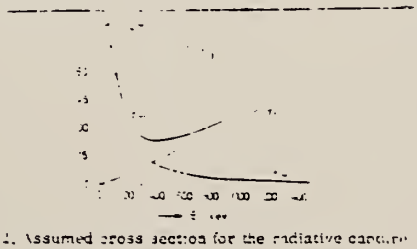

Fig. 2. Assumed cross section for the radiative capture Tid, γ. σ_{res} cross section for resonance capture. The shape of the curve is the same as given by Porter et al. [1] for $H^2(d,n)He^3$. σ_{dir} cross section for direct capture process. A linear increase with energy is assumed. The slope is adjusted to give the best fit for Y_{tot} (fig. 1) to the experimental points.
The absolute scale for σ_{res} + σ_{dir} is taken from the absolute value of the [illegible] cross section as given in the text.

REF. V. M. Bezotosnyi, V. A. Zhmailo, L. M. Surov, and M. S. Shvetsov
Yad. Fiz. 10, 225 (1969)
Sov. J. Nucl. Phys. 10, 127 (1970)

ELEM. SYM.	A	Z
He	5	2

METHOD

REF. NO.: 69 Be 10 egf

REACTION	RESULT	EXCITATION ENERGY	SOURCE		DETECTOR		ANGLE
			TYPE	RANGE	TYPE	RANGE	
D,G	ABX	17	D	999	NAI-D		
		(16.7)		(.025-.100)			

999 = 25-100 keV

We report the results of measurements of cross sections of the reaction $T(d,\gamma)He^5$ with emission of 16.7-MeV γ quanta at a deuteron energy 25—100 keV. The ratio of the cross sections of the reactions $T(d,\gamma)He^5$ and $T(d,n)He^4$ is found to be $\sigma(d,\gamma)/\sigma(d,n) = (2.1 \pm 0.6) \times 10^{-4}$, and the radiative width of the reaction $T(d,\gamma)He^5$ is $\Gamma_\gamma = 14 \pm 4$ eV. The results are compared with the data of other papers on the mirror reaction.

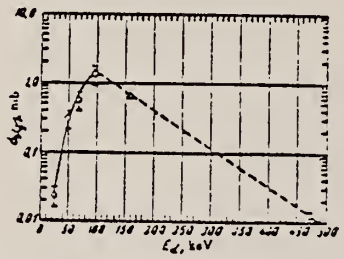

Cross section of the reaction $T(d,\gamma)He^5$ vs. the deuteron energy. Points: ○—present results, △—data of [1], □—data of [2].

[1] G. Sawyer and L. Burkhardt, Phys. Rev. 98, 1305 (1955).
[2] J. Coon and R. Davis, Bull. Amer. Phys. Soc. 4, 365 (1939).

REF. A. Kosiara and H. B. Willard
Phys. Letters 32B, 99 (1970)

ELEM. SYM.	A	Z
He	5	2

METHOD

REF. NO. 70 Ko 1 egf

REACTION	RESULT	EXCITATION ENERGY	SOURCE		DETECTOR		ANGLE
			TYPE	RANGE	TYPE	RANGE	
D,G	ABX	18	D	1	SCI		90
				(1.025)			

$\sigma^{3}H(^{2}H,G)^{5}He$ at 90° = 0.44±0.12 μb/sr

1 = 1025 KEV

HE
A=6

HE
A=6

REF. D. Renker, W. Dahme, W. Hering, H. Panke, C. Zupancic, J.C. Alder, B. Gabioud, C. Joseph, J.F. Loude, N. Morel, J.P. Perroud, A. Perrenoud, M.T. Tran, E. Winklemann, G. Strassner & P. Truöl
Phys. Rev. Lett. 41, 1279 (1978)

ELEM. SYM.	A	Z
He	6	2

METHOD

REF. NO. 78 Re 5 hmg

REACTION	RESULT	EXCITATION ENERGY	SOURCE		DETECTOR		ANGLE
			TYPE	RANGE	TYPE	RANGE	
PI,G	SPC	150	D	0	MGP-D		UKN

PI IS PI-

Partial rates for radiative capture from the 1s atomic level in ^{6}Li to the lowest two ^{6}He states have been determined by measuring, with the necessary energy resolution, x rays and high-energy photons in coincidence. A comparison of our results and other related experimental results with different theoretical approaches shows that phenomenological wave functions consistently describe photopion processes as well as electromagnetic and weak transitions between low-lying ^{6}Li and ^{6}He states.

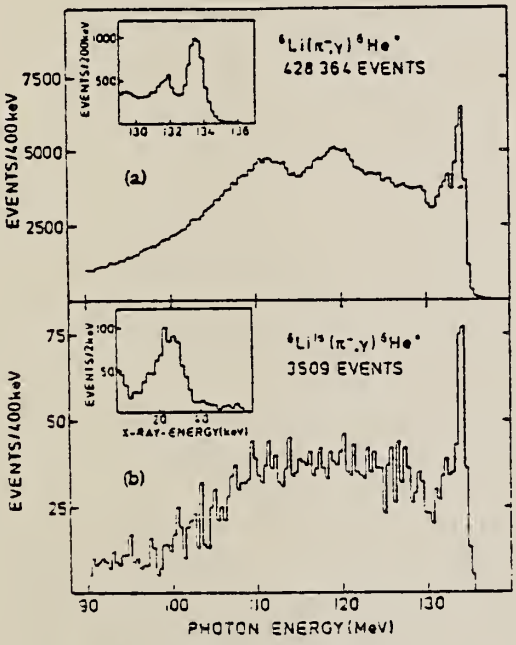

FIG. 1. Spectrum of high-energy photons from radiative pion capture in ^{6}Li. (a) Capture from all atomic levels. The inset shows the upper part of the spectrum measured with optimum resolution. (b) Capture from the atomic 1s level. The inset shows the x-ray spectrum from the coincidence measurement.

TABLE I. Comparison of our experimental results and recent theoretical predictions for the ^{6}He ground state and first excited state. Here, b is the harmonic-oscillator parameter. R_{1s}, R_{2p}, and R are the radiative-capture branching ratios from the atomic 1s level, the 2p level, and all levels, respectively. Λ_γ^{1s} and Λ_γ^{2p} are the absolute radiative-capture rates from the 1s and 2p levels, respectively. The theoretical values obtained in structure-type and phenomenological impulse-approximation calculations are indicated by St and Ph, Respectively. In the latter group, the calculation of Ref. 20 uses π-capture matrix elements directly obtained from other reactions.

Wave Function Components					b	Λ_γ^{1s}	Λ_γ^{2p}	Reference	Type
^{6}He(0⁺)		^{6}Li(1⁺)			[fm]	[s⁻¹]			
$^1S_0$	$^3P_0$	$^3S_1$	$^1P_1$	$^3D_1$		10^{15}	10^{10}		
.92	-.40	.95	.30	.02	1.95	1.70	5.4	16	St
.93	-.36	.99	.12	-.03	1.95	1.89	4.8	17	St
.92	-.40	.95	.30	.02	1.66	2.56	3.0	18	St
.84	-.54	.92	.37	.10	2.19	1.32		5	Ph
1.00	-.01	.92	.37	.10	2.30	1.45		5	Ph
1.00	.03	.92	.37	.10	2.03	1.60		13	Ph
1.00	.03	.92	.37	.10	-	1.45		13	Ph
-	-	-	-	-	2.05	1.51	5.3	20	Ph
.39	.45	.97	.25	.05	1.98	1.10	4.1	21	Ph
						1.60			EP
Experiment:		R = .34±.03							
		R_{1s} = .47±.05				1.39 ±.16	5.8 ±1.9	this work	
		R_{2p} = .26±.05							
^{6}He(2⁺)		^{6}Li(1⁺)							
$^1D_2$	$^3P_2$	$^3S_1$	$^1P_1$	$^3D_1$					
.83	.53	.99	.12	-.03	1.95	.61	3.5	17	St
Experiment:		R = .11±.01							
		R_{1s} = .11±.04				.33 ±.12	2.5 ±1.1	this work	
		R_{2p} = .11±.04							

DEFINITIONS OF ABBREVIATIONS AND SYMBOLS

Note: In this list definitions are given for various photoneutron reactions in which the following symbols are used: N, NL, nN, SN and XN. Corresponding definitions apply for reactions involving other nuclear particles where the symbols N (neutron) is replaced by, e.g. P, D, T, H3, A etc. Where unknown reactions result in the production of a specific radionuclide, the chemical symbol and mass number is listed as the reaction product, e.g. a G,NA22 reaction in ^{59}Co.

A	alpha particle
ANAL	analysis
ABI	absolute integrated cross-section data
ABX	absolute cross-section data
ABY	absolute yield data. Often means cross-section per equivalent quantum is listed.
ACT	measurement of induced radioactivity of the target
ASM	asymmetric, asymmetry
AVG	average
BBL	bubble chamber
BEL B(EL)	reduced electric radiative transition probability
BF3	BF_3 neutron counter with moderator e.g., Halpern detector, long counter
BML	reduced magnetic radiative transition probability, B(ML)
BREAKS	levels located by "breaks" in the yield curve
BRKUP	break up
BRMS	bremsstrahlung
BTW	between
C	continuous. Used to describe a photon source or a detector response function. Contrast with D = discrete.
CCH	cloud chamber
CF	compared with
CHRGD	charged
CMPT	Compton
COIN COINC	coincidence, coincide
COH	coherent
CK	Cerenkov
D	deuteron or discrete. When discrete, it is used to describe a photon source or a detector response function. Contrast with C = continuous.
DLTE	energy loss
DLTQ	momentum transfer
DST	distribution
DT BAL	detailed balance
E	electron
E/	inelastically scattered electron
E+	positron
EDST	energy distribution or spectrum
E/N	used only to indicate a coincidence experiment as in (E,E/N).

	N stands for any outgoing particle measured in coincidence with an inelastically scattered electron. Distinguish from eg., (E,N) which is used to represent an electron induced reaction when only the outgoing particle N is detected.
EMU	emulsions (photographic plates)
EXCIT	excited
F	fission
FMF	form factor
FM-1	inverse femtometers
FRAG	fragment
G	photon
G/	inelastically scattered photon
G-WIDTH	gamma-ray transition width
HAD	hadrons, hadron production
HE He3	^{3}He particle
INT	interaction, integral, intensity
INC	includes
ION	ionization chamber
ISOB	isobaric
ISM	isomer
J	multiplicity of particle defined by following symbol e.g. (G,PJN) with remark J = 2,3,5,7
JPI J-PI	spin and parity of a nuclear state
K	second multiplicity index, e.g. (G,JPKN) with both J & K positive integers greater than 1
KE	kinetic energy
L	may be an integer or zero that always follows a reaction product symbol. This is used to indicate transitions to specific states in the residual nuclide. When the letter is used as in (G,NL) the cross section given is that for the sum of transitions to two or more specific final states.
LFT	excited state lifetime
LIM	limit
LV,LVS	level, levels
LQD	liquid
MAG	magnetic spectrometer
MEAS	measurement(s)
MGC	magnetic Compton spectrometer
MGP	magnetic pair spectrometer
MOD	moderated neutron detector <u>not</u> employing a BF_3 counter, e.g. rhodium foil, Szilard-Chalmers reaction, ^{3}He, ^{6}Li reactions, GD loaded liquid scintillator, etc.
MSP	mass spectrometer
MULT	multiple, multipole, multiplicity
MU-T	used only in combination with G to indicate a total photon absorption cross section measurement, i.e. (G,MU-T)
N	neutron (see also XN and SN). The notation (G,N) is used to indicate a reaction in which only a single neutron is emitted, i.e. the reaction that can, in many cases, be measured by observing the radioactive decay of the residual nuclide.

nN	where n is any integer. (G,nN) indicates the sum over all reaction cross sections in which n neutrons are emitted.
NAI	NaI(Tl) spectrometer
NEUT	neutron(s)
NOX	no cross-section data
P	proton (see also XP)
PART	particle(s)
PHOT	photon(s)
PI	pion, usually written as PI+, PI-, PIO to indicate charge
POL	polarized or polarization
Q-SQUAR	momentum transfer squared (q^2)
RCL	recoil
REL	relative
RLI	relative integrated cross-section data
RLX	relative cross-section data
RSP	reaction spectrometer
RLY	relative yield data
SCTD	scattered
SCD	semiconductor (solid state) detector
SCI	scintillator detector other than NaI, e.g., CsI, KI, organic (liquid or solid), stilbene, He
SEP	separation
SEP ISOTP	separated isotope used
SIG	SIGMA (cross section)
SN	sum of neutron producing reactions, $\sigma(\gamma,SN)=\sigma(\gamma,N) + \sigma(\gamma,NP) + \sigma(\gamma,2N) + \sigma(\gamma,3N)$ + etc.
SPC	photon or particle energy spectrum
SPK	spark chamber
SPL	spallation
STAT	statistical
SYM	symetric, symmetry
T	triton
TEL	counter telescope
THR	threshold for reaction or threshold detector, e.g., $^{29}Si(n,p)^{29}Al$.
TOF	time-of-flight detector
TRK	tracks of particles or fragments observed in solid materials (glass, mylar, etc.)
TRNS	transition
UKN UNK	unknown
VIB	vibrational
VIR PHOT	virtual photon(s)
XN	all neutrons, total neutron yield, $\sigma(\gamma,XN) = \sigma(\gamma,N) + 2\sigma(\gamma,2N) + 3\sigma(\gamma,3N) + \sigma(\gamma,NP)$ + etc.
XP	all protons, total proton yield $\sigma(\gamma,XP) = \sigma(\gamma,P) + \sigma(\gamma,NP) + 2\sigma(\gamma,2P)$ + etc.
XX XXX	reaction products defined in REMARKS
YLD	yield

4PI	a 4π geometry was used or a method like radioactivity or a total absorption measurement		products was determined. The polarized particle is indicated in REMARKS.
999	energy defined in REMARKS	* or @	symbols used to indicate that the units associated with the numerals on one or both sides of the symbol in a specific column are not MeV. The units are defined in REMARKS.
$	indicates the measurement involved beams or targets that were either polarized or aligned, or that the polarization of the reaction		

NBS-114A (REV. 2-8C)

U.S. DEPT. OF COMM. BIBLIOGRAPHIC DATA SHEET (See instructions)	1. PUBLICATION OR REPORT NO. NBSIR 83-2742	2. Performing Organ. Report No.	3. Publication Date July 1983

4. TITLE AND SUBTITLE

Photonuclear Data-Abstract Sheets
1955-1982

5. AUTHOR(S)

E.G. Fuller and Henry Gerstenberg

6. PERFORMING ORGANIZATION (If joint or other than NBS, see instructions)

NATIONAL BUREAU OF STANDARDS
DEPARTMENT OF COMMERCE
WASHINGTON, D.C. 20234

7. Contract/Grant No.

8. Type of Report & Period Covered

9. SPONSORING ORGANIZATION NAME AND COMPLETE ADDRESS (Street, City, State, ZIP)

10. SUPPLEMENTARY NOTES

☐ Document describes a computer program; SF-185, FIPS Software Summary, is attached.

11. ABSTRACT (A 200-word or less factual summary of most significant information. If document includes a significant bibliography or literature survey, mention it here)

These abstract sheets cover most classes of experimental photonuclear data leading to information of the electromagnetic matrix element between the ground and excited states of a given nucleus. This fifteen volume work contains nearly 7200 abstract sheets and covers 89 chemical elements from hydrogen through americium. It represents a twenty-seven year history of the study of electromagnetic interactions. The sheets are ordered by target element, target isotope, and by an assigned bibliographic reference code. Information is given on the type of measurement, excitation energies studied, source type and energies, detector type, and angular ranges covered in the measurement. For a given reference, the relevant figures and tables are mounted on a separate sheet for each nuclide studied.

12. KEY WORDS (Six to twelve entries; alphabetical order; capitalize only proper names; and separate key words by semicolons)

data-abstract sheets, elements, experimental, isotopes, nuclear physics, photonuclear reactions

13. AVAILABILITY

☐ Unlimited

☒ For Official Distribution. Do Not Release to NTIS

☐ Order From Superintendent of Documents, U.S. Government Printing Office, Washington, D.C. 20402.

☐ Order From National Technical Information Service (NTIS), Springfield, VA. 22161

14. NO. OF PRINTED PAGES

15. Price